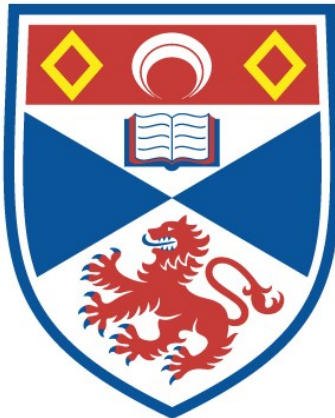


A STUDY OF THE ANCHIZONE-EPIZONE
METAMORPHIC TRANSITION

Charles William Ker Morrison

A Thesis Submitted for the Degree of PhD
at the
University of St Andrews



1990

Full metadata for this item is available in
St Andrews Research Repository

at:

<http://research-repository.st-andrews.ac.uk/>

Please use this identifier to cite or link to this item:
<http://hdl.handle.net/10023/15473>

This item is protected by original copyright

A STUDY OF THE
ANCHIZONE-EPIZONE METAMORPHIC
TRANSITION

by

CHARLES WILLIAM KER MORRISON

Thesis submitted for the
degree of Doctor of Philosophy

UNIVERSITY OF ST. ANDREWS
May 1989



ProQuest Number: 10170840

All rights reserved

INFORMATION TO ALL USERS

The quality of this reproduction is dependent upon the quality of the copy submitted.

In the unlikely event that the author did not send a complete manuscript and there are missing pages, these will be noted. Also, if material had to be removed, a note will indicate the deletion.



ProQuest 10170840

Published by ProQuest LLC (2017). Copyright of the Dissertation is held by the Author.

All rights reserved.

This work is protected against unauthorized copying under Title 17, United States Code
Microform Edition © ProQuest LLC.

ProQuest LLC.
789 East Eisenhower Parkway
P.O. Box 1346
Ann Arbor, MI 48106 – 1346

Th ~~A1014~~
A1016

THESIS DECLARATION

I Charles William Ker Morrison hereby certify that this thesis has been composed by myself, that it is a record of my own work, and that it has not been accepted in partial or complete fulfilment of any other degree or professional qualification.

Signed Date 15/5/89

I was admitted to the Faculty of Science of the University of St.Andrews under Ordinance General No 12 on Oct 1985 and as a candidate for the degree of Ph.D. on Oct 1986.

Signed Date 15/5/89

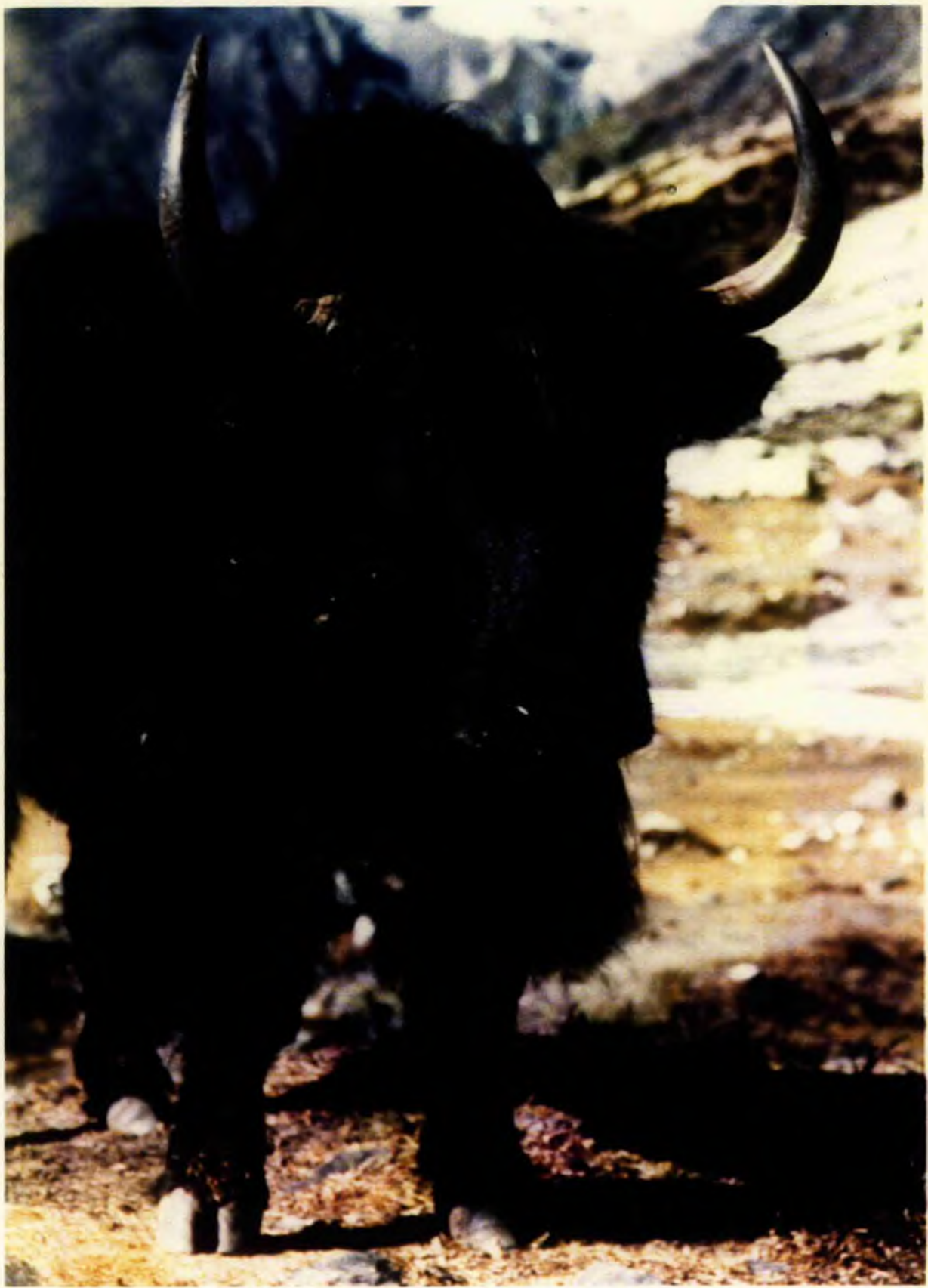
I hereby certify that the candidate has fulfilled the conditions of the Resolution and Regulations appropriate to the degree of Ph.D.

Signed Date 15/5/89

COPYRIGHT

Unrestricted

In submitting this thesis to the University of St.Andrews I understand that I am giving permission for it to be made available for use in accordance with the regulations of the University Library for the time being in force, subject to any copyright vested in the work not being affected thereby. I also understand that the title and abstract will be published, and that a copy of the work may be made and supplied to any bona fide library or research worker.



Frontispiece 1 - Yak

CONTENTS

CONTENTS -----	i
ABSTRACT -----	vi
ACKNOWLEDGEMENTS -----	vii
LIST OF FIGURES -----	viii
LIST OF TABLES -----	xii
LIST OF PLATES -----	xiii
LIST OF APPENDICES -----	xvii

<u>CHAPTER 1 - INTRODUCTION -----</u>	Page 1
---------------------------------------	--------

CHAPTER 2 - METHODS

2.1 PHYLLOSILICATES -----	3
2.1.1 Introduction -----	3
2.1.2 Polymorphs and Polytypes -----	3
2.1.3 Chemistry and Structure -----	5
2.1.4 Mixed-Layering (Interstratification) -----	9
2.1.5 Grade Transformations -----	10
2.2 X-RAY DIFFRACTION (XRD) -----	15
2.2.1 Aims -----	15
2.2.2 Introduction -----	15
2.2.3 Sample Preparation -----	15
2.2.4 Machine Conditions -----	18
2.2.5 Mineral Identification -----	18
2.2.6 Treatments -----	23
2.2.7 Illite Crystallinity -----	25
of the Anchizone -----	28
2.2.9 External Calibration of Quartz Standard -----	30
2.2.10 External Data Calibration -----	33
2.2.11 Factors Affecting Peak Width -----	36
2.2.12 Determination of b_0 -Spacing -----	38
2.2.13 Factors Affecting b_0 -Spacing -----	39
2.2.14 Anchizone Temperature Limits -----	41
2.3 FLUID INCLUSION METHODS -----	44
2.3.1 Aims -----	44
2.3.2 Introduction -----	44
2.3.3 Preparation of FI wafers -----	45
2.3.4 Optical Examination -----	45
2.3.5 Thermometric Measurements -----	47
2.3.6 Data Interpretation -----	49
2.3.7 Fluid Extraction -----	52

CHAPTER 3 - ISLE OF MAN

3.1 INTRODUCTION -----	54
3.2 GEOLOGICAL BACKGROUND -----	55
3.2.1 Previous Work -----	55
3.2.2 Stratigraphy -----	55
3.2.3 Age Constraints -----	57
3.2.4 Previous Structural Interpretation -----	57

3.3	FIELDWORK -----	58
3.3.1	Sample Collecting -----	58
3.3.2	Data Collecting -----	59
3.4	STRUCTURAL INTERPRETATION -----	60
3.4.1	Regional Structure -----	60
3.4.2	The Niarbyl Fault Zone (NFZ) -----	64
3.4.3	Sinistral Transcurrent (Transpressive) Faulting -----	70
3.4.4	Brittle Thrusting -----	72
3.4.5	Late Features -----	72
3.4.6	Thrust or Lag? -----	72
3.4.7	Textural Zones -----	73
3.4.8	Shear Sense Indicators -----	77
3.4.9	Structural Summary -----	77
3.5	PETROGRAPHY -----	80
3.5.1	Introduction -----	80
3.5.2	Thin Section Analysis -----	80
3.5.3	Conclusions -----	83
3.6	ILLITE CRYSTALLINITY -----	84
3.6.1	Introduction -----	84
3.6.2	The Crystallinity Map -----	84
3.7	PHYLLOSILICATE MINERALOGY -----	89
3.7.1	Mineralogy in Relation to Illite Crystallinity -----	89
3.7.2	Comparison with the Lake District and Wales -----	96
3.8	DISCUSSION -----	98
3.8.1	Areas of Low Isocryst Gradient and Higher Grade -----	98
3.8.2	Areas of High Isocryst Gradient and Lower Grade -----	99
3.8.3	The Anchizone-Epizone Transition -----	100
3.9	b_0 -SPACING -----	102
3.9.1	Introduction -----	102
3.9.2	Results -----	102
3.9.3	Discussion -----	106
3.9.4	Diastathermal Metamorphic Model -----	107
3.10	FLUID INCLUSIONS -----	110
3.10.1	Samples -----	110
3.10.2	Results Obtained -----	110
3.10.3	Discussion -----	116
3.10.4	Conclusions -----	117
3.11	SYNTHESIS -----	119
3.11.1	Aims -----	119
3.11.2	Introduction -----	119
3.11.3	Geological History -----	119
3.11.4	Conclusions - The Anchizone-Epizone Transition on the IOM -----	121

CHAPTER 4 - GLEN ESK

4.1	INTRODUCTION -----	123
4.1.1	Aims -----	123
4.1.2	Introduction -----	123
4.2	GEOLOGICAL BACKGROUND -----	126
4.2.1	History of Research on the HBC -----	126
4.2.2	Stratigraphy -----	130
4.3	FIELDWORK -----	138
4.3.1	Sample Collection -----	138
4.3.2	Data Collection -----	138
4.4	STRUCTURAL INTERPRETATION -----	140
4.4.1	Introduction -----	140
4.4.2	Discussion -----	140
4.4.3	Summary -----	146
4.5	PETROGRAPHY -----	148
4.5.1	Introduction -----	148
4.5.2	Thin Section Analysis -----	148
4.5.3	Conclusions -----	156
4.6	MINERAL CHEMISTRY -----	159
4.6.1	Aims -----	159
4.6.2	Introduction -----	159
4.6.3	White Mica -----	159
4.6.4	Chlorite -----	159
4.6.5	Biotite -----	166
4.6.6	Tourmaline -----	167
4.6.7	Almandine -----	169
4.6.8	Granditic Garnet -----	169
4.6.9	Pumpellyite -----	170
4.6.10	Epidote -----	171
4.6.11	Actinolite -----	171
4.6.12	Feldspar -----	174
4.6.13	Clinopyroxene -----	174
4.6.14	Albitisation -----	177
4.6.15	Controls on Metamorphic Assemblages -----	178
4.6.16	Equilibrium -----	179
4.6.17	HBC Metabasite Assemblages -----	180
4.6.18	Metamorphic Grade -----	183
4.6.19	Chlorite Geothermometer -----	185
4.6.20	Metabasite Mineral Assemblages -----	189
4.6.21	PT Estimate -----	190
4.6.22	Conclusions -----	193
4.7	PHYLLOSILICATE MINERALOGY -----	196
4.7.1	Introduction -----	196
4.7.2	Dalradian -----	196
4.7.3	HBC -----	198
4.7.4	Conclusions -----	203
4.8	ILLITE CRYSTALLINITY -----	204
4.8.1	Introduction -----	204
4.8.2	Illite Crystallinity -----	204
4.8.3	Discussion -----	208
4.8.4	Metamorphic Gradient -----	210

4.9	b_0 -SPACING -----	211
4.10	PRESSURE-TEMPERATURE (PT) CONDITIONS -----	215
4.11	SYNTHESIS -----	221
4.11.1	Aims -----	221
4.11.2	Geological History -----	221
4.11.3	Conclusions - The Anchizone-Epizone Transition in Glen Esk -----	224
 <u>CHAPTER 5 - NEPAL</u>		
5.1	INTRODUCTION -----	225
5.1.1	Aims -----	225
5.1.2	Introduction -----	225
5.2	GEOLOGICAL BACKGROUND -----	226
5.2.1	Stratigraphy -----	226
5.2.2	Position of the MCT -----	232
5.2.3	Present Knowlegde -----	235
5.2.4	Inverse Metamorphism Models -----	243
5.3	FIELDWORK -----	248
5.4	PETROGRAPHY -----	248
5.4.1	Introduction -----	248
5.4.2	Thin Section Analysis -----	248
5.5	PHYLLOSILICATE MINERALOGY -----	253
5.5.1	Kuncha Formation -----	253
5.5.2	Benighat Slates -----	253
5.5.3	Above the MCTII -----	257
5.6	ILLITE CRYSTALLINITY -----	257
5.7	b_0 SPACING -----	265
5.8	FLUID INCLUSIONS -----	270
5.8.1	Introduction -----	270
5.8.2	Geological History of Inclusions -----	270
5.8.3	Results -----	273
5.8.4	Discussion -----	281
5.8.5	Conclusions -----	287
5.9	ISOTOPIC AGES -----	288
5.9.1	Introduction -----	288
5.9.2	Sample Descriptions -----	288
5.9.3	Results and Discussion -----	288
5.10	DISCUSSION : INVERSE METAMORPHIC MODELS -----	291
5.10.1	Introduction -----	291
5.10.2	Discussion -----	291
5.11	SYNTHESIS -----	299
5.11.1	Geological History -----	299
5.11.2	Conclusion - The Anchizone-Epizone Transition in Nepal -----	303

CHAPTER 6 - DISCUSSION

6.1	INTRODUCTION -----	305
6.2	THE ANCHIZONE-EPIZONE METAMORPHIC TRANSITION -----	305
6.2.1	Lithology -----	307
6.2.2	Environment -----	307
6.2.3	Phyllosilicate Mineralogy, Hbre1, b_0 -----	308
6.2.4	Metabasite Mineralogy -----	309
6.2.5	Fluids -----	309
6.2.6	Pressure-Temperature Estimates -----	310
6.3	CONCLUSIONS -----	310
REFERENCES -----		313
APPENDICES -----		338

ABSTRACT

Field areas in the Isle of Man, Glen Esk, Scotland, and Nepal provided examples of the anchizone-epizone metamorphic transition under various tectonometamorphic conditions. The anchizone-epizone transition is best defined by the disappearance of 1Md white mica, and constrained using Hbrel, b_0 , phyllosilicate and metabasite mineralogy, fluid inclusion data, and PT estimates.

In the Isle of Man, pre- to syn-D1 anchizone to epizone regional diastathermal metamorphism is overprinted by post-D1 to syn-D2 epizone contact metamorphism. The anchizone-epizone transition corresponds to Hbrel 154 with a mean b_0 of 8.988 Å. Dominant phyllosilicate minerals are 2M₁ mica, chlorite, paragonite and paragonite-muscovite. Syn-D2 N₂ and saline aqueous fluid inclusions homogenise at up to 348 °C. Low temperature retrogressive cataclasis of anchizonal grade slates occurred in the sinistral transpressive Niarbyl Fault Zone, producing diagenetic grade illite.

At Glen Esk, collision between the Highland Border Complex (HBC) and the chlorite grade Dalradian along the Highland Boundary Fault produced prograde anchizone to epizone metamorphism in a sinistral transpressive fault zone within the HBC. The anchizone-epizone transition corresponds to Hbrel 135 with a mean b_0 of 9.029 Å. Phyllosilicate mineralogy is dominated by 2M₁ mica and chlorite. Metabasite mineralogy indicates pumpellyite-actinolite facies at c. 265 °C/>2.34 kb (supported by chlorite geothermometry), with H₂O-CO₂ fluids circulating.

In Nepal, the Main Central Thrust (MCT) zone formed during compressive collision between the Indian and Asian plates. Epizone Benighat Slates show re-crystallisation of white mica in the MCT zone. The anchizone-epizone transition has been tectonically removed, but epizone Benighat Slates range up to Hbrel 167, with a mean b_0 of 9.020 Å, and one anchizone sample, isolated by thrusts, has a Hbrel of 173. Phyllosilicate mineralogy is dominated by 2M₁ mica. Post-M1, syn-MCT zone H₂O-CO₂-NaCl equivalent inclusions homogenise at up to 367 °C and show higher CO₂ concentrations in the MCT zone.

ACKNOWLEDGEMENTS

I would like to offer my sincere thanks to my colleagues in the Geology Department of St. Andrews University. Their advice (both sought or volunteered) and assistance has helped this project on its way. I am particularly grateful to the following: Dr Grahame Oliver for his thorough supervision and encouragement; Dr Judith Kinnaird for guidance on the use and application of fluid inclusion microthermometry; Richard Batchelor for analysing my fluid extraction data; Jim Allan, Angus Calder, Donald Herd and Andrew Mackie for their technical assistance, without which this project would still be at the laboratory stage; Dr?? Martin Gillespie for his support during field work in Nepal and on many other expeditions.

Analytical work, assistance and advice were also given at a number of other institutions. Collaboration with Dr Brin Roberts resulted in comparative analyses of samples between St. Andrews and Birkbeck College, the testing of the St. Andrews quartz standard and the writing of a paper on the low grade metamorphism of the Manx Group, Isle of Man. Steven H irons gave technical assistance at Birbeck. Professor Bernard Kubler analysed both samples and the St. Andrews quartz standard. Dr Brian Bluck, Dr Chris Burton and Dr Peter Haughton (of Glasgow University) gave useful advice and stratigraphical information on the Highland Border Complex. At the Scottish Universities Research and Reactor Center Dr Tim Dempster and Dr Simon Kelley ran Rb/Sr and Ar/Ar analyses for me. The assistance freely given by these people has been much appreciated.

The receipt of NERC studentship GT4/85/GS/90 is gratefully acknowledged.

Most importantly I would like to thank my parents who have encouraged and supported me in my chosen academic career.

LIST OF FIGURES

2.1	Molecular structures of muscovite, montmorillonite and chlorite -----	4
2.2	TEMA milling versus jaw crushing, illite crystallinity values -----	17
2.3	Determination of illite crystallinity -----	26
2.4	External calibration of samples from the IOM ---	34
3.1	Geology of the Isle of Man -----	56
3.2	Structural map of the Niarbyl Fault Zone -----	65
3.2A	Sub-area A -----	67
3.2B	Sub-area B -----	68
3.2C	Sub-area C -----	69
3.3	Cross-section through the NFZ -----	71
3.4	Textural zones in the NFZ -----	74
3.5	Illite crystallinity map of the IOM -----	85
3.6	Hbrel traverses across the IOM -----	86
3.7	Hbrel values at the NFZ -----	88
3.8	Mineralogy versus Hbrel -----	90
3.9	Samples versus Hbrel -----	91
3.10	XRD trace of N8 (Hbrel 246) -----	93
3.11	XRD trace of M81 (Hbrel 145) -----	94
3.12	XRD trace of M87 (Hbrel 116) -----	95
3.13	b_o map of the IOM -----	103
3.14	Cumulative frequency curves of b_o values from the IOM, Glen Esk and Nepal -----	104
3.15	Hbrel versus b_o -----	105
3.16	Samples versus $T_m \text{ H}_2\text{O}$ -----	114
3.17	Samples versus Th TOT -----	115
4.1	Highland Border successions location map -----	124
4.2	Geology of the Burn Section, Glen Esk -----	125
4.3	Stratigraphy of the Dalradian, HBC and ORS -----	132
4.4	Structural measurements made on the HBC -----	139
4.5A	Field map A, Glen Esk -----	141
4.5B	Field map B, Glen Esk -----	141
4.5C	Field map C, Glen Esk -----	142
4.5D	Field map D, Glen Esk -----	142

4.6	Stereoplots of fault related folding, HBC -----	143
4.7	Sense of rotation of fault related folds, HBC ---	145
4.8	Microscopic shear sense indicators -----	146
4.9A	HBC white mica analyses plotted in terms of Al, K, and FeTOT + Mg -----	160
4.9B	Dalradian chlorite zone white mica analyses plotted in terms of Al, K, and FeTOT + Mg -----	160
4.9C	Dalradian biotite zone white mica analyses plotted in terms of Al, K, and FeTOT -----	161
4.9D	Dalradian garnet zone white mica analyses plotted in terms of Al, K, and FeTOT -----	161
4.10A	Hey plot of Glen Esk chlorites -----	163
4.10B	Comparative chlorite compositional fields -----	163
4.11	FeTOT versus Mg in Glen Esk chlorites -----	164
4.12	K versus (Mg + Fe) in Glen Esk biotites and chlorite after biotite -----	164
4.13	(Ca+Mg+Mn)-Al-FeTOT plot for Dalradian tourmalines -----	168
4.14	(Ca+Mg)-Al- Fe^{3+} plot for HBC granditic garnets ---	168
4.15	Fe^{2+} -Al-Mg plot for HBC pumpellyite -----	171
4.16	Fe^{2+} versus Al in HBC pumpellyite -----	171
4.17	Ca-Al-(Fe^{3+} +Mg) plot for HBC epidotes -----	173
4.18	Fe^{2+} -Al-Mg plot for coexisting HBC chlorite and actinolite -----	173
4.19	Na-K-Ca plot of Glen Esk feldspars -----	175
4.20	Mg-Ca-Fe plot of HBC clinopyroxenes -----	175
4.21	Mn-Ti-Na plot of HBC clinopyroxenes -----	176
4.22	F1 versus F2 in HBC clinopyroxenes -----	176
4.23A	Ca- Fe^{3+} -(Mg+ Fe^{2+})-Al cation proportion diagram for the pumpellyite-actinolite facies -----	182
4.23B	Ca- Fe^{3+} -(Mg+ Fe^{2+})-Al cation proportion diagram for granditic garnet bearing pumpellyite-actinolite facies -----	182
4.24	Tetrahedral aluminium versus octahedral vacancy in Glen Esk chlorites -----	187
4.25	Tetrahedral aluminium and octahedral vacancy temperature in Glen Esk chlorites -----	187
4.26	P (fluid)-T diagram of low grade metabasite facies -----	191

4.27	P (fluid)-T diagram showing the displacement of reaction curves and invariant points at the introduction of Fe_2O_3 into the model basaltic system -----	192
4.28	Mineralogy versus Hbrel -----	197
4.29	XRD trace of D11 (Hbrel 125) and D47 (Hbrel 115) -----	199
4.30	XRD trace of HBS12 (Hbrel 153) and HBS17 (Hbrel 226) -----	200
4.31	XRD trace of HBS42 (Hbrel 143) and HBS57 -----	202
4.32	Glen Esk Hbrel values ($<2\mu\text{m}$) -----	205
4.33	Glen Esk Hbrel values ($2\text{-}6\mu\text{m}$) -----	206
4.34	$2\text{-}6\mu\text{m}$ versus $<2\mu\text{m}$ Hbrel values -----	207
4.35	Histograms of Dalradian versus HBC Hbrel values ($<2\mu\text{m}$ and $2\text{-}6\mu\text{m}$) size fractions -----	209
4.36	Glen Esk b_o values -----	212
4.37	Cumulative frequency curves of b_o values from the IOM, Glen Esk and Nepal -----	213
4.38	Comparative histograms of b_o values -----	214
4.39	Metamorphism of the Dalradian and HBC in Glen Esk: model 1 -----	217
4.40	Metamorphism of the Dalradian and HBC in Glen Esk: model 2 -----	219
5.1	Geology of the Kathmandu Basin -----	227
5.2A	Sample traverse A, from Barahbise to the Bagmati river -----	228
5.2B	Sample traverse B, from Syabru to Betrawati -----	229
5.3	Stratigraphy of the Kathmandu area -----	230
5.4	Cross-section of Himalayan thrusts -----	233
5.5	Cross-section of metamorphic conditions -----	237
5.6	Thermal regime of two thrusted slabs -----	246
5.7	Mineralogy versus Hbrel -----	254
5.8	XRD trace of HS15 (Hbrel 179) and HS18 (Hbrel 157) -----	255
5.9	XRD trace of HS25 (Hbrel 126) and HS27 (Hbrel 176) -----	256
5.10	XRD trace of HS36 (Hbrel 114) and LH2 -----	258
5.11	Traverse A, Hbrel and b_o results -----	260
5.12	Traverse B, Hbrel and b_o results -----	258

5.13	Histograms of HbreI values from the Benighat Slates, Kuncha Formation and Kathmandu Klippe ---	262
5.14	Cumulative frequency curves of b_o values from the IOM, Glen Esk and Nepal -----	266
5.15	Histograms of b_o values from the Benighat Slates Kuncha Formation and Kathmandu Klippe -----	267
5.16	Samples versus T_m H_2O -----	275
5.17	Samples versus Th TOT -----	276
5.18	Samples versus Th CO_2 -----	279
5.19	Fluid inclusion salinity traverse -----	283
5.20	Fluid extraction plot of H_2O/CO_2 versus Na/K ----	283
5.21	Cross-section of Nepal in the Kathmandu region --	295

LIST OF TABLES

2.1	Illite crystallinity experimental conditions of various authors -----	19
2.2	Effect of quartz standard preparation on peak width and standard consistency; samples prepared and run at Birkbeck -----	31
2.3	Consistency of a quartz standard; samples prepared and run at Neuchatel -----	31
2.4	Anchizone temperature limits -----	41
2.5	Phase changes during fluid inclusion microthermometry -----	48
2.6	Typical microthermometry results -----	50
3.1	The Manx Group sucession -----	57
3.2	Comparative structural histories: Simpson (1963) and regional geology (this study) -----	61
3.3	Mean b values and pressure facies -----	106
3.4	Fluid inclusion trapping temperature estimates --	111
3.5	Microthermometric results for fluid inclusions from the IOM -----	112
4.1	References for Fig. 4.3 -----	133
4.2	Mineral assemblages for HBC metabasites samples -	181
4.3	Chlorite geothermometric estimates for HBC and Dalradian chlorites -----	188
4.4	Alternative metamorphic models for the Dalradian and HBC metamorphic events -----	220
5.1	Metamorphic conditions in Nepal -----	238
5.2	Isotopic ages from the Nepal Himalaya -----	241
5.3	Illite crystallinity ranges in Nepal -----	259
5.4	Microthermometric results for fluid inclusions from Nepal -----	271
5.5	Fluid inclusion trapping temperature estimates --	272
5.6	Fluid extraction results from Nepal -----	274
5.7	Fluid inclusions in relation to metamorphic grade -----	285
5.8	$^{40}\text{Ar}/^{39}\text{Ar}$ age dates from the Kuncha Formation -----	289
6.1	Conditions of the anchizone-epizone transition in the three field areas studied -----	306

LIST OF PLATES

Note: Captions to plates have been abbreviated. Descriptions of photomicrographs (with the plates) include the type of light used (PPL = plain polarised light, XPL = cross polarised light), the sample number and the length of the field of view (in mm). Plate numbers indicate which chapter the plate belongs to (e.g. plate 3.5 belongs to chapter 3).

Frontispiece 1 - Yak.

Frontispiece 3 - Chomolongma (8848m), with the Nuptse ridge in front (7879m).

Frontispiece 4 - Looking north towards Gyachung Kang (7922m).

Frontispiece 5 - Looking north towards part of the Nuptse-Lhotse wall.

Plate 2.1 - Phase changes in a fluid inclusion.

Plate 2.2 - Phase changes in a fluid inclusion.

Plate 3.1 - Re-folded slump fold in the Maughold Banded Group.

Plate 3.2 - Slump fold in the Maughold Banded Group.

Plate 3.3 - Slump breccia in the Barrule Slates.

Plate 3.4 - Coarse graded greywacke in the Lonan Flags.

Plate 3.5 - Large F1 fold in the Niarbyl Flags.

Plate 3.6 - Boudinaged quartz vein in the Maughold Banded Group.

Plate 3.7 - F2 fold in the Barrule Slates.

Plate 3.8 - Phyllonites of the Niarbyl Fault Zone disrupted by the later brittle thrusting on the Niarbyl Thrust.

Plate 3.9 - Textural zone 3 phyllonites of the Niarbyl Fault Zone.

Plate 3.10 - Textural zone 3 phyllonite quartz segregations.

Plate 3.11 - Sinistral Riedel shears cross-cut the phyllonitic fabric.

Plate 3.12 - Phyllonites of the Niarbyl Fault Zone showing macroscopic crumpling.

Plate 3.13 - Maughold Banded Group slates in a relatively undisturbed form.

Plate 3.14 - Maughold Banded Group slates (textural zone 1).

Plate 3.15 - Thin section showing grain reduction in a dismembered quartz vein in textural zone 1 slates.

Plate 3.16 - View towards the Niarbyl Flags from textural zone 2 slates.

Plate 3.17 - Textural zone 2 slates showing disruption of the bedding and the development of quartz segregations, and veins.

Plate 3.18 - Textural zone 3 mica rich phyllonite with abundant quartz segregation pods.

Plate 3.19 - Textural zone 3 phyllonite containing a strained monocrystalline quartz porphyroblast.

Plate 3.20 - Strained polycrystalline quartz porphyroblast showing sinistral shear sense in N4.

Plate 3.21 - M34 contains pre- to syn-D1 chlorite pods.

Plate 3.22 - M23 contains porphyroblasts of platy ilmenite which cross-cut the S1 foliation, but are crenulated by the S2 foliation.

Plate 3.23 - In M55 biotite porphyroblasts overgrow the S1 foliation.

Plate 3.24 - M45 contains early (?syn-D1) muscovite pods and later (post-D1) pyrites with quartz overgrowths.

Plate 3.25 - Muscovite bearing pegmatitic quartz vein cross-cutting the Foxdale granite.

PLate 3.26 - Syn-F2 quartz vein from Calf Sound.

Plate 4.1 - Fault foliation, in the HBC, is folded by a brittle fold with sinistral rotation.

Plate 4.2 - Fault foliation cross-cut by brittle extensional duplexes with a sinistral sense of movement.

Plate 4.3 - Feldspathic basalt showing a well developed sinistral S-C fabric.

Plate 4.4 - Purple shale containing a porphyrocryst which indicates sinistral shear.

Plate 4.5 - Purple shale containing porphyrocrysts (?amygdales) composed of chlorite and opaques.

Plate 4.6 - Mylonitic grain reduction in an Upper Margie psammite.

Plate 4.7 - Mylonitic grain reduction in a Lower Margie sandstone.

Plate 4.8 - Biotite grade pelitic schist.

Plate 4.9 - Biotite grade psammitic schist.

Plate 4.10 - Purple shale with chlorite/opaque pods (?amygdales).

Plate 4.11 - Upper Margie psammite with a feldspar phenocryst surrounded by grain reduced matrix.

Plate 4.12 - Pseudomorph after olivine in pillow basalt.

Plate 4.13 - Spherulitic clinopyroxene crystals growing on a skeletal albite crystal in pillow basalt.

Plate 4.14 - Two "arrow head" clinopyroxene crystals in basalt.

Plate 4.15 - Epidote vein fill in purple shale.

Plate 4.16 - Amygdale in green pelite.

Plate 4.17 - Dismembered feldspar phenocryst in green pelite.

Plate 5.1 - Re-folded fold in the Benighat Slates.

Plate 5.2 - A 1km high cross-section through the Kuncha Formation exposed by a rockslide.

Plate 5.3 - Euhedral garnet in muscovite schist from the Kuncha Formation.

Plate 5.4 - Chlorite pseudomorphs after garnet in chlorite schist from the Kuncha Formation.

Plate 5.5 - Crenulated garnet grade biotite rich schist from the Kuncha Formation.

Plate 5.6 - Benighat Slate showing a strongly developed foliation.

Plate 5.7 - Mylonitic muscovite rich schist in the Raduwa Formation.

Plate 5.8 - Biotite schist from the Kulikhani Formation.

Plate 5.9 - A plane of 'flat' secondary aqueous fluid inclusions confined to a healed fracture plane (LH1).

Plate 5.10 - Two inclusion populations. Earlier inclusions are strained and later inclusions form an undeformed plane (FI2)

Plate 5.11 - A mixture of regular and irregular H₂O-CO₂ fluid inclusions (FI3).

Plate 5.12 - Negative crystal inclusion with a CO₂ double bubble in an aqueous solution (FI3)

Plate 5.13 - Single bubble H₂O-CO₂ negative crystal inclusions. (FI4).

Plate 5.14 - A mixture of regular and irregular fluid inclusions. (FI5).

Plate 5.15 - A large irregular fluid inclusion with a CO₂ liquid phase in an aqueous liquid phase (FI7).

Plate 5.16 - The same field of view as in plate 5.15, but at -34.5°C (FI7).

LIST OF APPENDICES

2.1	XRD instrumental conditions -----	338
2.2	XRD sample preparation -----	339
2.3	Treatment for clay mineral determination -----	339
2.4	XRD peaks used to determine K white mica polymorphs -----	340
3.1	IOM sample map -----	341
3.2	IOM sample list -----	342
3.3	XRD analyses of samples from the IOM -----	343
3.4	Mean b_0 values and pressure facies -----	345
3.5	IOM fluid inclusion microthermometric data -----	346
4.1	Glen Esk sample map -----	347
4.2	Electron microprobe standards -----	348
4.3	White mica probe analyses -----	349
4.4	Chlorite probe analyses -----	353
4.5	Biotite probe analyses -----	356
4.6	Tourmaline and actinolite probe analyses -----	357
4.7	Grnaditic and almandine garnet probe analyses ---	358
4.8	Epidote and pumpellyite probe analyses -----	358
4.9	Feldspar probe analyses -----	359
4.10	Clinopyroxene probe analyses -----	360
4.11	XRD analyses of samples from Glen Esk -----	361
5.1	XRD analyses of samples from Nepal -----	362
5.2	Nepal fluid inclusion microthermometric data ----	363

CHAPTER 1

INTRODUCTION

The aim of this thesis is to investigate the anchizone-epizone metamorphic transition in a range of tectonic environments.

Field areas in the Isle of Man, Glen Esk, Scotland, and Nepal were selected for investigation. These field areas provided a variety of tectonometamorphic situations involving low grade metamorphic rocks. These included regional metamorphism, contact metamorphism and low temperature transcurrent fault cataclasis in the IOM, regional metamorphism and metamorphism in a sinistral transpressive fault zone at Glen Esk, and regional and thrust zone metamorphism in Nepal. The anchizone-epizone transition can be quantified using the parameters: 1. petrography, 2. mineral chemistry and thermometry, 3. metabasite mineralogy, 4. H₂O, 5. b_o, 6. fluid inclusion microthermometry and composition, and 7. fluid extraction data. Not all the possible techniques were applied to each field area, but were applied when considered viable. Comparisons and contrasts could be made between the field areas on the basis of the above parameters.

In chapter 2, methods are discussed in the following sections: 1. - phyllosilicate chemistry and structure; 2. - the application of XRD techniques to phyllosilicate mineralogy, illite crystallinity and b_o; 3. - the study of fluid inclusions by microthermometry and fluid extraction.

The results from each field area are presented and discussed in chapters 3, 4 and 5 (the Isle of Man, Glen Esk and Nepal respectively). Each chapter is subdivided into sections which cover the following (if appropriate): 1. - geological background and stratigraphy; 2. - fieldwork; 3. - structural interpretation; 4. - petrography; 5. - mineral chemistry; 6. - phyllosilicate mineralogy; 7. - illite crystallinity; 8. - b_o ; 9. - fluid inclusion results; 10. - metamorphic modelling; 11. - synthesis.

Similarities and contrasts between the anchizone-epizone transition in three field areas are discussed in chapter 6.

CHAPTER 2

METHODS

2.1 PHYLLOSILICATES

2.1.1 Introduction

The basic structure of phyllosilicate minerals is that of tetrahedrally and octahedrally coordinated sheets of atoms linked together in a 1:1 or 2:1 ratio to form layers (Longstaffe, 1981), for example two tetrahedral sheets linked with each octahedral sheet. The layers are linked together by interlayer material. This can take the form of cations, water molecules, hydroxy and hydrated complexes, and organic liquids. From these prototype structures layer silicates are formed. Cation substitutions and the presence of various interlayer materials produce the variety in layer silicates. In phyllosilicates cation substitutions (for example Al for Si and Mg for Al) result in a net negative layer charge, and this is balanced by having a compensating positive charge in the interlayers.

In Fig. 2.1 a schematic representation of the structures of muscovite, paragonite, montmorillonite and chlorite are shown. These four minerals are the commonest layer silicates, along with mixed-layer silicates, found in this study, and all have 2:1 type layer structures.

2.1.2 Polymorphs and Polytypes

Phyllosilicate minerals can show a variety of polymorphs and polytypes. Polymorphs are different crystal

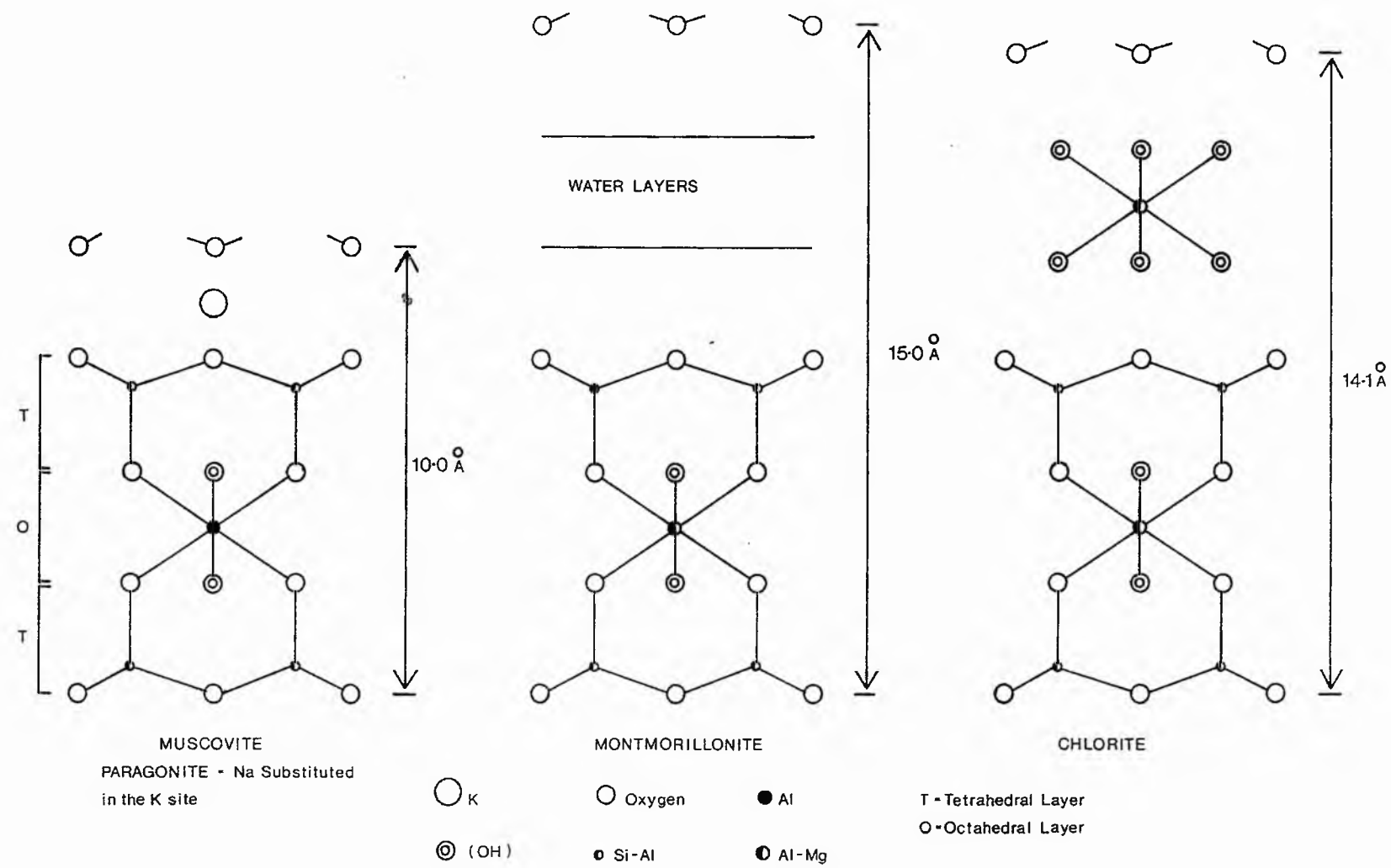


Fig. 2.1 - The molecular structures of muscovite, montmorillonite and chlorite.

forms of the same chemical substance. Polytypism is brought about by different stacking sequences of similar structural units and represents one type of polymorphism (Frey, 1987, p23). Polymorphism and polytypism are indicators of very low-grade metamorphism. Disordering is a form of polytypism and can occur in several forms (Brindley and Brown, 1980; Longstaffe, 1981).

1. At atomic level due to partial cation substitution.

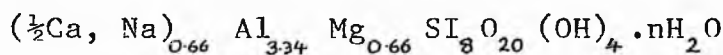
2. By 'mistakes' in the stacking sequence of layers.

3. The sequence of layer types in the interstratified structure may be ordered or disordered due to variable swelling conditions between the layers or by mixed layering.

2.1.3 Chemistry and Structure

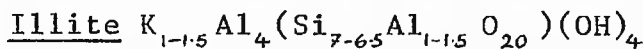
A brief description of the chemistry and structure of the layer silicates relevant to this study follows. More detailed descriptions can be found in Deer et al. (1962), Brindley (1980), Bailey (1980), and Reynolds (1980) in Brindley and Brown (1980).

Montmorillonite

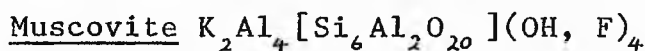


This is a dioctahedral 2:1 layer mica with charge balancing and exchanged cations between the layers, and showing random orientation of the expanded layer sequences. This is due to small layer charges, few inter-layer cations and its hydrated state. Mg for Al substitution occurs in

the octahedral site. The number of layers in a crystal are small ($N = 10$), so the (001) diffraction is always broad, and the broadening is increased by lack of layer homogeneity (Hower and Mowatt, 1966; Longstaffe, 1981).



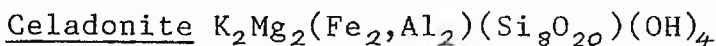
Illites have proved a problem to describe because they can form mixed-layer interstratifications, for example with montmorillonite, chlorite or paragonite, in variable proportions. They are generally classified by their polytypes, 1Md (disordered), 1M, 2M, 2M₁, and 3T, the first three being the most common in sub-greenschist facies rocks. Mixed-layering will be discussed more fully in section 2.1.4. Illites are characterised by the substitution of Si for Al in the tetrahedral site, Fe+Mg for Al in the octahedral site, a deficit of K compared to muscovite, and little or no inter-layer water. Surface held water contributes an appreciable amount of extra water to illites, in addition to a limited amount of interlayer water occupying vacant K sites (Hower and Mowatt, 1966). K deficiency results in weak inter-layer bonds producing a tendency for disordering. Hydro-muscovite is similar but the K deficiency is made up for by $(\text{H}_3\text{O})^+$ in the K site or replacement of $(\text{O})^{=2}$ by $(\text{OH})^{-1}$.



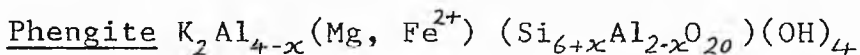
Polymorphs of muscovite are described under their own mineral names. In this study 2:1 dioctahedral muscovite was found to be of the 2M₁ variety, though the metastable polymorphs, 1Md, 1M and 3T occur less commonly.

Sericite

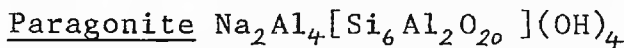
This is used as a informal term for fine white mica. Sericite tends to be high in SiO₂, MgO and H₂O, and low in K₂O compared to muscovite.



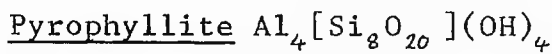
The main differences between celadonite and muscovite are that Mg substitutes for K and Fe substitutes for Al in the octahedral sites, and Si substitutes for Al in the tetrahedral sites. 1Md and 1M are the dominant polymorphs. The celadonite component of lowest grade metamorphic rock appers to decrease with increasing metamorphic grade.



Phengites are muscovites with a Si/Al ratio >3:1. The increase in Si is accompanied by substitution of Mg or Fe²⁺ for Al in the octahedral site. The 1M, 1Md and 3T polymorphs are most common, 2M and 2M, are less so.



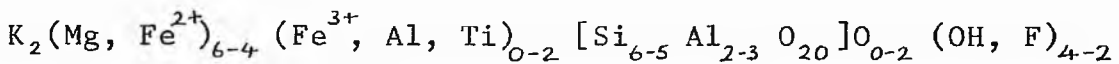
Paragonite is a simple variation on muscovite with the substitution of the smaller Na ion for K, in the 2M, polymorph. 1M paragonite also occurs, but less commonly. Paragonite is a common constituent of anchizonal slates, preferentially forming due to K deficiency in the slate. Mixed layering with muscovite is common.



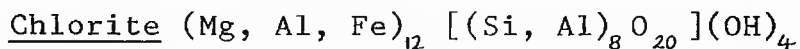
The relationship between polytype and grade of metamorphism in pelitic rocks is uncertain for pyrophyllite. This is partly to do with its uncommon

occurrence. Pyrophyllite can occur in monoclinic or triclinic form, the 2M₁ form being the commonest. A small amount of substitution of Al for Si in the tetrahedral site is common. Relatively weak interlayer bonds result in a tendency to disorder.

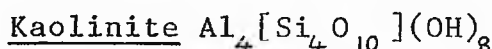
Biotite



Biotite and phlogopite are members of a continuous chemical and structural series. Ratios of Mg:Fe <2:1 fall in the biotite field. The 1M or 1Md form is most common while lesser amounts of 3T or 2M₁ can form. Substitutions are common with Fe decreasing while Mg and Ti increase with increasing metamorphic grade.



Chlorites are 2:1 layer silicates which show considerable cation replacement. Mg²⁺ is replaced by Fe²⁺ or Mn and Si by Al in the tetrahedral site, and Al by Fe³⁺ in the octahedral site. Mg:Fe proportions can reflect variations in lithology rather than metamorphic conditions (Cathelineau and Nieva, 1985). There are two main chlorite polymorphs, 7Å and 14Å chlorite. The 14Å polymorph shows the progressive polytype change Ibd (d = disordered) to Ib(97°) to Ib(90°) to IIb in conditions of incipient metamorphism.



The kaolinite group is composed of dioctahedral 1:1 layer silicates, commonly of the 1M and 2M₁ (dickite)

forms. Disordering, mixed-layering and minor cation replacements are common.

2.1.4 Mixed-Layering (Interstratification)

Mixed-layering (M-L) of phyllosilicate minerals is a common occurrence in low grade metamorphic rocks. Two component M-L is the most common though three component M-L can occur, for example smectite/illite/chlorite (Reynolds and Hower, 1970). With increasing temperature, M-L develops through a number of stages, as can be seen in the following example:

Smectite forms into random M-L illite/smectite at between 75 and 115°C, with >35-40% expanded layers (Kisch, 1983), and <20% illite (Reynolds and Hower, 1970). With increased temperature this develops into regular 1:1 M-L rectorite with <35-40% expanded layers. By about 230°C (McDowell and Elders, 1980; Kisch, 1983) an IMII type interstratification has formed with <10% smectite which is at the detection limit of XRD analysis (Reynolds and Hower, 1970; Perry and Hower, 1972). The progression from random to regular M-L occurs with the loss of water from the expanded layers, and can be measured using an order parameter (Corbato and Tettenhorst, 1987). The type of interstratification can also be measured directly by counting the layers using a TEM. This gives a direct measure of packet size, sequence of layers and periodicity (Ahn et al., 1988).

There are a number of possible combinations of phyllosilicates that can form M-L. These include

illite/smectite, chlorite/smectite or vermiculite, illite/chlorite (Ahn et al., 1988) and paragonite/mica (for example the M-L paragonite/phengite identified by Frey (1969)). The classification of some regular interstratifications can be quite tightly constrained allowing specific names to be given to them. These include the following (Bailey et al., 1982);

Low charge corrensite = regular 1:1 trioctahedral chlorite/trioctahedral smectite.

High charge corrensite = regular 1:1 trioctahedral chlorite/trioctahedral vermicularite.

Rectorite = regular 1:1 dioctahedral mica/dioctahedral smectite.

Tosudite = 1:1 regular dioctahedral chlorite/smectite.

2.1.5 Grade Transformations

Mineral Compositions and Abbreviations

For the sake of convenience, abbreviations have been used in this section as follows;

Compositions are shown when not previously given.

Ab = Albite	$\text{NaAlSi}_3\text{O}_8$	Bi = Biotite
Chl = Chlorite		Hy = Hydromica
Ill = Illite		Ka = Kaolinite
K-f = K-feldspar	(K, Na) AlSi_3O_8	
Mnt = Montmorillonite		Mu = Muscovite
Pa = Paragonite		Ph = Phengite
Py = Pyrophyllite		Qtz = Quartz SiO_2
Sm = Smectite	(as for montmorillonite)	
I/M = Illite/Montmorillonite		

Pa/Mu = Paragonite/Muscovite Rect = Rectorite
M-L = mixed-layer Det = Detrital
Reg = Regular Irreg = Irregular
Tri = Trioctahedral Di = Dioctahedral

Transformations

The progressive metamorphism of pelitic rocks from diagenetic to lowest greenschist grade can be recognised by a number of mineral transformations. Various hypothetical transformations have been proposed by a number of authors, and the following are some of the ones relevant to pelitic rocks;

Illite

Hower et al. (1976) produced the formula Sm + Det K-f + Det Mica = Ill + Chl + Qtz + H₂O. This transformation would take place progressively from late diagenesis to early anchizone.

Muscovite

The transition from illite to phengite has been modelled by a number of authors. Weaver (1984) deduced that Ill + Chl + Qtz = Ph + Chl + H₂O without going into details of ionic substitutions. Velde (1965) put forward Ill + Chl + K-f + H₂O = Ph + Chl (Al) + Qtz as appropriate for argillaceous sediments. Frey (1970) produced the same products from I/M. Weaver and Pollard (1973) produced, experimentally, a further transition Ph = Mu + Chl + H₂O being completed by 400°C (upper epizone by his reckoning).

The progressive development of white mica from diagenetic illite to epizonal muscovite is well illustrated

by Karpova (1969) with Al-Mg-Fe 1M (1Md) Ill to Fe-Al 1M Ill to Al 1M Ill to 2M, Hy to 2M, Mu. This reflects a decrease in Mg and Fe, and an increase in Al and K with increasing metamorphic grade. Hunziker et al. (1986) have found that diagenetic white mica has 6-8wt% K₂O, anchizonal has 8.5-10wt% and epizonal has 10-11.5wt%. When other important minerals are included in Karpovas model the overall grade transformations are as follows;

Diagenesis/Low Anchizone =

Mnt + Ka + M-L I/M + Fe 1Md Ill + orthohexagonal Ib Chl

Low/Med Anchizone =

Al 1M Ill + Ka + Mg-Fe monoclinic IIb Chl

Med/High Anchizone =

2M, Hy + Fe-Mg monoclinic IIb Chl

High Anchizone/Epizone =

2M, Mu + Pa + Fe-Mg monoclinic Chl.

The choice of facies is different to that of Karpova because of the availability of more recent data. Maxwell and Hower (1967) report that the 1Md to 2M, illite transformation is completed by the biotite isograd. Hunziker et al. (1986) give evidence that the transition is completed by the high anchizone. A compilation of data concerning the grade at which 1Md illite converts to 2M, mica has been made by Frey (1987), and the overall consensus is that the transition is completed at approximately the anchizone/epizone boundary.

Paragonite

Frey (1970, 1978, 1987) put forward a transformation sequence to explain the development of paragonite. Irreg M-L I/M to Rect to Reg M/L Pa/Mu to discrete Pa + Mu. The conversion to discrete paragonite would occur at a minimum temperature of 330 to 340°C and pressure of 1kb according to Hemley and Jones (1964; in Frey, 1987). Possible sources for paragonite include the following;

Mnt + NaCl + Qtz = Pa + Ab + Mu + Chl + salts + HCl + H₂O, at 350°C and 1kb (Althaus and Johannes, 1969; in Frey, 1987).

Na Mnt + 2Ab = 3Pa + 8Qtz = H₂O, at 335°C and 2kb (Chatterjee, 1973; in Frey, 1987).

These both suggest a transformation at between 330 and 350°C, and 1-2kb. Weaver (1984) suggested an additional source of paragonite from detrital biotite and albite : Bi + Ab + H₂O = Chl + Pa + K.

Pyrophyllite

Frey (1978) put forward three mechanisms for the development of pyrophyllite;

1. 2Det Mu + 6Qtz + 2H⁺ = 3PY + 2K⁺
2. 1Ka + 2Qtz = 1Py + 1H₂O
3. 1Pa + 4Qtz = 1Py + 1Ab

The second mechanism is probably the most significant contributor due to the common occurrence of kaolinite and quartz in diagenetic rocks. The coexistence of

pyrophyllite, paragonite and albite is indicative of low to medium pressure metamorphism (Frey et al., 1988).

Biotite

Ernst (1963) put forward the transformation $8\text{Ph} + \text{Chl} = 5\text{Mu} + 3\text{Bi} + 7\text{Qtz} + 4\text{H}_2\text{O}$ to produce biotite. An alternative formation mechanism can be found in Miyashiro (1981) : microcline + Chl = Bi + white mica + Qtz + H_2O . In the Dalradian the transformation Chl + Phengitic Mu = Less Phengitic Mu + Chl + Bi + H_2O , (Atherton, 1977), has been proposed.

2.2 X-RAY DIFFRACTION (XRD)

2.2.1 Aims

The aim of this section is to present an outline of the application of the techniques used and describe the information gained from them.

2.2.2 Introduction

XRD techniques were used to identify phyllosilicate minerals assemblages, and to obtain illite crystallinity and b_0 values. The operating conditions are given in Appendix 2.1, sample preparation techniques are given in Appendix 2.2, and the various clay mineral treatments are given in Appendix 2.3.

2.2.3 Sample Preparation

The reliability of the data obtained from an XRD scan can be influenced by the sample preparation technique used.

The first stage in this process is obtaining a suitable size fraction. Fresh samples are collected whenever possible, and excess weathering is removed from the samples by grinding. This is done to minimise the influence of weathering products on the scan. The sample is then reduced to a coarse powder in a jaw crusher. Mechanical milling in a tungsten-carbide mill may follow (Hunziker et al., 1986), but some authors prefer to avoid this, (Merriman and Roberts, 1985; Robinson and Bevins, 1986). Over milling reduces the crystallite size (see section 2.2.5), increases lattice distortion, and permits increased interparticle water by increasing the surface

area of particles (Reay, 1982). This last effect allows the appearance of pseudo mixed-layering, and the corresponding peak broadening, due to the XRD perception of interparticle diffraction (Nadeau et al., 1984).

During this study some of the samples were prepared using minimal (10 to 25 seconds) TEMA milling (as used by Johnson et al., 1985), while other samples were prepared just using a jaw crusher, as this was found to produce adequate fine powder. Fifteen samples were prepared both ways to test for variation in illite crystallinity values obtained (see Fig. 2.2). One sample seems to have been over TEMA'd, otherwise results are within c.10% of each other.

The powder was then disaggregated in an ultrasonic bath for ten minutes (Merriman and Roberts, 1985; Kemp et al., 1985; Robinson and Bevins, 1986). There is data suggesting that this causes a reduction in peak width (Toselli and Weber, 1982; in Frey, 1987, p301), but Frey also states that his own observations show no variation. The sample is then centrifuged to obtain the relevant size fractions (Thomas, 1985), and pipetted onto a glass slide (Kisch, 1980a, b; Thomas, 1985; Evans, 1987; Frey, 1987, p301). The thickness of the sediment appears to influence the peak width (Frey, 1987 p301). Smears, favoured by a number of authors (Merriman and Roberts, 1985; Robinson and Bevins, 1986), tend to result in broader peaks (Brime, 1980; in Frey 1987).

For illite crystallinity analysis the $<2\mu\text{m}$ size fraction was favoured to avoid contamination by detrital

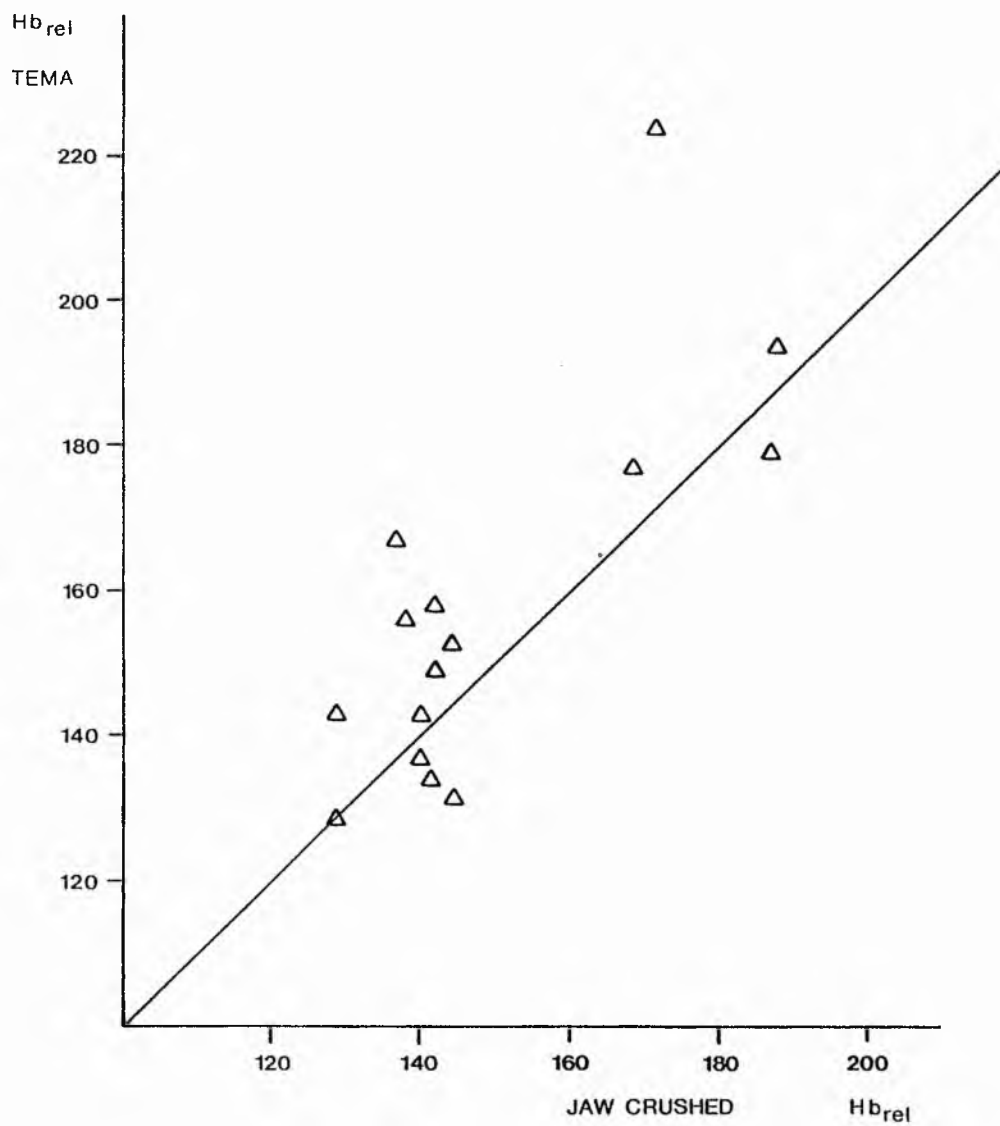


Fig. 2.2 - Plot of samples prepared for illite crystallinity using TEMA milling and jaw crushing to obtain a powdered sample.

mica (Weber, 1972; Frey et al., 1980b; Frey, 1987). For some samples the 2-6 μm size fraction (Johnson et al., 1985) and coarse powder were also used, and these samples had narrower peaks on average (see Fig. 4.34). For illite crystallinity, b_0 , 3-35° 2θ , 3-65° 2θ and 5-45° 2θ scans the <2 μm size fraction was used. The 2-6 μm slides and coarse powder packs were also used for illite crystallinity.

2.2.4 Machine Conditions

The various machine conditions used are shown in Appendix 2.1. Variations in machine conditions provide yet another source of variations in illite crystallinity results (Kisch, 1983). There appears to be a variety of preferred settings used by various authors, and this is probably due to the performance of different machines and attempts to optimise the internal consistency of results. A table of machine conditions (see table 2.1) has been prepared using data collected by Kisch (1983, p348) and data gathered from various other sources. Most authors favour conditions laid out by Kisch (1980b).

2.2.5 Mineral Identification

Machine conditions for mineral identification are given in Appendix 2.1. Minerals were identified by individual or a set of characteristic peaks located at various angles in ° 2θ on an XRD scan. The angle in ° 2θ is directly related to the unit cell spacing $d\text{\AA}$ by the Scherrer equation (a variation on the Bragg equation);

$$\beta = K\lambda/Ndc\cos\theta$$

Table 2.1 Experimental conditions adopted by various authors when determining "illite crystallinity" on the 10A peak. The limits of the anchizone, of Kübler (1967), are given

Author	Experimental conditions (see notes)	$1^{\circ}20$ on chart (in mm)	Low Anchizone boundary (in $^{\circ}20$)	High Anchizone boundary (in $^{\circ}20$)	Max. crystallinity in $^{\circ}20$
Weaver (1961)	1.	*	2.3mm*	12.1mm*	-
Kübler (1967a)	2.	10	0.4	0.25	0.18
Kübler (1968) Frey (1969, 1970)	3.	13.3	0.56	0.30	0.21
Dunoyer de Segonzac (1970)	4.	8.61	0.64	0.41	0.23
Chennaux et al. (1970)	5.	6.66	0.64	0.40	-
Sagon and Dunoyer de Segonzac (1972)	6.	10	0.32	0.27	0.16
Weber (1972)	7.	20	c.0.25 Hbrell 150-155	c.0.17 Hbrell 105-110	c.0.15
Aprahamain (1974)	8.	13.3	c.0.4	c.0.25	-
Kisch (1978)	9.	40	0.38	0.21	0.11
Merriman and Roberts (1985)	10.	40	0.43	0.26	0.144
Johnson et al. (1985)	11.	20	-	-	-
Thomas (1985)	12.	40	-	-	Hbrell 100
Robinson and Bevins (1986)	13.	-	0.34	0.18	0.11
Evans (1987)	14.	10	0.38** Hbrell 170	0.21** Hbrell 70	0.25 Hbrell 90
Roberts (pers. comm.)	15.	40	-	-	0.12
Rice et al (in press) 1989	16.	-	0.38**	0.21**	0.10
Blenkinsop (1988)	17.	-	0.40	0.215	-
This study	18.	20			0.20 Hbrell 114 Nepal
		,	0.37 Hbrell 208	0.27 Hbrell 154	0.21 Hbrell 107 IOM
	19.	,			0.26 Hbrell 110 Glen Esk

Key to table 2.1

1. No data available.
 2. Philips, XY units, $8^\circ/\text{min}$ (no further details provided).
 3. Philips, CuK_α , Slits: 1° divergence - 0.2mm receiving - 1° scatter, $\text{TC}=2$ or 4, Scan: $2^\circ 20/\text{min}$.
 4. Philips 1010, Ni filtered CuK_α , Slits: 2° - 0.1mm - 2° , $\text{TC}=10$ for $1 \times 10^2 \text{ c.p.s.}$, $\text{TC}=4$ for $1 \times 10^3 \text{ c.p.s.}$, Scan: $2^\circ 20/\text{min}$.
 5. Scan: $2^\circ 20/\text{min}$.
 6. $\text{TC}=2$ for $2 \times 10^3 \text{ c.p.s.}$, Scan: $2^\circ 20/\text{min}$.
 7. Philips, CuK_α , Slits: $\frac{1}{2}^\circ$ - 1° monochromator, $\text{TC}=4$ at Scan: $\frac{1}{2}^\circ 20/\text{min}$, $\text{TC}=2$ at $\frac{1}{2}^\circ 20/\text{min}$. For quartz (100) measurements the 1° divergence slit was used (pk width = 3.2-3.3mm). $2-6 \mu\text{m}$ size fraction or rock slices polished parallel to slaty cleavage used.
 8. Philips, Ni filtered CuK_α , Slits: 1° - 0.1mm - 1° , $\text{TC}=4$ for 4×10^2 to $2 \times 10^3 \text{ c.p.s.}$ (usually 1×10^3), Scan: $1^\circ 20/\text{min}$.
 9. Philips, Ni filtered CuK_α , Slits: 1° - 0.2mm - 1° , $\text{TC}=2$ for 1×10^3 or $2 \times 10^3 \text{ c.p.s.}$ (usually 1×10^3), or rarely $\text{TC}=4$ for $\text{c.p.s.} = 4 \times 10^2$, Scan: $\frac{1}{2}^\circ 20/\text{min}$.
 10. Philips PW 1130, Ni filtered CuK_α , 40kV 30mA, Slits: $\frac{1}{2}^\circ$ - 0.1mm - 1° , $\text{TC}=4$ for 4×10^2 to $1 \times 10^3 \text{ c.p.s.}$, Scan: $\frac{1}{2}^\circ 20/\text{min}$. Scans were made on $<2 \mu\text{m}$ smears forward and reverse from 7.5 to $10^\circ 20$ with 2 standards run at start and finish of 25 samples.
 11. Philips PW 1010, CuK_α , 36kV 18mA, Slits: 1° - 0.2mm - monochromator, $\text{TC}=4$ for 2×10^2 to $4 \times 10^2 \text{ c.p.s.}$, Scan: $\frac{1}{2}^\circ 20/\text{min}$.
 12. As for 11. but divergence slit of $1/6^\circ$ sometimes used, $4 \times 10^2 \text{ c.p.s.}$ and $40 \text{ mm} = 1^\circ 20$.
 13. Philips PW 1730/10, CuK_α , 40kV 30mA, automatic divergence - 0.1mm - monochromator, Scan: $\frac{1}{2}^\circ 20/\text{min}$. $<2 \mu\text{m}$ smears used and computer recorded data.
 14. As for 12. but 2° scatter instead of a monochromator and $10 \text{ mm} = 1^\circ 20$.
 15. Philips PW 1710, Ni filtered CuK_α , 40kV 30mA, $\frac{1}{2}^\circ$ - 0.1mm - 1° , $\text{TC}=4$ for $1 \times 10^3 \text{ c.p.s.}$, Scan: $\frac{1}{2}^\circ 20/\text{min}$. Chart recorder PM 8210 with heat sensitive paper.
 16. Philips PW 1790, CuK_α , 40kV 30mA, Slits: Automatic Divergence - 0.1mm - monochromator, $\frac{1}{2}^\circ 20/\text{min}$.
 17. Values in this study were derived by running polished standards obtained from Kisch.
 18. Philips PW 1010, CoK_α , 40kV 30mA, Slits: 1° - 0.2mm - monochromator, $\text{TC}=4$ for 4×10^2 to $2 \times 10^3 \text{ c.p.s.}$, Scan: $1^\circ 20$ or $\frac{1}{2}^\circ 20/\text{min}$.
 19. As for 17. except CuK_α , 36kV 18mA.
- * Values given in terms of sharpness ratio of Weaver(1961), which is taken as the ratio of the peak height (at 10Å) to the height of the low angle side at 10.5Å.
- ** Anchizone limits taken from Kisch (1980a).

Where K is a constant (0.91), λ = the radiation wavelength, N = the crystallite thickness consisting of a stack of $Nd\text{\AA}$ unit cells, d = the unit cell spacing (for example 10\AA^o for illite), and β = the peak width in $^o2\theta$. The Scherrer equation also explains how peak broadening on the chart can be related to a reduction in crystallite thickness (Roberts and Merriman, 1985), which will affect the illite crystallinity value obtained.

A brief summary of the peaks used to identify phyllosilicate minerals and their polymorphs is given. More detailed information can be obtained from Hutchinson (1976) and Thorez (1975).

Illite/Muscovite

The presence of illite or muscovite can be detected by the occurrence of major peaks at 10\AA^o (001), 5\AA^o (002) and 3.3\AA^o (003). The various polymorphs can be distinguished by a variety of basal reflections (see Appendix 2.4 for a list of examples). As a general rule the progression from 1Md to 1M to 2M₁ polymorphs is characterised by a sharpening of peaks and an increase in the number of basal reflections. Peaks at 3.89\AA^o , 3.74\AA^o , 3.00\AA^o , 2.87\AA^o , and 2.80\AA^o indicate the presence of the 2M₁ polymorph.

Montmorillonite

Montmorillonite can be recognised by a peak at 15 to 17\AA^o which expands to 18\AA^o on ethyl-glycolation.

Chlorite

Peaks at 14.20°A (001), 7.10°A (002), 4.73°A (003) and 3.55°A (004) can be used to identify chlorite. If the 003 peak is the strongest and the 002 peak is preserved after heat treatment to 600°C , then dioctahedral chlorite is present, otherwise the trioctahedral variety is present. Fe rich chlorite is indicated by the 002 and 004 peaks being larger than the 001 and 003 peaks.

Kaolinite

Kaolinite can be difficult to distinguish from chlorite due to its main peaks lying at 7.18°A (001) and 3.58°A (002), coinciding with the 002 and 004 peaks of chlorite (Biscay, 1964). HCl treatment will destroy chlorite 001 and 003 reflections while reducing the 002 and 004 reflections, and heat treatment will destroy all kaolinite reflections and all but the 001 reflection of chlorite.

Mixed-Layering

Owing to the possibilities of both random and regular mixed-layering in various proportions, a wide variety of peak positions and shapes can occur. The presence of random mixed-layering is usually recognised by broad humps or shoulders on better defined peaks. Regular mixed-layering is shown by sharper peaks. In both situations the peaks lie in a position between the peak positions of the two or more constituents involved in the mixed-layering. Some regular interstratifications have been named and these include corrensite, rectorite and tosudite (see section 2.1.4).

Paragonite

Paragonite can be identified by its $9.56\text{-}9.66\text{\AA}$ (001), 4.82\AA (002) and $3.21\text{-}3.20\text{\AA}$ (003) peaks (Zen and Albee, 1964), though small quantities will be swamped by larger muscovite and quartz peaks.

Mixed-Layer Paragonite/Muscovite

Paragonite/muscovite has peaks at $9.76\text{-}9.77\text{\AA}$, 4.88\AA and $3.25\text{-}3.26\text{\AA}$ for a 6:4 mix (Frey, 1969). It forms a shoulder on the muscovite peaks if there is >20% paragonite in the mixed-layer structure (Merriman and Roberts, 1985).

Pyrophyllite

Pyrophyllite can be recognised by, having a unique peak at 9.20\AA (001), as well as peaks at $4.46\text{-}4.60\text{\AA}$ (002) and $3.05\text{-}3.07\text{\AA}$ (003).

Biotite

Biotite can be masked by muscovite, having major peaks at 10.1\AA (001) and 3.37\AA (003), though its 2.66\AA ($20\bar{1}, 130$) peak is unique and allows its identification.

2.2.6 Treatments

To aid the identification of phyllosilicate minerals and their polymorphs a variety of treatments can be applied to the sample slides before XRD analysis, as described by Hutchinson (1974) and Thorez (1976), see Appendix 2.3. These include;

1. Ethyl-Glycolation - This is used to test for mixed-layer expandable clay minerals. The smectite (001)

peak expands from 15°A to 17°A . Illite, kaolinite and chlorite are unaffected.

2. Heat Treatment - This produces the dehydration of different clay species. It is useful in distinguishing between kaolinite and chlorite. The kaolinite diffraction pattern disappears whereas chlorite is little affected. The 15°A peak of montmorillonite disappears and is replaced by a 9°A peak.

3. Acid Treatment - Treatment with 2M HCl should produce the following results. Chlorite is destroyed, smectite attacked and kaolinite is unaffected.

2.2.7 Illite Crystallinity

The determination of illite crystallinity values was carried out using the methods of both Kübler (1968) and Weber (1972). The Kübler Index is a measure of the (001) white mica peak at half its height (see Fig. 2.3). Measurements are made in mm and converted into $^{\circ}2\theta$ to cancel out the effect of variable chart or scan speeds between laboratories. The Weber Index again measures the half height peak width, but in the St.Andrews lab an average of five scans is taken and this is divided by the average of three scans on the quartz (100) peak of a quartz standard, and multiplied by 100 to give a value in Hbrel (Halbwertsbreite).

Internal standardisation can be carried out using a variety of standards. Kübler uses roofing slate cut parallel to schistosity, and run with each batch of samples. The peak width is consistent to within < + or - 2% (Kübler, pers comm.), and has been made available to a number of other authors. Roberts and Merriman both use the same two powdered pelite standards prepared as $<2\mu\text{m}$ smears on glass slides (Roberts, pers comm.). BRM 147 is run with samples believed to be high anchizone/epizone, while BRM169 is run with low anchizone samples. These indicate a maximum machine error of + or - 0.02 $^{\circ}2\theta$ (Merriman and Roberts, 1985). For this study a quartz powder standard was used. This was packed into a sample holder and flattened off with a glass slide. The standard shows a variation of + or -

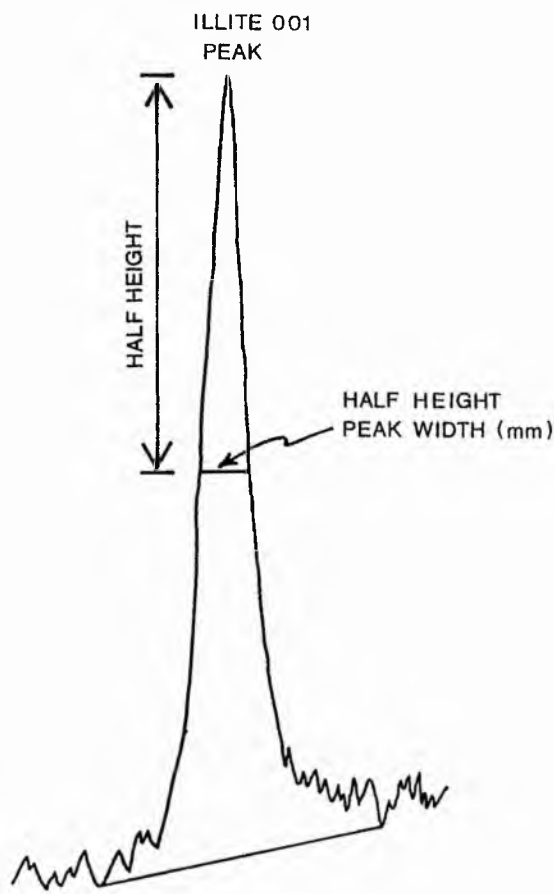


Fig. 2.3 - Determination of illite crystallinity values using the Kubler Index (KI) and the Weber Index (WI). The KI is obtained by measuring the half height peak width (mm) of the illite 10 \AA peak, and converting the value to $^{\circ}2\theta$. The WI is the same value divided by the half height peak width of the quartz (100) peak of a quartz standard as follows:

$$WI \text{ (Hbre1)} = \frac{\text{Width of illite (001) peak at } \frac{1}{2}ht}{\text{Width of quartz (100) peak at } \frac{1}{2}ht} \times 100$$

This figure is produced using the average of five measurements of the illite peak, and 3 measurements of the quartz peak.

0.0125 ° 2θ which could reflect variation in the machines performance or in the flattening of the standard.

External standardisation is much more problematical. In order to achieve universal standardisation the following requirements would ideally be met:

1. The machines used would be of the same type, and in similar states of wear and tear.

2. Detailed sample preparation, including how the samples are crushed and the size fractions are obtained, would have to be standardised.

3. Machine conditions would have to be standardised. This tends not to happen everywhere because the performance of various machines is usually compensated for by varying the machine conditions.

4. A suitable standard should be used which is immune to variation in peak width. This tends to rule out powdered samples due to the problems of preferred orientation and damage to the standard. The use of cut slate seems to provide an acceptable standard. A large enough supply of slate of consistent mica (001) peak width would have to be available to all illite crystallinity workers.

5. The illite crystallinity measurements should be made in the same way at different establishments. Both the Kübler Index and Weber Index could be applied to a set of samples. If a suitable standard could be established then variations in machine conditions could be compensated for. This would not cancel out variations in sample preparation.

2.2.8 Illite Crystallinity Limits of the Anchizone

The lower and upper limits of the anchizone were first defined by Kübler (1967a), on the basis of the illite 10 \AA half height peak width. This was measured in millimetres, though values in $^{\circ}2\theta$ were later adopted to simplify comparison between laboratories (see section 2.2.7). These limits were $0.42^{\circ}2\theta$ (lower) and $0.25^{\circ}2\theta$ (upper).

Blenkinsop (1988) examined the problems involved when comparisons are made between sets of data from different laboratories. The two major problems are the variety of values chosen for zone boundaries (see table 2.1) and the persistent use of three different crystallinity indices (see Blenkinsop, 1988).

The first problem is primarily due to the use of a range of measurement techniques, and variations in machine performance between laboratories. This is dealt with by inter-laboratory calibration using standards to get equivalent values, for the anchizone limits, in $^{\circ}2\theta$, to those used by Kübler. Theoretically inter-laboratory calibration should be straightforward, but it has been complicated by an absence of a consistent standard which is available to all laboratories.

The problem of using different indices (Kübler Index, Weaver Index and Weber Index) was dealt with by Blenkinsop by plotting the indices against each other for the same data sets. The Kübler versus Weber plot showed a linear relationship, while the Kübler versus Weaver plot showed a

power law relationship. These relationships can be used to deduce equivalent relative values of the anchizone boundaries, for the Weber and Weaver Indices, from the Kübler Index. The relationships are only valid for the data base from which they were derived.

The limits of the anchizone can also be constrained by phyllosilicate mineralogy. Merriman and Roberts (1985) and Robinson and Bevins (1986) made illite crystallinity surveys in Wales covering metapelites ranging from diagenetic grades to the high epizone. In both studies the lower and upper boundaries of the anchizone were defined using both crystallinity values and white mica polymorphs. The lower boundary of the anchizone was recognised by the first appearance of the 2M₁ polytype and the upper boundary was recognised by the last appearance of the 1Md polytype. The anchizone was characterised by the coexistence of both polytypopes in variable proportions.

The advantage of using white mica polytypes to define the anchizone limits is that their identification is not dependant on machine conditions. The main problem is that precise estimates of small quantities of 1Md or 2M₁ mica cannot be made by XRD.

By combining phyllosilicate mineralogy with illite crystallinity the limits of the anchizone can be placed with acceptable accuracy for each set of data investigated. This facilitates more meaningful comparisons between results from different laboratories.

2.2.9 External Calibration of Quartz Standard

The use of a reliable standard is essential when making illite crystallinity measurements. It provides internal calibration of machine conditions, as well as the potential for external calibration with other institutions.

In this study a degree of external calibration with other authors was achieved by sending samples of the quartz powder used at St.Andrews to Professor Kübler at the University of Neuchâtel, Switzerland, and to Dr Roberts at Birkbeck College, University of London. Instructions were given on how to prepare the samples for analysis (see section 2.2.7) in order to cancel out variation due to different preparation techniques. Peak measurements are made on the quartz (100) peak.

At Birkbeck the quartz standard was prepared in both the St.Andrews way, (quartz powder is packed into a sample holder and flattened by applying pressure directly onto the powder with a glass slide), and in the Birkbeck way, (an XRD sample holder is placed face down on a piece of glass, the back removed, quartz powder added and flattened using pressure from the back). The results are listed in table 2.2.

The results indicate that technique 2 produces a more random orientation of the quartz standard. The poorer standard deviation could be attributed to the limited number of scans made (5 scans).

Table 2.2 - The effect of quartz standard preparation techniques on peak width and consistency of the standard. Samples prepared and run at Birkbeck.

St Andrews	Birkbeck
Scans 5	5
Peak intensity (counts per second)	
Mean 403.4	445.4
Sample SD 4.615	2.793
% SD + or - 1.144%	+ or - 0.627%
Peak width ($^{\circ}2\theta$)	
Mean 0.148	0.1355
Sample SD 1.118×10^{-3}	3.260×10^{-3}
% SD + or - 0.775%	+ or - 2.410%

At Neuchatel a different approach was made. Six separate powder mounts were made using the St.Andrews technique. They were analysed by both automatic and manual diffractometer. The automatic diffractometer uses the APD 10 program which gives a value equivalent to the area under the peak. The results were as follows (see table 2.3):

Table 2.3 - Consistency of a quartz standard. Samples prepared and run at Neuchâtel.

Manual	Automatic
Scans 6	6
Peak intensity*	
Mean 162.83	4206.00
Sample SD 14.36	640.61
% SD + or - 8.8%	+ or - 15.2%
Peak width ($^{\circ}2\theta$)	
Mean 0.17	0.17
Sample SD 0.02	0.03
% SD + or - 11.8%	+ or - 17.6%

* Peak intensity equivalent to height for manual and to area for automatic.

It can be seen that automatic diffractometry produces more variability in the results. Kübler attributes this in part to the use of an automatic divergence slit. The larger standard deviation can alternatively be explained as the result of squaring the error by measuring an area as opposed to a height. When the square root of the six automatic scan results for peak intensity is taken a % SD of + or - 7.636% is produced which is compatible with the manual run.

The % SD on peak width for the manual technique which is compatible with that used at Birkbeck is over fifteen times as large. This must reflect error incurred as a result of producing separate standards as opposed to running the same standard a number of times. Kübler recommends the use of his roofing slate standard which has a % SD of + or - 2%.

Though the quartz standard is not ideal errors can be reduced by monitoring the peak height of the standard and remaking the standard if the height drops appreciably due to damage to the exposed surface.

The differences in mean peak width, for the same quartz standard run at St Andrews ($0.1875^{\circ}2\theta$), Birkbeck ($0.148^{\circ}2\theta$) and Neuchâtel ($0.17^{\circ}2\theta$) can be attributed to variations in machine conditions (see section 2.2.4). The age and state of repair of the machines used may also be a contributory factor.

2.2.10 External Data Calibration

A certain amount of external calibration was achieved by having samples analysed at Birkbeck College, London, under the supervision of Dr B. Roberts, as well as at St. Andrews University.

With Birkbeck College, London

Twenty-five samples, prepared and analysed at St. Andrews, were also analysed at Birkbeck. Smears were also made at Birkbeck from unprepared rock from the same twenty-five samples and analysed at Birkbeck. A further fifteen samples were prepared at Birkbeck and analysed at both institutions.

The results are shown in Fig. 2.4 as a graph of the Birkbeck analyses versus the St. Andrews analyses. These results are shown in $^{\circ}2\theta$ and also in Hbrel using a quartz standard run at both institutions (see section 2.2.9). Variations in the quartz standard value, with multiple runs, were within acceptable limits.

The data in $^{\circ}2\theta$ plots to one side of the X=Y line. This must reflect the difference in machine conditions between the two institutions, since the same prepared slips were used for both sets of analyses. The difference in machine conditions between the two institutions has been compensated for by plotting points in Hbrel using quartz standards appropriate to the respective institutions. This moves data points into relatively good correlation with the X=Y line. Ideally, for data measured in Hbrel, the points should plot along the X=Y line. In reality, the graph shows

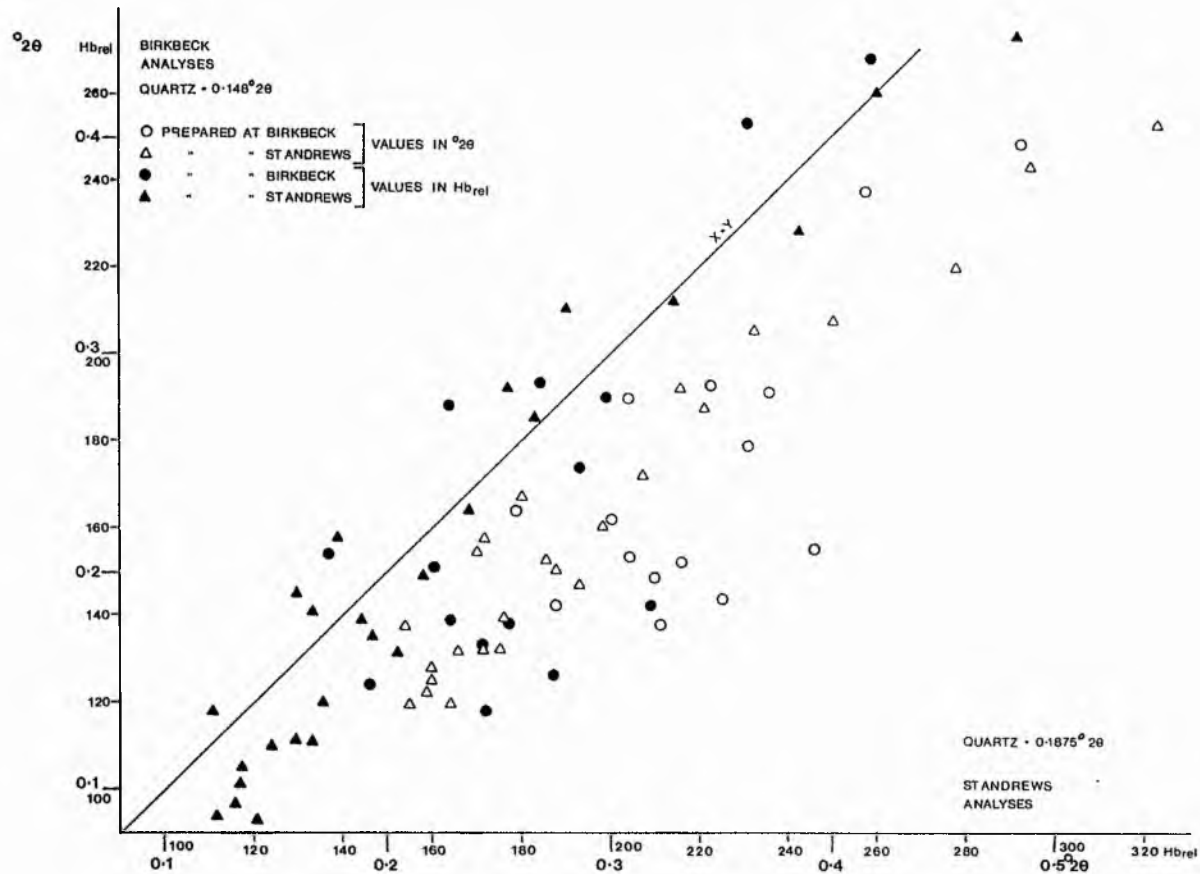


Fig. 2.4 - External calibration of samples from the Isle of Man. Samples were prepared at both Birkbeck and St. Andrews, and analysed at both institutions. Light symbols are values in $^{\circ}2\theta$ and dark symbols are values in Hbrel using mean quartz standard values for a quartz standard measured at both institutions.

a scatter around this line. Part of this scatter will have resulted from using an average quartz standard value for each institution, rather than analysing the standard with each sample run. Further potential sources of error are from orientation of the slip in its sample holder, and from damage to the surface of the sample between analyses runs.

2.2.11 Factors Affecting Peak Width

A number of factors can affect the peak width of the mica 10 \AA peak and are listed as follows:

1. Sample preparation: The processes involved in sample preparation and their effects on peak width are described in section 2.2.3. These include over milling, ultrasonic disaggregation and thickness of sedimentation.

2. Scan speed: Kisch (1980b) observed that for the same machine conditions as Kübler uses, his peak widths were approximately $0.05^\circ 2\theta$ narrower than Kübler's. The only difference was that his scan speed was $0.5^\circ 2\theta/\text{min}$ whereas Kübler's was $2^\circ 2\theta/\text{min}$. By using a standard, run with samples, scan speed effect can be adjusted for.

3. Crystallite size: Crystallite size can be directly related to peak width by the Scherrer equation (see section 2.2.5). Smaller crystallites are associated with broader peaks. Therefore the grade of metamorphism determined by illite crystallinity is a measure of crystallite size.

4. Weathering: Mixed-layer illite/montmorillonite may form as a hydration product of K-white mica, and result in peak broadening. To avoid this, weathered samples are avoided in the field, and excess weathering is ground off samples.

5. Detrital mica: Micas derived from other sources may be more crystalline than authigenic micas and therefore have correspondingly narrower peaks widths. This results in an increase in illite crystallinity where detrital mica is

a significant component of a sample. To avoid this the <2um size fraction is used, since detrital mica is usually coarser grained than this.

6. Lithology: Potassium is an essential element in the conversion of smectite in illite-smectite to illite (Whitney and Northrop, 1988) and therefore the amount of K available controls the level of crystallinity achieved at different grades. Porous sandstones receive a higher input of K and develop K-white mica more rapidly than pelitic rocks (Kübler, 1968; Dunoyer de Segonzac, 1970). Metacarbonate rocks tend to be K deficient and consequently suffer retarded illite growth (Frey, 1987). A similar retarding effect can be found in sediments with a high organic content, due to the isolation of illites from circulating solutions by hydrophobic organic material (Frey, 1987). Pelitic samples are collected to maintain consistent lithology.

7. Retrogression: Retrogressive hydration can reverse the process of illitisation with a corresponding reduction in crystallinity. The importance of this effect is uncertain.

8. Interparticle Diffraction: "Interparticle diffraction is considered to be the coherent diffraction of radiation by atomic planes of two or more adjacent, parallel particles" (Nadeau et al., 1984). This effect was studied by Nadeau et al. (1984) and has been touched on in section 2.2.5. If the number of unit cells per crystallite is less than 5 to 15, then a sedimented mixture of

elementary particles of illite and montmorillonite gives an identical XRD pattern to that of a randomly interstratified illite-smectite, which would appear as a broad 13 \AA peak as opposed to two discrete peaks at 10°A and 17°A .

9. Adjacent Peaks: Peak broadening can result from the presence of minerals with a similar d-spacing to that of muscovite (10.1 to 9.9°A). These include paragonite (9.7°A), paragonite-muscovite (9.9 to 9.8°A), biotite (10.1 to 9.9°A), and to a lesser extent pyrophyllite (9.2 to 9.1°A) (Dunoyer de Segonzac, 1970; Kisch, 1980a; Roberts and Merriman, 1985). Crystallinity measurements can be made in the presence of these minerals if their quantity is small, and their peaks can be resolved.

10. Stress: The effect of stress on illite crystallinity is not yet clear. Roberts and Merriman (1985) recorded increased crystallinity across the hinge zone of a tight anticline. Further discussion can be found in Frey (1987, p18 to 20).

2.2.12 Determination of b_0 -Spacing

The basal spacing (b_0) of the (060) peak of potassic white mica has now become an accepted measure of relative pressure in low grade metamorphic rocks. Cipriani et al. (1968; in Padan et al., 1982) adopted a b_0 -spacing parameter as a measure of the celadonite content in K-white mica. $b_0 = 8.990 + 0.327RM$ (in \AA), where RM is the celadonite content formed by mol. prop. $\frac{1}{2}\text{Fe}_2\text{O}_3$ + mol. prop. FeO + mol. prop. MgO. Frey et al. (1983) have produced a refined parameter, where $d(060, 331)\text{\AA} = 1.389 + 0.082RM$

which is equivalent to b_o (060, 331) $^{\circ}\text{A}$ = 8.988 + 0.492RM. This new parameter takes into account the presence of the (331) 2M, peak which cannot be separated from the (060) 2M, peak, and has an intensity of approximately double that of the (060) 2M, peak. An increase in celadonite content can be directly related to an increase in barometric pressure for rocks of uniform geochemistry, temperature of metamorphism and grain size (Sassi, 1972; Frey, 1987).

The b_o values were measured under the machine conditions shown in Appendix 2.1. By scanning from 59.0 to 62.5 $^{\circ}2\theta$, the quartz (211) peak could be used as an internal standard to correct the calibration of the $^{\circ}2\theta$ value of the mica (060) peak (Sassi, 1972; Johnson et al., 1985).

2.2.13 Factors Affecting b_o spacing

Bulk composition and mineral assemblage have to remain constant in order to obtain a reliable measure of pressure using b_o . A number of factors have to be taken into consideration when sampling and interpreting b_o values:

1. Samples rich in quartz, chlorite, or with significant K-feldspar content have higher b_o values (Sassi and Scolari, 1974).
2. Carbonate rich samples have lower b_o values (Sassi and Scolari, 1974).
3. Rocks with abundant paragonite, margarite or pyrophyllite have illite with lower celadonite content, and

therefore tend to give low b_o values (Guidotti and Sassi, 1976).

4. In hematite or magnetite bearing rocks it is difficult to differentiate between celadonitic muscovite and ferro-muscovite.

5. The temperature of metamorphism will affect the celadonite content of the K-white mica. Increased temperature produces a decrease in celadonite content and decrease in sensitivity of the method and these in turn determine the b_o value (Sassi, 1972).

6. As with illite crystallinity, detrital mica can influence the b_o spacing by having a different celadonite content from the authigenic mica (Padan et al., 1982).

7. The random mixed-layer illite (060)/smectite peak can obscure the (060) illite peak in diagenetic to low anchizone rocks (Padan et al., 1982).

Samples were collected from uniformly pelitic rocks where possible, both for the benefit of b_o and illite crystallinity measurements. The rocks were also collected from areas of anchizone to epizone rocks which minimises the effect of temperature. From petrographic examination detrital mica can be seen to be minimal in most samples, and its influence has been minimised by using the $<2\mu\text{m}$ size fraction. The grade of the rocks meant that there was very little mixed-layer illite/smectite.

2.2.14 Anchizone Temperature Limits

The upper and lower limits of the anchizone are defined by illite crystallinity values determined by Kübler (1967a) (see section 2.2.8). Over the last couple of decades a number of authors have put forward temperature limits for the lower and upper anchizone boundaries. The anchizone temperature limits are based on a variety of indicators:

1. Experimental data on mineral transformations, in particular zeolite minerals.

2. Vitrinite reflectance (VR), coal rank (CR), graptolite reflectance and various other organic indicators (eg. conodont colour alteration index).

3. $\delta^{18}\text{O}$ -isotopes.

4. Fluid inclusions (FI)

By applying temperature limits to the anchizone, illite crystallinity values can in turn be temperature constrained. Both Weaver (1984) and Kisch (1987) have reviewed much of this information, though on the basis of what they each reviewed, they favour quite different sets of limits. A table of limits reviewed by Weaver and Kisch is presented (Table 2.4).

Table 2.4 - Anchizone temperature limits.

Weaver, 1984

Source	Diagenesis	Anchizone	Epizone	Method
Weaver, 1984		280°C 190-300	360°C 300-400°C	$\delta^{18}\text{O}$ -isotope. Conodont colour alteration index.
Biotite appears at 420°C				

Black, 1974	250 °C	400 °C	O-isotope.
Frey, et al., 1980b	200 °C 1.2kb	270 °C	FI.
Winkler, 1979 Biotite appears at 425-450 °C		350-370 °C 2kb	
<u>Kisch, 1987 (in Frey, 1987)</u>			
Brauckmann, 1984 p150	145-155 °C 180-240 °C		Quartz-illite O-isotope. CR and VR.
Primmer, 1985	<200 °C (low epizone)	321-377 °C 300 °C	Quartz-illite O-isotope. Quartz-chlorite. O-isotope.
Durney, 1974	245 °C (high diagenesis)		FI.
Saliot et al., 1982	170-310 °C 200-650bars (high diagenesis)		FI.
Barlier, 1974	200 °C (high diagenesis)		FI and VR.
Robinson et al., 1980	150-250 °C		FI and CR.
Kisch (unpublished)	185-230 °C (low-medium anchizone)		FI.
Duba and Williams-Jones, 1983b	300 °C		FI and VR.
Mullis, 1979 and Frey et al., 1980b	200 °C min 1.2kb	270 °C min 1.7kb	FI and VR.
Niedermayr et al., 1984	180-200 °C (adopted)	300-350 °C	FI.

The fluid inclusion data reported by Frey et al. (1980b) represent the fluid inclusion homogenisation temperatures without pressure correction, and therefore represent minimum temperatures.

Weaver (1984) favours a lower anchizone boundary between 250 and 280 °C and upper anchizone boundary of 350

to 400 °C, whereas Frey (1987) concludes by favouring 200 to 250 °C and 300 °C for the lower and upper boundaries respectively. When both sets of conclusions are taken together they show how poorly constrained the limits of the anchizone are.

2.3 FLUID INCLUSION METHODS

2.3.1 Aims

The aims of this chapter are to outline the techniques used and describe the information gained from them.

2.3.2 Introduction

In the metamorphic environment fluid inclusions (FI's) are samples of fluids trapped during the crystallisation or recrystallisation of a host mineral. These trapped fluids are representative of the fluids circulating at the time of trapping, and therefore provide useful information on the conditions during metamorphism. On cooling, after trapping, the liquid shows a greater thermal contraction coefficient than the host mineral and forms a vapour bubble. The reversal of this process, by heating the inclusion to the homogenisation temperature, can give an estimate of the trapping temperature of the liquid. Further to this, the optical and thermal properties of the fluid can provide much information on its composition.

FI studies were undertaken using petrographic, thermometric and extraction techniques on quartz vein and segregation material. These techniques were applied to help determine the temperature and pressure conditions of the rocks studied, and the nature of the fluids circulating within them.

2.3.3 Preparation of FI Wafers

Double-sided polished wafers, 0.2 to 0.8mm thick were prepared from vein and segregation quartz samples. The details of the preparation process can be found in Crosbie (1981). A minimum thickness of 0.2mm prevents the wafer becoming over brittle and allows for the possibility of large inclusions. A maximum thickness of 0.8mm minimises thermal lag in the response of the inclusions to heating on the thermometric stage. The exact choice of thickness depends on the clarity of the quartz.

2.3.4 Optical Examination

Before a thermometric study is made a number of observations can be made from the optical examination of a fluid inclusion wafer using a standard petrographic microscope. These observations include the following:

1. Inclusion origin - Primary, secondary and pseudosecondary inclusions can be distinguished on the basis of their size, shape and distribution within a quartz crystal. The determination of the types of inclusions and the various pitfalls present are reviewed in Touret (1977), Roedder (1984) and Shepherd et al. (1985).

Primary inclusions are trapped during the crystal growth, and are therefore representative of the crystal precipitating fluids. They can be easily recognised if they are confined to recognisable growth zones. A three dimensional random distribution, with inclusions isolated by at least 5 times their diameter from the next inclusion,

is taken as indicative of primary inclusions. Negative crystal shape is not diagnostic of primary inclusions.

Secondary inclusions are formed later by the post-crystallisation introduction of fluids, into the host crystal, along fractures or cleavages. These form planar groups in healed fractures.

Pseudosecondary inclusions are inclusions formed during crystal growth along growth generated fractures giving them the appearance of secondary inclusions. They can be recognised by the abrupt termination of these fractures by later crystal growth.

In metamorphic quartz, secondary inclusions are by far the most common type.

2. Sequence of trapping - The relative ages of sets of inclusions can be determined by the way inclusion planes intercept, and by the extent of migration of inclusions away from a plane.

3. Phases present - A qualitative assessment of the composition of the fluids, as well as their relative proportions, can be made by observing the phases present. Water is the most common constituent, but the presence of CO and hydrocarbons can be recognised. Phase proportions of the various liquid and vapour phases can be estimated on suitable inclusions at room temperature (Shepherd et al., 1985; Craw, 1988).

4. Captured or daughter minerals - Minerals can occur individually, or in sets in inclusions, as a result of trapping during the formation of the inclusion or by growth

in the inclusion from oversaturated fluids. A trapped mineral can be recognised either by having an anomalously large size for the inclusion, or by occurring elsewhere in the host crystal as a solid inclusion. Daughter minerals can be recognised by their regular occurrence in inclusions and in relative proportions to the inclusion size.

5. Necking-down, leaking and autodecrepitation -

These three mechanisms all result in anomalous thermometric results. Necking-down can be detected by spikes in the inclusion wall or by variable phase proportions in adjacent inclusions. Autodecrepitation results from the fluid pressure exceeding the lithostatic pressure by enough to cause fracturing of the inclusion walls. This can result from rapid uplift or heating when at low pressure. A large irregular inclusion with small satellite inclusions would indicate this. Leaking, commonly due to gradual pressure release with uplift, is often impossible to detect because of the annealing of microfractures after the escape of a phase.

2.3.5 Thermometric Measurements

In this study a Linkam TH 600 heating and freezing stage was used with a Leitz microscope. Thermometric measurements are made on a small piece of wafer. The rest was saved in case more material is required. Up to seven different phase changes were recorded on a single inclusion (see table 2.5, and plates 2.1 and 2.2).

Th CO₂ and Th TOT can homogenise to the liquid (L) phase, vapour (V) phase or with critical behaviour (C), and

Plate 2.1 - A number of phase changes can be observed during the heating of a three phase fluid inclusion. This example, from sample FI3, is 100 μm long. The lower right inclusion would be unsuitable for thermometric measurements because it has been necked.

A - -11.5 $^{\circ}\text{C}$: Three phases are recogniseable at this temperature. The aqueous phase (upper) is frozen, the CO₂ phase (lower) is liquid, and there is also a crystalline gas clathrate phase growing on the CO₂ phase.

B - -3.3 $^{\circ}\text{C}$: At this temperature the aqueous phase is mostly liquid, though a last ice crystal is present (not very visible in this picture, but there). The clathrate is well developed.

C - 2.0 $^{\circ}\text{C}$: The aqueous phase is entirely liquid, and the CO₂ phase has started to seperate into a liquid and vapour phase.

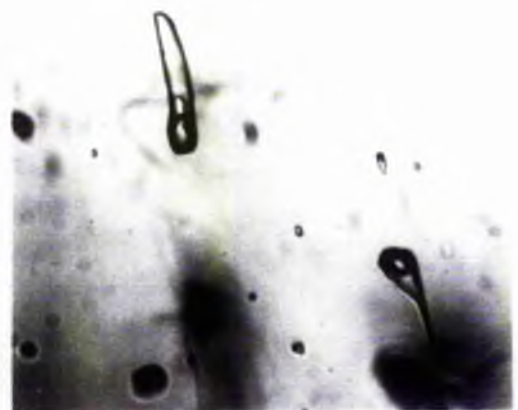
D - 11.0 $^{\circ}\text{C}$: the clathrate has now dissolved, and the inclusion now contains a vapour CO₂ bubble inside a liquid CO₂ bubble inside an aqueous liquid phase.

E - 32.3 $^{\circ}\text{C}$: The meniscus between the two CO₂ phases is faint. This indicates that homogenisation of the CO₂ phases, with critical point behaviour, is occurring.

F - 33.3 $^{\circ}\text{C}$: The CO₂ liquid and vapour phases have now homogenised (Th CO₂).



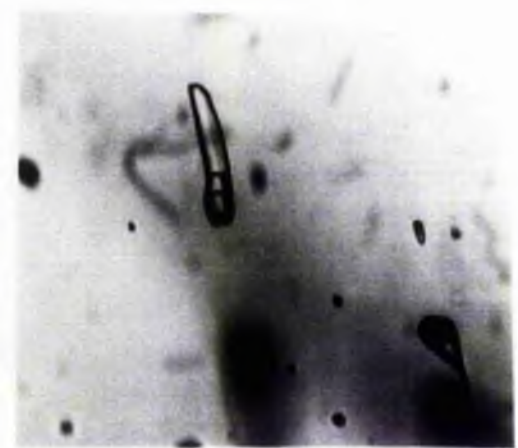
A



B



C



D



E



F

Plate 2.2 - In this example of a three phase fluid inclusion further phase changes are illustrated from plate 2.1. This example, from FI3, is 50 μm long.

A - 3.5 $^{\circ}\text{C}$: A CO₂ bubble, in an aqueous phase, is enclosed in a ragged clathrate.

B - 22.5 $^{\circ}\text{C}$: The CO₂ phase has formed a double bubble.

C - 32.2 $^{\circ}\text{C}$: The CO₂ double bubble is homogenising to the liquid state. The vapour phase forms a small bubble in the bottom left corner of the CO₂ liquid bubble.

D - 32.8 $^{\circ}\text{C}$: The CO₂ phase has now completely homogenised.

E - 278 $^{\circ}\text{C}$: Total homogenisation (ThTOT) of the inclusion, to the liquid phase, has nearly been achieved. The CO₂ phase forms a small bubble.

F - 285 $^{\circ}\text{C}$: The inclusion has homogenised to the liquid phase.



A



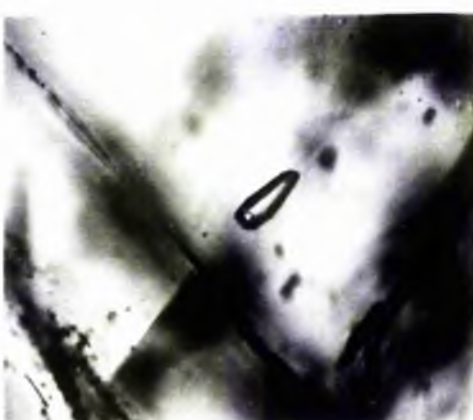
B



C



D



E



F

is expressed as Th CO₂ to L, for example. Critical behaviour can be recognised when the meniscus between the liquid and vapour phases fades on heating until it disappears.

Table 2.5 - Phase changes during fluid inclusion microthermometry.

Phase Change	Approx. Temp.	Description
Tff	-110 to -90°C	Freezing of CO ₂ liquid
T _m CO ₂	-62 to -56.6°C	Last melt of CO ₂ ice
T _e	-59 to -15°C	First melt of H ₂ O ice
T _m H ₂ O	-15 to 0°C	Last melt of H ₂ O ice
T _m Clath	+5 to +10°C	Last melt of gas clathrate
Th CO ₂	-5 to 31.1°C	Homogenisation of CO ₂ phases
Th TOT	> +100 °C	Total homogenisation

The number of phase changes that can be measured on an inclusion is determined by whether CO₂ is present and the viewing quality of the inclusion. The lower temperature changes are often difficult to see. A minimum sample population of thirty inclusions should be studied, though this is not always possible. For statistical purposes an inclusion should only be studied if it is unlikely that it has suffered fluid or vapour loss. It should thereby contain fluids representative of the fluids circulating when trapping occurred.

Observations are made while heating to avoid problems of cooling changes occurring only after supercooling. Th TOT should always be measured after all other measurements on a group of inclusions are made. In this way, any stretching or decrepitation during heating will only happen after all the data has been gathered. When measuring Th TOT, care

should be taken to observe the inclusions with lower homogenisation temperatures, since these will decrepitate while higher temperature inclusions are homogenising.

2.3.6 Data Interpretation

Aqueous inclusions observed in this study lie in the H₂O - CO₂ - NaCl system and so only the interpretation of data in this field will be discussed. The data gathered is plotted as a set of histograms showing phase changes versus number of samples. This helps clarify the inclusion populations. Next, for each population, a mean temperature, standard deviation and sample number can be determined for each phase change. Once the statistics of the initial data have been obtained further information can be gained using experimentally determined PVTX data. See Hollister and Crawford (1981) and Roedder (1984) for reviews of PVTX data. Unfortunately, for metamorphic environments, there are major gaps in this data. Experimental data is not well constrained for pressures greater than 2kb.

The example in table 2.6 illustrates the type of data that can be obtained.

In the example the phase proportions, measured as degree of fill (F), where $F = V_{liq} / (V_{liq} + V_{vap})$ and $V_{liq} + V_{vap} = V_{tot}$, are F = 0.65 (H₂O liq) and F = 0.35 (CO₂ liq + vap).

The eutetic for the CO₂ - CH₄ system is -56.6 °C, which would indicate the presence of pure CO₂, and therefore T_m CO₂ does not exceed this temperature. Likewise the eutectic for Th CO₂ is +31.1 °C. The errors present are within acceptable limits for the temperature ranges concerned.

Table 2.6 - The results of a typical sample analysed together with statistical data.

Sample Number : FI3

Phases Change	Mean Temp (x)	n	Pop SD
T _m CO ₂	-53.99 °C	24	0.5302
T _e	-25.39 °C	14	1.5829
T _m H ₂ O	-1.21 °C	11	0.3232
T _m Clath	+9.62 °C	20	0.3539
T _h CO ₂	+33.28 °C to L	35	0.2210
T _h H ₂ O	+285 °C to L	38	1.2620

The following data is interdependant and must be derived sequentially:

1. Salt System - From Shepherd et al. (1985, table 4.1, p74) the salt system H₂O - NaCl - KCl is appropriate for a T_e of -25.39 °C. This is close to the eutectic indicating that KCl is a minor component.
2. CO₂ -CH₄ - As stated above, the CO₂ phase appears to be pure (Touret, 1977). An increasing methane component would be recognised by a lowering of T_m CO₂ (see Shepherd et al., 1985; Fig. 4.11, p75).
3. Salinity - Shepherd et al. (1985, Fig. 6.22, p123) can be used to determine the salinity of the H₂O phase if either T_m H₂O or T_m Clath are known. T_m H₂O gives a value of 1.8wt% NaCl equivalent, while T_m Clath gives a value of 1.5wt% NaCl. The true value will lie somewhere between the two values because some of the H₂O will be trapped in the

CO_2 hydrate structure, producing a more saline residual aqueous solution than the original (Collins, 1979; Hedenquist and Henley, 1985).

4. Density - The density of the CO_2 phase can be determined from Th CO_2 to L or V using Shepherd et al. (1985, Fig. 6.17, p115). In FI3 the inclusions homogenise to the liquid near the eutectic indicating a density of 0.5g/cm^3 . The density of the H_2O phase can be roughly determined using wt% NaCl in conjunction with Th TOT on Fig. 6.24 (Shepherd, et al. 1985, p126. This gives a density value of 0.75g/cm^3 . Overall density can then be calculated with the aid of the relative phase proportions.

$$(0.5 \times 0.35) + (0.75 \times 0.65) = 0.6625\text{g/cm}^3.$$

$$(\rho_1 \times \text{vol}_1) + (\rho_2 \times \text{vol}_2)$$

From this wt% CO_2 can be determined as follows:

$$(0.5 \times 0.35)/0.6625 = 26.4\text{wt\%}.$$

5. Pressure (P) - Pressure determination has proved to be one of the problem areas in FI data gathering. The limitations of various techniques have been discussed in depth by Roedder and Bodnar (1980) and reviewed in Roedder (1984). Ideally an independant barometer should be used, though finding one and reliably relating it to the trapping age of the inclusions is more difficult. Certain inclusion assemblages can provide good pressure estimates. These include the trapping of two immiscible phases, and boiling assemblages, recognised by the presence of liquid rich and vapour rich inclusions that homogenise at similar temperatures (Bodnar et al., 1985; Craw, 1988). In this

example pressures at 1, 5 and 10km are given for hydrostatic and lithostatic heads.

	<u>1km</u>	<u>5km</u>	<u>10km</u>	
Hydrostatic P	98	490	980bars	(density = 1.00g/cm ³)
Lithostatic P	269	1343	2685bars	(density = 2.74g/cm ³)

6. Temperature - A minimum trapping temperature can be taken directly from Th TOT as 285°C. When pressure is taken into consideration, this temperature can be adjusted upwards using figures calculated by Potter II (1977). These figures cover a range of salinities and use P, Th TOT and salinity to give trapping temperature (TT).

	<u>1km</u>	<u>5km</u>	<u>10km</u>	
Hydrostatic	290	329	373°C	
Lithostatic	308	407	536°C	

2.3.7 Fluid Extraction

The bulk composition of the inclusion can be directly measured using fluid extraction techniques. Extractions were carried out by Mr R. A. Batchelor.

Quartz separates are prepared from the samples. Each sample is coarsely crushed, sieved and the -16 +30 mesh (1.0 - 1.5mm) fraction retained. Uncontaminated grains are hand picked under a binocular microscope, washed in 50% HNO₃, repeatedly rinsed in deionised distilled water and dried at 110°C.

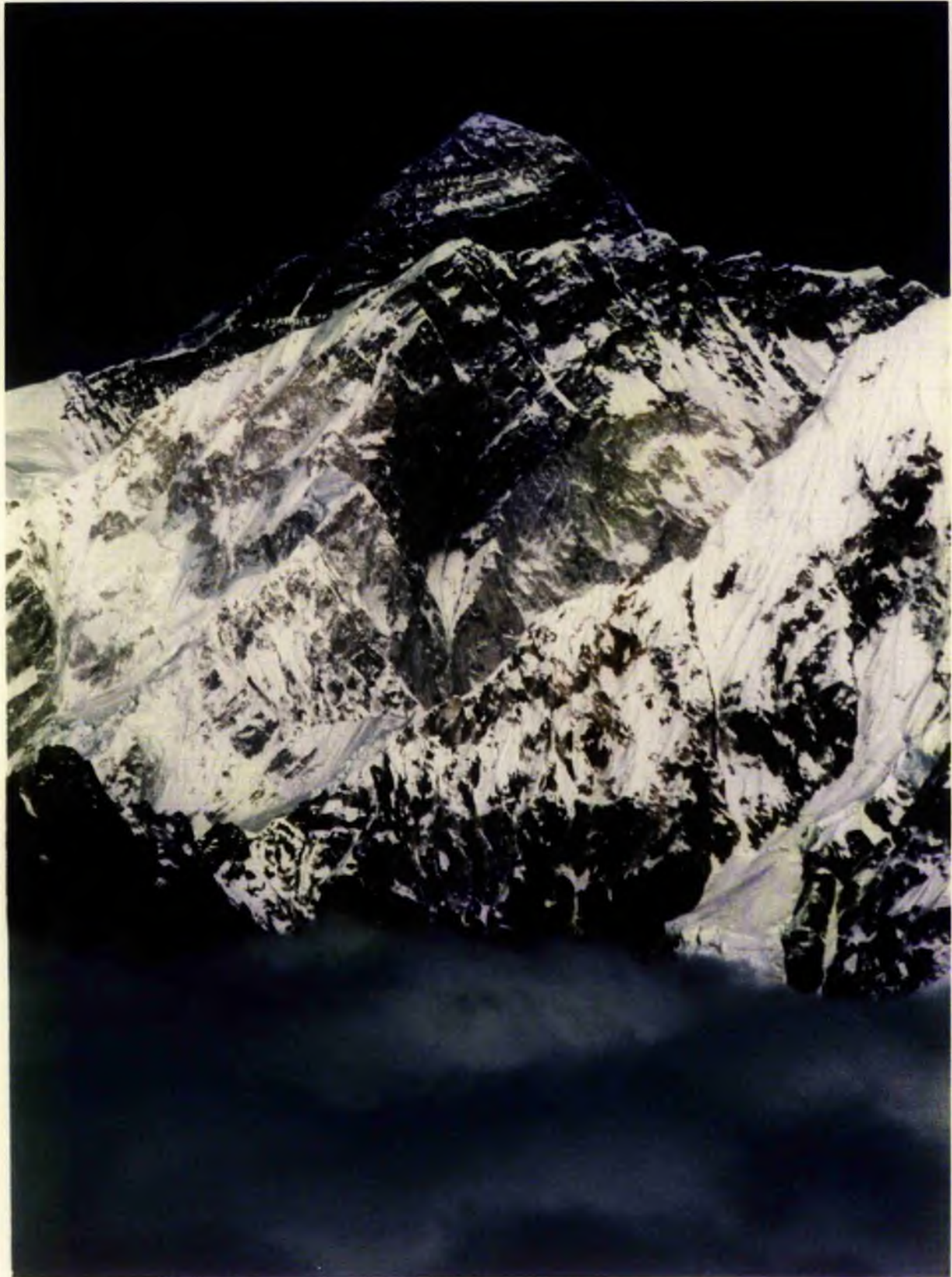
Approximately 0.1g of clean quartz grains are placed inside the vacuum train and degassed for 30 minutes at

110 °C. The sample is then heated to 450 °C and held there for 10 minutes while decrepitation takes place. The volatile phase is isolated in a liquid nitrogen trap (-196 °C). Any residual pressure represented non-condenseable gasses.

The fluid extraction line is linked to a Carlo-Erba gas chromatograph, fitted with a thermal conductivity detector. This is used to identify non-condensable gasses. Methane was detected on a 6' x 1/8" glass column packed with 80-100# Porapak Q, with a He flow of 25ml/min and isothermal oven temperature of 30 °C. The column was calibrated with standard gasses.

Volatile phases are then measured. On removal of the liquid nitrogen the pressure rises rapidly then stabilised after 30 seconds, remaining constant for 10 seconds. This value represents the CO₂ phase. Water is then released by rapid warming of the cold trap by hair drier to produce a transient maximum pressure.

The decrepitated grains are leached for 2 hours in deionised distilled water, at 80 °C, and acidified with 0.5ml 3M-HNO₃. The resulting solution was analysed for Na and K by atomic absorption spectrophotometry.



Frontispiece 3 - Chomolongma (8848m), with the Nuptse ridge in front (7879m), shows roughly 4km of Tibetan Slab succession. The N dipping limestones and slates of Chomolongma and Nuptse are intruded by tourmaline leucogranites (in the lower half of Nuptse), with an associated network of granitic veins.

CHAPTER 3

ISLE OF MAN

3.1 INTRODUCTION

The aims of this study were; 1. To map the low grade metamorphism of the Isle of Man (IOM). 2. To study the anchizone-epizone transition in the environment of a granite pluton. 3. To study illite crystallinity in a sub-epizone fault zone.

The lower Ordovician Manx Group of the IOM (Downie and Ford, 1966; Molyneux, 1979 and 1981) is well suited to a detailed study of anchizone-epizone metamorphism. This is because; 1. The island has been mapped in detail (Simpson, 1963). 2. The grade of metamorphism in the island ranges from chlorite, through biotite to garnet grade, and thus passes through the anchizone-epizone transition. 3. Lithologies are dominated by pelitic rocks. Even where the rocks are dominantly psammitic, pelitic sub-units can readily be found. Exposure is good enough to collect samples throughout the island, and geological knowledge is evolved enough to base a metamorphic interpretation. Previous attempts to interpret the metamorphism and structure of the IOM (Lamplugh, 1903; Gillott, 1955 and 1965a; Simpson, 1963a, 1964a and 1965a) have suffered from a lack of stratigraphical control, which, though still incomplete, is now better understood. The introduction of new XRD techniques to study low grade pelites has also benefitted this study.

3.2 GEOLOGICAL BACKGROUND

3.2.1 Previous Work

The first comprehensive geological survey of the Isle of Man was made by G. W. Lamplugh between 1892 and 1897. He interpreted the structure of the island as an inverted fan structure, effectively producing a synclinal structure with bedding dipping away from the core (Lamplugh, 1903). No further work was carried out on the Manx Group until that of Gillott (1955, 1956a and 1956b), who subdivided some of the units and noted the presence of slump breccias. The next major work was done by Simpson (1963a,b, 1964a,b and 1965a,b), and is discussed in section 3.2.4. Since Simpson's work stratigraphical refinements have been made by Downie and Ford (1966), and Molyneux (1979).

3.2.2 Stratigraphy

The Lower Palaeozoic Manx Group crops out throughout most of the IOM, though there are Pleistocene and Recent unconsolidated sediments in the North, Carboniferous limestones, sandstones and conglomerates in the South and West, and scattered intrusives of various ages (see Fig. 3.1). The succession is dominated by turbiditic mudstones with, to a lesser degree, siltstones, turbiditic sandstones, and minor andesitic and related volcanics.

A detailed succession has been produced by Simpson (1963) containing 11 formations totaling 8000m in thickness (see table 3.1). The oldest formation was the Lady Port Banded Group, and the youngest was the Glen Dhoo Flags. All



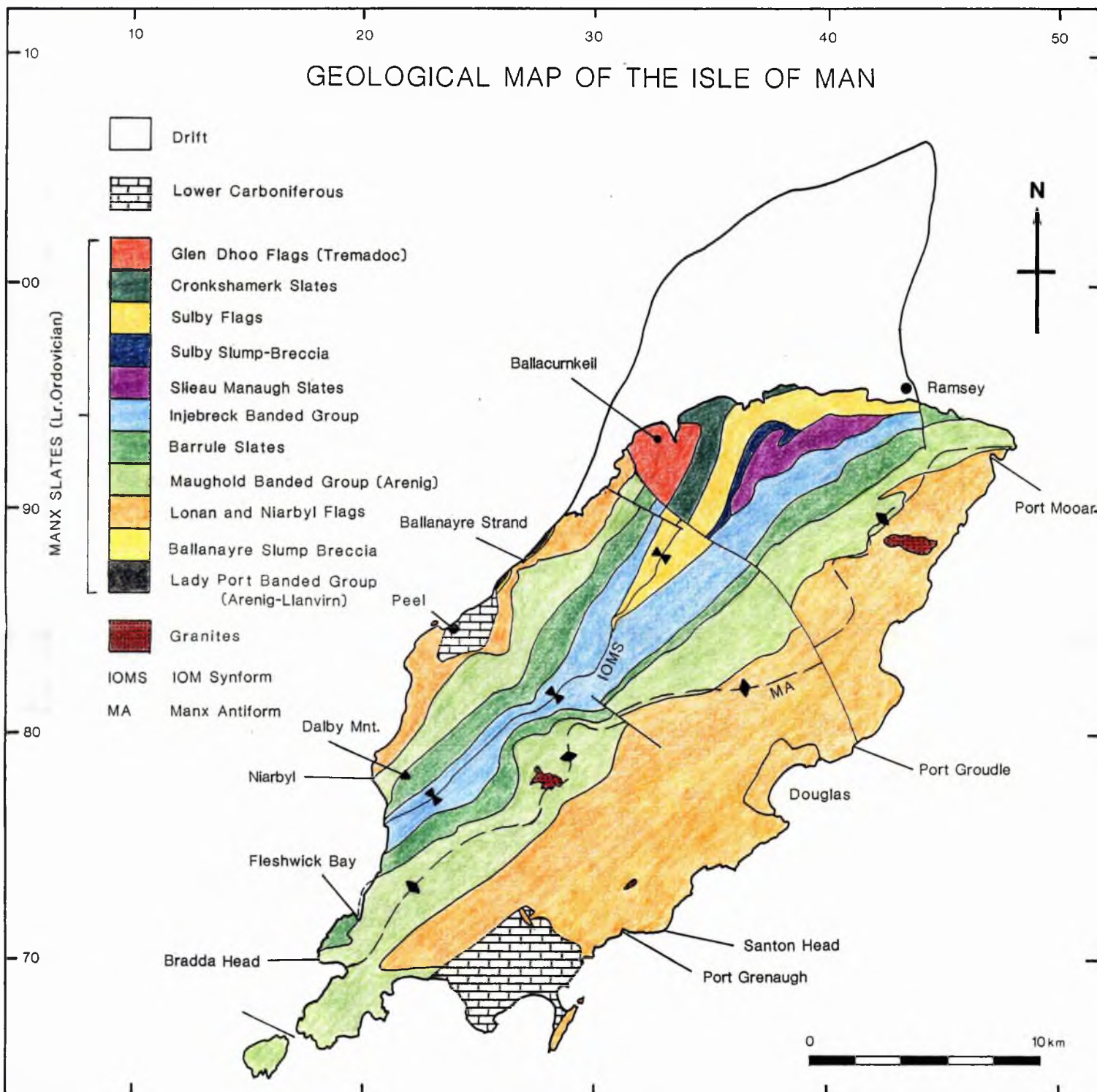


Fig. 3.1 - Geology of the Isle of Man after Simpson (1963a). IOMS and MA after this study.

were considered to be of Cambrian age in the absence of palaeontological constraints.

Table 3.1 - The Manx Group sucession after Simpson (1963a).

11	Glen Dhoo Flags	975m
10	Cronk Sumark Slate	460-560m
9	Sulby Flags	640m
8	Sulby Slump-Breccia	275-460m
7	Sileau Manaugh Slate	335m
6	Injebreck Banded Group	610-880m
5	Barrule Slate	160-925m
4	Maughold Banded Group	790-1830m
3	Lonan and Niarbyl Flags	600-3000m
2	Ballanayre Slump-Breccia	6-150m
1	Lady Port Banded Group	120m

3.2.3 Age Constraints

Acritarch faunas have been described from both the Lonan and Niarbyl Flags giving them an Arenig age (Downie and Ford, 1966), and a Tremadoc age (Molyneux, 1979) respectively. Further to this Molyneux was able to produce acritarch based Tremadoc ages for the Glen Dhoo Flags (making it one of the oldest units), Arenig ages for the Maughold Banded Group, and Arenig to Llanvirn ages for the Lady Port Banded Group (making the latter one of the youngest dated units). This indicates that the succession lies within the Lower Ordovician and that Simpson's original stratigraphy needs revision.

3.2.4 Previous Structural Interpretation

The most recent mapping done on the IOM was that of Simpson. He interpreted the structure and stratigraphy

(Simpson, 1963a), the metamorphism (Simpson, 1964a), and the granite intrusions (Simpson, 1965a).

The structural interpretation involved three phases of deformation. The Manx Group was folded around the D1 IOM Syncline, which trends NE-SW, with the youngest rocks in the core being the Glen Dhoo Flags. This was refolded by the low angle D2 Manx Synform with a similar trend. The whole structure has been subjected to weaker D3 folding with a NW-SE trend, and brittle faulting with the same trend.

Simpson's structural interpretation has been outdated by more recent age constraints. Rocks in the core of the IOM Syncline have been shown to be Tremadoc in age, whilst those in one limb are Arenig to Llanvirn in age (see section 3.2.3). This cannot match a simple synclinal structure. Therefore, whilst collecting samples for petrographic study, structural features were also mapped.

3.3 FIELDWORK

3.3.1 Sample Collecting

Fieldwork was undertaken on the IOM in order to provide the samples necessary for a metamorphic study, and also to provide a geological basis on which the metamorphism could be interpreted.

Samples were collected from the Manx Group on a rough grid with intervals between 0.5 and 2.5km, depending on the quality of exposure (see Appendix 3.1). Of the 158

samples collected, 141 were pelites, 8 were psammites, 4 were metabasites, 4 were vein quartz for fluid inclusion studies and one was from a lamprophyre dyke (see Appendix 3.2).

3.3.2 Data Collecting

While collecting samples field observations were made in an attempt to test Simpson's structural interpretation. It was observed that Simpson's F1 folds, including those from the type localities (Simpson, 1966), could be interpreted as slump folds. There was no S1 cleavage development in the cores of these folds. The F2 folds, with sub-horizontal axial planes, are the dominant fold phase, and have a strongly developed near horizontal cleavage.

An important fault zone at Niarbyl, in the west of the island, first described by Simpson (1963a), was mapped in detail during this study. The details of this are covered in the next section.

3.4 STRUCTURAL INTERPRETATION

3.4.1 Regional Structure

An outline of the main structural elements is presented in table 3.2, along with a summary of Simpson's interpretation.

Modification to Simpson's Interpretation

For the purposes of this study the interpretation of the regional structure has been modified from that of Simpson (1963a). The modifications and the reasons for them are as follows:

1. - Many of Simpson's F1 folds have been re-interpreted as slump folds. These include F1 folds, described at localities listed in Simpson (1966). Folds were complex but lacked axial planar cleavage (see plate 3.1). In addition, folds were confined to bedding planes without disrupting finely laminated beds above (or below) the folds (see plate 3.2).

2. - The IOM Syncline and Manx Synform have been re-interpreted and re-named the IOM Synform and Manx Antiform, and both attributed to D1 deformation. This is because: 1. Recent ages for some of the sedimentary units make Simpson's structural interpretation untenable (see section 3.2.4).; 2. Younging evidence also conflicts with Simpson's structural interpretation, particularly with the nature of the IOM 'Syncline'. At Niarbyl the rocks young to the NW. Between Port Grenaugh and Santon Head they young to the SE.; 3. There is no field evidence apparent to the writer that the Manx Antiform refolds the IOM Synform. In

Table 3.2 - Comparative structural histories: Simpson (1963a) and regional geology (this study).

SIMPSON	REGIONAL
<u>S0</u> - Turbiditic sediments including slump-breccias and "Greenstone dykes" (near concordant sills).	<u>S0</u> - As for Simpson, but slump-breccia made up of rip up clasts. Slump folds are present.
<u>D1</u> - Major structures = IOM Syncline, NE/SW trend (Caledonian). Steep axial planar cleavage dips to NW or SE. Folds are tight to isoclinal.	<u>D1</u> - Pre or syn-F1 quartz veining showing sinistral boudinaging. Major structures = IOM Synform and Manx Antiform (associated with Simpson's F2 folds. Minor folds show a NE/SW trend, shallow to steep axial planar dips to NW or SE. Pervasive cleavage may be domainal.
<u>Post-D1 to Syn-D2 granite intrusions.</u>	
<u>D2</u> - Major structures = Manx Synform. Axial planes dip gently to the NW, folds are tight to open with a NE/SW trend. Spaced cleavage (pervasive at times). Syn-F2 quartz veins in fold hinges. <u>Syn-D2</u> - granite intrusions.	<u>D2</u> - Axial planes dip at low angles to the SE or NW and plunge gently to the E or W. Folds tight to open. Syn-F2 quartz veins in fold hinges.
<u>D3</u> - Open folds, N to NW trend, axial planes dip steeply to E. Syn-F3 quartz veins	<u>D3</u> - Open folds, shallow plunge to the NNW, axial planes near vertical with E/W dip.
<u>D4</u> - Post-F3 quartz veins in tension gashes. <u>Pre-Carboniferous</u> NW-NNW trending transcurrent faults	Transcurrent sinistral faults Quartz and dolomite veins Quartz filled tension gashes. Kink bands.
<u>Post-Carboniferous</u> NW to NE trending normal faults with steep dips.	<u>Post-Carboniferous</u> normal faults. Quartz and dolomite brecciation.



Plate 3.1 - Re-folded slump fold in the Maughold Banded Group (GR 195 693) with a sub-horizontal S1 cleavage. The slump fold shows no axial planar cleavage.



Plate 3.2 - Slump fold in the Maughold Banded Group (GR 188 690) confined to the bedding plane. The slump fold has no axial planar cleavage, but is cross-cut by a pervasive S1 cleavage dipping at c.20° and a S2 cleavage dipping at c.70°.

Simpson's cross-section refolding has been inferred to accommodate his structural interpretation. 4. There are no clear lithological correlations across the IOM Synform. This is because of the poor inland exposure and the possibility of lateral facies changes. In addition, the Lonan and Niarbyl Flags vary from slates to coarse sandstones in the eastern outcrop, but are relatively uniform in the western outcrop. This makes correlation across the island tentative.

3. - The granite intrusions have been re-interpreted as post-D1 to syn-D2. Hornfelsic porphyroblasts mostly cross-cut the S1 foliation, but are deformed by the S2 foliation, though, according to Simpson (1964a, b) some also cut the S2 foliation.

These modifications have been made with the understanding that detailed lithostratigraphical mapping of the IOM is required before a proper structural interpretation can be made.

Regional Structure

So - The turbiditic metasediments that make up the Manx Group are dominated by slates (see plate 3.2), often with original bedding easily recogniseable due to colour variation. These slates make up the bulk of formations, 1,2,4,5,6,7,8 and 10 (table 3.1), which include slump-breccia units. The slump-breccias are composed of rip-up shale and siltstone clasts (plate 3.3), and are more extensive than Simpson documented (eg Fleshwick Bay, GR. 201 715). Also common are the siltstones and sandstones of



Plate 3.3 - Slump breccia in the Barrule Slates (GR 200 716) with rip-up clasts of shale and siltstone.



Plate 3.4 - Coarse graded greywacke in the Lonan Flags (GR 327 703) showing matrix supported grains and a normal younging direction.

the flaggy units 3, 9 and 11. The sandstones are coarse in localised areas (between Port Grenaugh and Santon Head on the SE coast, see plate 3.4). Throughout the succession slump folding is a common occurrence. "Greenstone dykes" (Lamplugh, 1903) occur either as concordant sills or mildly discordant dykes within the sedimentary succession. They have been subjected to the metamorphism and all the phases of deformation.

D1 - The first phase of regional deformation is also associated with the strongest cleavage development which, though pervasive, sometimes fractures to give a spaced appearance within slaty units. F1 folds are tight to isoclinal with a Caledonian NE-SW trend, and shallow to steep axial planes dipping to the NW. The folds plunge at a shallow angle to the NE or SW (see plate 3.5). The IOM Synform and Manx Antiform form a major fold pair apparently running the length of the island, though this relationship will not be confirmed until the stratigraphy of the island has been re-interpreted.

Associated with the folding are syn-tectonic quartz veins, which often concentrate on fold hinges in planes concordant to bedding or S1, as well as discordant masses. Bedding parallel quartz veins are often boudinaged, due to slip on the bedding surfaces during tightening of the F1 folds (see plate 3.6).

The intrusion of the Foxdale and Dhoon granites occurred post-D1 to syn-D2.



Plate 3.5 - Large F1 fold in the Niarbyl Flags (GR 227 805) with the axial planar cleavage dipping at 36° to the NW. Boudinaging can be seen in the upper limb and cleavage refraction in the lower limb. F2 and F3 folds cross-cut F1 on the right hand side of the picture.



Plate 3.6 - Boudinaged quartz vein in the Maughold Banded Group (GR 203 715). The quartz vein is syn- or post-D1.

D2 - The second phase of folding is characterised by open to tight folds gently plunging to the E or W, and with a low angle axial planar dip to the SE or NW. The cleavage is often weak, being mainly confined to fold hinges (see plate 3.7), and crenulates the earlier cleavage. Associated quartz veining is mainly confined to fold hinges. There are also post-F2 quartz and dolomite veins.

D3 - F3 folds are a set of open undulations with steep N/S striking axial planes, and low angle plunges to the N.

Subsequent to D3 further minor deformation took the form of D4 kink bands, with steep N/S trending axial planes and associated tension gashes. Tension gashes are sometimes filled with quartz. Transcurrent faults formed (mainly sinistral), associated with quartz and dolomite veining. This is all post-dated by post-Carboniferous normal faulting (Simpson, 1963a), with associated quartz and dolomite veining, and brecciation.

3.4.2 The Niarbyl Fault Zone (NFZ)

A fault structure was first observed at Niarbyl by Simpson (1963a). He interpreted it as a slide, formed during F1 folding as a vertical dislocation, and subsequently re-orientated, by the later F2 Manx synform, so that it dips steeply to the NNW.

A more detailed interpretation of the NFZ is presented here. Fig. 3.2 is a structural map of the area, Figs 3.2 A, B, C are enlargements of sub-areas within the



Plate 3.7 - This F2 fold in the Barrule Slates (GR 200 717) folds the S1 cleavage and has developed a S2 cleavage which is best developed in the fold hinge.



Plate 3.8 - Phyllonites of the Niarbyl Fault Zone (GR 212 777) have been disrupted by the later brittle thrusting of the Niarbyl Flags (towards the camera) on the Niarbyl Thrust (T).

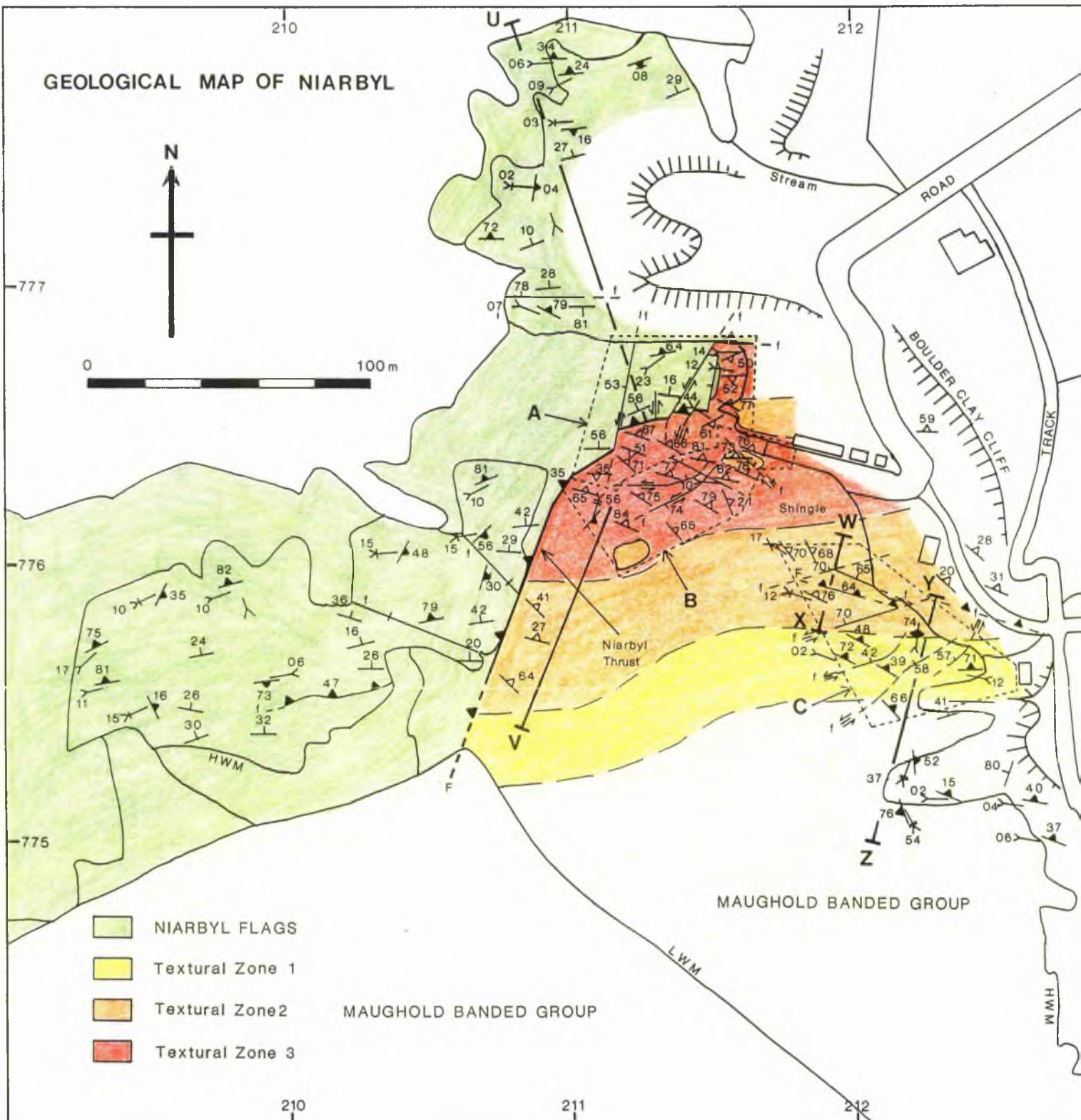


Fig. 3.2 - Structural map of the Niarbyl Fault Zone.

LEGEND

	Bedding		Vertical Bedding
			S ₁ S ₂ Staty Cleavage
	Axial Plane Plunge of Fold Hinge.		F ₁ Folding
	"		F ₂ Folding
	"		F ₃ Folding
	Late Kink Bands		Exposed
	Vertical		Unexposed
	"		Exposed
	Thrust Fault		Unexposed
● 195	Mica Crystallinity Value Measured in H _b _{rel}		Thrust Related Folding
			Younging Direction

Legend to Figs 3.2, 3.2A, B and C, and 3.7.

67

Fig. 3.2A

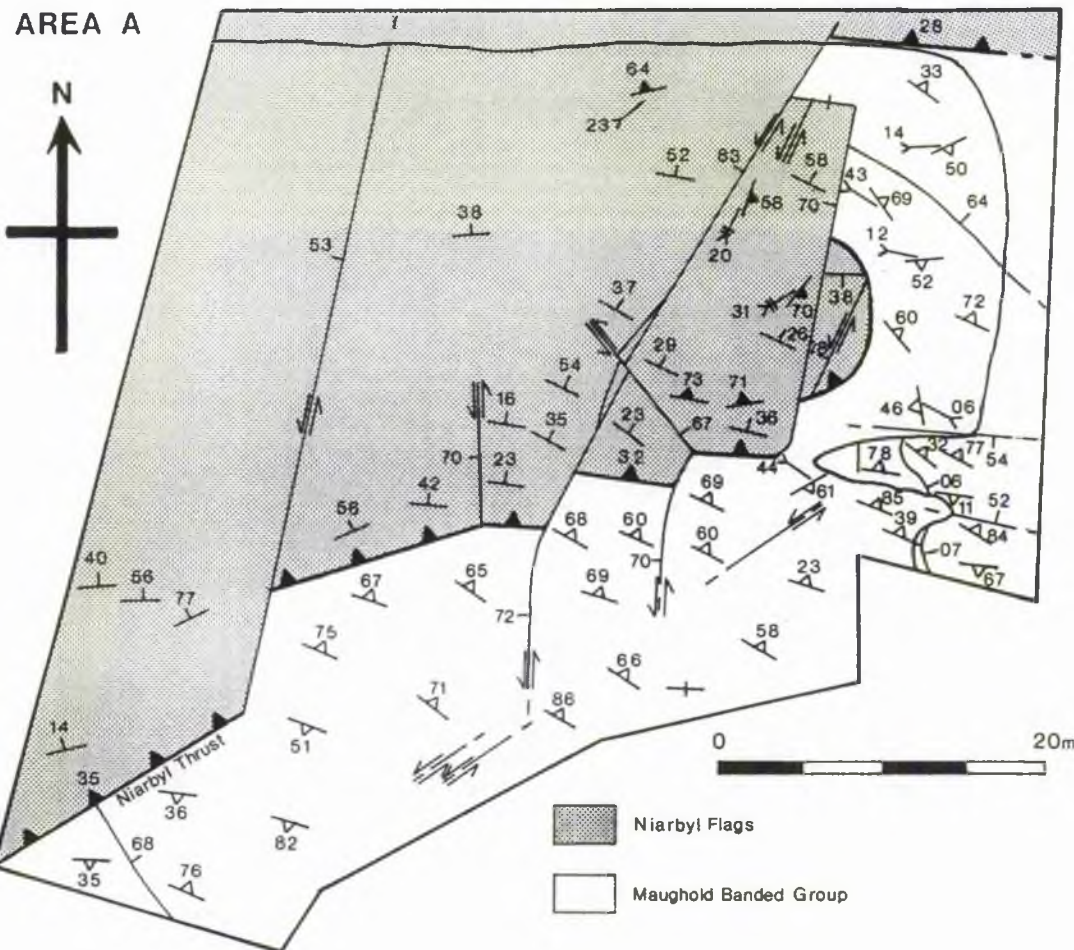
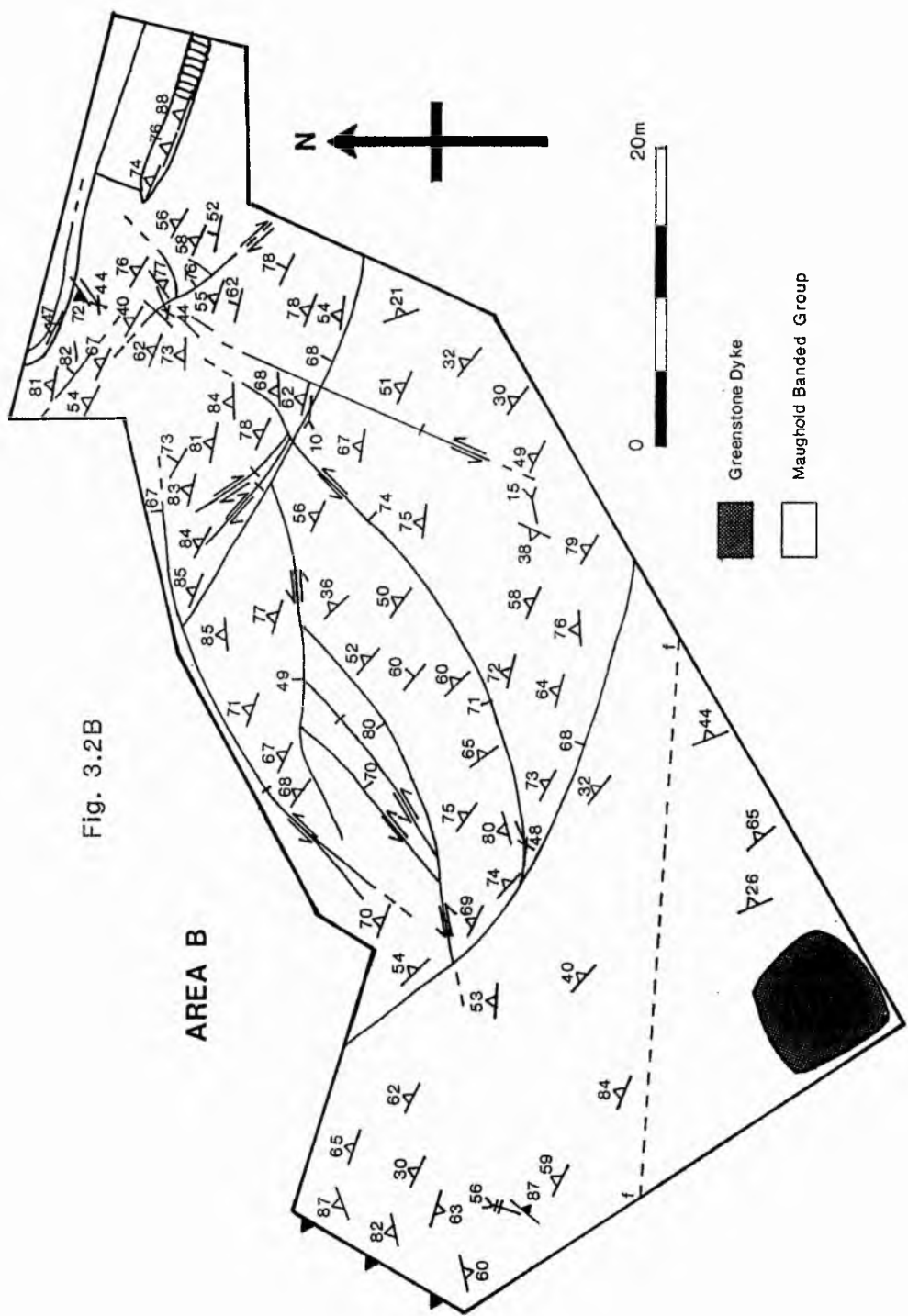


Fig. 3.2A, B, C - Enlargements of sub-areas within the Niarbyl Fault Zone see Fig. 3.2 for locations of sub-areas.

Fig. 3.2B



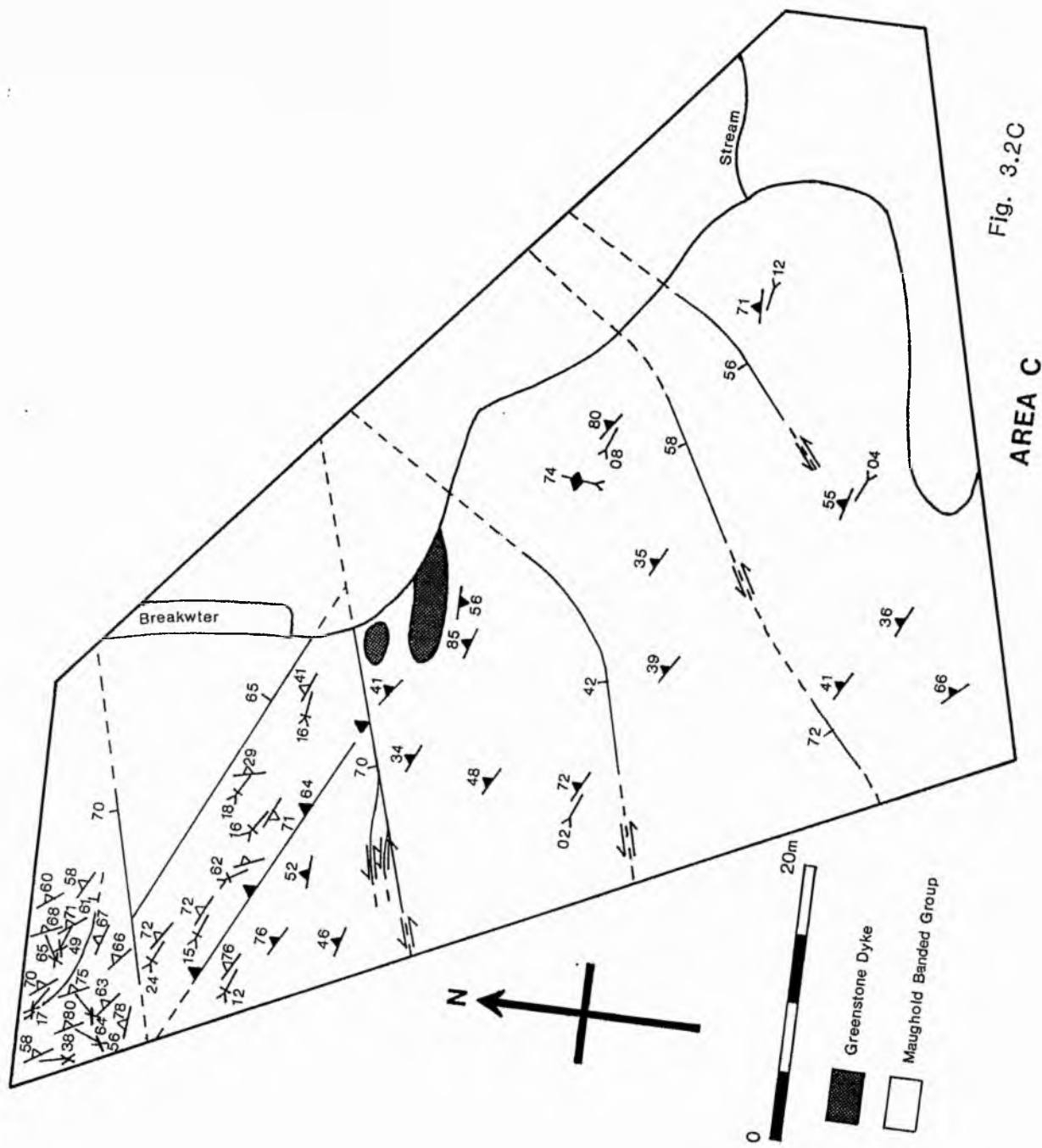


Fig. 3.2C

AREA C

fault zone and Fig. 3.3 is a set of cross sections across the fault zone.

The Niarbyl Thrust marks the boundary between the Niarbyl Flags and the Maughold Banded Group at Niarbyl Point. The obvious fault plane dips to the NW at 32 to 35°, and truncates an earlier mylonitic fault fabric, which relates to the main faulting at Niarbyl. The sequence of fault structures is as follows.

3.4.3 Sinistral Transcurrent (Transpressive) Faulting

A 100m wide belt of intensely sheared pelites formed in a WNW/ESE trend. This belt post-dates the main D1 deformation, and represents a zone of sinistral transcurrent movement (see section 3.4.8). The rocks involved were originally pelites, but have been cataastically comminuted to produce phyllonites (Higgins, 1971; Anderson and Oliver, 1986). The foliation terminates abruptly at a brittle fault, against the Niarbyl Flags (see below and plate 3.8). This indicates their subsequent tectonic contact, and also that the belt could extend further under the flags.

The history of movement along the shear zone could have been prolonged, and this is reflected by the presence of folding of the foliation, with movement at a low angle to the fault foliation (see plates 3.9 and 3.10), as well as later Reidel fractures (see plate 3.11) (Ghisetti, 1987) and extensional sinistral duplexes (see Fig. 3.2B) (Swanson, 1988).

71

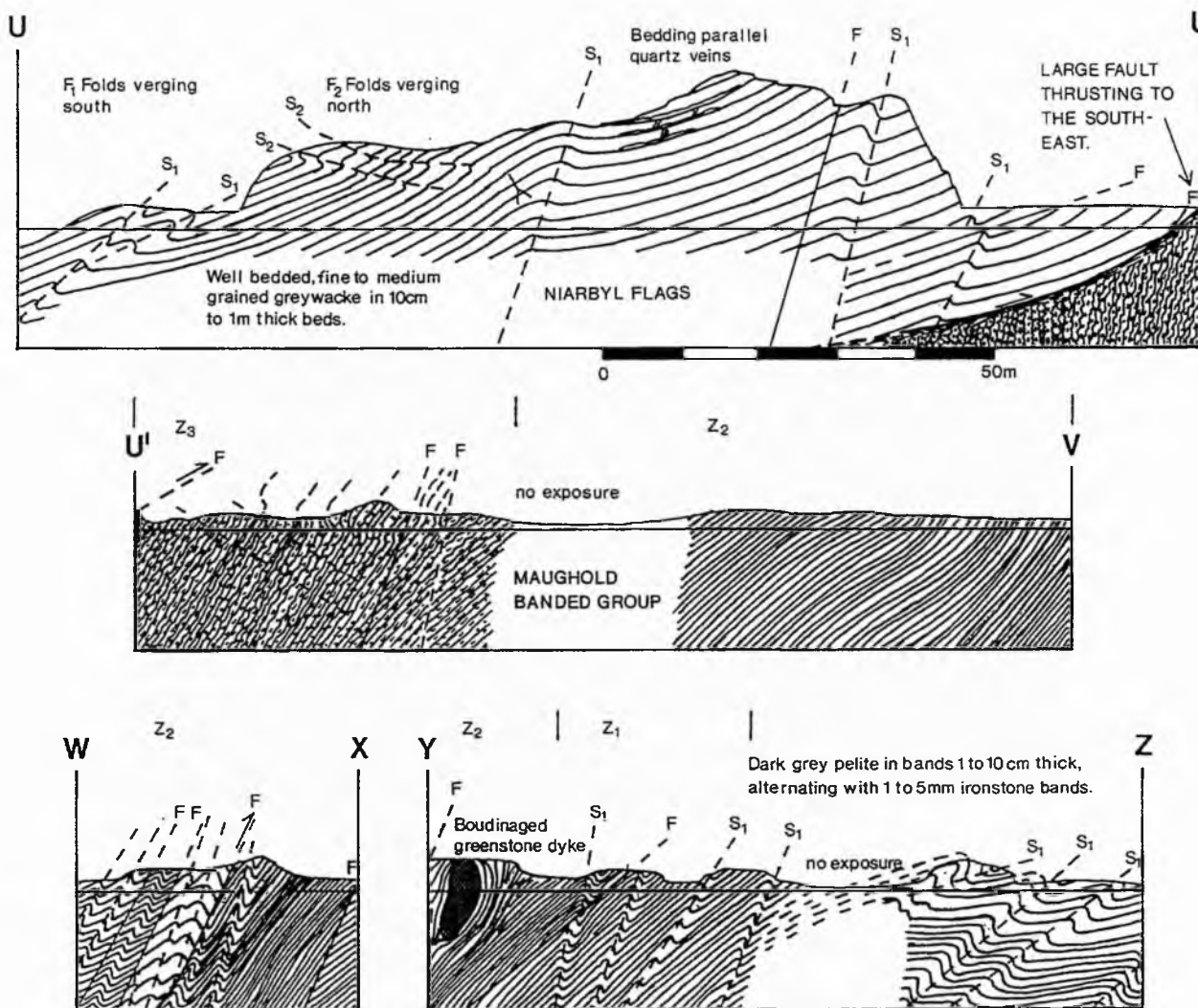


Fig. 3.3 - Cross-sections through the Niarbyl Fault Zone. See Fig. 3.2 for locations of cross-sections.



Plate 3.9 - Textural zone 3 phyllonites of the Niarbyl Fault Zone, containing abundant quartz segregations, have been folded by folds showing sinistral rotation.



Plate 3.10 - In this hand specimen of textural zone 3 phyllonite quartz segregations show sinistral macroscopic folding (F) and the development of stylolitic impingement points (St).



Plate 3.11 - Sinistral Riedel shears (R) cross-cut the phyllonitic fabric (textural zone 3) of the Niarbyl Fault Zone.



Plate 3.12 - Textural zone 3 phyllonites of the Niarbyl Fault Zone showing crumpling of the dominant foliation.

3.4.4 Brittle Thrusting

As previously mentioned, the main shear zone is truncated by a brittle thrust fault (the Niarbyl Thrust) that marks the boundary between the Niarbyl Flags and Maughold Banded Group. This thrust dips at between 32 and 35 to the NW. Before the initiation of thrusting, the shear zone was crumpled on a macroscopic scale (see plate 3.12 and Fig. 3.3).

3.4.5 Late Features

Subsequent to the transcurrent and thrust faulting, activity was limited to late (D3 onwards) regional deformation, though there is a local high concentration of transcurrent faults dissecting the earlier faulting. Again the sense of movement is dominantly sinistral (see Fig. 3.2A and section 3.4.8).

3.4.6 Thrust or Lag?

In interpreting the brittle thrust fault as a thrust the evidence is partly circumstantial. There is a lack of mylonitic fabrics at the fault contact that can be examined because of its brittle nature. Evidence favouring thrusting is the following;

1. The secondary fault associated foliation crumples the earlier shear fabric indicating a compressional environment in the same orientation as for thrusting.
2. Bedding cross-sections can be balanced on a local scale for minor thrusts.

3. The regional fold vergence, to the SE, accommodates a thrust mechanism.

From this, and lack of any evidence for a lag fault, a thrust interpretation has been made.

3.4.7 Textural Zones

An attempt was made to classify the intensity of the fault fabric by textural zones (Anderson and Oliver, 1986). Three zones were distinguished (Fig. 3.4), representing increasing levels of disruption due to shear movement. These zones are confined to the Maughold Banded Group, and therefore disrupt banded slates with occasional semi-pelitic units and greenstone dykes. The banded slate, in its least disturbed form, has numerous cycles of 1 to 10cm thickness, including thin (5mm) ironstone bands, of some lateral persistence, which are repeated throughout the succession (see plate 3.13). Cycles consist of a thin ironstone band followed by dark slate which gradually lightens upwards towards the next ironstone band. This appears to be a way up indicator. The three zones are as follows:

Textural Zone 1 - Zone 1 is the least affected by fault movement (see plate 3.14). Bedding is easily recognisable, but disrupted by numerous brittle C-planes (Lister and Snoise, 1984). The more competent ironstone bands fracture into rhomb shaped lithons of various length, and on a smaller scale, lenses, indicating extension roughly parallel to bedding, with a dominance of sinistral

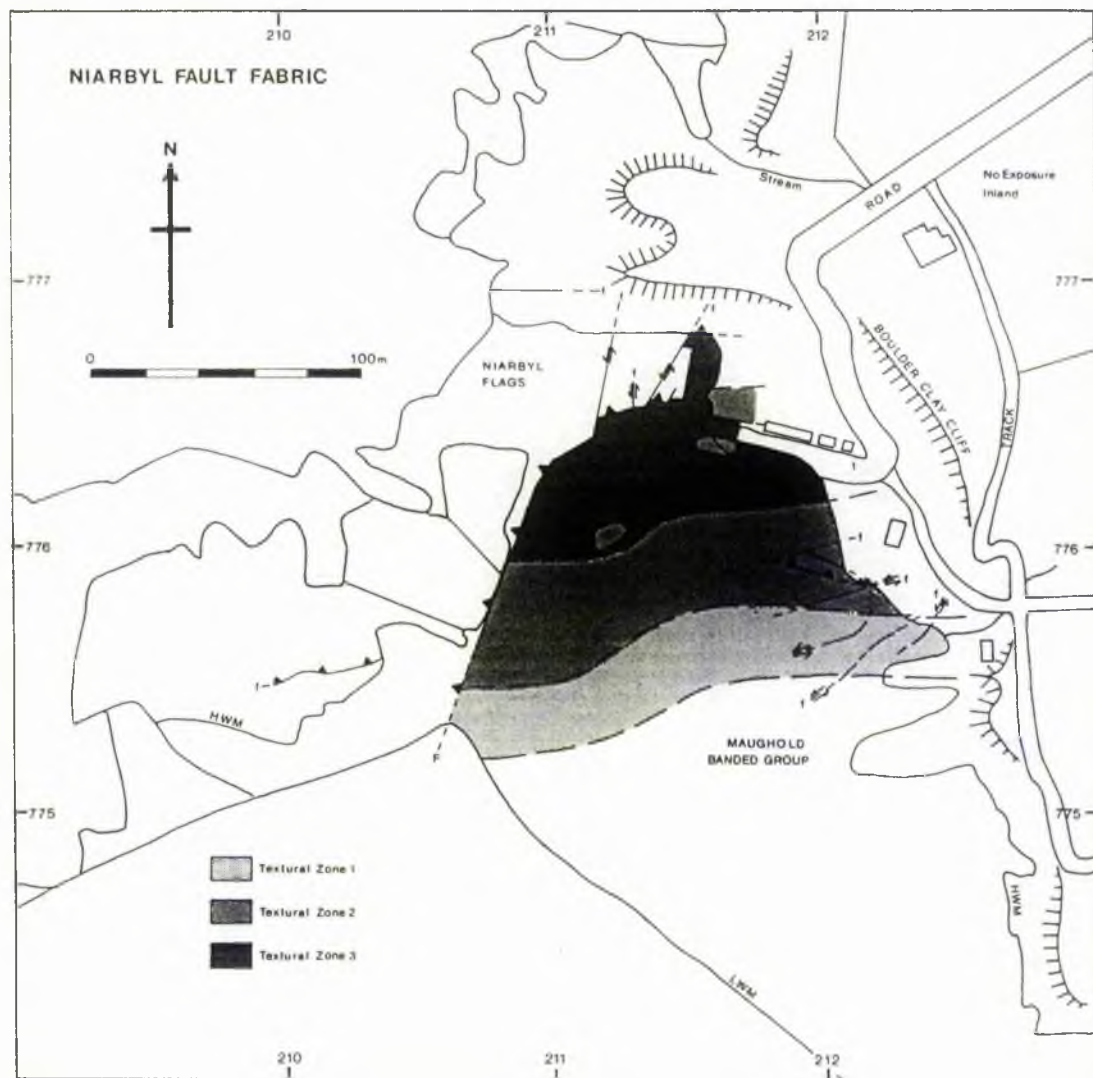


Fig. 3.4 - Textural zones indicating the intensity of shearing in the Niarbyl Fault Zone.



Plate 3.13 - Maughold Banded Group slates (GR 213 776) in a relatively undisturbed form. The slate has numerous cycles of 1 to 10cm thickness, with regularly occurring laterally persistent ironstone bands.



Plate 3.14 - Maughold Banded Group slates (textural zone 1) showing disrupted bedding folded by F4 kink bands.

shearing. At 90° to the fault fabric (a vertical plane running roughly N/S) the rock is crumpled by F2 folding.

In thin section S and C surfaces lie at about 5° to each other. Movement is illustrated by the offsetting of minor quartz veins along dark pressure solution seams. Fine arenaceous laminae are dismembered into trails of lenses, the margins of which have suffered grain reduction (see plate 3.15).

Textural Zone 2 - In zone 2 bedding is harder to recognise within the banded slate (see plates 3.16 and 3.17). C surfaces are more common, making the rock break along less predictable surfaces. These surfaces tend to concentrate opaques, and offset quartz veins. Greenstone dykes are boudinaged into isolated pods up to three meters in length, with the fault fabric flowing around them. Within this zone folded units occur. These show more obvious continuity of bedding, which is folded by steeply plunging chevron folds relating to the earliest folding of the fault foliation. Quartz segregations occur before folding, and minor veining after folding. Both are disrupted by shearing.

In thin section the rock is similar to that of textural zone 1. The exceptions are that C planes are more common and often near parallel to S1, and bedding is not so easily distinguished.

Textural Zone 3 - The rocks in this zone vary in appearance reflecting both compositional differences and intensity of shearing. Some rocks are characterised by

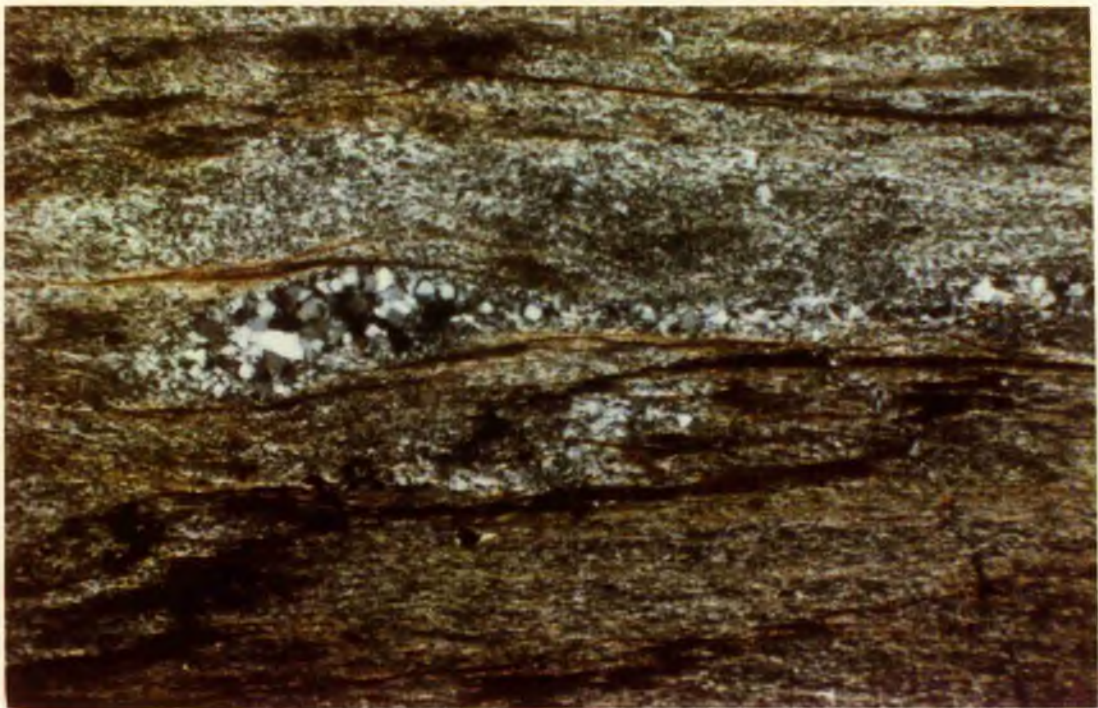


Plate 3.15 - Thin section N8 shows grain reduction in a dismembered quartz vein in textural zone 1 slates (field of view = 1.0mm).



Plate 3.16 - View towards the Niarbyl Flags from textural zone 2 slates. Exposures of textural zone 3 rocks, of the Niarbyl Fault Zone, run from the cottage to the left hand rocks in the middle distance.



Plate 3.17 - Textural zone 2 slates showing disruption of the bedding and the development of quartz segregations and veins.



Plate 3.18 - Textural zone 3 mica rich phyllonite with abundant quartz segregation pods.

abundant discontinuous and tightly folded quartz segregations comprising 20 to 50% of the whole rock. In places quartz segregations are isoclinally folded with stylolitic impingement points (see plate 3.10). The segregations have an average thickness of 5mm, ranging from 1 to 10mm, and are embedded in intensely foliated, micaceous grey-black phyllonite, as observed by Anderson and Oliver (1986). The fabric is cross-cut by Riedel fractures (Ghisetti, 1987). In more micaceous rocks the quartz segregations represent about 20% of the whole rock, and are in the form of well rounded pods from 1 to 10mm in size, embedded in a fine foliated micaceous matrix (see plate 3.18). In all cases the fabric is crumpled by the secondary fault-associated foliation (see plate 3.12). Greenstone dykes occur as large competent boudins with a uniform strongly developed foliation.

In zone 3 thin sections (see plates 3.19 and 3.20), quartz dominates, with fine muscovite, opaques, epidote and calcite also being common. Grain size reduction occurs throughout, the mica forming a felted fabric, while the groundmass quartz forms a fine granular texture. Quartz segregation pods and veins are composed of aggregates of quartz grains, showing undulose extinction and sutured margins. These subgrains are sometimes elongate at a low angle to the long axes of the pods. Quartz segregation veins are disrupted by pull-apart zones and Riedel fractures. C surfaces, rich in opaque material and muscovite, anastamose around quartz segregations and fine grained quartz rich microlithons (Hobbs et al., 1976),

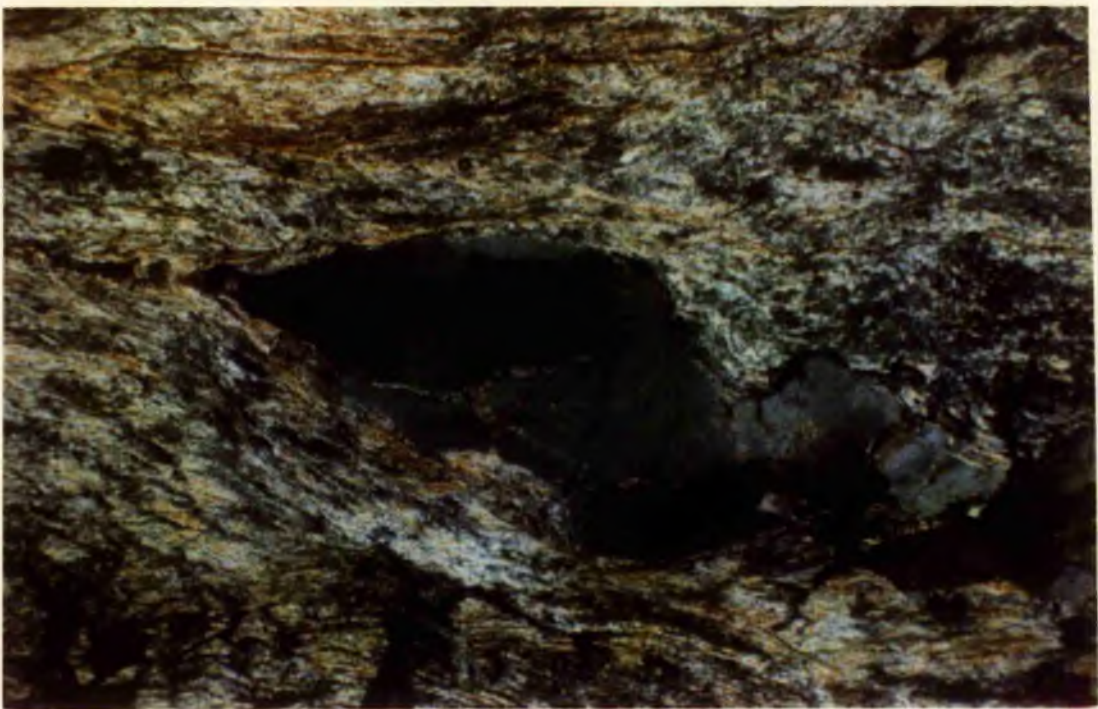


Plate 3.19 - In this field of view of N4, a textural zone 3 phyllonite, a strained monocrystalline quartz porphyroblast indicates sinistral shear sense (field of view = 2.5mm).

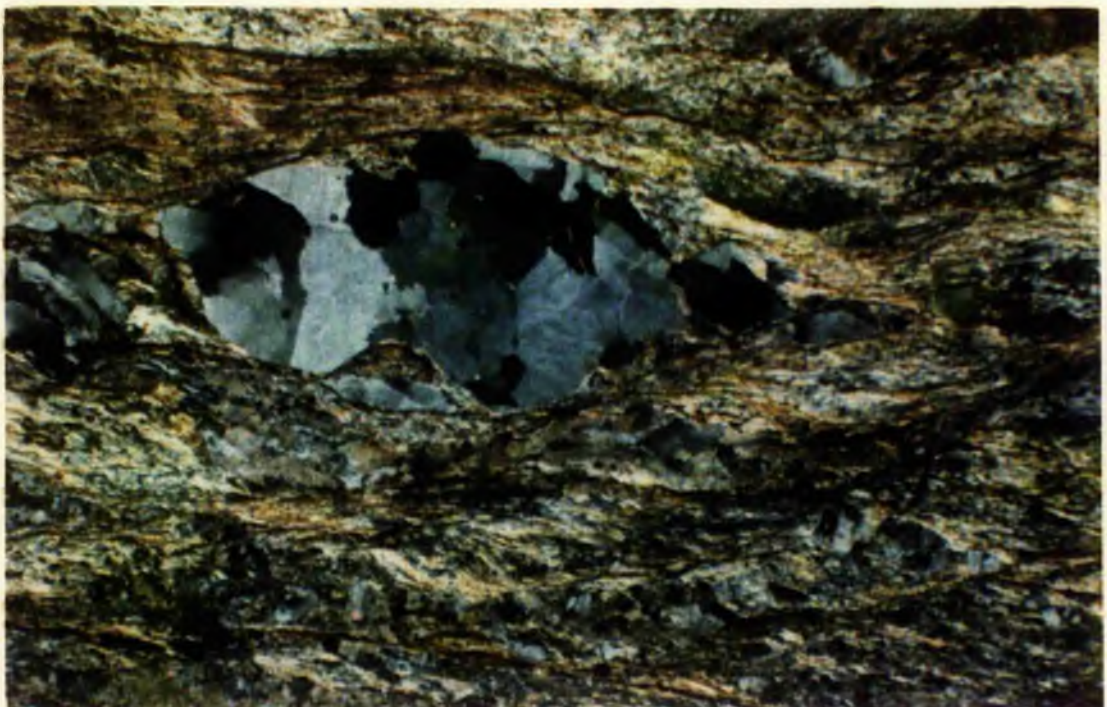


Plate 3.20 - This is an example of a strained polycrystalline quartz porphyroblast showing sinistral shear sense in N4 (field of view = 2.5mm).

which display S surfaces. Both sinistral and dextral movement can be seen in thin section (see section 3.4.8).

It should be noted that the intensity of shearing increases to the north towards the Niarbyl Flags, where it is abruptly truncated by the thrust fault contact. What happens to the shear zone inland is unknown, due to the total lack of exposure in the first kilometre from the coast, and poor exposure elsewhere inland.

3.4.8 Shear Sense Indicators

A qualitative assessment of the overall sense of movement on the Niarbyl Fault Zone was made using a number of parameters observed at the outcrop, in hand specimen and in thin section. These include S-C mylonites (Lister and Snoke, 1984), asymmetrical quartz, feldspar and lithic porphyroclasts (Simpson and Schmid, 1983), transcurrent faulting, and Riedel fractures in conjunction with S-C mylonites (Ghisetti, 1987). The parameters give both sinistral and dextral senses of movement, though the sinistral component dominates throughout the history of shear movement on the fault (of the 81 indicators that gave a clear sense of direction, 83% gave sinistral and 17% gave dextral movement).

3.4.9 Structural Summary

1. Regional Deformation - A distal turbiditic sequence formed during the Lower Ordovician. Most sediments were fine grained shales, mudstones and siltstones, though sandstones were not uncommon, particularly in the east of the island. Slump breccias and slump folds are present in a

number of places. The sequence was intruded by "Greenstone Dykes", probably during consolidation. Regional D1 deformation resulted in the development of pervasive cleavage and folds with a Caledonian strike. Fold plunges are at a shallow angle and cleavage tends to dip at a low angle to the NW or SE. Quartz veining occurred during D1. D2 is characterised by a weak cleavage dipping to the SE or NW, low angle plunges to the E or W and quartz veining. The Caledonian granites of the IOM were intruded pre- to syn-D2. More quartz, and dolomite veining occurred between D2 and D3. D3 resulted in open folds plunging steeply to the N or S. Later minor D4 deformation resulted in kink bands, tension gashes, brittle transcurrent and normal faults, and yet more quartz and dolomite veining with associated brecciation.

2. Niarbyl Fault Zone - As well as structures characteristic of regional deformation, the Niarbyl Fault Zone shows more localised structures. These include a 100m wide WNW trending zone of steeply dipping phyllonites showing variable degrees of shearing and lying within the Maughold Banded Group. This mylonitic fault fabric has been folded, firstly by folds complimentary to the sinistral shear movement of the fault, and then later crumpled by folds relating to the initiation of thrusting of the Niarbyl Flags over the Maughold Banded Group from the NW. Subsequent to thrusting the fault zone was dissected by a high concentration of sinistral transcurrent faults. Movement in the Niarbyl Fault Zone appears to have started

just after D1. There is no clear evidence for the timing of the later brittle thrust, relative to the D2 deformation.

3.5 PETROGRAPHY

3.5.1 Introduction

Forty six thin sections were prepared representing a broad coverage of the lithologies found within the Manx Group on the IOM. Localities are given Appendix 3.1 together with a sample map. These were examined to determine mineral occurrence and origin. The minerals could be either detrital, be due to contact metamorphism, have formed at various stages of regional metamorphism, or as the result of weathering.

3.5.2 Thin Section Analysis

The most common rocks of the Manx Group are the pelitic rocks. Variations in the proportions of metamorphic minerals can be seen within individual thin sections. This is due to the common occurrence of compositional banding in the form of sedimentary banding, slumping and rip-up clasts.

The fine mineralogy of the matrix is dominated by white mica (mainly muscovite), with common quartz, chlorite and opaques. Micas are strongly orientated by the strong S1 cleavage, usually close to bedding. In one thin section (M45) a chert band is present, partly disrupted by movement on the cleavage surfaces. S1 is commonly crenulated by a weaker S2 cleavage.

Calciferous or siliceous concretions, and porphyroblasts commonly occur. The latter include chlorite, muscovite and chlorite-muscovite pods, biotite, and opaques such as pyrite and ilmenite. Chlorite, muscovite and

chlorite-muscovite pods (see plate 3.21) range in size from 0.1 to 0.5mm and appear to have formed subsequent to lithification during anchizone to lowest greenschist facies metamorphism (Roy, 1978; Craig et al., 1982; Woodland, 1984). These pods represent areas of low strain, and if they occur commonly enough, they result in the development of domainal cleavage. They are characterised by having their (001) basal planes at a high angle to the cleavage folia. Their dimensions normal to (001) may equal or exceed the dimension parallel to (001). Woodland also observed siliceous concretions forming at the same time as the pods and refracting the cleavage around them. These concretions are usually composed of a polycrystalline mosaic of coarse grains with much finer grains at the margins. Some of the porphyroblastic opaques are disrupted by the primary cleavage foliation showing that they grew before or during S1 cleavage development. Porphyroblasts of platy ilmenite grow across the S1 foliation (see plate 3.22), and also the S2 crenulation cleavage in some slides. This growth occurred from the post-S1 until the post-S2 static interval. This tends to agree with Simpsons (1964a) interpretation. In places ilmenite has been replaced by leucoxene (Simpson, 1964a). Biotite crystals were found in one thin section, M55 from c. 500m to the south of the Foxdale granite (see plate 3.23). These appear to be post-D1, syn-D2 having suffered some D2 deformation. In more extensive studies both Gillott (1955) and Simpson (1964a, Fig. 3) found further porphyroblasts of garnet, muscovite, staurolite, chloritoid and cordierite. These lay in a zone

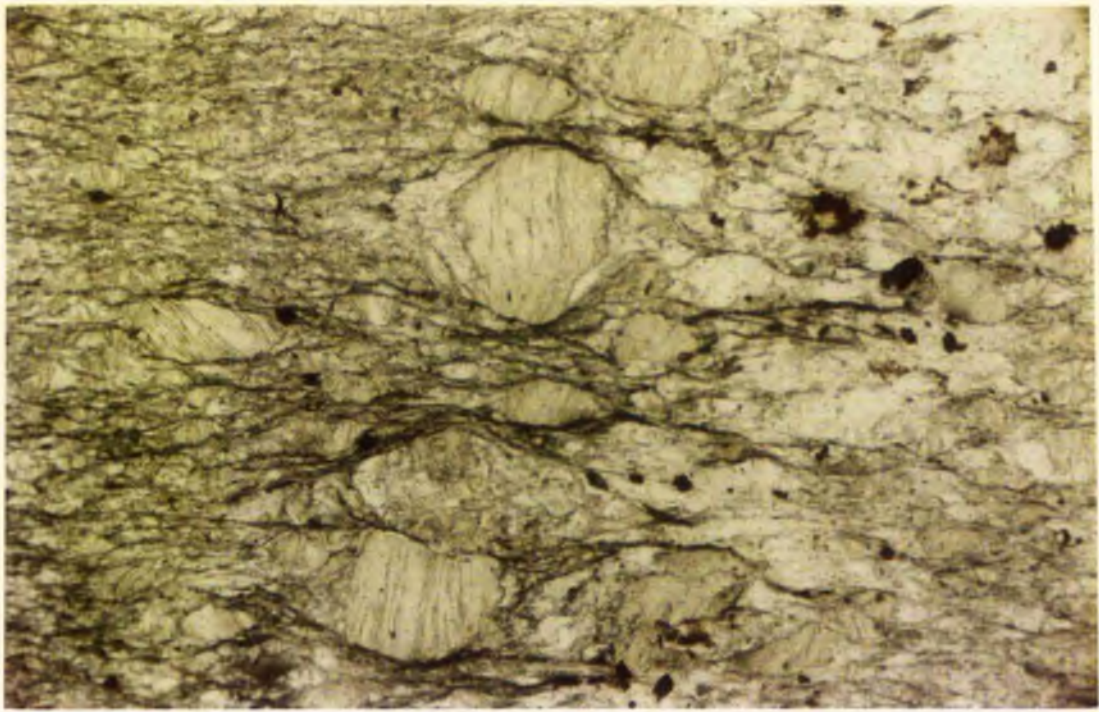


Plate 3.21 - M34 contains pre- to syn-D1 chlorite pods with cleavage at a high angle to the S1 foliation (field of view = 1.0mm).



Plate 3.22 - M23 contains small porphyroblasts of platy ilmenite which cross-cut the S1 foliation, but are crenulated by the S2 foliation (field of view = 1.0mm).

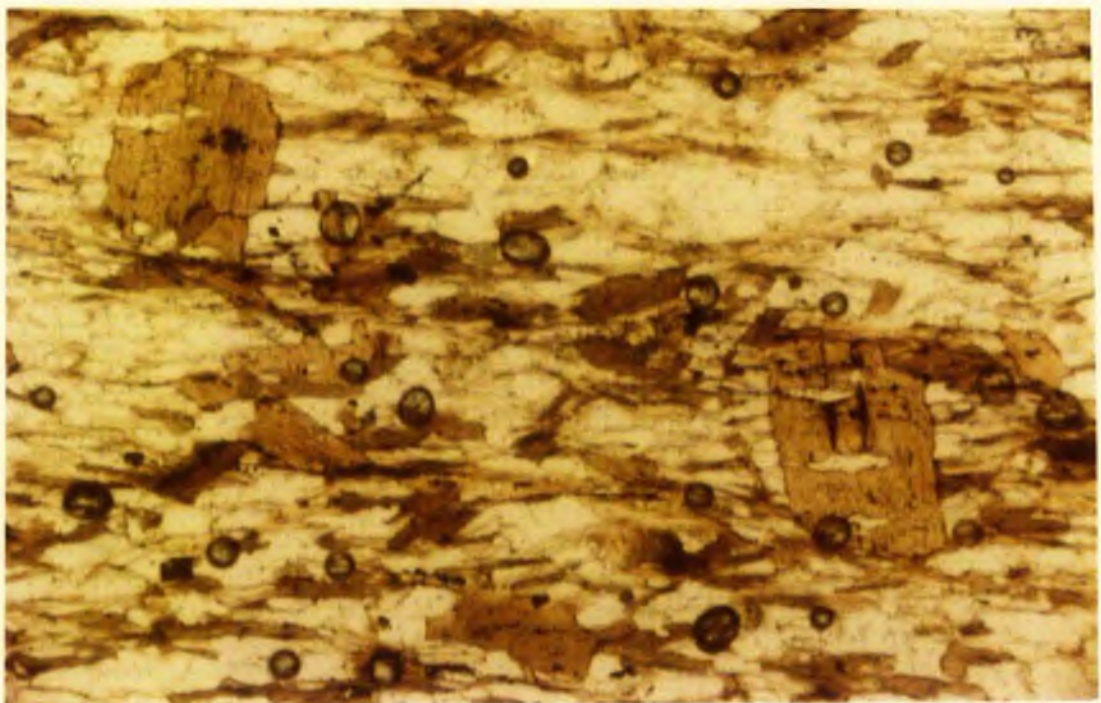


Plate 3.23 - In M55 biotite porphyroblasts overgrow the S1 foliation (field of view = 1.0mm).

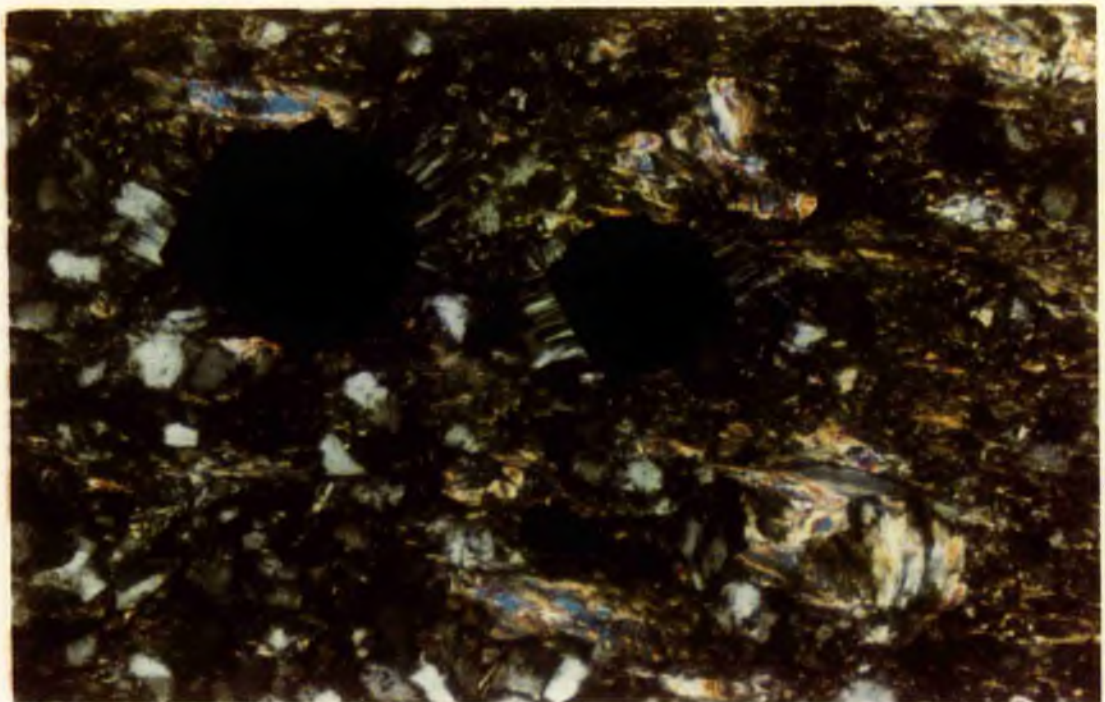


Plate 3.24 - M45 contains early (?syn-D1) muscovite pods (e.g. bottom right) and later (post-D1) pyrites with quartz overgrowths (field of view = 1.0mm).

from the 4km SW of the Foxdale granite to Ramsey in the NE. Both authors related them to granites and the D2 deformation.

Psammitic rocks are characterised by mixtures of medium grained (0.2mm), angular monocrystalline quartz grains of uniform size, and a finer grained groundmass rich in quartz with lesser amounts of muscovite, chlorite, feldspar and opaques. The coarser quartz grains are both matrix and clast supported depending on their concentration. There are also detrital grains of tourmaline, zircon and muscovite, though these are not common. Porphyroblasts of quartz, muscovite and calcite formed pre- or syn-D1, and euhedral pyrite formed post-D1 (see plate 3.24). Ilmenite porphyroblasts are not present, being confined to the pelitic samples studied.

Veining occurs throughout the structural history of the Manx Group. Details of timing have been described in section 3.4.1, and so only petrographic details will be briefly discussed here. Quartz is the most common vein material and is often strained showing undulose extinction. The quartz can be in association with earlier formed radial and acicular chlorite growth. In one slide a muscovite filled vein was observed with larger crystals of muscovite than that of the surrounding groundmass. This is due to more favourable growth conditions within the extensional environment of the vein (Roedder and Bodnar, 1980). Later formed veins often contain calcite, or dolomite rhombs as well as quartz.

One thin section, from a "Greenstone Dyke", was examined. This contained phenocrysts of plagioclase (up to 3mm) in a fine groundmass of quartz feldspar, chlorite and opaques with minor calcite. The plagioclase phenocrysts are strained showing undulose extinction and fracturing. These phenocrysts show partial replacement by fine chlorite, quartz and albite.

3.5.3 Conclusions

1. The growth of primary metamorphic minerals started subsequent to diagenesis and continued until the end of S1 cleavage development. This involved the growth of quartz and calcite concretions, chlorite and muscovite porphyroblasts, and the re-crystallisation of the fine detrital matrix. White mica is pervasively orientated to the S1 cleavage.

2. A second phase of metamorphism occurred during D2 and the static phase after this. This metamorphism was characterised by the growth of a variety of types of porphyroblast, some of which, according to Simpson, 1964a, cross-cut the S2 crenulation cleavage. These porphyroblasts are believed to have grown during contact metamorphism from the Dhoon and Foxdale granites.

3.6 ILLITE CRYSTALLINITY

3.6.1 Introduction

One of the main objectives of studying the IOM was to produce a crystallinity map of the Manx Group. While this research was in progress a similar study was underway at Birkbeck College, London. This study, made by Dr Brin Roberts, proved to be complimentary to the St Andrews study. The results correlated very well, providing evidence for the validity of illite crystallinity mapping and at the same time allowing direct comparison of data between two laboratories (Roberts, B., Morrison, C. W. K. and Hirons, S., in press).

Pelitic samples were collected on a grid spaced between 0.5 and 2.5km (see Appendix 3.1). A more detailed sampling of Niarbyl was carried out, with 13 samples collected across an area of <250m (see Fig. 3.7).

The results, in Hbre1, for 114 samples are listed in Appendix 3.3, and are plotted on a base map of the Isle of Man (Fig. 3.5) and in traverses X-X and Z-Z (see Fig. 3.6). Isocrysts were drawn by hand at an interval of 10 units of Hbre1. The methods of investigation are discussed in chapter 2.2.

3.6.2 The Crystallinity Map

The crystallinity values obtained ranged from Hbre1 298 (lowest grade) to 107 (highest grade), covering a wide range from diagenetic to epizone metamorphism. Values over 200 are very localised and have local explanations (see below). This leaves the metamorphism ranging from the

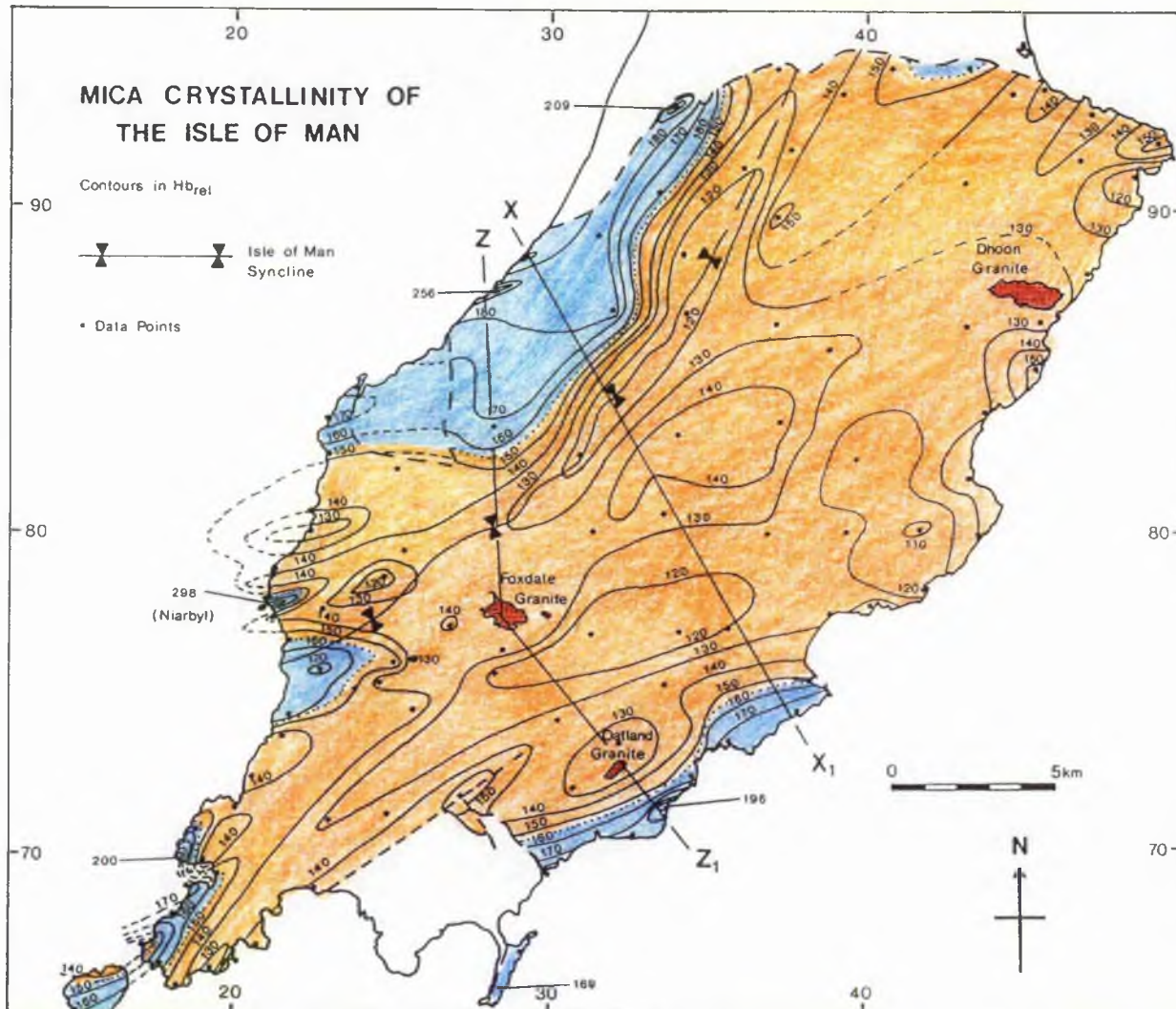


Fig. 3.5 - Isocryst map of illite crystallinity in the IOM (<2µm size fraction).
Contour interval of 10 Hb_{rel}. Orange areas are epizonal, blue areas are anchizonal.

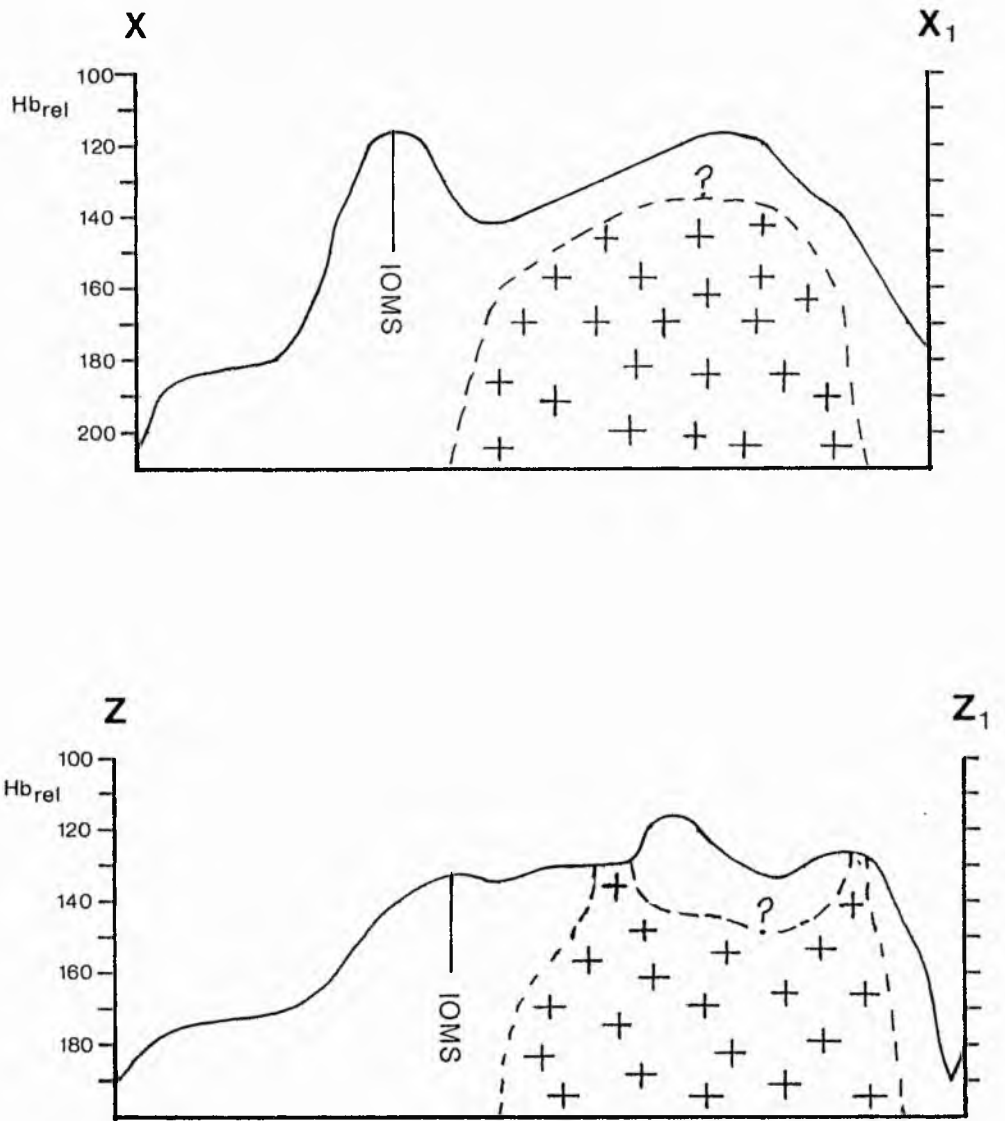


Fig. 3.6 - Contoured Hb_{rel} traverses across the IOM (locations shown on Fig. 3.5). This illustrates the effects of the IOM Synform and contact metamorphism from granite plutons.

anchizone to the epizone. Some samples have had to be omitted due to interference on the 10\AA ^o peak by paragonite or biotite.

The central and eastern part of the Manx Group shows a relatively low metamorphic gradient with extensive areas of low crystallinity values ($\text{Hbrel} < 130$) with a NE-SW trend. There are 3 main areas with crystallinity values $<\text{Hbrel} 120$, one lying along the line of the Isle of Man Synform, one associated with the Foxdale granite, and one extending NW for 5km from Port Groudle. Another 4 lesser areas occur being associated in the S with the Oatland granite, in the NE with the Dhoon granite, in the NE at Port Mooar, and in the W at Dalby Mountain. The Foxdale, Port Groudle, and Dhoon "highs" are not separated by values higher than $\text{Hbrel} 130$.

The rest of the Manx Group outcrop, along the whole of the western fringe and the southern fringe, is an area of steeper gradients and higher crystallinity values. The lowest crystallinity rocks ($\text{Hbrel} > 200$) occur in 4 very localised areas.

(1) In the SW, at Bradda Head ($\text{Hbrel} = 200$), high values are presumed to have been caused by hydrothermal alteration associated with vein quartz mineralisation.

(2) Further N at Niarbyl, values as high as 298 were obtained (see Fig. 3.7). There are clear correlations between increased shearing and cataclasis (cf. with a TEMA

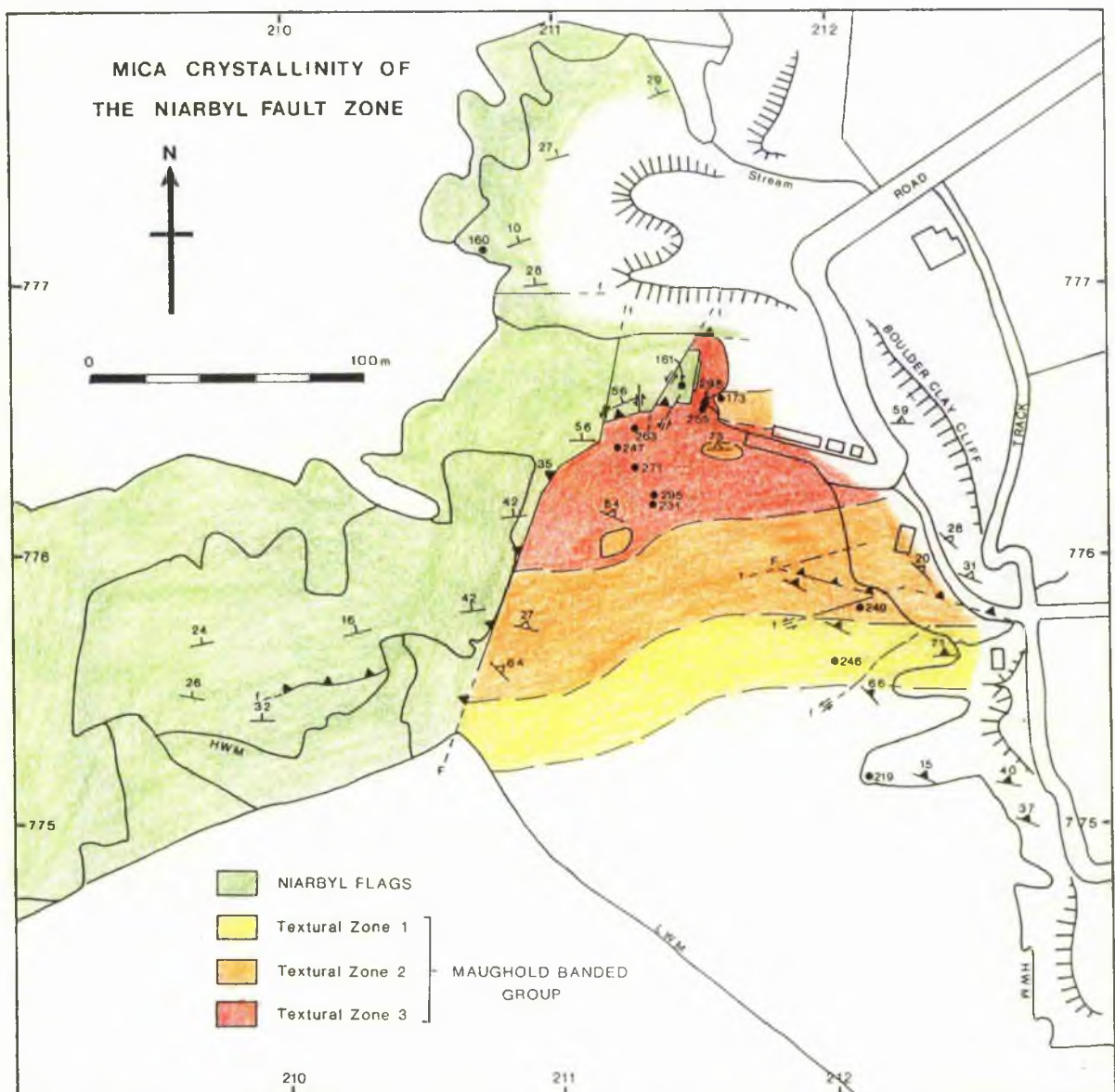


Fig. 3.7 - Illite crystallinity measurements from the Niarbyl Fault Zone. Structural symbols are explained with Fig. 3.2.

mill effect), and increased crystallinity values in the phyllonites associated with faulting at Niarbyl.

(3) Further NNE, at Ballanayre Strand (Hbrel 256), some of the rocks were recognisably phyllonitic, with quartz segregations, and therefore the low temperature crystallinity values may be associated with fault shearing and cataclasis.

(4) At Ballacurnkeil (Hbrel 209) a similar explanation to that for Ballanayre Strand may apply.

Grades of between 200 and 160 occur in belts along the west from Ballaugh in the north to the Calf of Man in the extreme SW, and in the SE from Douglas to Dreswick Point in the south. These areas reflect a regional increase in crystallinity values. The reasons for this are discussed in section 3.8.

3.7 MINERALOGY

3.7.1 Mineralogy in Relation to Illite Crystallinity

The mineralogy of 114 samples in relation to illite crystallinity (Hbrel) is summarised in Fig. 3.8. Histograms showing the number of samples of a given crystallinity is presented as Fig. 3.9. A list of samples examined by XRD and their respective Hbrel and b_o values, and mineralogy is given in Appendix 3.3. Relative proportions of minerals have been semi-quantified on a small, medium and large scale by visual inspection of XRD traces.

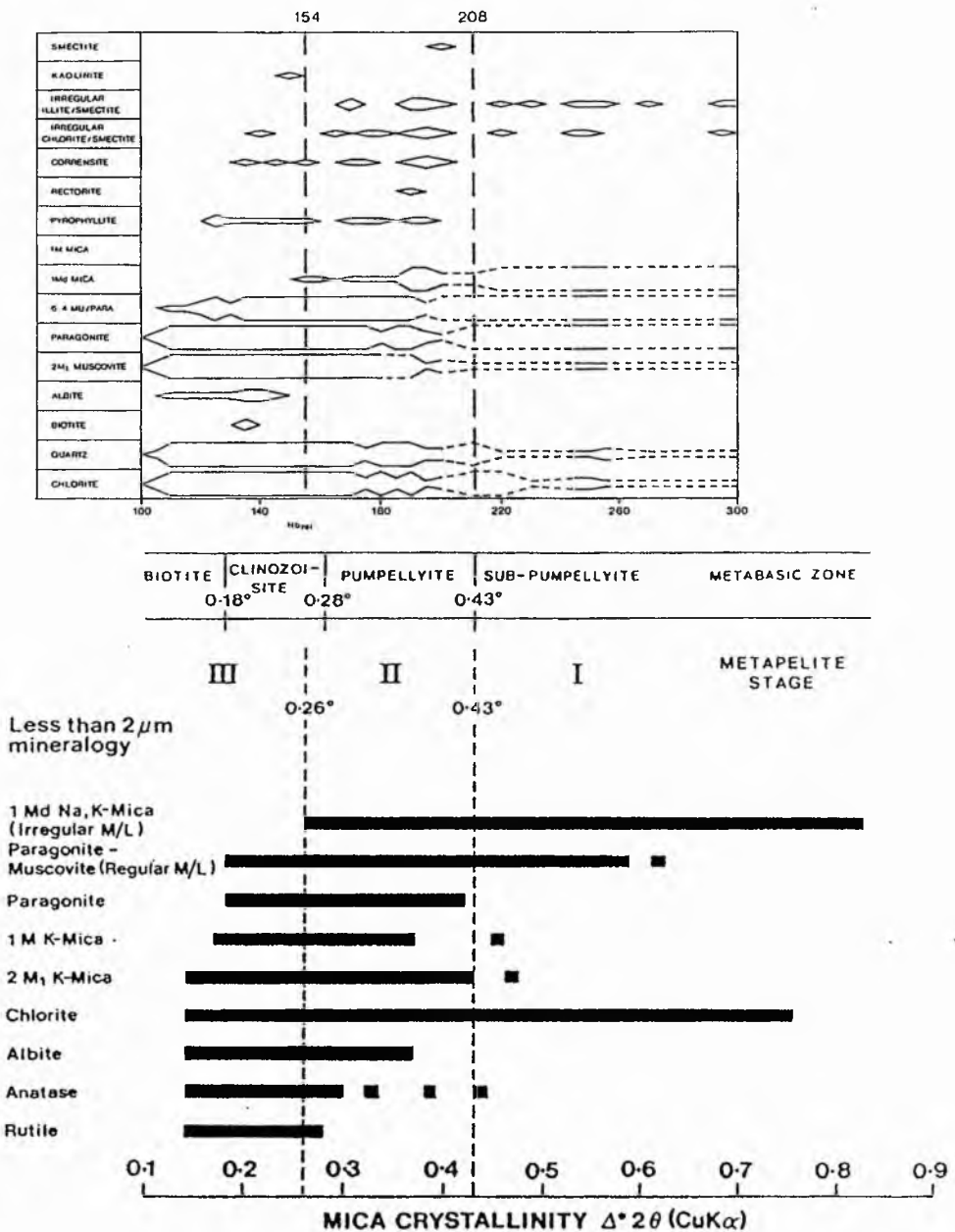


Fig. 3.8 - Mineralogy of the $<2\mu\text{m}$ size fraction compared to Hbrel. Relative proportions of minerals (shown by the width of bars) are quantified on a small, medium and large scale by visual inspection of XRD traces. A comparative table from Merriman and Roberts (1985) is included. Lower and upper limits for the anchizone (of $0.43^\circ 2\theta$ and $0.26^\circ 2\theta$) correspond to Hbrel 208 and 154 in this study.

GRANITE AUREOLE

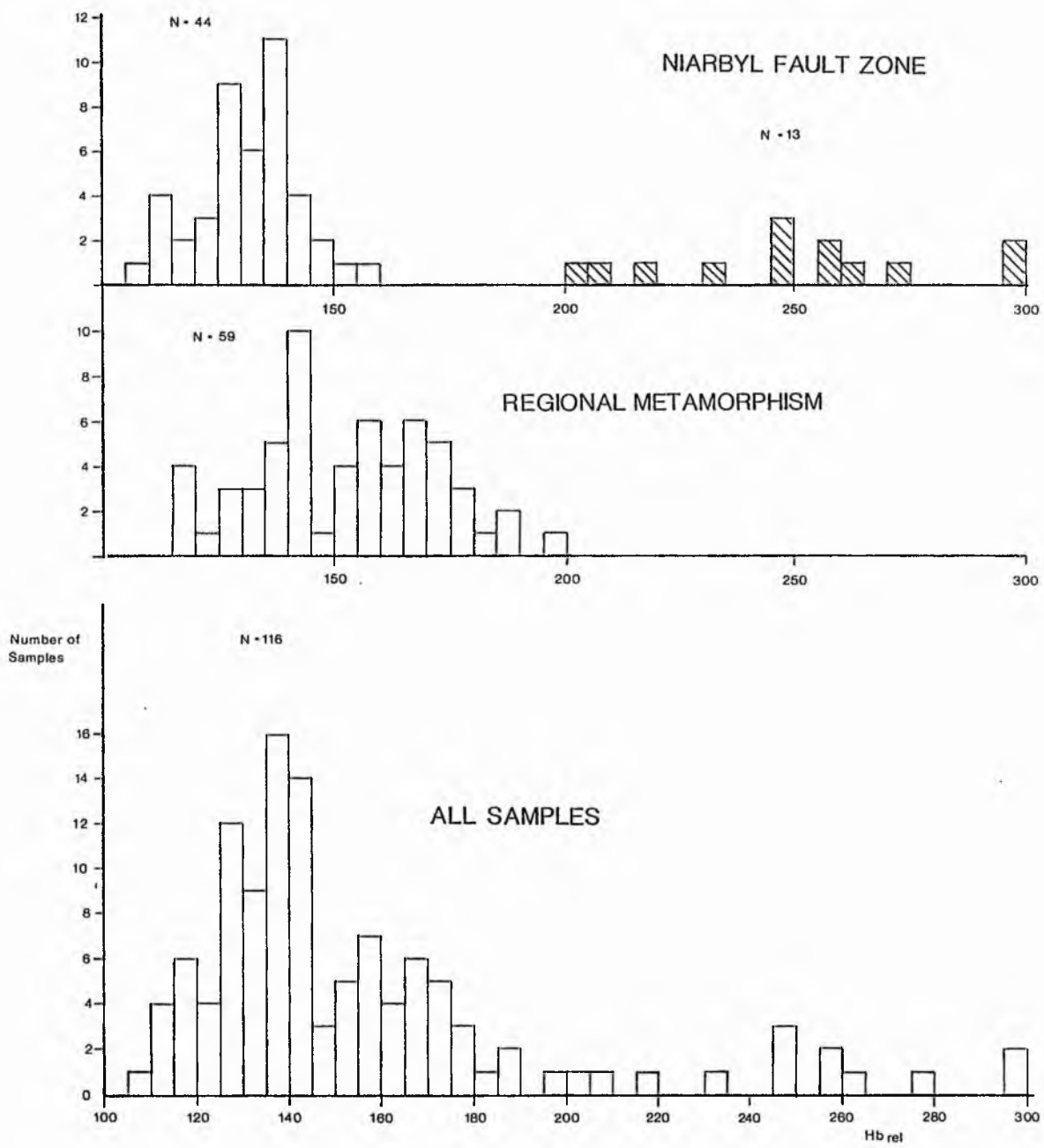


Fig. 3.9 - Histograms of samples versus Hb_{rel} values.

The lowest grades, Hbrel 298 to 209, are dominated by the phyllonites of the Niarbyl Fault Zone. 1Md mica polytypes occur as irregular interstratified Na-mica and K-mica with <10% smectite interlayers. Paragonite and regular paragonite-muscovite are present along with relict 2M, muscovite (see Fig. 3.10). Quartz and sporadic chlorite are present.

At higher grades, Hbrel 208 to 188, 1Md and 2M, polytypes coexist, and the 2M, /1Md ratio increases with advancing grade. Paragonite and regular (6:4) paragonite-muscovite occur in variable amounts. Pyrophyllite was detected at Hbrel 196 in one sample. A minor amount of rectorite was detected at Hbrel 188. Quartz and chlorite were also present.

From Hbrel 187 to 125 2M, muscovite, paragonite and regular (6:4) paragonite-muscovite dominate (see Fig. 3.11). 1Md illite is a minor phase becoming absent at Hbrel 154. Albite occurs frequently, in minor amounts, from Hbrel 143 onwards. Biotite was detected in two samples at Hbrel 134 and 173 (see plate 3.23). In these samples peak width has probably been affected by the biotite peak. Pyrophyllite occurs sporadically in minor amounts. Kaolinite occurs in one sample with Hbrel 153. This may be a weathering product. Ilmenite, detected in thin section, occurs in samples ranging from Hbrel 129 to 144, with one at Hbrel 163. Quartz and chlorite are present throughout.

At the highest grades, Hbrel <125, 2M, muscovite and paragonite dominate, and regular (6:4) paragonite-muscovite

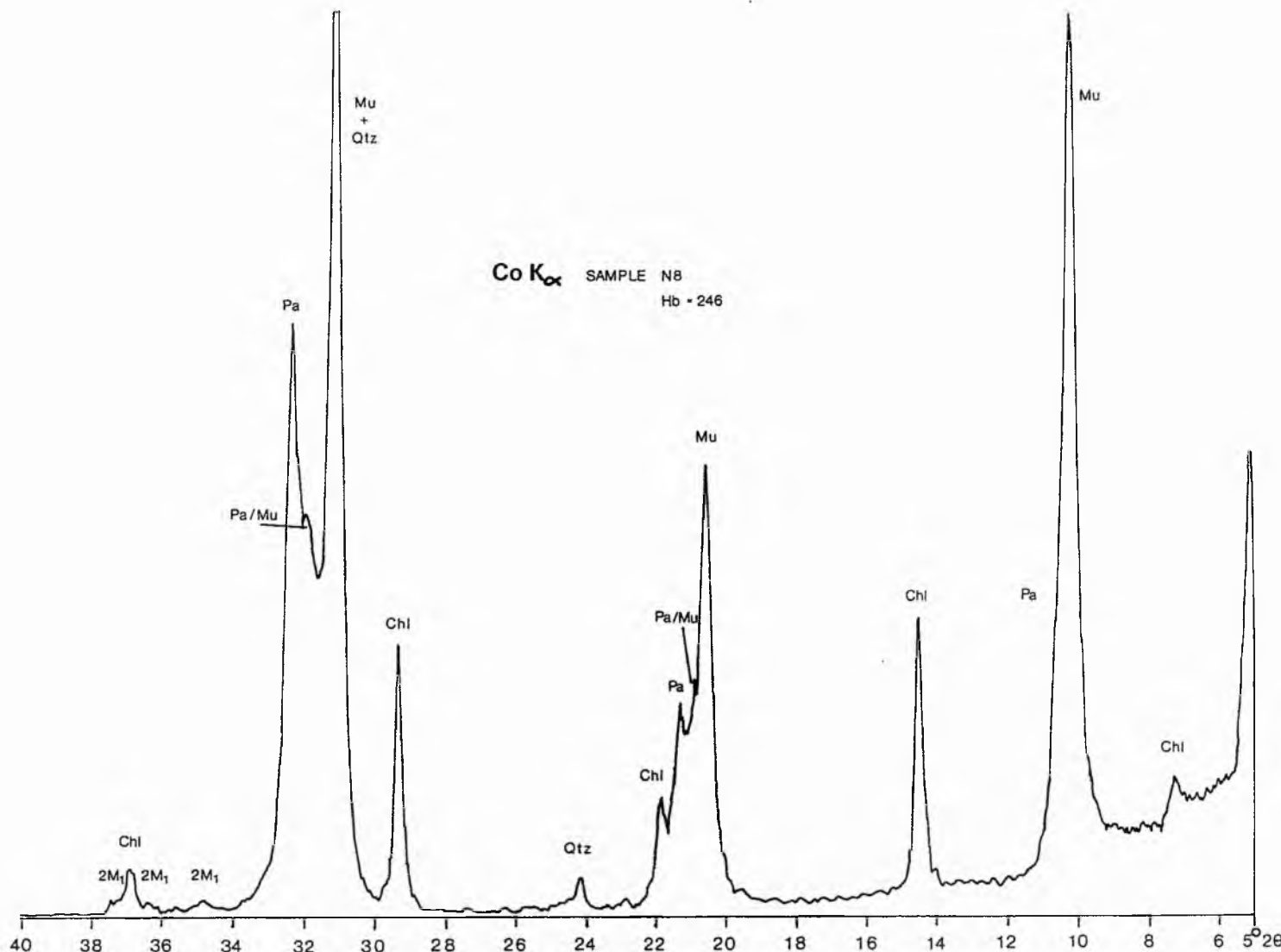


Fig. 3.10 - XRD trace from sample N8 (Hbrel 246) in the Niarbyl Fault Zone. Mu = illite or muscovite, Chl = chlorite, Pa = Paragonite, Pa/Mu = paragonite-muscovite, Q = quartz, 2M₁ = the 2M₁ polymorph of muscovite.

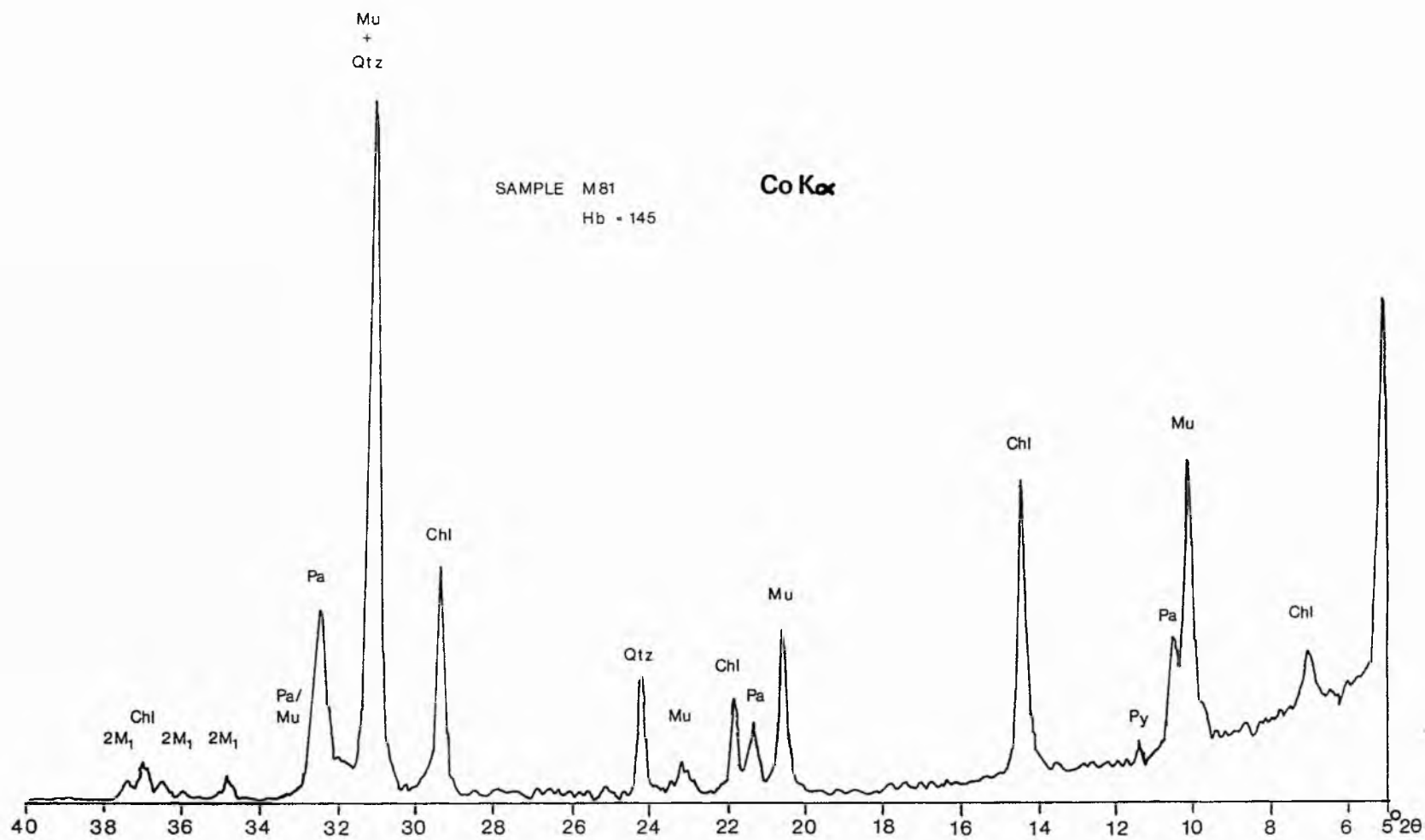


Fig. 3.11 - XRD trace from sample M81 (Hbrel 145). Abbreviations are explained with Fig. 3.10. In addition Py = pyrophyllite.

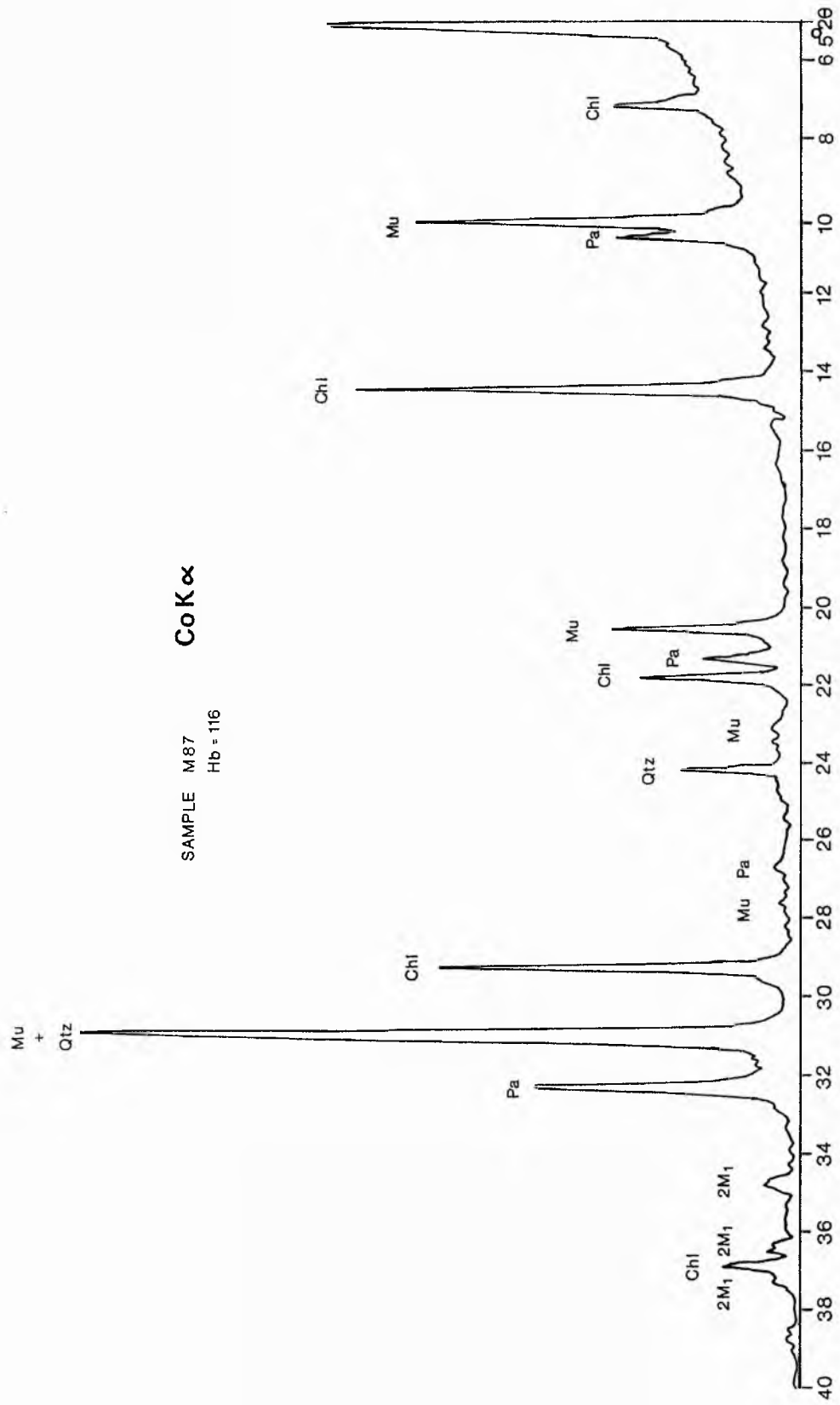


Fig. 3.12 - XRD trace from sample M87 (Hbrel 116). Abbreviations are explained with Fig. 3.10.

dissappears by 110 (see Fig. 3.12). The highest grade sample, Hbrel 107, has 2M₁ muscovite, paragonite, quartz and chlorite.

3.7.2 Comparisons with the Lake District and Wales

Comparisons are made here with rocks from the Lake District and Wales because: 1. - The rocks are lithologically similar. 2. - They have similar ages. 3. - They are at similar metamorphic grades. 4. - They are geographically close to the IOM.

The low grade metamorphic rocks of the Lake District include the Skiddaw Slates (Arenig to Llanvirn), the Borrowdale Volcanics (Llandeilo to ?Caradoc) and the Upper Ordovician and Silurian succession. According to Thomas (1986), these rocks fall in the anchizone and epizone. The Skiddaw Slates are dominantly anchizonal (mostly from Hbrel 107-177) and are associated with quartz, chlorite, 1Md and lesser 2M₁ white micas, mixed-layer paragonite/muscovite, paragonite, and minor pyrophyllite, illite/smectite and smectite. The Borrowdale Volcanics Group (Hbrel 100-143), and upper Ordovician and Silurian succession (Hbrel 100-149) are mostly epizonal and this is reflected by an increased 2M₁/1Md ratio. The absence of paragonite, mixed-layer paragonite/muscovite and pyrophyllite is not considered diagnostic of grade but of variation in rock composition.

Studies on the mainly Ordovician slates of the Welsh Basin by Merriman and Roberts (1985), Roberts and Merriman (1985) and Robinson and Bevins (1986) have resulted in

clear correlations between mineral assemblages and low grade metamorphic zones (see section 2.2.8 for further discussion). At diagenetic grades ($>0.43^{\circ}2\theta$ in Robinson and Bevins, 1986) mixed-layer illite/smectite and diagenetic clays, such as kaolinite, are present. At lower anchizone grades ($0.43-0.30^{\circ}2\theta$ in Robinson and Bevins, 1986; and $>0.43^{\circ}2\theta$ in Merriman and Roberts, 1985; Roberts and Merriman, 1985) 1Md K-Na micas are present in association with chlorite, minor 1M and 2M, muscovite, and minor regular mixed-layer paragonite/muscovite. At upper anchizone grades ($0.30-0.21^{\circ}2\theta$ in Robinson and Bevins, 1986; and $0.43-0.26^{\circ}2\theta$ in Merriman and Roberts, 1985; Roberts and Merriman, 1985) 2M, is dominant over 1Md mica. Paragonite, paragonite/muscovite and chlorite are common constituents, lesser 1M mica and albite are present, and minor anatase and rutile are present. Pyrophyllite, rectorite and corrensite are associated with larger intrusions. In epizone grade rocks ($<0.21^{\circ}2\theta$ in Robinson and Bevins, 1986; $<0.26^{\circ}2\theta$ in Merriman and Roberts, 1985; Roberts and Merriman, 1985) 2M, mica is the dominant polymorph, 1M is present and 1Md is absent, paragonite is more common than paragonite/muscovite, chlorite, anatase and rutile are common constituents, and albite is mostly present in paragonite free slates.

On the basis of the mineralogy of the metamorphic zone described above, for the Welsh Basin (see Fig. 3.8), the following zones are recognised in the IOM;

Hbre1 298-209 - These were once anchizonal grade rocks which have been reduced to diagenetic grade due to cataclastic grain size reduction (see section 3.8.2).

Hbre1 208-188 - Low anchizone.

Hbre1 187-154 - High anchizone.

Hbre1 <154 - Epizone.

3.8 DISCUSSION

The majority of samples collected were of similar pelitic composition, to minimise the effect of lithology on crystallinity values.

3.8.1 Areas of Low Isocryst Gradient, and Higher Grade.

As mentioned previously, many of the areas of high grade rocks are closely associated with the outcrops of the Foxdale, Dhoon and Oatland granites, and are most likley due to contact metamorphism associated with these granites and the sub-surface extension of them. Geophysical evidence of Cornwell (1972) suggests that the Foxdale and Dhoon granites each represent cusps on separate adjacent granite plutons. These plutons could account for the extensive area of higher grade rocks in the central part of the IOM. The Oatland granite provides a smaller example of the contact metamorphism (see Figs 3.5 and 3.6).

Another area of high grade rocks extends 5km NW from Port Groudle. Samples collected here show no evidence for above average strain, and thus the crystallinity values have been ascribed to another hidden igneous body.

A further area of high grade rocks lies in close association with the Isle of Man Synform. The concentration of higher grade rocks along its axis could be indicative of higher strain, though the cleavage intensity is not abnormally high.

3.8.2 Areas of High Isocryst Gradients, and Lower Grade.

Areas of higher isocryst gradient extend along the whole of the NW facing and the SE facing coasts of the Isle of Man. These areas are generally associated with metamorphic grades lower than Hbrel 140.

These areas lie outside the zone of influence of the granite plutons and are taken to represent anchizone to epizone grade regional metamorphism. Anchizone to epizone grades were attained before and during D1 deformation, which is associated with pervasive growth of white mica (see section 3.5.3) A possible explanation for this is that, after an initial burial metamorphism, temperatures continued to stay high during D1 deformation.

In the central part of the IOM epizone grade contact metamorphism was superimposed on the regional metamorphism (see above). This would have occurred pre- to syn-D2 (see section 3.4.1).

D2 deformation, associated with crenulation cleavage development but not with new mica growth, has not contributed to the regional metamorphic grade. Later deformations are weak or brittle events.

There are localised narrow belts of diagenetic grade rocks at Ballacurnkeil (Hbrel 209), Ballanayre Strand (256)

and at Niarbyl (289). The fault activity at Niarbyl has produced phyllonitic rocks with induced lowering of the metamorphic grade. A possible explanation for this is that since the cataclastic deformation occurred after the thermal high of regional metamorphism, a major portion of the higher grade 2M₁ mica was comminuted by the mylonitisation process. This, together with strain induced lattice defects, has resulted in peak broadening. Local decreases in crystallinity resulting from post-crystalline thrusting have been described by Teichmuller et al. (1979, p213) in Frey (1987, p264-265). The Ballanayre Strand "low" could be associated with transcurrent fault zones, since phyllonitic rocks were observed there.

3.8.3 The Anchizone-Epizone Transition in the IOM.

In Fig. 3.9 samples, illustrated on Fig. 3.5, have been subdivided into three groups. These are based on the likely importance of regional or contact metamorphism, or low temperature cataclasis on the Hbrel values. The division between the regional and contact metamorphic groups cannot be precisely made. For the purpose of this study a division has been made on the basis of the likely sub-surface extent of the granites. This was estimated from the distribution of porphyroblasts observed by Simpson (1964a) and is shown on Appendix figure 3.1. If the anchizone-epizone boundary is taken at Hbrel = 154 (see section 3.7.2), then regional metamorphism ranges from low anchizone to high epizone, with an absence of values between Hbrel 145 and 150. The contact metamorphic

overprint falls clearly in the epizone. Cataclastic rocks fall in the diagenetic zone (see above).

3.9 b_o SPACING

3.9.1 Introduction

A study of relative pressure conditions within the Manx Group was undertaken using the same set of samples that were used for illite crystallinity. 118 data points were obtained. The uniform composition of the rocks and grade of metamorphism allowed internal consistency of the results. From these results an iso- b_o map was produced for the IOM (Fig. 3.13), as well as a cumulative frequency plot (Fig. 3.14). Curves from Sassi and Scolari (1974), Fettes et al. (1976) and Robinson and Bevins (1986), and results from Glen Esk and Nepal produced during this study, are included for comparison.

Sassi and Scolari (1974) produced a set of b_o values that could be used to quantify the pressure facies of a metamorphic area (see table 3.3). Sassi et al. (1976) classified the pressure zones in simpler terms as follows:

Mean Value	Facies
$b_o < 9.000\text{\AA}^o$	Low P
$9.000\text{--}9.040\text{\AA}^o$	Med P
$b_o > 9.040\text{\AA}^o$	High P

3.9.2 Results

For the IOM the mean b_o value is 8.988\AA^o ($SD = 0.014$) which would indicate even lower pressure conditions than that of Bosot (see Appendix 3.4). Illite crystallinity appears to show a random relationship with b_o (see Fig. 3.15), and so the effect of temperature on b_o is considered to be negligible. Fig. 3.15 has been subdivided into

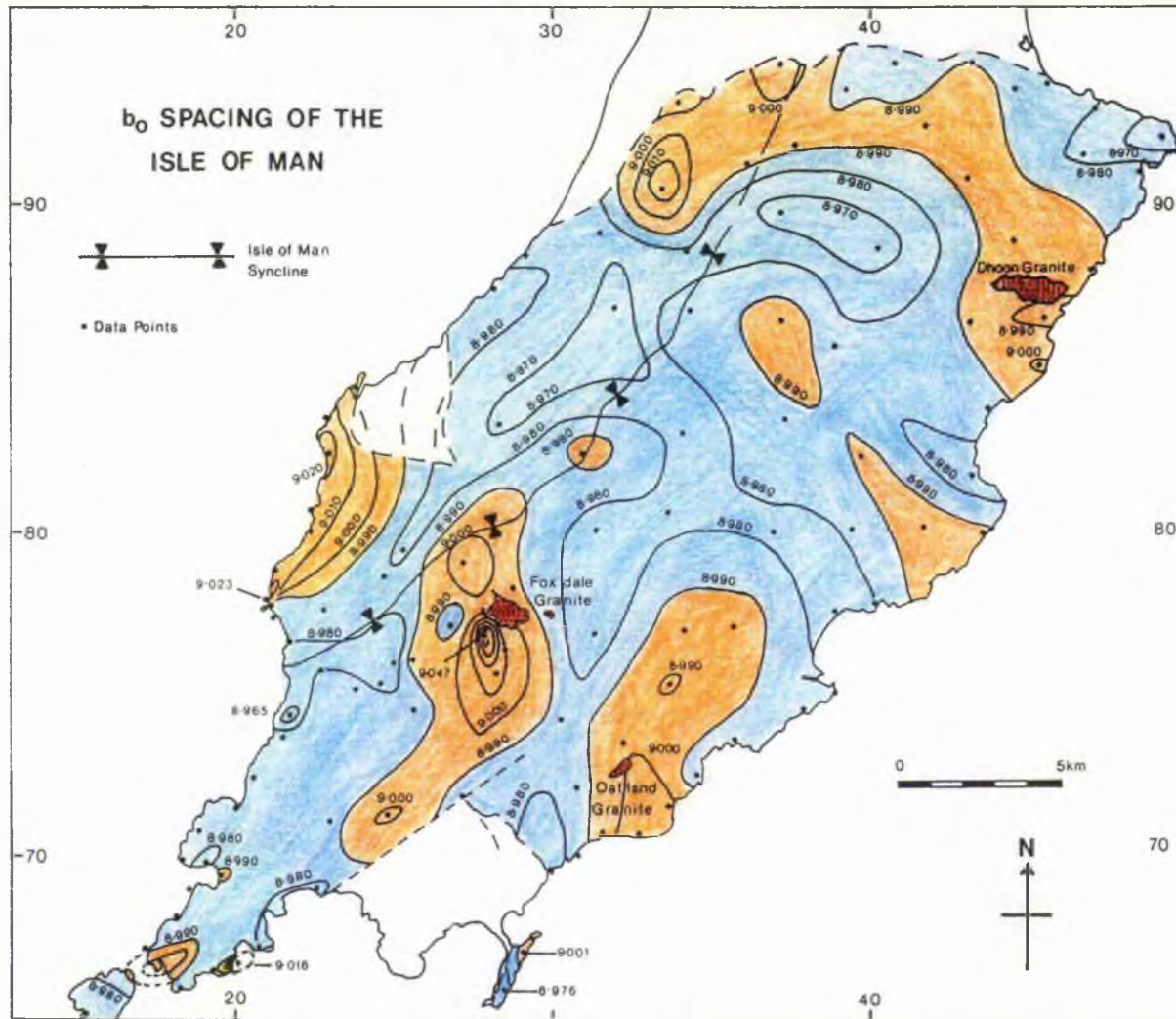


Fig. 3.13 - Map of b_0 in the IOM. Contour interval of $0.010 b_0 \text{ A}^{\circ}$. Orange and blue areas are areas of higher and lower b_0 values respectively.

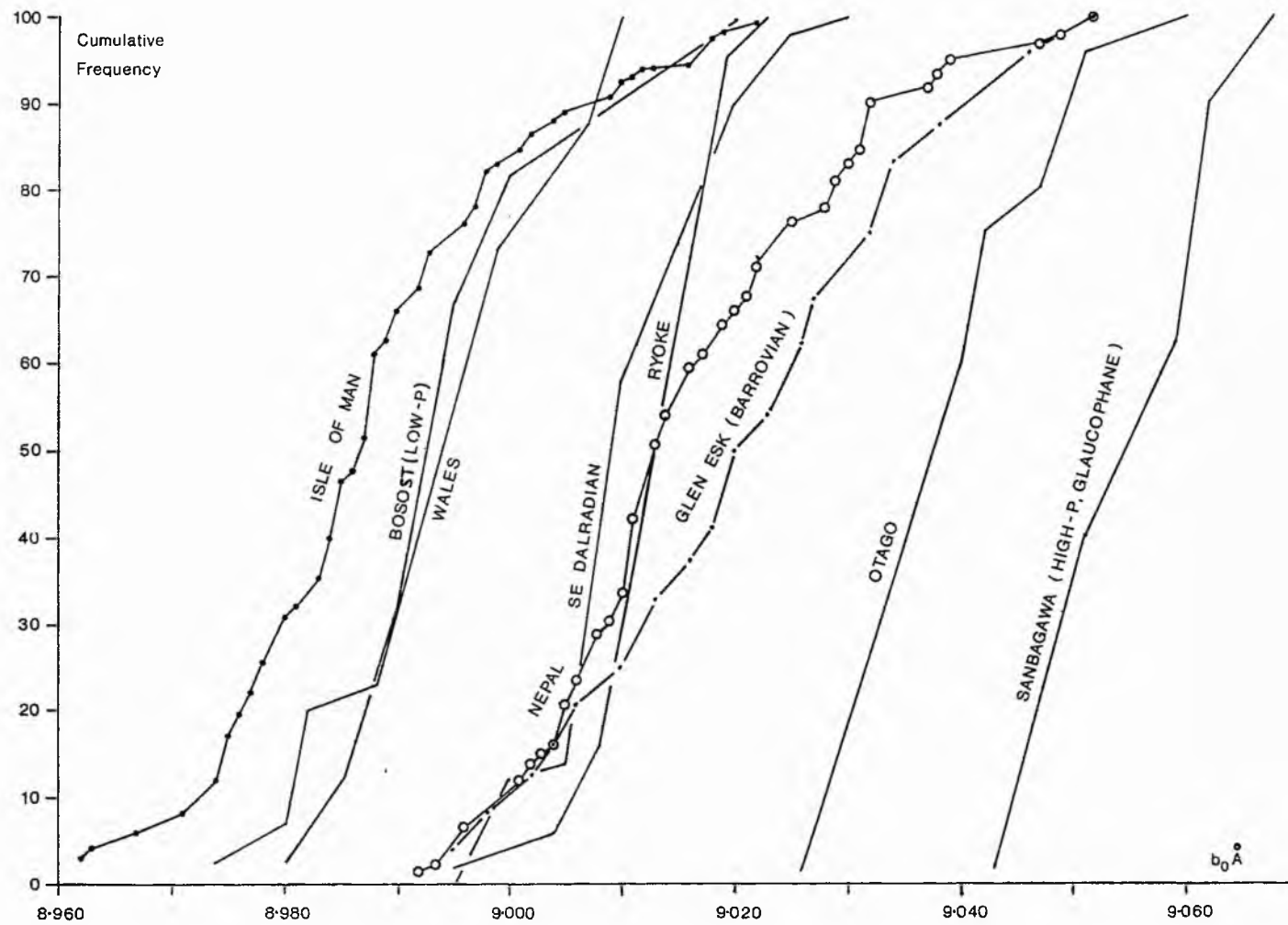


Fig. 3 14 - Cumulative frequency curves of b_0 values from: the IOM, Glen Esk and Nepal (this study), and also Bosost, Ryoke, Otago and Sanbagawa (Sassi and Scolari, 1974), Wales (Robinson and Bevins, 1986), and the SE Dalradian (Fettes et al., 1976).

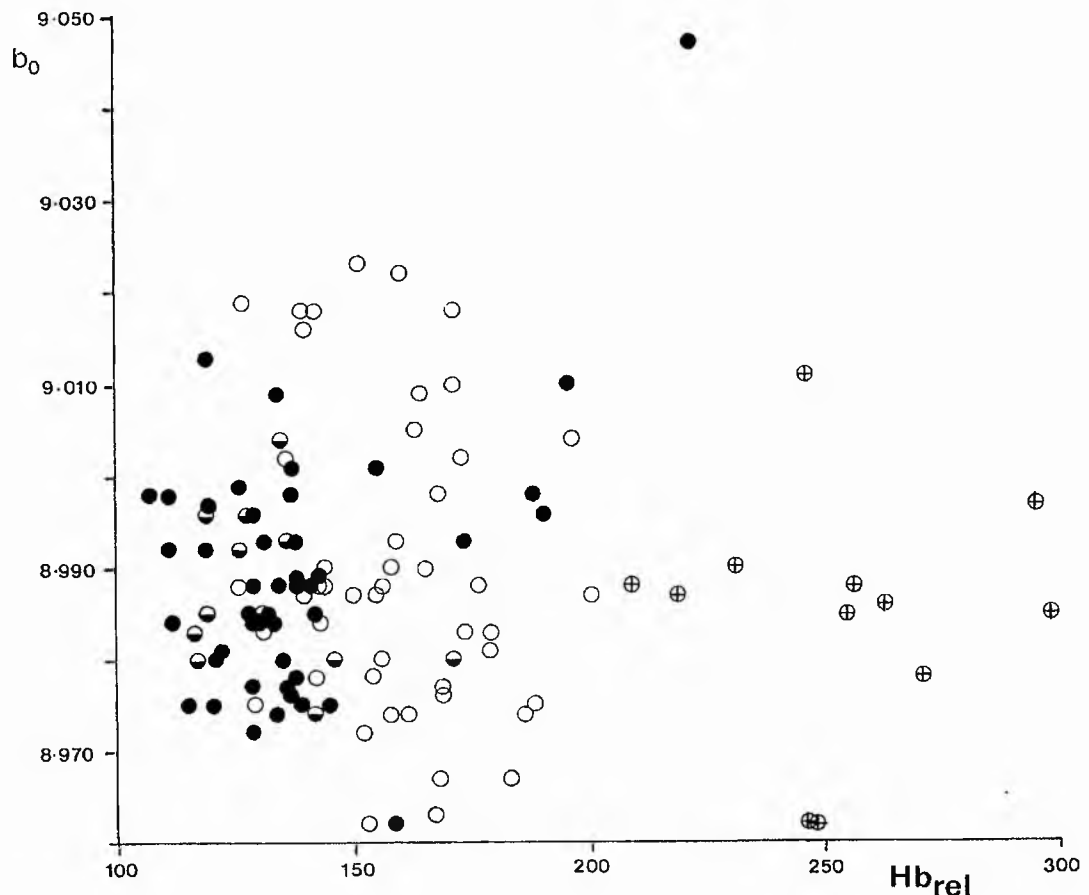


Fig. 3.15 - $H_{b\text{rel}}$ values plot against b_0 values from the IOM. \circ = Regional metamorphism, \bullet = Contact metamorphism, \ominus = samples from the IOM synform, \oplus = samples from the Niarbyl Fault Zone.

samples from the granite aureole (as described in section 3.8.3), from the Niarbyl Fault Zone, from areas of regional metamorphism and from the Isle of Man Synform (see Appendix 3.1). The random relationship between b_o and the subdivisions of the data in Fig. 3.15 show that neither contact metamorphism nor tectonic activity have altered the b_o values, though the strong relationship between Hbre1 and tectonometamorphic environment is clearly illustrated.

Table 3.3 - Mean b_o values and pressure facies determined by Sassi and Scolari (1974). Data included for comparison are: Thomas (1986) (#), from the Lake District; Fettes et al. (1976) (**), from the Scottish Dalradian; Robinson and Bevins (1986) (**), from Wales; and this study (*), from the IOM and Glen Esk

Mean Value	Facies	Study Area
8.988	Low P	IOM *
8.988	Low P	Skiddaw Slates #
c. 8.990	Low P	Bosot
c. 8.995	Low P	Hercynian of E. Alps
8.995	Low P	Welsh Basin **
9.003	Low P	Dalradian ***
c. 9.010	Low-Med P	New Hampshire
9.015	Low-Med P	Dalradian *
9.020-9.025	Barrovian	Scottish Dalradian
9.022	Medium-P	Borrowdale Volcanics #
9.029	Medium P	Highland Border Complex *
9.033	Med-High P	U. Ord/Sil Succession #
c. 9.035	Med-High P	Otago
c. 9.055	Glaucophane	Sanbagawa

3.9.3 Discussion

The very low b_o values in the IOM can partly be explained by the b_o lowering effect of abundant paragonite and para/mu throughout the Manx Group (see section 2.2.13).

Thomas (1986) also obtained a mean b_o value of 8.988\AA^o , for the Skiddaw Slates. This compared to b_o values of 9.022\AA^o and 9.033\AA^o for the Borrowdale Volcanics and the U. Ordovician and Silurian Succession respectively. The anomalously low b_o values for the Skiddaw Slates were attributed to the presence of abundant paragonite and pyrophyllite, and Thomas concluded that the Borrowdale Volcanics and U. Ordovician and Silurian Sucession gave a more reliable indication of the relative pressure conditions. It is questionable whether the effect of abundant paragonite and pyrophyllite would lower b_o values to the degree suggested by Thomas. In the Isle of Man there was no clear correlation between samples containing paragonite and low b_o values. A similar study to that of Thomas, in the Lower Palaeozoic of Wales, by Robinson and Bevins (1986), shows a mean b_o of 8.995\AA^o for 150 samples. While acknowledging the effects of paragonite (which was less common than in the IOM) they concluded that low pressure conditions did exist in the Welsh Basin. This was supported by the re-interpretation of the metabasite mineralogy of Bevins and Rowbotham (1983), which gave a PT estimate compatable with a high geothermal gradient (of c. 40°C/km).

3.9.4 Diastathermal Metamorphic Model

A low pressure facies series in the Manx Slates implies a higher rate of heatflow than would normally be achieved in a burial metamorphic environment with D1 deformation superimposed (see section 3.8.2). A possible solution lies in the modelling of Robinson (1987), and

Bevins and Robinson (1988). The low pressure diagenetic to low greenschist facies metamorphism of the Welsh Basin was attributed to diastathermal metamorphism. The Welsh Basin was modelled as a marginal basin in an extensional tectonic setting. High heat flow was generated by a process of lithospheric extension coupled with basaltic magmatic activity. Peak metamorphic conditions, of c.2kb (c.8km depth, based on the upper limit of the prehnite-actinolite facies) and 350°C at the base of the sedimentary pile, were attained during burial, with a concordance between depth of burial and metamorphic grade. Initial cooling in the basin was not initiated by uplift and erosion, but by slow thermal relaxation caused by a cessation of the extensional process. Compressional tectonics with uplift, cleavage development and final cooling caused local re-orientation and re-crystallisation of micas giving an apparent correlation between deformation and metamorphism.

In the IOM there are many similarities with the Welsh Basin. 1. The presence of slump breccias (the Sulby and Ballanayre slump breccias as well as those observed at Fleshwick Bay, see plate 3.3) implies syn-sedimentation faulting within the basin. 2. There is evidence, in the form of chlorite and chlorite/muscovite porphyroblasts, for metamorphic mineral growth before D1 deformation (see section 3.5). 3. The Manx Group sucession was interpreted as being c.8km thick, by Simpson (1963a), which is comparable with the depth of burial estimated for the Welsh Basin. 4. Anchizone to epizone metamorphism and low b_o values are similar to the metamorphic facies found in

Wales. 5. The sedimentary pile was intruded by basaltic 'sills' (see section 3.4.1).

On the basis of the above evidence it is considered likely that the Manx Group formed in an extensional basin, and that diastathermal metamorphism occurred during the formation of this basin. D1 deformation caused the recrystallisation of mica in parts of the sucession, but the relative importance of this overprint is uncertain. A concentration of higher grades along the IOM Synform may have resulted from deformation.

3.10 FLUID INCLUSIONS

3.10.1 Samples

One sample, from a muscovite bearing quartz vein, was collected from the Foxdale granite (see plate 3.24). A tourmaline bearing quartz vein sample was collected from the Dhoon granite. Two samples were prepared from quartz vein material from a large syn-F2 vein at the Calf Sound (see plate 3.25). From the Niarbyl Fault, two fluid inclusion wafers were made from quartz segregated pelites. These samples were chosen to compare veining associated with; 1. granite intrusion, 2. regional metamorphism and 3. major faulting. Methods used are described in chapter 2.3.

3.10.2 Results Obtained

In the 2 samples from Niarbyl the inclusions were too small for thermometric measurements. Mylonitisation probably prevented trapping of all but the smallest inclusions. The results from the remaining 4 samples are shown in Figs 3.16 and 3.17, tables 3.4 and 3.5, and Appendix 3.1.

Foxdale - Two distinct inclusion populations could be recognised. Primary inclusions could not be positively identified because possible candidates were usually too closely spaced. Fluid-rich H₂O-NaCl inclusions dominated, with mean salinities ranging from 1.6 to 23.0 wt% NaCl equivalent. KCl and CaCl salts were also present (from Te, see section 2.3.5). These are all secondary inclusions, since they frequently form as planar sets in annealed fractures. Th TOT ranged from 169 to 283°C to liquid (L). A



Plate 3.25 - Muscovite bearing pegmatitic quartz vein cross-cutting the Foxdale granite (GR 278 774).



PLATE 3.26 - Syn-F2 quartz vein from Calf Sound (GR 173 667).

limited number of CO₂ bearing inclusions were present. They have low salinities and decrepitate at > 300°C.

Table 3.4 - Trapping temperature estimates for hydrostatic and lithostatic pressure at depths of 1, 5 and 10km. The density of the Manx Slate was taken as 2.74g/cm³ (as for the Skiddaw Slate) and pressure corrections were taken from Potter II (1977). Values are given for the highest Th TOT populations of the main types of inclusions found in each sample.

Sample	Th TOT	NaCl	TT (1)	5	10km)
<u>Foxdale</u>	300°C	3.0 wt%			
Hydrostatic P			308	347	393°C
Lithostatic P			324	429	553°C
<u>Foxdale</u>	283°C	5.8 wt%			
Hydro			288	320	366°C
Litho			292	401	553°C
<u>Dhoon</u>	365°C	2.8 wt%			
Hydro			372	428	480°C
Litho			390	517	652°C
<u>Dhoon</u>	264°C	5.1 wt%			
Hydro			268	301	345°C
Litho			282	377	444°C
<u>Calf Sound A</u>	305°C	- wt%			
Hydro			312	352	399°C
Litho			328	435	562°C
<u>Calf Sound A</u>	249°C	2.5 wt%			
Hydro			253	289	330°C
Litho			273	363	478°C
<u>Calf Sound B</u>	348°C	- wt%			
Hydro			355	404	457°C
Litho			373	493	626°C
<u>Calf Sound B</u>	217°C	17.2 wt%			
Hydro			229	265	308°C
Litho			250	339	400°C

Table 3.5 - Microthermometric results for fluid inclusions from the IOM.

Sample	1	2	3	4	5	6	7	8	9	10	11	12	Remarks
<u>FOXDALE</u>													
A	A	1.6	0.88	-	-	-	191-L	98.4	1.6	0.0	0.95	6	
B	A	3.0	0.74	4.0	28.7-C	0.47	300-L	66.2	1.8	32.0	0.50	1	
C	C	17.0	1.03	-	-	-	172-L	83.0	17.0	0.0	0.95	3	Th TOT = Decrepitate
D	E	7.0	0.87	-	-	-	232-L	93.0	7.0	0.0	0.95	6	
E	D	23.5	1.00	-	-	-	258-L	76.5	23.5	0.0	0.95	1	
F	E	5.0	0.89	-	-	-	209-L	95.0	5.0	0.0	0.95	4	
G	-	5.8	0.77	-	-	-	283-L	94.2	5.8	0.0	0.95	1	
<u>DHOON</u>													
A ₁	E	4.5	0.86	-	-	-	200-L	95.5	4.5	0.0	0.95	6	A ₁ , A ₂ , A ₃ treated
A ₁	C	5.0	..	-	-	-	..	95.0	5.0	0.0	0.95	2	as same population
A ₃	B	4.6	..	-	-	-	..	95.4	4.6	0.0	0.95	9	for Th TOT.
B	B	2.8	0.8	-	21.3-V	0.20	324-V	36.4	1.1	62.5	0.60	1	
B	B	2.8	0.11	-	12.4-L	0.83	365-V	16.0	0.5	83.5	0.60	1	
C	B	5.1	0.83	-	-	-	264-L	94.9	5.1	0.0	0.95	4	
D	A	6.2	0.94	-	-	-	183-L	93.8	6.2	0.0	0.90	3	
<u>CALF</u>													
<u>Sound A</u>													
A ₁	C	16.5	1.00	-	-	-	183-L	83.5	16.5	0.0	0.95	14	
A ₂	D	12.3	0.97	-	-	-	179-L	87.7	12.3	0.0	0.95	4	
B	C	-	0.94	-	-	-	-	10.0	0.0	90.0	0.10	1	CO ₂ vapour
*C	C	15.8	0.95	-	-	-	220-L	84.2	15.8	0.0	0.95	4	
D	F	3.8	0.93	-	-	-	163-L	96.2	3.8	0.0	0.95	2	
E	F	2.5	0.83	-	-	-	249-L	97.5	2.5	0.0	0.95	1	
F	-	-	-	-	-	-	305-L	-	-	-	0.95	1	Nitrogen
<u>CALF</u>													
<u>Sound B</u>													
*A	C	17.2	0.96	-	-	-	217-L	82.8	17.2	0.0	0.95	18	Some salt crystals
B	-	-	-	-	-	-	348-L	-	-	-	0.70	9	Nitrogen
C	-	-	-	-	-	-	299-L	-	-	-	0.95	2	..
D	-	-	-	-	-	-	238-L	-	-	-	0.90	2	..
E	-	-	-	-	-	-	348-V	-	-	-	0.30	1	..

Key to table 3.5: Microthermometry Results

1. Salt System - A = H₂O-NaCl-KCl B = H₂O-KCl
C = H₂O-NaCl-CaCl D = H₂O-CaCl
E = H₂O-NaHCO₃ - NaCO₂ F = H₂O-NaCl-MgCl
2. Wt% NaCl equivalent present in the aqueous solution.
3. Density of the H₂O-NaCl liquid (g/cm³).
4. Mole% CH₄ in the CO₂ phase.
- 4a. Mole% CO₂ , for the whole FI wafer, determined by fluid extraction. The result is an average for the whole sample.
5. Homogenisation temperature of two CO₂ phases to liquid (L), vapour (V) or critical behaviour (C) (°C).
6. Density of CO₂ phase (g/cm³).
7. Total homogenisation temperature of the inclusion to liquid, vapour or critical (°C).
- 8 to 10. Estimated composition of the fluid phase in terms of the components H₂O-NaCL-CO₂ within the whole inclusion.
8. Wt% H₂O.
9. Wt% NaCl equivalent.
10. Wt% CO₂.
11. Degree of fill (F) of liquid phase in two phase inclusions, aqueous phase in three phase inclusions (1.00 = 100%).
12. Number of inclusions studied.

Dhoon - This has similar inclusion populations to Foxdale. There are many irregular and negative crystal inclusions with mean salinities ranging from 2.8 to 6.2 wt% NaCl equiv., and Th TOT ranging from 167 to 276°C to L. The few CO₂ bearing inclusions seem to contain appreciable CH₄ (from Tm CO₂, see section 2.3.5), and homogenise at up to 365°C.

Calf Sound A - This sample contained mainly small aqueous inclusions found as irregular clusters or in planes. These have mean salinities ranging from 2.5 to 16.5 wt% NaCl equiv., and ThTOT ranging from 156 to 249°C to L. CaCl is an important part of the salt component. One CO₂-CH₄ inclusion was observed, as well as one nitrogen bearing inclusion, which homogenised at 305 °C to L. N₂ was identified by the fact that no freezing or change in phase proportions occurred on cooling to -181°C (Bottrell et al., 1988). Some inclusions contain rhombic crystals, possibly of calcite. A number of liquid only, dark brown inclusions decrepitated at <200 °C. These probably contain higher hydrocarbons (HHC) (Roedder, 1984; Shepherd et al., 1985).

Calf Sound B - The generic similarity of Calf Sound B to Calf Sound A was apparent. Aqueous inclusions had a mean wt% NaCl of 17.2, and Th TOT ranged from 195 to 247°C. N bearing inclusions were common with variable phase proportions. Th TOT ranged from 227 to 375°C homogenising to liquid, with a value of 348 °C to vapour (V) in one sample. A similar set of HHC inclusions to Calf Sound A were present.

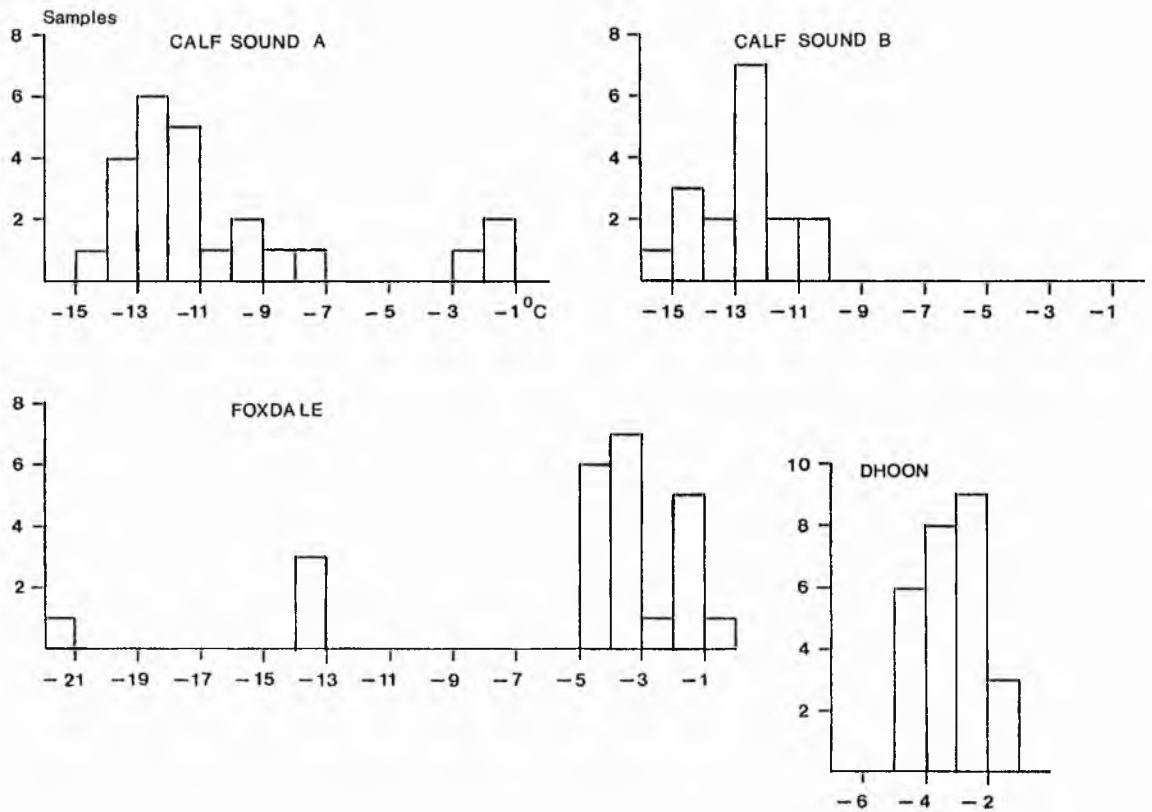


Fig. 3.16 - Histograms from IOM fluid inclusion samples. Numbers of analyses are plotted against temperature ($^{\circ}\text{C}$) for the last melt of ice ($\text{T}_m \text{ H}_2\text{O}$) in the fluid inclusions analysed.

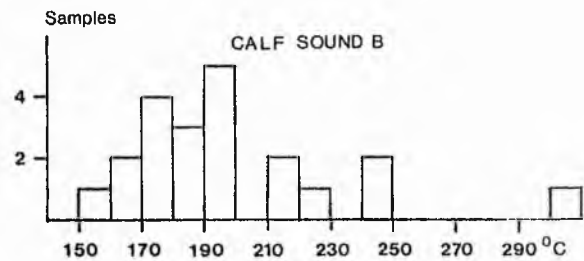
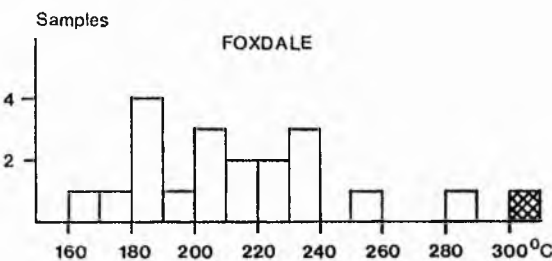
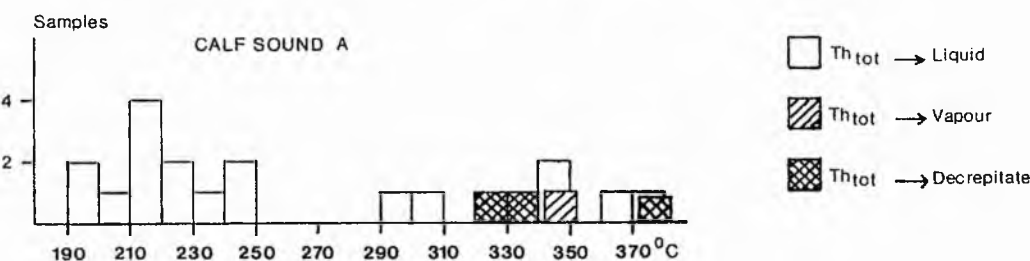
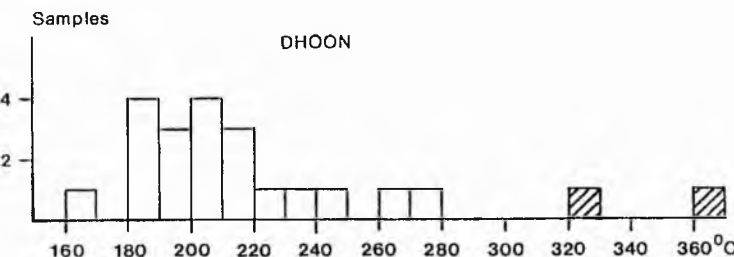


Fig. 3.17 - IOM fluid inclusion samples. Number of analyses versus temperature of total homogenisation (Th TOT) in fluid inclusions analysed. Inclusions homogenise to the liquid or vapour phase, or decrepitate before homogenisation is achieved.

3.10.3 Discussion

Granites - The fluids involved in late pegmatitic veining in the granites are appreciably different from those involved in syn-F2 country rock veining, though the two sets of veins have similar ages. CO₂ bearing inclusions are the earliest preserved and would therefore indicate the nature of the fluids circulating as the granite degassed on cooling. These are high CO₂, low salinity fluids with a minimum trapping temperature of 365°C in the Dhoon granite. Table 3.4 gives pressure corrected trapping temperatures applicable for a range of depths the granite could have degassed at. Low to medium salinity aqueous fluids, with no obvious salinity evolution, circulated once the CO₂ bearing inclusions had been trapped.

F2-Vein Quartz - Three distinct inclusion populations could be recognised. These are N₂ bearing, aqueous and HHC inclusions. Th TOT and decrepitation temperatures suggest that the inclusions were trapped in the order given above. N₂ inclusions homogenise at up to 348°C, which gives a minimum trapping temperature for syn-D2 vein quartz. The trapping temperature could easily be >400°C (see table 3.4). Dorobek (1989) found inclusions in a deformed sedimentary sequence, with well constrained paleotemperatures of c.150°C, homogenised at between 200 and 300+°C. He attributed this to the syn-deformational migration of hot brines, from a higher grade thrust zone c.100km from the sedimentary basin. In the IOM the quartz

precipitating fluids need only be derived from deeper in the sedimentary pile to have higher trapping temperatures.

The existence of N₂ bearing and aqueous inclusions coexisting in vein quartz in slates has only recently been documented. Bottrell et al. (1988) made a study on vein quartz from Llanbedr Formation slates in N. Wales. From microthermometry and Laser Raman analysis they concluded that N₂ was derived from organic matter in the sediments, and subsequently released to the fluid phase during metamorphism. Phase equilibrium calculations show that slate mineral assemblages can be in equilibrium with either N₂ or aqueous fluid depending on redox conditions.

The presence of HHC inclusions is puzzling. The HHC rich fluids must have circulated at a late stage, being trapped along annealing fractures, though there is no obvious source for the fluids. The Manx Slates have been subjected to too high a temperature of metamorphism for the preservation of HHC's (Frey et al., 1980a). HHC's could have been drawn into the circulation system from a higher level.

3.10.4 Conclusions

Fluids circulating during the cooling of the granites evolved from H₂O-CO₂-NaCl to H₂O-NaCl fluids. There is no thermometric or petrographic evidence to indicate the nature of country rock involvement. However in the syn-D2 veining it is most likely that N₂ and saline aqueous fluids were derived from the breakdown of organic matter in the sediments, and also from metamorphic dehydration processes.

Homogenisation temperatures are consistent with fluids migrating from a deeper, hotter source area. HHC fluids could have been drawn into the circulation system from a higher sedimentary source.

3.11 SYNTHESIS

3.11.1 Aim

In this section the different lines of investigation are brought together to produce a geological history of the Manx Group, IOM.

3.11.2 Introduction

A new interpretation of the metamorphic and structural history of the IOM is presented below.

3.11.3 Geological History

1. Sedimentary Environment - The turbiditic metasediments of the Manx Group are dominated by mudstones, with lesser amounts of siltstones and sandstones. Common sedimentary features are slump-breccias and slump folds. Pre-metamorphic "greenstone dykes" are found throughout the succession.

2. D1 - Subsequent to lithification, low-temperature diastathermal metamorphism occurred. Chlorite and chlorite-muscovite porphyroblasts grew before and during S1 cleavage development. Peak metamorphism was attained pre- or syn-D1, depending on the intensity of the cleavage overprint, and ranged from anchizone to high epizone in what was probably a low pressure environment. It was associated with the common occurrence of 2M, muscovite, paragonite, mixed-layer paragonite/muscovite, chlorite and quartz, and lesser amounts of albite, pyrophyllite and 1Md illite. Deformation took the form of tight to isoclinal folds with a Caledonian

trend and pervasive cleavage. Associated with this folding is a phase of quartz veining.

3. Niarbyl Fault Zone - Sinistral transcurrent faulting post-dated the main D1 deformation. This produced a 100m wide belt of mylonitised rocks trending ESE/WNW. These rocks show quartz segregations, folding and Riedel fractures. Within this belt, the cold re-working of the slates resulted in an induced reduction in metamorphic grade, to high diagenetic to low anchizone illite crystallinity values.

4. Granites - The intrusion of the Foxdale and Dhoon granites occurred post D1 to syn-D2. Much of the epizone grade metamorphism, along the central axis of the island, is due to contact heating from these granites, which seem to form extensive sub-surface bodies. Contact metamorphism resulted in the growth of porphyroblastic ilmenite, biotite, garnet, muscovite, staurolite, cordierite and chloritoid. Fluid inclusions in late pegmatitic veins indicate a minimum vein formation temperature of 365 °C. Fluids evolved from the CO₂-H₂O-NaCl system to the H₂O-NaCl system.

5. D2 - The second phase of deformation resulted in a crenulation cleavage. This is not pervasive, but is common to fold hinges. Folding is open to tight, plunges gently to the E or W with shallow dipping axial planes. Quartz veins are mainly confined to fold hinges. Fluid inclusion studies on vein material give a minimum syn-D2 vein formation temperature of 348 °C. N₂, found in inclusions, was derived

from the breakdown of organic matter in the sediments. Saline aqueous inclusions appear to have formed later. HHC rich inclusions may have been derived by circulation from overlying sediments.

6. Post-D2 - Within the NFZ the shear zone was crumpled on a macroscopic scale prior to brittle thrusting from the NW. This was associated with minor folding, duplexing and quartz veining. Regional quartz and dolomite veining also occurred.

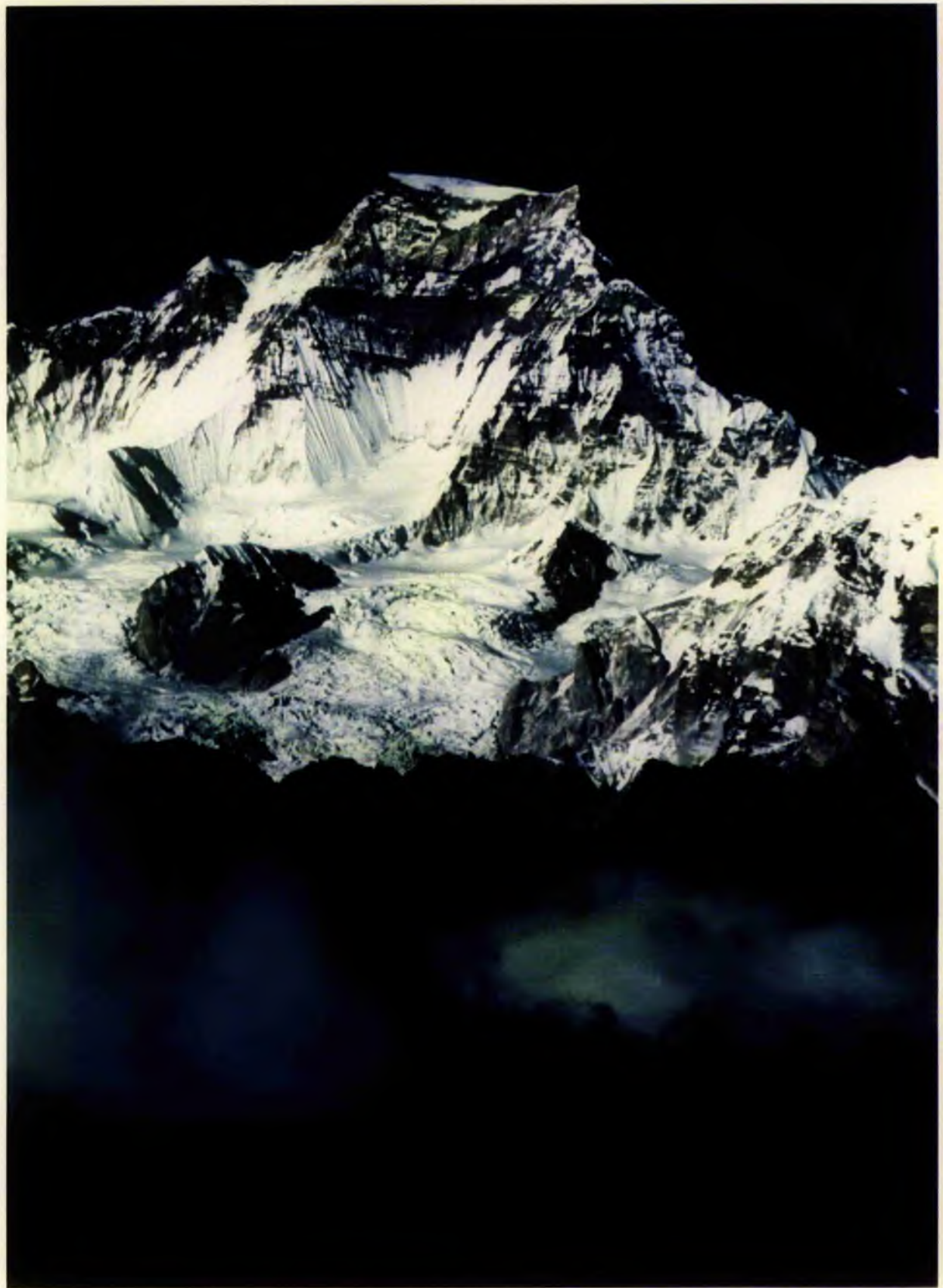
7. D3 - Late deformation took the form of shallow plunging open F3 folds with steep N/S trending axial planes.

8. D4 onwards - Late structural features include kink bands and small transcurrent to normal faults at Niarbyl. Regional features include less common transcurrent to normal faults, kink bands, tension gashes, and quartz and dolomite veins showing brecciation in places.

3.11.4 Conclusions - The Anchizone-Epizone Transition on the Isle of Man

In the Manx Slates the anchizone-epizone metamorphic transition is associated with regional burial or diastathermal metamorphism with a D1 deformational overprint. The growth of primary white mica started subsequent to lithification and continued until the end of S1 cleavage development. The anchizone/epizone transition is defined by the disappearance of 1Md white mica, which is replaced by 2M₁ white mica (see section 2.2.8). In the Manx Slates this occurs at Hbrel 154, and is associated with the

common occurrence of 2M, mica, paragonite, paragonite-muscovite and chlorite. Lesser mineral phases at the anchizone-epizone transition are pyrophyllite and corrensite. b_o values are suggestive of low pressure conditions, though may be anomalously low due to the chemical control of abundant paragonite. Syn-D2 vein quartz contains N₂ bearing fluid inclusions derived from the breakdown of organic matter in the sediments. Saline aqueous fluid inclusions dominate later. A minimum trapping temperature estimate of 348°C, for syn-D2 vein quartz, lies at the high end of temperature estimates for the anchizone-epizone transition (see section 2.2.14).



Frontispiece 4 - Looking north towards Gyachung Kang (7922m). The bulk of the mountain is composed of north dipping Tibetan Slab metasediments. Near the summit a slightly discordant leucogranite sheet cross-cuts the succession.

CHAPTER 4

GLEN ESK

4.1 INTRODUCTION

4.1.1 Aim

The aim of this chapter is to investigate the anchizone-epizone transition in a transpressive shear zone.

4.1.2 Introduction

The river North Esk, in Angus, was chosen as a suitable field area for an illite crystallinity study of the anchizone to epizone transition (see Fig. 4.1). Rocks of the Highland Border Complex (HBC) and the Dalradian are exposed along a nearly continuous river section of >2km (see Fig. 4.2). They show a change in grade from sub-greenschist HBC rocks in the S to biotite and higher grade rocks in the N. This rapid variation in grade provides an opportunity to test the sensitivity of illite crystallinity measurements. The study area was also attractive for another reason: The HBC contains spilites whose alumina silicates can be used as an independant metamorphic grade indicator. Understanding the tectonic and metamorphic relationships between the Dalradian and HBC is a key problem in explaining the Lower Palaeozoic history of Scotland. It was hoped that a metamorphic study of these rocks in their tectonic context would help to elucidate this problem.

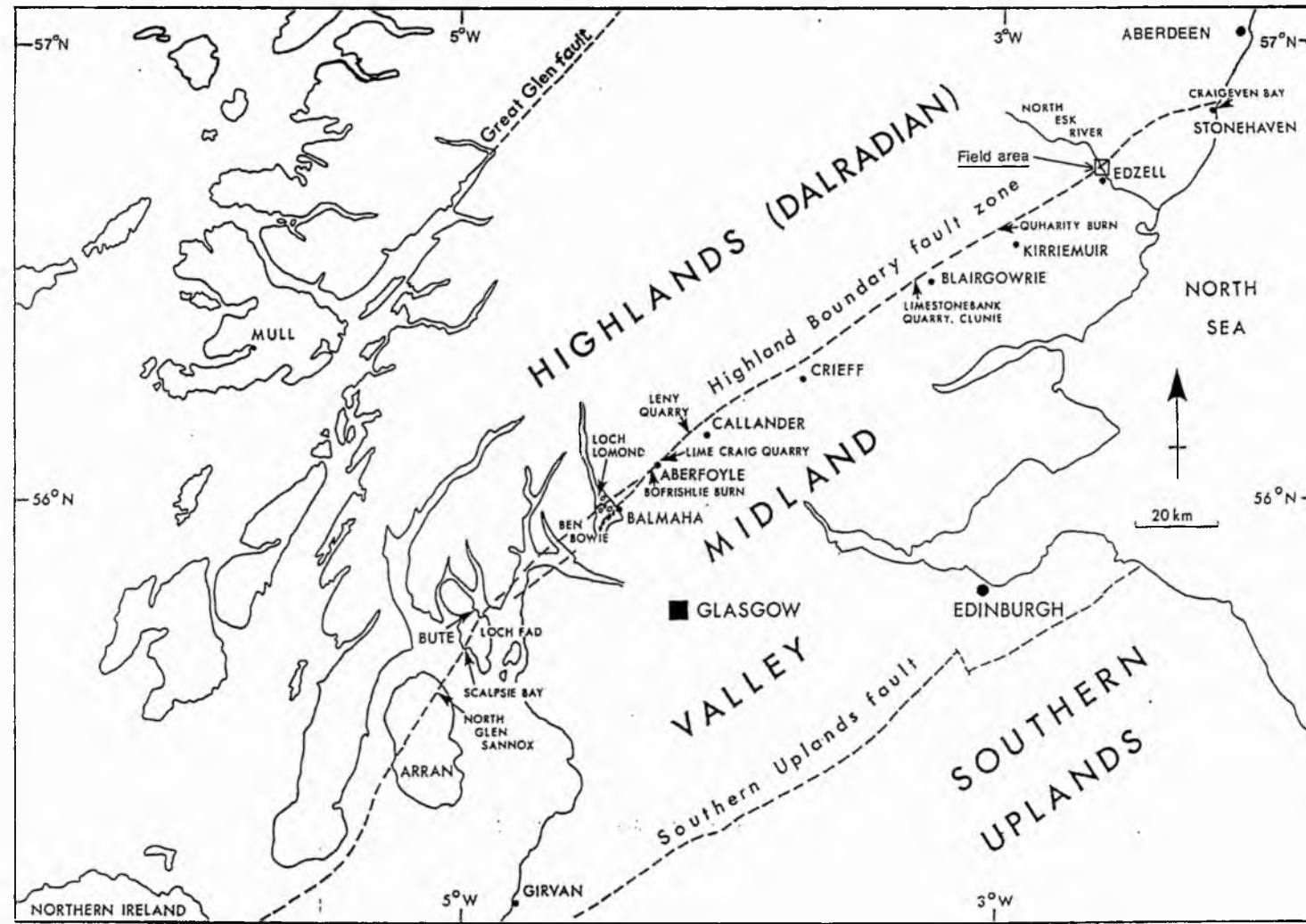


Fig. 4.1 - Outline map showing locations of Highland Border successions described in the text (after Curry et al., 1984).

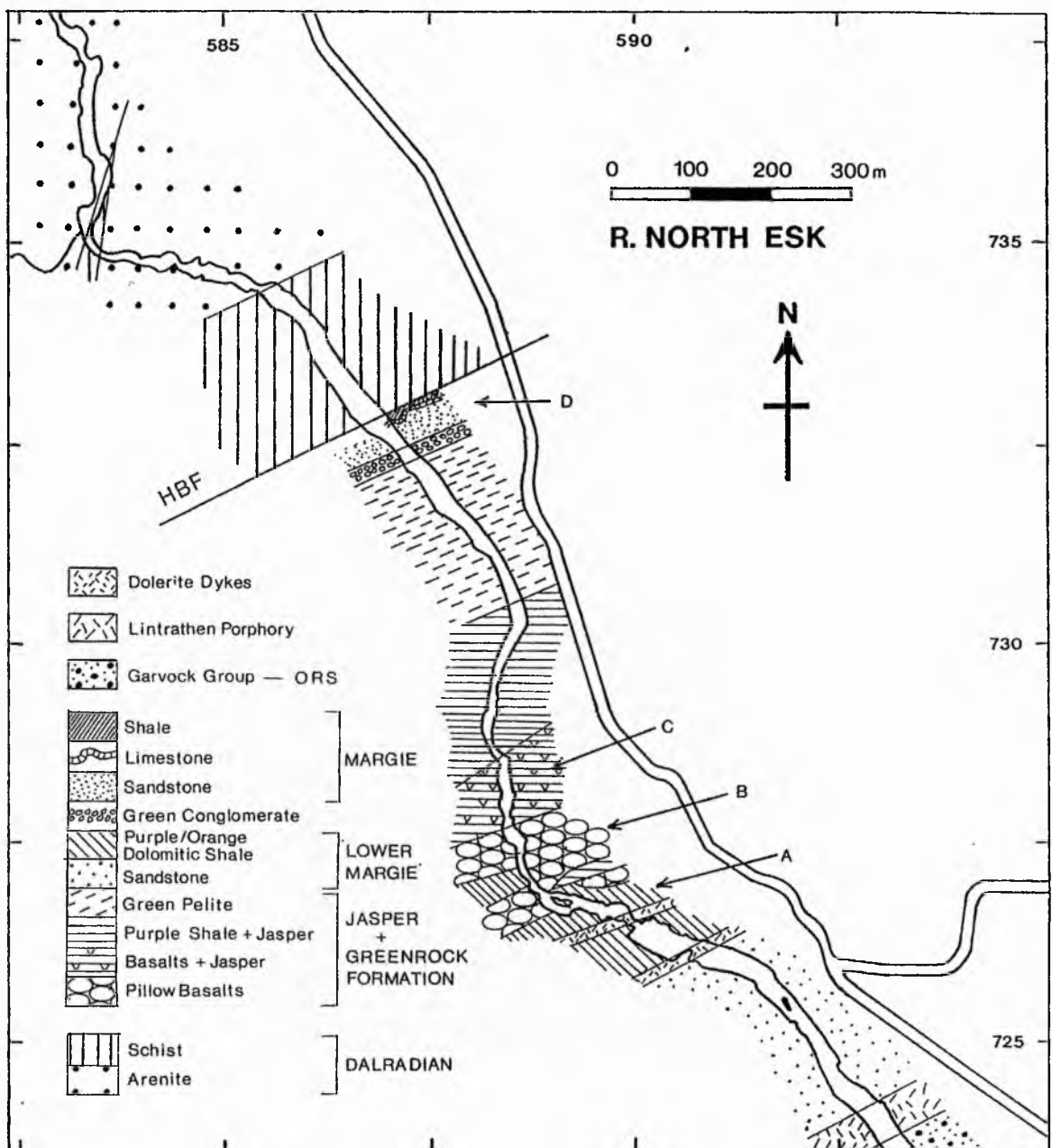


Fig. 4.2 - Geology of the Burn Section, Glen Esk. A, B, C and D are the locations of detailed maps presented in Figs 4.5A, B, C and D. HBF = Highland Boundary Fault.

4.2 GEOLOGICAL BACKGROUND

4.2.1 History of Research on the HBC

Attempts at unravelling the complex geological history of the HBC gained momentum at the start of the twentieth century with Barrow's work at Glen Esk. He named the main units and tentatively placed the HBC in the Ordovician (Barrow, 1901). He later opted for a Cambrian age on the basis of fossil evidence (Barrow, 1912). Jehu and Campbell (1917) re-affirmed an Ordovician age on further fossil evidence. Since then authors have favoured Cambrian (e.g. Henderson and Robertson, 1982) or Ordovician ages (e.g. Curry et al., 1984) for the HBC depending on whether they want to include the HBC within the Dalradian (e.g. Anderson 1947), or keep it separate (e.g. Longman et al., 1979). The controversy over the age continued with the discovery of Lower Cambrian trilobites and inarticulate brachiopods in the Leny Limestone (Pringle, 1939), and the later discovery that Jehu and Campbell had wrongly identified fossils from Aberfoyle (see Curry, 1986 for discussion). The only reliably dated unit, the Leny Limestone, could be part of the Dalradian or the HBC (see section 4.2.2).

With this uncertainty in the fossil evidence more recent efforts were concentrated on the structural affinities of the HBC. Both Kennedy (1958) and George (1960) tried to clarify the timing and senses of fault movement on the HBF. In the sixties detailed structural interpretations of the Grampian Orogeny were being made

(e.g. Harte and Johnson, 1969). Harte and Johnson's model involved five phases of deformation, the Tay Nappe was emplaced with F1 folding, and peak metamorphism was attained prior to D3. Johnson and Harris (1965) put forward the model that the Leny and Margie Limestones were formed before the 'post-Arenig' formation of the Tay Nappe. They later correlated structural elements in the Jasper and Greenrock Series, and Dalradian (Johnson and Harris, 1967). Harris (1969) took the age of the Leny Limestone as evidence that the Tay Nappe formed at the Highland Border during or after the Lower Cambrian.

Further developments in the interpretation of the HBC resulted from the constraining of the phases of deformation in the Dalradian with radiometric ages. Radiometric dates on igneous intrusions and phases of metamorphism showed that the main events (D1 to D3) of the Grampian Orogeny occurred between 510 and 480Ma (Dewey and Pankhurst, 1970). A range from pre-590 (Rodgers et al., in press) to 470Ma is currently more appropriate. To be part of the Dalradian, the HBC would have to be of Precambrian age or older to accommodate these events. At the time, this scenario was not inconsistent with the available palaeontological evidence.

The most significant recent developments have involved the acquisition of fresh palaeontological data, and an increased understanding of the significance of major transcurrent faults in plate tectonics. Downie et al. (1971) found achritarchs and chitinozoa in the Jasper and Greenrock Series at Glen Esk which they suggested had an Early Ordovician (Tremadoc-Llanvirn) age. Curry et al.

(1982) found an undoubted Early Arenig silicified fauna in the Dounans Limestone. At Bofrishlie Burn, Curry et al. (1984) found acritarchs of Llanvirn to Llandeilo age in a siltstone. Burton et al. (1984) found a chitinozoan assemblage of Mid-Caradoc to possibly Early-Ashgill age in the Margie Limestone at Glen Esk. The well constrained faunas in the Leny, Dounans and Margie Limestones show them to be three separate limestones, and that the HBC is not part of the Dalradian Supergroup as suggested by Henderson and Robertson (1982).

Recent palaeontological work by Whelan (1988) has resulted in the recovery of faunas from a number of lithologies in the HBC at Glen Esk. Chitinozoans and acritarchs of Llanvirn to Llandeilo age were found in shales below the Margie Limestone. In the Margie, south of the Jasper and Greenrock Series, a chitinozoan age of Llanvirn to Ashgill was obtained. Investigations were also made at Leny Quarry. Though no new age was obtained for the Leny Limestone, two species of *torellella* were recovered from another limestone. These date it to the Tommotian-Attabanian (late Precambrian-earliest Cambrian). This limestone and the surrounding detrital sediments are of uncertain affinities.

With the development of the 'Suspect Terranes' concept the relative proximities of the Dalradian, HBC and ORS has become an important source of discussion. Papers by Bluck (1983, 1984, 1985) and Curry et al. (1984) bring together many of the salient points. During the Ordovician, while the HBC was being deposited, the Dalradian terrane

was being uplifted with an erosion surface inclined to the SE (Dempster, 1984). Around 10-15km of sediments were eroded between 520 and 410Ma. It would be expected that much of this sediment, dispersed to the SE, would be deposited in the area of the HBC. The fact that there is no metamorphic debris in the HBC indicates that the HBC was remote from the Dalradian at least until the end of the Ordovician.

The Lower ORS lies unconformably on both the Dalradian and the HBC. This shows that major uplift in the Dalradian was completed by c.400Ma. The conglomeratic detritus was dispersed from both the north and south into the Strathmore Syncline. Conglomerates from both sources are dominated by volcanic, hypabyssal and plutonic clasts as well as metaquartzite and vein quartz clasts. Arbuthnot Group volcanics, in the Lower ORS, near Stonehaven, have been dated as Siegenian (c.401-394Ma), (Thirlwall, 1983a). The Stonehaven Group conglomerates, at the base of the Lower ORS, are considered of Pridoli (Upper Silurian) age, but could be as old as Llandovery (Thirlwall, 1981). Dunnottar Group conglomerates, sandwiched between the Stonehaven and Arbuthnot Groups are therefore of pre-Siegenian age. The Dunnottar Group forms two main lithological groups, one dispersed from the north, and the other from the south and east. The latter are derived from a hypothetical Midland Valley source (Bluck, 1984; Haughton, 1988). The former contains clasts of clear Dalradian origin (Haughton pers comm.). These include two mica and biotite granite clasts which are very similar

geochemically and isotopically to those of NE Scotland. Two mica granite clasts are Ordovician in age, and similar to the Aberdeen granite, while biotite granite clasts, similar to the Hill of Fare granite, date in the Upper Silurian. In addition to granite clasts there are jaspers and greenstones of likely HBC origin, and greenschist facies psammites derived from the Southern Highland Group with a cooling age of 460Ma. These conglomerates show that the Dalradian and HBC were in contact by the start of the Siegenian, and shedding debris into the Midland Valley.

The Upper ORS lies unconformably on the Lower ORS in scattered outcrops in the Midland Valley. In the Clyde area the sediments were dispersed from the SW along the Midland Valley. The conglomerates are dominated by vein quartz with important contributions from quartzites and greenschists. Again the provenance is uncertain. A breccia-conglomerate, <100 thick, with a south-easterly dispersal, is found at Balmaha. This fines upwards into a Carboniferous marine transgression sequence. The conglomerate contains slate and greywacke clasts of local Dalradian derivation. This shows that fault activity on the HBF was limited by Late Devonian-Early Carboniferous times, and that uplifting of the Dalradian had nearly finished.

4.2.2 Stratigraphy

The stratigraphy of the Dalradian and HBC has been treated by various authors as either a continuous succession (e.g. Henderson and Robertson, 1982), or as two

entirely different successions with independent origins (e.g. Curry et al., 1984). The detailed stratigraphy within each succession is summarised in Fig. 4.3 along with that of the Old Red Sandstone (ORS) of the Midland Valley. This stratigraphical column includes the most recent palaeontological and isotopic information.

A. Dalradian - The Dalradian Supergroup is composed of deformed and metamorphosed late Precambrian to Cambrian sediments and volcanics. Detailed stratigraphies of the Dalradian of Scotland can be found in Anderton et al. (1979) or Anderton (1985). The Southern Highland Group (SHG), the youngest Dalradian group, is exposed next to the HBC along its length. Lowest Cambrian (?) acritarchs in the Tayvallich Limestone (Anderton et al., 1979), at the top of the underlying Argyll Group, tentatively put the SHG in the Cambrian. The age of the top of the SHG is as yet unclear. The Ben Ledi Grits and Slates lie near the top of the SHG and are the youngest confirmed Dalradian rocks, pre-dating the start of regional deformation. Younger rocks lie next to the HBC and have uncertain affinities. The existing date for the start of regional deformation has very recently been revised by a post-D2 U/Pb age for the Ben Vuirich granite of 590 + or - 2Ma (Rodgers et al., in press). Because the Ben Vuirich granite post-dates the D2 deformation of the Dalradian, a date of 590Ma pushes back the start of Dalradian metamorphism and the age of the youngest Dalradian into the Precambrian. The Leny Limestone, containing early Cambrian trilobites (Downie et

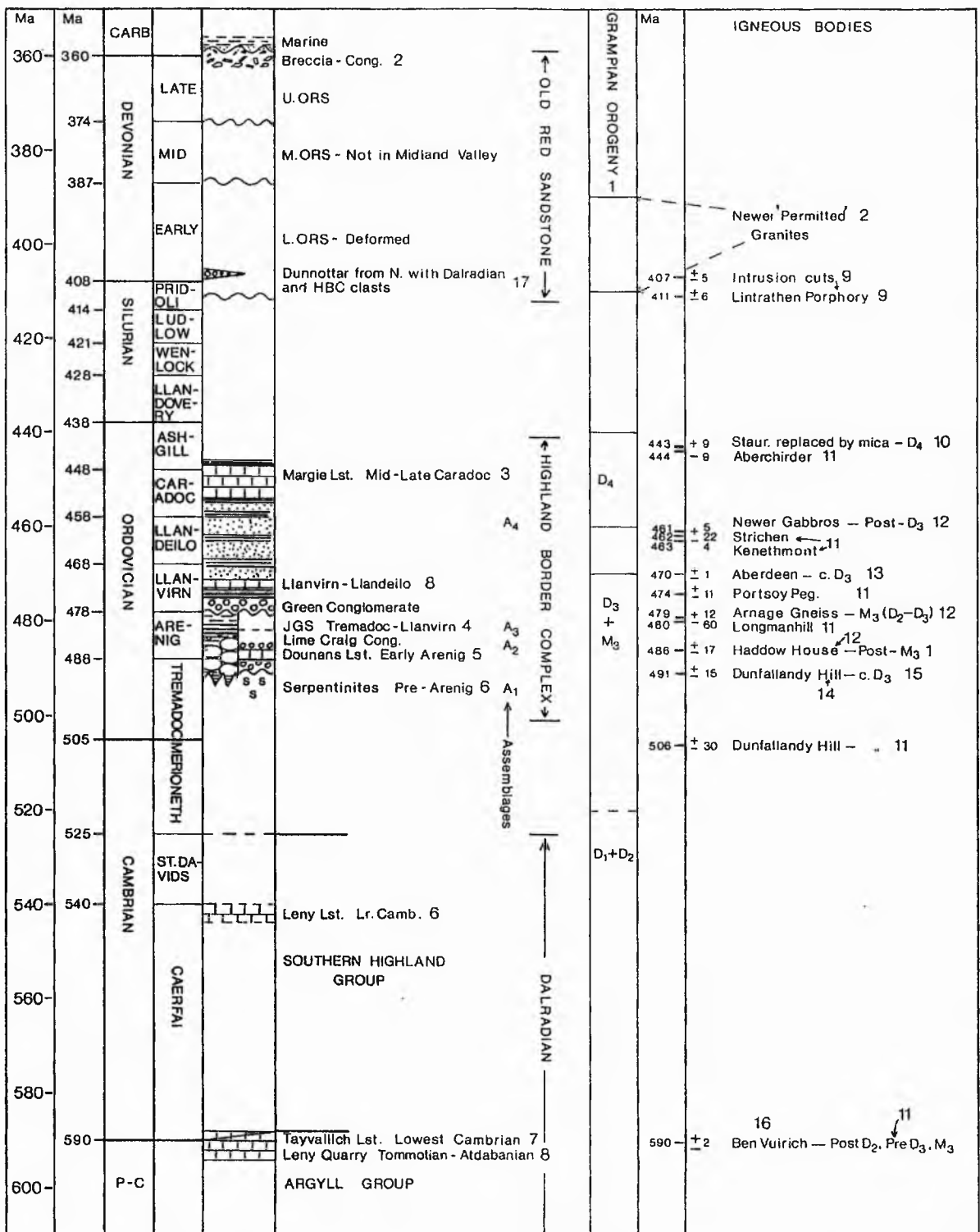


Fig. 4.3 - Stratigraphy of the Dalradian, Highland Border Complex and Old Red Sandstone. Isotopic ages constraining Dalradian events are presented along with references listed on table 4.1.

Table 4.1 - References appropriate to Fig. 4.3.

1. - Harte et al., 1984
2. - Bluck, 1984
3. - Burton et al., 1984
4. - Downie et al., 1971
5. - Curry et al., 1982
6. - Curry et al., 1984
7. - Anderton, 1985
8. - Whelan, 1988
9. - Thirwall, 1983a
10. - Dempster, 1983 (in Harte et al., 1984)
11. - Aftalion et al., 1984
12. - Pankhurst, 1970
13. - Kneller and Aftalion, 1987
14. - Pidgeon and Pankhurst, 1976
15. - Bradbury et al., 1976
16. - Rodgers et al., in press
17. - Haughton, pers comm.

al., 1971; Curry et al., 1984) could be part of the Dalradian or the HBC (Curry, 1986).

The sediments of the SHG, were deposited as quartz-feldspathic arenites, rudites, black shales and minor limestones (Henderson and Robertson, 1982). Blue quartz grains indicate a high grade source area for some of the material (Sutton and Watson, 1955).

B. Highland Border Complex - The HBC is a tectonically disrupted succession strung out along the length of the Highland Boundary Fault (HBF) in lenticular masses up to 2km across. Units can be correlated along the length of the HBC outcrop. The HBC has been divided into 4 assemblages separated by tectonic boundaries or unconformities (Bluck, 1984; Curry et al., 1984).

Assemblage 1 - Serpentinised ultra-basic rocks, interleaved with gabbroic and plagiogranitic slivers (Bluck, 1984), are believed to be the oldest rocks in the HBC. Serpentinite clasts, sometimes rounded (Henderson and Fortey, 1982), occur in a carbonate rich rock at Balmaha. This, or an associated carbonate at Lime Craig Quarry near Aberfoyle, has yielded an Early Arenig trilobite fauna (Curry et al., 1982). This implies that all or some of the HBC serpentinites are Early Arenig or older (Curry et al., 1984).

Assemblage 2 - The altered Dounans Limestone and conglomeratic rocks at Lime Craig Quarry, and serpentinite conglomerate at Balmaha are grouped together as an Early

Arenig assemblage which may be in unconformable contact with assemblage 1 (Curry et al., 1984, Fig. 9).

Assemblage 3 - At Glen Esk this assemblage is dominated by the "Jasper and Greenrock Series" (Barrow, 1901). This is a sequence of mafic volcanic rocks including sheared pillow lavas and more massive lavas. These are interbedded with red and black cherts, siliceous siltstones and mudstones. Highly sheared red, orange and black siltstones and mudstones form intercalations up to 6m thick (Henderson and Robertson, 1982). At Bofrishlie Burn, Aberfoyle, black shales, cherts and quartz-wacke turbidites have yielded a brachiopod and chitozoan fauna of Llanvirn-?Llandeilo age (Curry et al., 1984), with an unknown lower age limit. The relationship of this assemblage to assemblage 2 is also unclear, the boundary being either tectonically disrupted or unseen.

Assemblage 4 - This assemblage is represented at Glen Esk by the "Upper Margie" unit. A basal 'green conglomerate', containing basic and ultra-basic clasts, unconformably overlies the Jasper and Greenrock Series. This grades northwards into orange stained quartz-arenites. Within 15m of the fault bounded Dalradian, black and grey shales host a dark-grey limestone. A chitinozoan fauna of Mid to Late Caradoc or possibly Ashgill age, has been found (Burton et al., 1984).

Elsewhere assemblage 4 is represented by the "Loch Lomond clastics" (Balmaha) and the Achray Formation (Aberfoyle). These are dominated by sandstones with minor

shales present. A siltstone within the Achray sandstone at Lime Craig quarry has yielded blackened and deformed chitinozoa of Llanvirn-?Llandeilo age, as well as light-coloured, undeformed Caradoc-Ashgill fossils. This implies that the older fossils were derived from a low-temperature metamorphic source eroded before the Caradoc (Curry et al., 1984).

The "Lower Margie" unit, at Glen Esk, lies to the south of the Jasper and Greenrock Series. It is dominated by quartz-arenites and lutites. Closer to the Jasper and Greenrock Series, north of two dolerite dykes, purple-orange shales with quartz and carbonate segregation banding dominate. The age of this unit has not yet been established though many authors (e.g. Henderson and Robertson, 1982) have followed Barrow (1901) in including it in with the Upper Margie.

C. Old Red Sandstone - In the Midland Valley the Lower ORS lies unconformably on the HBC (Curry et al., 1984). The Lower ORS ranges in thickness from c.1.5km in Arran to c.9km at Stonehaven (Bluck, 1984). There is isotopic and fossil evidence to suggest that its deposition started in the Silurian. The 'Lintrathern porphyry', an ignimbrite according to Paterson and Harris (1969) and Watson (1984), has been dated at 411 + or - 6Ma (Thirlwall, 1983b). This overlies the Dalradian, but is also interbedded with the Lower ORS in the Strathmore Syncline (Thirlwall, 1983a). The lavas of the Arbuthnot Group, in the middle of the Lower ORS, are cut by an intrusion dated at 407 + or - 5Ma putting them in the Upper Silurian.

Fossil evidence tends to contradict these ages. Westoll (1977) placed the Stonehaven Group, at the base of the Lower ORS, in the uppermost Silurian on the basis of fossil fish, and the rest of the Lower ORS in the Lower Devonian (see Fig. 4.3).

North of the HBF outliers of the Lower and Middle ORS lie unconformably on the Dalradian. These sediments have been dated as basal Dittonian (Lower Devonian) or younger by Westoll (1977), but again overlying lavas have been dated at c.410Ma in the Pridoli (Upper Silurian), by Clayburn et al. (1983).

The Middle ORS is absent in the MV while the Upper ORS lies unconformably on the Lower ORS which was deformed during the Middle Devonian. The lack of plant spores to delineate the Devonian/Carboniferous boundary makes it possible that some of the Upper ORS lies in the Lower Carboniferous (Anderton et al., 1979, p117).

4.3 FIELDWORK

4.3.1 Sample Collection

Samples were collected at c.10m intervals along a near continuous river section of 1700m on the N. Esk, Angus. 142 samples were collected for a illite crystallinity study. A further 13 orientated samples were collected for fabric analysis, and 4 samples for petrographic study (see Appendix 4.1). Of the 159 samples, 70 were collected within the Dalradian adjacent to the North Esk Fault and the rest were collected from the HBC.

4.3.2 Data Collection

The HBC, at Glen Esk has been mapped intensively a number of times throughout the history of its study (for example Barrow, 1901; Johnson and Harris, 1967; Henderson and Robertson, 1982). This persistant attention reflects the importance and complexity of the area. The primary objectives of the present mapping have been to put the HBC in stratigraphical context and to compare the structural development of the HBC with that of the adjacent Dalradian. More recently, interpreting the amount and sense of fault movement on the HBF has become a prime research target. To this end field measurements were made on folds, and brittle and ductile fabrics in the HBC (see Fig. 4.4). A petrographic study of micro-fabrics was also made.

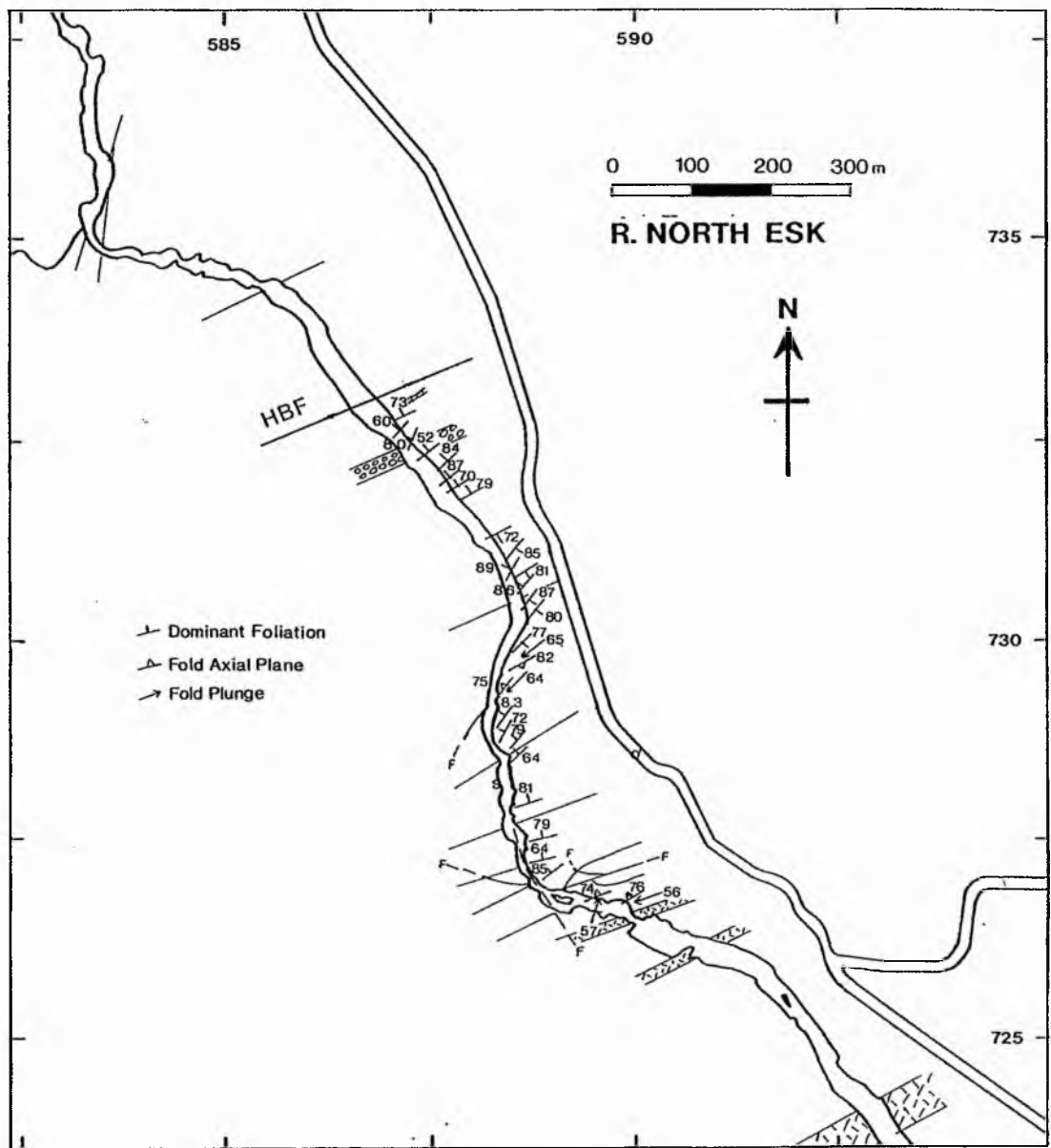


Fig. 4.4 - Structural measurements made on the HBC. Lithological boundaries are clarified with Fig. 4.2.

4.4 STRUCTURAL INTREPRETATION

4.4.1 Introduction

It is generally accepted that the HBF is an important zone of fault activity. What is not so certain is the nature of the activity. Understanding the following features is key to understanding fault movement at Glen Esk:

1. Evidence for fault movements.
2. The directions of fault movements.
3. The magnitude of fault movements.
4. The timing of movements.
5. The presence of ductile and brittle phases
6. The distribution of fault zones within the HBC.

Within this limited study it was hoped to clarify the information available, show some of the inherent problems in quantifying the fault movement and suggest areas for further research.

4.4.2 Discussion

To facilitate this investigation detailed field maps were prepared at a number of key localities (see Figs. 4.2 and 4.5A, B, C, D). Measurements were made on folds to produce a set of complimentary stereoplots (see Fig. 4.6). Orientated thin sections were prepared and examined for microscopic shear sense indicators.

(a) Field Maps and Stereoplots - The field maps A to D are taken from various units within the HBC. Folding

171

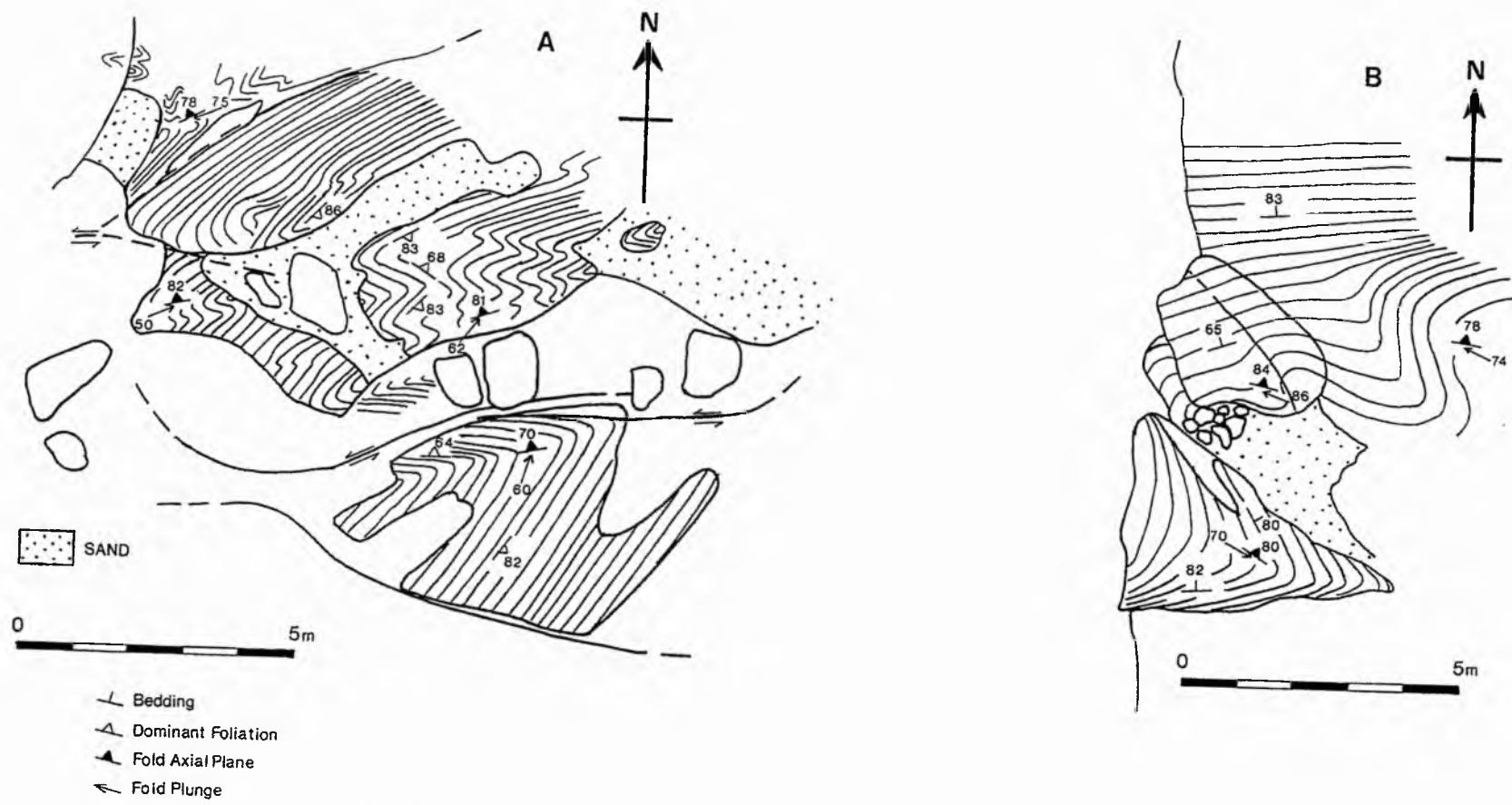


Fig. 4.5A and B - Detailed field maps from localities in the HBC at Glen Esk
(see Fig. 4.2 for locations).

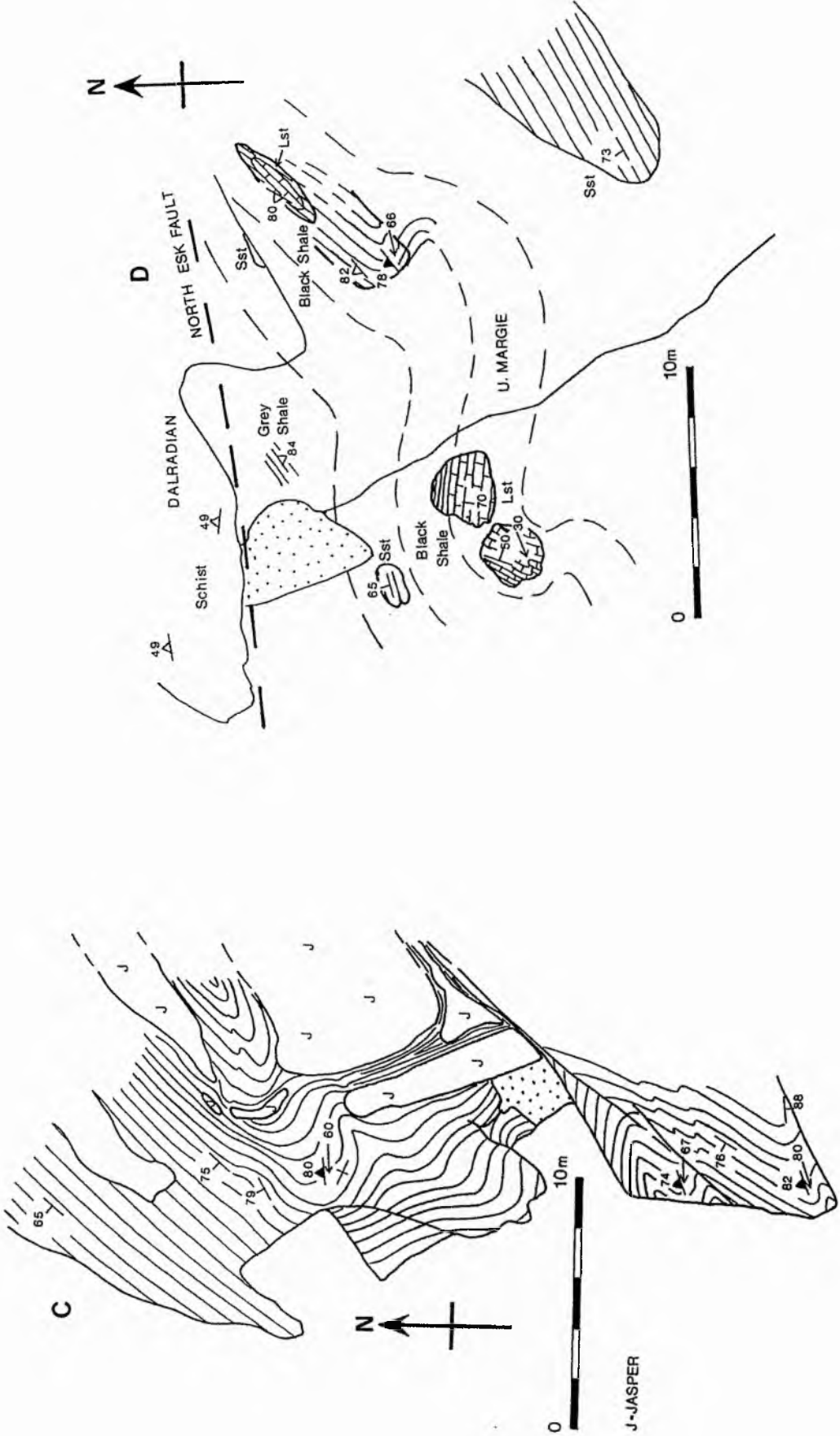
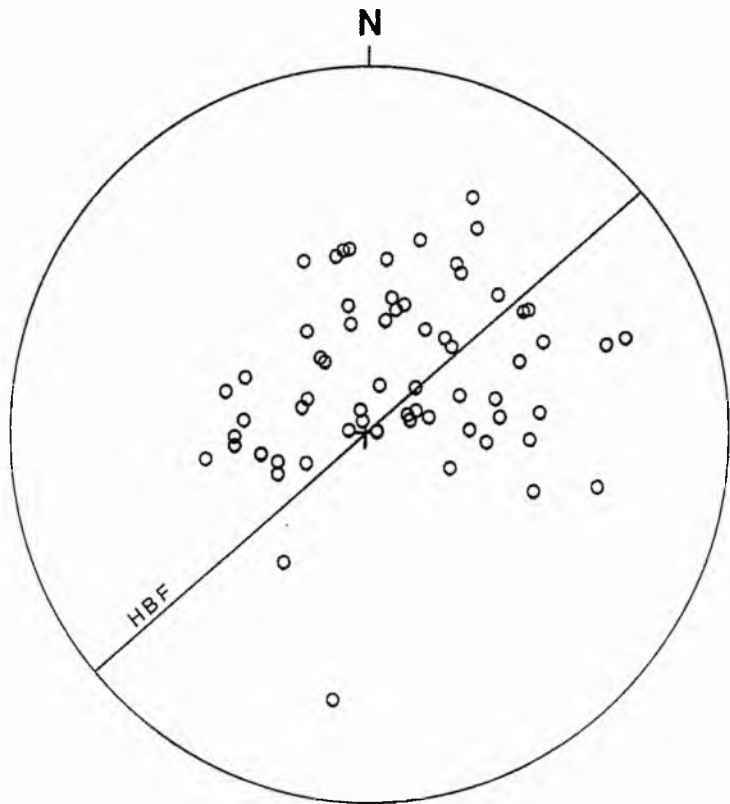


Fig. 4.5C and D - Detailed field maps from localities in the HBC at Glen Esk
 (see Fig. 4.2 for locations).

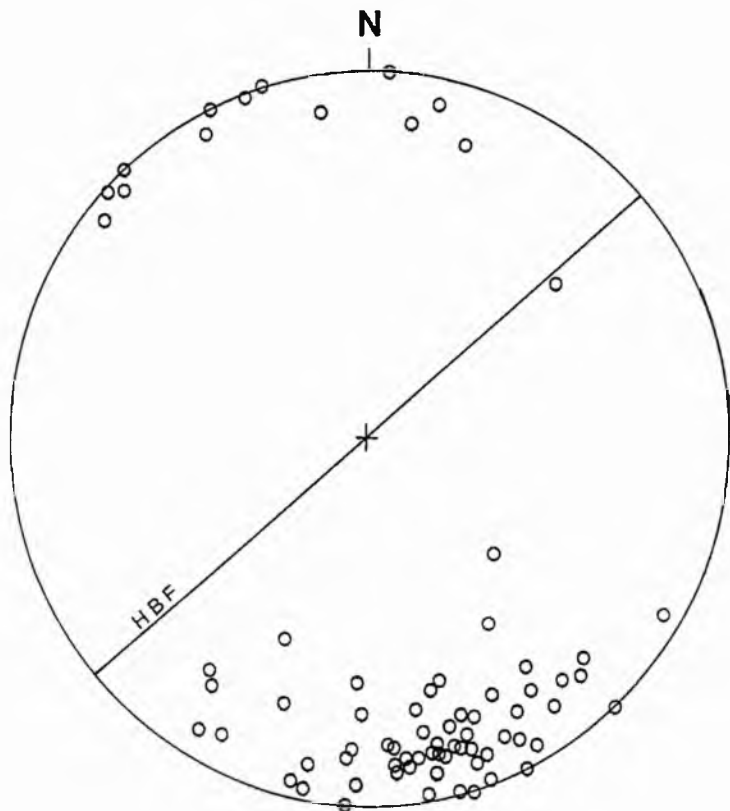
143



a o 63 Fault zone S-fold plunges.

HBF - Orientation of the Highland Bound Fault.

Fig. 4.6a, b - Fault related folding in



b ○ 71 Fault zone S-fold, poles to axial planes.

HBF • Highland Boundary Fault orientation.

the HBC, lower hemisphere stereoplots.

within these areas post-dates the dominant foliation. This foliation indicates variable intensities of strain in each area. Most folds plunge steeply to the NE, with axial planes dipping steeply to the NNW or SSE (see Fig. 4.6 and plate 4.1). These folds have an anti-clockwise sense of rotation, indicating sinistral movement (see Fig. 4.7). A weak axial planar cleavage is displayed. The sequence youngs to the N, on the basis of palaeontological evidence (see section 4.2.2), and folds face to the W.

The fault foliation is a ductile feature. Late sinistral extensional duplexes (Swanson, 1988) cut across the foliation with variable orientations (see plate 4.2). Late faults include high angle thrust faulting to the SSE. Thrust faults are characterised by sharp boundaries and slickenside surfaces, indicating their late brittle nature. Slickenside surfaces give the sense of movement. In the more pelitic units 'S-C' fabrics are common.

(b) Orientated Thin Sections - Thin sections CS1 to CS13 were examined for shear sense indicators. S-C mylonite fabrics (Lister and Snoke, 1984), with sinistral shear sense, were observed in thin sections CS12 and HBS36A (see plates 4.3). Porphyroclasts and porphyrocrysts can provide a clear indication of shear sense (see plate 4.4). Takagi and Ito (1988) have shown that the drag angle (A), and not the positions of the asymmetric pressure shadows on a porphyrocryst, provide an accurate measure of shear sense within a rock (see Fig. 4.8 and plate 4.5). Observations on HBC samples show porphyrocrysts to have dominantly sinistral shear sense (see plates 4.4 and 4.5). Many of the



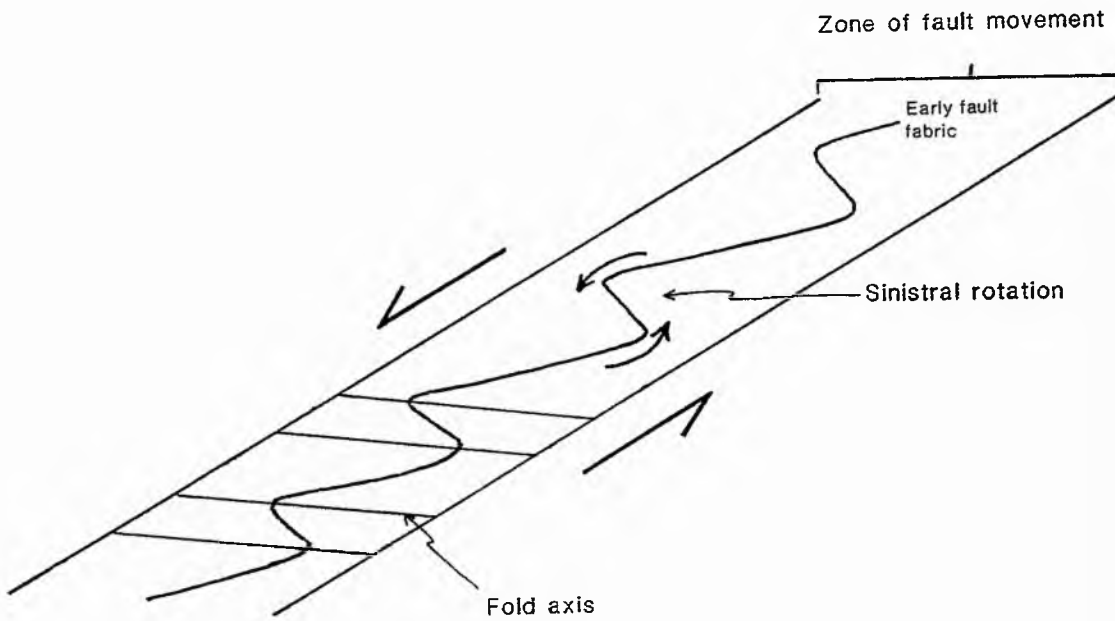
Plate 4.1 - Fault foliation (S), in the purple/orange dolomitic snails of the Highland Border Complex, is folded by a brittle fold (F) with sinistral rotation.



Plate 4.2 - Fault foliation (S) cross-cut by brittle extensional duplexes (D) with a sinistral sense of movement.

Transcurrent fault related folds

145



The earlier fault fabric is folded with a sinistral sense of rotation within the fault zone.

Fig. 4.7 - Anticlockwise sense of rotation of fault related folds in the HBC.



Plate 4.3 - Feldspathic basalt from the Jasper and Greenrock Series (JGS) showing a well developed sinistral S-C fabric (PPL, HBS36, 2.5mm).



Plate 4.4 - Purple shale from the JGS. The porphyrocryst is composed of calcite, opaques and chlorite and indicates sinistral shear (PPL, CS3, 2.5mm).



Plate 4.5 - Purple shale, from the JGS, containing porphyrocrysts (?amygdales) composed of chlorite and opaques. This example indicates sinistral shear (PPL, CS1, 2.5mm).

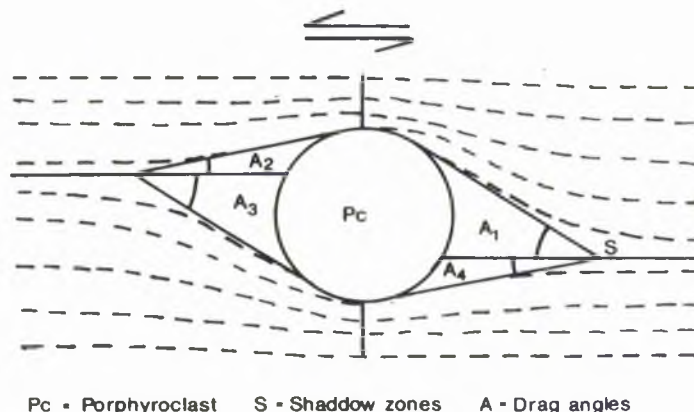


Fig. 4.8 - Microscopic shear sense indicators, after Takagi and Ito (1988). Angles A1 and A3 are larger than A2 and A4. This indicates sinistral shear. The reverse would indicate dextral shear.

unorientated thin sections prepared show characteristic quartz matrix grain reduction, indicative of patchy mylonitisation throughout the HBC (see plates 4.6 and 4.7).

It is possible to extrapolate sinistral shear to the whole of the HBC on the basis of this data. Analysis on a much larger scale along strike is necessary to establish a clear dominance of sinistral or dextral fault movement. What is clear is that simple shear is present in these rocks. This is indicative of ductile fault movement in a transpressional environment. The most significant question, the magnitude of fault movement, is the hardest to quantify. The extensive pelitic units of the HBC have the potential to accommodate very large amounts of fault movement without leaving much evidence of the activity. Large movements (10's of km's) are inferred since the HBC terrane is clearly exotic to the Dalradian terrane.

4.4.3 Summary

With regards to the six features listed in section 4.4.1, the following can be said:

1. There is evidence for a concentration of fault movements in the HBC. 2. Fault movement appears to involve sinistral transpressional faulting in an NE-SW direction, NNW dipping thrusts and a variety of brittle faults. 3. There is no clear indication of how much movement was taken up by transcurrent faulting. The need to bring two entirely separate terranes together would imply a large amount of movement. Thrust faulting represents a relatively minor stage with possibly c.100m of movement in the Late

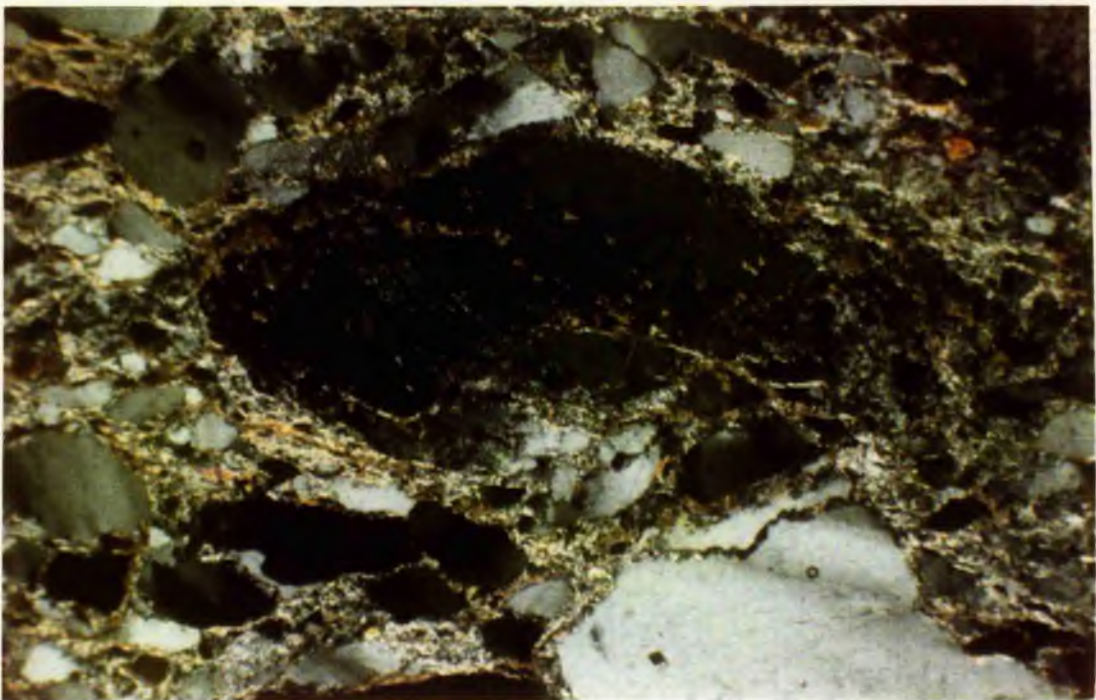


Plate 4.6 - Mylonitic grain reduction in an Upper Margie psammite. The central quartz clast shows grain reduction along stress induced fractures (XPL, HBS67, 2.5mm).

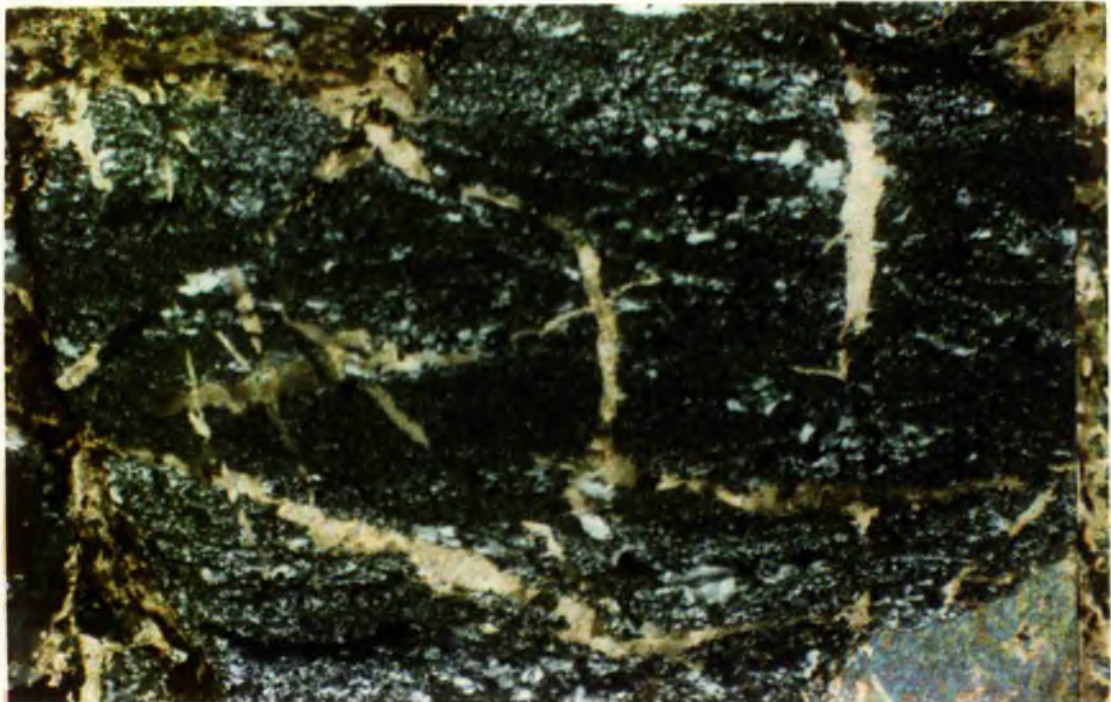


Plate 4.7 - This photomicrograph shows mylonitic grain reduction in a Lower Margie sandstone (XPL, HBS22, 2.5mm).

Devonian. This is shown by the deposition of c.100m of local Dalradian material in the Upper ORS conglomerates (Bluck, 1984). 4 and 5. Ductile transcurrent faulting is the earliest discernable fault phase in the HBC. Thrusting and minor faults are late brittle features. 6. Sinistral transcurrent faulting is found in zones throughout the HBC. Much of the movement may be hidden in pelitic units.

4.5 PETROGRAPHY

4.5.1 Introduction

41 thin sections were prepared from Dalradian samples and 42 from HBC samples collected along the River N. Esk. Sample localities are given in Appendix 4.1. Thin sections were examined to determine the mode of occurrence of minerals, and put them in metamorphic and structural context.

4.5.2 Thin Section Analysis

(A) Dalradian

The Dalradian samples collected are a mixture of greenschist facies pelites and arenites. The mineralogy of the pelitic samples is dominated by muscovite (c.5-50%), chlorite (c.5-45%), and quartz and feldspar (c.10-60%). There are lesser amounts of calcite, fine opaques (<1-c.6%), tourmaline and dertrital zircon. Porphyroblastic growth of pyrite occurs in some of the lower grade rocks and strained biotite porphyroblasts (c.0-15%) are common in higher grade samples.

A sequence of mineral growths and tectonic fabrics occur throughout the sample population. The following sequence is typical (e.g. sample D23) (see plate 4.8):

S1 cleavage develops in association with prograde metamorphic growth of fine chlorite and muscovite. Peak metamorphism is attained in a post-D1 static interval. This is indicated by the growth of porphyroblastic chlorite, biotite or garnet (see sample D3) depending on the

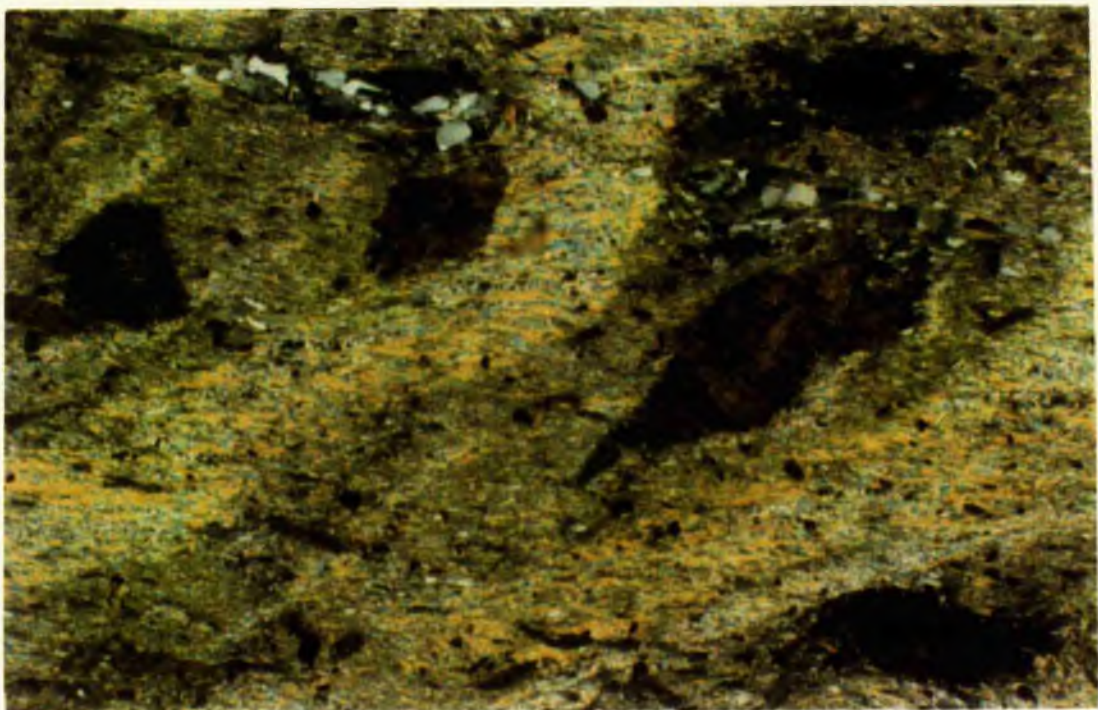


Plate 4.8 - Biotite grade pelitic schist. Biotite porphyroblast growth is post-D1 and pre- the D2 crenulation cleavage (XPL, D23, 2.5mm).

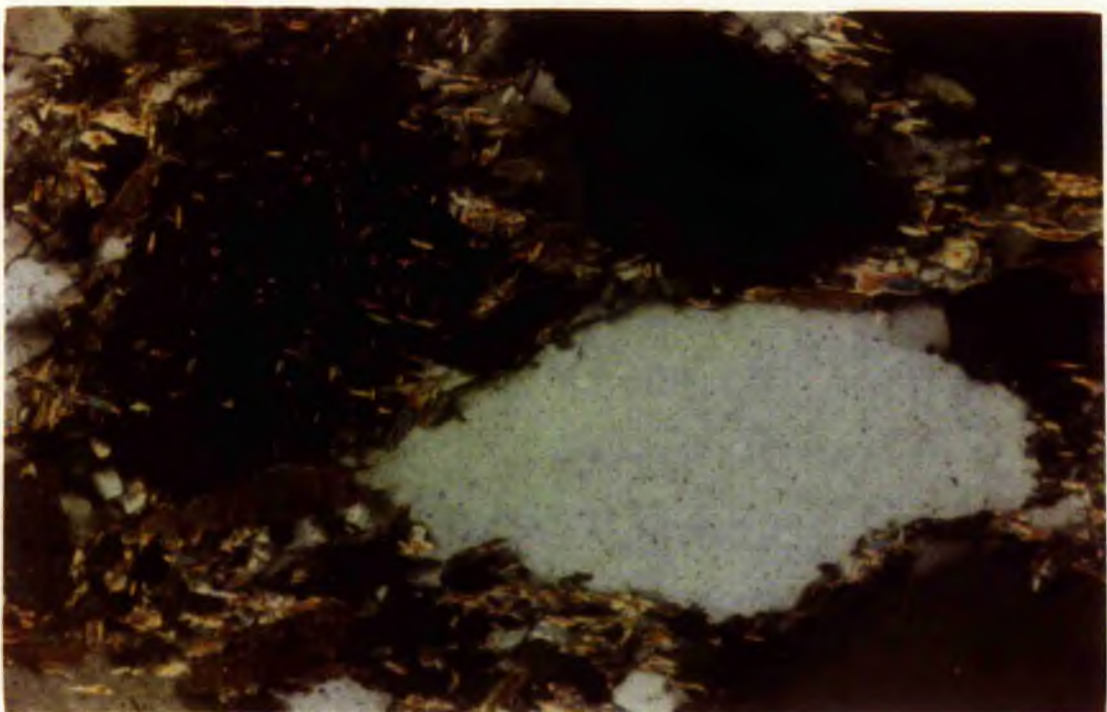


Plate 4.9 - Biotite grade psammitic schist. The effects of D2 are not recogniseable (XPL, D27, 2.5mm).

metamorphic grade attained. During this static interval quartz veining occurs, sometimes with chlorite or muscovite present. Crenulation cleavages (S2 and S3) are usually present. These re-orientate porphyroblasts and strain early vein quartz. The crenulations are also associated with the growth of retrogressive chlorite, replacing garnet and biotite. Late features include veins bearing quartz, chlorite, calcite and muscovite, and cavities filled by quartz and pyrite in that order (see D12), calcite replacement of quartz and feldspar in the groundmass, and kink bands.

Psammitic samples (eg D27) are dominated by quartz and feldspar (c.55-90%), with lesser amounts of muscovite (<1-c.25%), biotite (c.0-15%) and chlorite (<1-c.10%). Calcite is a common minor constituent, but attains c.40% in D13. Lesser amounts of opaques (<1-c.3%), and tourmaline and detrital zircon are present.

The same sequence of events recognised in pelitic samples can be seen in these samples, though a few different features are present. Biotite porphyroblasts are often smaller possibly reflecting deficiencies in K, Fe, Mg and Ti (see plate 4.9). Syn-D1? pyrite porphyroblasts and earlier chlorite pods sometimes occur.

These Dalradian samples reflect events from the Grampian orogeny.

(B) HBC

The HBC samples show a wide variety of lithologies within each assemblage. Sedimentary rocks contain both a

terrigenous clastic and argillaceous input. Basic volcanic rocks consist of pillow lavas, massive lavas and pyroclastic units.

Lower Margie

1. Sandstone - This is dominated by quartz and feldspar (c.40-60%) with lesser amounts of muscovite (c.10-25%), chlorite (c.5-10%), calcite (c.0-5%), haematite and opaques. Variable amounts of the muscovite are detrital. Occasional grains of detrital zircon and tourmaline also occur.

The sandstones are typified by HBS5 and HBS12. They contain a major component of detrital quartz and feldspar, as well as some detrital muscovite. A foliation is well developed and is associated with new muscovite and chlorite growth. Detrital grains show undulose extinction. This foliation is cross-cut first by quartz then by calcite veining. HBS20 and HBS22 contain c.70% quartz, c.20-30% calcite, c.0-10% muscovite, minor chlorite and opaques. They are strongly mylonitised with characteristic grain reduction of the quartz. Quartz and calcite veining and brecciation occurs with some mylonitisation of the earlier quartz.

2. Dolomitic Shales (see plate 4.10) - These purple and orange shales are characterised by a ferro-magnesian mineralogy. Quartz and feldspar ranges from c.20-25% with feldspar dominating. Chlorite (c.30-60%) is most common, with lesser calcite and dolomite (c.10-30%), haematite (c.10%), white mica (c.2-5%) and epidote (c.1-13%). Minor

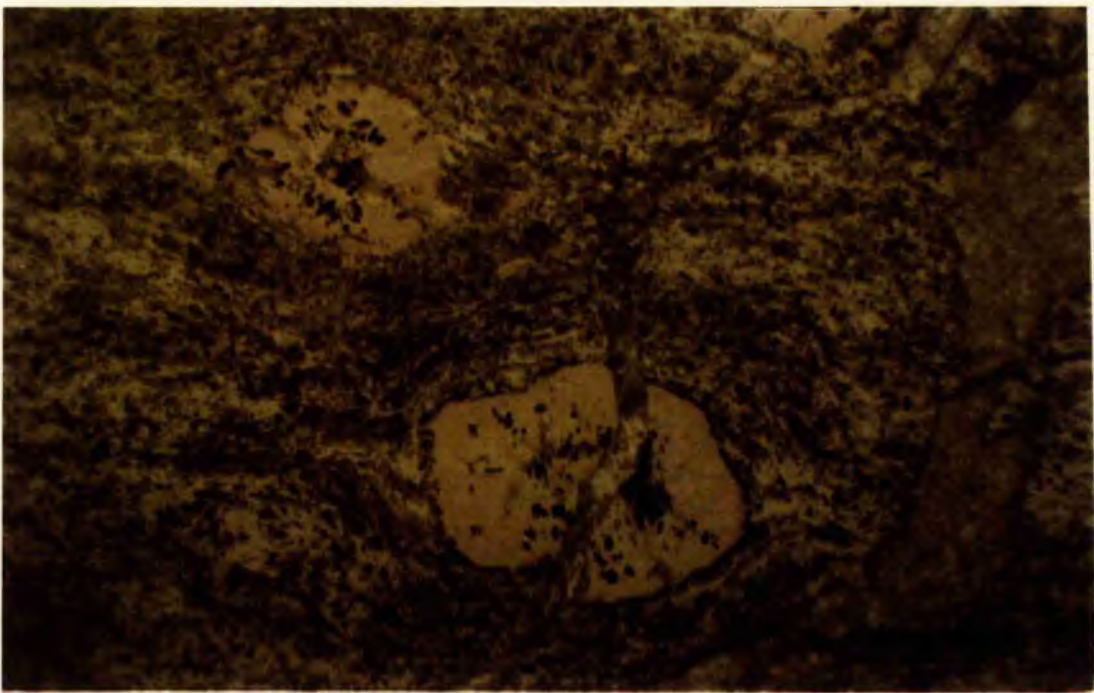


Plate 4.10 - Purple shale with chlorite/opaque pods (?amygdales). Later epidote and carbonate veins cross-cut (PPL, HBS26, 2.5mm).

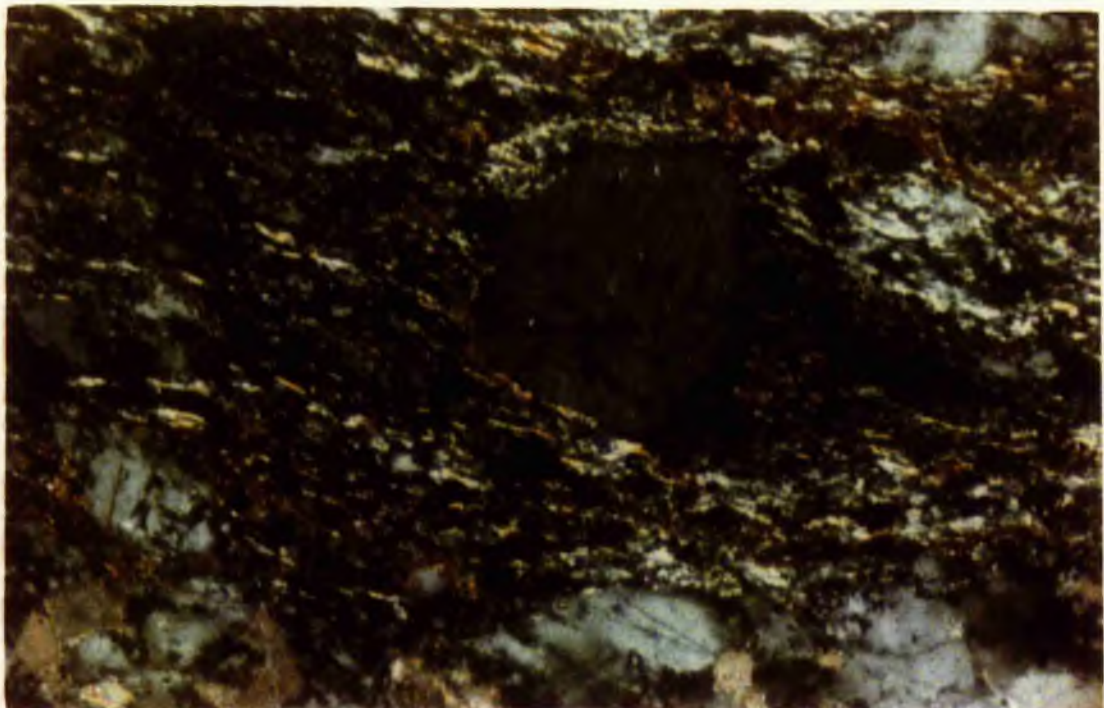


Plate 4.11 - Upper Margie psammite with a feldspar phenocryst surrounded by grain reduced matrix (PPL, CS12, 1.0mm).

amounts of graphite (up to 2%) and opaques (up to 5%) occur.

The composition of these shales implies a basic igneous origin for much of the material. A strong early foliation has developed in a fine matrix of chlorite, muscovite, haematite and feldspar. Within the foliation there are pods (0.5mm) of chlorite and opaques, or spherulitic quartz. These show rotation with asymmetric tails indicating the presence of sinistral simple shear. Pods are replaced in parts by later epidote and carbonate. Veins of calcite or dolomite with opaques, epidote and quartz show some tectonic disruption. The groundmass is patchily replaced by chlorite, quartz and calcite subsequent to any major tectonism. The latest features are brittle fractures, sometimes with concentrations of opaques and epidote along them.

Upper Margie

1. Sandstone - Quartz (c.60-70%), feldspar (c.5-20%), muscovite (c.2-20%) and chlorite (c.1-25%) are most common. Calcite (c.1-5%), epidote (c.0-2%) and opaques (c.1%) are usually present. Detrital zircon (<1%) also occurs.

These sandstones are dominated by detrital monocrystalline quartz and feldspar grains, and some detrital muscovite. A pervasive foliation is present, with the associated growth of new muscovite and chlorite. In places (see CS12) the characteristic grain reduction of mylonitisation is present (see plate 4.11). Later quartz, and quartz and calcite veining is common.

2. Limestone - This rock is composed of fine calcite (c.90%) and graphite (c.10%), with a strong foliation and accessory muscovite. The rock is heavily brecciated and infilled by coarse quartz and calcite. Some of the quartz shows tectonic grain reduction. The rock was mylonitised before brecciation.

3. Shale - This shale is a very uniform fine pelite with c.25% quartz, c.20% chlorite, c.30% muscovite, c.20% opaques, and minor epidote calcite and tourmaline. The strong S1 fabric, probably formed during faulting, is weakly crenulated. Later kink bands are associated with quartz and calcite veining. Epidote is confined to veins sub-parallel to the main foliation.

Jasper and Greenrock Formation

This formation is made up of a sequence of pillow basalts (c.10cm in diameter) with interbedded purple shales. Further up the sequence more massive lavas are present with jasper pods up to 6m across. These are overlain by purple then green chloritic shales.

1. Pillow Basalts - The pillow basalts (P1-P5) are characterised by the presence of skeletal feldspar (c.10-30%) and clinopyroxene (c.50-80%) forming a groundmass, with occasional euhedral pseudomorphs after olivine (see below) (c.1%) (see plate 4.12). These rocks have been spilitised and show pervasive metasomatic alteration. The sequential development of these basalts can be divided into a crystallisation and a spilitisation phase.

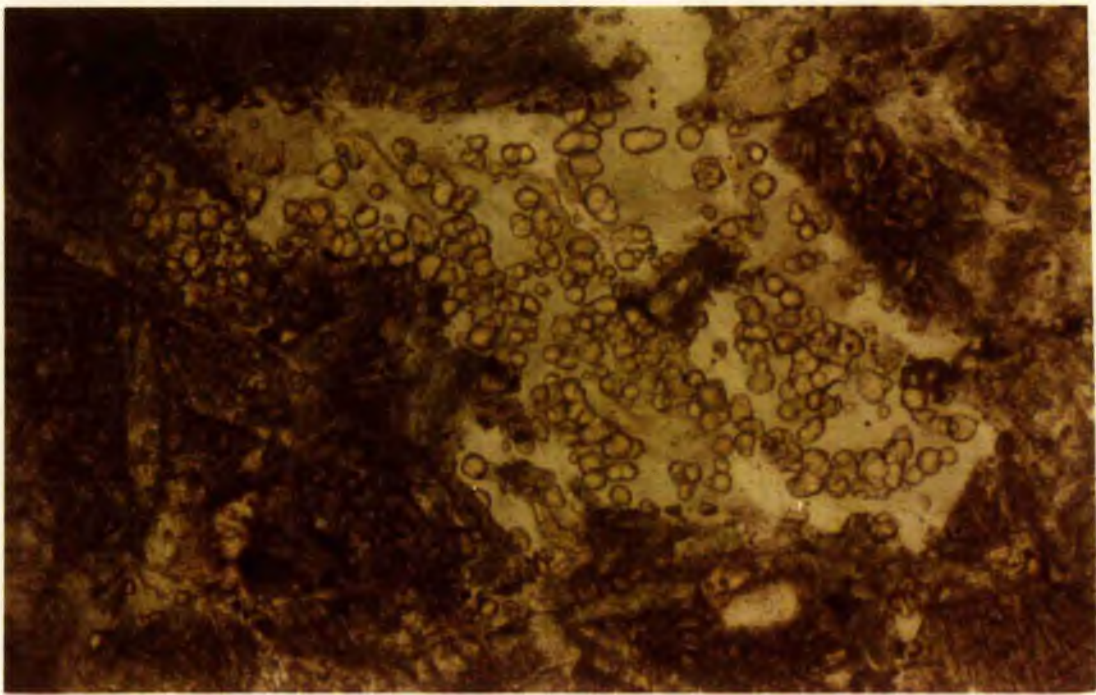


Plate 4.12 - Pseudomorph after olivine in pillow basalt. Olivine is replaced mainly by chlorite and high relief granitic garnet. The groundmass contains a mixture of primary clinopyroxene, and secondary albite and pumpellyite (PPL, P5, 1.0mm).

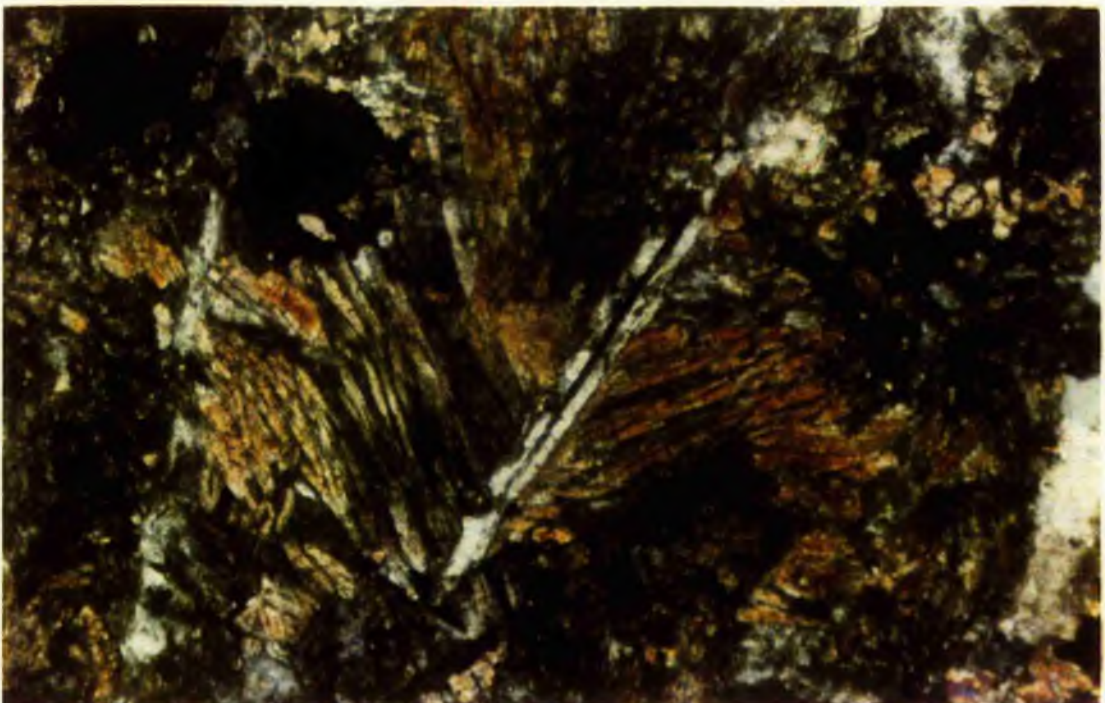


Plate 4.13 - Spherulitic clinopyroxene crystals growing on a skeletal albite crystal (white) in pillow basalt (XPL, P5, 1.0mm).

The crystallisation textures are typical of quenching of a basalt melt. The presence of small euhedral olivine phenocrysts (c.0.2mm) implies that the melt was held at temperatures just above 1200 °C (Lofgren, 1983). This allowed the relatively slow growth of olivine before the quenching of the rest of the melt. With rapid cooling, crystallisation of plagioclase and clinopyroxene occurred on heterogeneous nuclei to form the basalt groundmass. Plagioclase takes the form of intersertal small acicular and elongate skeletal crystals. These are intimately intergrown with fine fan and spherulite clinopyroxene crystal bundles (see plate 4.13). Experimental work on terrestrial basalt has allowed the tight constraining of this crystal morphological assemblage. Lofgren (1983) has shown that a basalt melt, held at 1195 °C for 24hrs or at 1205 °C for 7hrs, on cooling at a rate of 2-5 °C/hr, produces an almost identical set of crystal morphologies to the ones observed here. This tightly constrains the cooling history of these basalts. 'Bow tie' spherulites of plagioclase and CPX are found near the margins of some pillows. These are finer grained implying a slightly faster cooling rate at the margins (Lofgren, 1974). The presence of skeletal plagioclase crystals is particularly common to basalts erupted and cooled on the ocean floor (Lofgren, 1974).

On spilitisation, the plagioclase has been altered to albite. Relict plagioclase have a composition of labradorite (see section 4.6.12). The very fine interstitial material has been altered to chlorite, and

apple green pumpellyite (after plagioclase). The clinopyroxene component seems to have survived all alteration effects. Pseudomorphs after olivine are distinguished from clinopyroxenes by their morphology and the unaltered nature of groundmass clinopyroxenes. The altered olivines can be replaced by chlorite, granditic garnet, pumpellyite, epidote, minor actinolite and later calcite (see plate 4.12). Vesicles are also infilled with these minerals, except epidote. Late stage features include chlorite veins, and fractures sequentially filled with epidote, quartz and then calcite.

2. Lava - The more massive lava units overlying the pillow lavas consist of basalts and feldspathites. Slower cooling rates have resulted in the growth of euhedral plagioclase and plagioclase/clinopyroxene intergrowths.

HBS29 is composed of c.40% clinopyroxene, c.30% plagioclase, c.15% chlorite, c.12% epidote, c.2% quartz, and minor amounts of calcite, sphene, actinolite and opaques. The clinopyroxene takes the form of phenocrysts, up to 2mm long, made up of clusters of crystallites in optical continuity (see plate 4.14). The original skeletal crystals have been slightly deformed during metamorphism.

The groundmass is made up of irregular shaped feldspars, and alteration products of epidote, chlorite, actinolite and sphene. Veining also occurs with epidote, chlorite, quartz and calcite in various combinations, but forming in the order given.



Plate 4.14 - Two "arrow head" clinopyroxene crystals, in basalt, composed of crystallites in optical continuity. The original skeletal shape has been slightly flattened and stretched during metamorphism (XPL, HBS29, 2.5mm).



Plate 4.15 - Epidote vein fill (yellow), in purple shale, has broken from the lower vein wall, and has been successively enclosed in chlorite (green), quartz and calcite (off white) (PPL, HBS4, 2.5mm).

HBS36 is a feldspathic lava with c.75% feldspar, c.20% chlorite, c.3% calcite, c.2% opaques and minor white mica. The feldspar is partly re-crystallised and the matrix has taken on a sinistral S-C fabric. Opaques, chlorite and some calcite are present in the groundmass. Later vein calcite is also present.

3. Jasper - This is composed of haematite rich opaques and quartz, with minor amounts of calcite and chlorite. The rock shows evidence of brecciation, grain reduction of the brecciated fragments and veining.

Purple Shale

These shales contain c.15-70% calcite, c.10-40% haematite, c.5-15% white mica, c.5-10% quartz and feldspar, c.2-15% epidote, c.2-10% chlorite, c.0-10% sphene and minor clinzozoisite. The groundmass is dominated by calcite-rich or opaque-rich zones with a strong foliation. The groundmass contains most of the white mica, chlorite, haematite, epidote, sphene and detrital quartz. A weak crenulation cleavage is present. The history of vein filling is well illustrated in HBS4. Epidote has grown initially as granular crystals then later as acicular crystals. Fragments of this have broken free from the vein walls, and have been enclosed by chlorite, quartz and calcite in that order (see plate 4.15). Later veins of fine epidote and calcite are mildly tectonised.

Green Pelite - These have a basic composition and possibly represent tectonised pyroclastic units. The most common constituents are chlorite (c.10-30%), actinolite

(c.10-30%), pumpellyite (c.5-30%), feldspar (c.1-40%) and epidote (c.5-20%). Also present in some of the samples are clinopyroxene (up to 15%), sphene, opaques, white mica, calcite and quartz.

Clinopyroxene and relict feldspar form much of the original mineralogy. This groundmass has been metamorphosed to produce actinolite, which overgrows and replaces clinopyroxene as orientated sheaves (see plate 4.16), albite, brown or green pumpellyite, chlorite, epidote and sphene. Larger feldspar phenocrysts (see HBS57) have been partly replaced by pumpellyite, and pulled apart. The gaps are infilled with fresh albite, chlorite and calcite (see plate 4.17). There are a number of 'amygdales', of uncertain origin, which are orientated parallel to the main foliation. These show a progressive infilling with pumpellyite, epidote, chlorite, opaques, calcite and minor albite (see plate 4.16). Later veining also occurs with infills of quartz, calcite and epidote. Pods (up to 3mm) of pumpellyite are also present in HBS62.

4.5.3 Conclusions

1. Dalradian samples range from chlorite to garnet grade greenschist facies.

2. A sequence of events can readily be recognised in the Dalradian rocks. Prograde metamorphism was concurrent with the S1 cleavage development. Peak metamorphism was attained in the post-D1 static interval, with the growth of chlorite, biotite or garnet porphyroblasts.

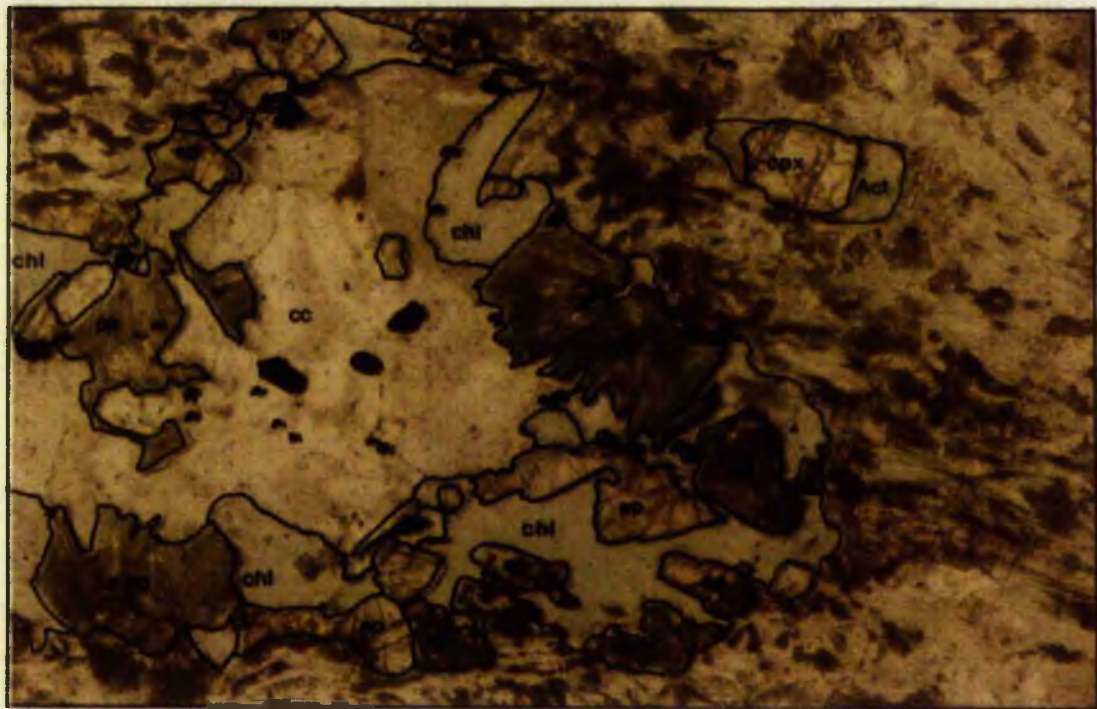


Plate 4.16 - Amygdale, in green pelite, with successive infillings of pumpellyite, epidote, chlorite, opaques and calcite. The groundmass contains chlorite, sphene, albite and clinopyroxene crystals overgrown by actinolite (PPL, HBS57, 1.0mm).



Plate 4.17 - Dismembered feldspar phenocryst in green pelite. The phenocryst has been partly replaced by pumpellyite and pulled apart. Gaps are infilled by albite, chlorite and calcite. Below the feldspar phenocryst are groundmass clinopyroxenes overgrown by actinolite (PPL, HBS57, 1.0mm).

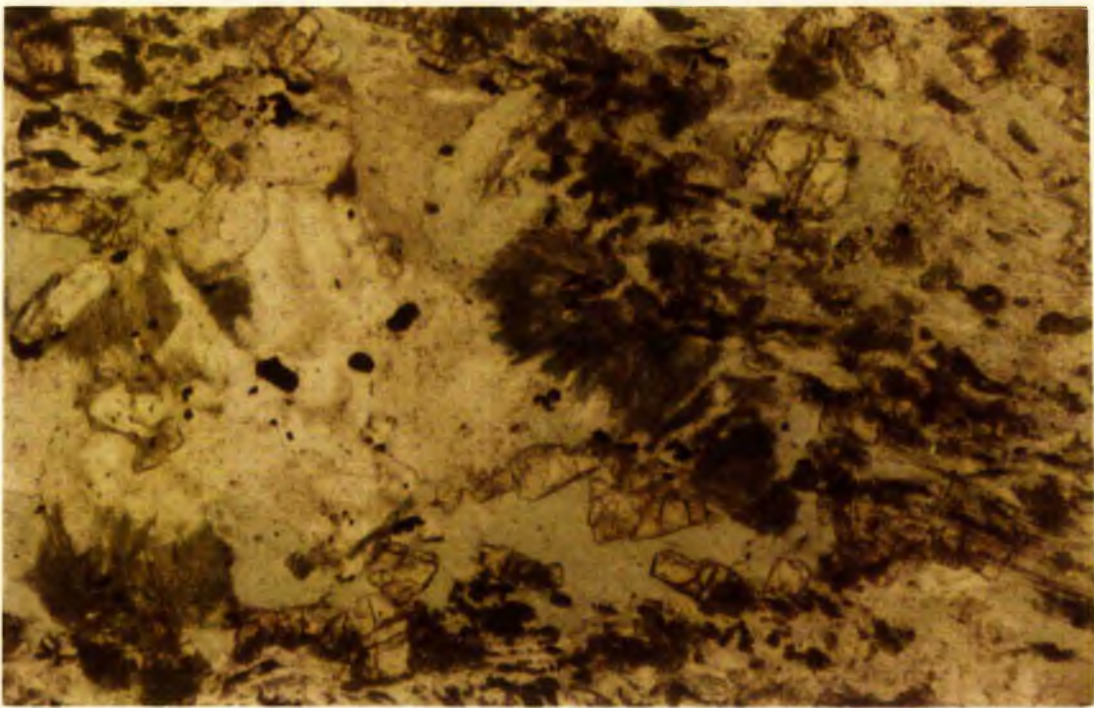


Plate 4.16 - Amygdale, in green pelite, with successive infillings of pumpellyite, epidote, chlorite, opaques and calcite. The groundmass contains chlorite, sphene, albite and clinopyroxene crystals overgrown by actinolite (PPL, HBS57, 1.0mm).

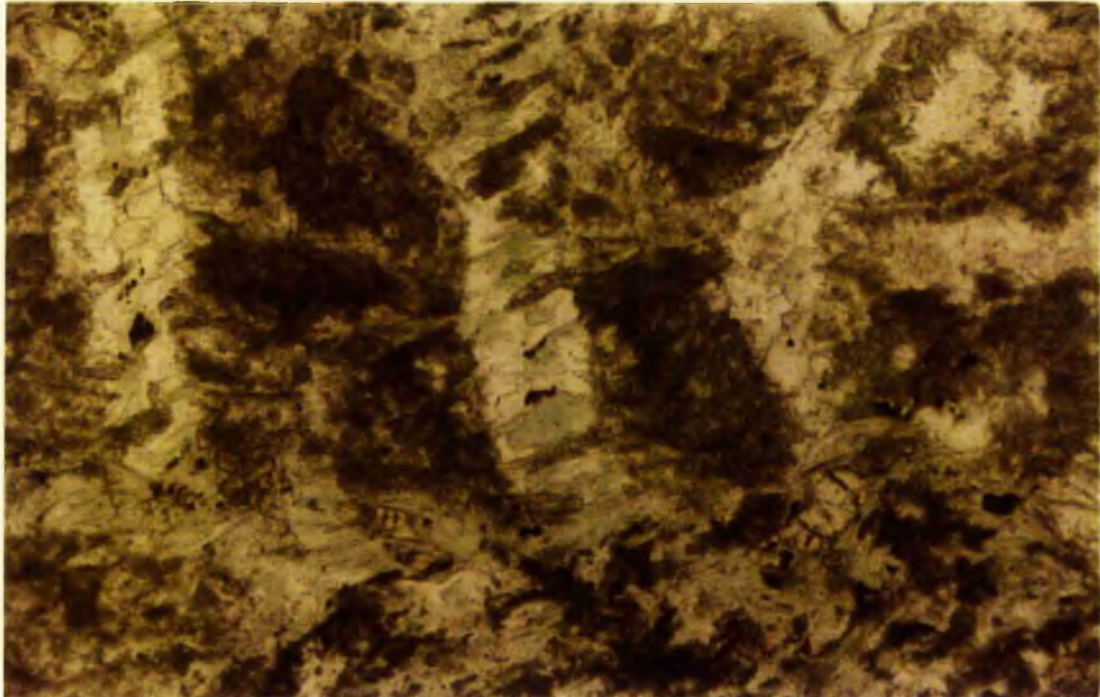


Plate 4.17 - Dismembered feldspar phenocryst in green pelite. The phenocryst has been partly replaced by pumpellyite and pulled apart. Gaps are infilled by albite, chlorite and calcite. Below the feldspar phenocryst are groundmass clinopyroxenes overgrown by actinolite (PPL, HBS57, 1.0mm).

3. Clastic samples contain detrital material, including muscovite. Most samples show a pervasive foliation associated with the growth of various combinations of muscovite, quartz, chlorite, epidote, carbonate, haematite and opaques, depending on the original lithology. A weak crenulation cleavage may also occur. Variable amounts of mylonitisation and brecciation can be seen. Later groundmass replacement and veining involves chlorite, epidote, quartz and calcite.

4. The growth of metamorphic minerals, in association with a pervasive foliation, in the HBC, indicates that peak metamorphic conditions were attained during the dominant phase of movement on the HBF. This presumably occurred during or immediately after the docking of the HBC with the Dalradian.

5. Lavas and pillow basalts have behaved with varying degrees of structural competence. They range from undeformed to S-C mylonitic fabrics.

6. The low grade of metamorphism is reflected by the survival of igneous clinopyroxene throughout the groundmass. Metamorphic minerals include albite, actinolite, pumpellyite, grandite, sphene, epidote, chlorite, white mica, calcite, quartz and opaques.

7. 'Pyroclastic' material also contains relict clinopyroxene. Metamorphism is characterised by the development of a pervasive foliation, with the growth of actinolite, pumpellyite, chlorite, albite, epidote, sphene, opaques and calcite.

8. The metamorphic and structural elements in the Dalradian and HBC samples do not clearly differentiate their separate tectonic histories. However stratigraphic considerations show that the two terranes evolved as separate terranes for much of their respective tectonic histories. All of the fault movement appears to be concentrated in the HBC. This may be because the already metamorphosed Dalradian behaved in a competent manner during transpressional faulting, whereas the HBC was metamorphosed and transpressed during docking with the Dalradian. Collision between the HBC and Dalradian occurred between the Ashgill (after HBC deposition) and the Siegenian (Dalradian detritus in the Lower ORS). Uplift associated with this collision was completed by the late Carboniferous (see section 4.2.1).

4.6 MINERAL CHEMISTRY

4.6.1 Aims

1. To assist in identifying minerals in thin section.
2. To clarify mineral intergrowths and textures.
3. To test for equilibrium assemblages.
4. To relate mineral chemistry to facies of metamorphism.

4.6.2 Introduction

The chemical compositions of minerals found in the HBC and Dalradian were determined using a JEOL Superprobe 733 (electron microprobe) with backscatter facilities. An operating current of 20nA at 15kV was used. Beam width was usually kept at $1\mu\text{m}$, but could be defocussed to $30\mu\text{m}$ to avoid disintergration of volatile rich minerals. Analyses were calibrated to a set of standards listed in Appendix 4.2.

4.6.3 White Mica

68 white mica analyses are presented in Figs 4.9A, B, C and D. Chemical formulae (Appendix 4.3) are recalculated on the basis of 24 oxygen atoms.

The dioctahedral micas show a range of substitutions which are characterised by the various end member compositions. Substitutions are described in section 2.1.3. In Figs 4.9B, C and D the Dalradian analyses plot in the phengite and muscovite fields. The pumpellyite-actinolite facies field of Upper Wakatipu, New Zealand (Kawachi, 1975), and the chlorite and biotite facies fields of eastern Otago, New Zealand (Brown, 1967) are included for

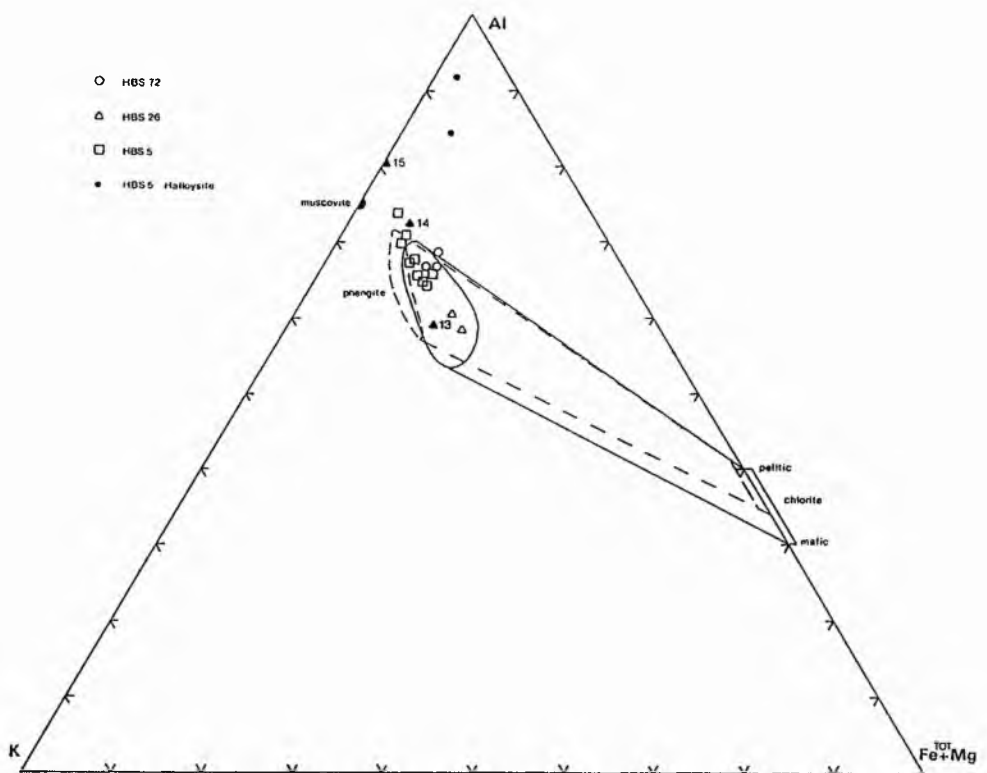


Fig. 4.9A - HBC white mica analyses (atomic proportions) plotted in terms of Al, K, and total Fe + Mg. Compositional fields, for coexisting white mica and chlorite, are included from the greenschist of Eastern Otago, New Zealand (Brown, 1967), dashed line, and the pumpellyite-actinolite facies of Upper Wakatipu, New Zealand (Kawachi, 1975), solid line. White mica analyses 13, 14 and 15 are from Deer, Howie and Zussman (1967). 13 is phengite from low grade psammitic schist, Morar Invernesshire, 14 is phengite from medium garnet grade schist, and 15 is from the sillimanite zone.

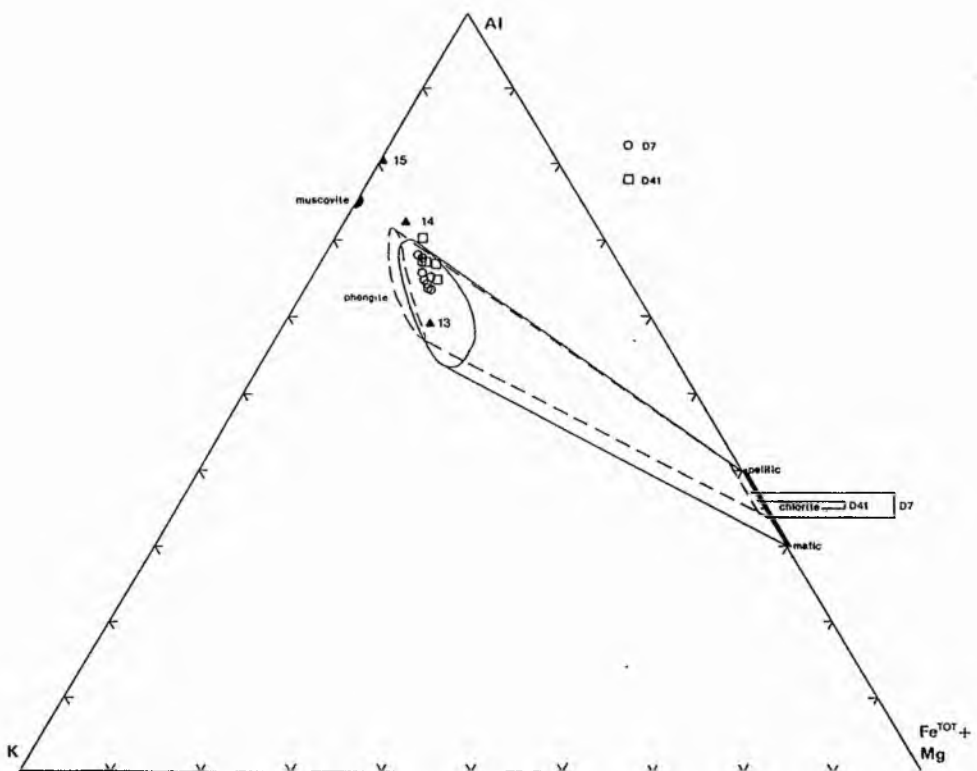


Fig. 4.9B - Chlorite grade Dalradian white mica analyses and coexisting chlorite analyses. Comparative data as in Fig. 4.9A.

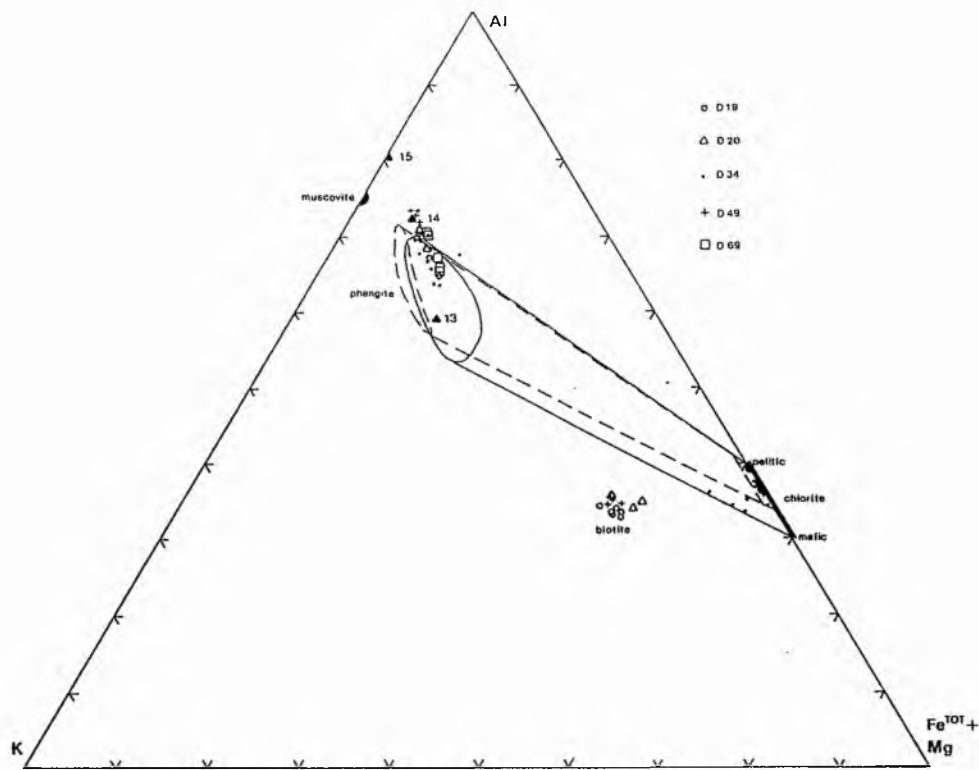


Fig. 4.9C - Biotite grade Dalradian white mica analyses, and coexisting chlorite and biotite analyses. Comparative data as in Fig. 4.9A.

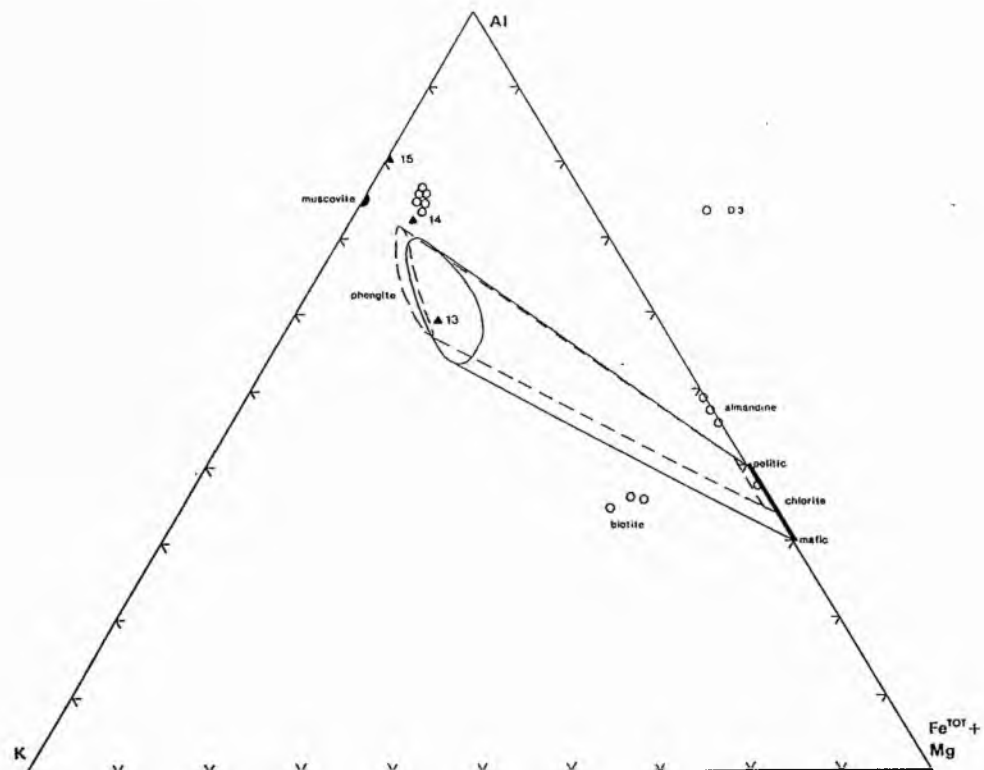


Fig. 4.9D - Garnet grade Dalradian white mica analyses, and coexisting chlorite, biotite and garnet analyses. Comparative data as in Fig. 4.9A.

comparison. Comparative analyses from Deer et al. (1967, p18) show a relative increase in Al, compared to K+Mg+FeTOT, with increasing metamorphic grade. The Dalradian analyses range in grade from chlorite (B) to biotite (C) to garnet grade (D). Increasing grade corresponds to a shift in the white mica fields towards a higher Al, less phengitic composition. This occurs with a decrease in the amount of Si substituting for Al in the tetrahedral site and Fe^{2+} + Mg for Al in the octahedral site.

Mixed chlorite-phengite analyses plot between the phengite and chlorite fields. Only TEM imagery could clarify the finer intergrowths of 14\AA chlorite and 10\AA phengite layers (see Franseschelli et al., 1986; and Ahn et al., 1988 for further discussion).

The HBC samples plot deeper into the phengite field. Greater variation within the group can be attributed to the presence of detrital mica. Samples are slightly biased towards K compared to Dalradian samples. Two halloysite analyses are possibly a product of tropical weathering in the Middle Devonian (Robertson and Henderson, 1984).

4.6.4 Chlorite

45 chlorite analyses are presented in Figs 4.10 and 4.11. Chemical formulae (Appendix 4.4) are recalculated on the basis of 28 oxygen atoms.

Chlorites are probably the most widespread minerals in the low grade assemblages at Glen Esk. Of the analyses made, 36 were from pelitic and psammitic Dalradian samples,

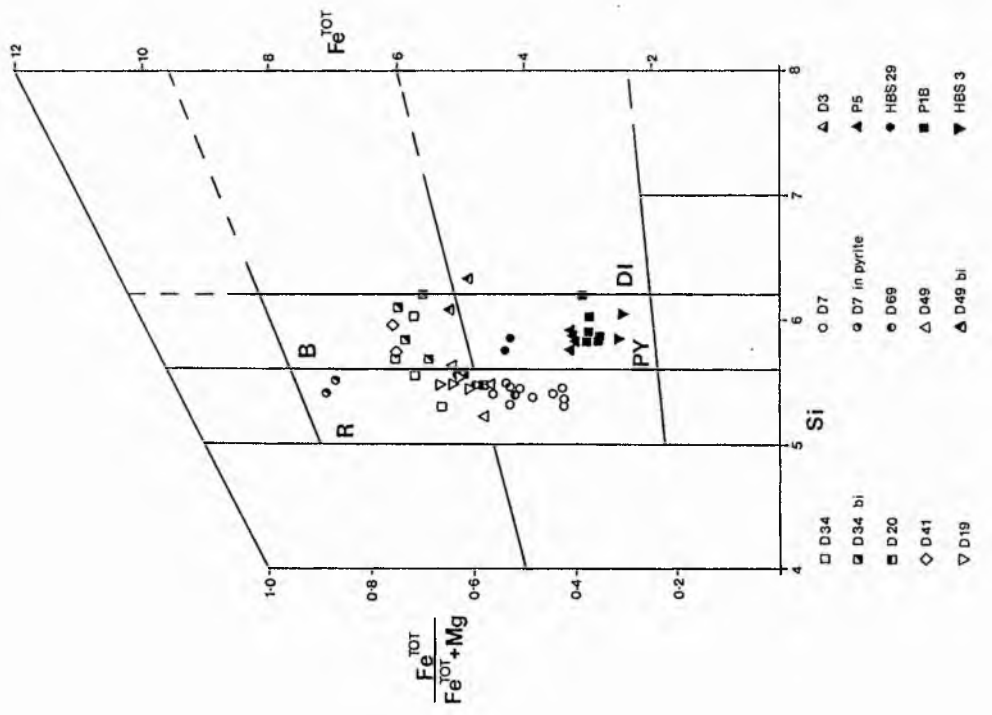


Fig. 4.10A - Glen Esk chlorite analyses (atomic proportions) plotted on Hey's (1953) diagram. R = Ripidolite, B = Brunsigtite, PY = Pyrochlorite and DI = Diabantite. P5, P1B, HBS3 and HBS29 are from the HBC, the remaining analyses are from Dalradian samples. BI = chloritised biotite.

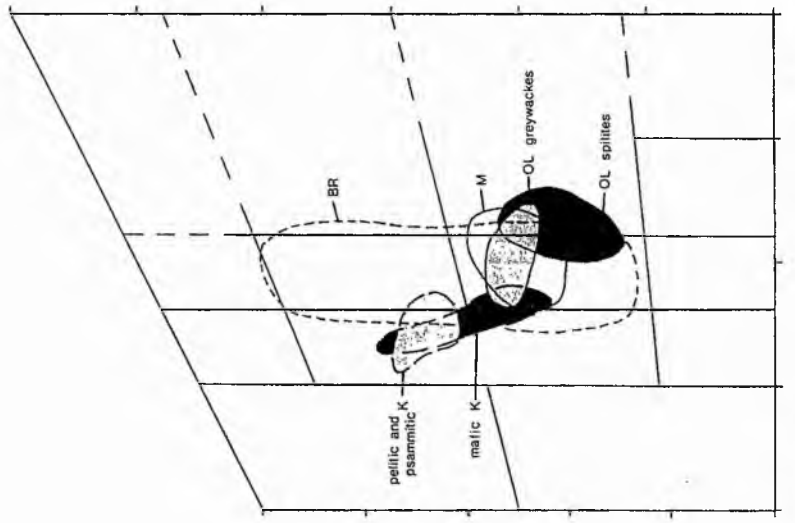


Fig. 4.10B - Comparative chlorite compositional fields from Wakanipu, New Zealand (K = Kawachi, 1975), the Southern Uplands (OL = Oliver and Leggett, 1980), Wales (BR = Bevins and Rowbotham, 1983), and Taly Fan, Wales (M = Merriman et al., 1986). Dark and light stipple indicates mafic and pelitic host rock composition.

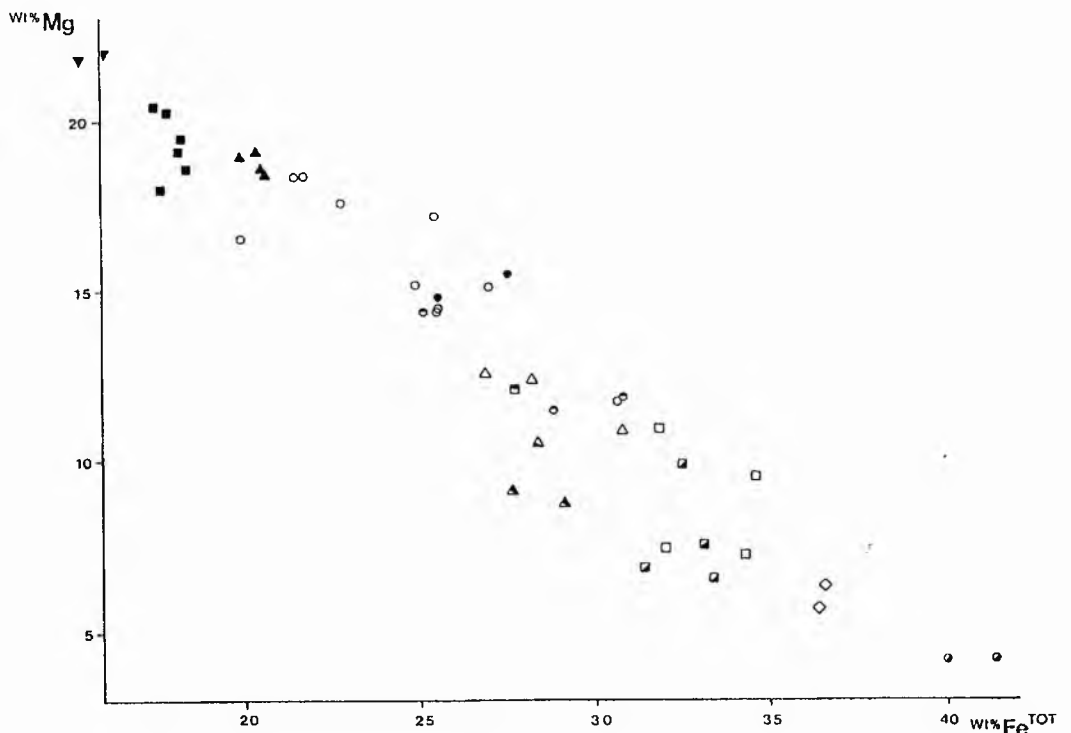


Fig. 4.11 - Fe substituting for Mg in Glen Esk chlorites.
An index of samples is given with Fig. 4.10A.

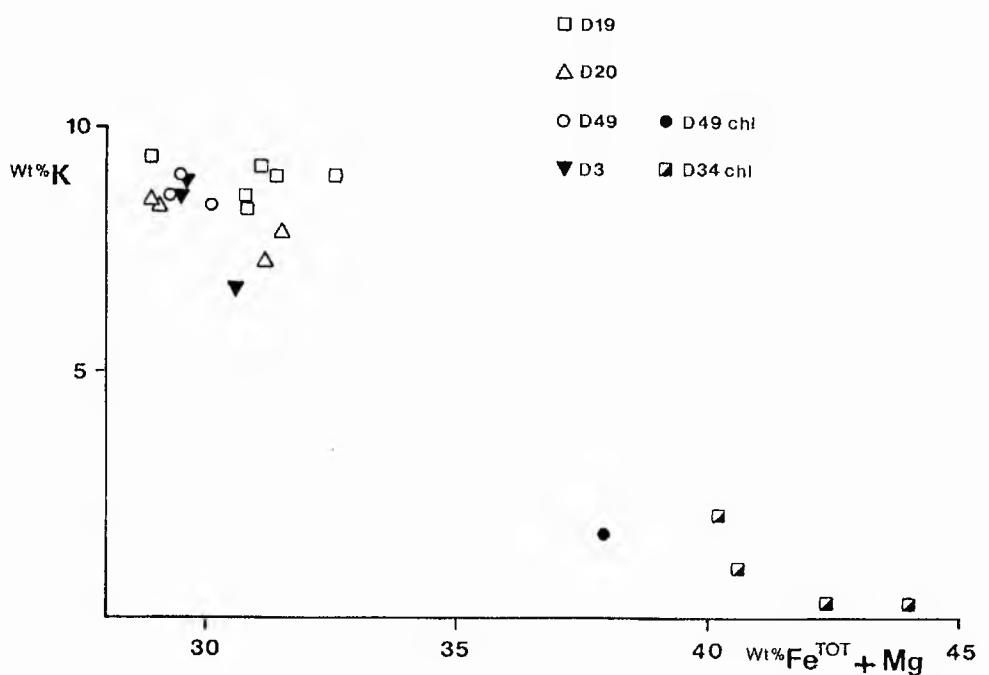


Fig. 4.12 - K plotted against Fe + Mg for Glen Esk biotites and chlorite after biotite. chl = chlorite after biotite.

and 14 were from basic samples from the HBC. The Dalradian chlorites plot in the ripidolite and brunsvigite fields (see Fig. 4.10), with one point, a chloritised biotite, falling in the diabantite field. Chlorites forming from the breakdown of biotite tend to have more SiO_2 . Late forming vein chlorites plot in the brunsvigite field and are more FeTOT rich than groundmass chlorites.

Chlorites in pelites and psammites, from Upper Wakatipu, fall mainly in the ripidolite field and overlap part of the Dalradian field. Chlorites in Southern Uplands greywackes (Oliver and Leggett, 1980) are pycnochlorites and diabantites, and are more mafic than Dalradian chlorites. The extensive field of chlorites from the Welsh paratectonic Caledonides (Bevins and Rowbotham, 1983) encompasses all but the more ripidolitic Dalradian chlorites.

The HBC chlorites all plot within the pycnochlorite field. They are only encompassed by the Welsh field. Upper Wakatipu mafic chlorites are mostly ripidolites with some pycnochlorites. Chlorites from the Tal y Fan metabasite intrusion, Wales (Merriman et al., 1986; Bevins and Merriman, 1988) are mainly pycnochlorites, but only overlap the field of chlorites from HBS29, a feldspathic lava. Southern Uplands spilites include both pycnochlorites and diabantites, and overlap part of the field of P1B, a pillow basalt.

Substitution of Si for Al is limited, but Fe for Mg substitution is widespread (see Fig. 4.11). The trend of Mg

for Fe substitution is accompanied by a general decrease in $\text{SiO}_2 / \text{Al}_2 \text{O}_3$ ratio (Kawachi, 1975). This compositional variation does not appear to be related to grade of metamorphism, but is primarily controlled by the host rock composition (Cathelineau and Nieva, 1985). The basic rocks contain Mg rich chlorites, and the pelites and psammites contain Fe rich chlorites.

Two chlorites analysed in D7 have grown in fractures in pyrite. These have the highest $\text{Fe}/(\text{Fe} + \text{Mg})$ ratios (c.0.88), and are quite different from the rest of the analyses from D7 (0.42-0.57) (see Fig. 4.11) This reflects a local control on chlorite growth, with Fe available from the breakdown of pyrite.

4.6.5 Biotite

22 biotite and chloritised biotite analyses are presented in Fig. 4.12. Coexisting biotite and chlorite analyses are also plotted on Figs 4.9 C and D. Chemical formulae are calculated on the basis of 24 oxygen atoms for biotite and 28 for chloritised biotite (see Appendix 4.5).

Biotite occurs commonly in the greenschist facies Dalradian pelites and psammites, but is not present in the HBC. Larger porphyroblasts tend to develop in the more pelitic units. This could be due to greater availability of K, Ti, Fe and Mg ions. At lower grades (anchizone) the reverse applies. Psammitic rocks crystallise micaceous minerals more readily, despite there being less suitable ions available. This is because ion bearing fluids can

circulate more freely in the psammitic rocks, making more ions available.

Partial retrogression of the Dalradian sequence is clearly shown by variable biotite alteration, in thin section, and in biotite analyses. A number of analyses are of unaltered biotites (see Fig. 4.12). There is also a range of analyses which probably reflect a fine scale mixed-layering of biotite and alteration chlorite. These retrogressive chlorites plot mainly in the brunsvigite field (Frey, 1987).

4.6.6 Tourmaline

5 tourmaline analyses are presented in Fig. 4.13. Chemical formulae (Appendix 4.6) are recalculated on the basis of 31 oxygen atoms.

Short prismatic tourmalines were found scattered in both Dalradian and HBC pelites and psammites. Their compositions lie mid-way along the dravite-schorl series. Data was too limited to show any trends. Kawachi (1975) found Wakatipu tourmaline colours, in plane polarised light, ranged from bluish-greens to browns with increasing grade. This reflects an increase in the $(\text{FeTOT}+\text{Mn})/(\text{Mg}+\text{Ca})$ ratio and a move towards the Schorl end member. The tourmalines analysed in D7, D19 and D69 are bluish-green, which is appropriate for the low grade rocks they occur in.

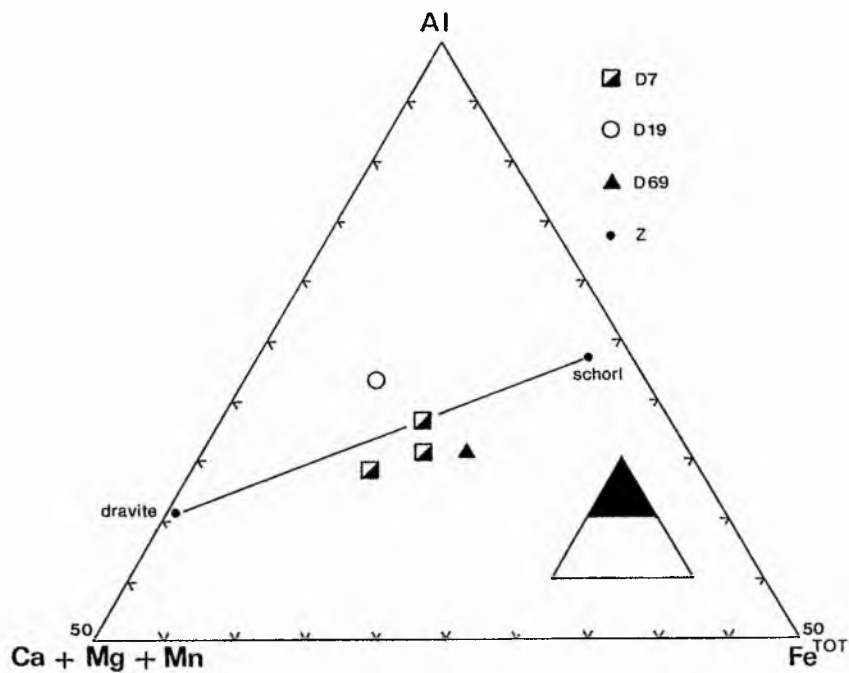


Fig. 4.13 - Tourmaline analyses (atomic proportions), from the Dalradian, plotted in terms of $\text{Ca}+\text{Mg}+\text{Mn}$, Al and total Fe. Schorl and dravite analyses (z), from Deer, Howie and Zussman (1975), are plotted for comparison.

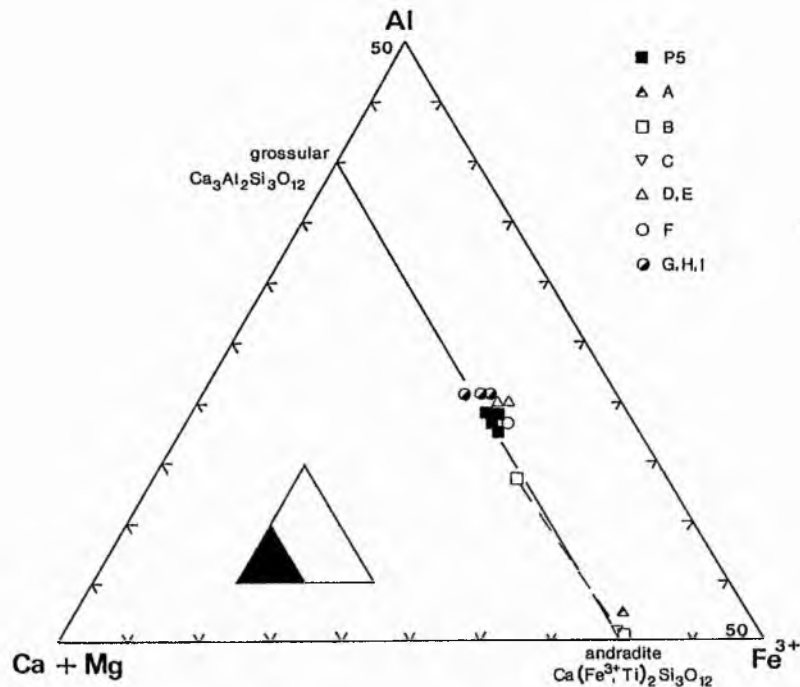


Fig. 4.14 - Granditic garnet analyses (atomic proportions), from P5 in the HBC, plotted in terms of $\text{Ca}+\text{Mg}$, Al and total Fe taken as Fe^{3+} . Comparative data is from the prehnite-actinolite facies (A, B, C) and the pumpellyite-actinolite facies (D to H) of southern New Zealand (Coombs et al., 1977). A = Harris Saddle, B = West Dome, C = Whare Creek, D, E = Gladstone Peak, F = Brown Peak, G, H, I = Upper Eglinton.

4.6.7 Almandine

3 almandine analyses are presented in Fig. 4.9 D. Chemical formulae (Appendix 4.7) are recalculated on the basis of 24 oxygen atoms.

The almandine garnet analyses are from small garnets in a Dalradian pelite (D3) and indicate that garnet schist grade is attained. Retrogressive chlorite is also associated with these garnets.

4.6.8 Granditic Garnet

4 grandite analyses, from P5, are presented in Fig. 4.14. Chemical formulae (Appendix 4.7) are recalculated on the basis of 24 oxygen atoms.

Granditic garnets occur in a number of HBC pillow basalt samples. Compositions show little variation and lie between andradite and grossular. $\text{FeTOT}/(\text{FeTOT}+\text{Al})$ ratios range from 0.51-0.55, compared to ratios of 0.48-0.55 for grandites described by Coombs et al. (1977). They commonly occur in amygdales and in pseudomorphs after olivine, but can also occur in the groundmass in close proximity to amygdales and pseudomorphs. Small rounded clear grains are usually enclosed in chlorite, but in addition can also be associated with epidote, calcite, actinolite, albite, pumpellyite and opaques. Quartz is present in veining not directly associated with grandite.

Coombs et al. (1977) described the assemblages grandite-chlorite-pumpellyite-epidote-calcite, and also prehnite, actinolite and quartz within a few millimetres of the other phases (D and E on Fig. 4.14), and grandite-

chlorite-epidote-actinolite-albite-quartz-pumpellyite, with relict actinolitic hornblende, and muscovite and zoisite within a few millimetres of the other phases (G, H and I on Fig. 4.14). D and E were in metabasites from the Gladstone Peak area, New Zealand, and G, H and I were in metabasites from the Upper Eglington area, New Zealand. These assemblages are very similar to those seen at Glen Esk. The Glen Esk assemblage falls into the pumpellyite-actinolite (PA) facies of metamorphism (see discussion in section 4.6.17).

4.6.9 Pumpellyite

A single pumpellyite analysis from HBS57 is presented in Figs 4.15 and 4.16. The chemical formula (Appendix 4.8) has been recalculated on the basis of 16 cations.

Pumpellyite occurs as a relatively common groundmass mineral, in the mafic rocks, associated with chlorite, albite, and various combinations of actinolite, epidote, sphene, opaques, calcite and relict clinopyroxene. It also occurs in amygdales and pseudomorphs after olivine in association with chlorite and opaques, and combinations of grandite, actinolite, epidote, albite, opaques and calcite. In HBS62 it is found in deformed veins associated with chlorite, epidote opaques, and later calcite and quartz. Colours range from brown to apple green. In pillow basalts groundmass pumpellyite is always apple green, while pumpellyite in amygdales and pseudomorphs are apple or olive green.

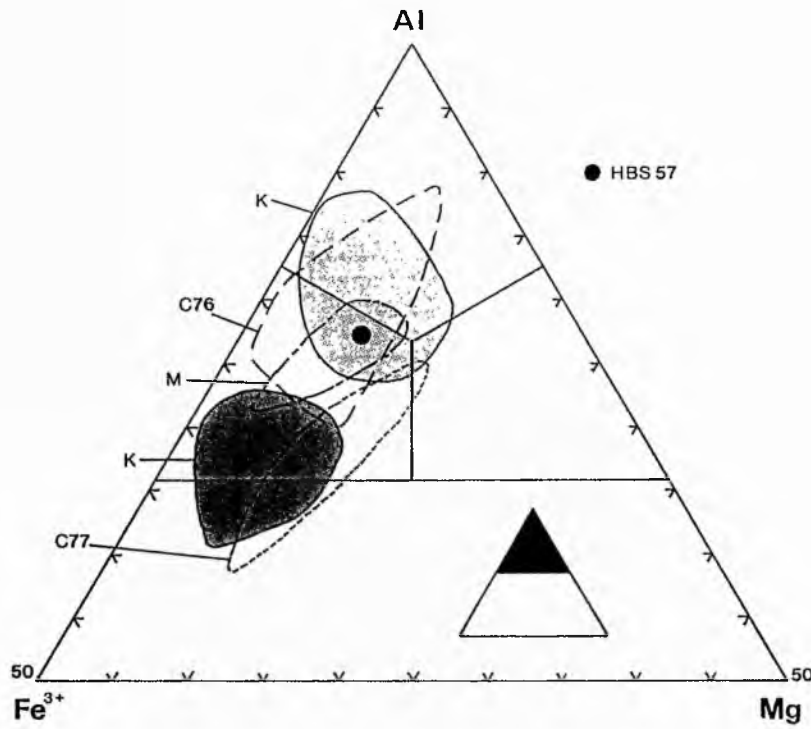


Fig. 4.15 - One pumpellyite analysis (atomic proportions), from HBS57 in the HBC, plotted in terms of Al, total Fe as Fe^{2+} , Mg. Comparative data is from zone I and II (dark stipple) and zone III (light stipple) of Upper Wakatipu, New Zealand (K = Kawachi, 1975), the pumpellyite-actinolite facies of Loeche, Switzerland (C76 = Coombs et al., 1976), southern New Zealand (C77 = Coombs et al., 1977), and Tal y Fan, Wales (M = Merriman et al., 1986).

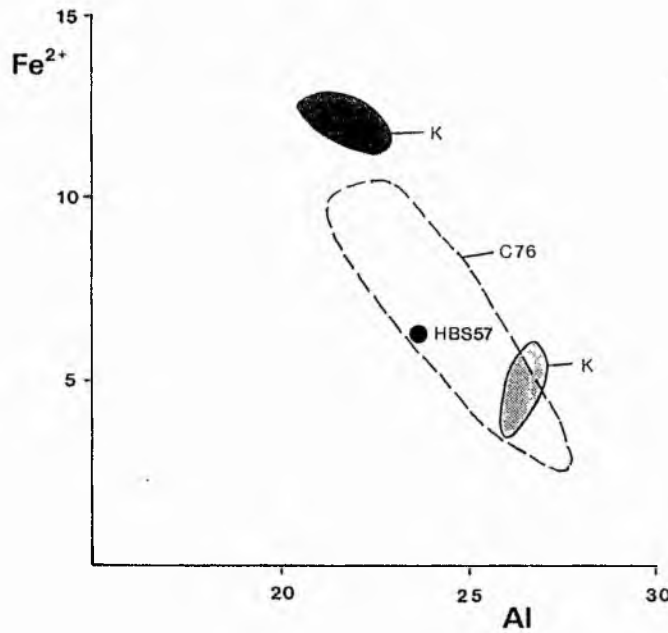


Fig. 4.16 - Total Fe as Fe^{2+} versus Al (wt%), in one pumpellyite analysis from HBS57. Comparative data from Kawachi (1975) and Coombs et al. (1976) as in Fig. 4.15.

4.6.10 Epidote

8 epidote analyses are presented in Fig. 4.17. Chemical formulae (Appendix 4.8) have been recalculated on the basis of 12.5 oxygen atoms.

Epidotes are a common groundmass, amygdale and vein mineral in mafic lithologies, purple shales and dolomitic shales. Analyses show limited compositional variation of these iron rich epidotes. On the assumption that all the iron is present as Fe³⁺ substituting for Al, the notional proportion of the Ca₂Fe₃Si₃O₁₂(OH) pistacitic (Ps) component is given by 100FeTOT/(FeTOT+Al). Compositions range from Ps 24-28 at Glen Esk.

4.6.11 Actinolite

3 actinolite analyses are pesented in Fig. 4.18. Chemical formulae (Appendix 4.6) are recalculated on the basis of 23 oxygen atoms.

Actinolites analysed have grown as colourless overgrowths on relict groundmass diopside in HBS3 and HBS57. Actinolite is also present in amygdales in metabasic rocks. In Fig. 4.18 comparative data from a number of localities is presented for actinolite in equilibrium with chlorite. Fe/Mg ratios for actinolite vary sympathetically with those of chlorite. Since the Fe/Mg ratio of chlorite is believed to be dominantly controlled by the bulk chemistry of the rock (see section 4.6.4), it is likely that the same control applies to actinolite.

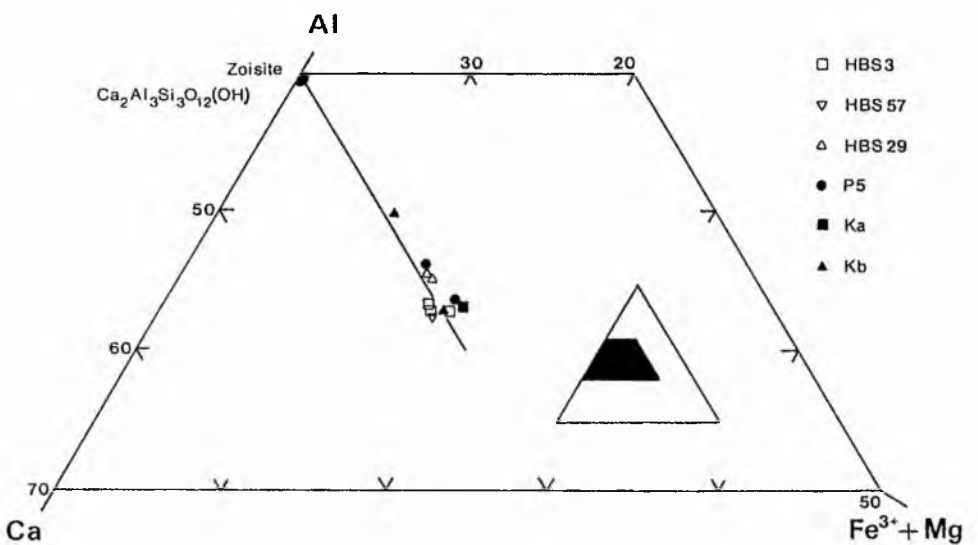


Fig. 4.17 - Epidote analyses (atomic proportions), from the HBC, plotted in terms of Ca, Al and Mg + total Fe as Fe^{3+} . Comparative analyses are from zone IIIa (Ka) and IIIb (Kb) of Upper Wakatipu, New Zealand (Kawachi, 1975). IIIb represent the range in compositions from a single epidote by rim (r) and core (c) analyses.

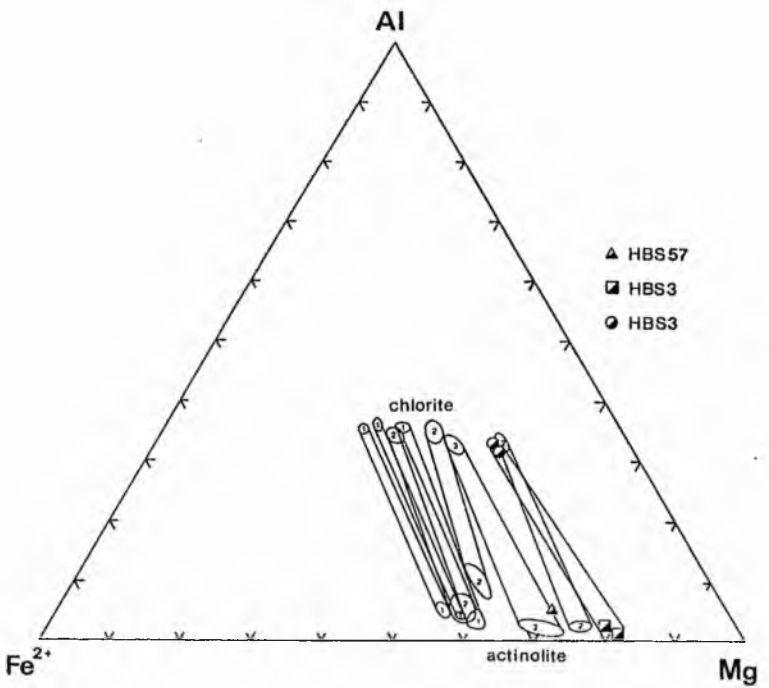


Fig. 4.18 - Coexisting chlorite and actinolite analyses (atomic proportions), from the HBC, plotted in terms of Al and total Fe as Fe^{2+} , Mg. Comparative data is from Loeche, Switzerland (1 = Coombs et al., 1976), Wales (2 = Bevins and Rowbotham, 1983), and southern New Zealand (3 = Coombs et al., 1977).

4.6.12 Feldspar

14 feldspar analyses are presented in Fig. 4.19. Chemical formulae (Appendix 4.9) are recalculated on the basis of 32 oxygen atoms.

5 Dalradian analyses fall in the albite field and one in the anorthoclase field. The latter is a detrital grain whereas the rest are metamorphic albite.

In the HBC, lithologies ranged from clastic sedimentary to pillow basalts. HBS5 yielded a detrital feldspar with Or97 and Ab3 components. In HBS29, a clinopyroxene rich lava, a groundmass feldspar has a composition in the labradorite field of An68, Ab32. This was the only unaltered plagioclase analysed. Other groundmass feldspars, some skeletal, ranged from An1 to An12. In P1B, a pillow basalt, 2 vein feldspars were analysed. One plotted at Ab97.8, An2.2, while the other plotted at Or89.3, Ab9.0, An1.7. The latter is possibly fine grained adularia.

4.6.13 Clinopyroxene

14 clinopyroxene analyses are presented in Figs 4.20, 4.21 and 4.22. Chemical formulae (Appendix 4.10) are recalculated on the basis of 6 oxygen atoms.

Relict clinopyroxene are common to most of the metabasic units. Analyses (see Fig. 4.20) plot in the diopside and augite fields as defined by the Subcommittee on Pyroxenes, IMA (Morimoto, 1988).

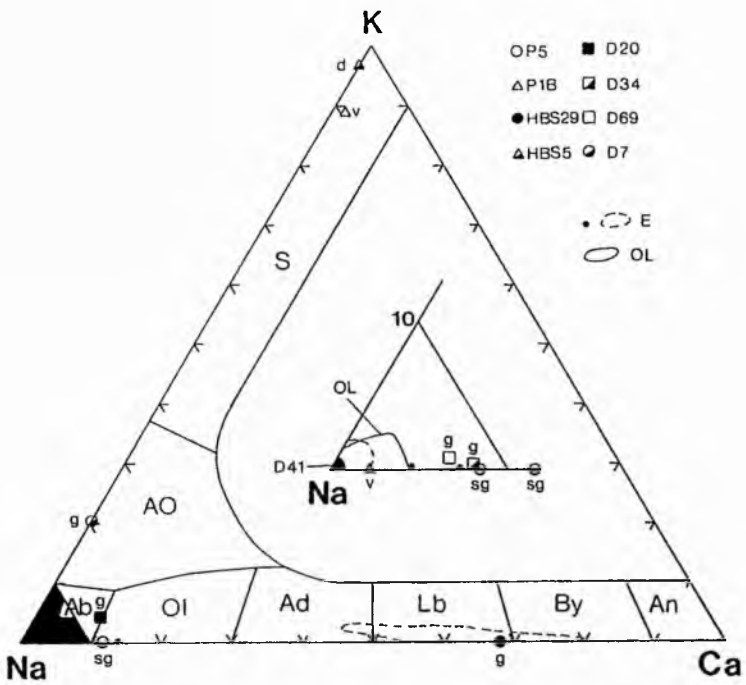


Fig. 4.19 - Feldspar analyses (atomic proportions), from Glen Esk, plotted in terms of K, Na and Ca. S = sanidine, AO = anorthoclase, Ab = albite, Ol = oligoclase, Ad = andesine, Lb = labradorite, By = bytownite, An = anorthite, g = groundmass, sg = skeletal groundmass, v = vein, d = detrital. Comparative data is from the Southern Uplands (OL = Oliver and Leggett, 1980), and the Midland Valley (E = Evans, 1987).

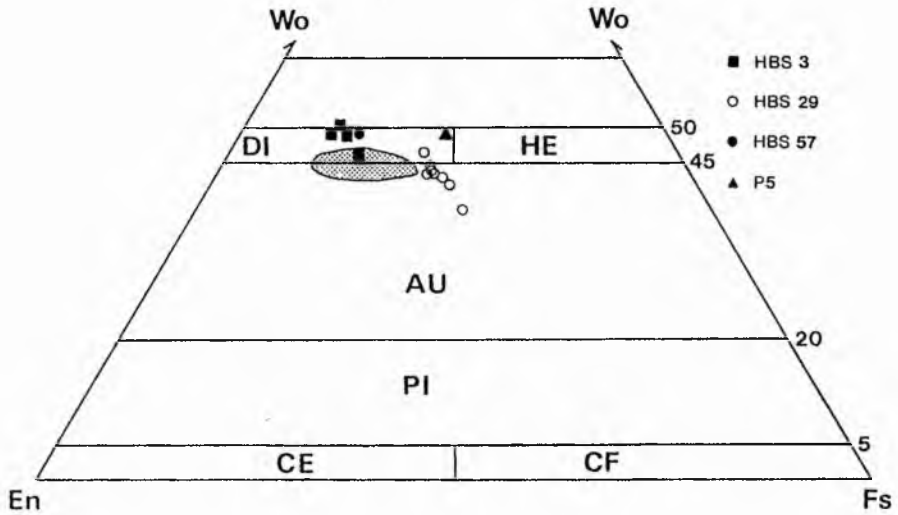


Fig. 4.20 - Clinopyroxene analyses (wt%), from the HBC, plotted in terms of Ca (Wo = wollastonite), Mg (En = enstatite), and Mn + total Fe as Fe^{2+} (Fs = ferrosilite). Clinopyroxene fields are after Morimoto (1988). DI = diopside, HE = hedenbergite, AU = augite, PI = pigeonite, CE = clinoenstatite, CF = clinoferrosilite. Comparative data from Tal y Fan, Wales (Merriman et al., 1986) is presented as a stippled area.

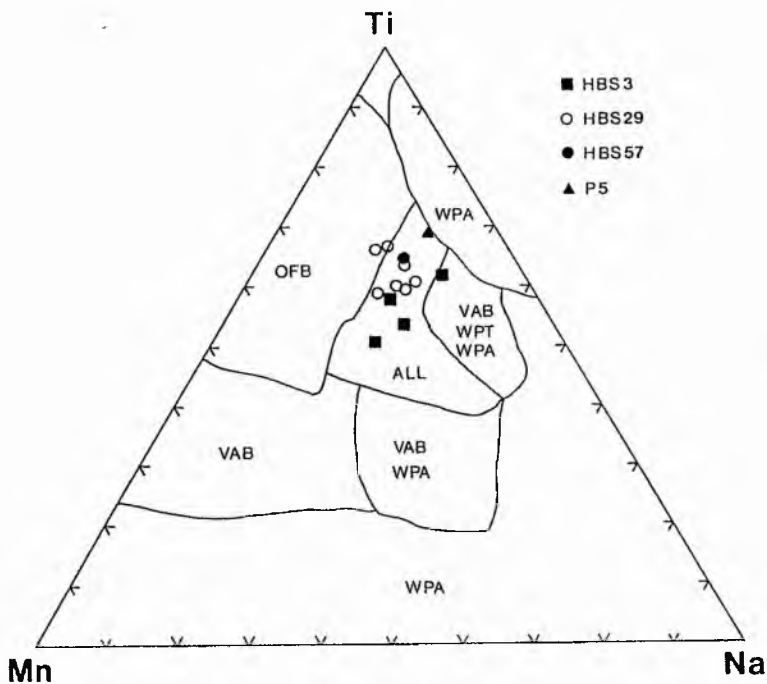


Fig. 4.21 - Clinopyroxene analyses (wt%), from the HBC, plotted in terms of Ti, Mn, Na. Fields are after Nisbet and Pearce (1977). OFB = ocean floor basalt, WPA = within plate alkali basalt, WPT = within plate tholeiitic basalt and VAB = volcanic arc basalt.

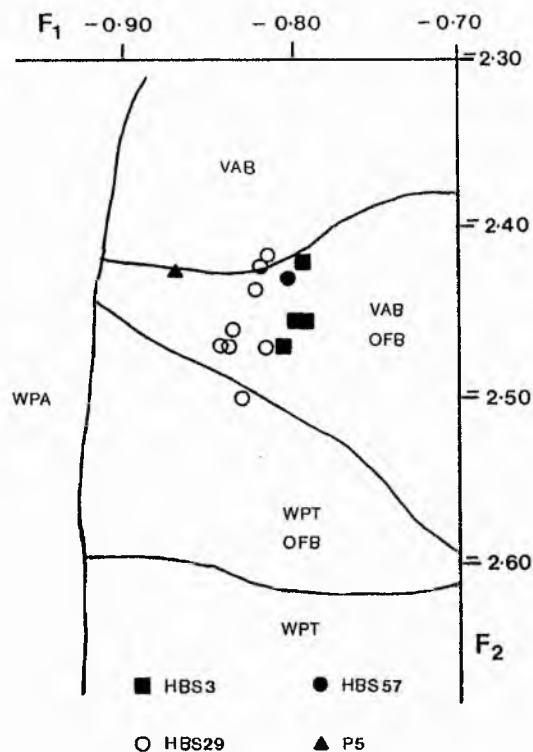


Fig. 4.22 - F1 versus F2 plot after Nisbet and Pearce (1977) for HBC clinopyroxenes. Fields as in Fig. 4.21.
 $F1 = -0.0120x\text{SiO}_2 - 0.0807x\text{TiO}_2 + 0.0026x\text{Al}_2\text{O}_3 - 0.0012x\text{FeO}^* - 0.0026x\text{MnO} + 0.0087x\text{MgO} - 0.0128x\text{CaO} - 0.0419x\text{Na}_2\text{O}$.
 $F2 = -0.0469x\text{SiO}_2 - 0.0818x\text{TiO}_2 - 0.0212x\text{Al}_2\text{O}_3 - 0.0041x\text{FeO}^* - 0.1435x\text{MnO} - 0.0029x\text{MgO} + 0.0085x\text{CaO} + 0.0160x\text{Na}_2\text{O}$.
* Total iron taken as FeO.

Bulk rock chemistry is the most commonly accepted and best constrained means of determining the tectonic setting of various basaltic lavas. Robertson and Henderson (1984) used this to categorise the basalts along the HBF in the field of Mid Ocean Ridge Basalts (MORB), with local occurrence of Within Plate Alkaline (WPA) basalts. Ikin (1983) described the suite as Ocean Floor Basalts (OFB) with local WPA. The tectonic settings of basalts have also been successfully constrained by microprobe chemistry on relict clinopyroxenes in metabasites. Nisbet and Pearce (1977) found correlation could be made with a 70% chance of success. Glen Esk clinopyroxenes have been plotted up in Figs 4.21 and 4.22 with data gathered by Nisbet and Pearce (1977) from various sources. Analyses show the strongest correlations with OFB and Volcanic Arc Basalts (VAB).

4.6.14 Albition

The albitisation of primary calcic plagioclase occurs as Fe^{2+} is made available to form pumpellyite. The process is summarised by the equation, plagioclase (An_{70}) + Fe^{2+} + Mg^{2+} + H_2O = Ab + pumpellyite (Kuniyoshi and Liou, 1976). This process requires the introduction of some Si, Fe, Mg, Na and H_2O , and the removal of Al. The necessary elements are probably supplied from the decomposition of earlier formed zeolites, interstitial glass and ilmenite. Released Al_2O_3 and CaO enters amygdales, veins and interstices, to crystallise pumpellyite, prehnite, chlorite, epidote or calcite.

Selective albitisation of some rocks or feldspars could be due to unequal distribution of interstitial water. Kuniyoshi and Liou (1976) propose that the concentration of Fe and Mg ions in the fluids is a critical factor. Primary oxides unmix into ilmenite and magnetite during cooling of the lava pile. With burial metamorphism, ilmenite is replaced by sphene, freeing Fe into the fluid, and obtaining Ca and Si from early formed zeolites or calcic plagioclase. The available Fe allows the conversion of the An plagioclase component to pumpellyite (+ chlorite).

Many albites at Glen Esk plotted outside the fields of albites found by others (e.g. Evans, 1987; Oliver and Legget, 1980). This may imply that the albitisation process was only partially completed. Evans (1987) found that plagioclase from zeolite facies basalts and tuffs were sometimes unaltered.

4.6.15 Controls of Metamorphic Assemblages

Under uniform pressure and temperature conditions variation in metabasite mineral assemblages can occur. This is due to the following factors:

1. Bulk Chemistry - Variations in the bulk chemistry of the rock, due to variation in original rock composition and the composition of fluids flushing through the rock, will result in variation in mineral assemblages.

2. $\text{Fe}^{3+}/\text{Fe}^{2+}$ Ratio - Increasing $\text{Fe}^{3+}/\text{Fe}^{2+}$ ratios lower invariant points in a modal system, and therefore can control the appearance and disappearance of minerals, as well as the minerals present.

3. Oxygen fugacity (fo_2) - This is the controlling factor on the Fe^{3+}/Fe^{2+} ratio. High fo_2 , usually due to water flushing through the rock, oxidises ilmenite to haematite and Ti compounds (Bevins and Merriman, 1988).

4. X_{CO_2} - With increasing X_{CO_2} the diagnostic Ca-Al silicates, epidote, prehnite, pumpellyite and actinolite, are suppressed (Roberts, 1981). Calcite grows instead. In addition the transition zone between the prehnite-pumpellyite and pumpellyite-actinolite facies expands, and the pumpellyite-actinolite facies is confined to higher pressures (Cho and Liou, 1987).

5. Rock Permeability - High permeability allows the movement of fluids through the rock resulting in the changes described above.

4.6.16 Equilibrium

Estimations of metamorphic grade in metabasites is dependant on whether or not the mineral assemblages studied are in equilibrium. It is debatable what constitutes an equilibrium assemblage. Nakajima et al. (1977) considered the area of a thin section to be in equilibrium, but Kawachi (1975) only accepted equilibrium between minerals in contact. Liou et al. (1985) and Cho and Liou (1987) found equilibrium in low variance buffered assemblages (for example in amygdales). The approach of Bevins and Merriman (1988) is perhaps most expedient for practical application. Uniform compositions of chlorite, epidote, prehnite, actinolite and pumpellyite, irrespective of growth site, is taken as indicating an approach to equilibrium.

4.6.17 HBC Metabasite Assemblages

A list of mineral assemblages from metabasic rocks in the HBC are presented in table 4.2. Dolomitic shales and purple shale both tend to be dominated by haematite and calcite. The original rock was probably permeable tuffaceous material. The growth of index minerals was suppressed by high f_{CO_2} and X_{CO_2} (see section 4.6.15). Pillow basalts and massive lavas contain no haematite and have well developed pumpellyite-actinolite facies mineralogies. These are characteristic of the low f_{CO_2} , low X_{CO_2} assemblages shown in Figs 4.23 A and B.

CO_2 , giving high f_{CO_2} values in dolomitic and purple shales, could have been derived from within the basaltic pile. Stopler and Holloway (1988) have shown experimentally that basaltic glass, erupted over a pressure range of 100 to 1500 bars, contains between c.25 and 550 ppm dissolved CO_2 , despite degassing of the basaltic magma. These values are a minimum. In examples of submarine basalts higher values are attributed to the incomplete degassing of the magma as it rapidly ascends. The CO_2 is released from the basalts during spilitisation. Additional CO_2 could have been derived by devolatilisation of carbonates in the HBC.

Equilibrium of metabasite mineral assemblages is shown by lack of chemical variation of epidote, chlorite and grandite, and textural equilibrium between coexisting chlorite and actinolite, within a thin section. The differences between groundmass, and amygdale or olivine pseudomorph assemblages reflects local variations in bulk

Table 4.2 - Mineral assemblages for HBC metabasite samples.
Samples are presented in stratigraphical order (i.e. from south to north).

Lithology and sample number	Location in thin section	Mineral Assemblage
<u>Dolomitic Shale</u>		
HBS26	Groundmass	Haem-Chl-Ab-Sph
	Amygdales	Haem-Chl
	Veins	Ep-Calc-Dol-WMica
<u>Pillow Basalts</u>		
P1A and B	Groundmass	Chl-Ab-Pump-Sph
	Veins	Chl-Ep-Calc-Ab
P2, P3	Groundmass	CPX*-Chl-Ab-Pump-Sph
	Amygdales	Chl-Calc
	Veins	Chl-Ep-Calc-Ab
P4	Groundmass	CPX*-Chl-Ab-Pump
	Amygdales	Chl-Grand-Act-Pump-Op-Calc
	Ol Pseudo	Chl-Grand-Act-Pump-Op-Ep- Calc
	Veins	Chl-Ep-Calc-Qtz
P5	Groundmass	CPX*-Chl-Ab-Act-Pump
	Amygdales	Chl-Grand-Op-Calc
	Ol Pseudo	Chl-Grand-Act-Pump-WMica- Ep-Op-Calc
	Veins	Ep-Calc-Qtz
<u>Lava</u>		
HBS29	Groundmass	CPX*-Lab*-Chl-Ab-Act-Ep- Sph
	Veins	Chl-Ep-Calc-Qtz
<u>Purple Shale</u>		
HBS42	Groundmass	Haem-Chl-Ep-WMica-Calc-Qtz
HBS46	Groundmass	Haem-Chl-Qtz-Calc
	Veins	Ep-Calc
HBS51	Groundmass	Haem-Chl-WMica-Calc-Qtz
	Veins	Ep-Calc
HBS4	Groundmass	Haem-Chl-WMica-Sph-Ep-Qtz
	Veins	Ep-Chl-Qtz-Calc
<u>Green Pelite</u>		
HBS53	Groundmass	Chl-Sph-Calc-Qtz-Op
	Veins	Calc-Qtz
HBS1	Groundmass	Chl-Ep-Calc-WMica-Qtz-Op
HBS2	Groundmass	Chl-WMica-Ep-Calc-Qtz-Op
HBS3	Groundmass	CPX*-Chl-Ab-Act-Ep-Sph
	Amygdales	Chl-Ep-Act-Sph
HBS57	Groundmass	CPX*-Chl-Ab-Pump-Act-Ep- Sph
	Amygdales	Pump-Ep-Chl-Op-Calc-Ab
	Feld Pheno	Pump-Ab-Chl-Calc-Op
HBS62	Groundmass	Pump-Chl-Ab-Ep-Act
	Vein	Pump-Chl-Ep-Op-Qtz-Calc

Abbreviations

Chl-Chlorite, Ab-Albite, Pump-pumpellyite, Act-Actinolite,
Ep-Epidote, WMica-white mica, Calc-calcite, Qtz-quartz,
Haem-Haematite, Op-opaques, Sph-sphene, CPX-clinopyroxene,
Lab-labradorite, Ol Pseudo-Olivine pseudomorph, Feld Pheno-
Feldspar phenocryst. * = Relict phase.

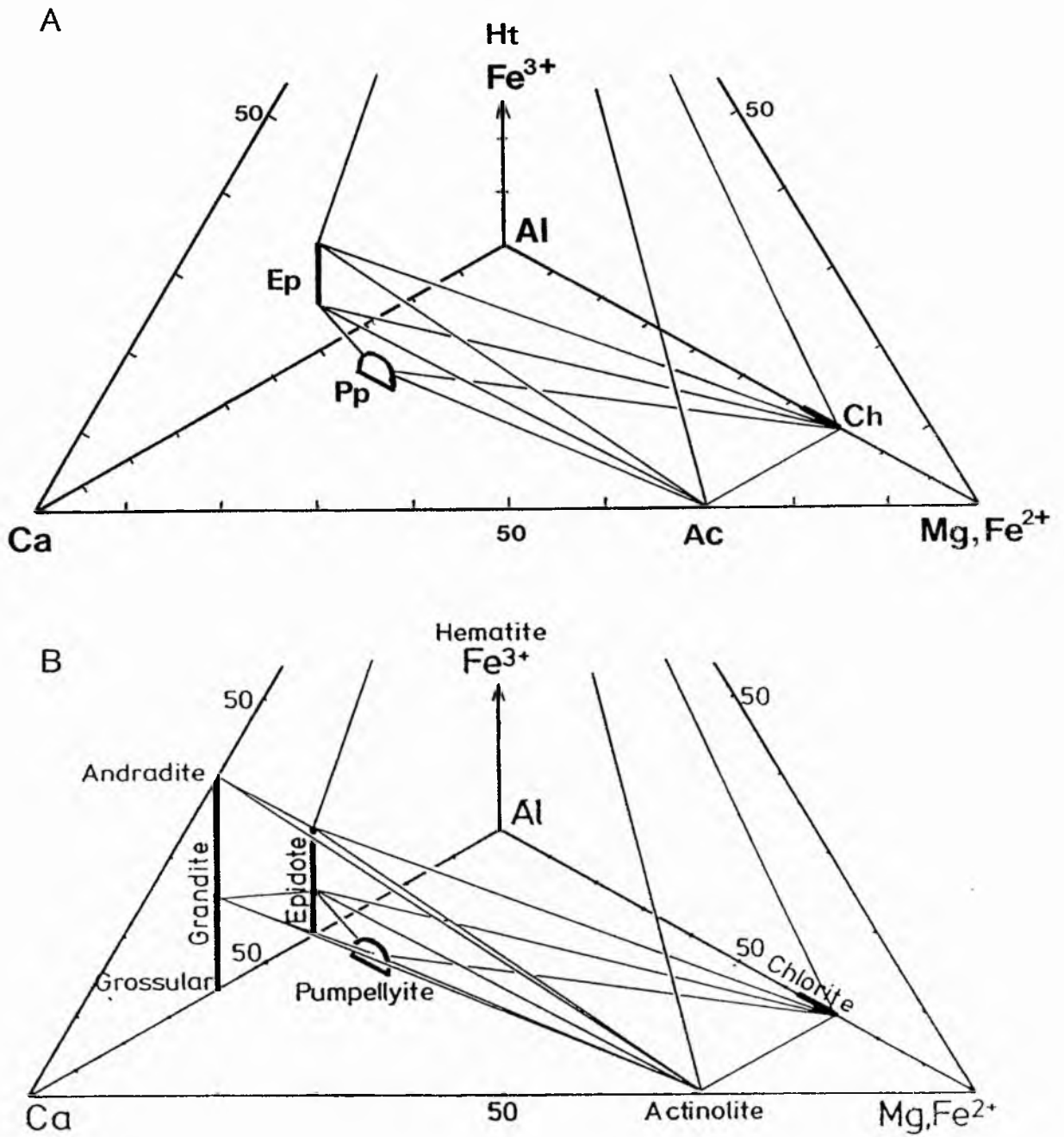


Fig. 4.23A, B - Ca, Fe^{3+} , $(\text{Mg}+\text{Fe}^{2+})$, Al cation proportion diagrams showing various phases stable in the pumpellyite-actinolite facies; tie lines join coexisting phases (after Coombs et al., 1977). FeO contents of grandite and epidote, and Fe_2O_3 content of chlorite are ignored. Ep = epidote, Ht = haematite, Pp = pumpellyite, Ch = chlorite, Ac = actinolite. In A, HBC pillow lavas, massive lavas and green pelites plot in the Ch, Ac, Ep, Pp field, and purple shales and dolomitic shales plot in the Ht, Ch, Ep, Ac field. In B, amygdales and olivine pseudomorphs from pillow lavas, plot in the Ch, Ac, Pp, Ep, Grandite field. Chlorite-grandite coexist in equilibrium despite being separated by planes joining Ep, Ht, Ac, Pp.

composition. This is visually apparent from the distribution of grandite. These garnets are mostly confined to amygdales and pseudomorphs, but are also sometimes found in the groundmass immediately adjacent to them. Well developed pumpellyite-actinolite facies assemblages are found in the green pelites. Pumpellyite is found in HBS57 and HBS62. These two samples are representative of the upper part of the green pelite sucession. The absence of pumpellyite in the lower part may be due to the supression of pumpellyite formation with slightly higher X_{CO_2} . It is less likely to indicate the attainment of greenschist facies because the pumpellyite bearing pillow basalts and lavas underly the green pelites.

4.6.18 Metamorphic Grade

A. Dalradian

Increasing grade of metamorphism in the Dalradian is demonstrated by the progression from chlorite to biotite to garnet zones. The temperatures and pressures at which biotite and garnet are first formed are poorly constrained. According to Winkler (1979, p.242 to 245) biotite is formed at between 420 and $450^{\circ}C$ for a large range of pressures for example at c.435 C/3.5kb). Almandine rich garnet becomes stable at $500^{\circ}C/4kb$, though the range of temperature and pressure at which it is stable is not known. Increasing grade is also characterised by a relative increase in the amount of Al in white mica compared to Mg, Fe and K. Atherton (1977), in a study of Dalradian metamorphism, found this was reflected by a reduction of the white mica

field towards the composition of muscovite (see Figs 4.9A to D).

B. HBC

Actinolite - Kawachi (1975) relates an increase in the % Al of actinolites to increasing metamorphic grade. His Wakatipu zone IIIa actinolites average 0.61% Al_2O_3 , while IIIb and IV average 1.61% Al_2O_3 . This trend may exist, though the 3 analyses from Glen Esk range from 0.29-1.45% Al_2O_3 , showing a considerable range of Al content for rocks of one grade.

Pumpellyite - The Fe/(Fe+Al) ratio of pumpellyites has been related by a number of authors to metamorphic grade (for example Kawachi, 1975; Coombs et al., 1976). Lower ratios are associated with increasing metamorphic grade. While this may be true other factors may contribute. Cho and Liou (1987) found that the Fe content of pumpellyite is also sensitive to effective bulk composition, showing wide ranges in composition within a thin section. The decrease in Fe in pumpellyite may also be attributed to decreasing f_{O_2} with increasing metamorphic grade. Decreasing f_{O_2} permits the preferential partitioning of ferrous iron into coexisting actinolite and chlorites (Schiffman and Liou, 1980).

The one pumpellyite analysis from Glen Esk plots in the IIIb pumpellyite field of Kawachi (1975) (see Fig. 4.15). This corresponds to the upper pumpellyite-actinolite facies, though colouration is more consistent with zone IIIa (lower pumpellyite-actinolite facies). Coombs et al.

(1977) described prehnite-pumpellyite facies pumpellyite with 9.9-14.7% FeTOT and 2.1-2.5% Mg, and upper pumpellyite-actinolite facies pumpellyite with 5.6% FeTOT and 3.7% Mg. These analyses have $100\text{Fe}/(\text{Fe}+\text{Al})$ ratios of 26-38 and 14 respectively. The Glen Esk analysis has 6.3% FeTOT and 2.0% Mg, and a ratio of 16. This would correspond well with medium to high pumpellyite-actinolite facies metamorphism. When the evidence gained from colour is also considered, the Glen Esk assemblage would probably fall in the medium pumpellyite-actinolite facies.

Epidote - Epidote compositions range from Ps 24-28 at Glen Esk. This compares with Ps 28-37 for pumpellyite-actinolite facies epidotes described by Coombs et al. (1976), and Ps 22-34 and Ps 11-18 (Fe-poor epidotes) for epidotes attributed to the upper part of the pumpellyite-actinolite facies (Coombs et al., 1977). Nakajima et al. (1977) have demonstrated that the Ps composition of epidotes steadily decreases with increasing metamorphic grade. The upper limit of the pumpellyite-actinolite facies has been correlated with Ps 10-15 and c. 390°C , with a lower limit of Ps 31-34 and c. 300°C . Below this temperature haematite-pumpellyite becomes stable. This implies that the Glen Esk samples lie in the middle of the pumpellyite-actinolite facies.

4.6.19 Chlorite Geothermometer

An attempt has been made to determine the temperature of metamorphism within the HBC and Dalradian using a chlorite geothermometer devised by Cathelineau and Nieva

(1985). They found that in chlorites, in andesites from a bore hole (where accurate temperature estimates could be made), variation of the site occupancy (mainly of Al_{IV} in the tetrahedral site and $6\text{-}\text{Al}_{\text{VI}}\text{-}[\text{Mg}+\text{Fe}^{2+}] = \text{vacancy (VAC)}$ in the octahedral site) were mainly temperature dependant.

In Fig. 4.24 Al_{IV} is plotted against the VAC value for both HBC and Dalradian chlorites. A line ($X=Y$) has been included. This line indicates what Al_{IV} and VAC values correspond to the same formation temperatures on the basis of Cathelineau and Nieva's data.

HBC chlorites correlate well with the $X=Y$ line, and have then been plotted on Fig. 4.25 to obtain absolute temperature estimates. They range from 220.5 to 272.5°C ($213\text{-}280$ C within error bars) and are presented in table 4.3 (error bars reflect the range in composition of chlorites from each sample).

Dalradian samples show relatively poor correlation with the $X=Y$ line. On Fig. 4.25 this is reflected by wide differences in the temperature estimates determined from the VAC site and the Al_{IV} site. D7 (from immediately adjacent to the HBC) shows the best correlation with temperature estimates ranging from 272.5 to 295.5°C ($258\text{-}305.5$ °C within error bars). Biotite and garnet grade samples gave lower temperature estimates with larger error bars.

The lack of correlation in Dalradian samples could be due to several reasons. 1. Chlorites could be interlayered with biotite or muscovite. To avoid this analyses with

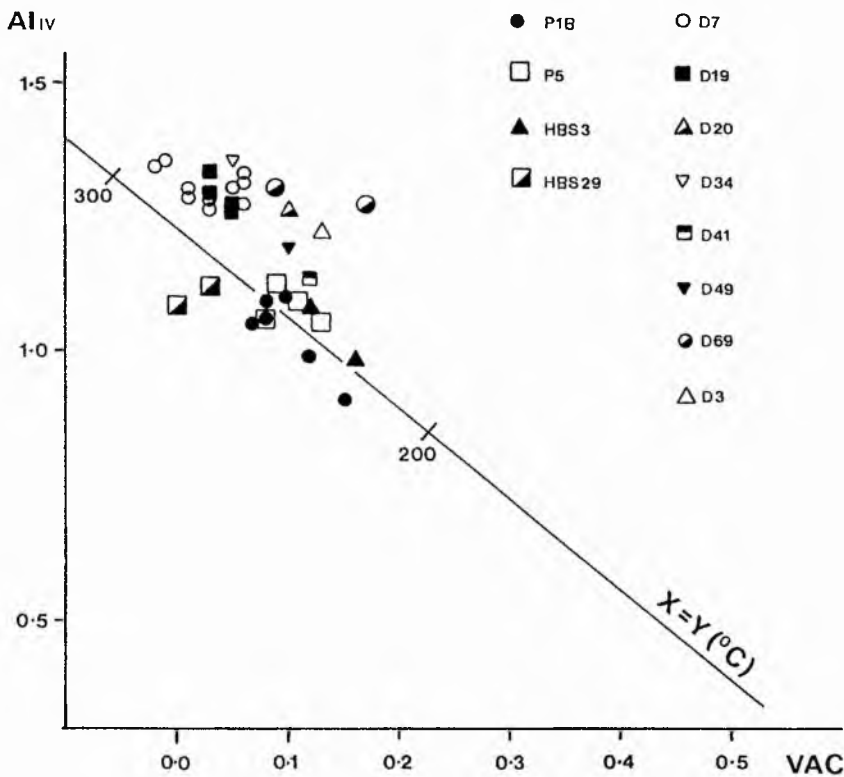


Fig. 4.24 - Correlation diagram showing variations in tetrahedral aluminium (Al_{IV}) as a function of octahedral vacancy (after Cathelineau and Nievea, 1985). $X = Y$ line indicates Al_{IV} and vacancy values corresponding to the same temperatures.

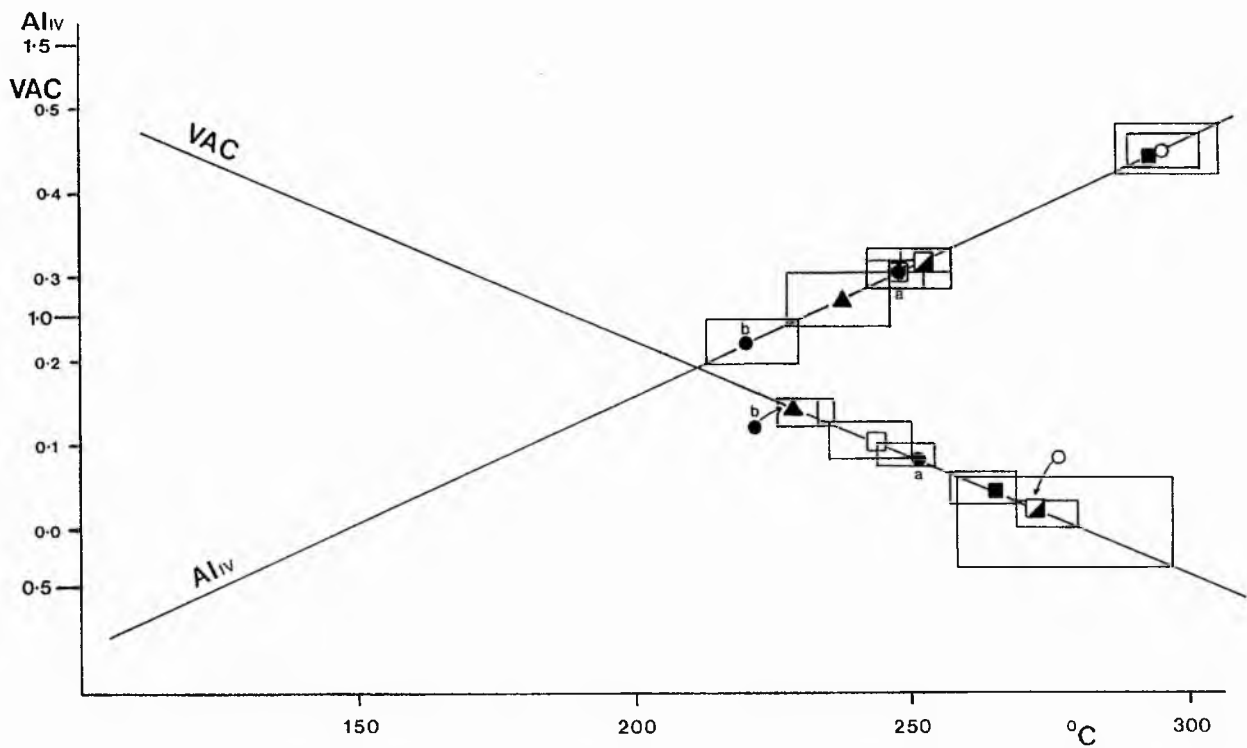


Fig. 4.25 - Plot of Al_{IV} and octahedral vacancy versus temperature for some HBC and Dalradian samples listed in Fig. 4.24 (after Cathelineau and Nievea, 1985). Rectangles indicates temperature ranges produced by compositional ranges within a population of analyses. Sample P1B has been subdivided into analysis populations a and b.

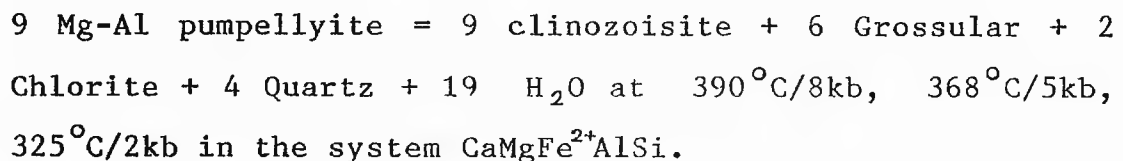
Table 4.3 - Chlorite geothermometric estimates for HBC and Dalradian chlorites, based on site occupancy of Al_V and octahedral vacancy (VAC) site (after Cathelineau and Nieva, 1985). Errors derived from the range of chlorite analyses within a sample (bracketed). These temperatures lie in the pumpellyite-actinolite field of Fig. 4.26.

Sample	Al _V	VAC Temperature (°C)
<u>Highland Border Complex</u>		
HBS29	252.5 (+ or -4.5)	272.5 (+7.5, -2.5)
P1Ba	248 (+4, -6)	251.5 (+2.5, -7.5)
P1Bb	220.5 (+9, -7.5)	229 (+7, -3)
P5	248 (+9, -6)	244 (+6, -9)
HBS3	238 (+8, -10)	229 (+4, -3)
<u>Dalradian</u>		
D7	295.5 (+10, -8.5)	272.5 (+24.5, -14.5)
D19	293 (+9, -4)	265 (+4, -7)
D20	287 (one analysis)	244
D3	287 (, ,)	233 garnet grade

abnormally high K content are omitted. 2. The geothermometer of Cathelineau and Nieva may only be appropriate for metamorphosed fine grained igneous rocks where pore fluids have had free flow, as in geothermal environments. Chlorites from metapelites may have different compositional controls or show different trends with temperature. 3. The study of Cathelineau and Nieva was limited to the temperature range 130-300°C. By the time 300°C is reached the octahedral vacancy site is filled. Again the behaviour of chlorite composition may be different at temperatures >300°C.

4.6.20 Metabasite Mineral Assemblages

Absolute PT values for the pumpellyite-actinolite facies have been based on experimental work. Schiffman and Liou (1980) attempted to constrain the upper boundary of the pumpellyite-actinolite facies with the disappearance of Mg-Al pumpellyite through the reaction:



This system does not take into account the effect of Fe_2O_3 in the system which would tend to lower the equilibrium temperatures.

Nakajima et al. (1977) modelled the stability field of coexisting pumpellyite-epidote-actinolite-chlorite, with a temperature range of 300-390°C.

Liou et al. (1983) found that the garnet-in, prehnite-out reaction occurred as a continuous reaction.

The reaction occurs at 325-343 °C/2kb, 353-375 °C/5kb and 373-395 °C/8kb P(fluid), and oxygen fugacity (f_{O_2}) of the haematite-magnetite (HM) buffer. Higher $Fe^{3+}/(Fe^{3+} + Al)$ ratios are associated with higher f_{O_2} and lower reaction temperatures within the ranges above. This system shows the depression of the reaction curve by the introduction of Fe_2O_3 .

Liou et al. (1985) have produced a petrogenetic grid for low grade metamorphic facies based on the system $Na_2O-CaO-MgO-Al_2O_3-SiO_2-H_2O$. (see Fig. 4.26). The pumpellyite-actinolite field ranges from c.2.4-8kb and c.250-370 °C. When Fe_2O_3 is introduced to the system reaction curves and invariant points are displaced (shown by the arrows on Fig. 4.26). For example, in Fig. 4.27, the addition of enough Fe_2O_3 to produce a P_s value of 26 in epidote results in a displacement of the invariant point VI from an original value of 340 °C/2.4kb to a new value of 297 °C/1.77 kb. The introduction of Fe_2O_3 to the system depresses the pumpellyite-actinolite field to a range of 210 to 320 °C/1.8 to c.7kb.

4.21 PT Estimate

An estimate of peak PT conditions in the metabasic assemblage at Glen Esk, based on the petrogenetic grid of Liou et al. (1985), would lie in the middle pumpellyite-actinolite facies (on the basis of epidote and pumpellyite compositions (see section 4.6.18) at c.265 °C. This temperature correlates well with the temperatures derived from chlorite geothermometry in section 4.6.19.

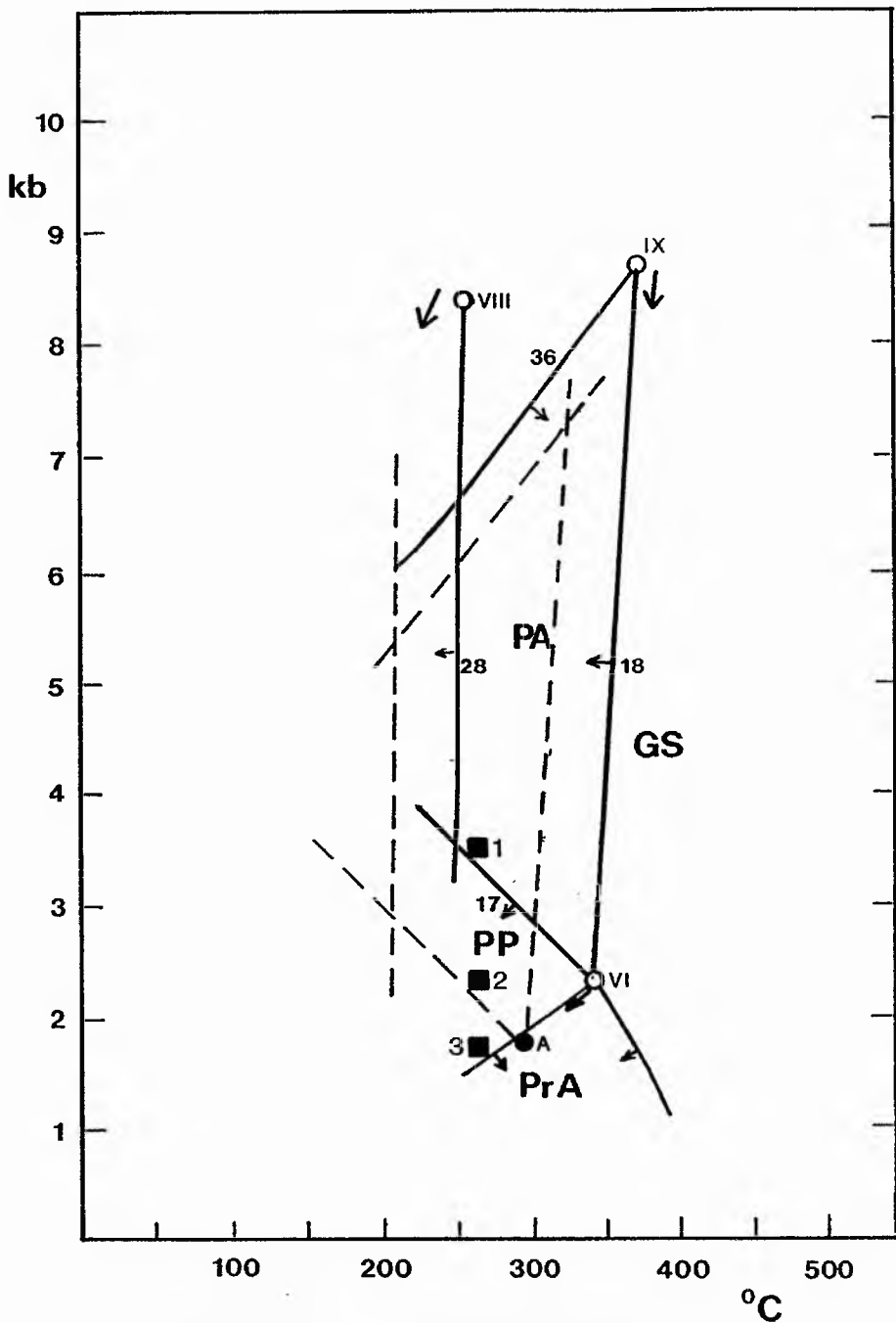


Fig. 4.26 - P (fluid)-T diagram showing a petrogenetic grid of various low-grade metamorphic facies in the system $\text{Na}_2\text{O}-\text{CaO}-\text{MgO}-\text{Al}_2\text{O}_3-\text{SiO}_2-\text{H}_2\text{O}$ (after Liou et al., 1985). PA = pumpellyite-actinolite facies, GS = greenschist, PP = prehnite-pumpellyite facies, PrA = prehnite-actinolite facies; VI, VIII and XI are invariant points; solid lines indicate metamorphic reactions:

- (17) prehnite + chlorite + quartz = pumpellyite + tremolite + H_2O .
- (18) pumpellyite + chlorite + quartz = tremolite + epidote + H_2O .
- (28) lawsonite + pumpellyite = zoisite + chlorite + quartz + H_2O .
- (36) Pumpellyite + glaucophane + quartz + fluid = tremolite + chlorite + albite.

Displacements of reaction curves and invariant points are shown by arrows. Point A and dashed lines indicates the displacement appropriate to a P_s value of 26 kb. The black squares 1, 2, 3 represent estimates of metamorphic grade for the HBC metabasic assemblages for different geothermal gradients. 1 = $20^\circ\text{C}/\text{km}$, 2 = $30^\circ\text{C}/\text{km}$, 3 = $40^\circ\text{C}/\text{km}$ (see text).

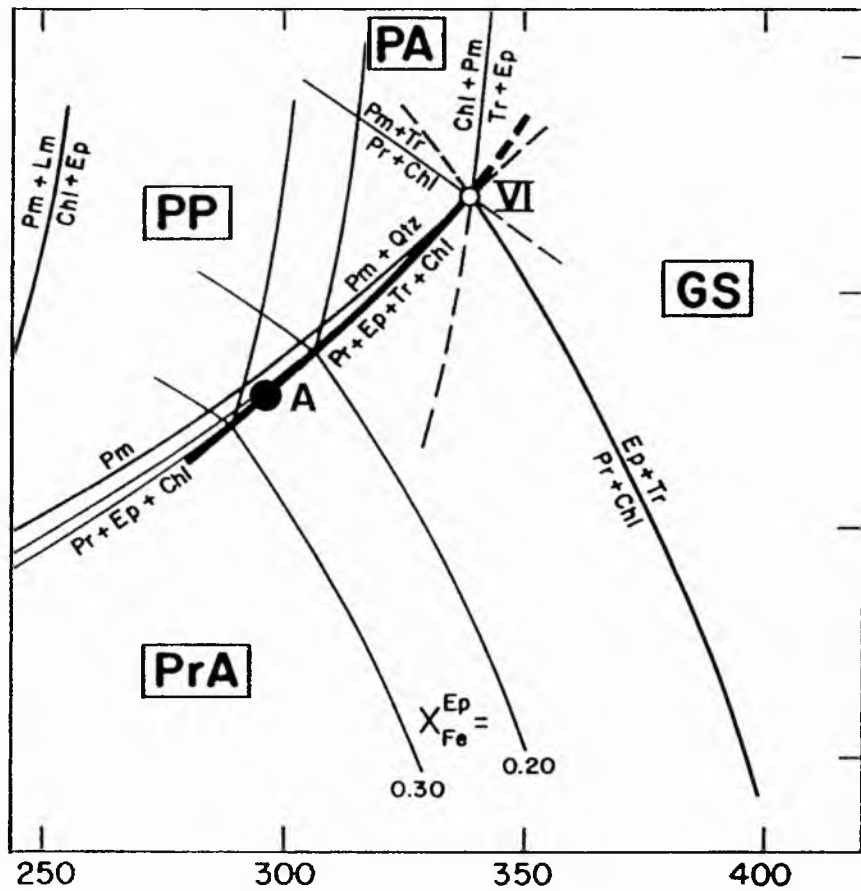


Fig. 4.27 - P (fluid)-T diagram showing the displacement of invariant point VI and reaction curves at the introduction of Fe_2O_3 into the model basaltic system (after Liou et al., 1985). Isopleths are designated as $\text{Ps} + \text{Fe}^{3+}/(\text{Fe}^{3+} + \text{Al})$ of epidote. For a Ps of 26 (0.26 on this diagram) Invariant point VI is displaced to A (at $297^\circ\text{C}/1.77\text{kb}$).

Estimates of pressure conditions are poorly constrained, ranging from c.2 to c.7kb in the pumpellyite-actinolite field (see Fig. 4.26). By taking three example geothermal gradients a selection of pressures and burial depths can be estimated (assuming an average rock density of 2.70g/cm³ and an increase in pressure of 265 bars/km) as follows:

Geothermal gradient	Pressure	Burial Depth
20° C/km	3.51kb	13.2km
30° C/km	2.34kb	8.8km
40° C/km	1.75kb	6.6km

A geothermal gradients of 30° C/km puts the pressure at the lower limit of the pumpellyite-actinolite field. Any higher geothermal gradient would put the pressure in the prehnite-pumpellyite field.

4.22 Conclusions

The metabasites of the HBC provide a control on PT conditions. The assemblage chlorite-actinolite-pumpellyite-epidote-albite-grandite-calcite-quartz lies clearly in the pumpellyite-actinolite facies. Compositional evidence from actinolites, pumpellyites and epidotes further constrain the grade to the middle part of the pumpellyite-actinolite facies. An estimate of temperature conditions, based on experimental work, puts peak metamorphism in the HBC metabasites at c.265° C. This corresponds to a pressure of 3.51kb, with a burial depth of 13.2km, for a geothermal gradient of 20° C/km, and a pressure of 1.75kb, with a burial depth of 6.6km, for a geothermal gradient of 40

$^{\circ}\text{C}/\text{km}$. On the basis of chlorite geothermometry, HBC chlorites give temperatures ranging from 220.5 to 272.5°C . If the temperature of 272.5°C is taken as indicative of peak metamorphism, then this temperature estimate correlates well with that determined by mineral assemblages. In section 4.5.3 the peak metamorphism was correlated with the collision of the Dalradian and HBC, and the major movement on the HBF that immediately followed collision. From this it can be inferred that the HBC, exposed today, collided with the Dalradian at a depth of $>8.8\text{ km}$.

PT conditions in the Dalradian are less easily quantified. Chlorite geothermometry has only limited success. D7, immediately adjacent to the HBC, gave temperature estimates of 272.5 to 295.5°C . Phyllosilicate mineralogy suggests that these temperatures are minima (see section 4.6.18). Samples from biotite and garnet grade rocks do not exceed this temperature estimate, and showed large error bars. It is likely that the controlling factors on chlorite composition, in Dalradian samples, are different from those controlling the composition of HBC chlorites, and that temperatures of 300°C have been exceeded.

If the biotite-in and almandine-in PT estimates considered in section 4.6.18 are taken as appropriate for the Dalradian, then:

1. - Biotite, forming at $435^{\circ}\text{C}/3.5\text{kb}$, would indicate a geothermal gradient of 33°C/km and a burial depth of 13.2km.

2. - Garnet, forming at $500^{\circ}\text{C}/4\text{kb}$, would indicate a geothermal gradient of 33°C/km and a burial depth of 15.1km.

Though there is no pressure control to test the above estimates they are not inappropriate for Barrovian metamorphic conditions. PT estimates are further discussed in section 4.10.

4.7 PHYLLOSILICATE MINERALOGY

(in relation to illite crystallinity)

4.7.1 Introduction

The $<2\mu\text{m}$ mineralogy of 35 Dalradian and 26 HBC samples was examined by XRD. Mineralogy, crystallinity and b_0 values are listed in Appendix 4.11, including those for analyses excluded from the illite crystallinity study. The mineralogy of 24 Dalradian and 23 HBC samples in relation to illite crystallinity are summarised in Fig. 4.28 along with comparative data from Wales and the IOM. The relative proportions of minerals are semi-quantified visually as small, medium or large scale.

The lithological complexities of the Dalradian and HBC have resulted in a broad overlap in the illite crystallinity values that does not necessarily reflect an overlap in metamorphic grade (see section 4.8). This broad scatter of results prevents a clear correlation between Hbrel and mineral paragenesis. Because of this the mineralogy of the Dalradian and HBC will be considered separately.

4.7.2 Dalradian

Of the Dalradian samples analysed D7 to D13 were collected from the chlorite zone, D14 to D69 were collected from the biotite zone (though biotite is not always present) and D3 was collected from the garnet zone. The Dalradian samples can be divided into two groups based broadly on the occurrence of biotite. D7 to D21 and D65 to D69 contain little or no biotite, and range in $<2\mu\text{m}$ Hbrel

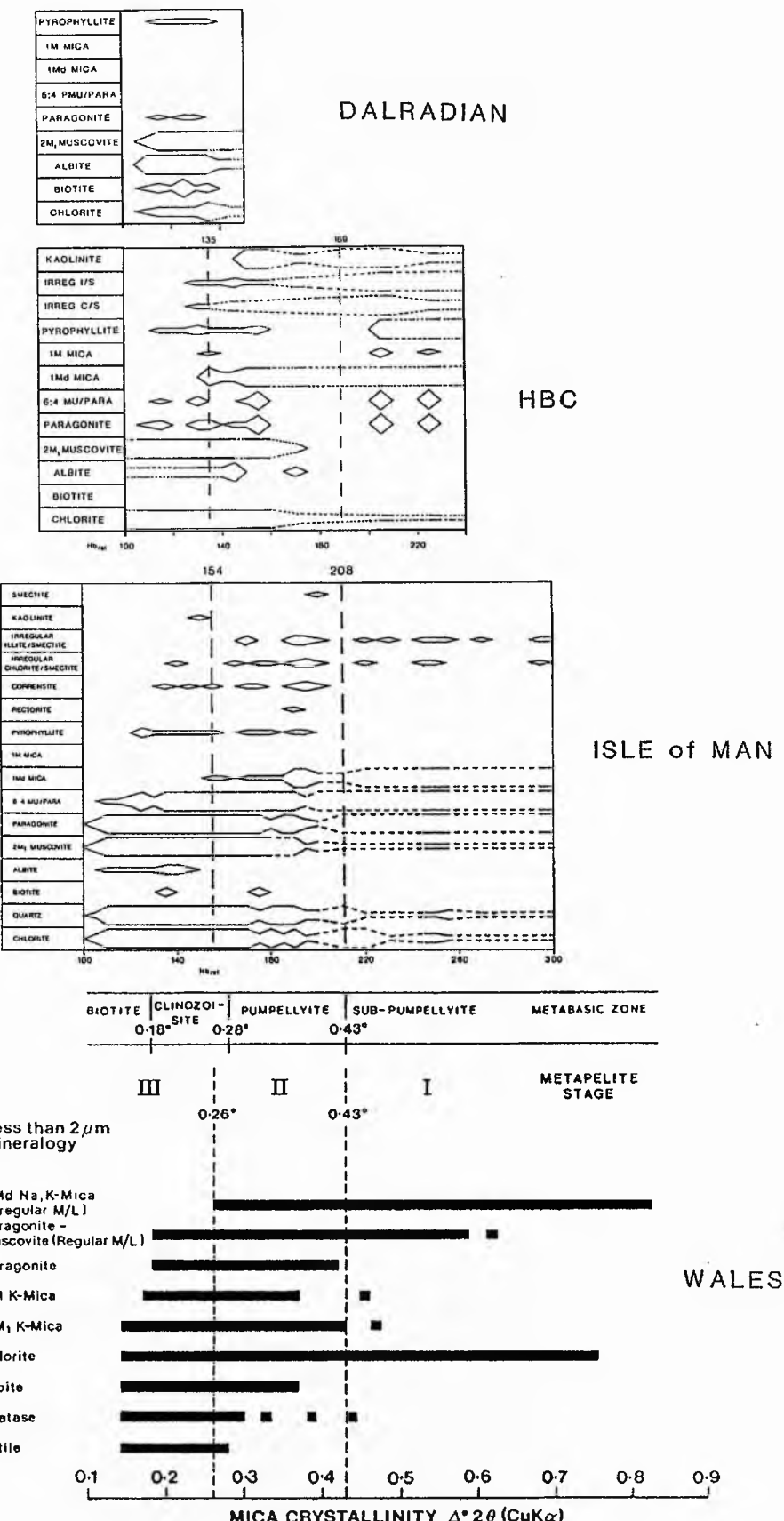


Fig. 4.28 - Mineralogy of the <2µm size fraction compared to Hbrel. Relative proportions of minerals (shown by the widths of bars) are quantified on a small, medium and large scale by visual inspection of XRD traces. Lower and upper limits of the anchizone are taken at Hbrel 135 and c.190. Comparative tables are from the Isle of Man (this study) and Merriman and Roberts (1985).

values from 111 to 134. These represent epizonal values (see section 4.7.4), clear of interference on the 10\AA white mica peak by biotite. D1 to D3 and D22 to D64 range in Hbrel from 115 to 179. These samples contain greater, though variable, amounts of biotite which has resulted in irregular biotite interference on the 10\AA peak.

The mineralogy of Dalradian samples is dominated by $2M_1$ mica with a complete absence of $1Md$ and $1M$ mica. Biotite is recogniseable in thin section from D14 onwards. Small amounts of paragonite are present in D7, 9, 10 and 68. Pyrophyllite occurs in small amounts throughout the sequence. Quartz and chlorite are present in variable amounts throughout (see Fig. 4.29).

4.7.3 HBC

The metamorphic mineralogy of the HBC is strongly controlled by origional lithology. HBS5 to HBS13 are dominantly psammites of the Lower Margie and range from Hbrel 129 to 157. Samples contain variable amounts of $1Md$ and $2M_1$ mica. Some $2M_1$ may be detrital. Paragonite and 6:4 paragonite-muscovite and kaolinite are present in variable amounts. Lesser amounts of illite-smectite and pyrophyllite also occur. Quartz and minor chlorite are present (see Fig. 4.30). Kaolinite may occur as a tropical weathering product (see Robertson and Henderson, 1984).

The mineralogy of HBS17, HBS19 and HBS20 is very different. Hbrel ranges from 155 to 226. Phyllosilicates in these psammitic rocks are dominated by $1Md$ mica with lesser $1M$ present. Illite-smectite, chlorite-smectite, kaolinite,

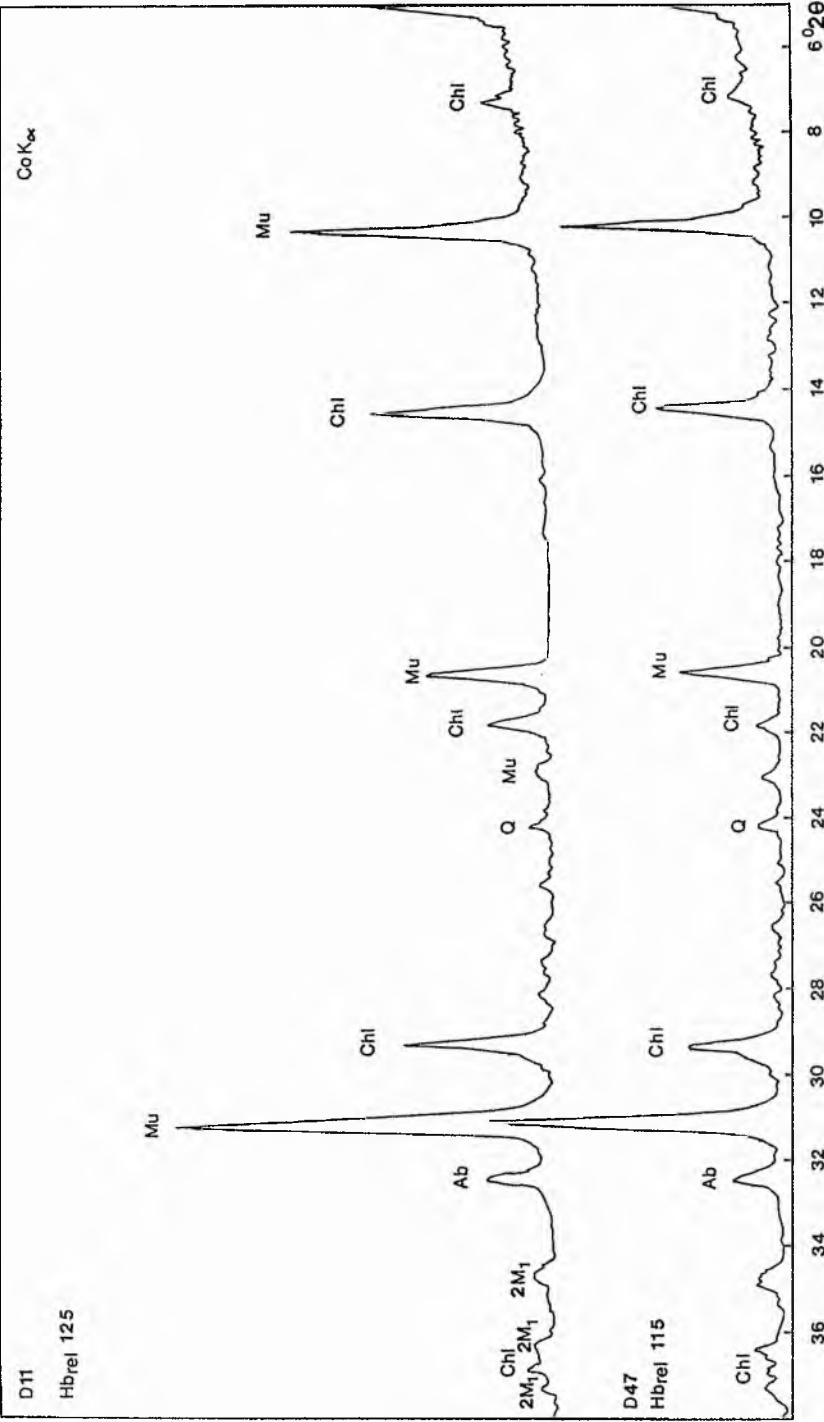


Fig. 4.29 - XRD traces for the <2 μ m Dalradian chlorite (D11) and biotite (D47) zones. Abbreviations explained with Fig. 4.30. In addition Mu = muscovite (or phengite) and 2M₁ indicates that the 2M₁ polymorph can be identified by these peaks. Despite the presence of biotite in thin section in D47 the muscovite peak gives a good crystallinity value. This is probably because the muscovite peak is strong and the coarser grained biotite component was removed from the <2 μ m size fraction. Both trace are very similar indicating the lack of variability in the epizone.

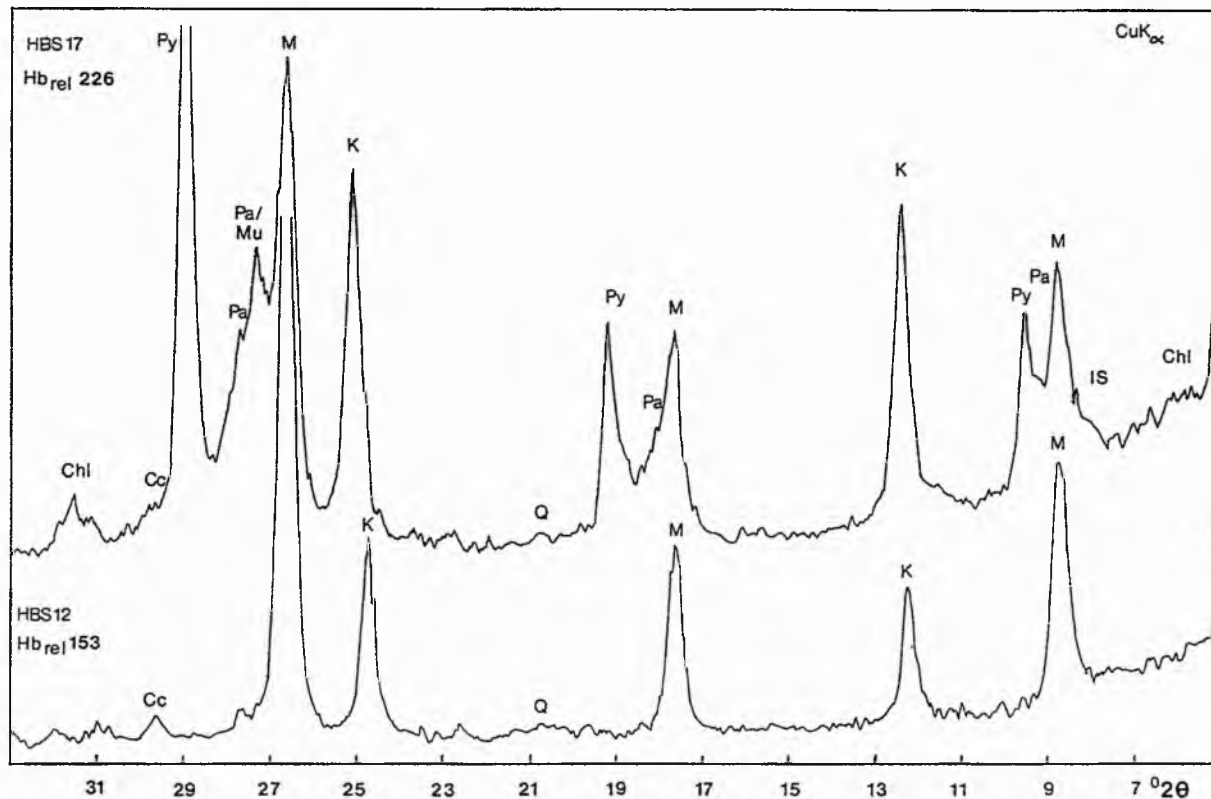


Fig. 4.30 - XRD traces from the Lower Margie (HBS12 and HBS17). M = 1Md and 2M illite in variable proportions, Chl = chlorite, IS = illite-smectite, Pa = paragonite, Py = pyrophyllite, K = kaolinite, Q = quartz, Pa/Mu = paragonite-muscovite, Cc = calcite. In both samples kaolinite is recognisable by the almost complete absence of a chlorite 14A peak ($6.3^{\circ} 2\theta$). In HBS17 the Hb_{rel} value is increased by the presence of strong paragonite, paragonite-muscovite and pyrophyllite peaks.

paragonite, M-L paragonite-muscovite and pyrophyllite, with minor chlorite, are all common constituents (see Fig. 4.30). This assemblage has been confirmed by Kübler in HBS19 (Kubler, pers comm.).

HBS25 is a Lower Margie dolomitic shale with Hbrel 172. 1Md mica is prevalent, and lesser amounts of 2M₁, illite-smectite, chlorite, kaolinite, dolomite and albite also occur in the <2µm size fraction. Quartz is a minor constituent.

HBS29 and HBS30 (Hbrel 122) are clinopyroxene bearing lavas. Chlorite, albite + or - 2M₁ mica dominate with minor amounts of quartz, kaolinite and pyrophyllite.

HBS4, and HBS42 to HBS51 are haematite-rich purple shales and range from Hbrel 126 to 157. 1Md and 2M₁ mica occur in variable proportions. Also present in significant quantities are chlorite, calcite and albite. Paragonite, illite-smectite, quartz pyrophyllite, and epidote are less common constituents (see Fig. 4.31).

HBS1 to HBS3 and HBS54 to HBS61 are green pelites with Hbrel ranging from 110 to 147. Common constituents are 2M₁ mica and chlorite, with lesser amounts of 1Md mica, paragonite and albite. Illite-smectite, chlorite-smectite, pyrophyllite, quartz and actinolite are present in lesser amounts (see Fig. 4.31).

HBS67 and HBS70 are Upper Margie psammites with Hbrel's of 130 and 145 respectively. Both 1Md and minor 2M₁ mica are present, along with illite-smectite, chlorite-smectite, chlorite, quartz and albite.

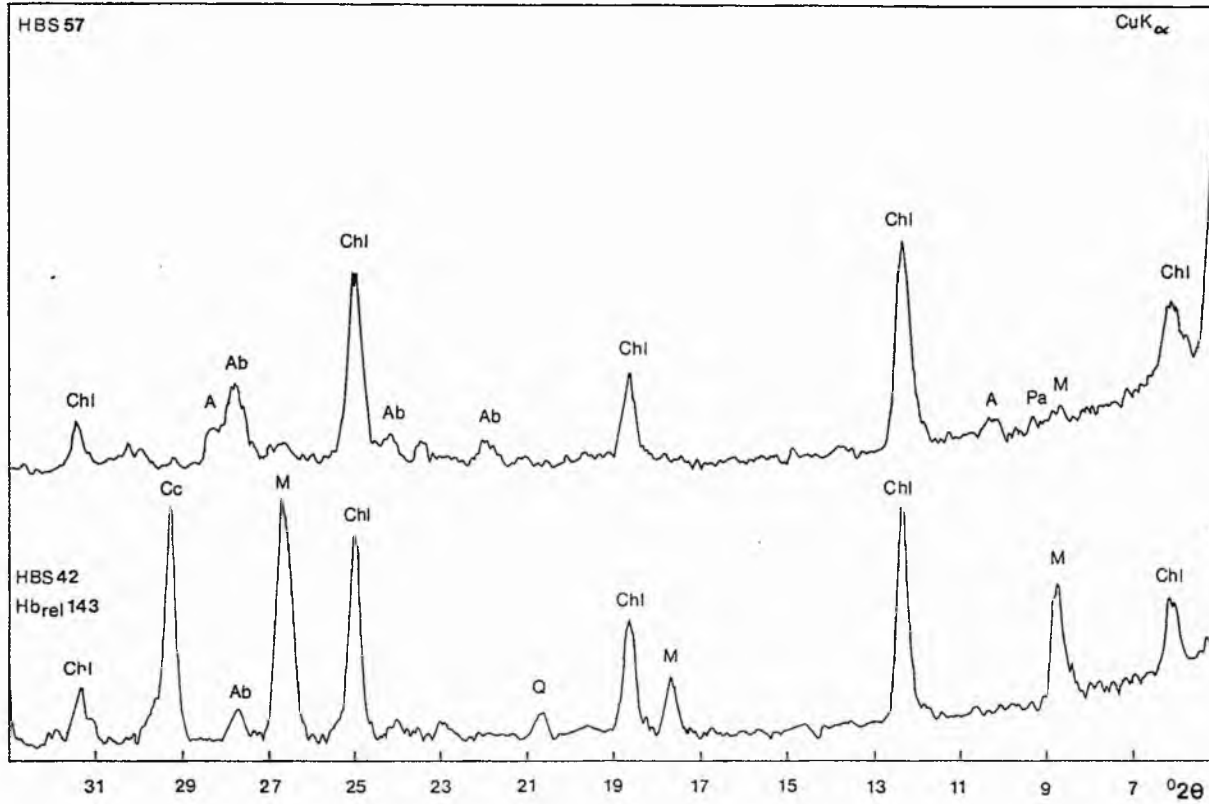


Fig. 4.31 - XRD traces for the purple shale (HBS42) and green pelite (HBS57). Abbreviations are explained with Fig. 4.30. In addition Ab = albite and A = actinolite.

HBS72 is a uniform grey pelite from the Upper Margie with Hbrel 131. Both 1Md and 2M, mica are present, with moderate amounts of illite-smectite, paragonite, paragonite-muscovite, pyrophyllite, chlorite and quartz.

4.7.4 Conclusions

The mineralogy of the Dalradian samples is relatively simple. The dominance of 2M, mica and complete absence of 1Md mica indicates that all samples lie in the epizone or above (see Fig. 4.28). The biotite isograd appears at D14, and though some samples lack biotite, this can be attributed to the effect of lithology on the formation of biotite close to the boundary.

The mineralogy of the HBC is very varied and this is reflected by the variable Hbrel values. Throughout the assemblage 2M, and 1Md mica (>Hbrel 135), illite-smectite, paragonite, pyrophyllite, albite and chlorite can be found. 2M, mica is more common than 1Md mica. Kaolinite, quartz, paragonite-muscovite, 1M mica, chlorite-smectite, calcite, dolomite actinolite and epidote are less common. On the basis of the disappearance of 1Md mica the anchizone-epizone boundary is taken at Hbrel 135. The diagenesis-anchizone boundary is not well constrained (because of a lack of diagenetic grade samples) and is taken at Hbrel c.190, by direct comparison with IOM boundaries (see Fig. 4.28). The HBC assemblage spans the anchizone-epizone transition. Further discussion can be found in section 4.8.3.

4.8 ILLITE CRYSTALLINITY

4.8.1 Introduction

The method of investigation is discussed in section 2.2. Sampling at Glen Esk was complicated by the wide variety of lithologies present. Pelitic samples could be readily obtained from the Dalradian, but suitable samples were less readily available in the HBC. This is reflected by gaps in the crystallinity traverse. Productive lithologies in the HBC include psammites, pelites, and micaceous units within purple and orange dolomitic shales, purple shales and green pelites (bearing c.10-20% white mica in thin section). Sample collecting is described in section 4.11.

Results, in Hbrel, are presented in Figs 4.32 and 4.33 for $46 <2\mu\text{m}$ and $46 2-6\mu\text{m}$ analyses, and are tabulated in Appendix 4.11.

4.8.2 Illite Crystallinity

Crystallinity values for the Dalradian $<2\mu\text{m}$ size fraction range from Hbrel 145 (lowest grade) to 111 (highest grade), and for the HBC Hbrel 172 to 110. A number of analyses were discarded due to poor peak height, interference on the 10\AA mica peak from paragonite (e.g. HBS 17 and 19) or biotite (e.g. D44). For the $2-6\mu\text{m}$ size fraction Dalradian values ranged from Hbrel 130-100, and HBC values ranged from Hbrel 146-100. Fig. 4.34 shows comparative analyses for both size fractions. Lower crystallinity values are biased towards the $2-6\mu\text{m}$ size fraction as would be expected (see section 2.2.10).

205

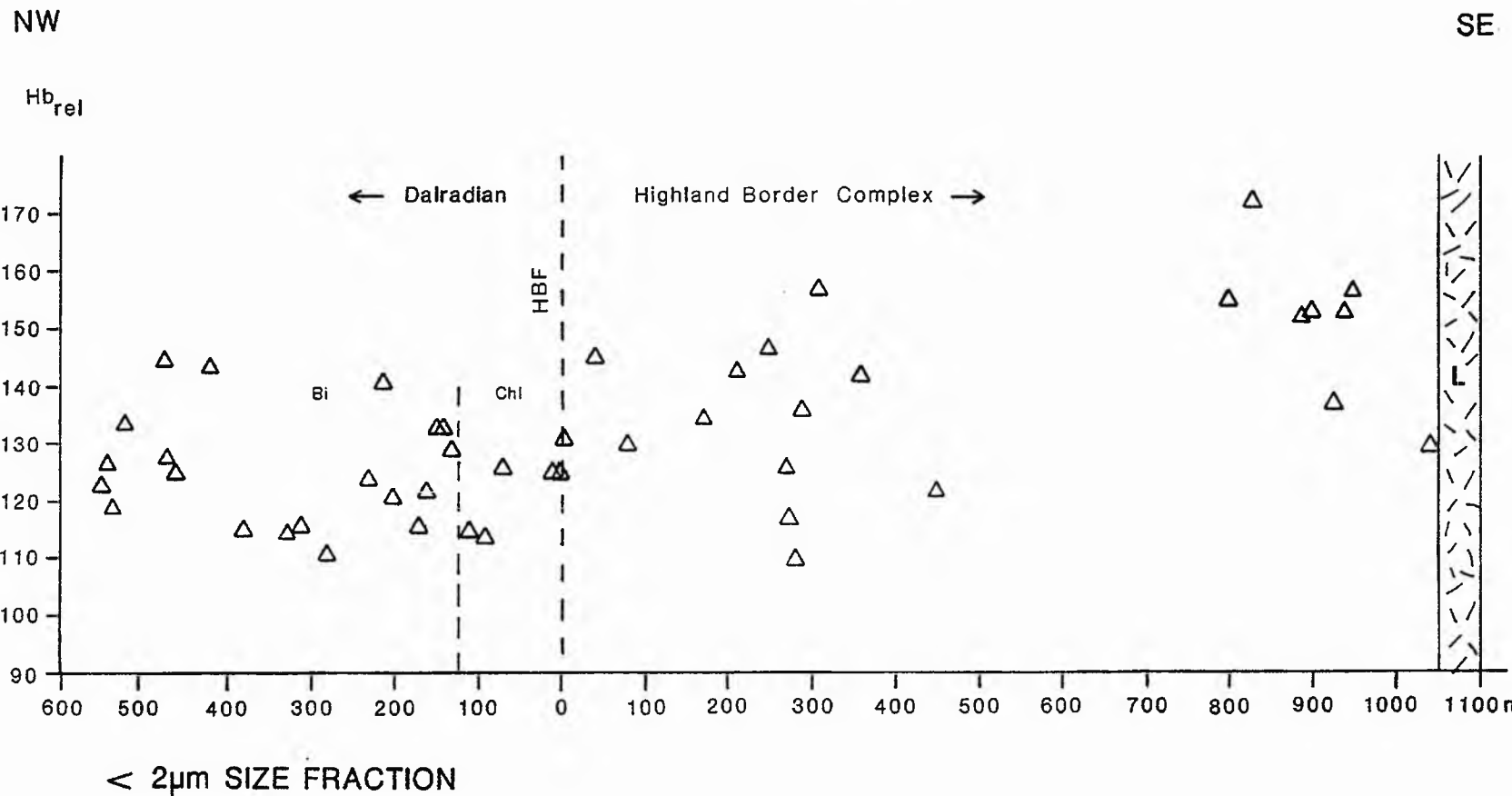


Fig. 4.32 - Glen Esk illite crystallinity values ($< 2\mu\text{m}$ size fraction). L = Lintrathern porphyry, Chl = chlorite zone, Bi = biotite zone. N = 46.

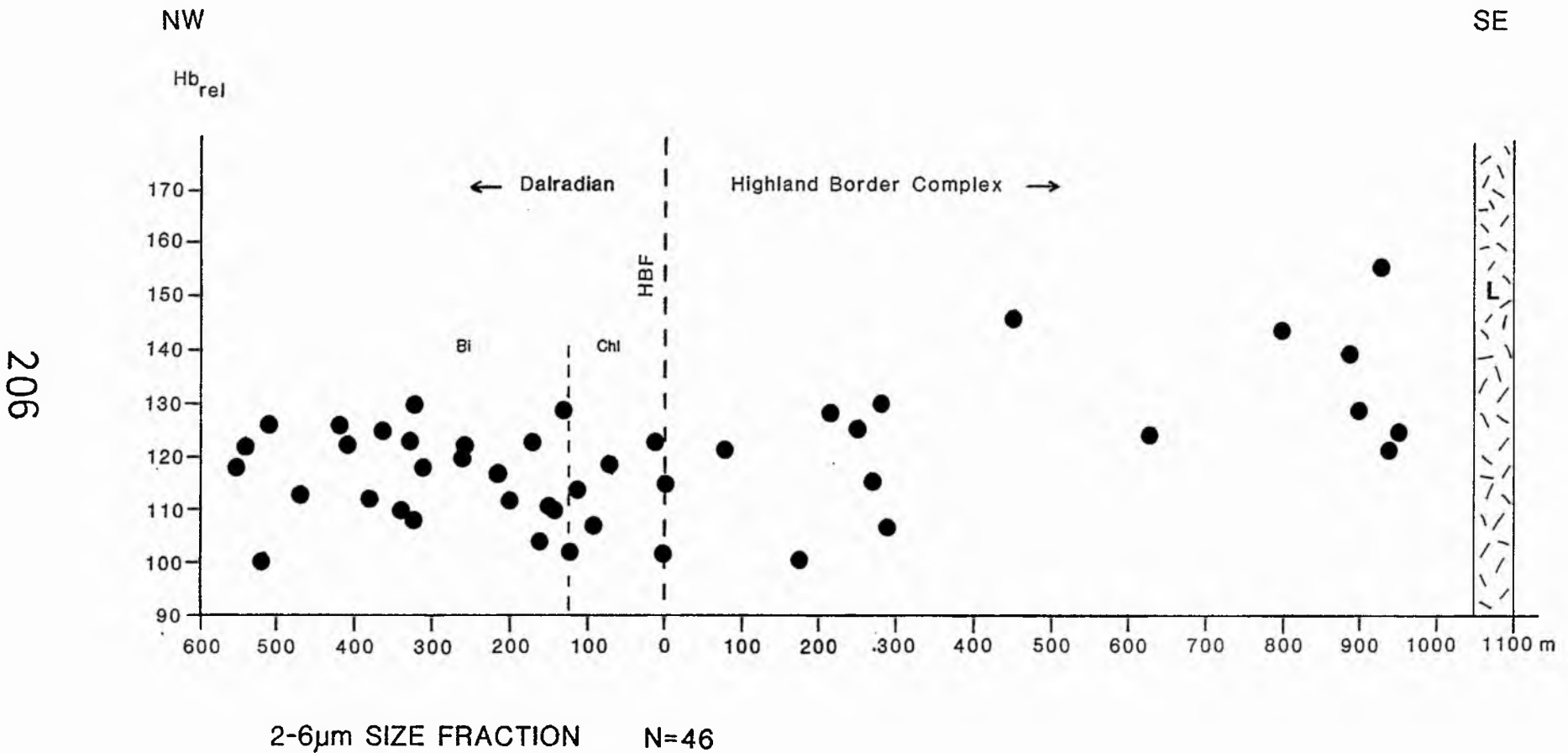


Fig. 4.33 - Glen Esk illite crystallinity values (2-6 μm). Chl and Bi as in Fig. 4.32. N = 46.

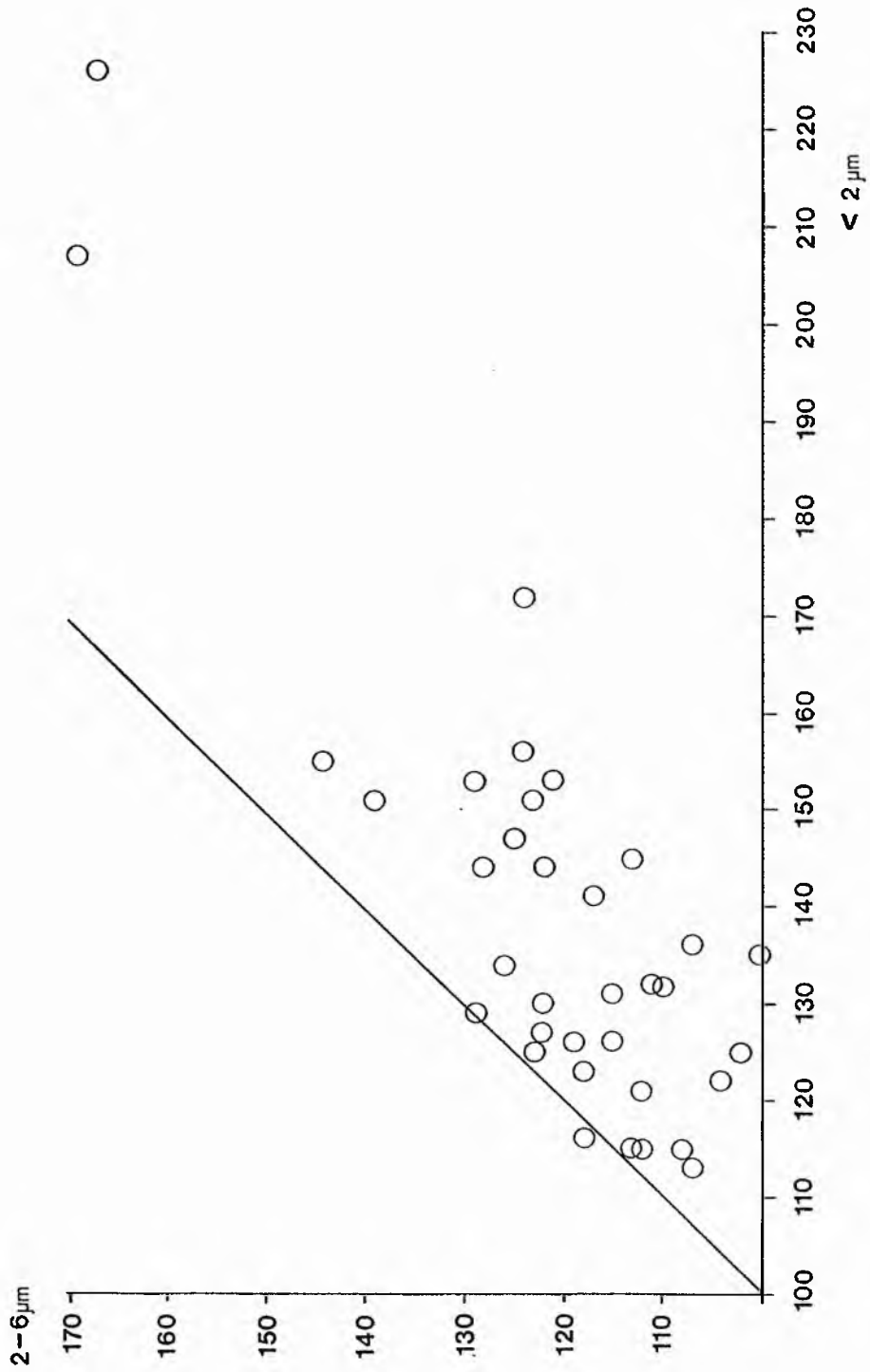


Fig. 4.34 - $2-6\mu\text{m}$ plot against $<2\mu\text{m}$ illite crystallinity results from Glen Esk. The $2-6\mu\text{m}$ fraction gives a higher grade due to the inheritance of clastic mica.

4.8.3 Discussion

A number of observations can be made based on the illite crystallinity values at Glen Esk:

1. - The grade of metamorphism is higher in the Dalradian than in the HBC (see Fig. 4.35). Dalradian samples are epizone grade or above. HBC samples range from the anchizone to the epizone, with epizone values concentrated towards the HBF.

2. - There is no significant break in crystallinity values across the HBF from the Dalradian to the HBC assemblages, or within either assemblage. This evidence, on its own, neither proves or disproves the possibility that the two assemblages could have been metamorphosed together. Palaeontological and isotopic evidence however, show that the Dalradian succession was metamorphosed before deposition of the HBC (see section 4.2.1).

3. - Mineralogical evidence shows a decrease in metamorphic grade in the Dalradian towards the HBC. This is not apparent from illite crystallinity results. This is because illite crystallinity loses its sensitivity in the epizone (Frey, 1987).

4. - Within the HBC the decrease in metamorphic grade appears to continue to the SE. This trend is most apparent in the $2-6\mu\text{m}$ size fraction. Apparently there is an inverse metamorphic gradient within the NW younging stratigraphic succession of the HBC (see Fig. 4.3).

5. - Within the HBC a broad local range in H_{Brel} can be attributed, in part, to lithological variations,

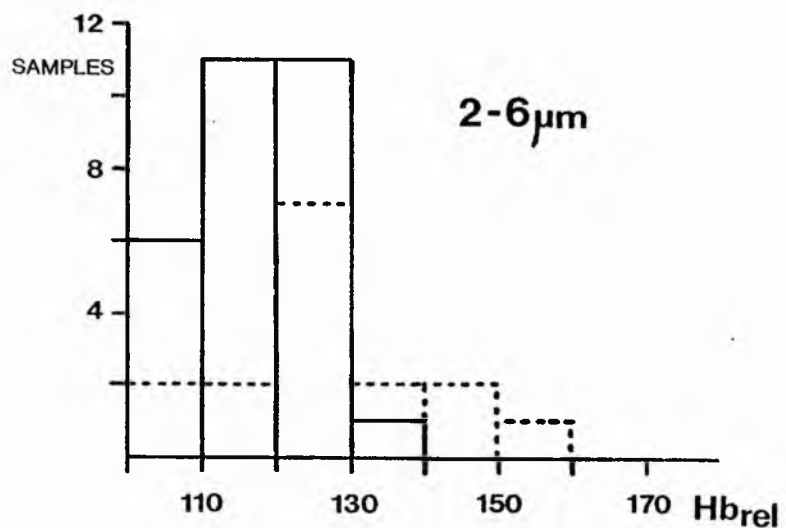
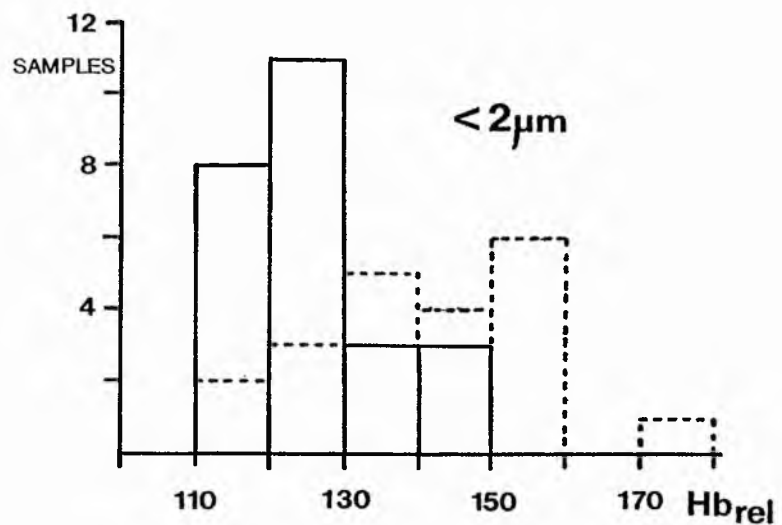


Fig. 4.35 - Histograms comparing illite crystallinity results for the HBC (dashed lines) and Dalradian (solid lines) in the <2μm and 2-6μm size fractions.

mylonitisation and the occurrence of detrital mica. Samples with petrographically identified detrital mica do not show serious discrepancies in HbreI values. From this it must be assumed that the use of the $<6\mu\text{m}$ size fractions effectively removes most detrital mica.

6. - In contrast to the Niarbyl Fault Zone, on the IOM, metamorphism of the HBC was prograde, and not a retrograde cataclastic metamorphism.

7. - The metamorphism of the HBC could have occurred before or during docking with the Dalradian. The latter possibility is favoured for the following reasons: 1. There is no jump in metamorphic grade between the Dalradian and the HBC. 2. Metamorphism of the HBC is associated with the dominant mylonitic fabric found in the HBC. The event most likely to produce such a fabric would be the docking of the Dalradian and HBC. 3. If the HBC was metamorphosed before docking with the Dalradian it seems likely that the HBC would behave competently, and that some of the faulting would have occurred in the Dalradian (see section 4.5.3).

8. - Syn-tectonic white mica growth in the HBC indicates that the metamorphism of the HBC occurred in a sinistral transpressive environment (see sections 4.4.3 and 4.5.3). This metamorphism must be post-Ordovician (post-Ashgill) and pre-Devonian (pre-Siegenian) (see section 4.2.1). An age close to the Siegenian is preferred.

4.8.4 Metamorphic Gradient

Within the scope of this study no attempt has been made to explain the steep metamorphic gradient in the

Dalradian adjacent to the HBF. Harte and Dempster (1987) provide a possible explanation. The prominent set of metamorphic zones dip steeply towards the HBC. These formed due to the presence of a cool block adjacent to the hot Dalradian block. The lateral heat flux, sustained by continuous or repetitive tectonic displacement between the blocks, produced the steep lateral temperature gradient preserved today. This implies that the southerly margin of the Dalradian block is much as it was 460Ma ago. The lack of a chlorite isograd at Stonehaven may indicate some loss from the edge of the Dalradian block by fault erosion. The block that the Dalradian cooled against must be older than the HBC and has therefore been faulted out.

4.9 b_o SPACING

Relative pressure conditions at Glen Esk were determined from 12 Dalradian and 12 HBC illite crystallinity samples. The application of b_o is described in section 2.2.11 and machine conditions are described in Appendix 3.1. A relative barometric traverse was produced (see Fig. 4.36) and the results are included on the cumulative frequency plot (Fig. 4.37). Histograms of HBC and Dalradian b_o values are compared with Dalradian b_o values of Fettes et al. (1976) (see Fig. 4.38).

The mean value for the HBC is 9.029\AA° ($SD = 0.014$) (medium P) and 9.015\AA° ($SD = 0.014$) (low-medium P) for the Dalradian. The difference in pressure conditions between the assemblages could have more than one explanation:

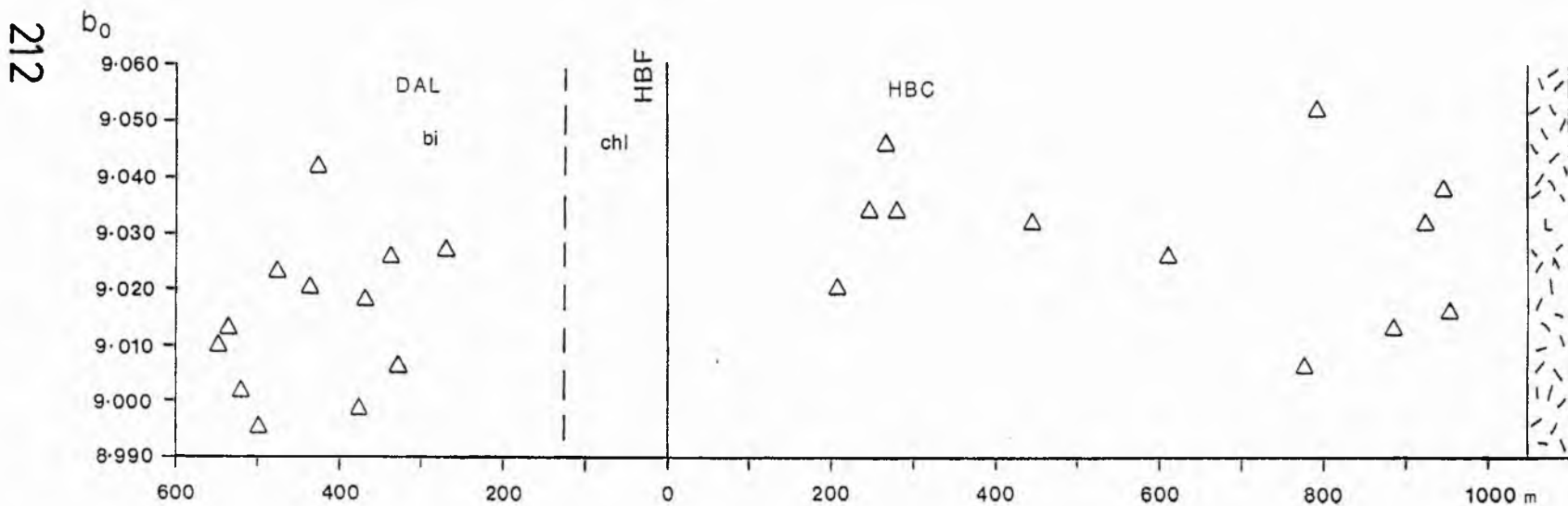


Fig. 4.36 - Glen Esk b_o values.

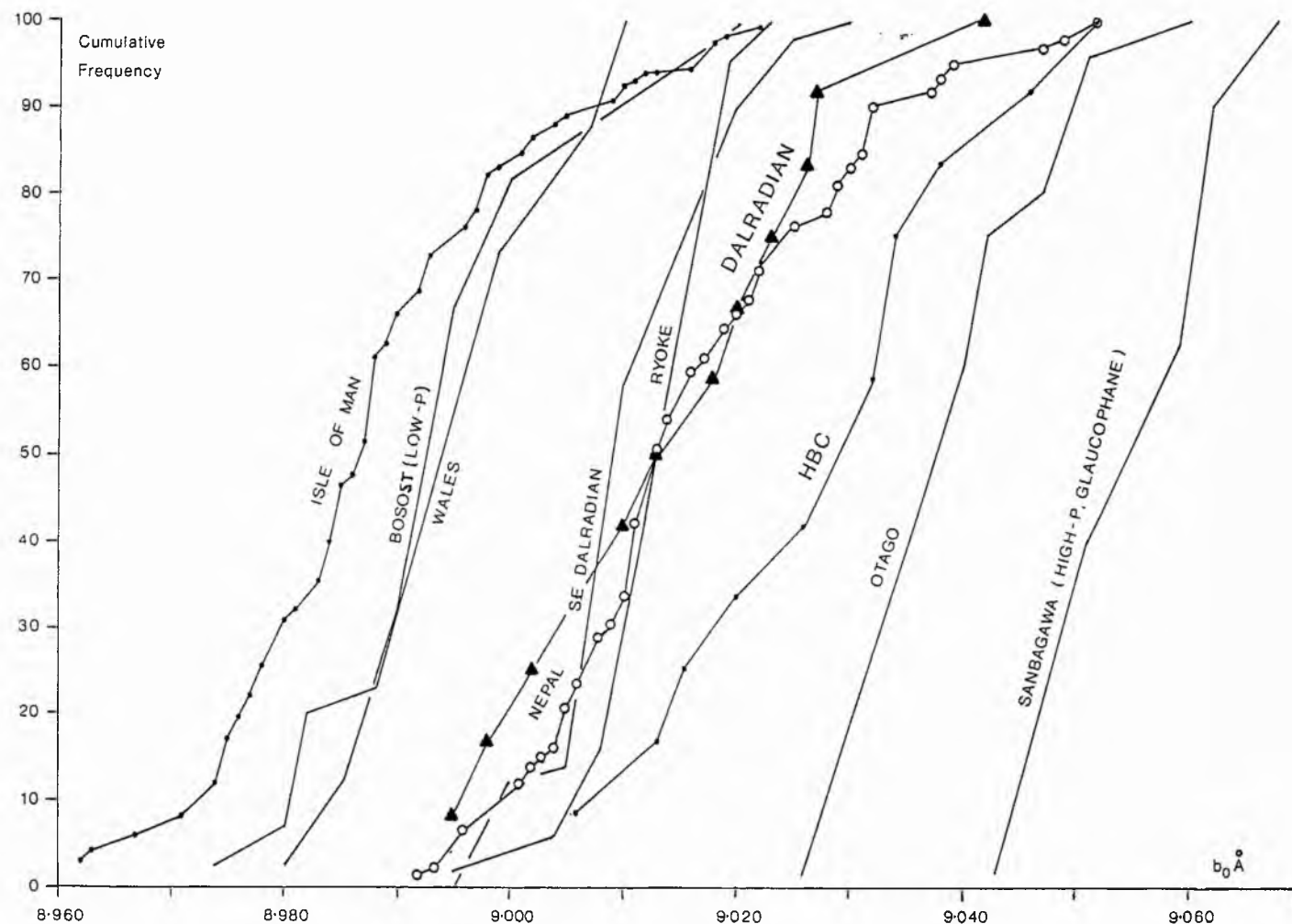


Fig. 4.37 - Cumulative frequency curves of b_0 values from: the IOM, Glen Esk and Nepal (this study), and also Bosost, Ryoke, Otago and Sanbagawa (Sassi and Scolari, 1974), Wales (Robinson and Bevins, 1986), and the SE Dalradian (Fettes et al., 1976). Glen Esk data has been divided into Dalradian samples and Highland Border Complex (HBC) samples.

ANALYSES

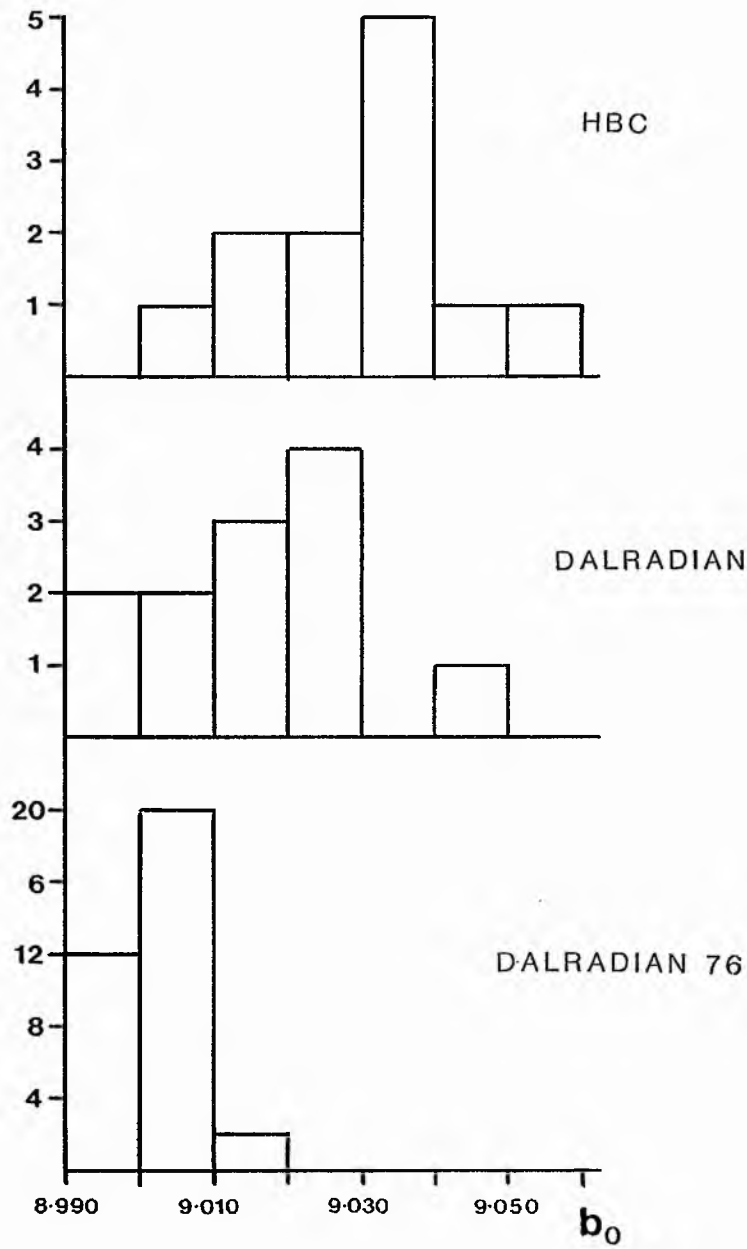


Fig. 4.38 - Histograms of samples versus b_0 values with comparative data (DALRADIAN 76) from Fettes et al. (1976).

1. It could reflect their separate metamorphic parageneses. The HBC may have been metamorphosed in a higher pressure environment than the Dalradian.
2. It could also be attributed to differences in mineralogy. HBC samples are more paragonite rich. This would tend to lower the b_o value (see section 2.2.12). The Dalradian samples are at a higher grade which has been correlated to a lowering in the celadonite content and therefore a lowering of the b_o values (see section 2.2.12). These two factors work against each other, but may be responsible for the difference in grades.

The Dalradian mean of 9.015°A ($\text{SD} = 0.014$) compares with 9.003°A ($\text{SD} = 0.006$) found by Fettes et al. (1976). This data was gathered from low grade rocks from Glen Esk and the surrounding area. An explanation for this difference is not immediately apparent. The former value is more compatible with Barrovian metamorphism.

4.10 PRESSURE-TEMPERATURE (PT) CONDITIONS

In section 4.6 estimates of PT conditions in the HBC were derived from metabasite mineral assemblages and chlorite geothermometry. Dalradian PT conditions are less well constrained, but are based on mineralogy and chlorite geothermometry. Using Hbrel data (section 4.8) and b_o data (section 4.9), and the information on the geothermal gradient produced by Harte and Dempster (1987) (section 4.8.4) further modelling of PT conditions can be made.

The HBC pelites lie mainly in the anchizone, which is correlated with the middle pumpellyite-actinolite facies of the HBC metabasites (c.265 °C). Grade increases to the epizone close to the HBF, and rapidly increases in the Dalradian, northwards, through the chlorite (epizone), biotite (c.435 °C) and garnet (c.500 °C) zones. Pressure conditions in the HBC are not well defined, but would need to exceed 2.34kb (at 265°C) for the HBC metabasites to fall in the pumpellyite-actinolite field (see Fig. 4.26), implying a geothermal gradient of 30°C/km or less. A mean b_0 of 9.029 \AA° suggests that medium pressure conditions would be appropriate, thus favouring a geothermal gradient of c.30 °C/km. A mean b_0 of 9.015 \AA° for the Dalradian suggests medium-low pressure conditions which would favour a slightly higher geothermal gradient than that of the HBC. The northwards temperature increase in the Dalradian has been attributed to lateral heat flux by Harte and Dempster (1987), and is therefore not accompanied by any great increase in pressure. The close spacing of the metamorphic zones also precludes any great pressure increase. The lateral heat flux in the Dalradian pre-dates the metamorphism of the HBC. Bearing the above in mind the following models could apply (see table 4.4 and Figs 4.39 and 4.40):

Model 1

In this model the pre-486Ma metamorphism of the Dalradian (see Fig. 4.3) occurred at a depth of around 11km. The depths of the chlorite, biotite and garnet zones have been taken as similar because the zones are

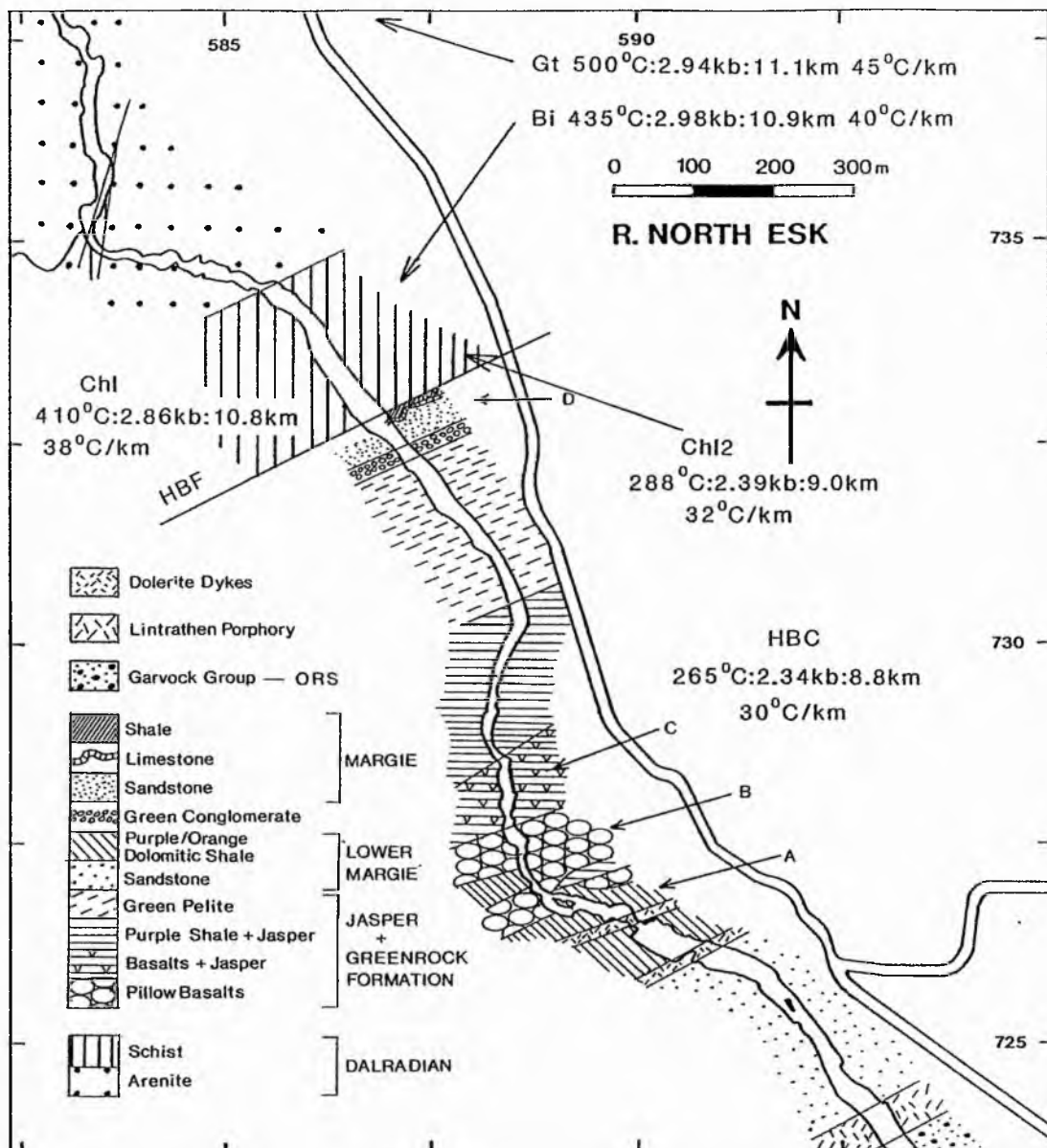


Fig. 4.39 - Metamorphism of the Dalradian and HBC at Glen Esk: Model 1. Model 1 is explained in section 4.10. HBF = Highland Boundary Fault; A, B, C and D are locations of detailed field maps (see Fig. 4.5).

PT estimates are as follows:

Gt = Dalradian garnet isograd (c.1km north of the HBF).

Bi = Dalradian biotite isograd.

Chl = Dalradian chlorite zone adjacent to the HBF.

Chl2 = Chlorite zone during metamorphism of the HBC.

HBC = Highland Border Complex metamorphism.

concentrated into a c.1km band (see Fig. 4.39), and are believed to have formed due to lateral heat flux. Geothermal gradients are controlled by temperature estimates, though the temperature of the chlorite zone has been derived from an estimate of the geothermal gradient (derived from the trend shown by the garnet and biotite zones).

The post-Ashgill (c.438Ma), probably late Silurian metamorphism of the HBC (see section 4.8.3) has been taken at the minimum pressure for the pumpellyite-actinolite field (2.34kb at 265°C). This gives a depth of 8.8kb and a geothermal gradient of 30°C/km. A PT estimate is also given for the chlorite zone of the Dalradian. This would correspond to retrogressive metamorphism of the Dalradian. A slightly higher geothermal gradient is taken because the temperature of the HBC increases towards the Dalradian up the stratigraphic sucession, implying that lateral heat flux applied. The depth of the Dalradian is taken at a slightly greater depth than the HBC because most of the fault movement is believed to be sinistral transpressive (see section 4.4.3), with late minor thrusting of the Dalradian over the HBC. The resultant temperature estimate (288°C) corresponds well with the results obtained for sample D7 from chlorite geothermometry (see section 4.6.19).

Model 2

In this model the same rules apply as those for model 1. The pressure conditions have been increased along with

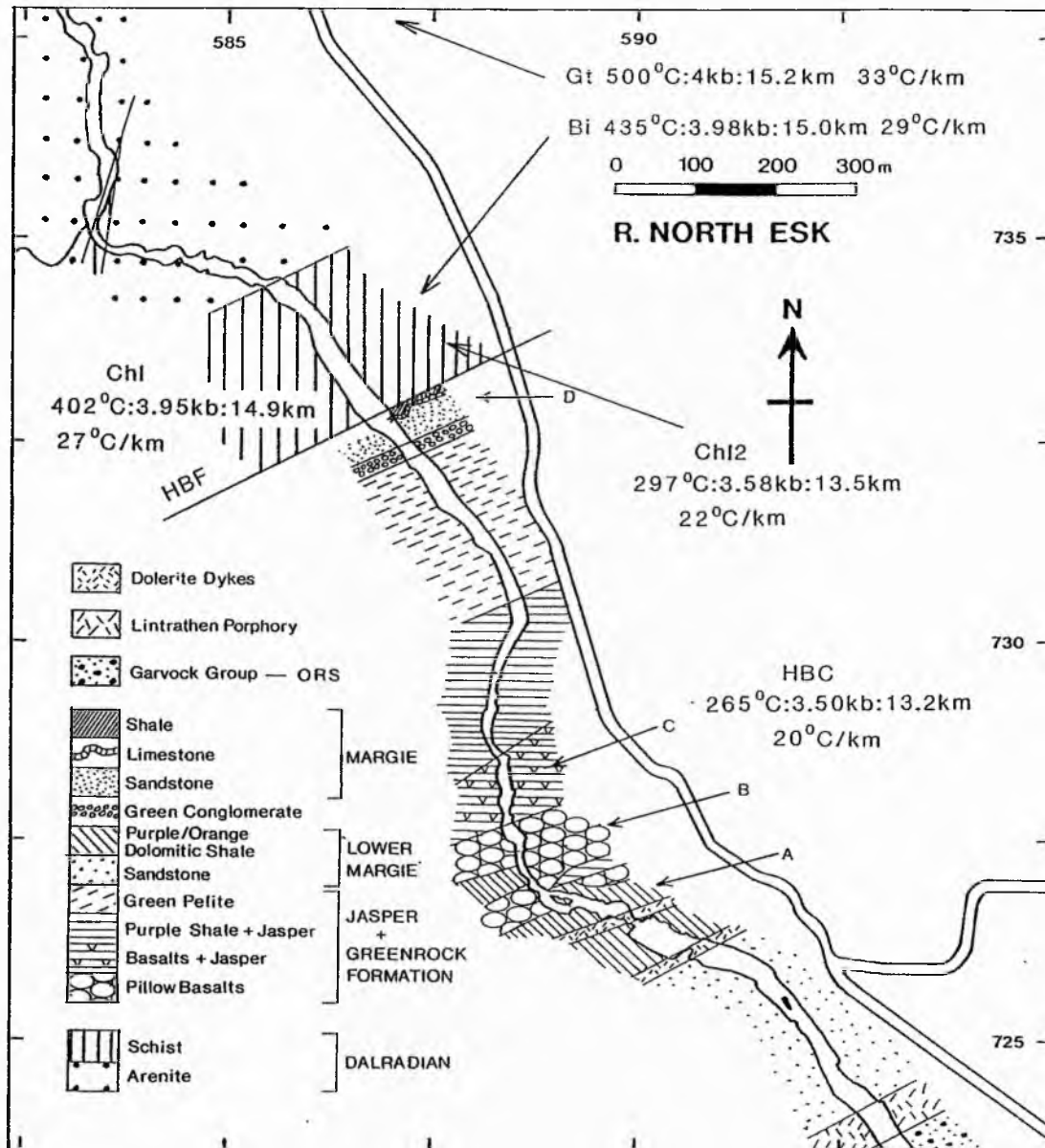


Fig. 4.40 - Metamorphism of the Dalradian and HBC at Glen Esk: Model 2. Model 2 is explained in the text and with Fig. 4.39.

corresponding burial depths, and the constrained temperatures have been maintained. New geothermal gradients have been extrapolated, and used to estimate the temperature of the Dalradian chlorite zone.

Table 4.4 - Alternative metamorphic models for the Dalradian and HBC metamorphic events. Dal (Gt) = Dalradian garnet isograd, Dal (Bi) = Dalradian biotite isograd and Dal (Chl) = Dalradian chlorite zone adjacent to the HBF. A lithostatic pressure gradient of 265kb/km is taken. The locations of PT conditions are shown on Figs 4.39 and 4.40.

Model 1

Location	T (°C)	P (kb)	Depth (km)	Geothermal Gradient
----------	--------	--------	------------	---------------------

Dalradian Metamorphism

Dal (Gt)	500	2.94	11.1	45 °C/km
Dal (Bi)	435	2.89	10.9	40 °C/km
Dal (Chl)	410	2.86	10.8	38 °C/km

HBC Metamorphism

HBC	265	2.34	8.8	30 °C/km
Dal (Chl)	288	2.39	9.0	32 °C/km

Model 2

Location	T (°C)	P (kb)	Depth (km)	Geothermal Gradient
----------	--------	--------	------------	---------------------

Dalradian metamorphism

Dal (Gt)	500	4.00	15.2	33 °C/km
Dal (Bi)	435	3.98	15.0	29 °C/km
Dal (Chl)	402	3.95	14.9	27 °C/km

HBC Metamorphism

HBC	265	3.50	13.2	20 °C/km
Dal (Chl)	297	3.58	13.5	22 °C/km

4.11 SYNTHESIS

4.11.1 Aims

In this section the different lines of investigation are brought together to synthesise a geological history of the HBF region in Glen Esk.

4.11.2 Geological History

1. Dalradian - Sedimentation of the Southern Highland Group, the youngest Dalradian group, is limited to the Precambrian by the age of the Ben Vuirich granite (Rodgers et al., *in press*). Structural and metamorphic events are also constrained by a number of igneous bodies. D1 and D2 pre-date 590Ma on the basis of the Ben Vuirich granite age date. D3 and M3 are well constrained by the Aberdeen granite at 470Ma or older, and D4 by a mica cooling age of 443 + or - 9Ma (Harte et al., 1984).

D1 is associated with prograde ripidolitic chlorite, and phengite or muscovite growth. Peak metamorphism is attained in the post-D1 static interval with the growth of chlorite, biotite ($c.435^{\circ}\text{C}$) or almandine porphyroblasts ($c.500^{\circ}\text{C}$), depending on the metamorphic grade attained. Veining, crenulation cleavages and partial retrogression of biotite to brunsvigite post-dates the peak of metamorphism.

Metamorphism in the chlorite and biotite grade Dalradian ranges from Hbrel 111 to 145. This covers a range of epizone and biotite grade rocks. Chlorite geothermometry shows that temperatures of 273°C are exceeded in the Dalradian immediately adjacent to the HBC. It is likely that temperatures exceeded 300°C throughout the Dalradian

sample population. Pressure is given by a mean b_0 of 9.015A° , which is equivalent to low-medium pressure conditions. The steep metamorphic gradient at the SE margin of the Dalradian is explained by Harte and Dempster (1987) as being due to lateral heat flux between the hot Dalradian block and a cool block, since faulted out.

2. HBC - The HBC covers an age range of formation from Tremadoc to Early Ashgill. Both the Lower Cambrian Leny Limestone and end Precambrian limestone in Leny Quarry could be precursors to the HBC. The HBC has previously been described in 4 main assemblages. 1. contains pre-Arenig serpentinites. 2. contains early-Arenig limestones and conglomerates. 3. is represented at Glen Esk by Tremadoc to Llanvirn mafic volcanics, red cherts and shales. 4. is represented at Glen Esk by Llanvirn to early-Ashgill green conglomerate, arenites, shales and limestone.

Lithologies are complex and preserve both original and metamorphic minerals. Clastic lithologies variously contain both detrital muscovite, quartz and feldspar, metamorphic phengite, paragonite, paragonite-phengite, pyrophyllite, illite-smectite, chlorite-smectite, albite, epidote and chlorite, and authigenic kaolinite. A wide variety of mafic rocks are present. Pillow lavas show quench textures, with an original mineralogy of skeletal diopside/augite and labradorite, and minor olivine. Metamorphic minerals consist of albite, pumpellyite, pycnochlorite, granitic garnets, epidote (Ps 24-28), actinolite, sphene, calcite, and quartz. Massive lavas and green pelites contain similar mineralogies, but with

different proportions and textures. A range of phyllosilicate minerals are also present in some of the green pelites. Purple shales are rich in haematite, chlorite, white mica, epidote, albite, calcite and quartz.

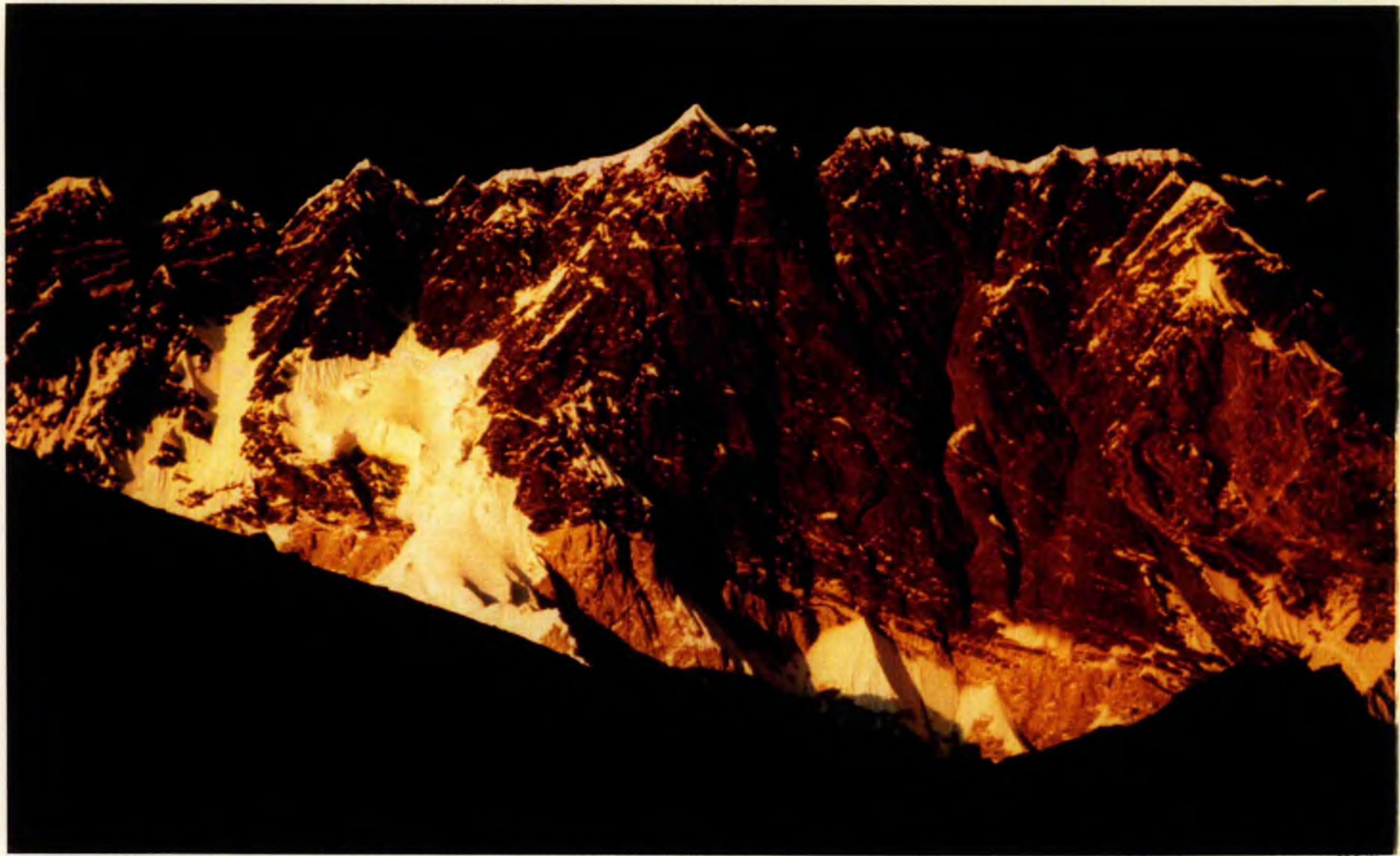
Hbrel values range from 110 to 172 with a trend of decreasing Hbrel towards the SE away from the Dalradian. Mineralogy, in conjunction with Hbrel, puts the HBC mostly in the anchizone, with epizone values concentrated close to the HBF. Mineral geochemistry puts the mafic assemblages in the middle pumpellyite-actinolite (PA) metamorphic field. On the basis of chlorite geothermometry and metabasite mineral assemblages, the HBC reached a maximum metamorphic grade of c.265 °C at a minimum of 2.34kb (equivalent to a depth of 8.8km and geothermal gradient of 30 °C/km). The growth of white mica, in the HBC, is syn-tectonic with the main phase of fabric formation in the HBF zone. It is therefore likely that peak metamorphism in the HBC occurred during, or immediately after, the pre-Siegenian collision between the Dalradian and the HBC. The HBC has a mean b_0 of 9.029A[°] (medium pressure) which could represent a genuine higher pressure facies than the adjacent Dalradian.

3. Faulting - The HBC shows NE-SW trending sinistral transpressive fault movement. The lack of interaction between the uplifting Dalradian and deposition in the HBC implies separation between the two terranes at least until the early Silurian. By the Siegenian the terranes are brought into contact along the HBF. Further transcurrent movement in the Devonian is limited to 10's of km's and is most likely to have been dextral. By the late Devonian

movement was limited to c.100m of brittle thrusting to the SE. This deposited locally derived Dalradian at the top of the Upper ORS. Later tectonic activity is limited to minor brittle features.

4.11.3 Conclusions - The Anchizone-Epizone Transition in the HBC

In the HBC the anchizone-epizone metamorphic transition is associated with sinistral transpressive fault movement resulting from collision between the Dalradian metamorphic terrane and the low-temperature HBC terrane. Prograde metamorphic growth and re-crystallisation of white mica occurred in the HBC during the main phase of transpressive fault movement in the HBF zone. The anchizone-epizone transition is defined by the disappearance of 1Md white mica, which is replaced by 2M, white mica (see section 2.2.8). In the HBC this occurs at Hbre1 135, and is associated with the common occurrence of chlorite. Lesser mineral phases at the anchizone-epizone transition are paragonite, paragonite-muscovite, albite, pyrophyllite, 1M mica, chlorite-smectite and illite-smectite. b_0 values correspond to medium pressure conditions. Metabasite mineralogy is consistent with middle pumpellyite-actinolite facies with a PT estimate of c. 265°C at >2.3kb. Chlorite geothermometry gives a temperature range of 221 to 273°C . Fluids circulating in the metabasite pile were $\text{H}_2\text{O-CO}_2$ rich. CO_2 may have been derived from dissolved CO_2 in the basaltic magma or by devolatilisation of carbonates in the HBC.



Frontispiece 5 - Looking north towards part of the Nuptse-Lhotse wall. The section of mountain shown is roughly 5km by 2km. Folding of the Tibetan Slab sucession can be seen on the right hand side of the wall. The base of the wall is intruded by a large north dipping sheet of leucorite associated with minor sheets.

CHAPTER 5

NEPAL

5.1 INTRODUCTION

5.1.1 Aims

A study of the inverse metamorphism associated with the Main Central Thrust (MCT), in Nepal, was undertaken for various reasons. A number of models have been proposed to explain the inverse metamorphism, but as new data has been added to the still incomplete body of information, these models have proved to be oversimplifications. There is a lack of detailed mapping of the rocks immediately below and above the MCT. Thermobarometry has been applied to the higher grade rocks of the hanging wall, but the sub-garnet grade assemblages found in the footwall have been comparatively neglected. Lack of palaeontological control has limited the understanding of the stratigraphy, and the timing of structural and metamorphic events. This project has been aimed at: 1. A study of the anchizone-epizone transition in an inverted metamorphic zonation. 2. A study of the metamorphism of low-grade rocks found both above and below the MCT zone, and reconciliation with previously published results.

5.1.2 Introduction

The Main Central Thrust (MCT), extending 2400km along the length of the Himalaya, represents a major tectonic boundary associated with the collision of India with Asia

during the Tertiary. After the initial collision over 100km of crustal shortening was taken up by intraplate subduction along the MCT (Hodges et al., 1988). Though the MCT is still active, intraplate subduction has migrated to the south, and has been centered on the Main Boundary Thrust (MBT) and Himalayan Frontal Thrust (HFT) since the late Tertiary.

An inverted metamorphic zonation is intimately associated with the MCT (Le Fort, 1975). In the footwall it ranges from epizonal to garnet grade schists, with the highest grades closest to the MCT. In the hanging wall metamorphism increases structurally upwards, over several km's, from kyanite to sillimanite grade gneisses, associated with migmatites and peraluminous granites.

5.2 GEOLOGICAL BACKGROUND

5.2.1 Stratigraphy

The geology of the Kathmandu region has recently been mapped in detail by Stöcklin et al. (1980). For the purposes of this project the mapwork and stratigraphy described by Stöcklin (1980) have been adopted. A location map and a simplified geological map of the Kathmandu basin are presented in Fig. 5.1. Cross-sections appropriate to two sampling traverses made are presented in Figs 5.2A and B, and the stratigraphy is presented in Fig. 5.3.

A. Below the MCT - Below the MCT lies the Midland Formation, known locally as the Nawakot Complex (Stöcklin, 1980). This complex lacks palaeontological control, but

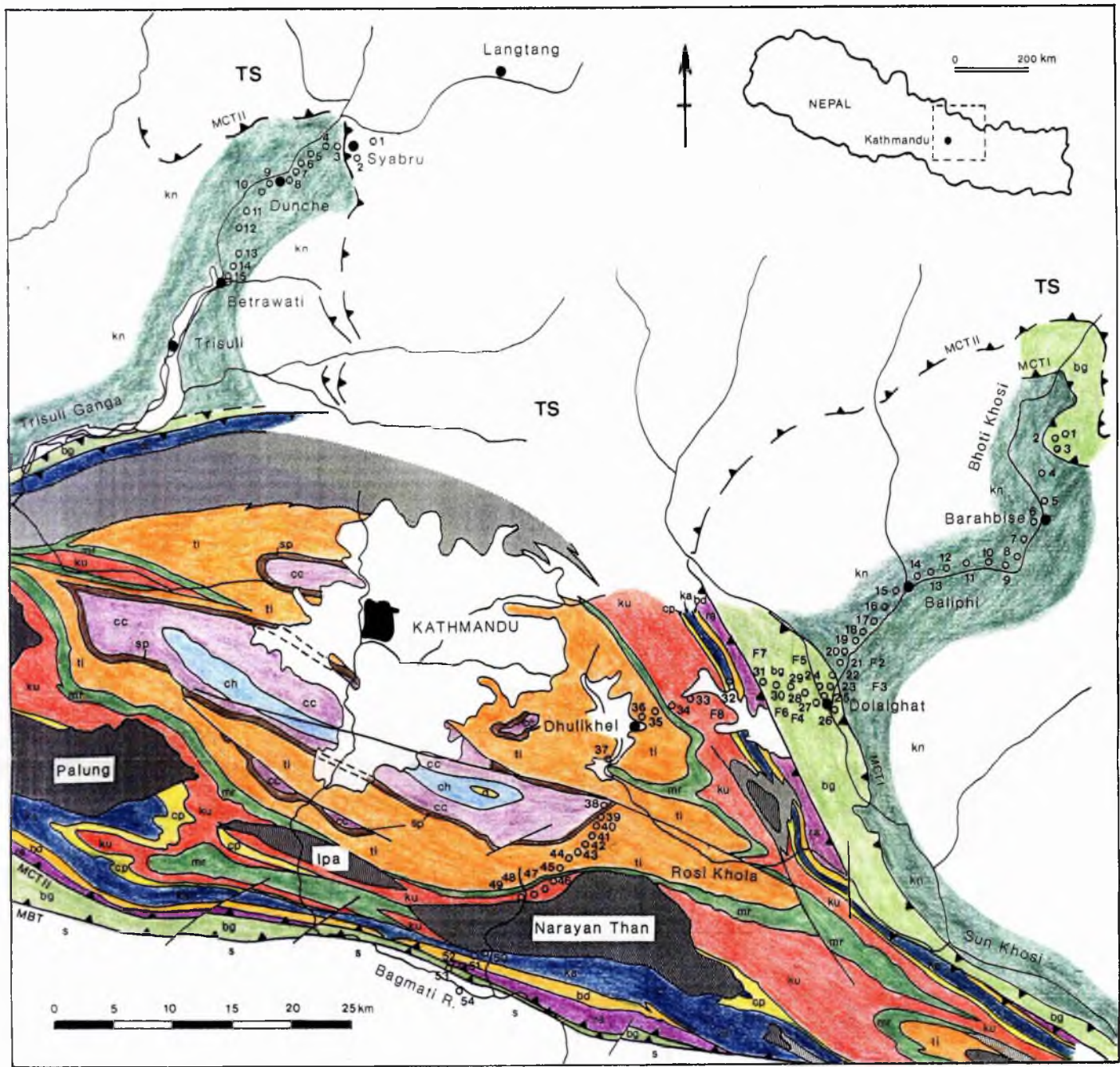


Fig. 5.1 - Geology of the Kathmandu basin (adapted after Stoklin, 1980). Dark stippled areas are Cambro-Ordovician leucogranites, light stippled areas are gneisses. Lithological units are as follows: kn = Kuncha Formation, bg = Benighat Slates, TS = Tibetan Slab (undifferentiated), ra = Raduwa Formation, bd = Bhainsedobhan Marble, ka = Kalitar Formation, cp = Chisapani Quartzite, ku = Kulikhani Formation, mr = Markhu Formaiton, ti = Tistung Formation, sp = Sopyang Formation, cc = Chandragiri Limestone, ch = Chitlang Slates, d = Devonian Limestone. MCTI and MCTII are the lower and upper Main Central Thrusts, described in section 5.2.3, and MBT is the Main Boundary Thrust. Sample traverse A is from the Barahbise area to the Bagmati River and B is from Syabru to Betrawati. In traverse A sample numbers are prefixed by HS in the text and fluid inclusion samples (F2 to F8) are called FI2 to FI8 in the text. In traverse B sample numbers are prefixed by LH in the text and LH1 was also used to make a fluid inclusion wafer.

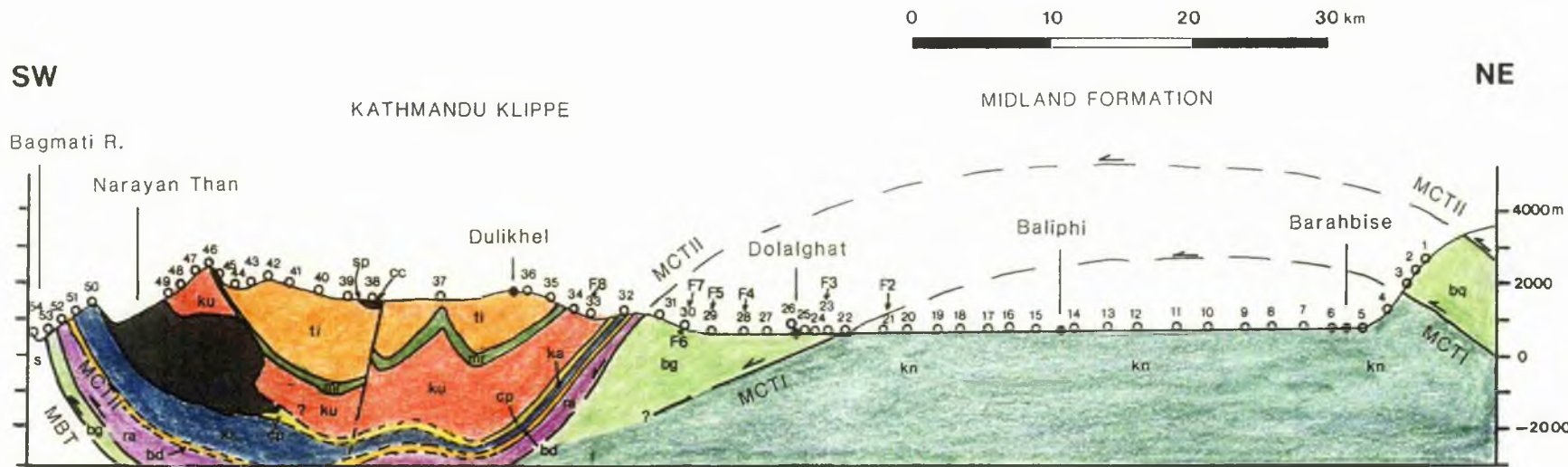


Fig. 5.2A - Sample traverse A, from the Barahbise area to the Bagmati River (the traverse is shown on map, Fig. 5.1). Samples 1 to 54 are prefixed by HS in the text. Samples F2 to F8 are called FI2 to FI8 in the text and are fluid inclusion vein samples. Other abbreviations are as in Fig. 5.1.

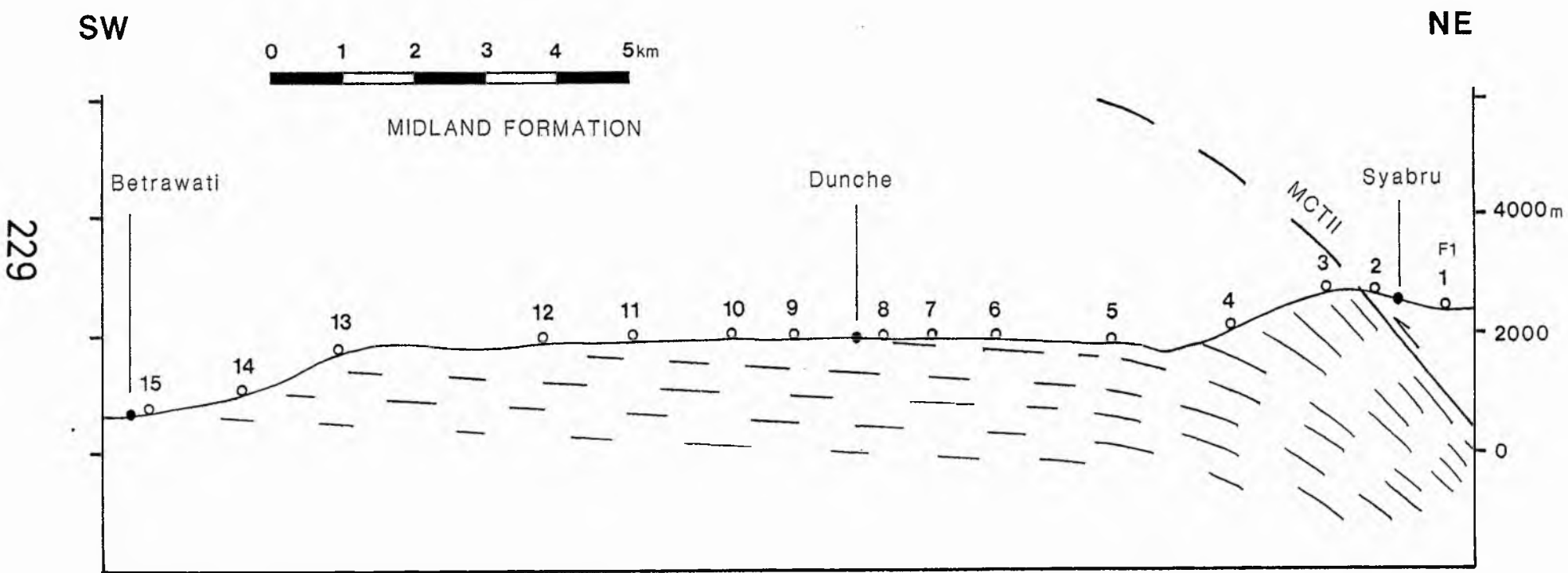
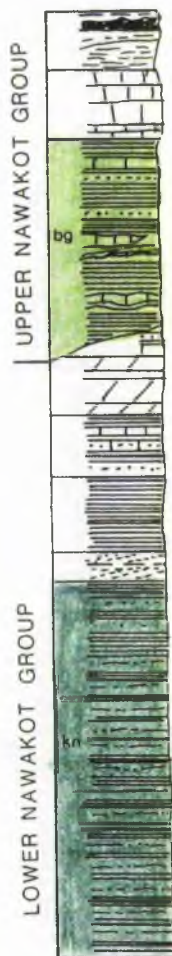


Fig. 5.2B - Sample traverse B, from Syabru to Betrawati (the traverse is shown on map, Fig. 5.1). Samples 1 to 15 are prefixed LH in the text. F1 is a quartz segregation from LH1 and is called LH1 in the text. Samples LH1 and LH2 are from the Tibetan Slab, other samples are from the Kuncha Formation.

MIDLAND FORMATION

U. Pre-Camb. Lr.Palaeozoic



KATHMANDU KLIPPE

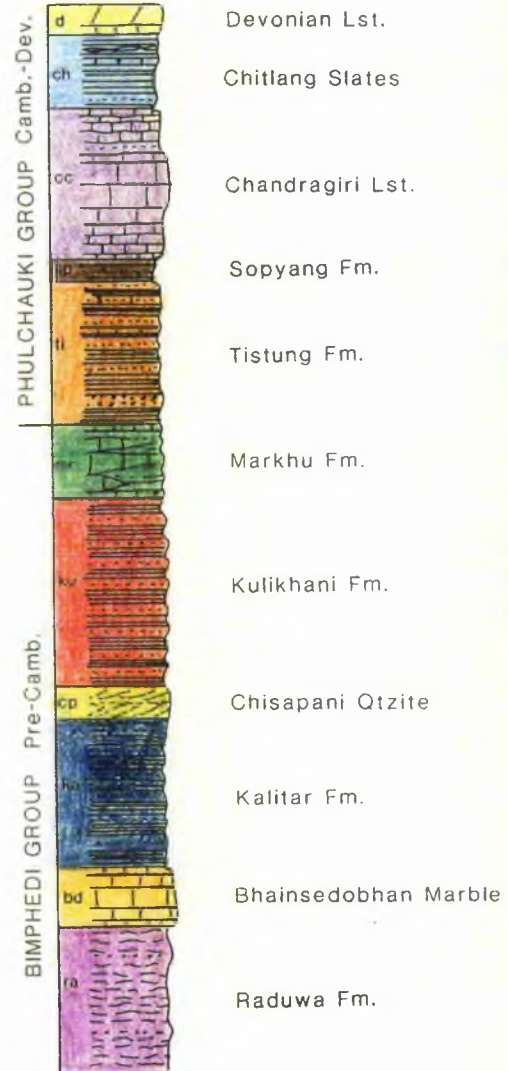


Fig. 5.3 - Stratigraphy of the Kathmandu area (after Stoklin, 1980). Details of the stratigraphy are given in Stoklin (1980). Coloured units are included in Fig. 5.1.

ranges from the late Precambrian to early Palaeozoic age on the basis of evidence from stromatolites, conodonts, acritarchs and shelly microfaunas (Le Fort et al., 1986a). Correlations have been made with the late Precambrian/early Cambrian Krol and Tal formations of the Kumaun Himal, India (Brasier and Singh, 1987, and Bhat, 1987). The lower Nawakot Group is dominated by the Kuncha Formation which is predominantly made up of psammitic and pelitic schists ranging from chlorite to garnet grade. Within the Upper Nawakot Group the Benighat Slate were sampled. These consisted of dark-grey slates and phyllites, local black carbonaceous slates, and calc-phyllites. One sample was collected of Neogene Siwalik sandstone.

B. Above the MCT - Above the MCT lie the kyanite to sillimanite schists and gneisses of the Bhimphedi Group in the Tibetan Slab. Within the Kathmandu basin the succession is known as the Kathmandu Complex. This complex shows a normal metamorphic succession from garnet grade to the anchizone in the core of the Maharabhat Syncline. The lower Bhimphedi Group is of late Precambrian age. Formations sampled include the garnet schists of the Raduwa formation, biotite schists of the Kalitar Formation and garnet biotite schists of the Kulikhani Formtion associated with tourmaline bearing granite pegmatites. The Cambrian to Devonian Phulchauki Group, overlying the Bhimphedi Group conformably, was sampled for biotite schists from the Tistung Formation and medium crystalline marble of the Chandragiri Limestone. The tourmaline bearing two mica Narayan Than granite was also sampled.

5.2.2 Position of the MCT (see Fig. 5.4)

Despite its tectonic importance there has been considerable variation in the choice of which thrust to call the MCT. Confusion has resulted for a number of reasons. Work has been done by research groups at restricted locations along the Himalayas. This has resulted in sets of local names for lithological groups and thrusts, which has hindered attempts at lateral correlation along the Himalayas. Local variations in tectonic sequences and apparent importance of tectonic boundaries has further added to the confusion.

Heim and Gansser (1939) identified the MCT, in the Kumaun Himal, as lying within the equivalent of the Midland Formation, at the top of the Berinag quartzites. Indian researchers have followed this lead. Recently Valdiya (1980, p336) re-designated the MCT as the Munsiari Thrust in the Kumaun. This lies between the lower and upper Midland Formation. French and Japanese researchers in Nepal (e.g. Hashimoto, 1973; Le Fort, 1975; Pecher, 1979) did not recognise a tectonic break between the lower and upper Midland Formation, but recognised a significant break where the kyanite grade rocks of the Tibetan Slab were thrust over the upper Midland Formation. This Nepali MCT has been correlated by Valdiya (1980) with the Vaikrita Thrust in the Kumaun, which lies above the Munsiari Thrust. Though the importance of the Vaikrita Thrust is not so apparent in the Kumaun, Valdiya (1980, p339) favours designating it as

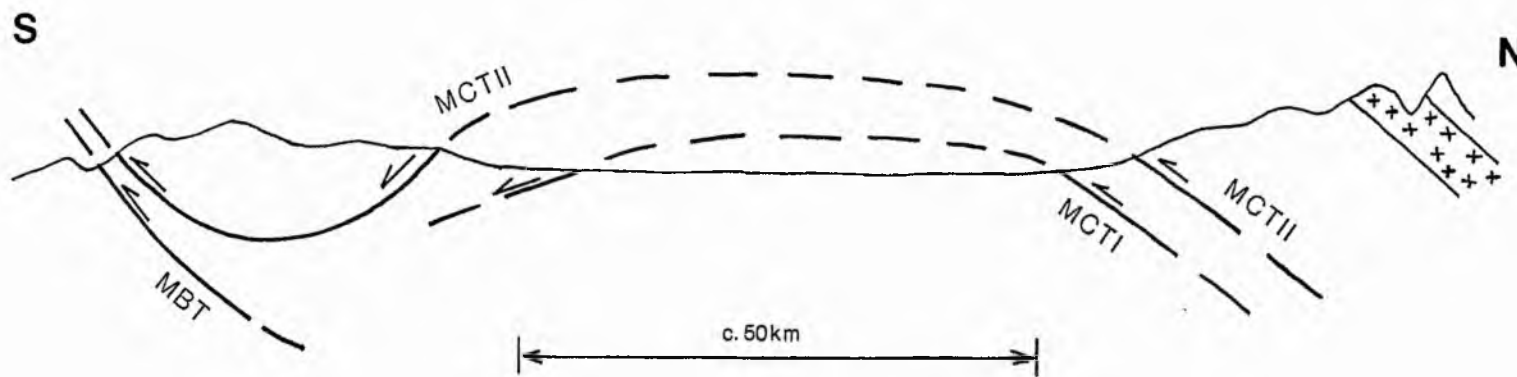


Fig. 5.4 - Sketch map after cross-section, Fig. 5.2A, to illustrate the thrusts discussed in the text (see Valdiya, 1980). The Main Central Thrust (MCTII) is equivalent to the Vaikrita Thrust of the Kumaun, India or the MCT of French authors in Nepal. The MCTI is equivalent to the Munsiari Thrust of the Kumaun or to the Benighat Thrust in Nepal. The Main Boundary Thrust (MBT) is equivalent to the Krol Thrust of the Kumaun or the Kathmandu Thrust in Nepal. The patterned area represents High Himalayan leucogranite.

the MCT instead of the lower level Munsiari Thrust, thus superceeding his designation of p336.

In Nepal most authors place the MCT at the base of the Tibetan Slab. Sinha-Roy (1982) favoured a position for the MCT at the base of the Ulleri Augen Gneiss in the Midland Formation (Munsiari Thrust of the Kumaun). Arita (1983) chose a compromise option by recognising a thrust zone bounded by the MCTI and MCTII (equivalent to the Munsiari Thrust and Vaikrita Thrust of the Kumaun).

For the purpose of this project the MCT is taken as lying at the base of the Tibetan Slab (equivalent to the Vaikrita Thrust or MCTII), and for further discussion will be called the MCTII. In addition the MCTI is recognised, after Arita (1983) and the term MCT zone is used when referring to the general zone of thrusting that incorporates the MCTI and MCTII. Tectonic disruption within the upper Midland Formation is taken to represent the later propagation of thrust slices in the footwall of the MCT (Pecher and Le Fort, 1986).

5.2.3 Present Knowledge

Over the years a large body of Himalayan "facts" has been built up. These have formed the basis for tectonometamorphic modelling.

A Dimensions

The MCTII and MBT can both be traced for 2400km along the Himalaya (Valdiya, 1980). The Tibetan Slab has been thrust SSW over the Indian Plate, on the MCTII, by >100km (Andrieux et al., 1977). The transportation direction was deduced from tectonic indicators (according to Bouchez and Pecher (1981) quartz rich tectonites show a southerly sense of movement). A minimum transportation distance of 100km is deduced from the distal position of the Kathmandu Klippe (Stöcklin, 1980). Crustal shortening within the Indian Plate south of the Indus-Tsangpo suture has been estimated at >500km since the Eocene (Searle et al., 1987), thickening the crust to c.60km under the High Himalaya (Pecher and Le Fort, 1986).

The Midland Formation, underlying the MCTII, forms a sequence up to 20km thick (Stöcklin, 1980). Above the MCTII the Tibetan Slab forms a continuous pile of gneisses, granites and Tethyan sediments c.20km thick (Arita, 1983).

The shear zone associated with the MCT zone ranges in thickness from 3-7km in the Midland Formation and 4-6km in the Tibetan Slab (Bouchez and Pecher, 1981). Bhattacharya (1987) described the MCT zone as a zone of homogeneous ductile shearing resulting in a vertical displacement of c.18km. Pre-thrust folds show flattening towards the MCTII,

which dips N at c.45°. Exposures in the Burhi Gandaki region indicates thrusting was initiated at depths up to 27km (Hodges et al., 1988). This estimate was based on mineral thermobarometric evidence.

B Metamorphism

A number of phases of metamorphism have been identified in units above and below the MCTII. Thermobarometric measurements made by a number of authors are presented in table 5.1 and Fig. 5.5. Arita (1983) found pyrope cores to almandine garnets which he associated with high grade Precambrian Barrovian metamorphism within the Tibetan Slab. Cambrian Rb/Sr whole rock ages for S-type orthogneisses are compatible with this. These include 550 + or - 16Ma (Ferrara et al., 1983) and 517 + or - 62Ma (Debon et al., 1986) for Dudh Kosi gneisses, and 513 + or - 30Ma (Le Fort et al., 1986a) for Manaslu gneisses.

In contrast to the Tibetan Slab Le Fort (1986) recognises only anchizonal grades in the Midland Formation until the Jurassic.

A second metamorphic event has been associated with the collision of the Indian and Asian plates at c.50Ma. This is believed to have been a high grade metamorphism in the Tibetan Slab (Le Fort, 1986). Arita (1983) associated this with the growth of almandine margins on pyrope cores in the Tibetan Slab of Nepal. In the Midland Formation this may have produced epizone to biotite grade metamorphism.

Movement on the MCTII was initiated during the late stage of this second phase of metamorphism. This produced a

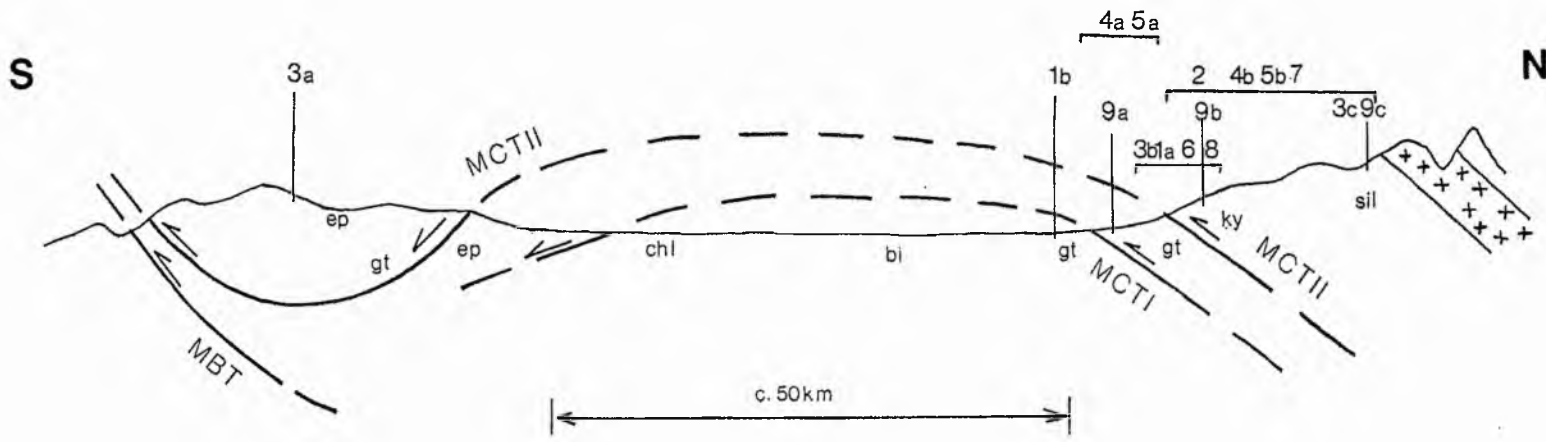


Fig. 5.5 - Sketch map after cross-section, Fig. 5.2A, showing the locations of the metamorphic conditions discussed in table 5.1. Thrusts are as in Fig. 5.4. ep = epizone, chl = chlorite zone, bi = biotite zone, gt = garnet zone, ky = kyanite zone, sil = sillimanite zone. The patterned area represents High Himalayan leucogranite.

Table 5.1 - Metamorphic Conditions

Temperature and pressure conditions, and index minerals at localities above and below the MCTII (see location map Fig. 5.5). These results were produced by various authors from research at a number of localities on the MCTII in Nepal.

Arita (1983)

1a - Chlorite-biotite-garnet grade (500-550 °C) in the Upper Nawakot Group jumps to kyanite grade across the MCTII into the Tibetan Slab and progresses upwards to sillimanite grade.

1b - Grade in the Lower Nawakot Group increases up the structure to a maximum of biotite grade (400-450 °C), at the MCTII. Paragonite content increases towards the MCTII.

Bouchez and Pecher (1981)

2 - In the Tibetan Slab early kyanite and garnet are stretched by shearing. Later minerals range from garnet, staurolite and chloritoid above the MCTII to sillimanite veins higher in the Tibetan Slab. Parts of the MCT zone at temperatures above 450 °C show large plastic strain in quartz.

Brunel and Kienast (1986)

Thermobarometric measurements were made in the Everest region using microprobe analyses of plagioclase, biotite, garnet, kyanite, sillimanite and cordierite. Results were as follows;

3a - 550-650 °C, 6-9kb.
3b - 510-720 °C, 5-8kb.
3c - 510-720 °C, 3.5-5kb.

Pressure conditions are similar in both proximal and distal (e.g. the Kathmandu Klippe) parts of the Tibetan Slab.

Hodges et al. (1986)

Thermobarometric measurements were made in the Manaslu area.

4a - Minerals range from chlorite to garnet-kyanite-staurolite as the MCTII is approached.

4b - From 1-12km above the MCTII the temperature is constant at c.600 °C while pressure ranges from 7.23-3.8kb. This gives a pressure gradient of 270b/km. Temperatures of 630-780 °C are near anatetic gneisses which have thermal buffering effect.

Le Fort et al. (1986b)

5a - Temperatures increase from 550 to 650 °C in the Upper Midland Formation approaching the MCTII.

5b - At the MCTII there is a small temperature jump to 670 °C. Temperatures increase for 1km to 720 °C, then decrease upwards across 4km, at 34 °C/km, to 580 °C. This decrease occurs in the local absence of the thermal buffering effect of anatetic granite (according to Hodges et al., 1988).

Mariuo and Kiazaki (1983)

6 - A traverse over c.3km through the Upper Nawakot Group and the Lower Tibetan Slab gave a continuous zone of inverse metamorphism ranging from c.530-650 °C below the MCTII and 650-720 °C above the MCTII, with no temperature jump detected in this study.

Pavlis (1986)

7 - Temperatures range from >650 °C to 700 °C across the Tibetan Slab. At lower levels a high P and T duplex formed (see section 5.2.4).

Pecher (1979)

8 - Temperatures increased from 400-710 °C through the Upper Nawakot Group into the Lower Tibetan Slab while pressure ranged irregularly from 2.2-4.5kb. Temperatures are based on fluid inclusion homogenisation temperatures (ThTr) and mineralogical evidence, while pressure was based on fluid inclusion density data. Salinities ranged from 1-8wt% NaCl, while CO₂ was most abundant closest to the MCTII.

Pecher and Le Fort (1986)

9a - Immediately below the MCTII a maximum temperature of 630 °C was achieved in the Midland Formation. This is associated with brown biotite, staurolite, garnet and plagioclase (An10).

9b - Above the MCTII the temperature jumps to 650-700 °C at high pressure (8kb). This has been subject to retrograde metamorphism at 500-550 °C.

9c - High in the Tibetan Slab temperatures remain high, but pressure drops to 6.5kb.

third phase of metamorphism, involving inverse prograde metamorphism, up to garnet grade, in the Midland Formation (Pecher and Le Fort, 1986), and retrogression, associated with chloritisation of garnets, at the base of the Tibetan Slab (Arita, 1983). The inverse metamorphism was primarily caused by the thrusting of the hot Tibetan Slab over the Midland Fomation (see section 5.2.4 for discussion).

Hodges et al. (1988) sampled a 12km thick section, in the Manaslu region, through the Tibetan Slab from the MCT zone to the High Himalayan granites, for thermobarometry (see table 5.1 for details). Pressure conditions ranged from 7.2kb immediately above the MCTII to 3.8kb at the top of the pile. This corresponds to a depth range of c.27 to c.14km. Temperature conditions remained constant at c.600°C throughout the pile. The values of 7.2kb and 600°C were related to the c.50Ma metamorphism of Le Fort (1986), but the presence of high temperatures at the top of the pile was attributed to the thermal buffering effect of the Manaslu granite. Samples collected 120km to the W, at the same stratigraphic level in the Kali Gandaki area, show no signs of the buffering effect (Le Fort et al., 1986).

Late movement in the MCT zone is associated with brittle shearing and a rapid drop in pressure in the Tibetan Slab. This pressure drop was facilitated by erosion and tectonic denudation of the Tibetan Slab. The latter occurred by gravity sliding on earlier formed sillimanite coated shear planes, and produced N verging recumbent folds

extending laterally for up to 200km and with inverted limbs up to 25km thick (Pecher and Le Fort, 1986).

C Ages

Isotopic ages obtained from the Tibetan Slab and Midland Formation provide some control on the timing of events during the Tertiary. A reliable body of data has now been collected for leucogranites of the Higher and Lesser Himalayas. Metamorphic mineral closure ages are less abundant. Ages are presented in Table 5.2.

The sequence of events during the Tertiary can be summarised as follows:

75-60Ma - Tethyan sedimentation in NW India (Searle, 1986).

Eocene (c.50-40Ma) - Collision of India with Asia. This is indicated by: 1. A change from marine to continental sedimentation.; 2. A change from I-type granitic intrusion to Eocene S-type anatectic granites (of the Transhimalaya). This reflects melting of sedimentary rocks, due to crustal thickening and burial of sediments with collision tectonics.; 3. Initiation of compression tectonics in the Indus-Tsangpo suture zone is shown by the syn-deposition deformation and thrusting of Eocene sediments (Searle et al., 1987).

Oligocene (after 38Ma) - Initiation of movement on the MCTII (Searle et al., 1987). This pre-dates the High Himalayan granites which are believed to have formed due to wet granitic melt temperatures being exceeded on the MCTII (Le Fort, 1975), (see section 5.2.4). Metamorphism of the

Table 5.2 - Isotopic ages from the Nepal Himalayas

Rock type	System	Age	Authors
<u>High Himalayan Leucogranites</u>			
Lhotse Granite	Rb/Sr whole rock (4)*	52 + or - 1Ma	Ferrara et al. (1983)
Everest Granite	Rb/Sr whole rock, mica	16-17 Ma	Bortolami et al. (1983)
,	U/Pb zircon/monazite	14.3 + or - 0.6Ma	Scharer et al. (1986)
Manaslu Granite	Rb/Sr whole rock	15-20 Ma	Debon et al. (1986)
,	,	17-20.5Ma	Le Fort (1986)
,	,	c.25Ma	Hodges et al. (1988)
,	,	18.1 + or - 0.5Ma	Deniel et al. (1987)
,	U/Pb monazite	25.0 + or - 0.5Ma	,
Nialam Migmatite	U/Pb zircon/monazite	16.8 + or - 0.6Ma	Scharer et al. (1986)
Makalu Granite	,	21.9 + or - 0.2Ma	,
,	,	24.0 + or - 0.4Ma	,
,	?	18.1 + or - 0.5Ma	Searle et al. (1987)
(U/Pb ages were derived from hand picked zircons to obtain data free from the influence of detrital zircons.)			
<u>Old Orthogneisses</u>			
Dudh Kosi	Rb/Sr whole rock	550 + or - 16Ma	Ferrara et al. (1983)
Manaslu	,	517 + or - 52Ma	Debon et al. (1986)
Manaslu augen gneiss	,	513 + or - 30Ma	Le Fort et al. (1986a)
<u>Granites thrust with the Kathmandu Klippe</u>			
Simchar	Rb/Sr whole rock (5)*	466 + or - 40Ma	Le Fort et al. (1983)
,	, (7)*	511 + or - 55Ma	,
Ipa	Rb/Sr whole rock, biot	14Ma (reset)	,
Palung	Rb/Sr whole rock	486 + or - 21Ma	Debon et al. (1986)
,	U/Pb zircon, monazite	470 + or - 4Ma	,
<u>Metamorphism</u>			
Midland Formation	K/Ar muscovite	3.7Ma	Arita (1983)
Inverse metamorphism	K/Ar mu, bi, Rb/Sr biot	15-20 Ma	Le Fort (1986)

* Number of analyses where known.

Midland Formation will have occurred as the Tibetan Slab was thrust over it. A K/Ar muscovite cooling age of 3.7Ma (Arita, 1983) indicates that temperatures over 350 °C were sustained until the Pliocene.

Lower Miocene (25-14Ma) - Formation of anatectic granites in the High Himalaya (Scharrer et al., 1986).

Pliocene (5Ma) - Initiation of movement on the MBT, involving Pliocene or early Pleistocene Siwalik rocks (Stöcklin, 1980).

5.2.4 Inverse Metamorphism Models

A number of models have been proposed to explain the formation of the inverted metamorphic isograds:

Auden (1935) suggested contact metamorphism from the Higher Himalayan granites. This is unlikely because the zone of inverse metamorphism is over 10km thick in places and extends along the whole of the Himalaya, and in any case the granites have minor contact aureoles (Bortolami et al., 1983).

Heim and Gansser (1939) suggested recumbent folding, but, according to Le Fort (1975), the succession has not been inverted. Searle et al. (1987), using Pakistan and Ladakh as examples, support the inversion of isograds by recumbent folding.

Wager (1965) proposed a model involving post-metamorphic inter-zonal thrusting. Thin tectonic slices of higher grade rocks could be superimposed on lower grade rocks to give the appearance of a gradual upward increase in metamorphic grade. Lal et al. (1981), and Andrieux et al. (1980) and (1981) adopted this model, but also recognised retrogression in the hanging wall. To produce the zone of inverse metamorphism a broad zone of major tectonic disruption is required, but according to Pécher and Le Fort (1986), this has not been observed.

Maruo (1979) attributed the inverse metamorphism to shear heating during thrusting (see also Maruo and Kiazaki, 1983). Shear heating should raise the temperature of the rocks by c.200°C, and thrusting should be rapid enough to

counter heat loss through conduction. This model has also been applied by Aprahamin and Paris (1981) to thrusting in the Haute-Savoie, France. Typical values considered appropriate for a thrust on the scale of the MCTII were: displacement rate of 0.1-10cm/yr, thickness of 20km or more for the thrust pile and millions of years of displacement. Models involving shear heating have been applied by a number of Himalayan researchers. Bouchez and Pêcher (1981) suggest 3-5cm/yr displacement rate for 2-3Ma to produce c.100km thrusting, with thrusting initiated at c.20km depth and c.700°C. Arita (1983) suggests 5-10cm/yr displacement rate, for 2½-5Ma producing c.250km of thrusting at temperatures around 550°C.

Pavlis (1986) has produced a more elaborate model. Initial movement on the MCTII produces shear heating under conditions of 3-10cm/yr displacement rate for 1-3Ma on a 20° to 30° thrust plane to produce c.100km of thrusting and 200°C of strain heat in a zone a few km wide. At 20km depth 650-700°C would be attained. A second phase develops. Wet upper crustal (footwall) rocks, taken down to c.20km, lose water into the hanging wall. Wet granitic melt temperatures are exceeded and anatectic plutons, formed in the hanging wall, rise to form the High Himalayan granites (see also Debon et al., 1986). At the same time high pressure and temperature duplexes accrete to the base of the hanging wall. Rapid uplift at this time results in the successive accretion of lower pressure and temperature rocks, resulting in apparent inverse metamorphic zonation.

Arguments against a significant heat contribution from shearing are: 1. insufficient strain could be concentrated in a shear zone several km thick, and 2. a negligible rise in temperature could be achieved in an initially hot shear zone (Bouchez and Pêcher, 1981). High stress and/or strain rates were only achieved in the late stages of movement on the MCTII when it was a narrow cold brittle fault zone (Bouchez and Pêcher, 1981).

Le Fort (1975) produced a model in which S-shaped isograds were formed during rapid syn-metamorphic ductile underthrusting of the Indian Slab under the Tibetan Slab. Heat is supplied by the hot Tibetan Slab. The speed of underthrusting and uplift prevented re-equilibration of the isograds (see Fig. 5.6). This model was favoured by Pêcher (1979), Stöcklin (1980) and Sinha-Roy (1982).

Le Fort's model has subsequently been adapted and refined to suit a growing body of data. Pêcher and Le Fort (1986) recognised variable tectonometamorphic conditions at different depths on the MCTII. As before, prograde metamorphism was associated with early movement on the MCTII. In deep areas initial temperatures are high on both sides of the MCTII (600 - 630°C) and thermal equilibration across a broad zone of inverted isograds was easily achieved. Closer to the thrust front, equilibration to c. 500 - 550°C was achieved by retrogression of the base of the Tibetan Slab and the formation of a narrow zone of inverted isograds under the MCTII. Still closer to the thrust front (e.g. the Kathmandu Klippe) hot shearing is replaced by cold thrusting of gneisses over anchizone to

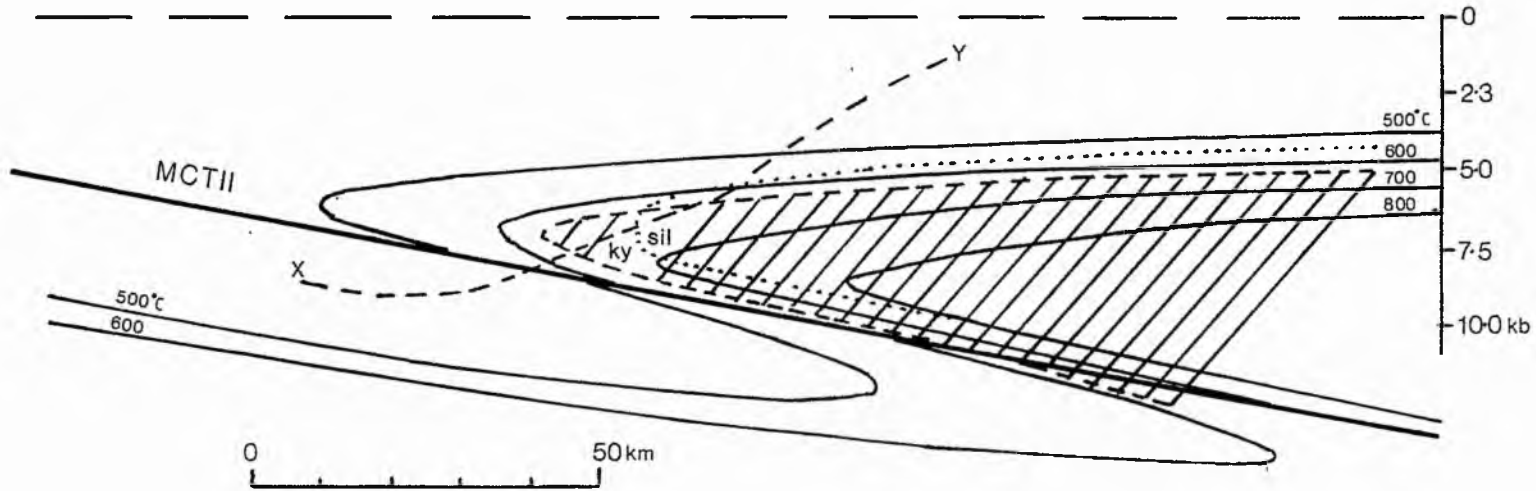


Fig. 5.6 - Thermal regime of two thrusted slabs (after Le Fort, 1975). Temperature isograds are tentatively drawn together with the corresponding kyanite-sillimanite boundary, and the muscovite granite excess water solidus (shaded). Heat transfer by magma and water movement is not taken into account. The present topographical surface for the Manaslu area is also indicated.

epizone rocks, with a sharp jump in grade. After ductile shearing has finished shortening in the Indian plate is taken up by brittle fault planes within the MCTII zone and below it in the Midland Formation. (No doubt the MBT is active at this stage).

Mason (1984) has proposed a model for a zone of inversion in the Sulitjemla area in Norway. The isograds were simply rotated by thrusting in a shear zone initiated in the crystalline basement. This would also imply inversion of the succession.

The results from this study, presented here (chapter 5), allow some assessment of these models.

5.3 FIELDWORK

Samples were collected along two traverses for illite crystallinity and petrographic studies (see Figs 5.1 and 5.2A and B, and Appendix 5.1). In traverse A, from Barahbise to the Bagmati River, 54 samples were collected at roughly 1-1.5km intervals (see plate 5.1). Sampling gaps occur where drift covers the exposure and where the Narayan Than granite is exposed. A further 8 samples of vein quartz were collected between Balephi and Dhulikhel for fluid inclusion studies. In traverse B, from Syabru to Betrawati, 15 samples were collected at roughly 2km intervals (see plate 5.2).

5.4 PETROGRAPHY

5.4.1 Introduction

36 thin sections were prepared from traverse A and thin sections were prepared from all 15 samples of traverse B. These were examined to determine mineral paragenesis and for evidence of fault fabrics.

5.4.2 Thin Section Analysis

A. Below the MCTII

Kuncha Formation (HS4-HS21 and LH3-LH15) - The schists of the Kuncha Formation show a decrease in metamorphic grade southwards (see below). Samples collected in traverse B were generally more pelitic than those of traverse A. Lithological variations account for much of the irregularities in the occurrence of index minerals.



Plate 5.1 - Re-folded fold in the Benighat Slates.

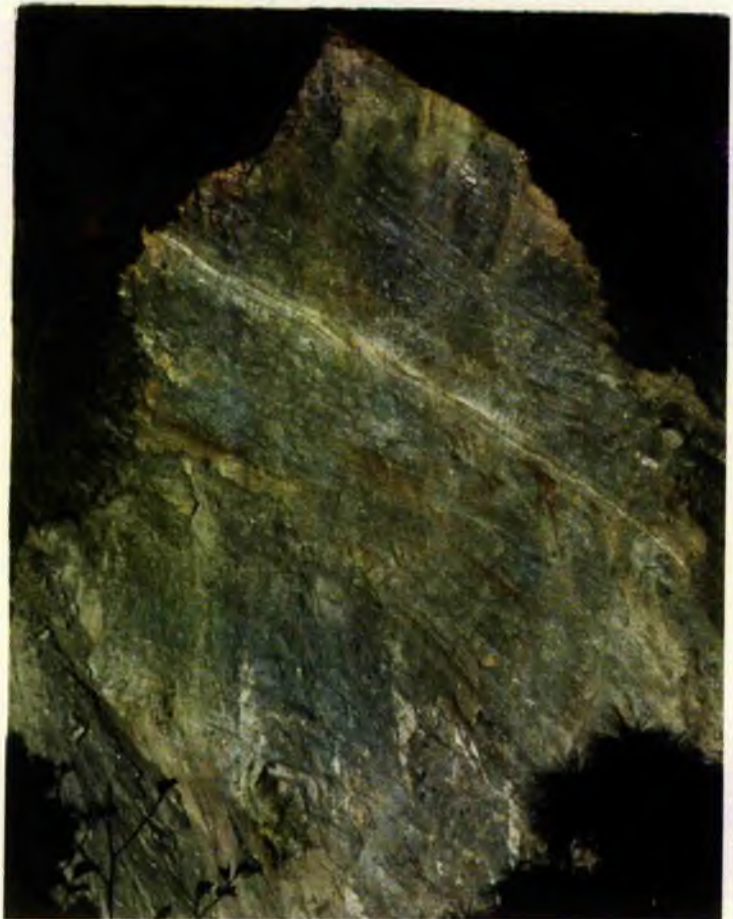


Plate 5.2 - A 1km high cross-section through the Kuncha Formation exposed by a rockslide (note the houses and terraced fields in the top right corner). This exposure lies close to the MCTI and shows isochlinal folding of the beds which dip at c.20° to the NE.

In traverse A, garnet grade rocks range from HS4 to HS10. Samples are mostly psammitic and contain detrital feldspar, quartz and zircons. Metamorphic minerals include poorly formed garnets, biotite, muscovite and albite. Chlorite is uncommon. HS4 came from the MCTI, and shows total re-crystallisation, a mylonitic fabric and chlorite retrogression of garnet margins.

Garnet grade rocks, in traverse B, range from LH3 to LH9 (see plate 5.3) and LH12. These rocks are more pelitic, and contain euhedral garnet in association with biotite, muscovite, quartz, feldspar, tourmaline and minor cordierite.

In traverse A, biotite grade rocks range from HS11 to HS17, and are characterised by the presence of biotite and muscovite with minor retrogressive chlorite. In contrast HS18 to HS21 are very rich in muscovite and chlorite while biotite is absent. HS18 shows chlorite pseudomorphs after garnet which indicates strong retrogression (see plate 5.4).

Biotite grade rocks, in traverse B, range from LH10 to LH12. No retrogressive chlorite is present. LH13 to LH15 are heavily weathered fine grained muscovite and chlorite schists.

Throughout the Kuncha Formation metamorphic tourmaline and detrital zircon are common, a crenulation cleavage is usually present (see plate 5.5), and quartz veining is surprisingly uncommon.

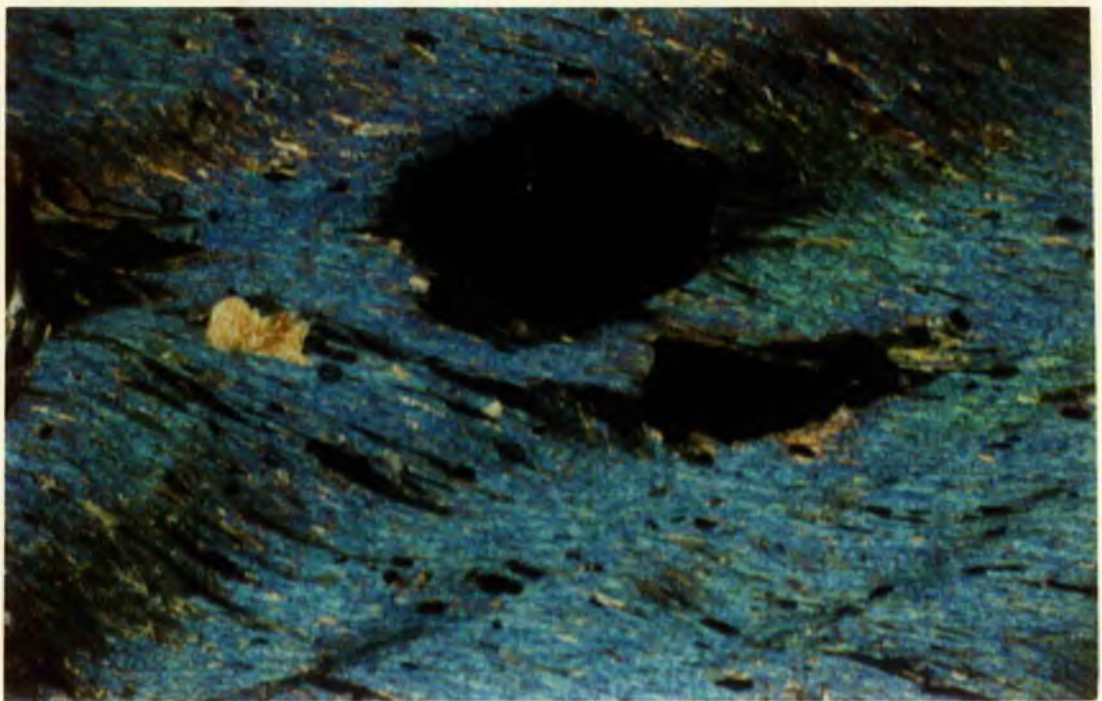


Plate 5.3 - Euhedral garnet, with chlorite in the pressure shadows, in crenulated muscovite schist from the Kuncha Formation (XPL, LH9, 2.5mm).

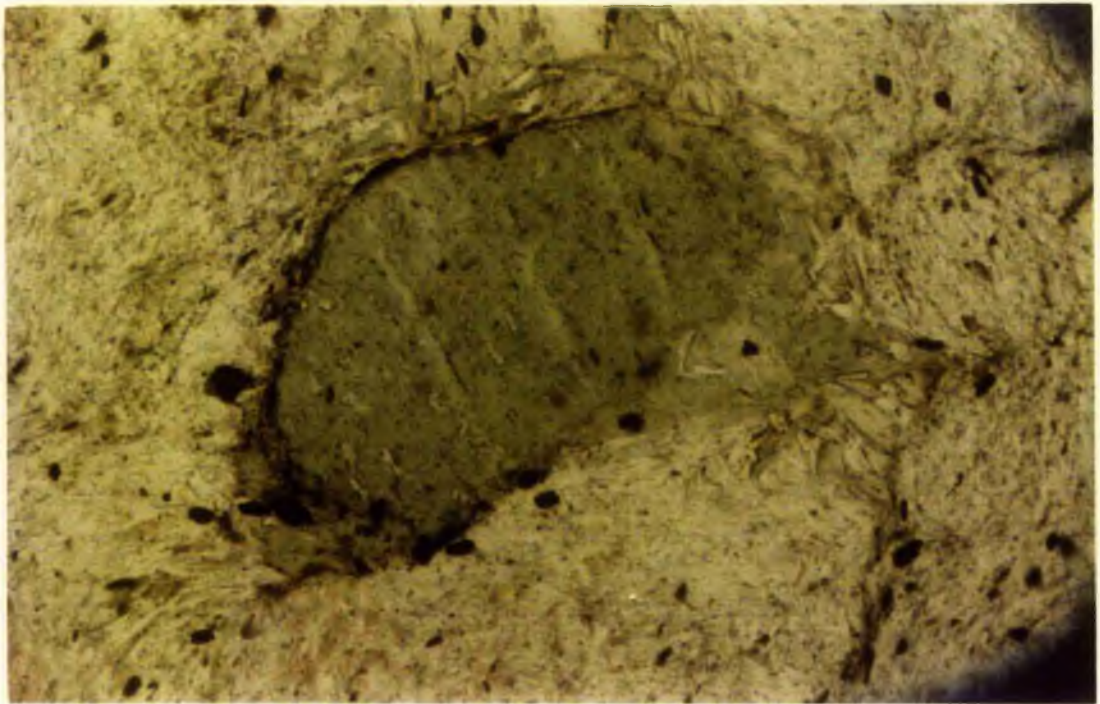


Plate 5.4 - Chlorite pseudomorphs after garnet in chlorite schist from the Kuncha Formation (PPL, HS18, 2.5mm).



Plate 5.5 - Crenulated garnet grade biotite rich schist from the Kuncha Formation (note the lack of retrogression) (PPL, LH7, 2.5mm).

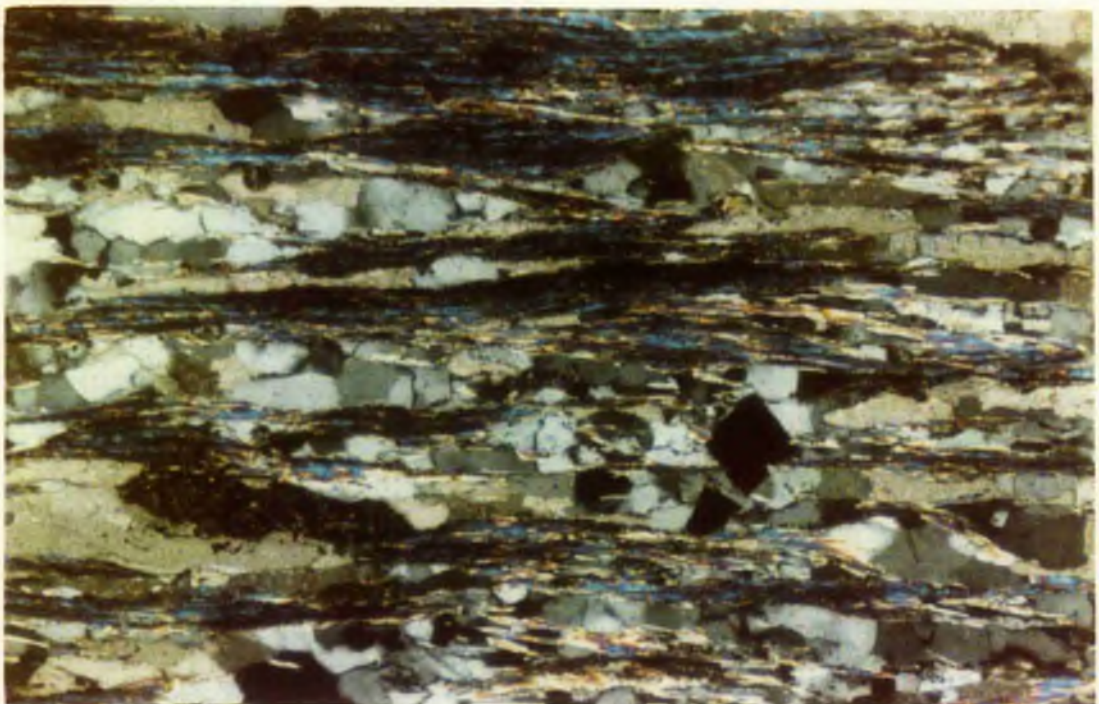


Plate 5.6 - Benighat Slate showing a strongly developed foliation with white mica, re-crystallised quartz, carbon, calcite and later pyrite (XPL, HS29, 1.0mm).

Across the Kuncha Formation there is a decrease in metamorphic grade from north to south. This metamorphism has frequently been interpreted as a zone of inverse metamorphism, and is associated with the prograde metamorphic growth of garnet, biotite or chlorite, depending on the grade attained. Only limited retrogressive chlorite is present in biotite and garnet grade rocks. The presence of chlorite pseudomorphs after garnet in HS18 (at the chlorite-biotite zone boundary) is difficult to explain on the basis of a single thin section.

Benighat Slates (HS1-HS3, HS22-HS31 and HS53) - A clear jump in grade occurs between the Kuncha Formation and the Benighat Slates. Near Barahbise, chlorite schists, carbonates and black carbonaceous slates overly garnet grade schists of the Kuncha Formation. In the Dolalghat area the boundary between the chloritic schists of the Kuncha Formation and the black Benighat Slates is only apparent from the change in lithology. The slates are characterised by large amounts of fine white mica, recrystallised quartz, black carbon, carbonate (including dolomite) and opaques (including pyrite) (see plate 5.6). Minor epidote, chlorite and tourmaline is also present. HS27 and HS28 also contain fine grained brown biotite. The biotite grade may have only been achieved in favourable lithologies. A sub-phyllonitic foliation is frequently developed, and is associated with common quartz veining and polyphase folding.

B. Above the MCTII

LH1 and LH2 are samples from immediately above the MCTII (immediately above the footwall) in a position proximal to its root zone (close to the High Himalaya). LH1 is a garnet kyanite gneiss with abundant biotite, quartz and feldspar, lesser muscovite, and detrital zircon. LH2 is an unusual crenulated chlorite epidote schist. It contains abundant chlorite, epidote and quartz, lesser muscovite and opaques, and minor biotite and tourmaline.

In the Kathmandu Klippe, distal to the root zone of the MCT, a number of formations were sampled:

Raduwa Formation (HS52) - This one sample, lying south of the Narayan Than granite and close to the southern limit of the MCTII, is a strongly mylonitic biotite schist. Total recrystallisation has occurred with strongly orientated biotite and muscovite crystals, quartz trails and occasional muscovite 'fish' (see plate 5.7).

Kalitar Formation (HS32, HS50 and HS51) - Samples are composed of medium grade weathered biotite muscovite schists. HS50 is an augen gneiss local to the southern margin of the Narayan Than granite. It contains feldspar porphyroblasts in a groundmass of quartz, feldspar, biotite, muscovite, tourmaline and epidote. It may represent part of the tectonised margin of the Narayan Than granite.

Kulikhani Formation (HS33, HS34 and HS46-HS49) - This is composed of weathered biotite schists (see plate 5.8). Biotite is often very dark brown, and in association with

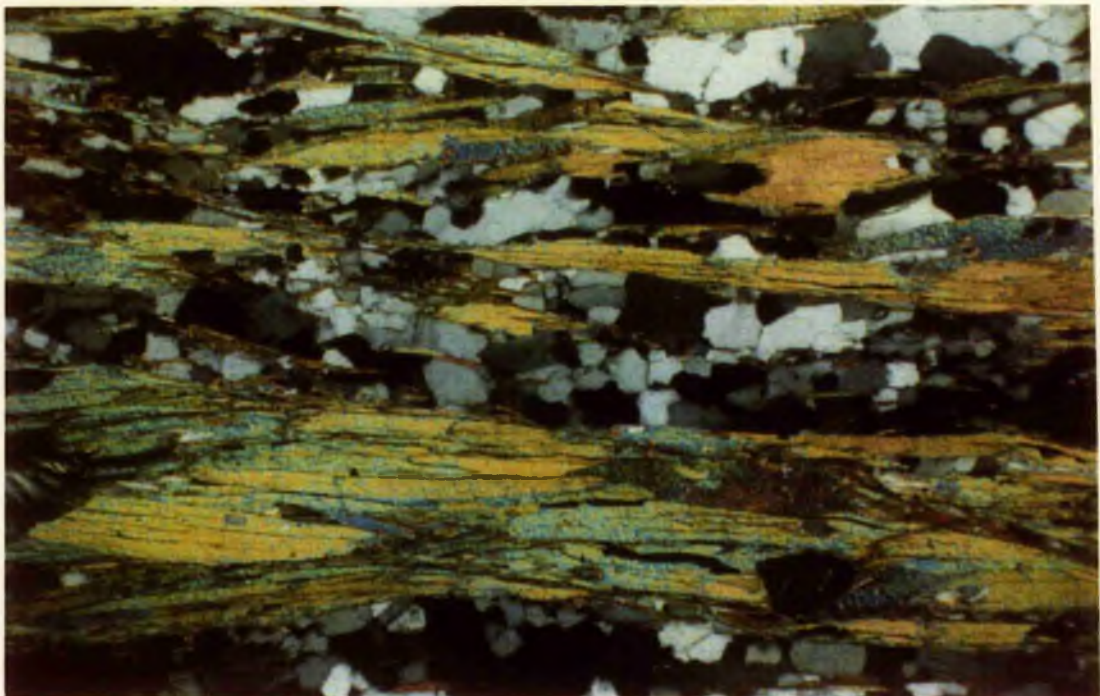


Plate 5.7 - Mylonitic muscovite rich schist in the Raduwa Formation. Quartz is completely re-crystallised, muscovite forms elongate aggregates and occasional 'fish' (XPL, HS52, 2.5mm).



Plate 5.8 - Biotite schist, from the Kulikhani Formation, with abundant dark grey/brown biotite and a weakly developed foliation (PPL, HS34, 2.5mm).

lesser muscovite and epidote. At higher stratigraphic levels muscovite and chlorite dominate over biotite. The control of lithology on the presence of biotite is shown by HS48. Two lithological bands are present in one thin section. One is dominated by fine muscovite with minor chlorite and no biotite, while the other is rich in medium grained biotite. Seen separately the two bands might be assigned to separate metamorphic grades.

Tistung Formation (HS35-HS37 and HS39-HS45) - The lower grade biotite and muscovite schists of the Tistung Formation lie higher in the succession. Biotite makes a variable appearance, and minor epidote, tourmaline, calcite and pyrite also occur.

Chandragiri Limestone? (HS38) - one sample of a massive medium crystalline limestone was sampled. Impurities of detrital quartz and feldspar, and metamorphic opaques and muscovite were present.

Siwalik Sandstone (HS54) - One sample of Siwalik Sandstone was collected close to the MBT. This had no foliation, and was rich in detrital monocrystalline and polycrystalline quartz, feldspar, muscovite and zircon. Secondary clay minerals, chlorite, calcite and epidote were also present.

5.5 PHYLLOSILICATE MINERALOGY

The $<2\mu\text{m}$ mineralogy of all the samples gathered (excepting HS1, HS3, HS9, HS38, HS50 and LH1) was examined by XRD. Mineralogy, crystallinity and b_0 values are listed in Appendix 5.1. The relative proportions of minerals are semi-quantified visually on a small, medium or large scale, and compared with Hbrel values in Fig. 5.7.

5.5.1 Kuncha Formation

The mineralogy of the Kuncha Formation can be considered in terms of the garnet, biotite and chlorite zones. In the garnet zone the major constituents are 2M, muscovite, albite and quartz (see Fig. 5.8). Biotite is often hard to detect by XRD, but present in thin section. Chlorite and paragonite are regularly present in small amounts. The biotite zone is similar, but has marginally more chlorite and less paragonite. The chlorite zone differs by having greater amounts of chlorite, less albite, and no biotite or garnet (see Fig. 5.8). HS20 contains halloysite which probably formed from the decomposition of alkali feldspar with tropical weathering. Small amounts of mixed-layer illite/smectite occur sporadically throughout the Kuncha Formation. This may have formed from the weathering and breakdown of 2M, muscovite.

5.5.2 Benighat Slates

The $<2\mu\text{m}$ mineralogy of the Benighat Slates is dominated by 2M, muscovite and quartz (see Fig. 5.9). Chlorite and paragonite are usually present in minor amounts. Albite, 6:4 paragonite/muscovite and pyrophyllite

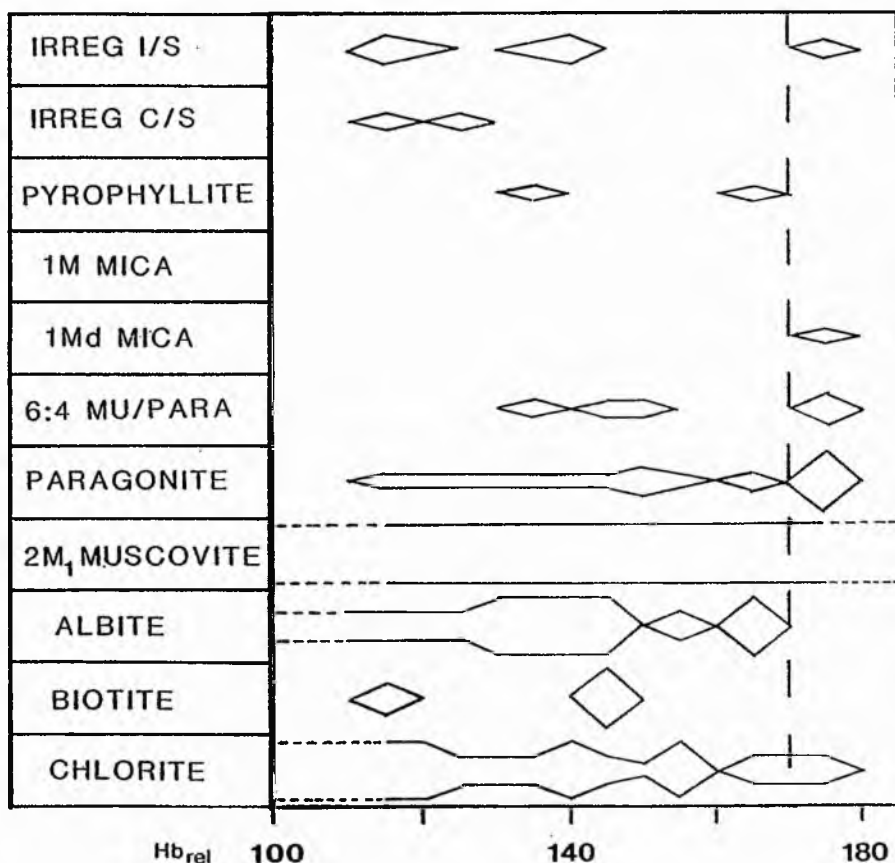


Fig. 5.7 - Mineralogy of the <2µm size fraction compared to Hbrel. Relative proportions of minerals (shown by the width of the bars) are quantified on a small, medium and large scale by visual inspection of XRD traces. A value of Hbrel 170 is taken as the anchizone-epizone boundary (see text).

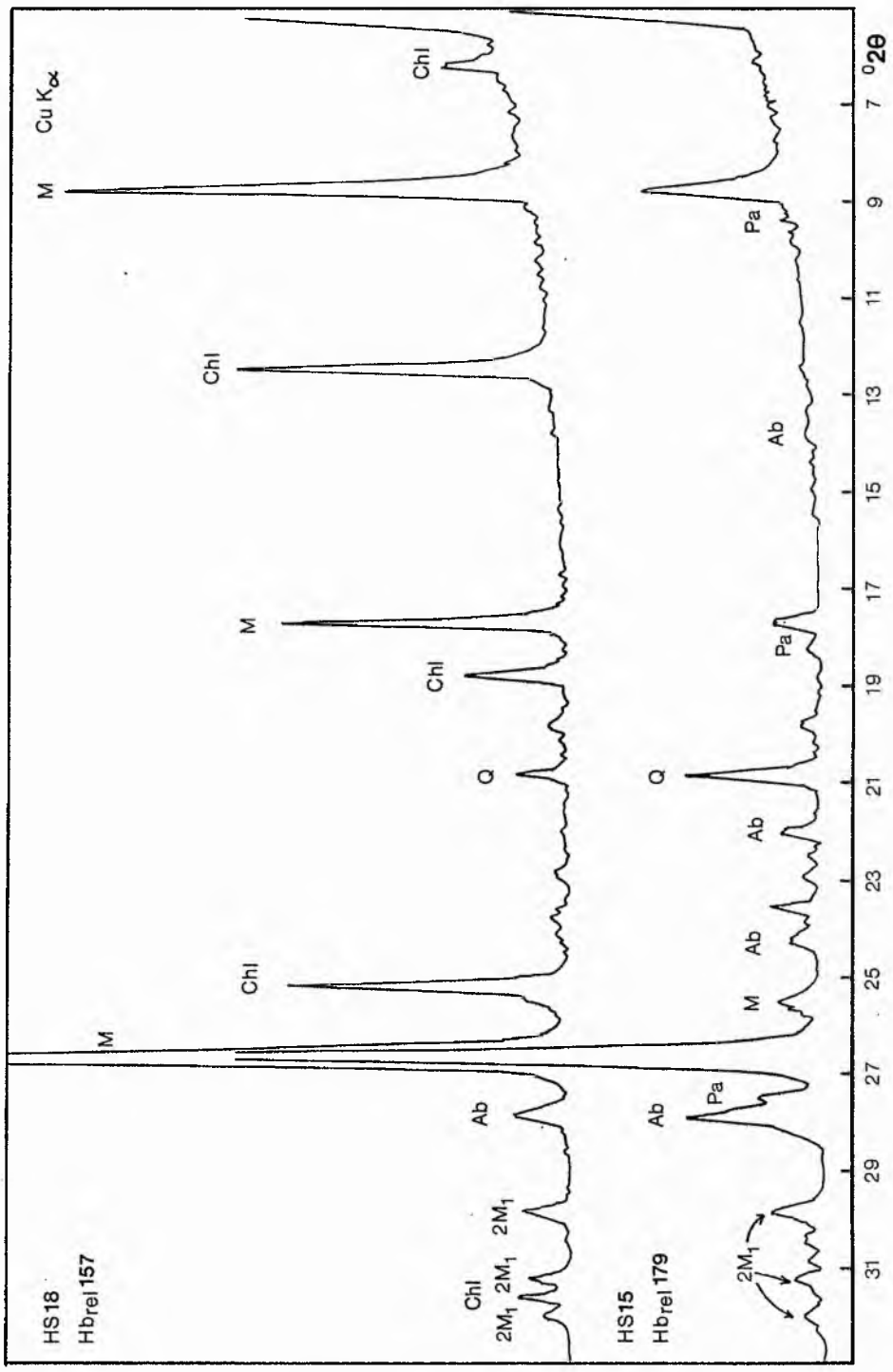


Fig. 5.8 - XRD traces from samples HS15 and HS18 from the Kuncha Formation. M = muscovite, $2M_1$ = the $2M_1$ polymorph of muscovite, Chl = chlorite, Q = quartz, Pa = paragonite, Ab = albite. HS15 is from the biotite zone. Chlorite is absent, albite is abundant and biotite cannot be distinguished from the muscovite peaks. HS18 is from the chlorite zone. Chlorite and $2M_1$ muscovite are abundant.

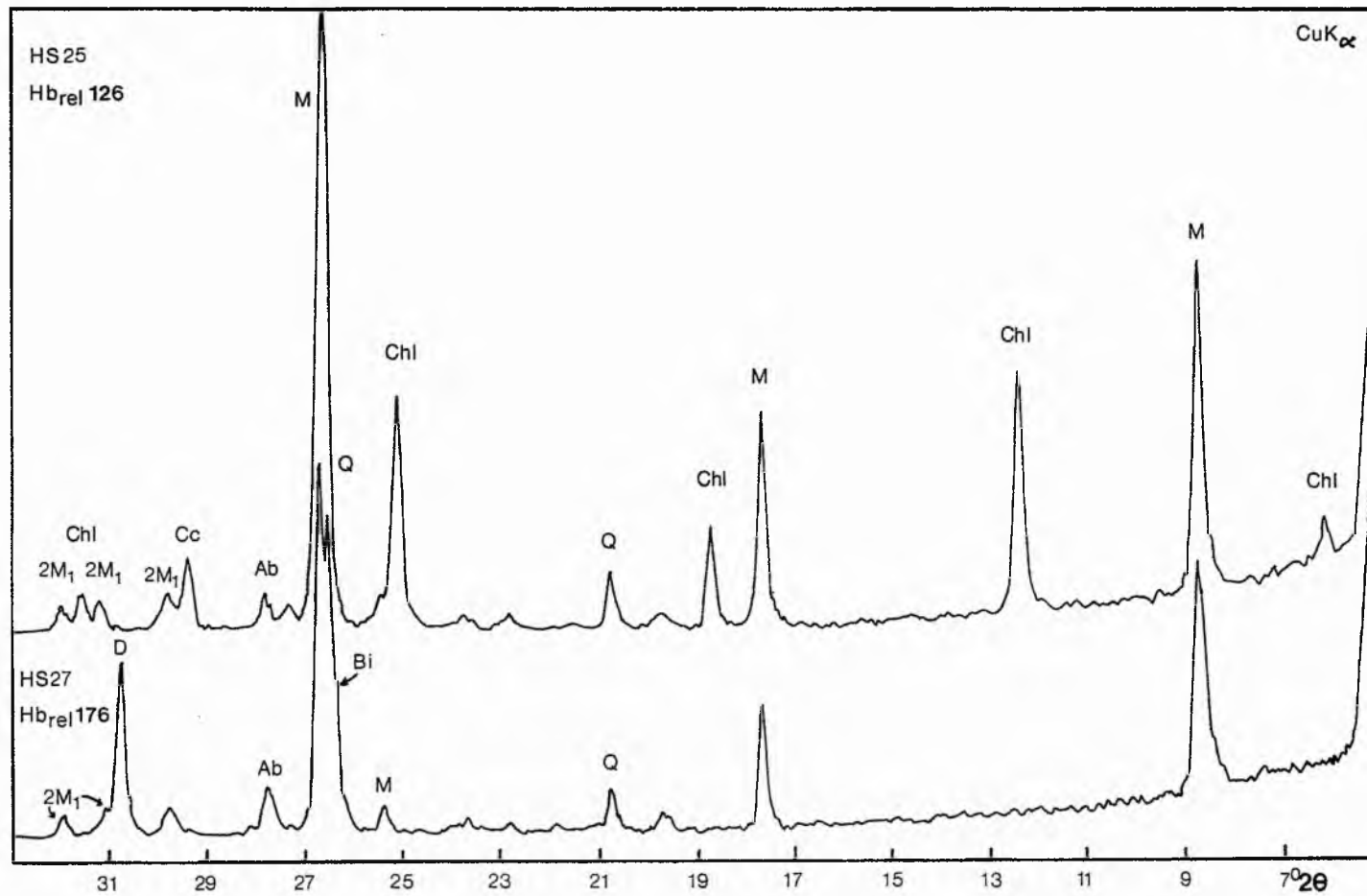


Fig. 5.9 - XRD traces from samples HS25 and HS27 from the Benighat Slates. Abbreviations are explained with Fig. 5.8. In addition Bi = biotite, Cc = calcite and D = dolomite. Between 26 and $27^\circ 2\theta$, in HS27, overlapping muscovite, quartz and biotite peaks can be distinguished.

occur sporadically, and mixed-layer chlorite/smectite occurs only in HS24. Dolomite and calcite are prominent in some of the samples. Strong biotite peaks are present in HS27 and HS28 (see Fig. 5.9). The small grain size of the biotite has favoured preferential trapping in the <2µm size fraction and this accounts for the strong biotite peaks.

The abundance of 2M₁ mica in these samples indicates that they are epizonal. HS53, from the most southerly outcrop of the Benighat Slates, contains small amounts of 1Md mica in addition to common 2M₁ mica, paragonite, chlorite and minor illite/smectite. This sample is likely to be upper anchizonal.

5.5.3 Above the MCTII

The garnet and biotite schists of the Kathmandu Klippe are dominated by 2M₁ muscovite with more variable amounts of albite, quartz and paragonite. Chlorite is a frequent minor constituent, and biotite is only confirmed in HS34 despite its common occurrence in thin section. Other less common minerals were calcite, dolomite (HS34) and mixed-layer illite/smectite (see Fig. 5.10). The latter mineral is likely to be a weathering product. The chlorite grade schists contained more abundant albite, less chlorite, paragonite and mixed-layer illite/smectite, and no pyrophyllite or biotite.

5.6 ILLITE CRYSTALLINITY

The method of investigation is described in section 2.2.7. Crystallinity analyses were obtained from all

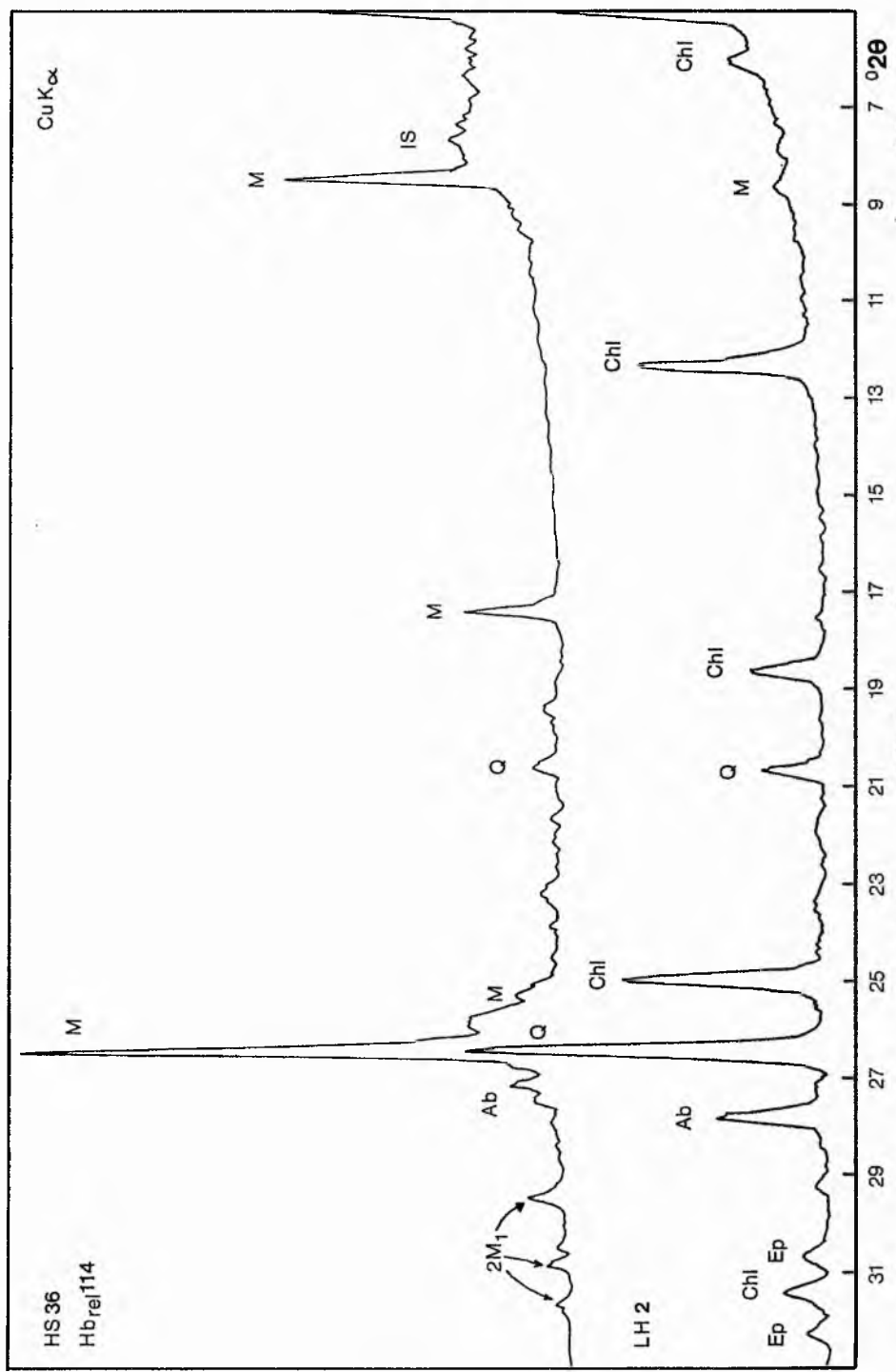


Fig. 5.10 - XRD traces from samples HS36 and LH2 from the Kathmandu Klippe and Tibetan Slab, at Syabru, respectively. Abbreviation are explained with Fig. 5.8. In addition IS = mixed-layer illite/smectite and Ep = epidote. Illite-Smectite in HS36 is likely to be a tropical weathering product. LH2 contains abundant quartz, feldspar, chlorite and epidote in thin section.

samples (excepting HS1, HS3, HS38, HS44, HS50, LH1 and LH2 because of poor 10 \AA ^o mica peaks). Hbrel values from samples in which biotite was subsequently identified, and have interfered with the 10 \AA ^o muscovite peak, have been omitted, though are included in Appendix 5.1. Results, in Hbrel, for the <2 μm size fraction are presented in Figs 5.11, 5.12 and 5.13, and are tabulated in Appendix 5.1. Table 5.3 shows the range of crystallinity values within each formation.

Table 5.3 - Illite Crystallinity Ranges (in Hbrel)

Benighat Slates (Barahbise area)	124
Kuncha Formation (chlorite zone)	117-167
Benighat Slates (Dolalghat area)	117-151
Tistung Formation (chlorite zone)	114-164
Benighat Slates (Bagmati R. area)	173
Siwalik Sandstone	144

From the results the following observations can be made:

1. - Below the MCTI, in the Kuncha Formation, metamorphic grade increases steadily northwards towards the MCTI. This is reflected in traverses A and B by a northwards decrease in Hbrel values in the chlorite zone (values indicate epizonal conditions). North of the chlorite zone the occurrence of biotite, at 425-450°C (see section 2.2.14) and then garnet, at 500-550°C (Arita, 1983) indicates that grade continues to increase northwards.

2. - Between the MCTI and MCTII are the Benighat Slates. In traverse A these outcrop at three localities. At Barahbise, proximal to the MCTII root zone, one Hbrel value of 124 was recorded in a muscovite chlorite schist. This,

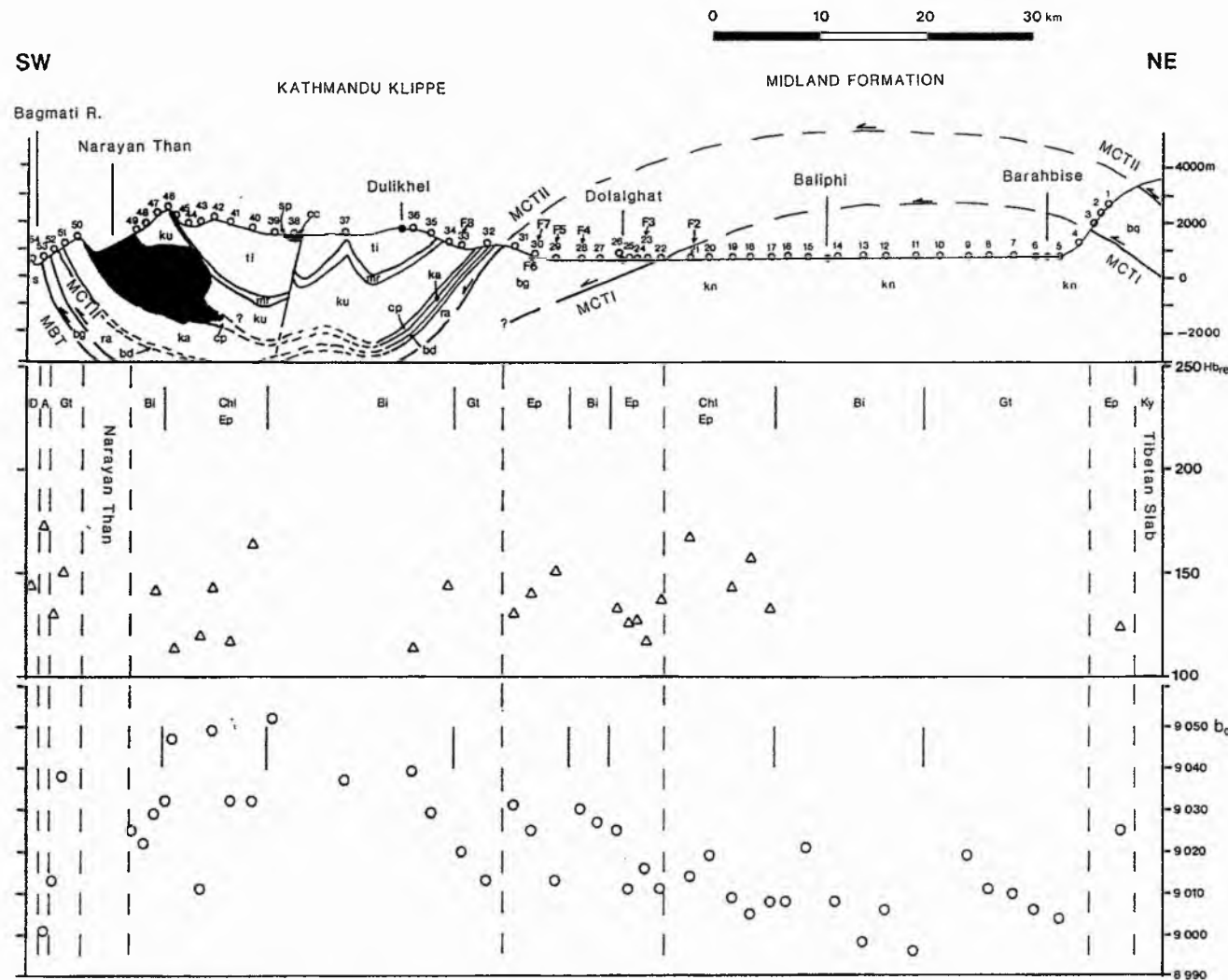


Fig. 5.11 - Traverse A, from the Barahbise area to the Bagmati River, with HbreI and b₀ data. Traverse A is explained in Fig 5.1. Additional abbreviations are as follows: d = diagenesis, A = anchizone, Ep = epizone, Chl = chlorite zone, Bi = biotite zone, Gt = garnet zone, Ky = kyanite zone. Dashed lines indicate lithological boundaries on the HbreI and b₀ traverses.

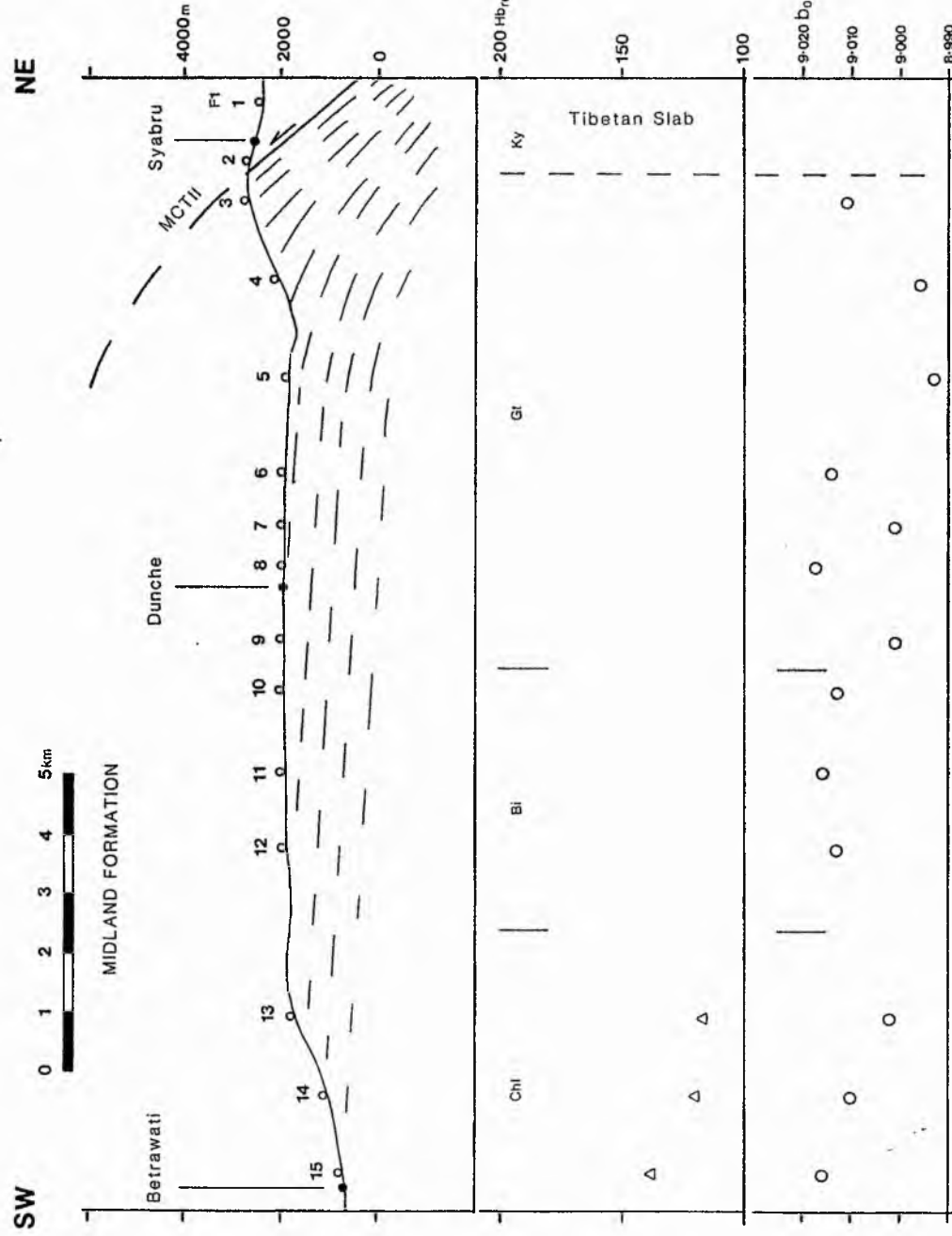


Fig. 5.12 - Traverse B, from Syabru to Betrawati, with HbreI and b_o data. Abbreviations are explained with Figs 5.1 and 5.11.

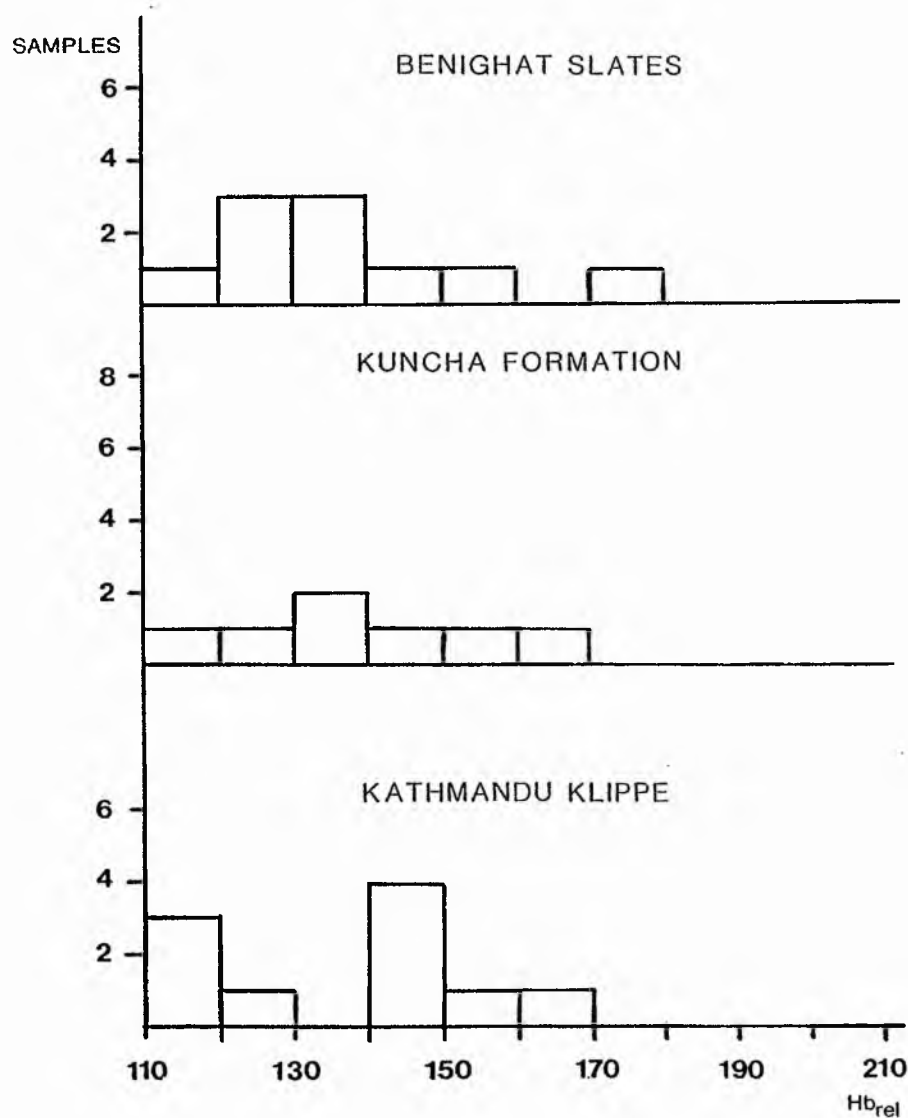


Fig. 5.13 - Histograms comparing the Hb_{rel} values of the Benighat Slates, Kuncha Formation and Kathmandu Klippe.

and the presence of black carbonaceous slates, indicate that epizonal conditions are unlikely to have been exceeded. In the Dolalghat area, NE of the Kathmandu Klippe, Hbrel values ranged from 117-151, with two samples with values of 170 and 176 respectively. The former samples fall into the epizone, whereas the latter two contain fine biotite and fall in the biotite zone (upper epizone at 425-450 °C). Biotite interferes with the 10 \AA muscovite peak resulting in larger Hbrel values. Across the outcrop Hbrel values are relatively uniform. The presence of biotite in two samples may reflect relatively minor variations in grade, or lithological differences. The most distal occurrence of the Benighat slates is to the south of the Kathmandu Klippe at the Bagmati River. Slates are bound by the MCTII and MBT. The one sample analysed had a Hbrel of 173 which indicates anchizonal conditions.

Across the three outcrops of the Benighat Slates, which are spaced over 100km from proximal to distal positions below the MCTII, there is very little change in metamorphic grade. This could indicate that the MCTII was a very low angle thrust plane. Alternatively, metamorphism of these rocks is pre-Himalayan and temperatures during the formation of the MCTII did not exceed the older temperatures. Since they immediately underly the MCTII, this would imply that the inverse zonation in the Kuncha Formation was not caused by metamorphism during the formation of the MCTII. This is contrary to all the various hypotheses put forward for Himalayan metamorphism.

The Benighat Slates reach a maximum grade of upper epizone. Near Barahbise these slates are sandwiched between the MCTII and the garnet grade Kuncha Formation. This implies that the MCTII could not have imposed the inverse zonation on the Kuncha Formation because the grade in the overlying Benighat Slates is lower.

3. - Above the MCTII, in the Kathmandu Klippe, the grade of metamorphism decreases upwards through the succession. The Kathmandu Klippe forms a synclinal structure up to 45km across. In traverse A the grade decreases from garnet grade, immediately above the MCTII, to epizonal conditions in the Tistung Formation, near the core of the syncline. Closer to the core of the syncline, in the younger Silurian and Devonian rocks, a maximum of anchizonal grades are probably achieved, on the basis of petrographic evidence (Stöcklin, 1980).

Metamorphism in the Kathmandu Klippe is believed by Stöcklin (1980) to pre-date the emplacement of the Cambro-Ordovician granites of the Lesser Himalaya. It follows that it also pre-dates movement on the MCT zone and folding of the Kathmandu Klippe into a syncline. This evidence is compatible with a decrease in metamorphic grade towards the core of the Kathmandu Klippe, as described above.

4. - Sample LH1, from immediately above the MCTII in the High Himalaya, lies in the kyanite grade which corresponds to the observation of previous authors (e.g. Le Fort, 1975).

5. - Sample HS54, a Siwalik sandstone, has a HbreI of 144. This is due to the presence of detrital mica which has swamped diagenetic clays.

6. - The anchizone-epizone transition was not observed in the field area though HS53 and HS54 were sub-epizone samples. Anchizone Benighat Slates are in tectonic contact with garnet grade rocks (e.g. the Raduwa Formation), or diagenetic grade rocks (e.g. the Siwaliks). Epizone rocks either increase in grade (e.g. in the Kuncha Formation), or are in tectonic contact with similar or higher grade rocks (e.g. the Benighat Slates and the Tibetan Slab).

5.7 b_o SPACING

b_o spacings were determined on samples used for illite crystallinity. The method of investigation is described in section 2.2.12 and 2.2.13, and machine conditions are given in Appendix 2.1. Two b_o traverses are presented in Figs 5.11 and 5.12, and results are included on the cumulative frequency plot (Fig. 5.14) and Fig. 5.15. Mean b_o values for the Kuncha Formation, Benighat Slates and Kathmandu Klippe are presented in Appendix 3.4. Biotite bearing samples are included because they can be used without prejudicing the results (the 060 white mica peak is not obscured by a biotite peak).

In traverse A the Kuncha Formation has a mean b_o value of 9.009\AA° ($SD = 0.008$, low-medium P), similar to 9.008\AA° ($SD = 0.007$, low-medium P) in traverse B (see table

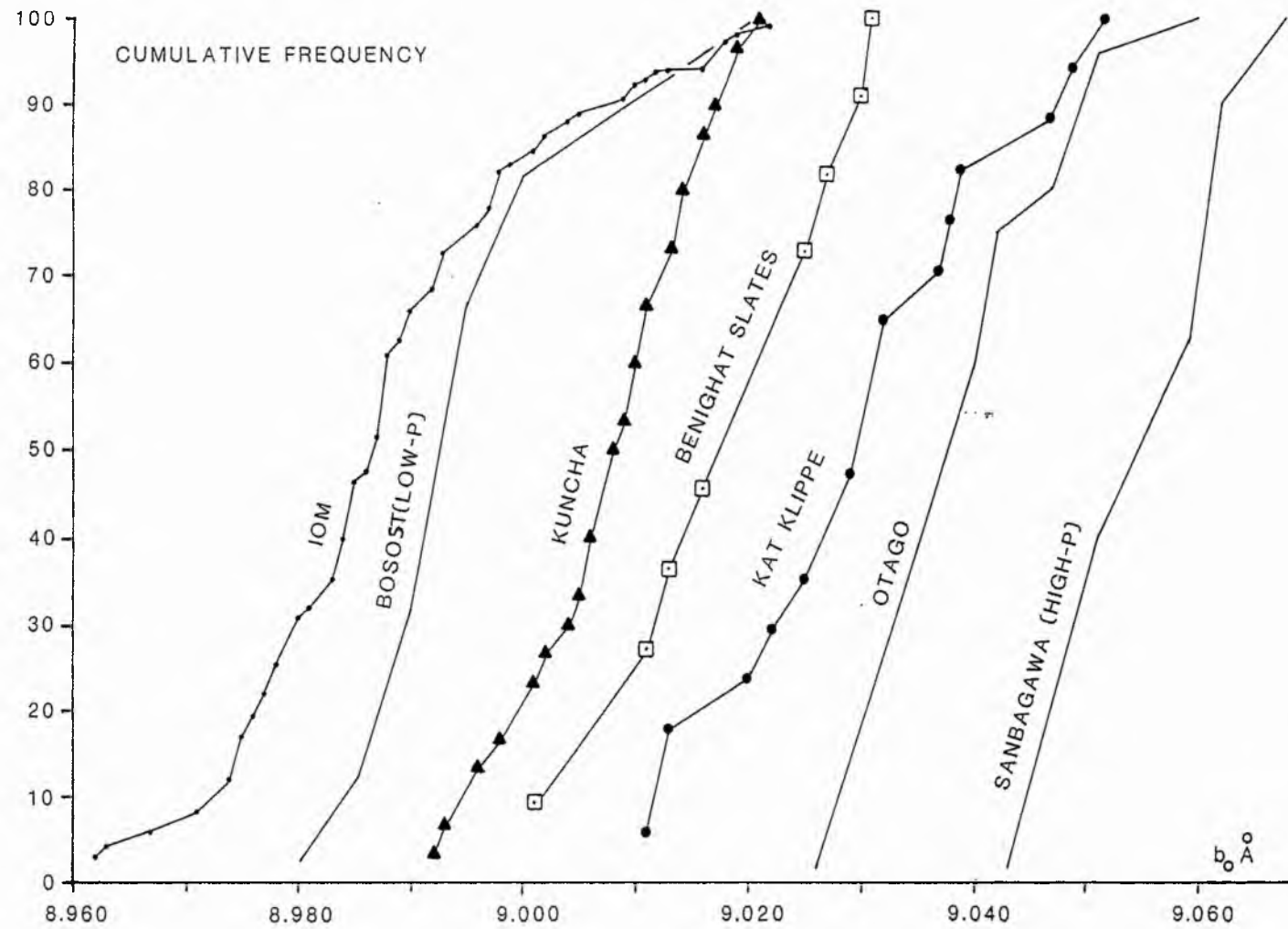


Fig. 5.14 - Cumulative frequency curves of b_o values from: Nepal and the IOM (this study), and also Bosost, Otago and Sanbagawa (Sassi and Scolari, 1974). Nepal samples have been divided up into those from the Kuncha Formation, the Benighat Slates and the Kathmandu Klippe.

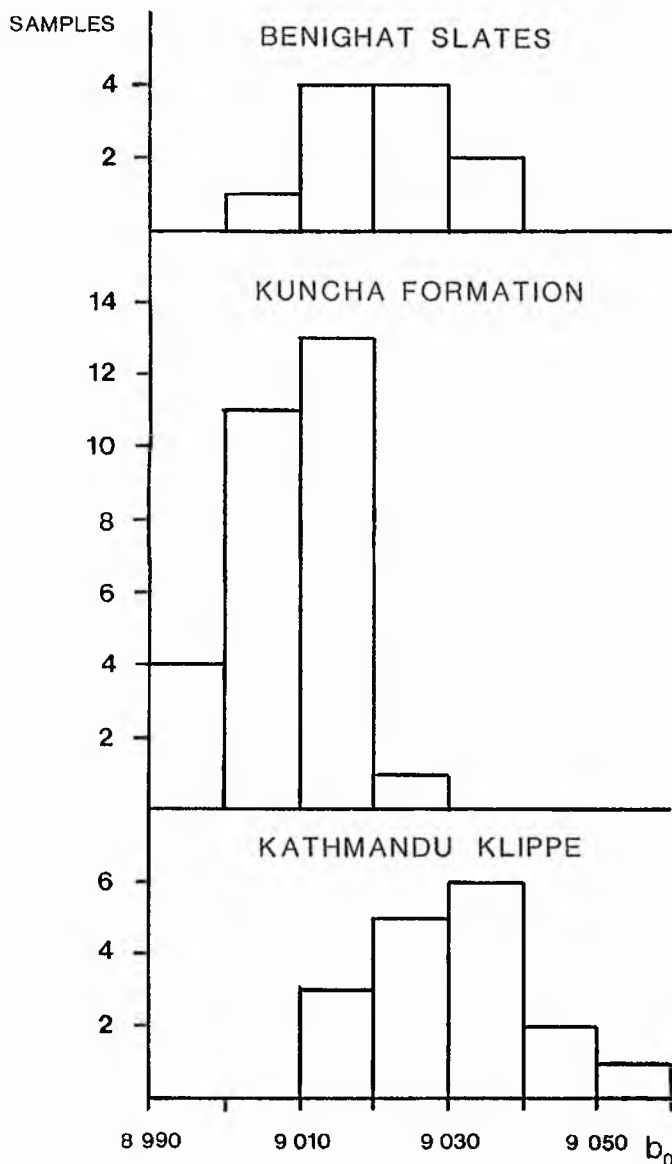


Fig. 5.15 - Histograms comparing the b_0 values of the Benighat Slates, Kuncha Formation and Kathmandu Klippe.

3.7 for pressure conditions, after Sassi and Scolari, 1974). The Benighat Slates had a mean b_o value of 9.020 \AA° ($SD = 0.009$, medium P), and the Kathmandu Klippe a value of 9.032 \AA° ($SD = 0.015$, medium-high P). From Figs 5.11 and 5.12 the following observations can be made:

1. A medium pressure b_o value reflects the pressure conditions in the Kuncha Formation.

2. - The Benighat Slates show suitable lithological homogeneity and temperature conditions for a b_o study, and therefore probably accurately reflect relatively medium pressure metamorphism. The slight trend of increasing pressure upwards through the sucession is unlikely to reflect an inverse pressure gradient. The explanation may be the limited size of the sample population, or minor lithological variations which are unavoidable.

3. - The rocks of the Kathmandu Klippe show a trend of increasing b_o towards the core of the syncline. This, again, is likely to reflect the range of temperature conditions. Overall these rocks lie in a relatively medium to high pressure range.

Previous pressure studies based on mineralogy and fluid inclusions are presented in section 5.2.3. These studies have mostly been limited to the higher grade assemblages of the Tibetan Slab. Hodges et al. (1988) show that pressure decreases upwards through the Tibetan Slab (from 7.2 to 3.8kb across 12km of the sucession) without any change in temperature ($c.600^\circ\text{C}$), (see section 5.2.3 for an explanation). These results are compatable with those of

Brunel and Kienast (1986), (from 5-8kb to 3.5-5kb with temperature in the range 510-720^oC across the lower part of the Tibetan Slab). Brunel and Kienast (1986) also found that pressure conditions were still high in distal parts of the Tibetan Slab (6-9kb for 550-650^oC). This is compatable with the findings of this study.

5.8 FLUID INCLUSIONS

5.8.1 Introduction

8 samples were made into fluid inclusion wafers. These included 7 quartz vein samples, collected between Baliphi and Dhulikhel, of which FI2 came from the Kuncha Formation, FI3-FI7 came from the Benighat Slates and FI8 came from the Kulikhani Formation in the Kathmandu Klippe. The last sample, LH1, was collected from a quartz segregation in garnet kyanite gneiss from the lower Tibetan Slab in the Syabru area (see Figs 5.1 and 5.2). Methods used are discussed in section 2.3. Results are presented in Figs 5.16; 5.17, 5.18, 5.19 and 5.20, in tables 5.4, 5.5, 5.6 and 5.7, and Appendix 5.2. These should be frequently consulted when reading the rest of this chapter.

5.8.2 Geological History of Inclusions

Quartz, collected for fluid inclusion analysis, came from various tectonic settings. LH1, is a pre- or syntectonic gneissose, quartz segregation from the lower Tibetan Slab, orientated parallel to the strong fabric associated with the MCTII (Pecher, 1979). FI2, from the Kuncha Formation, cross-cuts the main foliation and is post-M_I, but is deformed by a later fold phase. In the Benighat Slates FI5, FI6 and FI7 come from deformed syn-MCT zone veins, whereas FI3 and FI4 are from undeformed veins which cross-cut all ductile fabrics associated with the MCT zone. FI8 is from a post-ductile deformation vein in the Tistung Formation of the Kathmandu Klippe. The structural position of these vein samples has been constrained to syn-

Table 5.4 - Microthermometric results for fluid inclusions from Nepal

Sample	1	2	3	4	4a	5	6	7	8	9	10	11	12	Remarks	
LH1	A	12.5	-	-	2.1	-	-	-	-	-	-	-	-	21 Inclusions necked	
FI2	A	2.0	0.81	9.1	3.0	-4.8-L	0.96	253-L	75.2	1.5	23.3	0.80	18	Strain orientated.	
	B	A	5.7	0.92	-	3.0	-	-	193-L	92.4	5.6	2.0	0.98	5	
FI3	A	1.5	0.75	0.0	9.0	33.3-L	0.50	285-L	72.1	1.1	26.8	0.65	50		
FI4	A	4.0	0.74	-	7.9	0.35-L	0.92	287-L	73.2	3.1	23.7	0.80	25		
FI5	A	A	2.0	0.58	14.3	33.1	24.3-L	0.71	367-V	29.6	0.6	69.8	0.35	11	Decrepitate 430°C
	B	A	2.0	0.83	12.0	33.1	21.6-L	0.67	240-L	54.1	1.1	44.8	0.50	11	Th TOT = Dec.
	C	-	-	-	5.0	33.1	26.6-V	0.26	-	-	-	-	0.30	1	
FI6	A	-	0.6	0.85	-	39.8	26.7-L	0.67	227-L	91.5	0.5	8.0	0.90	3	
	B	A	2.8	0.58	4.6	39.8	13.1-L	0.85	303-V	39.8	1.1	59.1	0.50	14	Strain orientated.
	C	-	5.0	0.97	-	39.8	21.3-L	0.77	108-L	91.5	4.8	3.7	0.95	2	
	D	-	-	-	-	39.8	-	-	205-L	-	-	-	0.90	1	
	E	-	3.9	-	3.0	39.8	25.1-L	0.72	-	9.6	0.4	90.0	0.10	1	
FI7	A	B	2.0	0.80	-	4.8	-	-	258-L	c.90	c.2	c.8	0.90	15	
	B	B	4.0	0.78	-	4.8	-1.1-L	0.94	278-L	84.7	3.5	11.8	0.90	8	
	C	B	3.8	0.64	-	4.8	-	-	353-L	c.81	c.3	c.16	0.85	3	
	D	B	3.8	0.77	-	4.8	-	-	284-V	c.70	c.3	c.27	0.70	3	
	E	-	3.5	0.72	-	4.8	-	-	316-L	c.87	c.3	c.10	0.90	1	
FI8	A	A	4.5	0.80	2.8	2.2	24.1-L	0.73	279-L	91.1	4.3	4.6	0.95	15	
	B	-	-	-	-	2.2	-	-	316-L	-	-	-	0.70	2	

Key to table 5.4: Microthermometry Results

1. Salt System - A = H₂O-NaCl-KCl B = H₂O-KCl
 C = H₂O-NaCl-CaCl D = H₂O-CaCl
 E = H₂O-NaHCO₃ -NaCO F = H₂O-NaCl-MgCl

2. Wt% NaCl equivalent present in the aqueous solution.

3. Density of the H₂O-NaCl liquid (g/cm³).

4. Mole% CH₄ in the CO₂ phase.

4a. Mole% CO₂, for the whole FI wafer, determined by fluid extraction. The result is an average for the whole sample.

5. Homogenisation temperature of two CO₂ phases to liquid (L), vapour (V) or critical behaviour (C) (°C).

6. Density of CO₂ phase (g/cm³).

7. Total homogenisation temperature of the inclusion to liquid, vapour or critical (°C).

8 to 10. Estimated composition of the fluid phase in terms of the components H₂O-NaCl-CO₂ within the whole inclusion.

8. Wt% H₂O.

9. Wt% NaCl equivalent.

10. Wt% CO₂.

11. Degree of fill (F) of liquid phase in two phase inclusions, aqueous phase in three phase inclusions (1.00 = 100%).

12. Number of inclusions studied.

Table 5.5 - Trapping temperature estimates for hydrostatic and lithostatic pressure at depths of 1, 5 and 10km. Rock density is assumed to be 2.74g/cm³ (Thomas, 1985).

Sample	Th TOT	wt% NaCl	TT (1)	5	10 km
<u>FI2 A</u>	253	2.0			
Hydrostatic P			261	293	336°C
Lithostatic P			275	368	485°C
<u>FI2 B</u>	193	5.7			
Hydro			203	234	273°C
Litho			216	303	406°C
<u>FI3</u>	285	0.5			
Hydro			293	330	375°C
Litho			307	408	530°C
<u>FI4</u>	287	4.0			
Hydro			296	323	373°C
Litho			304	406	531°C
<u>FI5 A</u>	367	2.0			
Hydro			374	432	485°C
Litho			388	523	665°C
<u>FI6 A</u>	227	0.6			
Hydro			235	265	306°C
Litho			249	337	449°C
<u>FI6 B</u>	303	2.8			
Hydro			311	351	400°C
Litho			325	433	558°C
<u>FI6 C</u>	108	5.0			
Hydro			122	157	192°C
Litho			140	221	320°C
<u>FI7 A</u>	258	2.0			
Hydro			266	299	342°C
Litho			280	376	492°C
<u>FI7 B</u>	278	4.0			
Hydro			287	314	362°C
Litho			295	395	516°C
<u>FI7 C</u>	353	3.8			
Hydro			362	396	452°C
Litho			369	492	648°C
<u>FI7 D</u>	284	3.8			
Hydro			293	320	368°C
Litho			301	402	524°C
<u>FI7 E</u>	316	3.5			
Hydro			325	355	405°C
Litho			332	443	578°C
<u>FI8 A</u>	297	4.5			
Hydro			288	315	363°C
Litho			295	396	517°C

ductile movement in the MCT zone. Further constraints are prevented by a lack of detailed structural control for the area.

5.8.3 Results

LH1 - Inclusion in this pre- or syn- MCT zone sample were limited to planes of irregular 'flat' inclusions up to 1mm long (see plate 5.9). These are secondary inclusions confined to healed fracture planes. Extensive necking is recogniseable from spiked inclusion walls, partially necked inclusions, and erratic phase proportions of liquid and vapour phases. Many inclusion have no vapour bubbles, while a few have large bubbles. The liquid phase forms >95% of the mean inclusion fill. Thermometric measurements were limited because of necking. Only T_m H_2O could be determined (see Fig. 5.16), indicating a mean salinity of 12.5 wt% NaCl equivalent (see sections 2.3.5 and 2.3.6). Fluid extraction data (table 5.6) give 2.1 mole% CO_2 , 96.7 mole% H_2O and 1.2 mole% non-condensable gasses. NaCl-KCl salts are present in greater concentrations than in any of the vein quartz samples.

FI2 - Two populations of inclusions were identified in this deformed post-M₁ sample (see plate 5.10). The bulk of inclusions (pop. A) showed variable amounts of strain orientation. Pop. B inclusions are undeformed. All inclusions lie in planes and are probably secondary. Pop. A has 1.5 wt% NaCl equiv., a Th TOT of 253°C to Liquid (L) (see Fig. 5.17), 75.2 wt% H_2O , and 23.3 wt% CO_2 , of which CH_4 makes up 9.1 wt % of the CO_2 phase. Pop. B has 5.6 wt%

Plate 5.9 - A plane of 'flat' secondary aqueous fluid inclusions, confined to a healed fracture plane, in a quartz segregation. Inclusions show extensive necking, with only a few containing bubbles. Sample = LH1, Temp = 50 °C, Length of field of view = 1.0mm.

Plate 5.10 - Two inclusion populations (inclusions are hard to distinguish in this plate). Earlier inclusions are strained and later inclusions form an undeformed plane (part of which is in focus). Sample = FI2, Temp = 20.9 °C, Length of field of view = 300µm.

Plate 5.11 - A mixture of regular and irregular H₂O-CO₂ fluid inclusions. Irregular inclusions show necking. The lower middle inclusion is 60µm long. Sample = FI3, Temp = 22.2 °C, Length of field of view = 400µm.

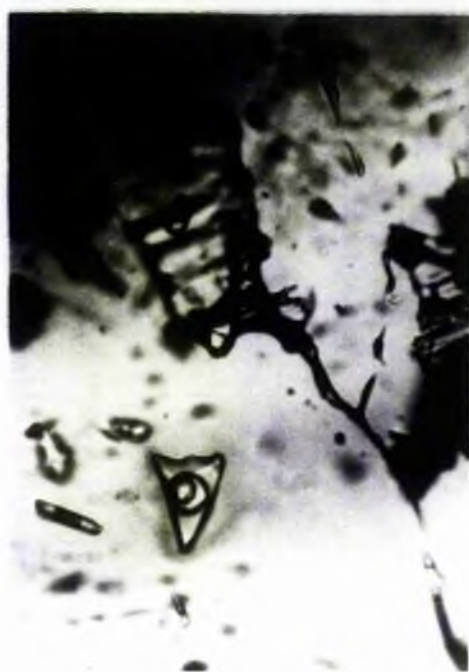
Plate 5.12 - Possible primary inclusions. The central inclusion is a 35µm negative crystal inclusion with a CO₂ double bubble (liquid and vapour phase) in an aqueous solution. Sample = FI3, Temp = 20.4 °C, Field of view = 400µm.



5.9



5.10



5.11



5.12

Table 5.6 - Fluid extraction results for bulk inclusion populations. Values are given as molecular percentages. Non-condensables (N-C) include nitrogen, methane (CH_4), carbon monoxide (CO) and oxygen in order of likely importance. Ratios are given for $\text{H}_2\text{O}/\text{CO}_2$ and atomic Na/K in NaCl and KCl salts.

Sample	N-C	CO_2	H_2O	$\text{H}_2\text{O}/\text{CO}_2$	Atomic	Na/K
LH1	1.2	2.1	96.7	46		3.20
FI2	0.3	3.0	96.7	32		3.77
FI3	0.2	9.0	90.8	10		2.94
FI4	3.2*	7.9	88.9	11		3.32
FI5	3.2	33.1	63.7	1.9		4.16
FI6	3.5	39.8	56.7	1.4		1.70
FI7	0.8	4.8	94.4	20		7.34
FI8	1.0	2.2	96.8	43		1.39

* CH_4 positively identified by gas chromatography (see section 2.3.7).

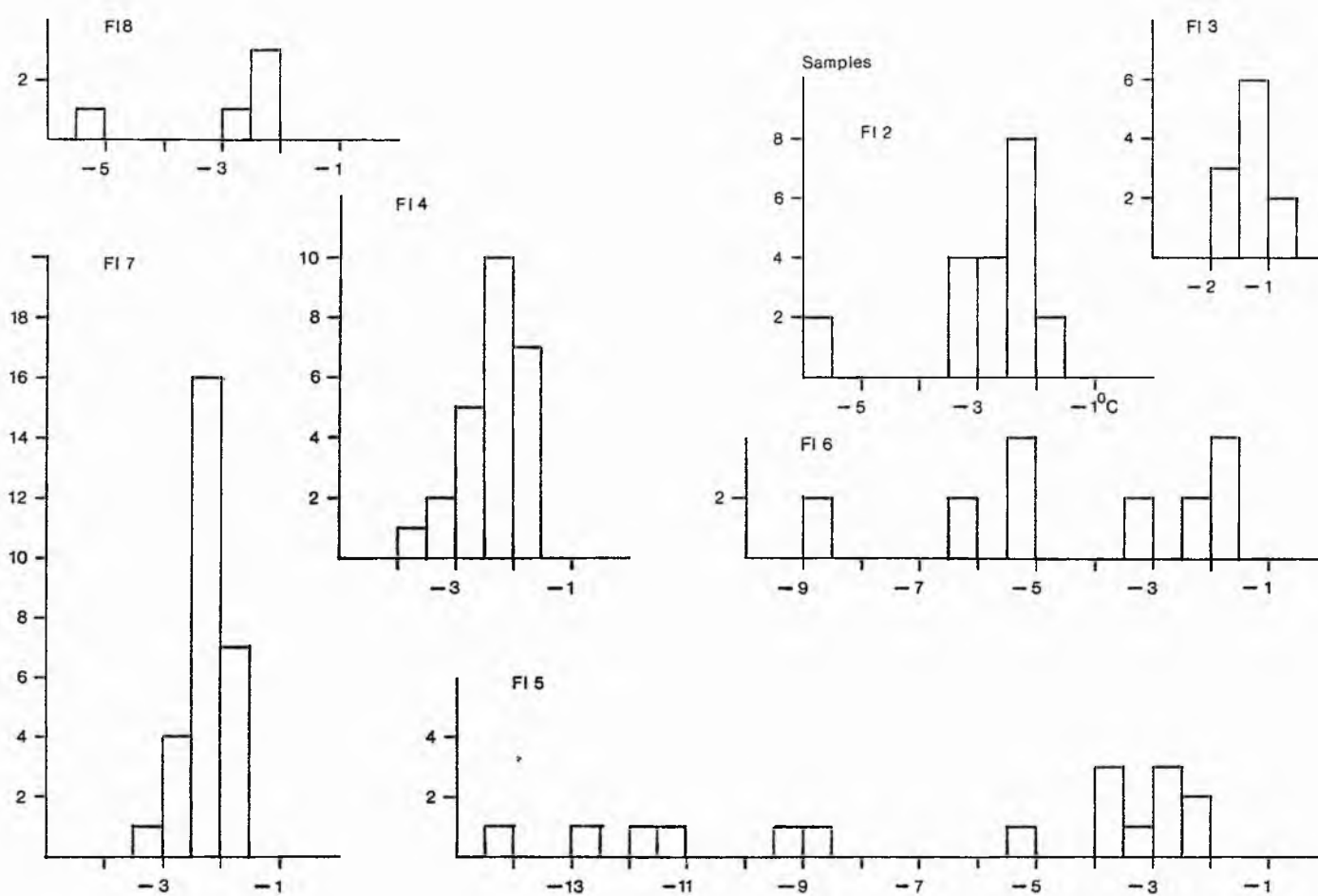


Fig. 5.16 - Histogram of last melt temperatures of ice ($T_m H_2O$) for Nepal fluid inclusion samples. Numbers of analyses are plotted against temperature.

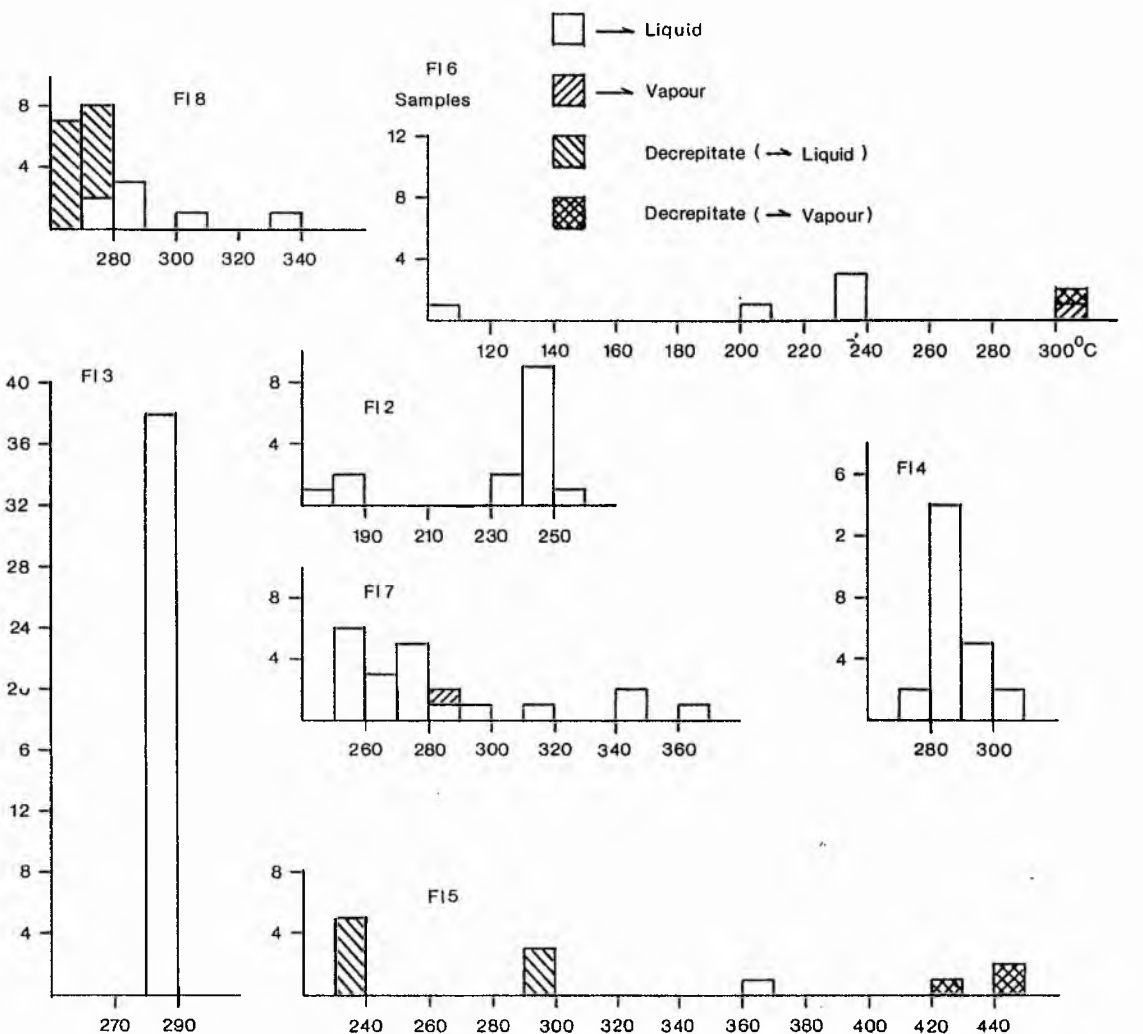


Fig. 5.17 - Histogram of total homogenisation temperatures (Th TOT) for Nepal fluid inclusions. Number of analyses are plotted against temperature.

NaCl equiv., a Th TOT of 193°C to L, 92.4 wt% H₂O, and 2.0 wt% CO₂. Fluid extraction results (see table 5.6) for a bulk analysis of the whole sample gives 3.0 mole% CO₂, 96.7 mole% H₂O and 0.3 mole% non-condensables. The disparity between CO₂ values obtained by microthermometry compared to extraction can be explained two ways. It can be attributed to preferential sampling of CO₂ rich inclusions during microthermometry or to CO₂ loss during extraction.

FI3 - FI3, a post-MCT zone undeformed vein sample, contained an abundant population of irregular and negative-crystal inclusions (see plates 5.11 and 5.12). These occurred as planes of secondary inclusions up to 250µm in size and usually showing gradation of size within a plane. Inclusions analysed had 1.1 wt% NaCl equiv., a Th TOT of 285°C to L, 72.1 wt % H₂O and 26.5 wt% CO₂ with no CH₄. Fluid extraction data gives a low mole% CO₂ value (9.0%), with 90.8 mole% H₂O and 0.2 mole% non-condensables. In this instance CO₂ rich inclusions are dominant in FI3. Therefore the difference in results between the two analyses can mainly be attributed to CO₂ loss during extraction, rather than to preferential sampling of CO₂ rich inclusions during microthermometry.

FI4 - The inclusions in FI4 (a post-MCT zone undeformed vein sample) are very similar to those found in FI3 (see plate 5.13). Inclusions all appear to have formed as secondary planes with inclusions up to 150µm across. Inclusions are mostly negative-crystals, with larger inclusions tending to be more irregular. Inclusions have 3.3 wt% NaCl equiv., a Th TOT of 287°C to L, 73.2 wt% H₂O

and 26.5 wt% CO₂. Fluid extraction data gives 7.9 mole% CO₂, 88.9 mole% H₂O, and 3.2 mole % non-condensables, some of which was positively identified as CH₄. Comparative CH₄ data could not be obtained by microthermometry (T_m CO₂ was not observable).

FI5 - FI5 is a syn-MCT zone vein sample. Large inclusions (c.50μm) are similar to but less abundant than in FI3 and FI4. There are numerous planes of small inclusions (<10μm). As in other samples larger inclusions are often irregular shaped (see plate 5.14). Inclusions fall into two distinct populations on the basis of microthermometric measurements. Pop. A has 0.6 wt% NaCl equiv., a Th TOT of 367°C to Vapour (V), 29.6 wt% H₂O, and 69.8 wt% CO₂, of which 14.3 wt% is CH₄. These tend to be small negative-crystal inclusions and may be primary. Pop. B includes both large irregular inclusions and small negative-crystal inclusions. The latter clearly form secondary planes. They have 1.1 wt% NaCl equiv., a Th TOT of 240°C to L, 54.1 wt% H₂O, and 44.8 wt% CO₂, of which 12.0 wt% is CH₄. Inclusion C, contained 5.0 wt% CH₄ in the CO₂ phase and Th CO₂ homogenised at 26.6°C to V (see Fig. 5.18). Other data could not be obtained. Fluid extraction data gave 33.1 mole% CO₂, 63.7 mole% H₂O and 3.2 mole% non-condensables.

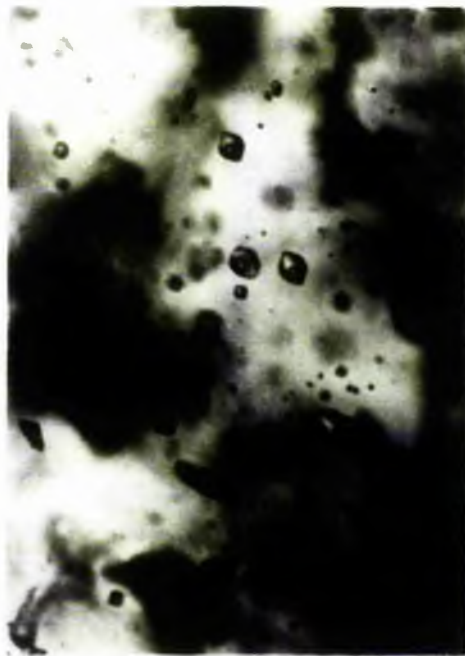
FI6 - In this syn-MCT zone sample few inclusions were of a workable size (>5μm). The earliest formed inclusions show strain orientation. There are also numerous planes of undeformed secondary inclusions. Pop. A has 0.5 wt% NaCl equiv., a Th TOT of 227°C to L, 91.5 wt% H₂O and 8 wt% CO₂.

Plate 5.13 - Single bubble H₂O-CO₂ negative crystal inclusions. The double bubble homogenised at 0.35°C to the liquid phase of CO₂. Sample = FI4, Temp = 15.0°C, Length of field of view = 300µm.

Plate 5.14 - A mixture of regular and irregular fluid inclusions. Some of these inclusions contain CO₂ double bubbles (not recogniseable in this plate). Sample = FI5, Temp = 12.8°C, Length of field of view = 300µm.

Plate 5.15 - A large irregular fluid inclusion with a CO₂ liquid phase in an aqueous liquid phase, and planes of smaller regular inclusions. Sample = FI7, Temp = 21.7°C, Length of field of view = 300µm.

Plate 5.16 - The same field of view as in plate 5.15. In the large inclusion the aqueous phase is frozen, and the CO₂ phase has seperated out into a liquid and a vapour phase. The CO₂ liquid phase is distorted by the frozen aqueous phase. Sample = FI7, Temp = -34.5°C, Length of field of view = 300µm.



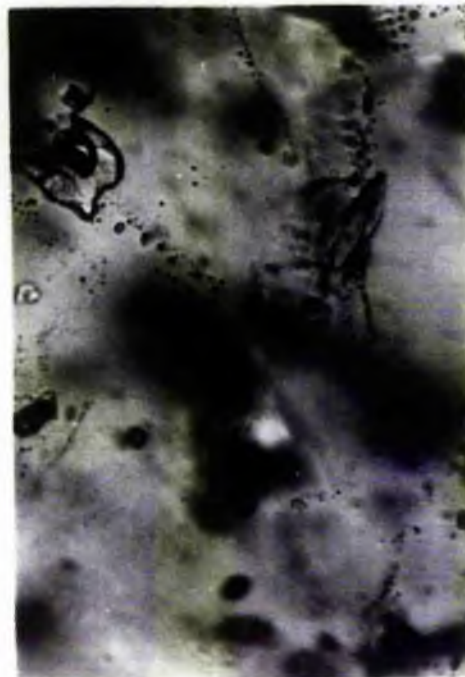
5.13



5.14



5.15



5.16

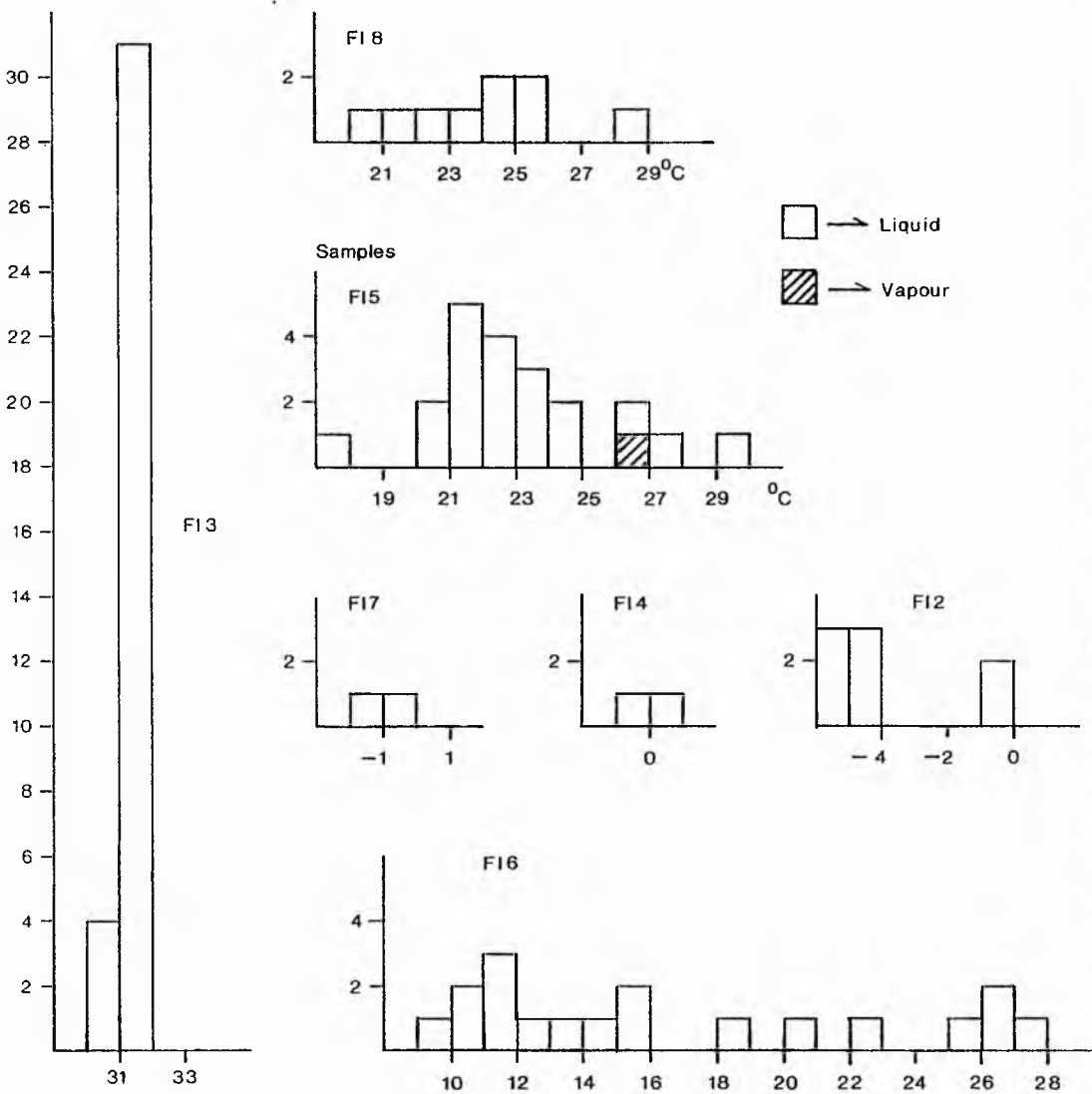


Fig. 5.18 - Histogram of homogenisation temperatures of the CO_2 phase (Th CO_2) for Nepal fluid inclusions. Number of analyses are plotted against temperature.

Pop. B, the strained inclusions, represents the majority of analyses, primarily because inclusions tend to be larger. They have 1.1 wt% NaCl equiv., a Th TOT of 303°C to V, 39.8 wt% H₂O, and 59.1 wt% CO₂, of which 4.6 wt% is CH₄. Pop. C has 4.8 wt% NaCl equiv., a Th TOT of 108°C to L, 91.5 wt% H₂O and 3.7 wt% CO₂. Inclusion D has a Th TOT of 205°C to L. Inclusion E is CO₂ rich, and has c.0.4 wt% NaCl equiv., c.9.6 wt% H₂O, and c.90 wt% CO₂, of which 3.0 wt% is CH₄. Fluid extraction results give 39.8 mole% CO₂, 56.7 mole% H₂O and 3.5 mole% non-condenseables.

FI7 - FI7 is a syn-MCT zone vein sample. Like many of the other samples FI7 contains larger (c.50µm) inclusions with a range from irregular to negative-crystal shapes, and planes of secondary inclusions (see plates 5.15 and 5.16). Pop. A has c.2.0 wt% NaCl equiv., a Th TOT of 258°C to L, c.90 wt% H₂O and c.8 wt% CO₂. Pop. B has 3.5 wt% NaCl equiv., a Th TOT of 278°C to L, 84.7 wt% H₂O and 11.8 wt% CO₂. These two populations form the majority of inclusions and are found as planes of secondary inclusions. Pop. C has c.3 wt% NaCl equiv., a Th TOT of 353°C to L, c.81 wt% H₂O, and c.16 wt% CO₂. These are the highest temperature inclusions and may be primary. Pop. D has c.3 wt% NaCl equiv., a Th TOT fo 284°C to V, c.70 wt% H₂O, and c.27 wt% CO₂. Inclusion E has c.3 wt% NaCl equiv., a ThTOT of 316°C to L, c.87 wt% H₂O and c.10 wt% CO₂. Fluid extraction data gave 4.8 mole% CO₂, 94.4 mole% H₂O and 0.8 mole% non-condensables.

FI8 - In this post-ductile deformation vein sample inclusions were mostly negative-crystal, confined to

annealed fractures planes and were mostly $<5\mu\text{m}$ in size. Between the inclusion planes the quartz was completely free from fluid inclusions. Results were obtained from two of the secondary inclusion populations. Pop. A had 4.3 wt% NaCl equiv., a Th TOT of 279°C to L, 91.1 wt% H₂O, and 4.6 wt% CO₂, of which 2.8 wt% is CH₄. Pop. B has a Th TOT of 316°C to L and a larger vapour phase (c.30% volume at room temperature). Fluid extraction data gives 2.2wt% CO₂, 96.8 wt% H₂O and 1.0 wt% non-condensables.

5.8.4 Discussion

In the Benighat Slates inclusion populations are often very similar in appearance and compositions (i.e. FI3, FI4, and FI7B). The highest temperature inclusions homogenise between 300 and 370°C to V or L. They are low salinity (0.6-c.3 wt% NaCl equiv.) and are rich in CO₂ (c.10-69.8 wt% CO₂). These inclusions are found in syn-ductile MCT zone quartz veins in epizone rocks. Trapping temperatures, up to 523°C for 5kb of lithostatic pressure (see table 4.5), are high relative to the peak metamorphic conditions that could be expected in the epizonal grade Benigat Slates. The onset of epizone conditions has been estimated at between 270 and 370°C , with biotite appearing at 425 to 450°C (see section 2.2.14). The high trapping temperatures of syn-MCT zone quartz veins could be due to the upwards migration of hot fluids from deeper in the MCT zone (see Dorobek 1989). Planes of second generation secondary inclusions commonly homogenise in the temperature range $240-290^\circ\text{C}$ to L. These tend to be low salinity inclusions (1.1-3.1 wt% NaCl equiv.) with significant

amounts of CO_2 present (c.8-44.8 wt% CO_2). They are the most common inclusions analysed. Subsequent generations of secondary inclusions mostly homogenise between 200 and 230°C to L (two analyses in FI6 homogenise at 108°C to L), with a mean salinity of 0.5 wt% NaCl equiv., and less CO_2 (2.0-8.0 wt% CO_2).

FI2, in the Kuncha Formation, has similar inclusion types to the Benighat Slates inclusions (Th TOT of 253°C to L, 1.5 wt% NaCl equiv. and 23.3 wt% CO_2 , and Th TOT of 193°C to L, 5.6 wt% NaCl equiv. and 2.0 wt% CO_2). Above the MCTII, LH1 only provided salinity information (12.5 wt% NaCl equiv.). FI8 has similar temperature secondary inclusions to the Benighat Slate inclusions ($279\text{-}316^{\circ}\text{C}$, 4.3 wt% NaCl and 4.6 wt% CO_2). From microthermometry there are few differences between inclusions from above and below the MCTII. This is perhaps due to the limited sample population above the MCTII. Salinities are generally lower in the Benighat Slates (see Fig. 5.19).

From extraction data, a plot of mole% $\text{H}_2\text{O}/\text{CO}_2$ versus atomic Na/K (see Fig. 5.20) effectively separates out the different sample populations on the basis of $\text{H}_2\text{O}/\text{CO}_2$. Samples from the Benighat Slates are richer in CO_2 than FI2 (the Kuncha Formation) which is in turn richer in CO_2 than samples from above the MCTII. Much movement related to the MCT zone has been taken up by the Benighat Slates (as mentioned in sections 5.2.2, 5.2.3 and 5.4.2). It therefore seems possible that shear movement has concentrated CO_2 into thrust zones. Pecher (1979), in studies in the Annapurna and Manaslu areas, found a close correlation

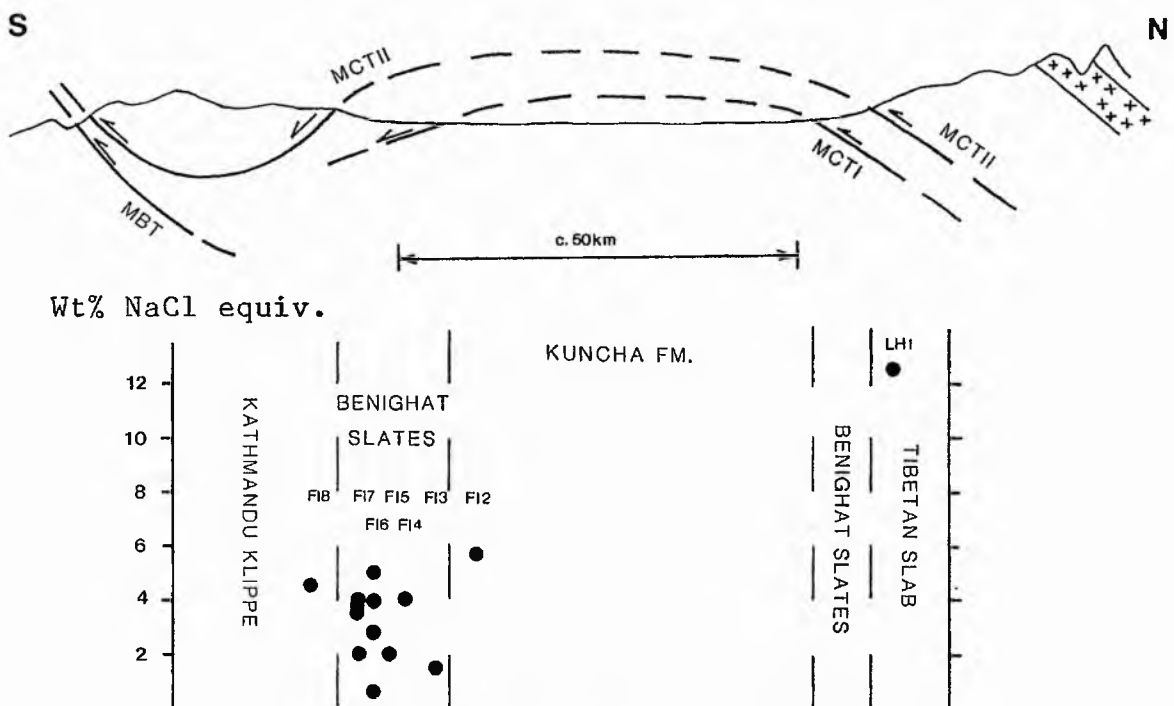


Fig. 5.19 - Sketch map (explained with Fig. 5.4) to illustrate variations in the salinities (wt% NaCl equiv.) of fluid inclusions studied from Nepal. See table 5.4 for specific values.

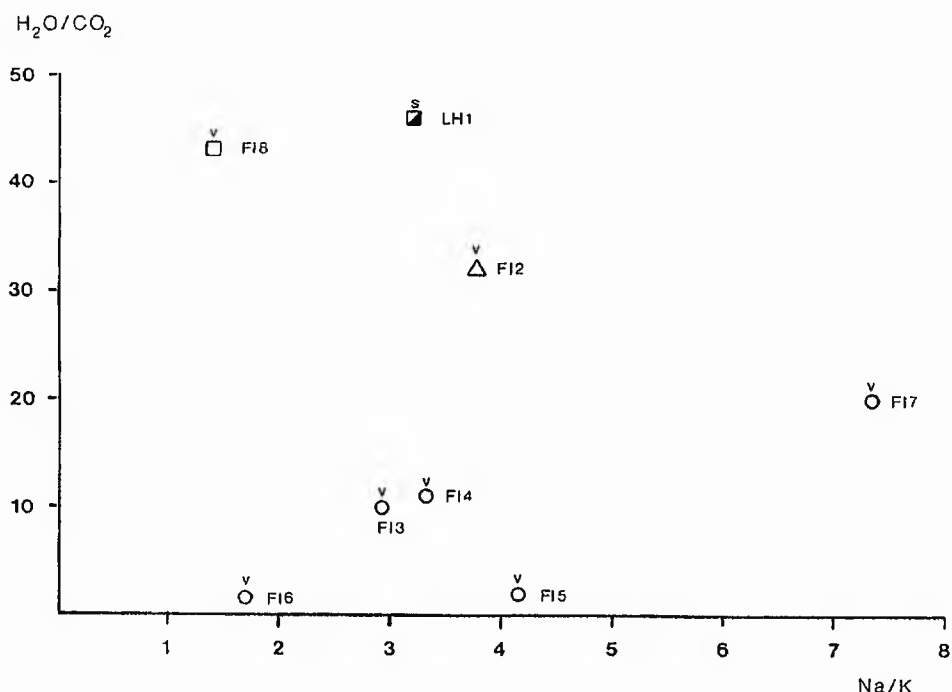


Fig. 5.20 - Fluid extraction data, for Nepal fluid inclusions, from the bulk analysis of quartz samples. Mole% H₂O/CO₂ is plotted against atomic Na/K. v = vein quartz, s = quartz segregation. Circles are from the Benighat Slates, FI2 is from the Kuncha Formation, FI8 is from the Kathmandu Klippe and LH1 is from the Tibetan Slab at Syabru.

between high CO₂ concentrations in inclusions and proximity to the MCTII (i.e. intensity of shearing). The highest CO₂ concentrations occurred in the lower part of the Tibetan Slab and the Upper Nawakot Group which contains the Benighat Slates.

Before considering the source of the high CO₂ concentrations in the MCT zone it is worth considering the position of CO₂ in a regional metamorphic environment. Poty et al. (1974) and Frey et al. (1980a) studied the compositions of fluid inclusions across a range of rocks from diagenetic to upper amphibolite grade metamorphism. Both studies were carried out along similar traverses through the central Swiss Alps. From their results a metamorphic scale of inclusion types was deduced (see table 5.7).

In a regional metamorphic environment CO₂ is only present in large amounts at staurolite or higher metamorphic grades. The composition of inclusions appears to be primarily governed by a series of reactions (listed below) which occur with increasing metamorphic grade (see Frey, 1980a):

1. HHC inclusions form from the breakdown of organic matter present in the source rocks.

2. CH₄ inclusions reflect the cracking of the HHC's with increased temperatures and pressures.

3. The CH₄ to H₂O transition is probably controlled by the presence of graphite under relatively oxidising

Table 5.7 - Fluid inclusions in relation to metamorphic grade. After Frey et al. (1980a).

Inclusion Type	Composition	metamorphic grade	zone
HHC*	c.1 to >80 mole% HHC (CH ₄ , H ₂ O, CO ₂ , NaCl)**	sub-anchizone	zeolite
CH ₄	c.1->90 mole% CH ₄ , <1 mole% HHC, (H ₂ O, CO ₂ , NaCl).	low and medium anchizone 250-300 °C, 1.5-2kb	prehnite-pumpellyite-chlorite
H ₂ O	c.90->99 mole% H ₂ O, <1 mole% CH ₄ , (CO ₂ , NaCl).	high anchizone and epizone*** 300-450 °C, 2-3kb***	chlorite, biotite
CO ₂	c.10->60 mole% CO ₂ , (CH ₄ , H ₂ O, NaCl).	mesozone 500-650 °C, 5-7kb	staurolite, kyanite, sillimanite

* HHC = Higher Hydrocarbons.

** In brackets: additional species found in inclusions. Furthermore, small amounts (<3 mole%) of H₂S and N₂ may also be present.

*** P/T estimates are based on fluid inclusion studies in fissure quartz, mineral assemblages and oxygen isotope thermometry (see Frey et al., 1980a for discussion).

**** It should be noted that epizonal grades included the presence of green biotite.

conditions. CO_2 from this reaction was probably fixed in carbonates.

4. CO_2 rich inclusions may have formed from decarbonisation reactions or the oxidation of graphite.

5. CO_2 in inclusions can be derived from a mantle source (Roedder, 1984).

Within the above constraints the situation of the Benighat Slates can now be considered. Within the succession both graphite and carbonates are present in significant quantities. Though the rocks are at a metamorphic grade appropriate to the presence of H_2O rich inclusions, the abundance of graphite and carbonate probably resulted in decarbonisation reactions. This provides a local source for CO_2 rich inclusions in the Benighat Slates. Other possible CO_2 sources would be deeper in the metamorphic pile or a mantle source. Whichever source is appropriate, the CO_2 rich fluids were concentrated along the MCT 'escape' zone. Upwards migration of the fluids will have taken place, but the scale of this migration is unclear.

High CO_2 concentrations related to major thrust zones have been documented from other parts of the world. Craw (1988) studied shallow level metamorphic fluids adjacent to the Alpine Fault, New Zealand. He envisaged a situation where CO_2 rich fluids migrated upwards from depth along numerous fractures. Fluid flow processes were made possible by high uplift rates ($>10\text{mm/yr}$ on the Alpine Fault) bringing hot rocks close to the surface. This is a post-peak metamorphic process which allowed the

transportation and deposition of quartz, calcite and metals (including gold) across a 12km wide zone (Craw and Koons, 1988). Oxygen isotope data indicate a source area in high grade metamorphic rocks with CO₂ derived from decarbonisation and/or graphite oxidation (reaction 4 above). In the MCT zone case veins are syn- and post-peak metamorphism. Oxygen isotope data could resolve the source area.

There is an overall trend of greater wt% CO₂ in Nepalese inclusions with higher homogenisation temperatures. This may reflect a greater abundance of CO₂ in the earlier (higher temperature) fluids circulating and precipitating vein quartz.

Salinities are irregular and low. The Na/K ratio shows limited variation except in FI7, close under the MCTII, which is richer in Na. On the basis of the Poty et al. (1974) Na-K geothermometer this would indicate lower temperature trapping conditions, but this is not apparent from inclusion homogenisation temperatures.

5.8.5 Conclusions

The carbonate and graphite rich Benighat Slates are a potential source area for CO₂ rich fluids. Movement on the MCT zone, particularly within the Benighat Slates, permitted the upwards migration and concentration of CO₂ rich fluids. This was a syn- to post-peak metamorphic event.

5.9 ISOTOPIC AGES

5.9.1 Introduction

The age of metamorphism in the Midland Formation was of particular interest to this project. Previous work (Arita, 1983; Le Fort, 1986) using K/Ar dating on muscovite and biotite, and Rb/Sr dating on biotite gave closing ages (at c.300 to 350°C) ranging from c.20 to 3.7Ma. These ages are related to uplift associated with the MCT zone.

In the present study muscovite and biotite separates were prepared from two samples (HS4 and LH9). These were sent to the Scottish Universities Research and Reactor Center, at East Kilbride, where $^{40}\text{Ar}/^{39}\text{Ar}$ analyses were carried out by Dr S. Kelley using a laser probe. The details of the technique can be found in Kelley and Bluck (in press).

5.9.2 Sample Descriptions

HS4 is a garnet biotite schist from Kuncha Formation immediately below the MCTI in the Barahbise area. Muscovite and biotite are strongly orientated by a mylonitic fabric, quartz is completely re-crystallised, and garnet shows minor chlorite retrogression.

LH9 is a garnet (biotite) schist from the Kuncha Formation. Euhedral garnets are enclosed in crenulated muscovite (see plate 5.3) with very little biotite or quartz in the sample.

5.9.3 Results and Discussion

The following results were obtained (see table 5.8):

Table 5.8 $^{40}\text{Ar}/^{39}\text{Ar}$ age dates from the Kuncha Formation.

<u>Sample</u>	<u>Mineral</u>	<u>Age</u>
HS4	Muscovite	14.6 + or - 0.6 Ma
HS4	Biotite	21.2 + or - 0.7 Ma
LH9	Muscovite	6.9 + or - 0.3 Ma

The three ages obtained are consistent with the results of Arita (1983) and Le Fort (1986). These ages could be cooling ages, but may more accurately indicate the re-crystallisation of mica in the MCT zone. Kelley (1988) found that micas from close to the Moine Thrust produced a range of ages. Smaller micas (biotite or muscovite) produced younger age dates. He interpreted the range of ages as being due to variable Ar loss through volume diffusion and re-crystallisation of the mica. Fine grained mica was completely re-crystallised whereas larger grains retained sectors which escaped complete re-crystallisation. From this it can be inferred that younger ages can be attributed to re-crystallisation associated with fault movement, while older ages are likely to fall between the mineral cooling age and re-crystallisation age. Samples LH9 and HS3 were collected on separate traverses, and so age differences may simply reflect variations in the timing of events in different parts of the MCT zone.

The older biotite cooling age in HS4 is anomalous because the $^{40}\text{Ar}/^{39}\text{Ar}$ isotopic system closes at a lower temperature in biotite ($\text{c.}300^\circ\text{C}$) compared to muscovite ($\text{c.}350^\circ\text{C}$) (Cliff, 1985). Anomalously old ages in biotites are usually attributed to the preferential uptake of excess ^{40}Ar by the biotite from mobile Ar in the host rock. This

occurs when temperatures exceed the biotite blocking temperature (see Roddick et al., 1980). Muscovite takes up very little excess ^{40}Ar and therefore provides more reliable blocking ages.

An estimate of the rates of uplift can be made on the basis of the muscovite ages. Given that the closing temperature for muscovite is 350°C the rate of uplift can be estimated for a particular geothermal gradient. For example for a geothermal gradient of 35°C/km (giving a closure depth of 10km) HS4 would be uplifted at a rate of 0.69mm/yr over the last 14.6Ma. LH9 would be uplifted at a rate of 1.46mm/yr over the last 6.9Ma. These rates are not incompatible with the estimates of 0.6 to 0.8mm/yr since the late Oligocene to early Miocene of Hodges et al. (1988b).

5.10 DISCUSSION : INVERSE METAMORPHIC MODELS

5.10.1 Introduction

A variety of models, put forward to explain the inverse metamorphism associated with the MCTII, have been described in section 5.2.4. The aim of this section is to relate the findings of this study to the inverse metamorphic models.

5.10.2 Discussion

The key to explaining the inverse metamorphism is the constraining of the relative timing of events in the Himalaya. Unfortunately there is still much uncertainty over the chronology of events, particularly concerning the timing and nature of metamorphic events.

Within the Tibetan Slab there is evidence for a number of metamorphic events. It is well established that the Tibetan Slab was subjected to Cambrian or earlier medium to high grade metamorphism (eg Debon et al., 1986). This has been recognised from Cambrian orthogneisses in the High Himalaya, and from chlorite to garnet grade metamorphism in the Kathmandu Klippe, intruded by dated younger Cambro-Ordovician leucogranites. Further metamorphic events have been related to the collision of India with Asia and are discussed later.

There is evidence for pre-MCT zone metamorphism of the Midland Formation. The Midland Formation consists of a sequence, up to 20km thick, of Late Pre-Cambrian to Early Palaeozoic metasediments (Stöcklin, 1980). Under burial metamorphic conditions (of $30^{\circ}\text{C}/\text{km}$, 265 bars/km) the base

of this sequence would have been subjected to a temperature of c.600°C and pressure of c.5.3kb. This exceeds the grade of metamorphism currently exposed in the Midland Formation suggesting that the 20km thickness has been overestimated. It seems likely that much of the metamorphism exposed in the Midland Formation is pre-MCT zone. Further evidence can be seen in the Kumaun Himal. A study by Oliver and Johnson (Oliver, pers comm.), using illite crystallinity and b_0 spacing to recognise differences in metamorphic grade, has shown that pre-Eocene epizone metamorphism occurred in the equivalent of the Midland Formation. The Lower Eocene Subathu Formation shows diagenetic grades compared to anchizone and epizone grades in the Precambrian to Early Palaeozoic Baini and Krol Formations. These Midland Formation units have been tectonically dismembered to form a series of thrust slices, with alternating anchizone and epizone metamorphism, in the footwall of the MCTII. There is no evidence for MCTII related inverse metamorphism within these thrust slices.

The grade of metamorphism observed in the Benighat Slates directly conflicts with the evidence for the inverse metamorphism in the Midland Formation resulting from the MCTII. The Benighat Slates are confined to the epizone in both proximal and distal positions with respect to the root zone of the MCTII. Since the Benighat Slates are caught between the MCTII and Kuncha Formation, this precludes heat, derived from above or within the MCTII, inversely metamorphosing the Kuncha Formation to garnet grade or higher. It is still possible that the Benighat Slates, in

the Barahbise area (proximal to the root zone), form a relatively narrow zone of inverse metamorphism caused by the MCTII. In the Kumaun, Oliver and Johnson (Oliver, pers comm.) found inverse metamorphism, from biotite to kyanite grade, restricted to a 1100 to 1200m zone between the MCTI and MCTII.

It should be noted that authors working in other parts of Nepal, adjacent to the High Himalaya, found a zone of inverse metamorphism between the MCTI and MCTII. Hubbard (in Hodges et al., 1988b) found this zone to be 3 to 5km thick and separating kyanite + or - sillimanite grade hanging wall rocks from garnet or biotite grade footwall rocks.

The model of Pecher and Le Fort (1986) is reasonably compatible with the evidence of this study (see section 5.2.4). Thrusting of the Tibetan Slab over the Midland Formation resulted in prograde inverse metamorphism of the latter, heat being supplied from the Tibetan Slab. The grade and thickness of this zone of inverse metamorphism is determined by the depth at which it was formed. In traverse A the grade of metamorphism jumps from epizonal in the Benighat Slates, to kyanite grade in the Tibetan Slab in the Barahbise area. This implies that the Tibetan Slab was thin and relatively cool when thrust over the Midland Formation. In the Kathmandu Klippe cold thrusting, with no inverse metamorphism, was recognised by Pecher and Le Fort (1986). These two areas are 60km apart in traverse A. The apparent lack of grade increase in the Benighat Slates between the two areas could be attributed to very low angle

thrusting on the MCTII. This may have resulted from a high rate of uplift and tectonic denudation of the High Himalaya due to ramping on the MCTII and lower thrust sheets, as footwall failure proceeded to successively higher levels (Johnson, 1986; Hodges et al., 1988b).

Thrusting may produce local inversion of the isograds in the Benighat Slates, near Barahbise, but does not immediately explain the inverse metamorphic zones in the Kuncha Formation. These zones could be an artifact of the variable rates of uplift in the Himalaya. If the rate of uplift, before and during thrusting, increases from south to north across the Midland Formation and Higher Himalaya, then the chlorite to garnet grade zones of the Kuncha Formation (Lower Midland Formation) would correspond to southerly dipping isograds (see Fig. 5.21), giving a false impression of inverse metamorphism. Additionally the isograds would be further rotated by shearing in the Kuncha Formation, associated with thrusting (Mason, 1984). This is assuming that the Kuncha Formation was metamorphosed up to garnet grade before the MCTII formed.

The younging direction in the Kuncha Formation could be used to establish the presence of inverse metamorphic isograds, but the poor stratigraphic control in the Kuncha Formation make the younging direction uncertain. In addition, if the succession is inverted, this could be attributed to tectonic rotation by shearing.

Evidence for higher rates of uplift in the High Himalaya, compared to the foreland is:

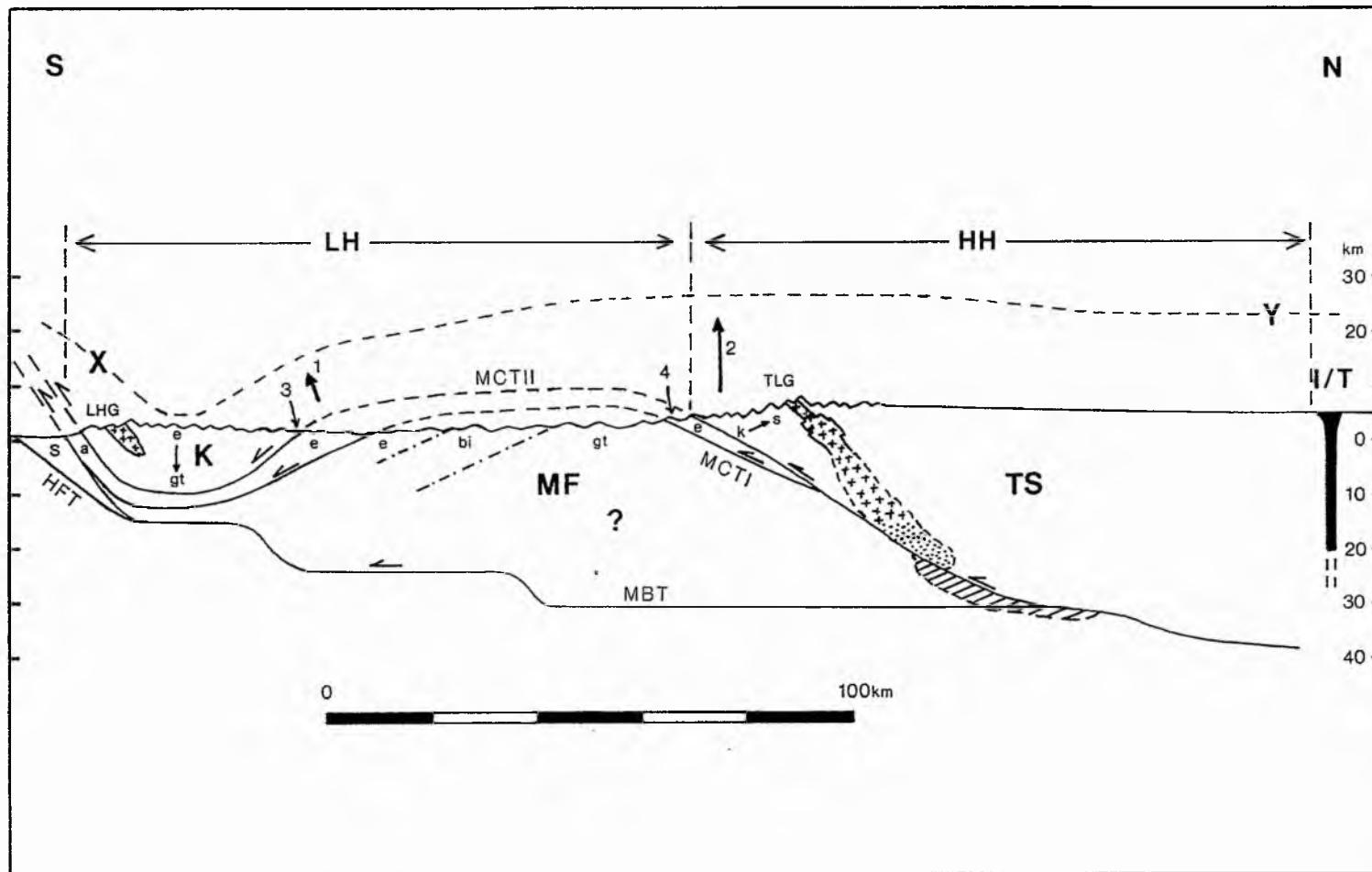


Fig 5.21 - A cross-section of the Nepal Himalaya in the Kathmandu Region.

Abbreviations are: LH = Lesser Himalaya, HH = Higher Himalaya, s = Siwaliks, K = Kathmandu Klippe, MF = Midland Formation, TS = Tibetan Slab, I/T = Indus/Tsangpo Sutre zone, MCTI and MCTII = Main Central Thrust I and II respectively, MBT = Main Boundary Thrust, HFT = Himalayan Frontal Thrust, TLG = Tourmaline Leucogranite of the High Himalaya, LHG = Lesser Himalayan Granite, a = anchizone, e = epizone, bi = biotite zone, gt = garnet zone, k = kyanite zone, s = sillimanite zone.

Dashed line XY represents the depth of cover removed over the last 25Ma. Arrows 1 and 2 indicate relative magnitudes of uplift (up to 15 to 20km in the High Himalaya); 3 is the zone of cold thrusting; 4 is the zone of inverse metamorphism associated with the MCTII. This ranges from 1 to 5km in the footwall. In the Kathmandu area the 'inverse' zone reached epizone (+ biotite) grade. Other authors found biotite to kyanite or staurolite grade.

In the Midland Formation a ? indicates thickening of the pile by thrust stacking. Increasing uplift rates to the north, thrust stacking and shearing may have rotated the isograds in the Lower Midland Formation to dip southwards.

The Miocene leucogranites of the High Himalaya may have formed as a result of fluid release in the footwall rocks (lined area) producing anatexis in the hanging wall (stippled area), though there is doubt that the previously metamorphosed epizone or higher grade footwall rocks could contribute very much fluid. The leucogranites form sheets which are roughly concordant with the N dipping Tibetan Slab succession, and this may indicate oblique migration of the granitic magma with a N to S bias.

1. - Simple isostatic adjustment of the thickened crust under the High Himalaya.

2. - Movement over ramps in structurally lower major faults (eg the MBT).

3. Tectonic denudation of the High Himalaya on northwards verging nappes and gravity slides (see section 5.2.3).

4. - Pressure estimates, from petrology, show that the High Himalaya has had 15 to 20km of uplift since the late Oligocene to early Miocene (Hodges et al., 1988b). This gives a mean uplift rate in the High Himalaya of 0.6 to 0.8mm/yr. This compares well with the estimates of section 5.9.

The Miocene and Pliocene Rb/Sr, K/Ar and Ar/Ar ages, for Midland Formation muscovites and biotites, indicate that closing temperatures, of 350°C , were exceeded during MCTI and MCTII thrusting. This metamorphism, up to biotite grade, would be hard to distinguish from an earlier metamorphism and may represent the maximum grade of metamorphism, of the Midland Formation, that can be attributed to tectonic burial during thrusting.

The Miocene generation of the Higher Himalayan leucogranites has previously been related to movement on the MCTII. A popular model (e.g. Pecher and Le Fort, 1986) involves wet upper crustal footwall rocks, taken down to c.20km, dewatering into the hanging wall, lowering the granitic melt temperature and inducing anatetic plutons which rise from the lower hanging wall. It is questionable

whether the previously metamorphosed epizone or higher grade footwall rocks could contribute much fluid.

Evidence for a source area for the granitic magma to the north of the High Himalaya is that the granite sheets are roughly concordant with the northwards dipping Tibetan Slab sucession. This implies that the magma migrated obliquely with a north to south bias (see Fig. 5.21).

5.11 SYNTHESIS

In this section the different lines of investigation are brought together to produce a geological history of the MCT zone.

5.11.1 Geological History

Pre-Collision - The pre-collision stratigraphy of the Indian plate contained the following components:

1. Precambrian to Early Palaeozoic metasediments of the Midland Formation

2. Precambrian to Devonian gneisses and schists of the Tibetan Slab

3. Triassic to Eocene Tethyan sediments deposited on the NW margin of the Indian plate. The lower Tibetan Slab was metamorphosed to high grades in the Precambrian to Cambrian and includes Cambro-Ordovician leucogranitic plutonism. The base of the 20km thick Midland Formation could potentially have been burial metamorphosed up to 600 °C and 5.3kb before the Eocene collision (see section 5.10.2).

Collision of India with Asia (50-40Ma) - Collision of the Indian plate with the Asian plate was characterised by:

1. A change from marine to continental sedimentation.

2. Compression tectonics in the Indus/Tsangpo suture zone.

3. The end of I-type granite plutonism and beginning of S-type anatexic plutonism in the Transhimalaya.

4. High pressure and temperature metamorphism in the Tibetan Slab associated with the growth of almandine and kyanite.

5. Possible initiation or reactivation of epizone to biotite grade metamorphism in the Midland Formation.

Oligocene (post-38Ma) - Movement on the MCT zone was initiated. Overall >100km of thrusting, with a zone of shearing up to 10km thick, occurred between the Oligocene and Pliocene. This was associated with inverse prograde metamorphism in the Upper Midland Formation up to almandine and kyanite grade ($550-650^{\circ}\text{C}$, 5-8kb), in a zone ranging from 1 to 5km thick, at the base of the MCTII.

Along the Barahbise to the Bagmati River traverse, the Midland Formation shows irregularities in the inverse metamorphism. In the Kuncha Formation grades increase steadily northwards, towards the MCTI, from epizone (Hbrell 117-179) to garnet grades with medium pressures metamorphism (mean b_0 of 9.009\AA°). Overlying the Kuncha Formation, immediately below the MCTII, are anchizone (Hbrell 173) and epizone (Hbrell 117-151) grade Benighat Slates. These show medium pressure metamorphism, with a mean b_0 of 9.020\AA° . In the Kathmandu Klippe the jump in grade from epizonal Benighat Slates to the garnet grade Raduwa Formation, of the Tibetan Slab, is attributed to cold thrusting at a high level in the MCTII (Pecher and Le Fort, 1986). In the Barahbise area, 60km further north, there is little difference in the grade of the Benighat Slates. This could be attributed to higher rates of uplift

and tectonic denudation as the High Himalaya is approached. This would also indicate that any Himalayan overprint could only have reached epizonal conditions.

The chlorite to garnet zones of the Kuncha Formation could reflect the rotation of earlier isograd surfaces to dip southwards. This may have occurred as a result of the variable uplift rates, suggested above, and MCT zone associated shearing in the Kuncha Formation.

In the overlying Tibetan Slab temperatures ranged from 630-710°C at the base of the pile and were associated with continued garnet and kyanite growth, and fresh growth of staurolite. In the Kathmandu Klippe a normal metamorphic succession, with a maximum grade of 550-650°C, 6-9kb at the base, most likely reflects Precambrian to Cambrian metamorphism. A mean b_0 value of 9.032 \AA reflects relatively medium to high pressure conditions. Movement on the MCTII at the Kathmandu Klippe involved cool shearing with little metamorphic impact on the Tibetan Slab, or the footwall Benighat Slates or Kuncha Formation.

25-14Ma - This phase overlaps movement on the MCTII. Water release from the underlying Midland Formation, due to heat conduction from the Tibetan Slab and possibly shear heating, produced retrogression at the base of the Tibetan Slab (chloritisation of garnet margins). Hydration of the base of the Tibetan Slab may also have generated anatetic plutonism which produced the tourmaline leucogranites of the Higher Himalaya between 25 and 14Ma. These granites may have produced a thermal buffering effect in the Tibetan

Slab. Metamorphic grades range from kyanite grade (630-710 °C, 5-8kb) at the base of the Tibetan Slab to sillimanite grade (630-780 °C, 3.5-5kb) below the anatetic plutons. Where no granites or buffering effect are present, temperatures range from 670 to 720 °C for the first km above the MCTII, to 580 °C at the stratigraphic level of the granites.

The dewatering of the Midland Formation below the MCTII produced quartz veining in rocks below and above the MCTII. Veining was particularly common in the Benighat Slates. These veins are post-peak metamorphism. They contain H₂O-CO₂-NaCl fluid inclusions which indicate a minimum vein formation temperature of 367 °C, though temperatures could be as high as 523 °C (at 5km lithostatic pressure). This is hotter than the epizonal rocks they intrude. Salinities are low while CO₂ concentrations are high. Pecher (1979) correlated high CO₂ concentrations in inclusions with close proximity to the MCT shear zone. In this study the Benighat Slates were particularly rich in CO₂. CO₂ was probably derived from decarbonisation and/or graphite oxidation reactions in the carbonate and graphite rich Benighat Slates. Movement in the MCT zone permitted the upwards migration and concentration of CO₂ rich fluids within the broad zone of shearing related to the MCTII.

Miocene and Pliocene Rb/Sr, K/Ar and Ar/Ar muscovite and biotite closing ages (at 350 °C), for the Midland Formation, indicate that burial metamorphism associated with the MCT zone exceeded 350 °C. This was superimposed on, but did not exceed, grades in the Lower Midland Formation.

Metamorphism of the Benighat Slates could be attributed to the MCTII in the Barahbise area.

Rapid uplift of the High Himalaya occurred as a result of ramping as footwall failure proceeded to successively higher levels. This produced the folding of the Kathmandu Klippe and Midland Formation, and resulted in 15 to 20km of uplift in the High Himalaya since c.25Ma.

Pliocene (post-5Ma) - Movement on the MBT was initiated during the late stages of movement on the MCTII. Late movement on the MCTII was restricted to narrow cold brittle fault zones. A rapid pressure drop in the Tibetan Slab was facilitated by ramping on younger thrusts (see above), erosion, and gravity sliding which produced large northwards verging recumbent folds in the Tibetan Slab.

5.11.2 Conclusions - The Anchizone-Epizone Transition

in Nepal

In the Nepal the anchizone-epizone metamorphic transition was not actually observed, the transition always being cut out by thrusting. The anchizone and epizone Benighat Slates are associated with strain induced recrystallisation of white mica in the MCT zone which was formed during collision between the Indian and Asian plates. The anchizone-epizone transition is defined by the disappearance of 1Md white mica, which is replaced by 2M, white mica (see section 2.2.8). In the Benighat Slates there is one sample, isolated by thrusts, which contains minor 1Md white mica and 2M, white mica at Hbre1 173.

Epizone grade Benighat Slates are associated with the common occurrence of 2M₁ mica and lesser occurrences of chlorite, paragonite, paragonite-muscovite and pyrophyllite, and a lack of 1Md white mica. b_o values correspond to medium pressure conditions. Post-M₁, syn-MCT zone quartz veins are dominated by H₂O-CO₂-NaCl (equiv.) inclusions. CO₂ is concentrated in the MCT zone and shows a decrease in abundance in lower temperature inclusions. A minimum trapping temperature estimate of 367°C, for syn-MCT zone vein quartz, is compatible with epizone conditions.

CHAPTER 6

DISCUSSION: THE ANCHIZONE-EPIZONE METAMORPHIC TRANSITION

6.1 INTRODUCTION

The three field areas investigated during this study provided examples of the anchizone-epizone metamorphic transition under various tectonometamorphic conditions. For the purposes of this study the anchizone-epizone transition was defined by the disappearance of 1Md white mica, which was replaced by 2M₁ white mica. Hbrel values appropriate to the anchizone-epizone transition in each area were obtained by considering Hbrel in conjunction with the phyllosilicate mineralogy of each sample. Constraints on the recognition of the metamorphic grade include Hbrel, b_0 , phyllosilicate and metabasite mineralogy, fluid inclusion data and PT estimates. The relationship between the anchizone-epizone transition and the tectonometamorphic environments of the three field areas is discussed in the following sections.

6.2 THE ANCHIZONE-EPIZONE METAMORPHIC TRANSITION

Table 6.1 lists the tectonometamorphic events that produced anchizone to epizone metamorphism in each field area. Also listed are the parameters with which the anchizone-epizone transition was constrained in each field area. Diagenesis and biotite or higher grade metamorphism is not discussed here.

Table 6.1 - Conditions of the anchizone-epizone metamorphic transition in the three field areas studied. In Nepal the transition was not observed though the Benighat Slates span the transition.

Conditions	Isle of Man	Glen Esk	Nepal
Lithology	Manx Slates	HBC (pelites, psammites and metabasites)	Benighat Slates
Environment	Regional diasthermal metamorphism (pre- to syn-D1) with post-D1 to syn-D2 contact metamorphism	Sinistral transpressive collisional fault zone metamorphism	MCT compressive, collisional metamorphism superimposed on regional metamorphism.
A/E trans. (HbreI)	154	135	c.170
b_0	8.988	9.029	9.020
Phyllosilicate Mineralogy	<u>2M, mica, Chl, Para,</u> Para/Mu, Py, <u>1Md mica,</u> <u>Ab, (I/S), (C/S), (Corr)</u> (Kao).	<u>2M, mica, 1Md mica, Chl,</u> <u>Ab, Para, I/S, Py, Kao,</u> Para/Mu, (C/S), (1M).	<u>2M, mica, Chl, Para, (Ab),</u> <u>(Para/Mu), (Py), (1Md Mica),</u> (C/S).
Metabasite Mineralogy		Chl-Ab-Ep-Act-Pump-Grand-Haem-Calc-WMica-Sph-Op-Qtz.	
Facies		Pumpellyite-Actinolite	
Fluids	N_2 , H_2O -NaCl equiv. fluid inclusions in syn-D2 quartz veins.	CO_2 - H_2O fluids in low permeability basalts. Greater fluid flow in Dolomitic and Purple Shales	H_2O - CO_2 -NaCl equiv. fluid inclusions in syn-MCT zone, post-M1 quartz veins.
PT	syn-D2 quartz >348°C.	Metabasite assemblage c.265°C, >2.34kb	Post-M1, syn-MCT zone quartz >367°C.
		Chlorite Geothermometry 221 to 273°C.	

Phyllosilicate minerals are given in order of abundance in the <2µm size fraction. Underlined minerals are abundant, those not underlined are common, but often in small quantities, and bracketed minerals are uncommon and in small and in small quantities. Abbreviations are: Chl = chlorite, Para = paragonite, Para/Mu = paragonite/muscovite, Py = pyrophyllite, Kao = kaolinite, I/S = illite/smectite, C/S = chlorite/smectite, Ab = albite, Corr = corrensite, 1M = 1M mica, Ep = epidote, Act = actinolite, Pump = pumpellyite, Grand = granditic garnet, Haem = Haematite, Calc = Calcite, WMica = white mica, Sph = Sphene, Op = opaques, Qtz = quartz, A/E trans = anchizone-epizone transition, PT = pressure/temperature conditions.

6.2.1 Lithology

Apart from temperature, lithology is the most important factor in controlling the recognition of the anchizone-epizone transition. The consistency of HbreI and b_o values, and phyllosilicate mineralogy, at a specific grade, is dependant on the uniformity of the original lithology and bulk composition of the rocks studied. In the three areas studied sampling was concentrated on pelitic samples with some psammitic samples. This was done to obtain optimum HbreI and b_o measurements, and allow comparison between the different sets of data. At Glen Esk metabasite samples were also collected from a sucession of pillow lavas, lavas, green chloritic shales and heamatite rich purple shales.

6.2.2 Environment

The driving force behind the metamorphism in each of the study areas is the tectonic environment. In all three areas the anchizone-epizone transition is pressure-temperature driven, but in widely different tectonic environments. 1. In the IOM the anchizone-epizone transition is associated with diastathermal metamorphism with regional D1 deformation superimposed. Epizone contact metamorphism was superimposed on much of the regional metamorphism, and in the Niarbyl Fault Zone diagenetic grades were produced by the low-temperature retrogressive cataclasis of anchizone grade slates. 2. At Glen Esk the anchizone-epizone transition is associated with sinistral transpressive fault movement resulting from the collision

between the Dalradian metamorphic terrane and the Highland Border Complex terrane. Prograde metamorphic growth and re-crystallisation of white mica, in the HBC, occurred during the main phase of transpressive fault movement in the Highland Boundary Fault zone. 3. The collision between the Indian and Asian continental plates resulted in the formation of the Main Central Thrust zone. In the Benighat Slates epizone metamorphism was synchronous with strain induced re-crystallisation of white mica in the MCT zone. This may have overprinted existing epizone metamorphism.

6.2.3 Phyllosilicate Mineralogy, H_{Brel} , b_o

As stated in section 6.1, the determination of the anchizone-epizone transition (in H_{Brel}) was dependant on the last appearance of 1Md white mica. The H_{Brel} values for the anchizone-epizone transition in the three field areas range from H_{Brel} 135 to c.170. The phyllosilicate mineralogy presented in table 6.1 spans the anchizone-epizone transition. 2M₁ mica is the dominant polymorph in the three field areas. In the Manx Slates paragonite and paragonite/muscovite are abundant, while in the HBC and Benighat Slates they represent either irregular or minor constituents. Chlorite is abundant in the Manx Slates and HBC, but less important in the Benighat Slates. 1Md mica is only abundant in the anchizone grade HBC samples. The distribution of minor mineral phases can be seen from table 6.1. Both the HBC and Benighat Slates have b_o values comparable with medium pressure facies. The Manx Slates have b_o values indicative of a low pressure facies, but

this could be partly attributed to the compositional control of abundant paragonite.

6.2.4 Metabasite Mineralogy

Metabasites were examined from the HBC. The mineral assemblages were indicative of middle pumpellyite-actinolite facies which was correlated with the upper anchizone.

6.2.5 Fluids

Evidence for the composition of fluids present during metamorphism was based on fluid inclusion evidence and metabasite mineralogy. 1. In the Manx Slates syn-D2 vein quartz contained early formed nitrogen bearing inclusions. These formed from the breakdown of organic matter in the slates. Later inclusions were dominated by saline aqueous fluids. 2. In the HBC the mineralogy of the metabasites is comparable with the circulation of H_2O-CO_2 rich fluids. Differences in rock composition and permeability of the original rocks are reflected in the metabasite mineralogy. More permeable rocks have abundant haematite and calcite reflecting a high H_2O and CO_2 fluid flow rate. The metabasite mineralogy of the pillow basalts and green pelites is comparable with lower fo_2 and fco_2 values. 3. - In the Benighat Slates syn-MCT zone, post-M1 quartz veins are dominated by H_2O-CO_2-NaCl (equiv.) inclusions. Inclusions are dominated by H_2O , but show an evolution towards less abundant CO_2 in lower temperature inclusions. CO_2 rich inclusions tend to be associated with nearness to the MCT zone.

6.2.6 Pressure-Temperature Estimates

There has been little constraint on the PT conditions in the IOM and Nepal. Fluid inclusions provide a direct measurement of temperature conditions, but in both field areas vein samples are post-M1. In the IOM, inclusions give a minimum trapping temperature of 348 °C for syn-D2 vein quartz. In Nepal inclusions give a minimum trapping temperature of 367 °C for syn-MCT vein quartz. These temperatures are at the higher end of temperature estimates for the anchizone-epizone transition (see section 2.2.14). Vein forming fluids may have circulated at higher temperatures than those of the host rocks. In the HBC metabasite mineralogy and probe analysis of metabasite minerals has produced good constraints on temperature conditions. A temperature of c.265 °C at >2.34kb (derived from the metabasite facies of Liou et al., 1985) is compatible with upper anchizone conditions. Chlorite geothermometry, using the method of Cathelineau and Nieva (1985), gives a temperature range of 221 to 273 °C which correlates with metabasite mineralogy.

6.3 CONCLUSIONS

Three field areas were selected to investigate the anchizone-epizone metamorphic transition in different tectonometamorphic regimes. As a result of this study the following can be concluded:

1. - Metamorphic facies concept should not be thought of in terms of exact temperatures and pressures, but as

changes represented by mineral facies (i.e. the 1Md to 2M, white mica change at the anchizone-epizone transition). This need not correspond to a consistent HbreI value, but may vary with metamorphic environment.

Mineral assemblages in metapelites, at the anchizone-epizone transition, are very similar despite the variations in tectonic control in the three field areas. The anchizone-epizone transition is characterised by the disappearance of 1Md mica. The mineralogy is dominated by 2M₁ mica which is usually associated with chlorite, paragonite and paragonite-muscovite, and less reliably albite, pyrophyllite and chlorite-smectite. Variations in original lithology account for the greatest variation in metamorphic mineral assemblages.

2. - Peak metamorphic conditions in the IOM were attained during burial in an extensional, diastathermal metamorphic environment. D1 regional deformation caused the re-crystallisation of white mica in parts of the succession (e.g. the IOM Synform), but the relative importance of this overprint is uncertain. Low-pressure b_o values from the Manx Slates may be partly misleading because of the abundance of paragonite throughout the sequence. b_o values are compatible with a high heat flow diastathermal metamorphic environment. In both the HBC and Benighat Slates b_o values correspond to medium pressure facies conditions. The anchizone and epizone metamorphism of Glen Esk and Nepal is related to the tectonic re-crystallisation

of white mica during the main phases of fault movement in the respective fault zones.

3. - In the IOM, nitrogen bearing and saline aqueous fluids were derived from the breakdown of organic matter in the sediments, and also from metamorphic dehydration process. In the fault controlled areas (Glen Esk and Nepal) CO₂ is a major component of the fluids. In Glen Esk this may be attributed to the presence of CO₂ trapped in the basic rocks and carbonates of the HBC. In Nepal this may be attributed to the abundance of carbonate and graphite in the Benighat Slates. Fault movement permitted the upwards migration and concentration of CO₂ rich fliuds.

4. - In this study constraints on PT conditions are dependant on either suitable mineral assemblages or fluid inclusion microthermometry. In the HBC metabasite mineralogy and chlorite geothermometry support a PT estimate, for the upper anchizone, of c.265°C and >2.34kb. In the Manx Slates and Benighat Slates PT estimates are dependant on fluid inclusions. In the Manx Slates and Benighat Slates vein quartz is post-M1. Fluid inclusions give minimum temperature estimates of 348 °C and 367 °C respectively. The higher temperatures obtained from fluid inclusions, compared to metabasite minerals, may be due to higher temperatures in the vein forming fluids.

REFERENCES

- Aftalion, M., van Breeman, O. and Bowes, D.R. 1984.
Age constraints on the basement of the
Midland Valley of Scotland. Trans. R. Soc.
Edinburgh, Earth Sci. 75: 53-64.
- Ahn, J. H., Peacock, D. R., Coombs, D. S. 1988.
Formation mechanisms of illite, chlorite
and mixed-layer illite-chlorite in Triassic
volcanogenic sediments from the Southern
Syncline, New Zealand. Contrib. Mineral.
Petrol. 99: 82-89.
- Althaus, E., and Johannes, W. 1969.
Experimental metamorphism of NaCl bearing
aqueous solutions by reaction with
silicates. Amer. J. Sci. 267: 87-98.
- Anderson, J. G. C. 1947.
The geology of the Highland Border:
Stonehaven to Arran. Trans. R. Soc.
Edinburgh, Earth Sci. 61: 479-515.
- Anderson, T. B. and Oliver, G. J. H. 1986.
The Orlock Bridge Fault: a major late
Caledonian sinistral fault in the Southern
Upland terrane, British Isles. Trans. R.
Soc. Edinburgh 77: 203-222.
- Anderton, R. 1985.
Sedimentation and tectonics in the Scottish
Dalradian. Scott. J. Geol. 21: 407-463.
- Anderton, R., Bridges, P. H., Leeder, M. R. and Sellwood,
B. W. 1979.
A Dynamic Stratigraphy of the British
Isles. George Allen and Unwin, London:
301pp.
- Andrieux, J., Brunel, M. and Hamet, J. 1977.
Metamorphism, granitisation and relations
with the Main Central Thrust in Central
Nepal: $^{87}\text{Rb}/^{87}\text{Sr}$ age determinations and
discussion. In: Écologie et géologie de
l'Himalaya. Colloques internat. du CNRS no.
268.
- Andrieux, J., Arthaud, F., Brunel, M. and Sauniac, S. 1980.
Le caractère postmétamorphique des grandes
chevauchements himalayen dans l'Himalaya du
Nord-Ouest. Aperçu sur les relations
possible avec le métamorphisme inverse du
Népal. Cr. Acad. Sci. Paris 291: 525-528.

Andrieux, J., Arthaud, F., Brunel, M. and Sauniac, S. 1981.
Géométrie et cinématique des chevauchements, end Himalaya du Nord-Ouest.
Bull. Soc. Géol. Fr. 23: 651-661.

Aprahamian, J. 1974.
La Crystallinité de l'illites et les minéraux argileux en bordure des massifs cristallins externes de Belledonne et du Pelvoux. Géol. Alpine 50: 5-15.

Aprahamian, J. and Paris, J. L. 1981.
Very low grade metamorphism with a reverse gradient induced by an overthrust in Haute-Savoie (France). In: Thrust and Nappe Tectonics, Geol. Soc. Lond. 1981: 159-165.

Arita, K. 1983.
Origin of the inverted metamorphism of the Lower Himalayas, Central Nepal. Tectonophysics 95: 43-60.

Atherton, M. P. 1977.
The Metamorphism of the Dalradian rocks of Scotland. Scott. J. Geol. 13(4): 331-370.

Auden, J. B. 1935.
Traverse in the Himalaya. Rec. Geol. Surv. India 69: 123-167.

Bailey, S. W. 1980.
Structure of layer silicates. In: Crystal Structures of Clay Minerals and their X-Ray Identification. Eds. Brindley, G. W. and Brown, G., Min. Soc. Lond. Monograph 5: 1-124.

Bailey, S. W., Brindley, G. W., Kodama, H., Martin, R. 1982.
Report of the clay mineral society nomenclature committee for 1980-81. Nonenclature for regular interstratifications. Clays and Clay Minerals 30: 76-78.

Barlier, J. 1974.
Recherches paléothermométriques dans le domaine des Terres Noires subalpines méridionales. Thèse Doct. 3e Cyde, Univ. Paris-Sud (Centre d'Orsay).

Barrow, G. 1901.
On the occurrence of Silurian (?) rocks in Forfarshire-Kinkardineshire along the eastern border of the Highlands. Q. J. Geol. Soc. Lond. 57: 328-345.

- Barrow, G. 1912.
On the geology of the lower Dee-side and
the Southern Highland border. Proc. Geol.
Assoc. 23: 268-284.
- Berry, L. G., (Ed). 1974.
Selected powder diffraction data for
minerals. Joint Committee on powder
Diffraction Standards. 833pp.
- Bevins, R. E. and Rowbotham, G. 1983.
Low-grade metamorphism within the Welsh
sector of the Paratectonic Caledonides.
Geol. J. 18: 141-167.
- Bevins, R. E. and Merriman, R. J. 1988.
Compositional controls on coexisting
prehnite-pumpellyite facies assemblages in
the Tal y Fan metabasite intrusion, North
Wales: implication for Caledonian
metamorphic field gradients. J. Metamorph.
Geol. 6: 17-39.
- Bevins, R. E. and Robinson, D. 1988.
Short paper: Low grade metamorphism of the
Welsh Basin Lower Palaeozoic sucession: an
example of diastathermal metamorphism? J.
Geol. Soc. 145: 363-366.
- Bhat, M. I. 1987.
Spasmodic rift reactivation and its role in
the pre-orogenic evolution of the Himalayan
region. Tectonophysics 134: 103-127.
- Bhattacharya, A. R. 1987.
A "ductile thrust" in the Himalaya.
Tectonophysics 135: 37-45.
- Biscay, P. E. 1964.
Distinction between kaolinite and chlorite
in recent sediments by X-ray diffraction.
Amer. Mineral. 49: 1281-1289.
- Black, P. M. 1974.
Oxygen isotope study of metamorphic rocks
from the Ouégoa District, New Caledonia.
Contrib. Mineral. Petrol. 47: 197-206.
- Blenkinsop, T. G. 1988.
Definition of low-grade metamorphic zones
using illite crystallinity. J. Metamorphic
Geol. 6: 623-636.
- Bluck, B. J. 1983.
The role of the Midland Valley of Scotland
in the Caledonian orogeny. Trans. R. Soc.
Edinburgh. 74: 119-136.

- Bluck, B. J. 1984.
Pre-Carboniferous history of the Midland Valley of Scotland. Trans. R. Soc. Edinburgh 75: 275-295.
- Bluck, B. J. 1985.
The Scottish paratectonic Caledonides. Scott. J. Geol. 21: 437-464.
- Bodnar, R. J., Reynolds, T. J. and Kuehn, C.A. 1985.
Fluid inclusion systematics in epithermal systems. Reviews in Economic Geology 2: 73 -98.
- Bortolami, G., Lombardo, B. and Poloni, R. 1983.
The granite of the Upper Imja Khola (Everest Region), Eastern Nepal. In: Shams, F. A. (Ed). Granites of the Himalayas, Karokorum and Hindu Kush. Inst. of Geol., Punjab Univ., Lahore, Pakistan: 257-269.
- Bottrell, S. H., Carr, L.P. and Dubessy, J. 1988.
A nitrogen-rich metamorphic fluid and coexisting minerals in slates from North Wales. Mineral. Mag. 52: 451-457
- Bouchez, J. L. and Pecher, A. 1981.
The Himalayan Main Central Thrust pile and its quartz rich tectonites in Central Nepal. Tectonophysics 78: 23-50.
- Bradbury, H. J., Smith, R. A. and Harris, A. L. 1976.
'Older' Granites as time-markers in Dalradian evolution. J. Geol. Soc. Lond. 132: 677-684.
- Brasier, M. D. and Singh, P. 1987.
Microfossils and Precambrian-Cambrian boundary stratigraphy at Maldeota, Lesser Himalaya. Geol. Mag. 124: 323-345.
- Brauckmann, F. J. 1984.
Hochdiagenese im Muschelkalk der Massive von Bramsche und Vlotho. Bochumer Geol. Geotech. Arb. 14.
- Brime, C. 1980.
Influencia del modo de preparación de la muestras en la relación $I(002)/I(001)$ de las ilitas. Breviora Geol. Asturica 24, (3-4): 24-28.
- Brindley, G. W. 1972.
The structure of micas and related minerals - a review. Materials Res. Bull. 7: 1191-1200.

- Brindley, G. W. 1980.
Order-disorder in clay mineral structures.
In: Crystal Structures of Clay Minerals and
their X-Ray Identification. Eds. Brindley,
G. W. and Brown, G., Min. Soc. Lond.
Monograph 5: 126-195.
- Brindley, G. W. and Brown, G. 1980. (Eds.)
The Crystal Structures of Clay Minerals and
their X-Ray Identification. Min. Soc.
Lond.. Monograph 5.
- Brown, E. H. 1967.
The greenschist facies in part of eastern
Otago, New Zealand. Contrib. Mineral.
Petrol. 14: 259-292.
- Brunel, M. and Kienast, J. R. 1986.
Etude pétro-structurale des chevauchements
ductile himalayens sur la transversale de
l'Everest-Makalu (Népal oriental). Can. J.
Earth Sci. 23: 1117-1137.
- Burton, J. C., Hocken, C., MacCallum, D. and Young, M. E.
1984.
Chitinozoa and the age of the Margie
Limestone of the N. Esk. Proc. Geol. Soc.
Glasgow 124/125: 27-32.
- Cathelineau, M. and Nieva, D. 1985.
A chlorite solid solution geothermometer.
The Los Azufres (Mexico) geothermal system.
Contrib. Mineral. Petrol. 91: 235-244.
- Chatterjee, N. D. 1973.
Low temperature compatibility relations of
the assemblage quartz-paragonite and the
thermodynamic status of the phase
reectorite. Contrib. Miner. Petrol. 42: 259-
271.
- Chennaux, G., Dunoyer de Segonzac, G. and Petracco, F.
1970.
Genèse de la pyrophyllite dans le
Paleozoïque du Sahara occidental. C. R.
Acad. Sci. Ser D, 270: 2405-2408.
- Cho, M. and Liou, J. G. 1987.
Prehnite-Pumpellyite to Greenschist facies
transition in the Kamutsen metabasite,
Vancouver Island, B. C. J. Petrol. 28(3):
417-443.
- Cipriani, C., Sassi, F. P. and Viterbo-Bassini, C. 1968.
La composizione delle miche chiare in
rapporto con le costanti reticolari e col
grado metamorfico. Rend. Soc. Ital.
Mineral. Petrol. 24: !53-187.

Clayburn, J. A. P., Harmon, R. S., Pankhurst, R. J. and Brown, F. J. 1983.

Sr, O and Pb isotope evidence for the origin and evolution of the Etive Igneous Complex, Scotland. *Nature* 303: 492-497.

Cliff, R. A. 1985.

Isotopic dating in metamorphic belts. *J. Geol. Soc. Lond.* 142: 97-110.

Collins, P. L. F. 1979.

Gas hydrates in CO₂-bearing fluid inclusions, and the use of freezing for estimating salinity. *Econ. Geol.* 74: 1435-1444.

Coombs, D. S., Nakamura, Y. and Vuagnat, M. 1976.

Pumpellyite-Actinolite facies schists of the Taveyanne Formation near Loeche, Valais, Switzerland. *J. Petrol.* 17: 440-471.

Coombs, D. S., Kawachi, Y., Houghton, B. F., Hyden, G., Pringle, I. J. and Williams, J. G. 1977.

Andradite and andradite-grossular solid solution in very low-grade regionally metamorphosed rocks in southern New Zealand. *Contrib. Mineral. Petrol.* 63: 29-246.

Corbató, C. E., and Tettenhorst, R. T. 1978.

Analysis of illite-smectite interstratification. *Clay Minerals* 22: 269-285.

Cornwell, J. D. 1972.

A gravity survey of the Isle of Man. *Proc. Yorks. Geol. Soc.* 39: 93-106.

Craig, J., Fitches, W. R. and Maltman, A. J. 1982.

Chlorite-mica stacks in low-strain rocks from central Wales. *Geol. Mag.* 119 (3): 234-256.

Craw, D. 1988.

Shallow-level metamorphic fluids in a high uplift rate metamorphic belt; Alpine Schist, New Zealand. *J. Metam. Geol.* 6: 1-16.

Craw, D. and Koons, P. O. 1988.

Tectonically induced gold mineralisation adjacent to major fault zones. *Bicentennial Gold 88*, Melbourne.

- Crawford, M. L. 1981.
Fluid inclusions in metamorphic rocks - Low to medium grade. In: Short Course in Fluid Inclusions: Applications to Petrology. Hollister, L. S. and Crawford, M. L., (Eds.) Min. Assoc. Canada.
- Crosbie, T.R. 1981.
Polished wafer preparation for fluid inclusion and other studies. Trans. Inst. Min. Metall. 90: B82-83.
- Curry, G. B. 1986.
Fossils and tectonics along the HBF in Scotland. J. Geol. Soc. Lond. 143: 193-198.
- Curry, G. B., Ingham J. K., Bluck, B. J. and Williams, A. 1982.
The significance of a reliable Ordovician age for some Highland Border Rocks in Central Scotland. J. Geol. Soc. Lond. 139: 453-456.
- Curry, G. B., Bluck, B. J., Burton, C. J., Ingham, J. K., Siveter, D. J. and Williams, A. 1984.
Age, evolution and tectonic history of the Highland Border Complex, Scotland. Trans. R. Soc. Edinburgh 75: 113-133.
- Debon, F., Le Fort, P., Sheppard, S. M. F. and Sonet, J. 1986.
The four plutonic belts of the Transhimalaya-Himalaya: a chemical, mineralogical, isotopic and chronological synthesis along a Tibet-Nepal section. J. Petrol. 27, part 1: 219-250.
- Deer, W. A., Howie, R. A. and Zussman, J. 1963.
Rock-Forming Minerals, Framework Silicates. Longmans, 4: 435pp.
- Deer, W. A., Howie, R. A. and Zussman, J. 1967.
Rock-forming Minerals, Sheet Silicates. Wiley, NY.: 270pp.
- Deer, W. A., Howie, R. A. and Zussman, J. 1975.
Rock-Forming Minerals, Ortho and Ring Silicates. Longmans, 1: 331pp.
- Dempster, T. J. 1983.
Studies of orogenic evolution in the Scottish Dalradian. Unpubl. PhD thesis, Edinburgh University (in Harte et al., 1984).
- Dempster, T. J. 1984.
Localised uplift in the Scottish Dalradian. Nature 307: 156-159.

Deniel, C., Vidal, P., Fernandez, A., Le Fort, P. and Peucat, J-J. 1987.

Isotopic study of the Manaslu granite (Himalaya, Nepal): inferences on the age and source of the Himalayan leucogranites. Contrib. Mineral. Petrol. 96: 78-92.

Dewey, J. F. 1971.

A model for the Lower Palaeozoic evolution of the southern margin of the early Caledonides of Scotland and Ireland. Scott. J. Geol. 7: 219-240

Dewey, J. F. and Pankhurst, R. J. 1970.

The evolution of the Scottish Caledonides in relation to their isotopic age pattern. Trans. R. Soc. Edinburgh 68: 361-387.

Dorobek, S. 1989.

Migration of orogenic fluids through the Siluro-Devonian Helderberg Group during late Paleozoic deformation: constraints on fluid sources and implications for thermal histories of sedimentary basins. Tectonophysics 159: 25-45.

Downie, G. and Ford, T. D. 1966.

Microfossils from the Manx Slate. Proc. of the Yorkshire Geol. Soc. 35, (3), no. 13: 307-322.

Downie, G., Lister, T. R., Harris, A. L. and Fettes, D. J. 1971.

A palynological investigation of the Dalradian rocks of Scotland. Rep. Inst. Geol. Sci. No17/9.

Duba, D. and Williams-Jones, A. E. 1983b.

The application of illite crystallinity, organic matter reflectance, and isotopic techniques to mineral exploration: a case study in southwestern Gaspe, Quebec. Econ Geol. 78: 1350-1367.

Dunoyer de Segonzac, G. 1969.

Les mineraux argileux dans la diagenese; passage metamorphisme. Mém. Serv. Carte Geol. Alsace Lorraine 29: 320pp.

Dunoyer de Segonzac, G. 1970.

The transformation of clay minerals during diagenesis and low-grade metamorphism. Sedimentology 15: 281-344

- Durney, D. 1974. Relations entre les températures d'homogénéisation d'inclusions fluides et les minéraux métamorphiques dans les nappes hélvetiques du Valais. Bull. Soc. Geol. Fr. 16 (7): 269-272.
- Ernst, W. G. 1963. Significance of phengitic white micas from low-grade schists. Am. Mineral. 48: 1357-1373.
- Evans, L. J. 1987. Low grade regional metamorphism of Paleozoic rocks of the Midland Valley of Scotland. Unpublished PhD thesis, St Andrews University.
- Ferrara, G., Lombardo, B. and Tonarini, S. 1983. Rb/Sr geochronology of granites and gneisses from the Mount Everest Region, Nepal Himalaya. Geol. Rdsch. 72: 119-136.
- Fettes, D. J., Graham, C. M., Sassi, F. P. and Scolari, A. 1976. The basal spacing of potassic white mica and facies series variation across the Caledonides. Scott. J. Geol. 12: 227-236.
- Franceschelli, M., Mellini, M. Memmi, I. and Ricci, C. A. 1986. Fine-scale chlorite-muscovite association in low-grade metapelites from Nurra (NW Sardinia), and the possible missidentification of metamorphic vermiculite. Contrib. Mineral. petrol. 93: 137-143.
- Frey, M. 1969. A mixed-layer paragonite/phengite of low-grade metamorphic origin. Contrib. Mineral. Petrol. 24: 63-65.
- Frey, M. 1970. The step from diagenesis to metamorphism in pelitic rocks during Alpine orogeny. Sedimentology 15: 261-279.
- Frey, M. 1978. Progressive low-grade metamorphism of a black shale formation, central Swiss Alps, with special reference to pyrophyllite and margarite bearing assemblages. J. Petrol. 19: 95-135.
- Frey, M. 1987. Low temperature metamorphism. Blackie and Son. Glasgow. 351pp

- Frey, M., Bucher, K., Frank, E. and Mullis, J. 1980a.
Alpine metamorphism along the Geotraverse
Basel-Chiasso - a review. *Eclogae Geol.*
Helv. 73: 527-546.
- Frey, M., Teichmüller, M., Teichmüller, R., Mullis, J.,
Künzi, B., Breitschmid, A., Gruner, U. and Schwizer, B.
1980b.
Very low-grade metamorphism in external
parts of the central Alps: Illite
crystallinity, coal rank and fluid
inclusion data. *Eclogae Geol. Helv.* 73:
173-203.
- Frey, M., Hunziker, J. C., Jaeger, E. and Stern, W.B. 1983.
Regional distribution of white K-mica
polymorphs and their phengite content in
the central Alps. *Contrib. Mineral. Petrol.*
83: 185-197.
- Frey, M., Saunders, J. and Schwanders, H. 1988.
The mineralogy and metamorphic geology of
low grade metasediments, Northern Range,
Trinidad. *J. Geol. Soc. Lond.* 145: 563-575.
- George, T. N. 1960.
The stratigraphical evolution of the
Midland Valley. *Trans. Geol. Soc. Glasgow*
24: 32-107.
- Ghisetti, F. 1987.
Mechanisms of thrust faulting in the Gran
Sasso chain, Central Apennines, Italy. *J.
Struct. Geol.* 9: 955-967.
- Gillott, J. E. 1955.
Metamorphism of the Manx Slate. *Geol. Mag.*
92: 141-154.
- Gillott, J. E. 1965a.
Structural geology of the Manx Slate. *Geol.
Mag.* 93: 301-313.
- Gillott, J. E. 1965b.
Breccias in the Manx Slate: their origin
and stratigraphic relations. *L'pool
Man'ch'r geol. J.* 1: 370-380.
- Gudotti, C. V. and Sassi, F.P. 1976.
Muscovite as a petrogenetic indicator
mineral in pelitic schists. *Neues. Jb.
Miner. Abh.* 127: 97-142.
- Harris, A. L. 1969.
The relationship of the Leny Limestone to
the Dalradian. *Scott. J. Geol.* 5: 187-190.

- Harte, B. and Johnson, M. R. W. 1969.
Metamorphic history of the Dalradian rocks
in Glens Clova, Esk and Lethnot, Angus,
Scotland. Scott. J. Geol. 5: 54-80.
- Harte, B., Boothe, J. E., Dempster, T. J., Fettes, D. J.,
Mandin, J. R. and Watts, D. 1984.
Aspects of post-depositional evolution of
Dalradian and Highland Border Complex Rocks
in the Scottish Caledonides. Trans. R. Soc.
Edinburgh 75: 151-163.
- Harte, B. and Dempster, T. J. 1987.
Regional metamorphic zones: tectonic
controls. Phil. Trans. R. Soc. Lond. A321:
105-127.
- Hashimoto, S. (Ed) 1973.
Geology of the Nepal Himalayas. Hokkaido
Imp. Univ., Sapporo, Tokyo Saikou publ.
co.: 383pp
- Haughton, P. W. D. 1988.
A cryptic Caledonian flysh terrane in
Scotland. J. Geol. Soc. Lond. 145: 685-703.
- Hedenquist, J.W. and Henley, R.W. 1985.
The importance of CO₂ in freezing point
measurements of fluid inclusions: evidence
from active geothermal systems and
implications for epithermal ore deposits.
Econ. Geol. 80: 1379-1406.
- Heim, A. and Gansser, A. 1935 (1975).
Central Himalaya. Geological observations
of the Swiss expedition. Mem. Soc. Helv.
Sci. Nat., Zurich 73(1): 245pp. Reprinted :
Hindustan Publ. Corp., Delhi.
- Hemley, J. J. and Jones, W.R. 1964.
Chemical aspects of hydrothermal alteration
with emphasis on hydrogen metasomatism.
Econ. Geol. 59: 538-569.
- Henderson, W. G. and Fortey, N. J. 1982.
Highland Border rocks at Loch Lomond and
Aberfoyle. Scott. J. Geol. 18: 227-245.
- Henderson, W. G. and Robertson, A. H. F. 1982.
The Highland Border rocks and their
relation to marginal basin development in
the Scottish Caledonides. J. Geol. Soc.
Lond. 139: 433-450.
- Hey, M. H. 1954.
A new review of the chlorites. Mineral.
Mag. 30: 277-292.

- Higgins, M. W. 1971.
Cataclastic rocks. Prof. Pap. US Geol. Surv. 687: 3-21.
- Hobbs, B. E., Means, W. D. and Williams, P. F. 1976.
An outline of structural geology. John Wiley and Sons. 571pp.
- Hodges, K. V., Le Fort, P. and Pêcher, A. 1988a.
Possible thermal buffering by crustal anatexis in collision orogens: Thermobarometric evidence from the Nepalese Himalaya. *Geology* 16: 707-710.
- Hodges, K. V., Hubbard, M. S. and Silverberg, D. S. 1988b.
Metamorphic constraints on the thermal evolution of the central Himalayan Orogen. *Phil. Trans. R. Soc. Lond.* A326: 257-280.
- Hollister, L.S. and Crawford, M. L. 1981.
Short Course in Fluid Inclusions: Applications to Petrology. Min. Assoc. Canada.
- Hower, J. H. and Mowatt, T. C. 1966.
The mineralogy of illite and mixed-layer illite/montmorillonites. *Am. Mineral.* 51: 825-854.
- Hower, J. H., Eslinger, E. V., Hower, M. E. and Perry, E. A. 1976.
Mechanism of burial metamorphism of argillaceous sediments: 1. Mineralogical and chemical evidence. *Geol. Soc. Am. Bull.* 87: 725-737.
- Hunziker, J.C., Frey, M., Clauer, N., Dallmeyer, R. D., Friedrichsen, H., Flehmig, W., Hochstrasser, K., Roggweiler, P. and Schwander, H. 1986.
The evolution of illite to muscovite: mineralogical and isotopic data from the Glarus Alps, Switzerland. *Contrib. Mineral. Petrol.* 92: 157-180.
- Hutchinson, C. S. 1974.
Laboratory handbook of petrogenetic techniques. Wiley and Sons.: 527pp.
- Ikin, N. P. 1983.
Petrochemistry and tectonic significance of the Highland Border Suite mafic rocks. *J. Geol. Soc. Lond.* 140: 267-278.
- Jehu, T. J. and Campbell, R. 1917.
The Highland Border rocks of the Aberfoyle district. *Trans. R. Soc. Edinburgh* 52: 175-212.

- Johnson, M. R. W. 1986.
The structural evolution of the Kumaun Lesser Himalaya. Current trends in Geology Vol IX; Himalayan thrusts and associated rocks: Saklani, P. S. (ed) : 27-39.
- Johnson, M. R. W. and Harris, A. L. 1965.
Is the Tay Nappe post-Arenig? Scott. J. Geol. 1: 217-219.
- Johnson, M. R. W. and Harris, A. L. 1967.
?Arenig relations in parts of the Highland Border, Scotland and their significance in the chronology in the Caledonian orogeny. Scott. J. Geol. 3: 1-16.
- Johnson, M. R. W., Kelley, S. P., Oliver, G.J.H. and Winter, D. A. 1985.
Thermal effects and timing of thrusting in the Moine Thrust zone. J. Geol. Soc. Lond. 142 (5): 863-873.
- Karpova, G. V. 1969.
Clay mineral post-sedimentary rank in Terrigenous rocks. Sedimentology 13: 5-20.
- Kawachi, Y. 1975.
Pumpellite-actinolite and contiguous facies metamorphism in parts of upper Wakatipu District, South Island, New Zealand. New Zealand J. Geol. Geophys. 18 No 3: 401-441.
- Kelly, S. 1988.
The relationship between K-Ar mineral ages, mica grain size and movement on the Moine Thrust Zone, NW Highlands, Scotland. J. Geol. Soc. Lond. 145: 1-10.
- Kelly, S. and Bluck, B. J. 1989.
Short Paper: Detrital mineral ages from the Southern Uplands using ^{40}Ar - ^{39}Ar laser probe. J. Geol. Soc. Lond. 146: 401-404.
- Kemp, A.E.S., Oliver, G.J.H. and Baldwin, J.R. 1985.
Low-grade metamorphism and accretionary tectonics: Southern Uplands-Longford down terrain, British Isles. Min. Mag. 49: 335-344
- Kennedy, W. Q. 1958.
The tectonic evolution of the Midland Valley. Trans. Geol. Soc. Glasgow 23: 106-133.

Kisch, H. J. 1978.

Incipient metamorphism of Cambro-Silurian clastic rocks from Jämtland Supergroup, central Scandinavian Caledonides, western Sweden: illite crystallinity and vitrinite reflectance. IGCP Project Caledonide Orogen Conf. "The Caledonides of the British Isles Reviewed, and Deformation Metamorphism of the Caledonide Orogen", Dublin Aug. 1978, Abs: 29-30.

Kisch, H. J. 1980a.

Illite crystallinity and coal rank associated with lowest grade metamorphism of the Taveyannne greywacke in the Helvetic zone of the Swiss Alps. Eclogae Geol. Helv. 73: 753-777.

Kisch, H. J. 1980b.

Incipient metamorphism of Cambro-Silurian clastic rocks from the Jämtland Supergroup, central Scandinavian Caledonides, western Sweden: Illite crystallinity and vitrinite reflectance. J. Geol. Soc. Lond. 137: 271-288.

Kisch, H. J. 1983.

Mineralogy and petrology of burial diagenesis (burial metamorphism and incipient metamorphism in clastic rocks). In: Larson, G. and Chilingar, G. V. (Eds) Diagenesis in sediments and sedimentary rocks 2, Ch 5: 239-493. Developments in Sedimentology 25B 1983, Elsevier, Amsterdam.

Kisch, H. J. 1987.

Correlation between indicators of very low-grade metamorphism. In: Frey, M. (ed), Low Temperature Metamorphism. Blackie and Son Ltd., Glasgow: 227-304.

Kneller, B. C. and Aftalion, M. 1987.

The isotopic and structural age of the Aberdeen Granite. J. Geol. Soc. Lond. 144: 717-721.

Kübler, B. 1967a.

La crystallinité de l'illite et les zones tout à fait supérieurs du métamorphisme. In: Etages Tectoniques. Ala Baconniere, Neuchâtel (Suisse): 105-121.

Kübler, B. 1967b.

Anchimétamorphisme et schistosité. Bull. Centre Rech. Pau-SNPA 1 (2): 259-278.

- Kübler, B. 1968.
 Evaluation quantitatative du métamorphisme par le cristallinité de l'illite. Bull. Centre Rech. Pau-SNPA 2: 385-397.
- Kuniyoshi, S. and Liou, J.G. 1976.
 Burial metamorphism of the Kamusten volcanic rocks, Northeastern Vancouver Island, British Columbia. Am. J. Sci. 276: 1096-1119.
- Lal, R. K., Mukerji, S. and Ackerman, C. 1981.
 Deformation and Barrovian metamorphism at Takdah, Darjeeling (eastern Himalaya). In: Skalami, P. S. (Ed). Metamorphic tectonites of the Himalaya. Today and Tomorrows printers and publ., New Delhi: 231-278.
- Lamplugh, G. W. 1903.
 The Geology of the Isle of Man. Mem. Geol. Surv. UK.
- Le Fort, P. 1975.
 Himalayas: The collide range. Present knowledge of the continental arc. Am. J. Sci. 275A: 1-44.
- Le Fort, P. 1986.
 Metamorphism and magmatism during the Himalayan collision. In: Coward, M. P. and Ries, A. C. (Eds), Collision Tectonics, Geol. Soc. Lond. Spec. Publ. 19: 159-172.
- Le Fort, P. 1988.
 Granites in the tectonic evolution of the Himalaya, Karakoram and southern Tibet. Phil. Trans. R. Soc. Lond. A326: 281-299
- Le Fort, P., Debon, F. and Sonet, J. 1983.
 The Lower Palaeozoic "Lesser Himalayan" Granitic Belt: emphasis on the Simchar pluton of Central Nepal. In: Shams, F. A. (Ed), Granites of Himalaya, Karakorum and Hindu Kush. Punjab Univ., Lahore, Pakistan: 235-255.
- Le Fort, P., Debon, F., Pécher, A., Sonet, J. and Vidal, P. 1986a.
 The 500Ma magmatic event in the Alpine Southern Asia: a thermal episode at Gondwana scale. Sci. de la Terre, Mém. 47: 191-209.
- Le Fort, P., Pécher, A. and Upreti, B. N. 1986b.
 A section through the Tibetan Slab in Central Nepal (Kali Gandaki Valley): Mineral, chemistry and thermobarometry of the Main Central Thrust zone. Sci. de la Terre, Mém. 47: 211-228.

- Liou, J. G., Kim, H. S. and Maruyama, S. 1983.
Prehnite-Epidote equilibria and their petrologic applications. *J. Petrol.* 24: 321-342.
- Liou, G. S., Maruyama, S. and Cho, M. 1985.
Phase equilibria and mineral parageneses of metabasites in low-grade metamorphism. *Mineral. Mag.* 49: 321-333.
- Lister, G. S. and Snook, A. W. 1984.
S-C Mylonites. *J. Struct. Geol.* 6, No 6: 617-638.
- Lofgren, G. E. 1974.
An experimental study of plagioclase crystal morphology: isothermal crystallisation. *Am. J. Earth. Sci.* 247: 243-273.
- Lofgren, G. E. 1983.
Effect of heterogeneous nucleation on basaltic textures: A dynamic crystallisation study. *J. Petrol.* 24 pt3: 229-255.
- Longman, C. D., Bluck, B. J. and van Breeman, O. 1979.
Ordovician conglomerates and the evolution of the Midland valley. *Nature* 80: 578-581.
- Longstaffe, F. J. (ed) 1981.
Clays and the resource geologist. Mineral. Assoc. Canada, Short Course Handbook 7.
- Maruo, Y. 1979.
Geology and metamorphism of the Nanda Devi region, Kumaun Higher Himalaya, India. *Himalayan Geol.* 9(1): 3-17.
- Maruo, Y. and Kiazaki, K. 1983.
Thermal structure in the nappes of Eastern Nepal Himalayas. In: Shams, F. A. (Ed), *Granites of Himalaya, Karakorum and Hindu Kush*. Punjab Uni., Lahore, Pakistan: 271-285.
- Mason, R. 1984.
Inverted isograds at Sulitjelma, Norway: the result of shear zone metamorphism. *J. Met. Geol.* 2, no.2: 75-82.
- Maxwell, D. T. and Hower, J. 1967.
High-grade diagenesis and low-grade metamorphism of illite in the Precambrian Belt series. *Amer. Mineral.* 52: 843-857.

- Merriman, R. J. and Roberts, B. 1985.
A survey of white mica crystallinity and polytypes in pelitic rocks of Snowdonia and Llŷn, N. Wales. Min. Mag. 49: 305-319.
- Merriman, R. J., Bevins, R. E. and Ball, T. K. 1986.
Petrological and geochemical variation within the Tal y Fan intrusion: a study of element mobility during low-grade metamorphism with implications for petrotectonic modelling. J. Petrol. 27: 1409-1436.
- Miyashiro, A. 1973.
Metamorphism and Metamorphic Belts. George Allen and Unwin, Lond. 492pp.
- Molyneux, S. G. 1979.
New evidence for the age of the Manx Group, Isle of Man. The Caledonides of the British Isles Reviewed, Geol. Soc. Lond.
- Morimoto, N., Chairman. 1988.
Subcommittee on Pyroxenes, IMA. Mineral. Mag. 52: 535-550.
- Mullis, J. 1979.
The system methane-water as a geologic thermometer and barometer from the external part of the Central Alps. Bull. Mineral. 102: 526-536.
- McDowell, S. D. and Elders, W. A. 1980.
Authigenic layer silicates in borehole Elmore 1, Salton Sea geothermal field, California, USA. Contrib. Mineral. Petrol. 74: 293-310.
- Nadeau, P. H., Tait, J. M., McHardy, W. J. and Wilson, M. J. 1984.
Interstratified XRD characteristics of physical mixtures of elementary clay particles. Clay Minerals. 19: 67-76.
- Nakajima, T., Banno, S. and Suzuki, T. 1977.
Reactions leading to the disappearance of pumpellyite in low-grade metamorphic rocks of the Sanbagawa metamorphic belt in Central Shikoku, Japan. J. Petrol. 18: 263-284.
- Niedermayr, G., Mullis, J., Niedermayr, E. and Schramm, J. M. 1984.
Zur Anchimetamorphose permo-skythoischer Sedimentgesteine im westliche Drauzug Karnten- Osttril (Österreich). Geol. Rundsch. 73 (1): 207-221.

- Nisbet, E. G. and Pearce, J. A. 1977.
Clinopyroxene composition in mafic lavas from different tectonic settings. Contrib. Mineral. Petrol. 63: 149-160.
- Oliver, G. J. H. and Leggett, J. K. 1980.
Metamorphism in an Accretionary prism: prehnite-pumpellyite facies metamorphism of the Southern Uplands of Scotland. Trans. R. Soc. Edinburgh Earth Sci. 71 (4): 235-246.
- Padan, A., Kisch, H. J. and Shargam, R. 1982.
Use of lattice parameter b of dioctahedral illite/muscovite for the characterisation of P/T gradients of incipient metamorphism. Contrib. Mineral. Petrol. 79: 85-95.
- Pankhurst, R. J. 1970.
The geochronology of the basic igneous complexes. Scott. J. Geol. 6: 83-107.
- Pankhurst, R. J. and Pidgeon, R. T. 1976.
Inherited isotope systems and the source region prehistory of early Caledonian granites in the Dalradian Series of Scotland. Earth Planet. Sci. Lett. 31: 55-68.
- Paterson, I. B. and Harris, A. L. 1969.
Lower Old Red Sandstone ignimbrites from Dunkeld, Perthshire. Rep. Inst. Geol. Sci. No67/7.
- Pavlis, T. L. 1986.
The role of strain heating in the evolution of megathrusts. J. Geophys. Res. 91 no.B12: 12407-12422.
- Pêcher, A. 1979.
Les inclusions fluides des quartz d'xsudation de la zone du MCT himalayen au Népal central: données sur la phase fluides dans une grande zone de ciasaillement crustal. Bull. de Minéral. 102: 537-554.
- Pêcher, A. and Le Fort, P. 1986.
The metamorphism in the central Himalaya: its relation with the tectonics. Sci. de la Terre, Mem 47: 285-309.
- Perrey, E. A. and Hower, J. 1972.
Late stage dehydration in deeply buried pelitic sediments. Am. Assoc. Petr. Geol. Bull. 56: 2013-2021.

- Potter II, R. W. 1977.
Pressure corrections for fluid-inclusion homogenisation temperatures based on the volumetric properties of the system NaCl-H₂O. U. S. Geol. Surv. Res. J. 5: 603-607.
- Poty, B., Stalder, H. A. and Weisbrod, A. M. 1974.
Fluid inclusion studies in quartz from fissures of Western and Central Alps. Schweiz Mineral. Petrog. Mitt 54: 717-752.
- Primmer, T. J. 1985.
A transition from diagenesis to greenschist facies within a major Variscan fold/thrust complex in south-west England. Miner. Mag. 49 (3): 365-374.
- Pringle, J. 1939.
The discovery of Cambrian trilobites in the Highland Border rocks near Callander, Perthshire. Pept. Br. Ass. Advmt. Sci. p252.
- Reay, A. 1982.
The effect of disc mill grinding on some rock forming minerals. Min. Mag. 44: 179-182.
- Reynolds, R. C. 1980.
Interstratified clay minerals. In: Crystal Structures of Clay Minerals and their X-Ray Identification. Brindley, G. W. and Brown, G. (Eds), Monograph 5, Min. Soc. Lond. : 249-303.
- Reynolds, R. C. and Hower, J. 1970.
The nature of interlayering in mixed-layer illite-montmorillonite. Clays Clay Minerals 18: 25-36.
- Rice, A. H. N., Bevins, R. E., Robinson, D. and Roberts, D. 1989.
Evolution of low-grade metamorphic zones in the Caledonides of Finmark, North Norway. In Gayer, R. A., The Caledonian Geology of Scandinavia, Graham and Trotman: 177-191.
- Roberts, B. 1981.
Low-grade and very low grade regional metabasic rocks of Llyn and Snowdonia, Gwynedd, North Wales. Geol. Mag. 118: 189-200.
- Roberts, B. and Merriman R. J. 1985.
The distinction between Caledonian burial and regional metamorphism in metapelites from North Wales: an analysis of isocryst patterns. J. Geol. Soc. Lond. 142: 615-624.

- Robertson, A. H. F. and Henderson, W. G. 1984.
Geochemical evidence for the origins of igneous and sedimentary rocks of the Highland Border, Scotland. Trans. R. Soc. Edinburgh, Earth Sci. 75: 135-150.
- Robinson, D. 1987.
Transition from diagenesis to metamorphism in extensional and collision settings. Geology 15: 866-869.
- Robinson, D., Nicholls, R. A. and Thomas L. J. 1980.
Clay mineral evidence for low-grade Caledonian and Variscan metamorphism in southwestern Dyfed, South Wales. Min. Mag. 43: 857-863.
- Robinson, D. and Bevins, R.E. 1986.
Incipient metamorphism in the Lower Palaeozoic marginal basin of N. Wales. J. Metamorphic Geol. 4: 101-113
- Roddick, J. C., Cliff, R.A. and Rex, D. C. 1980.
The evolution of excess argon in Alpine biotites - a ^{40}Ar - ^{39}Ar analysis. Earth Planet. Sci. Letts. 48: 185-208.
- Roedder, E. 1984.
Fluid Inclusions. Reviews in Mineralogy 12, Min. Soc. of Amer.: 644pp.
- Roedder, E. and Bodnar, R.J. 1980.
Geologic pressure determination from fluid inclusion studies. Ann. Rev. Earth Planet. Sci. 8: 263-301.
- Rogers, G., Dempster, T. J., Bluck, B. J. and Tanner, P. W. G. (in press).
A high precision U/Pb age for the Ben Vuirich Granite: Implications for the evolution of the Scottish Dalradian. J. Geol. Soc. Lond.
- Roy, A. B. 1978.
Evolution of slaty cleavage in relation to diagenesis and metamorphism: A study from the Hunsrück-schiefer. Geol. Soc. Amer. Bull. 89: 1775-1785.

- Sagon, J. P. and Dunoyer de Segonzac, G. 1972.
 La crystallinité des micas dans les schistes paleozoïques et briovériens du Bassins de Châteaulin (Massifarmoricain). C. R. Acad. Sci., Sér D, 275: 1023-1026.
- Saliot, P., Guilhamou, M. and Barbillat, J. 1982.
 Les inclusions fluides dans les minéraux des métamorphisme à laumonite-prehnite-pumpellyite des Grès du Champsaur (Alpes du Dauphiné). Etude du mécanisme de circulation des fluides. Bull. Minéral. 105: 648-657.
- Sassi, F. P. 1972.
 The petrologic and geologic significance of b_0 value of potassium white micas in low grade metamorphic rocks. An application to the Eastern Alps. Tschermaks. Mineral. Petrogr. Mitt 18: 105-113.
- Sassi, F. P. and Scolari, A. 1974.
 The b_0 value of potassic white mica as a barometric indicator in low-grade metamorphism of pelitic schists. Contrib. Mineral. Petrol. 45: 143-152.
- Sassi, F. P., Kraütner, H. G. and Zirpoli, G. 1976.
 Recognition of pressuren character in greenschist facies metamorphism. Schweiz. Miner. Petrol. 45: 143-152.
- Schärer, U., Xu, R. H. and Allégre, C. T. 1986.
 U-(Th)-Pb systematics and ages of the Himalayan leucogranites, South Tibet. Earth. Planet. Sci. Letts. 77: 35-48.
- Schiffman, P. and Liou, J. G. 1980.
 Synthesis and stability relations of Mg-Al pumpellyite, Ca Al MgSiO(OH) . J. Petrol. 21: 441-474.
- Searle, M. P. 1986.
 Structural evolutin and sequence of thrusting in the High Himalayan, Tibetan-Tethys and Indus sutre zones of Zanskar and Ladakh, Western Himalaya. J. Struct. Geol. 8: 923-936.
- Searle, M. P., Windley, B. F., Coward, M. P., Cooper, D. J. W., Rex, A. J., Rex, D., Tingdong Li, Xuchang Xiao, Jan, M. Q., Thakur, V. C. and Kumar, S. 1987.
 The closing of Tethys and the tectonics of the Himalaya. Geol. Soc. Am. Bull. 98: 678-701.
- Shepherd, T. J., Rankin, A. H. and Alderton, D. H. M. 1985.
 A practical guide to fluid inclusion studies. Blackie, Glasgow: 239pp.

Simpson, A. 1963a.

The stratigraphy and tectonics of the Manx Slate Series, Isle of Man. J. Geol. Soc. Lond. 119: 367-400.

Simpson, A. 1963b.

F2 Quartz veining in the Manx Slate Series. Nature 199, No 4896: 900-901.

Simpson, A. 1964a.

The metamorphism of the Manx Slate Series, Isle of Man. Geol. Mag. 101: 21-36.

Simpson, A. 1964b.

Deformed acid intrusions in the Manx Slate Series, Isle of Man. Geol. Jour. 4: 189-206.

Simpson, A. 1965a.

The syntectonic Foxdale-Archallagan Granite and its metamorphic aureole, Isle of Man. Geol. Jour. 4: 415-434.

Simpson, A. 1965b.

F1 Cross-folding in the Manx Slate Series, Isle of Man. Geol. Mag. 102: 440-444.

Simpson, A. 1966.

Summer field meeting in the Isle of Man. Proc. Geol. Assoc. 77: 217-227.

Simpson, C. and Schmid, S. M. 1983.

An evaluation of criteria to deduce the sense of movement in sheared rocks. Geol. Soc. Amer. Bull. 94: 1281-1288.

Sinha-Roy, S. 1982.

Himalayan Main Central thrust and its implications for Himalayan inverted metamorphism. Tectonophysics 84: 197-224.

Stöcklin, J. 1980.

Geology of Nepal and its regional framework. J. Geol. Soc. Lond. 137: 1-34.

Stöcklin, J., Bhattarai, K. D., Singh-Chettri, V. and Bhandari, A. N. 1980.

Geological map of Kathmandu area and Central Mahabharat Range. Sajedian Cartographic Co. Ltd. Tehran.

Stopler, E. and Holloway, J. R. 1988.

Experimental determination of the solubility of carbon dioxide in molten basalt at low pressure. Earth Planet. Sci. Lett. 87: 397-408.

- Sutton, J. and Watson, J. 1955.
The deposition of the Upper Dalradian rocks
of the Banffshire coast. Proc. Geol. Assoc.
Lond. 66: 101-133.
- Swanson, M. P. 1988.
Pseudotachylite-bearing strike-slip duplex
structures in the Fort Foster Brittle Zone,
S. Maine. J. Struct. Geol. 10 no.8: 813-
846.
- Takagi, H. and Ito, M. 1988.
The use of assymetric pressure shaddows in
mylonites to determine the sense of shear.
J. Struct. Geol. 10, No4: 347-360.
- Teichmüller, M., Teichmüller, R. and Weber, K. 1979.
Inkhaltung und Illit-Kristallinität -
Vergleichende Untersuchugen im Mesozoikum
und Paläozoikum von Westfalen. Fortschr.
Geol. Rheinld. Westf. 27: 201-276.
- Thirwall, M. F. 1981.
Implications for Caledonian plate tectonic
models of chemical data from volcanic rocks
of the British Old Red Sandstone. J. Geol.
Soc. Lond. 138: 123-138.
- Thirwall, M. F. 1983a.
Discussion on implications on Caledonian
tectinic models of chemical data from
volcanic rocks of the British Old Red
Sandstone. J. Geol. Soc. Lond. 140: 315-
318.
- Thirwall, M. F. 1983b.
Isotope geochemistry and origin of
calkalkaline lavas from Caledonian
continental margin volcanic arc. J.
Volcanol. Geotherm. Res. 18: 589-613.
- Thomas, L. J. 1985.
Low-grade metamorphism and the stable
isotopic composition of alteration fluids,
Lower Palaeozoic sucession, English Lake
District. Unpubl. PhD thesis, St.Andrews
University.
- Thorez, J. 1976.
Pratical Identification of Clay Minerals.
G. Lelotte, Dison, Belgum.
- Toselli, A. J. and Weber, K. 1982.
Anquimétamorfismo en rocas del Paleozoico
inferior en el noroeste de Argentina-Valor
de la cristalinidad de la illita como
índice. Acta. Geol. Lilloana (Argentina)
14: 187-200

- Touret, J. 1977.
The significance of fluid inclusions in metamorphic rocks. In: Fraser, D. G., Ed. Thermodynamics in Geology. D. Riedel Publ. Co. Dordrecht, Netherlands: 203-227.
- Valdiya, K. S. 1980.
The two intracrustal boundary thrusts of the Himalayas. Tectonophysics 66: 323-348.
- Velde, B. 1965.
Phengite micas: synthesis, stability, and natural occurrence. Amer. J. Sci. 263: 886-913.
- Wager, L.R. 1965.
Injected granite sheet of the Ronbuk valley and the north face of Mount Everest. D. N Wadia commemorative vol: India Min. Geol. and Met. Inst.: 358-379.
- Watson, J. V. 1984.
The ending of the Caledonian orogeny in Scotland. J. Geol. Soc. Lond. 141: 193-214.
- Weaver, C. E. 1961.
Clay minerals of the Ouachita structural belt and adjacent foreland. In: Flawn, P. T., Goldstein, A. Jr., King, P. B. and Weaver, C. E., The Ouachita Belt. Univ. Texas Publ. 6120: 147-160.
- Weaver, C. E. 1984.
Shale-slate metamorphism in southern Appalachians. Developments in Petrology 10, Elsevier, Amsterdam, 239pp.
- Weaver, C. E. and Pollard, L. D. 1973.
The Chemistry of Clay Minerals. Elsevier, New York, 213pp.
- Weber, K. 1972.
Notes on determination of illite crystallinity. Neues Jahrb. Mineral. Monatsh: 267-272.
- Westoll, T. S. 1977.
Northern Britain. In House, M. R. (ed). A correlation of the Devonian rocks in the British Isles. Spec. Rep. Geol. Soc. Lond. 7: 66-93.
- Whelan, G. M. 1988.
The biostratigraphy and palaeontology of organic-walled microfossils from selected Ordovician localities in Scotland. Unpubl. PhD thesis, Glasgow University.

- Whitney, G. and Northrop, H. R. 1988.
Experimental investigation of the smectite
to illite reaction: Dual reaction
mechanisms and oxygen-isotope systematics.
Amer. Mineral. 73: 77-90.
- Winkler, H. G. F. 1979.
Petrogenesis of metamorphic rocks.
Springer-Verlag, NY, 248pp.
- Woodland, B. G. 1985.
Relationships of concretions and chlorite
muscovite porphyroblasts to the development
of domainal cleavage in low-grade
metamorphic deformed rocks from north-
central Wales, Great Britain. J. Struct.
Geol. 7: 205-215.
- Zen, E-An and Albee, A. L. 1964.
Coexistent muscovite and paragonite in
pelitic schists. Amer. Mineral. 49: 904-
925.

APPENDIX 2.1 - XRD INSTRUMENTAL CONDITIONS

Phillips PW 1010 X-Ray diffractometer

Co-K α radiation	Cu-K α radiation
1° divergence slit	1° divergence slit
monochromator	monochromator
0.2mm receiving	0.2mm receiving
40kV, 30mA	36kV, 18mA

Instrumental conditions for illite crystallinity determination.

Angular goniometer speed	1°2θ/min or $\frac{1}{2}$ °2θ/min
Scanning range	<u>Co-tube</u> 23.5-25°2θ Quartz standard 9-11.5°2θ Mica peak
	<u>Cu-tube</u> 20-21.5°2θ Quartz standard 7.5-10°2θ Mica peak
Chart speed	5 x 240 or 5 x 120 mm/hr
Attenuation	4 x 10 ² , 1 x 10 ³ or 2 x 10 ³
Time constant	2 or 4

Instrumental conditions for b₀ determination

Angular goniometer speed	$\frac{1}{2}$ °2θ/min
Scanning range	59.0-62.5°2θ (Cu-tube)
Chart speed	5 x 120 or 5 x 240
Attenuation	4 x 10 ²
Time constant	4

Instrumental conditions for mineral identification

Angular goniometer speed	1°2θ/min
Scanning range	3-35°2θ or 3-65°2θ (Cu-tube) 5-45°2θ (Co-tube)
Chart speed	5 x 120 or 5 x 240
Attenuation	1 x 10 ³ or 4 x 10 ²
Time constant	2

APPENDIX 2.2 - XRD SAMPLE PREPARATION

Samples were collected from the more pelitic units whenever possible, and weathering was also avoided as much as possible. The samples were prepared as follows:

Rock powders were produced by grinding off excess weathering, jaw crushing the sample, and then TEMA milling for 10 to 25 seconds depending on the hardness off the rock. This produced a coarse powder. With later samples, from Nepal and the IOM, powders were obtained by repeated jaw crushing. This avoided the possibility of over grinding in the TEMA. The resultant coarse powder was then put in an ultasonic bath to disaggregate for 10 minutes, before being centrifuged to obtain the 2-6 μm and <2 μm size fractions (Thomas, 1986). The few samples that required a dispersant (calgon) were noted. The resultant slurries were pippetted onto glass slips, and air dried at 20 to 25°C.

APPENDIX 2.3 - TREATMENT FOR CLAY MINERAL DETERMINATION

Ethylene glycolation - (Hutchison, 1974)

Samples were placed in a dessicator containing $\frac{1}{2}$ pint of ethylene glycol, and heated to 60°C for 2 hours. Samples were stored in the dessicator until required.

Heat treatment - (Brindley, 1972)

Samples were heated to 600°C for one hour, and allowed to cool in the furnace to room temperature before being removed. Samples were stored in a dessicator until required

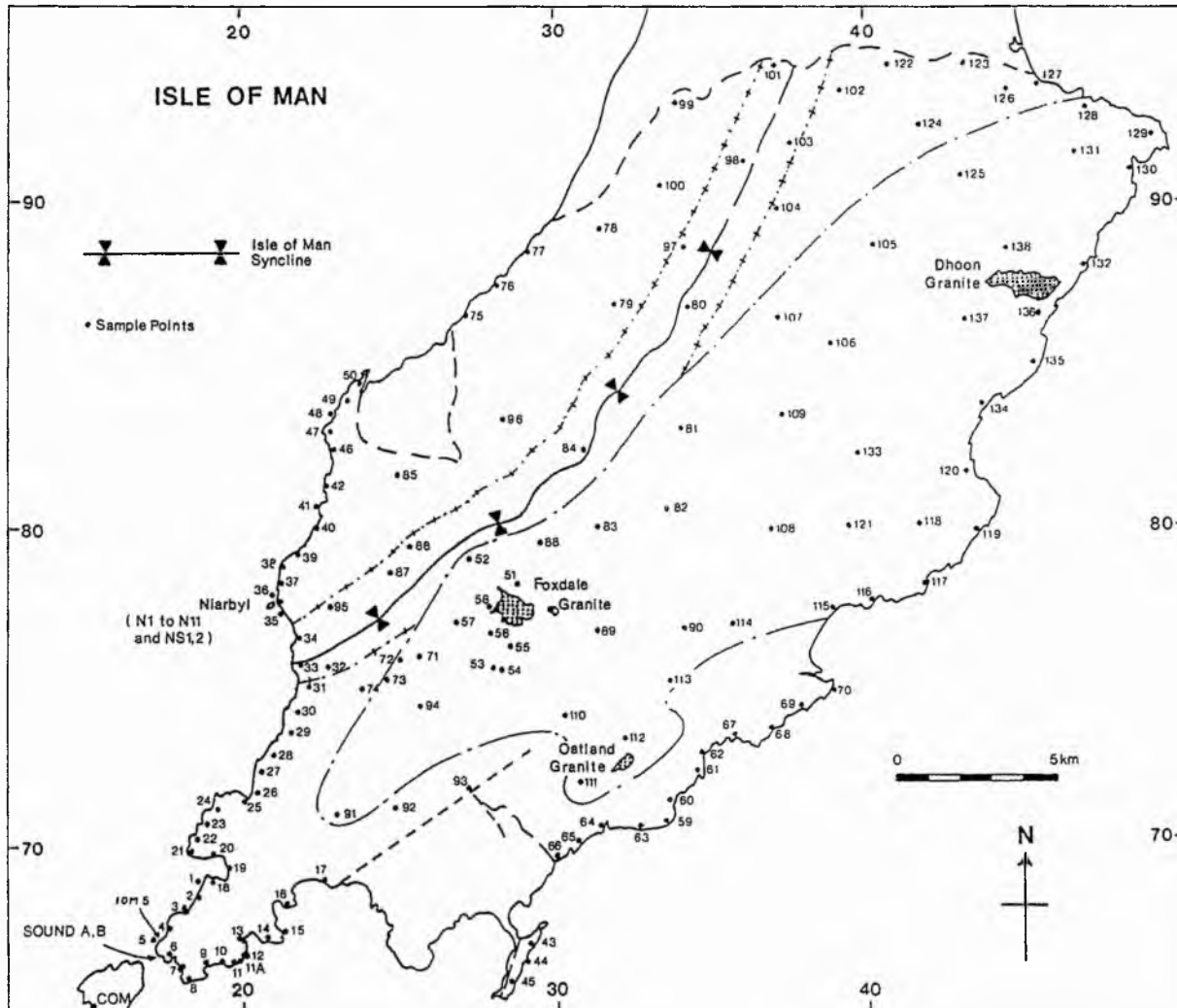
HCl dissolution - (Biscaye, 1964)

Whole rock powder was placed in a test tube with 2M HCl, and heated to 80°C for 8 hours. This was then filtered, washed and precipitated onto a glass slip, as before.

APPENDIX 2.4 - XRD peaks (in d \AA) used to identify polymorphs of potassic white mica (after Thorez, 1976 and Berry, 1974).

Peak	<u>Illite</u>				<u>Muscovite</u>							
	1Md	1M	2M _I	+1M	1Md	1M	1M	2M _I	2M _I	2M _I	3T	3T
001/002	10.1	10.1	10.0	10.0	10.08	10.08	10.00	10.00	9.95	9.90	9.97	10.00
002/004	4.98	4.98	4.98	4.98	5.04	5.04	5.03	5.02	4.97	4.90	4.99	4.95
020/110	4.48	4.48	4.48	4.48	4.52	4.49	4.52	4.48	4.47		4.49	4.48
111/110								4.46		4.46	4.46	
021								4.39				
111/111				4.29			4.35	4.30	4.30	4.29		
022/021							4.11		4.11	4.11	4.11	
112									3.95	3.95		
113			<u>3.89</u>						<u>3.89</u>	<u>3.88</u>	<u>3.88</u>	3.87
023/113			<u>3.74</u>	<u>3.75</u>					<u>3.74</u>	<u>3.73</u>		3.69
112/023		3.66	3.66	3.66	3.36	3.66	3.63				3.65	3.60
114			3.54	3.50					3.50	3.48		
003/006							3.36	3.36	3.35	3.34	3.36	
006	3.33	3.33	3.33							3.32		3.33
114			3.21	3.20					3.21	3.19		3.17
112/115		3.07	.	3.07			3.07	3.10		3.12	3.10	3.10
025			<u>3.01</u>						<u>3.00</u>	<u>2.99</u>		
113							2.93					
115/113		2.87	<u>2.87</u>	<u>2.89</u>				2.90	<u>2.87</u>	<u>2.86</u>	<u>2.86</u>	2.88
116									<u>2.80</u>	<u>2.79</u>		
023							2.69					
130/131	2.58	2.58			2.58	2.58	2.60	2.60	2.60		2.59	2.61
202/116				2.55					2.58	2.57	2.57	2.56

Peaks used to identify the 2M_I polymorph are underlined.



APPENDIX 3.1 - Sample localities on the IOM. Sample numbers are prefixed by M except where otherwise shown. The dot/dash line indicates the zone of contact metamorphism extrapolated from the distribution of porphyroblasts shown in Simpson (1964a). The dot/cross line indicates the zone of the IOM Synform.

APPENDIX 3.2

Samples collected on the Isle of Man (OS sheet 95). Grid references are prefixed with SC. TS = thin section, FI = fluid inclusion wafer, Altered Dyke = metamorphosed Greenstone dyke.

Sample	TS	Grid Ref	Lithology	Sample	TS	Grid Ref	Lithology
M1	-	188 690	Banded Slate	M55	yes	287 762	Slate
M2	-	186 685	,	M56	-	280 768	,
M3	-	184 681	,	M57	-	269 769	,
M4	yes	177 675	Altered Dyke	M58	-	282 776	Chloritic Slate
M5	,	174 672	Banded Slate	M59	yes	337 706	Slate
IOM5	,	174 672	Altered Dyke	M60	-	338 718	,
M6	,	178 665	Slate	M61	yes	346 721	,
M7	-	181 662	,	M62	-	347 728	,
M8	yes	183 658	Banded Slate	M63	-	326 703	Semi-pelite
M9	-	187 668	,	M64	-	317 705	Slate
M10	yes	192 663	Slate ,	M65	-	308 698	,
M11	-	198 663	Psammite	M66	-	330 693	,
M11A	yes	198 664	Biotitic Dyke	M67	yes	358 731	,
M12	,	201 667	Semi-pelite	M68	-	368 733	,
M13	-	202 672	Slate	M69	-	379 740	,
M14	-	207 670	,	M70	-	389 747	,
M15	-	212 672	,	M71	-	257 759	,
M16	yes	213 682	Semi-pelite	M72	-	253 757	,
M17	,	225 688	Banded Slate	M73	yes	247 752	,
M18	-	190 690	,	M74	-	240 750	,
M19	-	196 693	,	M75	-	259 861	Altered Dyke
M20	yes	192 697	Rip-up Slate	M76	-	280 871	Slate
M21	,	184 698	Slate	M77	-	295 883	,
M22	-	185 703	,	M78	-	317 890	Semi-pelite
M23	yes	190 708	,	M79	-	323 861	Slate
M24	-	196 713	,	M80	-	347 865	,
M25	yes	200 715	,	M81	-	342 829	,
M26	-	207 716	,	M82	-	337 805	,
M27	-	208 723	,	M83	-	314 800	,
M28	-	211 728	,	M84	-	310 823	,
M29	yes	217 735	,	M85	-	253 817	Chloritic slate
M30	-	219 742	,	M86	-	255 793	Slate
M31	-	223 747	,	M87	-	248 784	,
M32	-	228 757	,	M88	-	297 796	,
M33	-	219 759	,	M89	-	314 786	,
M34	yes	218 767	,	M90	-	341 769	,
M35	,	215 772	,	M91	-	231 710	,
M36	,	211 788	,	M92	-	249 791	,
M37	-	212 782	,	M93	-	273 717	,
M38	yes	213 787	,	M94	-	258 744	,
M39	,	219 792	Semi-pelite	M95	-	229 775	,
M40	,	224 799	,	M96	-	285 830	,
M41	,	226 806	Slate	M97	-	334 884	,
M42	-	227 811	,	M98	-	368 914	Banded Slate
M43	yes	293 669	,	M99	-	342 929	Slate
M44	-	290 663	Psammite	M100	-	338 902	,
M45	yes	287 658	Slate	M101	-	372 942	,
M46	,	231 882	,	M102	-	399 940	,
M47	-	231 872	,	M103	-	383 920	,
M48	-	233 833	Psammite	M104	-	375 896	,
M49	-	236 839	,	M105	-	404 886	Psammite
M50	-	251 844	Slate	M106	-	390 854	Slate
M51	-	288 780	,	M107	-	374 862	,
M52	-	276 792	Semi-pelite	M108	-	371 798	Semi-pelite
M53	-	283 756	Slate	M109	-	375 883	Psammite
M54	-	284 755	,	M110	-	303 740	Banded Slate
M111	-	308 720	Slate	M135	-	455 846	Semi-pelite
M112	-	323 733	,	M136	-	457 862	Slate
M113	-	337 752	Banded Slate	M137	-	434 816	,
M114	-	358 769	Slate	M138	-	452 887	Psammite
M115	-	393 773	Banded Slate	COM	-	151 651	Slate
M116	-	405 777	Psammite	NS1	-	2112 7760	Phyllonite
M117	-	421 781	Banded Slate	NS2	-	2111 7760	,
M118	-	418 799	Mudstone	N1	-	2115 7762	Altered Dyke
M119	-	437 798	Banded Mudstone	N2	-	2113 7763	Semi-Pelite
M120	-	425 815	Banded Slate	N3	-	2114 7762	Phyllonite
M121	-	397 799	Slate	N4	-	2114 7762	,
M122	-	410 943	,	N5	-	2110 7759	,
M123	-	435 924	,	N6	-	2111 7759	,
M124	-	425 925	,	N7	-	2118 7756	,
M125	-	434 907	,	N8	-	2117 7752	,
M126	-	449 934	,	N9	-	2120 7750	,
M127	-	462 934	,	N10	-	2112 7758	,
M128	-	474 928	Banded Slate	N11	-	2112 7758	,
M129	-	496 917	Slate	FOXDALE	FI	288 773	Quartz vein
M130	-	487 909	Banded Slate	DHOON	FI	459 871	,
M131	-	474 912	Slate	CALF			
M132	-	473 878	Chloritic Slate	SOUND A	FI	174 667	,
M133	-	399 822	Slate	CALF			
M134	-	440 834	Slate	SOUND B	FI	174 667	,

APPENDIX 3.3 - XRD analyses of samples from the IOM
($<2\mu\text{m}$ size fraction).

1 = Kaolinite, 2 = Illite/Smectite, 3 = Chlorite/Smectite, 4 = Corrensite
 5 = Rectorite, 6 = Pyrophyllite, 7 = 1M Mica, 8 = 1Md, K, Na Mica
 9 = 6:4 Muscovite/Paragonite, 10 = Paragonite, 11 = 2M, Mica, 12 = Albite
 13 = Biotite, 14 = Quartz, 15 = Chlorite.
 S, M and L (Small, Medium and Large) indicates a qualitative estimation of
 mineral proportions based on relative peak sizes. Im = ilmenite, CC = calcite,
 Mu = muscovite, Chl = chlorite, Bi = biotite, K-feld = K-feldspar.

Sample	H ₂ O b ₀	1	2	3	4	5	6	7	8	9	10	11	12	13	14	15	Remark
M1	176	8.988	-	-	-	-	-	-	S	L	L	L	-	-	S	S	
M3	165	8.990	-	-	-	-	-	-	-	L	L	L	-	-	M	L	
M5	134	8.988	-	-	-	-	S	-	-	S	L	L	S	-	M	L	Im, CC
M6	163	9.005	-	-	-	-	-	-	S	L	L	L	-	-	S	M	Im, CC
M8	142	8.985	-	-	-	-	-	-	-	-	M	L	-	-	S	M	
M10	126	8.988	-	-	-	-	S	-	-	-	L	L	-	-	M	M	
M12	142	9.018	-	-	-	-	S	-	-	S	M	L	-	-	L	L	
M14	146	8.980	-	-	S	-	-	-	-	L	M	L	-	-	M	L	
M17	142	8.978	-	-	S	-	-	-	-	L	L	L	-	-	M	L	
M19	159	8.993	-	-	-	-	-	-	-	L	L	L	-	-	M	L	
M20	129	8.975	-	-	-	-	-	-	-	-	L	L	-	-	L	L	Im, CC
M21	200	8.987	-	S	S	S	-	-	M	-	M	S	-	-	M	M	Im, CC
M23	144	8.988	-	-	-	-	-	-	-	S	L	L	-	-	M	L	Im, CC
M25	144	8.990	-	-	S	-	-	-	-	L	L	L	-	-	S	M	Im, CC
M27	131	8.983	-	-	-	-	S	-	-	M	L	L	S	-	L	L	
M29	138	8.988	-	-	-	-	-	-	-	L	M	-	-	M	M	Im	
M30	167	8.963	-	-	-	-	-	-	-	M	L	L	-	-	L	M	
M32	171	8.980	-	-	-	-	S	-	-	M	L	L	-	-	M	L	Mu needles
M34	156	8.980	-	-	-	-	-	-	S	L	L	L	-	-	M	M	Chl pods
M35	140	8.987	-	-	-	-	S	-	-	L	L	L	-	-	L	L	
M37	160	9.022	-	-	-	-	-	-	S	M	L	L	-	-	S	M	
M38	139	9.018	-	-	-	-	S	-	-	S	L	L	S	-	M	M	
M40	127	9.019	-	-	-	-	M	-	-	S	L	L	-	-	M	M	
M41	140	9.016	-	-	-	-	S	-	-	S	L	L	-	-	M	L	
M43	137	9.001	-	-	-	-	-	-	-	S	L	L	-	-	L	L	
M45	169	8.976	-	-	-	-	S	-	S	S	L	L	-	-	L	L	
M46	151	9.023	-	-	-	-	S	-	-	S	L	L	-	-	M	L	
M48	171	9.008	-	-	-	-	S	-	S	L	L	-	-	L	M		
M50	168	8.988	-	-	-	-	S	-	-	S	M	L	-	-	S	L	
M51	173	8.993	-	-	-	-	-	-	S	S	S	L	M	M	M	S	Bi in TS
M52	195	9.010	-	M	M	M	-	-	L	M	M	S	-	-	M	S	
M54	119	9.013	-	-	-	-	-	-	-	-	L	L	-	-	S	L	Labradorite
M55	134	9.009	-	-	-	-	-	-	-	S	M	L	-	M	M	M	Bi in TS
M56	222	9.017	-	-	-	-	-	-	-	-	-	-	-	-	S	L	
M57	143	8.984	-	-	-	-	-	-	-	-	L	M	-	-	M	L	
M58	137	8.998	-	-	-	-	S	-	-	S	L	L	-	-	M	M	
M60	196	9.004	-	-	-	-	S	-	S	M	M	S	-	-	S	S	K-Feld
M61	156	8.998	-	-	-	-	-	-	-	L	L	L	-	-	L	L	
M63	171	9.010	-	S	-	-	-	-	M	-	M	M	-	-	M	M	
M65	-	8.981	-	-	-	-	-	-	-	-	-	-	-	-	S	L	
M66	188	8.975	-	M	S	S	S	S	-	L	L	L	S	-	-	S	L
M67	179	8.983	-	-	S	-	-	-	-	S	S	M	-	-	M	M	
M69	179	8.981	-	-	-	-	S	-	-	S	L	L	-	-	L	L	
M70	173	8.983	-	M	-	-	S	-	-	S	L	L	-	-	M	M	
M71	129	8.996	-	-	-	-	-	-	-	S	L	L	S	-	L	L	
M72	154	8.978	-	-	-	-	S	-	-	S	L	L	-	-	L	M	
M73	138	8.978	-	-	S	-	-	-	-	S	L	L	-	-	L	M	

M74	150	8.987	-	-	-	-	-	-	-	L	L	-	-	L	L	
M76	256	8.988	-	-	-	-	-	-	L	L	M	-	-	M	L	
M77	169	8.977	-	S	-	-	-	S	-	S	L	M	-	-	M	L
M78	186	8.974	-	-	-	-	-	-	S	S	S	L	-	-	L	S
M79	183	8.967	-	-	-	-	-	-	S	L	L	-	-	M	L	
M80	119	8.985	-	-	-	-	-	-	-	M	L	-	-	L	L	
M81	145	8.975	-	-	-	-	S	-	-	S	L	L	-	-	L	M
M82	134	8.974	-	-	-	-	-	-	-	M	L	L	-	-	M	L
M83	139	8.975	-	-	-	-	-	-	-	L	L	L	-	-	L	L
M84	119	8.996	-	-	-	-	-	-	-	M	M	L	-	-	M	L
M85	144	-	-	-	-	-	S	-	-	M	M	L	-	-	S	L
M86	142	8.974	-	-	-	-	S	-	-	L	L	L	S	-	L	L
M87	116	8.983	-	-	-	-	-	-	S	L	L	S	-	-	L	L
M88	-	-	S	S	-	-	M	-	S	-	L	M	S	-	M	L
M89	115	8.975	-	-	-	-	-	-	-	L	M	S	-	-	M	L
M90	111	8.998	-	-	-	-	-	-	-	S	L	M	S	-	L	M
M91	129	8.984	-	-	-	-	-	-	-	S	L	L	S	-	M	L
M92	136	9.002	-	-	-	S	-	-	-	S	L	L	-	-	L	L
M93	155	8.987	-	-	-	S	-	-	-	M	L	L	S	-	M	1
M94	142	8.985	-	-	-	-	-	-	-	L	M	L	-	-	L	L
M95	131	8.985	-	-	-	-	-	-	-	L	L	L	S	-	L	L
M96	168	8.967	-	-	-	-	-	-	-	L	L	L	-	-	L	L
M97	117	8.980	-	-	-	-	-	-	-	M	L	L	S	-	L	L
M98	121	8.993	-	-	-	-	-	-	-	M	M	M	-	-	L	L
M99	209	8.988	-	-	-	-	-	-	-	M	L	L	-	-	L	L
M100	164	9.019	-	-	-	-	-	-	-	L	L	L	-	-	M	L
M101	135	9.004	-	-	-	-	-	-	-	M	L	L	-	-	M	L
M102	141	8.988	-	-	-	-	-	-	-	L	L	L	S	-	M	L
M103	136	8.993	-	-	-	-	S	-	-	L	L	L	-	-	L	L
M104	153	8.962	S	-	-	-	-	-	-	S	L	L	-	-	M	M
M105	-	8.965	-	-	-	-	-	-	-	S	S	S	-	-	M	L
M106	132	8.985	-	-	-	-	-	-	-	S	L	L	-	-	M	L
M107	128	8.996	-	-	-	-	S	-	-	M	L	L	-	-	M	L
M108	129	8.977	-	-	-	-	-	S	-	M	L	L	-	-	M	L
M109	143	8.988	-	-	-	-	-	S	-	M	L	M	-	-	L	L
M110	133	8.984	-	-	-	-	-	-	-	L	L	L	-	-	M	L
M111	128	8.985	-	-	-	-	-	-	-	M	M	L	-	-	M	L
M112	126	8.999	-	-	-	-	S	-	-	L	L	L	-	-	M	L
M113	138	8.989	-	-	-	-	-	-	-	L	L	L	-	-	M	L
M114	120	8.999	-	-	-	-	-	-	-	S	L	L	S	-	M	L
M115	129	8.972	-	-	-	-	-	-	-	M	M	L	-	-	M	L
M116	135	8.975	-	-	-	-	-	-	-	M	M	L	-	-	M	L
M117	111	-	-	-	-	-	-	-	-	S	M	M	S	-	S	M
M118	107	8.998	-	-	-	-	-	-	-	S	M	M	-	-	S	M
M119	130	8.992	-	-	-	-	-	-	-	S	L	M	S	-	L	L
M120	135	8.975	-	-	-	-	-	-	-	L	M	L	S	-	S	L
M121	122	8.981	-	-	-	-	-	-	-	M	L	L	M	-	S	M
M122	152	8.981	-	-	-	-	-	-	-	L	L	M	-	-	L	L
M123	158	8.990	-	-	-	-	-	-	-	L	L	M	-	-	L	M
M124	190	8.996	-	-	-	-	-	-	S	L	L	L	-	-	L	M
M125	136	8.989	-	-	-	-	-	-	-	L	L	M	-	-	M	L
M126	138	8.988	-	-	-	-	-	-	-	L	M	L	-	-	M	M
M127	143	8.989	-	-	-	-	-	-	-	L	L	M	-	-	L	L
M128	121	8.980	-	-	-	-	-	-	-	M	L	L	-	-	M	L
M129	159	8.962	-	-	-	-	-	-	-	L	L	L	-	-	M	L
M130	112	8.984	-	-	-	-	-	-	-	S	L	L	L	-	M	S
M131	137	8.976	-	-	-	-	-	-	-	S	L	L	S	-	M	S
M132	138	8.993	-	-	-	-	-	-	-	L	L	S	M	-	S	S
M133	111	8.992	-	-	-	-	-	-	-	S	L	M	S	-	M	L
M134	130	8.984	-	-	-	-	-	-	-	M	M	L	-	-	M	M
M135	155	9.001	-	-	-	-	-	-	-	M	L	L	-	-	M	L
M136	129	8.988	-	-	-	-	-	-	-	M	L	L	S	-	L	S
M137	126	8.992	-	S	-	-	-	-	-	M	L	L	S	-	M	M
M138	188	8.998	-	S	-	-	-	-	-	S	L	S	S	-	L	L
N1	173	9.002	-	S	S	-	S	-	S	L	L	S	-	-	S	M
N2	161	8.988	-	S	-	-	-	-	-	M	L	S	-	-	S	S
N3	298	8.985	-	S	-	-	-	-	-	L	L	L	-	-	S	S
N4	255	8.985	-	S	-	-	-	-	-	L	L	L	-	-	-	-
N5	247	8.962	-	S	-	-	-	-	-	L	L	L	-	-	-	-
N6	271	8.978	-	S	-	-	-	-	-	L	L	L	-	-	S	-
N7	249	8.962	-	S	S	-	-	-	-	L	L	L	-	-	S	M
N8	246	9.011	-	S	S	-	-	-	-	L	L	L	-	-	S	S
N9	219	8.987	-	S	S	-	-	-	-	L	L	L	-	-	S	L
N10	231	8.990	-	S	-	-	-	-	-	L	L	L	-	-	S	S
N11	295	8.997	-	S	S	-	-	-	-	L	L	L	-	-	S	S
NS2	263	8.987	-	-	-	-	-	-	-	-	-	-	-	-	-	-
COM	158	8.974	-	-	-	-	-	-	-	-	-	-	-	-	-	-

Gypsum

APPENDIX 3.4 - Mean b_o values (* = this study) and pressure facies determined by Sassi and Scolari (1974). Comparative data is from Thomas (1986)[#] from the Lake District, Fettes et al. (1976)^{***} from the Scottish Dalradian, and Robinson and Bevins (1986)^{**} from the Welsh Basin.

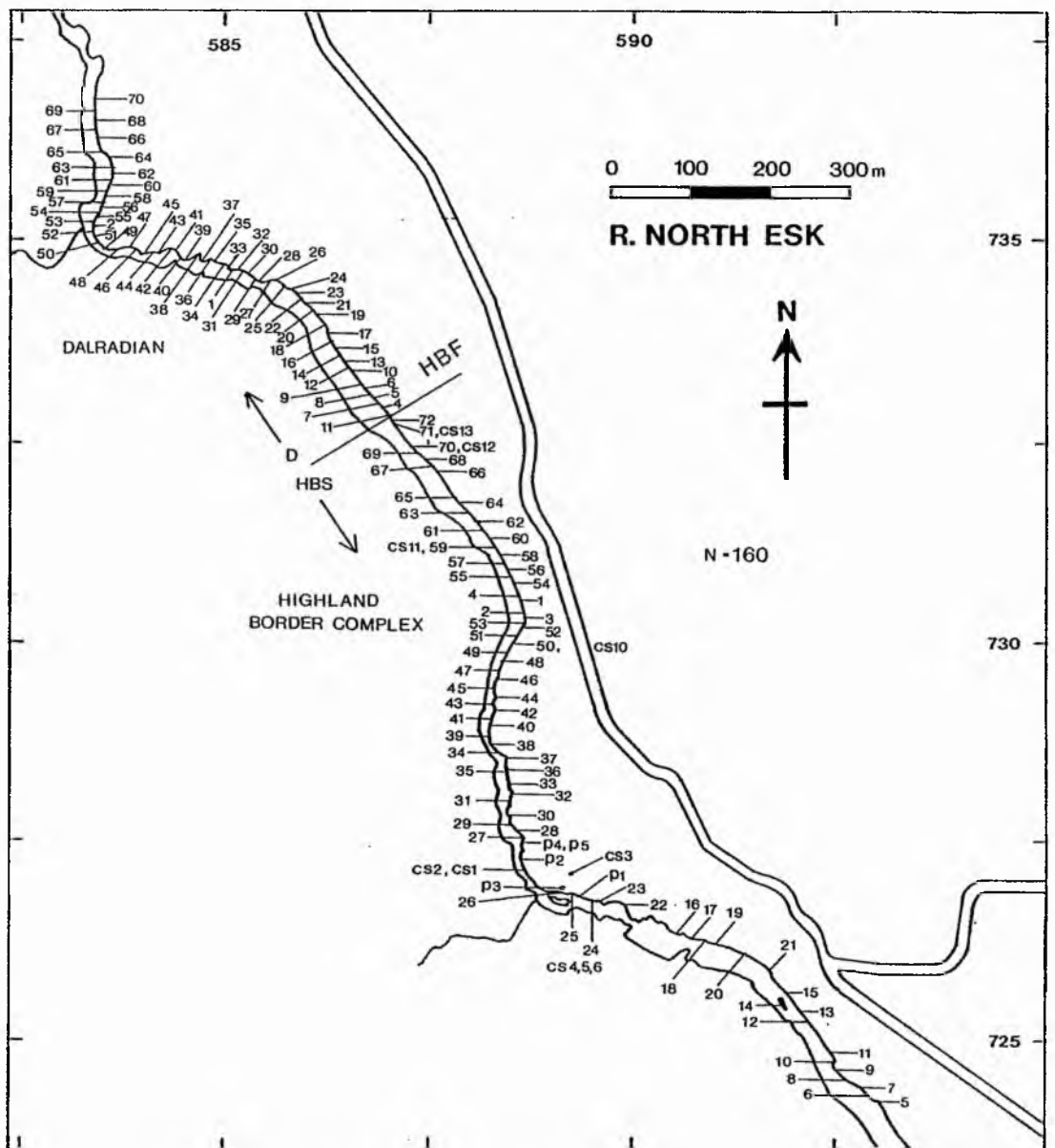
<u>Stratigraphic Unit</u>	<u>SNo.</u>	<u>Mean</u>	<u>PSD</u>	<u>Pressure</u>
Lake District#	46	8.988	0.008	Low
<u>Manx Slate*</u>	120	8.988	0.014	Low
Bosot	132	8.994	0.009	Low
Wales**	c.150	8.995	-	Low
Dalradian***	34	9.003	0.006	Low-Med
Ryoke	46	9.013	0.006	Low-Med
<u>Nepal*</u>				
Kuncha Formation*	30	9.008	0.007	Low-Med
Langtang*	14	9.008	0.008	Low-Med
Kuncha*	16	9.009	0.007	Low-Med
Benighat Slate*	11	9.020	0.009	Med
Kathmandu Klippe*	17	9.032	0.015	Med-High
<u>Glen Esk*</u>				
Dalradian*	12	9.015	0.014	Low-Med
H B C*	12	9.029	0.014	Med
Otago	35	9.039	0.005	Med-High
Sanbagawa	34	9.054	0.006	High

The Kuncha Formation was collected on two traverses 70km apart. PSD = Population Standard Deviation, SNo = Sample number.

APPENDIX 3.5 - Fluid inclusion microthermometric data for samples from the Isle of Man.

Sample	Te (H ₂ O 1st Melt)			Tm H ₂ O (H ₂ O last melt)			Th TOT (Total homogenisation)			
	PSD	M	SNo.	PSD	M	SNo.	PSD	M	SNo.	
FOXDALE										
A	0.96	-31.3	5	0.49	-1.12	6	8.09	191-L	6	
B	1.40	-31.7	2	0.21	-3.27	3	-	300-L	3	
C	-	<-60.0	3	0.05	-13.2	3	2.00	172-L	2	
D	0.52	-6.10	4	0.20	-4.37	6	5.04	232-L	5	
E	-	-48.0	1	-	-22.3	1	-	258-L	1	
F	0.42	-6.13	4	0.15	-2.93	4	1.48	209-L	4	
G	-	-	-	-	-3.70	1	-	283-L	1	
DHOON										
A ₁	1.15	-7.2	5	0.37	-2.72	6	13.85	200-L	14	
A ₂	-	-56.2	2	0.65	-3.25	2	-,	-,	,	
A ₃	2.35	-16.5	8	0.88	-2.61	8	-,	-,	,	
B	0.25	-16.8	2	0.65	-2.95	2	-	-	-	
C	1.67	-16.2	3	0.81	-3.45	4	11.67	264-L	3	
D	1.24	-25.3	3	0.26	-4.17	3	-	183-L	2	
CALF										
SOUND A	A ₁	2.11	-57.0	14	0.93	-12.44	14	11.53	183-L	9
	A ₂	4.62	-46.3	4	1.48	-9.03	4	5.25	179-L	3
	C	0.24	-57.6	3	1.59	-11.6	3	12.05	220-L	4
	D	-	-38.1	1	0.35	-2.05	2	-	163-L	2
	E	-	-35.4	1	-	-1.60	1	-	249-L	1
	F	-	-	-	-	-	-	-	305-L	1
SOUND B	A	1.76	-55.1	7	1.38	-12.64	15	16.90	217-L	9
	B	-	-	-	-	-	-	-	348-L	2
	C	-	-	-	-	-	-	-	299-L	2
	D	-	-	-	-	-	-	-	238-L	2
	E	-	-	-	-	-	-	-	348-V	1
Tm CO₂ (CO₂ last melt)										
FOXDALE	B	0.17	-61.0	3	0.05	8.77	3	0.25	28.5-C	3
DHOON	B	0.10	-62.0	2	0.05	9.25	2	-	12.4-L	1
CALF	SOUND A	B	0.55	-61.35	2	-	-	-	0.6-C	1

PSD: Population Standard Deviation, M: Mean Value (°C), SNo: Sample Number. Samples are subdivided into inclusion population A, B, C, etc. A₁, A₂ etc. is used for inclusion grouped together for some measurements. L: Liquid, V: Vapour, C: Critical behaviour.



APPENDIX 4.1 - Sample locations for samples collected from Glen Esk. Samples from south of the Highland Boundary Fault (HBF) are prefixed with HBC unless otherwise shown. Samples from north of the HBF are prefixed with D.

APPENDIX 4.2 - Electron Microprobe standards.

Si	Wollastonite
Ti	Rutile
Al	Corundum
Fe	Metal
Mn	Metal
Mg	Periclase
Ca	Wollastonite
Na	Jadeite
K	Orthoclase

APPENDIX 4.3 - Electron microprobe analyses.

WHITE MICA

Point	D7 (1)	D7 (2)	D7 (3)	D7 (5)	D7 (6)	D7 (8)	D7 (14)	HBS5 (4)	HBS5 (5)
SiO ₂	47.20	47.10	46.90	47.73	45.14	47.76	47.29	48.11	46.86
TiO ₂	0.27	0.25	0.25	0.32	0.42	0.43	0.28	0.07	0.10
Al ₂ O ₃	28.08	29.32	28.83	31.55	32.11	31.11	31.03	34.54	35.86
FeTOT	4.15	4.11	4.33	3.94	5.27	3.83	4.07	1.49	0.69
MnO	0.07	-	0.10	-	-	-	0.09	-	0.02
MgO	1.65	1.80	1.70	1.61	1.14	1.60	1.61	0.79	0.29
CaO	0.03	-	0.04	0.08	-	-	0.02	0.09	0.08.
Na ₂ O	0.43	0.29	0.30	0.42	0.50	0.28	0.19	0.03	0.09
K ₂ O	10.16	10.69	10.30	10.04	10.65	10.34	10.27	3.99	2.23
TOTAL	92.04	93.55	92.75	95.69	95.19	95.36	94.84	89.11	86.21

Atomic proportions calculated on the basis of 22 oxygen atoms

Si	6.60	6.49	6.52	6.39	6.20	6.43	6.41	4.14	4.10
Ti	0.03	0.03	0.03	0.04	0.05	0.05	0.03	-	-
Al	4.63	4.77	4.72	4.98	5.17	4.93	4.95	3.51	3.70
Fe	0.46	0.48	0.50	0.44	0.61	0.43	0.46	0.04	0.06
Mn	0.01	-	0.01	-	-	-	0.01	-	-
Mg	0.35	0.38	0.35	0.32	0.23	0.32	0.33	0.10	0.04
Ca	-	-	0.01	0.01	-	-	-	0.01	-
Na	0.11	0.07	0.08	0.11	0.13	0.07	0.05	-	0.01
K	1.81	1.88	1.82	1.71	1.90	1.78	1.78	0.58	0.25
TOTAL	14.00	14.09	14.04	14.11	14.23	14.01	14.00	8.24	8.16

WHITE MICA

Point	D7 (17)	D7 (19)	D7 (20)	D7 (23)	D7 (24)	D7 (29)	D7 (31)	D7 (32)	D7 (33)
SiO ₂	47.87	45.79	47.25	46.80	47.05	47.26	47.26	45.56	48.43
TiO ₂	0.29	0.13	0.38	0.37	0.32	0.39	0.55	0.54	0.15
Al ₂ O ₃	30.50	33.21	31.16	30.63	29.46	31.56	30.61	31.49	28.54
FeTOT	4.14	4.31	4.63	4.42	4.65	3.84	4.65	4.06	4.18
MnO	-	0.11	-	0.03	0.01	0.06	-	0.08	-
MgO	1.47	0.88	1.74	1.97	2.02	1.29	1.67	1.35	2.23
CaO	0.05	-	0.05	-	0.07	0.02	0.01	0.03	0.01
Na ₂ O	0.15	0.45	0.17	0.08	0.30	0.36	0.09	0.39	0.41
K ₂ O	10.22	10.45	10.41	10.77	10.38	9.82	10.52	10.18	10.05
TOTAL	94.69	95.32	95.80	95.05	94.29	94.61	95.36	93.67	94.00

Atomic proportions calculated on the basis of 22 oxygen atoms.

Si	6.48	6.23	6.36	6.36	6.43	6.39	6.39	6.27	7.21
Ti	0.03	0.02	0.04	0.04	0.04	0.04	0.06	0.06	0.02
Al	4.86	5.30	4.94	4.90	4.76	5.03	4.69	5.11	4.59
Fe	0.47	0.49	0.52	0.50	0.53	0.44	0.52	0.47	0.48
Mn	-	-	-	-	-	0.01	-	0.01	-
Mg	0.30	0.17	0.35	0.40	0.41	0.27	0.34	0.28	0.46
Ca	0.01	-	0.01	-	0.01	-	-	0.01	-
Na	0.04	0.11	0.05	0.02	0.08	0.09	0.03	0.10	0.11
K	1.77	1.81	1.79	1.87	1.82	1.70	1.81	1.79	1.75
TOTAL	13.96	14.10	14.05	14.10	14.09	13.95	14.03	14.07	14.01

WHITE MICA

Point	D19 (1)	D19 (3)	D19 (6)	D19 (9)	D20 (5)	D20 (6)	D20 (9)	D20 (10)	D34A (2)
SiO ₂	48.96	51.08	49.03	47.57	49.38	47.87	50.44	49.22	46.51
TiO ₂	0.27	0.11	0.30	0.25	0.18	0.63	0.14	0.36	0.44
Al ₂ O ₃	31.00	27.56	31.81	32.44	31.28	32.57	28.09	31.74	31.43
FeTOT	3.65	4.40	2.83	2.99	3.07	2.52	4.39	1.61	4.47
MnO	0.03	0.04	0.01	0.01	-	0.01	0.01	0.03	0.06
MgO	1.63	2.67	0.88	1.18	1.73	1.47	2.87	2.23	1.36
CaO	0.06	0.15	0.04	0.01	-	0.02	0.06	-	0.05
Na ₂ O	0.37	1.17	0.54	0.65	0.48	0.55	0.22	0.51	0.28
K ₂ O	10.14	10.21	9.41	10.10	9.77	10.18	10.19	9.99	10.48
TOTAL	96.10	97.39	94.86	95.21	95.89	95.81	96.41	95.69	95.09

Atomic proportions calculated on the basis of 22 oxygen atoms.

Si	6.38	6.51	6.76	6.54	6.54	6.36	6.49	6.71	6.32
Ti	0.02	0.02	0.02	0.02	0.02	0.06	0.04	0.02	0.05
Al	5.13	4.85	4.29	5.00	4.88	5.11	4.93	4.40	5.03
Fe	0.33	0.39	0.49	0.31	0.33	0.28	0.17	0.49	0.50
Mn	-	-	-	-	-	-	-	-	0.01
Mg	0.24	0.33	0.52	0.17	0.35	0.28	0.44	0.57	0.28
Ca	-	-	0.02	-	-	-	-	-	0.01
Na	0.17	0.09	0.31	0.13	0.13	0.13	0.13	0.66	0.07
K	1.71	1.17	1.71	1.60	1.65	1.71	1.67	1.74	1.82
TOTAL	13.98	13.92	14.12	13.77	13.90	13.94	13.87	14.58	14.08

WHITE MICA

Point	D34A (4)	D34A (7)	D34 (2)	D34 (3)	D34 (8)	D34 (9)	D34 (10)	D34 (12)	D34 (13)
SiO ₂	47.82	47.63	46.79	49.80	49.81	48.46	48.76	46.89	48.01
TiO ₂	0.36	0.26	0.32	0.27	0.20	0.30	0.22	0.24	0.35
Al ₂ O ₃	30.30	30.45	33.53	33.50	33.58	34.94	32.63	34.55	32.71
FeTOT	4.63	5.22	5.72	4.15	3.49	3.20	3.45	3.35	4.33
MnO	-	0.12	0.02	-	-	-	0.01	-	0.03
MgO	1.81	1.71	1.53	0.76	1.11	0.84	1.34	0.62	1.25
CaO	0.02	-	0.02	0.03	0.01	0.01	0.04	0.06	0.01
Na ₂ O	0.05	0.07	0.29	0.41	0.2	0.18	0.01	0.62	1.25
K ₂ O	10.75	10.66	9.25	10.21	10.26	10.41	10.81	9.96	10.83
TOTAL	95.74	96.12	98.24	99.28	98.99	98.97	97.85	96.20	97.67

Atomic proportions calculated on the basis of 22 oxygen atoms.

Si	6.43	6.40	6.25	6.42	6.44	6.34	6.47	6.22	6.33
Ti	0.04	0.03	0.04	0.03	0.02	0.03	0.02	0.03	0.04
Al	4.81	4.83	5.29	5.10	5.13	5.39	5.11	5.40	5.08
Fe	0.52	0.59	0.64	0.45	0.37	0.35	0.38	0.37	0.48
Mn	-	0.02	-	-	-	-	-	-	-
Mg	0.36	0.35	0.30	0.14	0.22	0.16	0.27	0.12	0.25
Ca	-	-	-	-	-	-	-	0.01	-
Na	0.01	0.02	0.07	0.10	0.06	0.05	-	0.14	0.04
K	1.85	1.83	1.58	1.69	1.70	1.74	1.83	1.78	1.82
TOTAL	14.03	14.08	14.17	13.94	13.94	14.05	14.08	14.06	14.02

WHITE MICA

Point	D41 (7)	D41 (8)	D41 (9)	D41 (11)	D49 (7)	D49 (9)	D49 (11)	D49 (12)	D49 (13)
SiO ₂	48.93	48.98	48.82	46.16	49.33	47.02	46.71	46.54	47.62
TiO ₂	0.38	0.33	1.58	1.04	0.19	0.27	0.27	0.41	0.23
Al ₂ O ₃	30.71	30.72	29.08	32.24	31.67	35.53	35.58	35.71	34.07
FeTOT	4.06	3.46	4.24	3.44	2.20	1.85	2.21	2.19	2.25
MnO	0.01	-	-	-	0.04	0.01	-	-	-
MgO	2.02	2.06	2.25	1.19	1.78	0.73	0.76	0.68	1.13
CaO	-	0.03	0.06	0.05	-	0.01	-	-	-
Na ₂ O	0.10	0.10	0.11	0.42	0.27	0.84	0.64	0.72	0.44
K ₂ O	9.20	9.79	9.39	8.99	9.77	9.75	9.67	9.46	9.44
TOTAL	95.41	95.42	95.51	93.53	95.22	96.01	95.81	95.71	95.18

Atomic proportions calculated on the basis of 22 oxygen atoms.

Si	6.51	6.54	6.54	6.27	6.55	6.20	6.17	6.16	6.32
Ti	0.05	0.02	0.15	0.11	0.02	0.03	0.05	0.03	0.02
Al	4.82	4.82	4.57	5.17	4.96	5.52	5.55	5.57	5.33
Fe	0.46	0.38	0.46	0.39	0.25	0.20	0.25	0.24	0.25
Mn	-	-	-	-	0.01	-	-	-	-
Mg	0.39	0.42	0.44	0.24	0.35	0.14	0.14	0.14	0.22
Ca	-	-	-	-	-	-	-	-	-
Na	0.02	0.02	0.02	0.11	0.06	0.22	0.15	0.18	0.12
K	1.54	1.67	1.59	1.54	1.65	1.64	1.63	1.59	1.59
TOTAL	13.81	13.86	13.78	13.85	13.83	13.95	13.99	13.91	13.84

WHITE MICA

Point	D69 (2)	D69 (3)	D69 (4)	D69 (5)	D69 (8)	D69 (11)	D3 (2)	D3 (4)	D3 (9)
SiO ₂	48.88	47.55	49.91	50.28	47.77	47.65	46.04	46.93	46.80
TiO ₂	0.46	0.36	0.20	0.14	0.33	0.31	0.26	1.31	0.23
Al ₂ O ₃	31.13	33.73	30.58	31.18	33.75	33.56	35.10	35.51	34.44
FeTOT	4.23	3.47	4.25	3.71	3.75	3.17	2.75	2.19	2.43
MnO	0.08	0.04	0.07	-	0.02	0.10	-	-	0.01
MgO	2.01	1.20	2.09	2.05	1.22	1.19	0.81	0.68	0.91
CaO	-	0.01	-	-	0.02	0.02	-	0.01	0.03
Na ₂ O	0.04	0.51	0.30	0.43	0.50	0.48	0.68	1.08	0.97
K ₂ O	9.97	9.54	10.10	9.68	9.72	9.67	9.15	9.08	8.47
TOTAL	96.80	96.40	97.51	97.48	97.08	96.16	94.75	96.78	94.29

Atomic proportions calculated on the basis of 22 oxygen atoms.

Si	6.47	6.27	6.55	6.55	6.27	6.32	6.16	6.14	6.25
Ti	0.05	0.05	0.02	0.02	0.05	0.02	0.02	0.13	0.02
Al	4.84	5.26	4.73	4.80	5.23	5.23	5.55	5.48	5.43
Fe	0.46	0.37	0.46	0.39	0.42	0.35	0.33	0.24	0.27
Mn	-	-	-	-	-	-	-	-	-
Mg	0.39	0.24	0.42	0.39	0.24	0.24	0.15	0.13	0.17
Ca	-	-	-	-	-	-	-	-	-
Na	-	0.13	0.06	0.02	0.13	0.13	0.17	0.27	0.24
K	1.65	1.59	1.67	1.59	1.63	1.63	1.54	1.50	1.43
TOTAL	13.88	13.93	13.95	13.78	13.98	13.92	13.93	13.91	13.83

WHITE MICA

Point	D3 (11)	D3 (14)	D3 (15)	HBS5 (1)	HBS5 (2)	HBS5 (6)	HBS5 (7)	HBS5 (8)	HBS5 (11)
SiO ₂	45.97	45.95	46.01	50.99	47.31	50.82	51.33	50.58	49.52
TiO ₂	0.21	0.23	0.24	0.20	0.01	0.14	0.08	0.62	0.10
Al ₂ O ₃	35.40	36.26	35.02	28.80	34.70	28.56	28.71	31.03	29.50
FeTOT	2.15	2.67	2.05	2.08	1.59	3.69	3.70	1.93	3.11
MnO	-	-	-	0.05	0.08	0.06	-	0.08	0.05
MgO	0.55	0.56	0.70	2.86	0.79	2.04	1.86	2.49	1.80
CaO	-	0.04	-	0.02	0.05	0.03	0.11	-	0.06
Na ₂ O	1.28	1.07	1.03	0.03	0.15	0.06	0.05	0.08	0.05
K ₂ O	8.04	8.43	8.48	10.30	9.89	10.32	9.47	10.60	9.46
TOTAL	93.60	95.20	93.52	95.24	94.57	95.72	95.30	97.41	93.68

Atomic proportions calculated on the basis of 22 oxygen atoms.

Si	6.18	6.10	6.18	6.77	6.32	6.77	6.86	6.58	6.69
Ti	0.02	0.02	0.02	0.02	-	0.02	-	0.06	-
Al	5.61	5.67	5.56	4.51	5.45	4.49	4.49	4.75	4.71
Fe	0.23	0.29	0.22	0.24	0.17	0.42	0.42	0.22	0.33
Mn	-	-	-	-	-	-	-	-	-
Mg	0.11	0.11	0.13	0.57	0.12	0.39	0.37	0.49	0.35
Ca	-	-	-	-	-	-	0.02	-	-
Na	0.33	0.27	0.27	-	0.05	0.02	0.02	0.02	0.02
K	1.38	1.43	1.45	1.74	1.67	1.76	1.59	1.76	1.63
TOTAL	13.86	13.99	13.82	13.85	13.81	13.88	13.75	13.88	13.73

WHITE MICA

Point	HBS5 (12)	HBS5 (13)	HBS26 (9)	HBS26 (11)	HBS72 (1)	HBS72 (3)	HBS72 (4)
SiO ₂	48.47	49.88	51.23	51.18	48.18	48.96	48.01
TiO ₂	0.40	0.13	0.04	0.07	0.11	0.16	0.08
Al ₂ O ₃	32.52	29.20	27.02	24.25	30.17	30.74	28.79
FeTOT	2.98	3.66	4.70	5.10	3.53	3.60	3.43
MnO	0.12	-	-	0.01	0.01	0.02	0.03
MgO	1.36	1.85	3.16	3.17	1.77	1.75	2.07
CaO	-	0.03	0.10	0.12	0.09	0.05	0.05
Na ₂ O	0.19	0.08	0.05	1.12	0.22	0.13	0.16
K ₂ O	10.71	10.41	9.83	9.16	8.59	9.91	9.84
TOTAL	96.75	95.23	96.12	94.18	92.67	94.52	91.45

Atomic proportions calculated on the basis of 22 oxygen atoms.

Si	6.40	6.69	6.86	6.98	6.58	6.55	6.65
Ti	0.05	0.02	-	-	0.02	0.02	-
Al	5.06	4.62	4.24	3.82	4.86	4.86	4.71
Fe	0.33	0.42	0.53	0.57	0.39	0.39	0.39
Mn	0.02	-	-	-	-	-	-
Mg	0.27	0.37	0.62	0.74	0.35	0.35	0.64
Ca	-	-	0.02	0.02	0.02	-	-
Na	0.05	0.02	0.02	0.29	0.06	0.05	0.05
K	1.80	1.78	1.67	1.57	1.49	1.54	1.54
TOTAL	13.97	13.93	13.92	14.07	13.78	13.78	14.00

APPENDIX 4.4 - Electron microprobe analyses.

CHLORITE

Point	D7 (4)	D7 (9)	D7 (10)	D7 (11)	D7 (12)	D7 (13)	D7 (18)	D7 (21)	D7 (22)
SiO ₂	26.37	25.61	24.02	24.92	25.98	26.13	25.53	25.42	25.22
TiO ₂	0.06	0.12	0.02	0.01	0.07	0.08	0.08	0.07	0.09
Al ₂ O ₃	21.07	21.77	20.04	20.67	20.87	20.70	20.83	20.66	20.95
FeO*	21.70	21.45	41.26	39.91	22.77	25.40	24.84	25.45	30.52
MnO	0.21	0.23	0.01	0.07	0.27	0.29	0.19	0.15	0.11
MgO	18.38	18.32	4.19	4.17	17.58	17.15	15.12	14.34	11.73
CaO	-	0.03	0.03	0.03	-	0.01	-	0.04	0.09
Na ₂ O	-	-	0.08	-	-	-	-	-	-
K ₂ O	0.02	0.02	-	0.04	0.01	-	-	0.09	0.12
TOTAL	87.82	87.55	89.64	89.81	87.64	89.75	86.59	86.23	86.82

Atomic proportions calculated on the basis of 28 oxygen atoms.

Si	5.44	5.30	5.41	5.53	5.40	5.38	5.44	5.46	5.39
Ti	0.01	0.01	-	-	0.01	0.01	0.01	0.01	0.01
Al	5.12	5.31	5.32	5.41	5.14	5.02	5.23	5.23	5.28
Fe ²⁺	3.74	3.71	7.77	7.41	3.96	4.37	4.43	4.57	5.46
Mn	0.04	0.04	-	0.01	0.05	0.05	0.04	0.03	0.02
Mg	5.65	5.65	1.41	1.38	5.45	5.26	4.80	4.59	3.74
Ca	-	0.01	0.01	0.01	-	-	-	0.01	0.02
Na	-	-	0.03	-	-	-	-	-	-
K	0.01	0.01	-	0.01	-	-	-	0.03	0.04
TOTAL	20.01	20.04	19.95	19.76	20.01	20.09	19.95	19.93	19.96

* Total iron taken as FeO.

CHLORITE

Point	D7 (26)	D7 (27)	D19 (12)	D19 (13)	D19 (14)	D19 (15)	D20 (7)	D3 (5)	HBS3 (4)
SiO ₂	25.18	25.46	24.79	25.39	25.38	25.69	25.40	24.82	29.06
TiO ₂	0.03	0.03	0.04	0.02	0.07	0.11	0.14	0.03	0.03
Al ₂ O ₃	20.83	20.33	21.41	20.93	20.55	20.64	20.90	20.04	19.12
FeO*	26.93	25.48	30.00	29.80	32.17	31.46	27.72	28.35	16.11
MnO	0.15	0.30	0.46	0.26	0.37	0.35	0.41	0.15	0.38
MgO	15.10	14.42	11.41	12.18	10.34	11.37	12.11	10.55	21.97
CaO	0.02	0.02	0.06	0.02	0.02	0.06	0.03	0.04	0.05
Na ₂ O	0.01	0.12	-	0.05	0.02	-	0.01	0.07	0.02
K ₂ O	0.04	0.04	-	0.02	0.03	0.02	0.02	0.03	-
TOTAL	88.29	86.19	88.18	88.66	88.95	89.70	86.73	84.15	86.89

Atomic proportions calculated on the basis of 28 oxygen atoms.

Si	5.32	5.48	5.35	5.43	5.46	5.46	5.49	5.57	5.85
Ti	0.01	-	-	-	-	0.03	0.03	-	-
Al	5.19	5.17	5.43	5.26	5.24	5.18	5.32	5.19	4.54
Fe ²⁺	4.76	4.59	5.40	5.32	5.80	5.60	5.01	5.32	2.72
Mn	0.03	0.06	0.08	0.06	0.06	0.06	0.08	0.03	0.06
Mg	4.76	4.63	3.67	3.86	3.33	3.61	3.89	3.53	6.61
Ca	-	0.01	0.03	-	-	0.03	-	-	-
Na	0.04	0.05	-	0.03	-	-	-	0.03	-
K	0.01	0.01	-	-	-	-	-	-	-
TOTAL	20.12	20.00	19.96	19.96	19.89	19.97	19.82	19.67	19.78

* Total iron taken as FeO.

CHLORITECHLORITE after BIOTITE

Point	D34A (1)	D34A (3)	D34B (4)	D34A (5)	D34A (6)	D34B (6)	D34B (7)	D34B (11)	D49 (1)
SiO ₂	27.76	25.54	25.15	26.34	28.25	29.63	25.49	25.84	28.62
TiO ₂	0.74	0.11	0.08	0.71	1.20	1.20	0.11	0.25	0.41
Al ₂ O ₃	18.66	19.56	22.11	18.67	18.15	19.33	20.03	18.70	19.97
FeO*	31.92	34.19	31.77	33.06	33.43	31.36	34.51	32.44	29.11
MnO	0.20	0.24	0.34	0.25	0.14	0.53	0.28	0.25	0.24
MgO	7.40	7.24	10.93	7.53	6.57	6.89	9.51	9.88	8.77
CaO	0.06	0.19	0.04	0.01	0.04	0.12	0.04	0.01	0.05
Na ₂ O	-	0.10	-	-	-	0.06	0.18	0.11	0.04
K ₂ O	1.64	0.44	0.14	1.02	2.09	2.94	0.31	0.26	1.66
TOTAL	88.38	87.60	90.55	87.59	89.86	91.59	90.62	87.74	88.87 .

Atomic proportions calcualted on the basis of 28 oxygen atoms.

Si	6.04	5.68	5.30	5.83	6.10	6.20	5.54	5.68	6.07
Ti	0.12	0.02	0.01	0.12	0.08	0.19	0.02	0.04	0.07
Al	4.78	5.12	5.50	4.87	4.62	4.77	5.13	4.84	4.99
Fe ²⁺	5.81	6.35	5.60	6.10	6.04	5.49	6.27	5.96	5.17
Mn	0.04	0.04	0.06	0.05	0.03	0.01	0.05	0.05	0.04
Mg	2.40	2.40	3.44	2.48	2.12	2.15	3.08	3.24	2.78
Ca	0.02	0.05	0.01	-	0.01	0.03	0.01	-	0.01
Na	-	0.04	-	-	-	0.02	0.06	0.05	0.02
K	0.46	0.12	0.04	0.29	0.58	0.79	0.01	0.07	0.45
TOTAL	19.67	19.82	19.96	19.74	19.58	19.65	20.17	19.93	19.60

* Total iron taken as FeO.

CHLORITE

Point	D49 (5)	D49 (6)	D49 (10)	D41 (3)	D41 (4)	D69 (6)	D69 (7)	D69 (10)	HBS3 (10)
SiO ₂	25.45	24.77	26.18	25.26	26.47	24.80	25.88	25.36	29.62
TiO ₂	0.11	0.04	0.16	0.03	0.08	0.16	0.05	0.06	0.01
Al ₂ O ₃	21.14	23.09	20.06	18.21	18.28	20.11	19.47	21.16	17.77
FeO*	26.82	28.14	30.79	36.52	36.35	28.73	30.71	25.08	15.44
MnO	0.29	0.33	0.27	0.10	0.02	0.39	0.35	0.45	0.29
MgO	12.58	12.43	10.92	6.39	5.69	11.50	11.84	14.37	21.84
CaO	0.03	0.01	0.04	0.04	0.04	0.01	0.03	0.02	0.79
Na ₂ O	-	0.07	-	0.05	-	-	0.06	0.02	0.03
K ₂ O	0.02	-	0.14	0.02	0.37	0.02	0.02	0.03	-
TOTAL	88.46	88.88	88.55	86.62	87.29	85.72	88.41	86.55	85.87

Atomic proportions calculated on the basis of 28 oxygen atoms.

Si	5.48	5.22	5.62	5.74	5.96	5.46	5.57	5.40	6.05
Ti	0.02	0.01	0.03	-	-	0.03	-	-	-
Al	5.37	5.74	5.08	4.87	4.84	5.24	5.96	5.32	4.28
Fe ²⁺	4.83	4.96	5.53	6.94	6.83	5.29	5.54	4.48	2.63
Mn	0.05	0.06	0.05	0.03	-	0.08	0.06	0.08	0.06
Mg	4.04	3.90	3.49	2.16	1.90	3.78	3.81	4.56	6.64
Ca	0.01	-	0.01	-	-	-	-	-	0.17
Na	-	0.03	-	0.03	-	-	0.03	-	-
K	0.01	-	0.04	-	0.11	-	-	-	-
TOTAL	19.81	19.92	19.85	19.77	19.64	19.88	20.97	19.84	19.83

* Total iron taken as FeO.

CHLORITE

Point	P1B (2)	P1B (8)	P1B (9)	P5 (2)	P5 (6)	P5 (12)	P5 (13)	HBS29 (8)	HBS29 (14)
SiO ₂	28.53	28.22	28.27	28.88	27.78	28.13	28.69	27.82	27.36
TiO ₂	-	-	-	-	0.01	-	-	0.01	0.01
Al ₂ O ₃	17.38	18.30	19.29	19.66	19.15	18.32	18.99	18.61	18.06
FeO*	18.30	17.60	17.86	20.41	20.66	19.97	20.54	27.49	25.50
MnO	0.36	0.24	0.17	0.27	0.26	0.28	0.24	0.31	0.40
MgO	19.50	20.38	20.26	19.14	18.40	18.97	18.60	15.47	14.76
CaO	0.15	0.10	0.07	0.13	0.12	0.10	0.16	0.11	0.20
Na ₂ O	0.03	-	-	0.01	0.06	0.04	-	0.05	0.11
K ₂ O	0.03	0.01	0.03	0.03	0.03	0.02	0.03	0.01	0.03
TOTAL	84.28	84.85	85.93	88.51	86.46	85.82	87.24	89.88	86.43

Atomic proportions calculated on the basis of 28 oxygen atoms.

Si	6.02	5.88	5.82	5.82	5.77	5.88	5.91	5.77	5.85
Ti	-	-	-	-	-	-	-	-	-
Al	4.31	4.51	4.68	4.68	4.70	4.51	4.59	4.54	4.56
Fe ²⁺	3.22	3.08	3.08	3.44	3.58	3.50	3.53	4.76	4.56
Mn	0.06	0.06	0.03	0.06	0.06	0.06	0.03	0.06	0.03
Mg	6.13	6.33	6.22	5.77	5.71	5.91	5.71	4.79	4.98
Ca	0.03	0.03	0.03	0.03	0.03	0.03	0.03	0.03	0.06
Na	-	-	-	-	0.03	0.03	-	-	-
K	-	-	-	-	-	-	-	-	-
TOTAL	19.77	19.89	19.86	19.80	19.88	19.92	19.80	19.95	20.04

* Total Iron taken as FeO.

APPENDIX 4.5 Electron microprobe analyses.

BIOTITE

Point	D19 (7)	D19 (8)	D19 (10)	D19 (11)	D19 (16)	D19 (17)	D49 (2)	D49 (3)	D49 (4)
SiO ₂	35.81	34.67	35.49	35.61	35.59	35.80	34.81	34.87	35.36
TiO ₂	1.80	1.96	1.44	1.61	1.36	1.53	1.59	1.64	1.88
Al ₂ O ₃	17.99	17.48	18.09	18.01	18.03	18.00	18.47	18.67	18.38
FeTOT	23.39	23.50	25.13	23.74	21.35	24.13	21.18	20.93	21.36
MnO	0.19	0.17	0.14	0.16	0.18	0.25	0.14	0.21	0.17
MgO	7.41	7.33	7.47	7.36	7.57	7.26	8.88	8.32	8.12
CaO	0.06	0.04	0.07	0.04	0.05	0.05	-	0.06	0.02
Na ₂ O	-	-	0.15	-	0.07	0.12	0.09	0.38	-
K ₂ O	8.63	8.31	9.04	9.20	9.40	9.04	8.37	8.60	9.00
TOTAL	95.27	93.48	97.02	95.73	93.60	96.17	93.53	93.69	94.29

Atomic proportions calculated on the basis of 22 oxygen atoms.

Si	5.48	5.52	5.45	5.50	5.56	5.52	5.43	5.44	5.48
Ti	0.24	0.20	0.18	0.20	0.16	0.17	0.18	0.19	0.22
Al	3.25	3.28	3.28	3.28	3.32	3.25	3.39	3.43	3.36
Fe	3.10	3.02	3.23	3.06	2.80	3.06	2.76	2.73	2.77
Mn	0.02	0.02	0.02	0.02	0.02	0.02	0.02	0.03	0.02
Mg	1.71	1.70	1.71	1.70	1.76	1.67	2.06	1.93	1.88
Ca	-	-	0.02	-	-	-	-	0.01	-
Na	-	-	0.05	-	0.02	0.05	0.03	0.12	-
K	1.67	1.70	1.76	1.81	1.87	1.78	1.67	1.71	1.78
TOTAL	15.47	15.44	15.70	15.57	15.53	15.56	15.54	15.59	15.51

BIOTITE

Point	D20 (1)	D20 (2)	D20 (8)	D20 (11)	D3 (3)	D3 (8)	D3 (11)
SiO ₂	35.95	34.22	35.02	33.33	32.83	34.16	34.47
TiO ₂	1.54	1.52	1.57	1.74	1.45	1.48	1.56
Al ₂ O ₃	18.48	18.03	18.38	17.94	18.82	18.33	18.32
FeTOT	21.11	23.50	21.42	23.21	23.96	21.89	21.96
MnO	0.16	0.19	0.17	0.13	0.13	0.14	0.12
MgO	7.75	7.98	7.64	8.02	7.68	7.70	7.59
CaO	0.02	0.07	-	0.07	-	-	-
Na ₂ O	0.06	0.04	0.02	0.14	0.05	0.04	0.13
K ₂ O	8.51	7.84	8.41	7.07	6.68	8.88	8.65
TOTAL	93.58	93.38	92.62	91.65	91.60	92.59	95.80

Atomic proportions calculated on the basis of 22 oxygen atoms.

Si	5.59	5.39	5.50	5.34	5.28	5.44	5.45
Ti	0.17	0.17	0.17	0.22	0.17	0.17	0.22
Al	3.39	3.35	3.41	3.39	3.57	3.43	3.41
Fe	2.75	3.10	2.81	3.10	3.21	2.91	2.86
Mn	0.02	0.02	0.02	0.02	0.02	0.02	-
Mg	1.81	1.87	1.78	1.92	1.85	1.82	1.87
Ca	-	0.02	-	0.02	-	-	-
Na	0.02	0.02	-	0.05	0.02	-	0.27
K	1.70	1.59	1.70	1.45	1.37	1.81	1.43
TOTAL	15.45	15.53	15.39	15.51	15.49	15.85	15.52

APPENDIX 4.6 - Electron microprobe analyses.

<u>TOURMALINE</u>	<u>ACTINOLITE</u>							
Point	D7 (15)	D7 (16)	D7 (25)	D19 (2)	D69 (9)	HBS3 (3)	HBS3 (6)	HBS57 (14)
SiO ₂	36.08	36.64	36.02	36.44	35.72	56.37	55.86	54.99
TiO ₂	0.42	0.05	0.57	0.61	0.52	-	0.01	0.05
Al ₂ O ₃	30.10	31.02	29.36	33.98	28.94	0.29	0.86	1.45
FeTOT*	10.24	8.93	8.03	5.71	11.82	7.51	7.79	10.25
MnO	-	0.03	0.01	0.05	0.06	0.15	0.25	0.26
MgO	6.40	6.21	7.77	6.60	5.31	19.61	18.93	16.46
CaO	0.18	0.03	1.03	0.80	0.25	12.79	13.25	12.12
Na ₂ O	2.38	2.75	2.19	1.93	2.53	0.07	0.12	0.48
K ₂ O	0.04	0.01	0.04	0.05	0.05	0.02	0.01	0.05
TOTAL	85.83	85.66	85.20	86.17	85.20	96.93	97.17	96.15

Atomic proportions calculated on the basis of 31 oxygen atoms for tourmaline and 23 oxygen atoms for actinolite.

Si	7.63	7.69	7.63	7.47	7.69	7.96	7.91	7.94
Ti	0.07	0.01	0.09	0.09	0.09	-	-	-
Al	7.50	7.68	7.33	8.22	7.35	2.19	2.20	2.21
Fe ²⁺	1.81	1.57	1.42	0.99	2.14	0.90	0.92	1.24
Mn	-	0.01	-	-	-	0.02	0.02	0.02
Mg	2.02	1.94	2.45	2.02	1.71	4.14	4.00	3.54
Ca	0.04	0.01	0.23	0.19	0.06	1.93	2.00	1.86
Na	0.98	1.12	0.90	0.78	1.05	0.02	0.02	0.14
K	0.01	-	0.01	-	-	-	-	-
TOTAL	20.05	20.03	20.05	19.76	20.09	17.16	17.07	16.95

*FeTOT taken as FeO for actinolites.

APPENDIX 4.7 - Electron microprobe analyses.

GRANDITIC GARNET					ALMANDINE		
Point	P5 (1)	P5 (7)	P5 (8)	P5 (9)	D3 (1)	D3 (6)	D3 (10)
SiO ₂	36.31	36.59	36.51	36.13	36.42	37.71	36.58
TiO ₂	0.58	0.47	0.99	0.80	0.08	-	0.05
Al ₂ O ₃	9.66	10.05	9.53	9.30	20.37	21.26	20.33
Fe ₂ O ₃ *	15.52	15.08	15.30	16.07	-	-	-
FeO*	-	-	-	-	29.53	33.01	27.38
MnO	0.21	0.11	0.19	0.16	6.93	6.54	7.33
MgO	0.13	0.09	0.08	0.14	1.47	1.55	1.36
CaO	33.84	34.62	33.96	33.97	2.18	2.02	2.15
Na ₂ O	-	0.02	-	-	0.02	-	-
K ₂ O	0.01	0.01	-	-	-	-	-
TOTAL	96.25	97.02	96.55	96.57	97.01	102.10	95.18

Atomic proportions on the basis of 24 oxygen atoms

Si	6.22	6.19	6.22	6.19	6.07	6.00	6.14
Ti	0.07	0.05	0.12	0.10	-	-	-
Al	1.94	2.02	1.92	1.87	4.01	3.98	4.03
Fe ³⁺	2.23	2.14	2.18	2.30	-	-	-
Fe ²⁺	-	-	-	-	4.10	4.39	3.86
Mn	0.02	0.02	0.02	0.02	0.98	0.89	1.06
Mg	0.02	0.02	0.02	0.05	0.36	0.36	0.34
Ca	6.22	6.29	6.19	6.26	0.38	0.34	0.38
Na	-	-	-	-	-	-	-
K	-	-	-	-	-	-	-
SUM	16.72	16.73	16.67	16.79	15.90	15.96	15.81

* Fe TOT taken as Fe O or FeO where appropriate.

APPENDIX 4.8 - Electron microprobe analyses.

<u>EPIDOTE</u>										<u>PUMPELLYITE</u>	
Point	HBS3 (1)	HBS3 (5)	HBS3 (9)	HBS57 (17)	HBS29 (1)	HBS29 (2)	P5 (3)	P5 (14)	HBS57 (16)		
SiO ₂	37.79	37.54	37.72	37.45	38.69	38.21	38.24	37.98	36.23		
TiO ₂	-	0.05	0.02	0.02	0.14	0.03	0.04	0.04	0.02		
Al ₂ O ₃	22.27	22.26	22.67	22.45	24.59	24.06	24.17	22.98	23.60		
FeO*	11.99	11.58	12.66	12.52	10.82	11.42	10.64	12.06	6.29		
MnO	0.08	0.15	0.10	-	0.20	0.03	0.07	0.17	0.06		
MgO	0.18	0.13	0.16	0.01	0.07	-	0.02	0.36	1.97		
CaO	23.23	23.00	22.87	23.65	23.38	23.29	22.80	21.96	22.24		
Na ₂ O	0.02	0.02	-	-	-	-	-	0.0	0.01		
K ₂ O	-	-	0.02	-	0.02	0.03	-	0.02	0.01		
TOTAL	95.56	94.73	96.22	96.11	97.90	97.05	95.97	95.57	90.55		

Atomic proportions calculated on the basis of 12.5 oxygen atoms for epidotes, and 16 cations for pumellyite.

Si	3.15	3.15	3.13	3.12	3.12	3.12	3.13	3.15	5.99
Ti	-	-	-	-	0.01	-	-	-	0.01
Al	2.19	2.20	2.21	2.20	2.33	2.31	2.34	2.24	4.60
Fe ²⁺	0.84	0.81	0.88	0.88	0.73	0.78	0.73	0.84	0.87
Mg	-	0.01	0.01	-	0.01	-	-	0.01	0.08
Mn	0.03	0.01	0.03	-	0.01	-	-	0.05	0.49
Ca	2.08	2.06	2.03	2.10	2.01	2.04	2.00	1.95	3.94
Na	-	-	-	-	-	-	-	-	-
K	-	-	-	-	-	-	-	-	-
TOTAL	8.29	8.24	8.29	8.30	8.22	8.25	8.20	8.24	16.00

APPENDIX 4.9

FELDSPAR - Ao = anorthoclase, Ab = albite.

Point	Ao D7 (1)	Ab D20 (4)	Ab D34B (1)	Ab D41 (2)	Ab D41 (5)	Ab D41 (6)	Ab D69 (1)
SiO ₂	68.82	63.21	66.87	67.72	67.20	64.73	62.24
TiO ₂	0.10	0.06	0.01	0.03	0.01	0.01	0.01
Al ₂ O ₃	17.04	22.87	21.21	20.80	20.49	19.11	20.03
FeTOT	1.33	0.47	0.58	0.50	0.31	0.33	0.32
MnO	-	-	-	-	0.08	-	0.02
MgO	0.46	0.37	-	0.05	0.01	0.01	0.03
CaO	0.01	0.85	1.75	0.04	0.03	0.07	1.24
Na ₂ O	6.89	9.46	11.07	11.40	11.76	10.43	10.35
K ₂ O	2.64	1.56	0.06	0.07	0.03	0.04	0.13
TOTAL	97.27	98.85	101.96	100.61	99.90	94.73	94.37

Atomic proportions calculated on the basis of 32 oxygen atoms.

Si	12.37	11.30	11.68	11.78	11.78	11.94	11.62
Ti	0.01	-	-	-	-	-	-
Al	3.60	4.83	4.37	4.26	4.22	4.16	4.42
Fe	0.20	0.06	0.08	0.06	0.03	0.06	0.06
Mn	-	-	-	-	-	-	-
Mg	0.12	0.10	-	-	-	-	-
Ca	-	0.16	0.33	-	-	-	0.26
Na	2.40	3.26	3.75	3.84	4.00	3.71	3.74
K	0.61	0.35	0.01	-	-	-	0.03
TOTAL	19.31	20.06	20.22	19.94	20.03	19.87	20.13

FELDSPARS - Ab = albite, Lb = labradorite, S = sanidine.

Point	Ab HBS26 (12)	Ab P5 (4)	Ab P5 (10)	Lb HBS29 (5)	S HBS5 (3)	Ab P1B (7)	S P1B (6)
SiO ₂	67.45	66.71	67.79	49.21	61.15	72.03	64.81
TiO ₂	0.02	0.04	0.03	0.06	0.12	0.03	0.09
Al ₂ O ₃	20.29	22.41	22.39	26.67	20.64	16.33	18.32
FeTOT	0.12	0.37	0.25	2.22	3.36	1.34	0.39
MnO	0.01	0.02	-	0.07	0.02	0.03	0.02
MgO	-	0.02	0.02	0.47	1.15	0.61	0.32
CaO	0.09	2.35	1.82	16.06	-	0.28	0.40
Na ₂ O	11.53	10.19	10.40	4.19	0.20	8.60	0.98
K ₂ O	0.05	0.07	0.04	-	8.67	0.04	14.80
TOTAL	99.54	102.18	102.74	98.97	95.57	99.30	110.12

Atomic proportions calculated on the basis of 32 oxygen atoms.

Si	11.84	11.49	11.58	9.28	11.55	12.34	11.94
Ti	-	-	-	-	0.03	-	-
Al	4.19	4.54	4.51	5.92	4.61	3.36	3.97
Fe	0.03	0.06	0.03	0.35	0.58	0.19	0.06
Mn	-	-	-	-	-	-	-
Mg	-	-	-	0.13	0.32	0.10	0.09
Ca	0.45	0.49	0.32	3.23	-	0.16	0.06
Na	3.39	3.39	3.46	1.54	0.06	3.26	0.35
K	-	-	-	-	2.08	0.35	3.49
TOTAL	19.90	19.97	19.90	20.45	19.20	19.76	19.96

APPENDIX 4.10

CLINOPYROXENE

Point	HBS29 (3)	HBS29 (4)	HBS29 (7)	HBS29 (9)	HBS29 (10)	HBS29 (11)	HBS29 (12)	HBS29 (13)
SiO ₂	50.85	49.89	49.82	50.39	49.69	49.87	50.27	49.23
TiO ₂	1.01	0.94	1.07	1.08	1.01	1.05	1.07	1.02
Al ₂ O ₃	2.95	3.22	3.23	3.25	3.20	2.79	3.22	3.92
FeO*	12.64	10.63	12.00	10.76	10.87	13.89	11.52	9.69
MnO	0.38	0.23	0.34	0.27	0.28	0.31	0.28	0.26
MgO	13.51	13.55	13.43	13.76	13.72	13.42	13.68	13.07
CaO	19.39	18.55	19.21	19.77	19.29	17.31	19.18	20.29
Na ₂ O	0.33	0.31	0.38	0.27	0.23	0.40	0.42	0.26
K ₂ O	-	0.03	0.01	-	0.01	-	0.01	-
TOTAL	101.07	97.44	99.48	99.51	98.31	99.04	99.65	97.84

Atomic proportions calculated on the basis of 6 oxygen atoms.

Si	1.90	1.90	1.89	1.90	1.90	1.91	1.90	1.88
Ti	0.03	0.03	0.03	0.03	0.03	0.03	0.03	0.03
Al	0.13	0.14	0.14	0.14	0.14	0.13	0.14	0.17
Fe ²⁺	0.40	0.34	0.38	0.34	0.35	0.44	0.37	0.31
Mn	0.01	0.01	0.01	0.01	0.01	0.01	0.01	0.01
Mg	0.75	0.77	0.76	0.77	0.78	0.76	0.77	0.74
Ca	0.77	0.78	0.78	0.80	0.79	0.71	0.77	0.83
Na	0.02	0.02	0.03	0.02	0.02	0.03	0.03	0.02
K	-	-	-	-	-	-	-	-
TOTAL	4.01	3.99	4.02	4.02	4.02	4.02	4.02	3.99

* Total iron taken as FeO.

CLINOPYROXENE

Point	P5 (11)	HBS3 (2)	HBS3 (7)	HBS3 (8)	HBS3 (11)	HBS57 (13)
SiO ₂	47.30	52.17	51.24	52.67	52.88	50.72
TiO ₂	1.71	0.45	0.46	0.42	0.44	0.66
Al ₂ O ₃	6.80	1.91	3.74	2.13	2.11	4.17
FeO*	10.01	6.81	4.80	4.87	5.64	6.06
MnO	0.25	0.24	0.18	0.08	0.16	0.16
MgO	11.18	16.99	16.79	17.66	17.12	15.99
CaO	20.84	20.79	22.16	21.66	21.63	21.45
Na ₂ O	0.52	0.20	0.22	0.18	0.16	0.21
K ₂ O	0.01	0.01	-	-	0.01	0.01
TOTAL	98.63	99.59	100.39	99.90	100.36	99.54

Atomic proportions calculated on the basis of 6 oxygen atoms.

Si	1.81	1.93	1.88	1.93	1.93	1.88
Ti	0.05	0.01	0.01	0.01	0.01	0.02
Al	0.31	0.08	0.16	0.09	0.09	0.18
Fe ²⁺	0.32	0.21	0.15	0.17	0.17	0.19
Mn	0.01	0.01	0.01	-	0.01	0.01
Mg	0.64	0.94	0.94	0.92	0.97	0.94
Ca	0.85	0.82	0.87	0.85	0.85	0.85
Na	0.04	0.01	0.02	0.01	0.01	0.01
K	-	-	-	-	-	-
TOTAL	4.03	4.01	4.05	3.98	4.04	4.08

* Total iron taken as FeO.

APPENDIX 4.11 - XRD analyses of samples (<2µm size fraction) from Glen Esk.

1 = Kaolinite; 2 = Illite/Smectite; 3 = Chlorite/Smectite; 4 = Pyrophyllite; 5 = 1M mica, 6 = 1Md, K, Na Mica; 7 = 6:4 Muscovite/Paragonite; 8 = Paragonite; 9 = 2M, Mica; 10 = Albite; 11 = Biotite; 12 = Chlorite.

S, M and L (small, medium and large) indicates a visual estimate of mineral proportions based on relative peak sizes. TS = thin section. Thin sections were also made for HBS22, HBS26, HBS29, HBS46, HBS62, HBS65, HBS71, P1 to P5, and CS1 to 15.

Highland Border Complex

Sample	Hbre1	b ₀	1	2	3	4	5	6	7	8	9	10	11	12	Lithology	TS
HBS1	117	-	-	-	S	-	-	S	M	L	-	-	L	Green pelite	yes	
HBS2	110	9.034	-	-	-	-	-	-	S	L	M	-	L	,, (+ act)	yes	
HBS3	-	-	S	S	S	-	S	-	M	S	S	-	L	,, (+ act and CPX)	yes	
HBS4	126	9.046	-	-	-	-	-	-	-	L	M	-	M	Purple shale (+ he)	yes	
HBS5	129	-	-	S	S	-	-	-	-	L	-	-	M	Psammite	yes	
HBS8	157	9.016	L	-	-	-	M	-	-	L	-	-	-	,		
HBS9	153	9.038	M	-	-	-	M	-	S	L	-	-	S	,		
HBS10	135	9.032	-	-	-	-	M	-	M	L	-	-	S	,		
HBS12	153	-	L	S	-	S	-	L	-	S	S	-	S	,	yes	
HBS13	152	9.013	L	S	-	-	-	S	S	L	-	-	S	,		
HBS17	226	9.006	M	L	M	L	S	L	L	-	-	-	S	,		
HBS19	207	9.052	L	L	L	M	L	L	L	-	-	-	S	,		
HBS20	155	-	M	S	-	M	-	M	L	S	-	-	-	,		
HBS25	172	9.026	M	M	-	-	L	-	-	M	M	-	M	Dolomitic shale		
HBS29	-	-	S	-	-	-	-	-	-	L	-	L	M	CPX Lava		
HBS30	122	9.032	-	-	S	-	-	-	-	L	M	-	M	,		
HBS42	143	-	-	S	-	S	-	M	-	M	M	-	L	Purple shale (+ cc, ep)	yes	
HBS51	157	-	-	S	-	S	-	L	-	S	S	-	L	,	yes	
HBS53	136	-	-	S	-	S	S	L	-	S	S	-	M	,	yes	
HBS55	147	9.034	-	-	-	-	M	-	S	S	M	-	L	Green pelite (+ act)		
HBS57	-	-	-	S	M	-	-	S	-	S	S	M	-	,	yes	
HBS58	143	9.020	-	-	-	-	S	-	S	L	M	-	M	,		
HBS61	135	-	-	S	-	-	M	-	-	L	M	-	M	,		
HBS67	130	-	-	S	S	-	-	-	-	L	M	-	S	Psammite	yes	
HBS70	145	-	-	M	M	-	M	-	-	S	L	-	S	,	yes	
HBS72	131	-	-	S	-	M	-	M	M	L	-	-	M	Pelite	yes	

Dalradian - Biotite was identified in thin section where possible, but may not reflect the amount present in the <2µm size fraction. Thin sections were also made for D2, D3, D8, D13, D19, D22, D24, D33, D37, D45, D49, D51 and D65.

Sample	Hbre1	b ₀	1	2	3	4	5	6	7	8	9	10	11	12	Lithology	TS
D1	111	-	-	-	-	-	-	-	-	M	L	S	S	Pelite	yes	
D7	125	-	-	-	-	-	-	-	S	L	M	-	S	,	yes	
D9	126	-	-	-	S	-	-	-	S	L	M	-	S	,	yes	
D10	114	-	-	-	S	-	-	-	S	L	M	-	M	,	yes	
D11	125	-	-	-	-	-	-	-	-	L	M	-	M	,	yes	
D12	115	-	-	-	-	-	-	-	-	L	M	-	M	,	yes	
D14	129	-	-	-	S	-	-	-	-	L	M	-	M	,	yes	
D15	133	-	-	-	S	-	-	-	-	L	M	S	M	,	yes	
D16	133	-	-	-	-	-	-	-	-	L	M	M	M	,	yes	
D17	122	-	-	-	S	-	-	-	-	L	M	S	M	,	yes	
D18	116	-	-	-	-	-	-	-	-	L	M	-	M	,	yes	
D20	167	-	-	-	-	-	-	-	-	S	L	M	S	Psammite	yes	
D21	121	-	-	-	-	-	-	-	-	L	M	S	M	Pelite	yes	
D23	143	-	-	-	S	-	-	-	-	M	M	M	M	,	yes	
D25	124	-	-	-	S	-	-	-	-	S	L	S	S	Psammite	yes	
D27	158	-	-	-	S	-	-	-	-	S	L	M	S	,	yes	
D29	-	9.027	-	-	S	-	-	-	-	S	L	M	S	,	yes	
D31	136	-	-	-	-	-	-	-	-	S	M	S	S	,	yes	
D35	116	-	-	-	S	-	-	-	-	S	L	-	S	,	yes	
D38	115	9.006	-	-	-	-	-	-	-	L	L	-	S	Pelite		
D39	151	9.026	-	-	-	-	-	-	-	M	L	S	S	,	yes	
D41	154	-	-	-	-	-	-	-	-	S	M	-	S	Psammite	yes	
D43	-	9.018	-	-	S	-	-	-	-	M	L	S	S	Pelite	yes	
D44	179	8.998	-	-	-	-	-	-	-	S	L	L	M	,		
D47	115	-	-	-	-	-	-	-	-	L	M	M	M	,	yes	
D50	144	9.042	-	-	-	-	-	-	-	M	M	S	M	,		
D53	-	-	-	-	-	-	-	-	-	S	L	M	-	Psammite	yes	
D57	125	-	-	-	-	-	-	-	-	M	M	L	M	Pelite	yes	
D59	128	9.023	-	-	-	-	-	-	-	L	L	-	M	,		
D60	145	-	-	-	-	-	-	-	-	L	M	S	M	,		
D61	153	-	-	-	-	-	-	-	-	M	M	L	S	,	yes	
D64	-	8.995	-	-	-	-	-	-	-	S	L	-	M	Psammite		
D66	134	9.002	-	-	-	-	-	-	-	M	L	S	L	Pelite		
D67	119	9.013	-	-	-	-	-	-	-	L	L	-	M	,	yes	
D68	127	9.010	-	-	-	-	-	-	-	S	M	L	-	S	,	
D69	123	-	-	-	-	-	-	-	-	S	M	-	S	Psammite	yes	

APPENDIX 5.1 - XRD analyses of samples (<2µm size fraction) from Nepal.

1 = Illite/Smectite; 2 = Chlorite/Smectite; 3 = Pyrophyllite; 4 = 1M Mica; 5 = 1Md, K, Na Mica; 6 = 6:4 Muscovite/Paragonite; 7 = Paragonite; 8 = 2M₁ Mica; 9 = Albite; 10 = Biotite; 11 = Chlorite. S, M and L (small, medium and large) indicates a visual estimate of mineral proportions based on relative peak sizes. Biotite was identified in thin section where possible, but may not reflect the amount present in the <2µm size fraction. TS = thin section, Ky = kyanite zone Gt = garnet zone, Bi = biotite zone, Chl = chlorite zone.

Traverse A - Barabise to the Bagmati River.

Sample	Hbrel	b ₀	1	2	3	4	5	6	7	8	9	10	11	Lithology	TS	
HS1														Benighat Slate (graphitic)		
HS2	142	9.025	-	-	-	-	-	-	L	M	-	S		Benighat Slate	yes	
HS3														" "	(graphitic)	
MCTI																
HS4	151	8.992	-	-	-	-	-	S	M	L	-	L	S	Kuncha (Gt)	pelite	yes
HS5	192	9.004	-	-	-	-	-	-	M	M	M	L	S	" "	"	yes
HS6	209	9.006	-	-	S	-	-	-	S	L	M	L	S	" "	"	
HS7	167	9.010	-	-	-	-	-	-	-	L	L	L	S	" "	psammite	yes
HS8	251	9.011	-	-	-	-	-	-	-	M	L	M	S	" "		
HS9	187	9.019	-	-	-	-	-	S	L	L	-	S	" "	pelite		
HS10	189	-	-	-	-	-	-	-	-	-	-	-	-	semi-pelite	yes	
HS11	189	8.996	-	-	-	-	-	S	M	M	-	S	Kuncha (Bi)	" "	"	
HS12	176	9.006	-	-	-	-	-	-	-	L	M	M	S	" "	pelite	
HS13	183	8.998	-	-	-	-	-	-	-	S	L	-	S	" "	psammite	
HS14	181	9.008	S	-	-	-	-	-	S	M	L	L	S	" "	psammite	yes
HS15	179	9.021	-	-	S	-	-	-	S	L	L	-	S	" "	"	
HS16	173	9.008	-	-	-	-	-	-	-	L	M	M	M	" "	"	yes
HS17	133	9.008	S	-	S	-	-	-	S	M	L	-	M	Kuncha (Chl)	" "	yes
HS18	157	9.005	-	-	-	-	-	-	S	L	M	-	L	" "	pelite	yes
HS19	143	9.009	-	-	-	-	-	-	S	L	S	-	M	" "	"	
HS20	179	9.019	-	-	-	-	-	-	S	L	S	-	M	" "	"	yes
HS21	167	9.014	-	-	-	-	-	-	S	L	M	-	M	" "	"	yes
MCTI																
HS22	137	9.011	-	-	-	-	-	-	L	M	-	M		Benighat Slate	yes	
HS23	117	9.016	-	-	-	-	-	-	S	L	-	L		" "	"	yes
HS24	127	-	-	S	-	-	-	-	-	L	S	-	M	" "		yes
HS25	126	9.011	-	-	-	-	-	-	S	L	S	-	M	" "	(+ calcite)	yes
HS26	133	9.025	-	-	S	-	-	-	S	S	L	-	S	" "	"	yes
HS27	176	9.027	-	-	-	-	-	-	S	S	L	-	S	" "	(+ dolomite)	yes
HS28	170	9.030	-	-	S	-	-	-	-	L	-	L	S	" "	(+ calcite)	yes
HS29	151	9.013	-	-	-	-	-	S	M	L	-	S	" "	"	(+ dolomite)	yes
HS30	140	9.025	-	-	-	-	-	-	S	L	-	S	" "	"	(+ dolomite)	yes
HS31	139	9.031	-	-	-	-	-	-	S	L	S	-	S	" "	"	yes
MCTII																
HS32	276	9.013	-	-	-	-	-	S	M	S	L	S	Kalitar (Gt)		yes	
HS33	209	9.020	-	-	-	-	-	-	S	L	S	L	S	Kulikhani (Gt)		yes
HS34	144	-	-	-	-	-	-	S	S	L	L	S	" "	(Bi) (+ dolomite)		yes
HS35	186	9.029	-	-	-	-	-	-	L	S	S	L	S	Tistung (Bi)		yes
HS36	114	9.039	M	S	-	-	-	-	-	L	M	L	S	" "	(+ calcite)	yes
HS37	186	9.037	-	-	-	-	-	-	S	L	L	L	S	Chandragiri Limestone		yes
HS38	181	9.052	-	-	S	-	-	-	S	M	S	-	S	Tistung (Chl)		yes
HS40	164	9.032	-	-	S	-	-	-	S	M	L	-	-	" "	"	yes
HS41	117	9.032	-	-	-	-	-	-	-	L	M	-	-	" "	(+ dolomite)	
HS42	143	9.049	-	-	-	-	-	-	-	L	L	-	-	" "	"	yes
HS43	120	9.011	-	-	-	-	-	-	-	L	M	-	S	" "	(+ calcite)	yes
HS44	114	9.047	-	-	-	-	-	-	S	M	M	-	-	" "	"	yes
HS46	-	9.032	S	-	-	-	-	-	S	S	L	-	-	Kulikhani (Bi)		yes
HS47	141	9.029	S	-	-	-	-	-	-	L	L	-	L	" "	(+ calcite)	yes
HS48	165	9.022	S	-	-	-	-	-	-	M	L	M	-	" "	"	yes
HS49	179	9.025	S	-	-	-	-	-	-	L	L	M	-			
HS50	151	9.038	-	-	S	-	-	-	-	L	M	M	L	Kalitar (Gt)	gneiss	yes
HS51	140	9.013	S	-	-	-	-	-	-	M	L	M	S	Kalitar (Gt)		yes
HS52														Raduwa (Gt)		yes
MCTII																
HS53	173	9.001	S	-	-	-	-	M	L	L	-	M		Benighat Slate		
MBT																
HS54	144	-	-	-	-	-	-	S	M	M	-	M		Siwalik (+ cc)	yes	

Traverse B - Syabru to Betrawati.

Sample	Hbrel	b ₀	1	2	3	4	5	6	7	8	9	10	11	Lithology	TS	
LH1														Tibetan Slab (Ky)	yes	
LH2	-	-	-	-	-	-	-	-	S	-	M	L		" "	epidote schist	yes
MCTII																
LH3	160	9.011	S	-	S	-	-	-	S	S	M	L	-	Kuncha (Gt)	pelite	yes
LH4	189	8.996	-	-	S	-	-	-	S	L	-	L	S	" "	"	yes
LH5	164	8.993	-	-	-	-	-	-	M	L	M	S		" "	"	
LH6	166	9.014	-	-	S	-	-	-	M	L	L	L	S	" "	"	yes
LH7	156	9.001	-	-	-	-	-	-	L	L	L	L	S	" "	"	yes
LH8	191	9.017	-	-	S	-	-	-	S	M	L	L	-	semi-pelite	yes	
LH9	179	9.001	S	S	-	-	-	-	-	L	M	M	L	" "	pelite	yes
LH10	160	9.013	-	-	-	-	-	-	L	S	L	S	-	(Bi)	"	yes
LH11	191	9.016	-	-	-	-	-	-	S	L	L	S	-	" "	semi-pelite	yes
LH12	188	9.013	S	-	-	-	-	-	S	M	M	M	S	" "	pelite	yes
LH13	117	9.002	-	-	-	-	-	-	L	S	-	M	-	(Chl)	"	yes
LH14	120	9.010	S	-	-	-	-	-	S	M	S	-	L	" "	"	yes
LH15	138	9.016	M	-	-	-	-	-	S	L	S	-	L	" "	"	yes

APPENDIX 5.2 - Fluid inclusion microthermometric data for samples from Nepal.

Sample	Te (H_2O 1st Melt)			SNo.	Tm H_2O (H_2O last melt)			Th TOT (Total homogenisation)		
	PSD	M	SNo.		PSD	M	SNo.	PSD	M	SNo.
LH1	-	-	-	-	-	-	-	-	-	-
FI2	A 1.67	-24.1	5		0.44	-2.29	14	4.55	253-L	12
	B 2.30	-22.3	2		1.06	-3.50	5	4.3	193-L	3
FI3	1.58	-25.4	14		0.32	-1.21	11	1.26	285-L	38
FI4	1.71	-26.1	5		0.50	-2.32	25	7.21	287-L	23
FI5	A 1.88	-24.2	6		0.59	-3.07	9	-	367-V	1
	B 0.79	-27.8	4		2.80	-10.3	7	-	240-L	1
	C -	-	-		-	-	-	-	-	Dec. at 240°C
FI6	A -	-	-		-	-1.90	1	1.70	227-L	3
	B 1.05	-27.3	2		2.01	-5.80	4	-	303-V	1
	C -	-	-		-	-5.30	1	-	108-L	1
	D -	-	-		-	-	1	-	205-L	1
	E -	-	-		-	-2.10	1	-	-	-
FI7	A 2.31	-14.5	13		0.43	-2.21	22	2.64	258-L	8
	A 1.51	-14.9	6		''	-2.25	2	7.37	278-L	8
	B 0.35	-15.4	2		0.15	-2.25	2	9.72	353-L	3
	C -	-	-		0.49	-2.23	3	-	284-V	1
	D -	-	-		-	-1.90	1	-	316-L	1
FI8	A 0.20	-23.2	2		1.12	-2.80	2	-	279-L	15
	B -	-	-		-	-	-	11.5	315-L	2
	Tm CO_2 (CO_2 last melt)			Tm Clath (Clathrate melt)			Th CO_2 (CO_2 homogenisation)			
LH1	PSD	M	SNo.	PSD	M	SNo.	PSD	M	SNo.	
	-	-	-	0.17	2.51	20	-	-	-	
FI2	A -	-	-	0.51	9.09	7	0.55	-4.83-L	6	
FI3	0.53	-56.99	24	0.35	9.62	20	0.22	31.1-L	35	
FI4	-	-	-	0.48	10.64	23	-	0.35-L	2	
FI5	A 0.62	-59.03	11	0.92	8.74	7	2.50	24.3-L	11	
	B 0.51	-59.55	11	0.61	8.77	7	1.56	21.6-L	10	
	C -	-	-	-	-	-	-	26.6-V	1	
FI6	A -	-	-	0.31	9.53	3	0.83	26.7-L	3	
	B 0.68	-60.43	12	1.44	8.74	7	2.82	13.1-L	12	
	C -	-	-	-	7.60	1	0.70	21.3-L	2	
	E -	-	-	-	-	-	-	25.1-L	1	
FI7	A -	-	-	-	8.90	1	0.25	-1.05-L	2	
	B -	-	-	-	1.80	1	-	-	-	
FI8	A -	-	-	0.21	7.53	3	2.16	24.1-L	9	

PSD = Population Standard Deviation, M = Mean Value ($^{\circ}C$), SNo = Sample Number. Samples are subdivided into inclusion populations A, B, C etc. L = liquid, V = vapour.